toth.zsuzsanna.emese_174_24

MTA DOKTORI ÉRTEKEZÉS

Neuromodulátorok az energiaháztartás és a stresszválasz szabályozásában

Dr. Tóth Zsuzsanna

Semmelweis Egyetem
Általános Orvostudományi Kar
Anatómiai, Szövet- és Fejlődéstani Intézet

Budapest
2024

toth.zsuzsanna.emese_174_24

TARTALOM

1. RÖVIDÍTÉSEK JEGYZÉKE

2TDM: 2-es típusú diabetes mellitus

ACTH: adrenokortikotrop hormon

ADX: adrenalektómia

AGRP: aguti-kapcsolt fehérje (*agouti-related protein*)

AP: area postrema

ARC: nucleus arcuatus hypothalami

AV3V: anteroventrális periventrikuláris area

AVP: (arginin)-vazopresszin

CART: kokain és amfetamin regulált transzkript (*cocaine- and amphetamine-regulated transcript)*

Cat #: katalógus szám

Core: Nac központi magja

CRH: kortikotropin-felszabadító (*releasing*) hormon

cVLM: kaudalis ventrolaterális medulla oblongata

D1R/D2R: 1-es/2-es típusú dopamin receptor

DHA: dorzális hipotalamikus area

DI: AVP hiányos homozigóta (-/-) Brattleboro patkány

DLH: dorzolaterális hipotalamusz

DM: nucleus dorsomediális hypothalami

DMX: nucleus dorsalis nervi vagi

dp: dorzális parvocelluláris PVN

EchoMRI: Echo mágneses rezonancia mérés

EEG: elektronkefalográfia

EMG: elektromiográfia

FISH: fluoreszcens *in situ* hibridizáció

fMRI: funkcionális mágneses rezonancia képalkotás (*functional magnetic resonance imaging*)

GFP: zöld fluoreszcens protein (*green fluorescent protein*)

GPCR: G-fehérje-kapcsolt receptor (*G protein-coupled receptor*)

H: a nucleus accumbens Héj (*shell*) régiója

HPA tengely: hipotalamusz-hipofízis-mellékvese tengely (*hypothalamic-pituitary adrenal axis*)

HRP: tormaperoxidáz enzim (*horseradish peroxidase enzyme*)

HS: krónikus sóterhelés (*high salt*)

icv: intracerebroventricularis (oldalkamrába történő)

IHC: immunhisztokémia (*immunohisochemistry*)

IP-GTT: intraperitoneális glükóz tolerancia teszt

IP-ITT: intraperitoneális inzulin tolerancia teszt

ISH: *in situ* hibridizáció

IUGR: intrauterin növekedési retardáció (*intrauterine growth retardation*)

KO: géndeficiens (*knockout*)

KP: kis platform (alvásmegvonás)

KPR: KP után alvás pótlás (*rebound*) saját ketrecben

LH: laterális hipotalamusz

LHA: laterális hipotalamikus area

LPS: bakteriális lipopoliszacharid

M: a nucleus accumbens Mag (*core*) régiója

MCH: melanin-koncentráló hormon (*melanin-concentrating hormone*)

mHéj: a nucleus accumbens mediális Héj régiója

mpdd: magnocelluláris dorzális preautonóm PVN

mpdv: magnocelluláris ventrális PVN

mpPVN: mediális parvocelluláris PVN

mpv: magnocelluláris pre-autonóm PVN

mPVN: magnocelluláris (nagysejtes) PVN

MWT: mikrohullámú kezelés (*microwave treatment*)

NA: noradrenalin

Nac: nucleus accumbens

NP: nagy platform (alvásmegvonás)

NPFF2R: 2-es típusú neuropeptid FF receptor

NPR: NP után alvás saját ketrecben

NPY: neuropeptid Y

NS: nem-sós (csap-) vízzel itatott állat

NT: normál táplált

NTS: nucleus tractus solitarii

NUCB2: nucleobindin'-2 fehérje

OVX: ovariektómia

PBS: 0,1 M sós foszfát puffer (pH 7,4)

PFA: perifornikális area

POMC: pro-opiomelanokortin

pPVN: parvocelluláris (kissejtes) PVN

PR: 50% protein redukált (*protein reduced*) táppal etetett anyától származó utód

PrRP/PRLH: prolaktin-felszabadító (*releasing*) peptid /hormon

PrRPR: a PrRP saját receptora (GPR10)

PT: patkány táp

pTH-Ser31: szerin 31-es helyen foszforilált tirozin hidroxiláz enzim

pv: periventrikuláris parvocelluláris PVN

PVN: nucleus paraventricularis hypothalami (*hypothalamic paraventricular nucleus)*

REM alvás: gyors szemmozgásos (*rapid eye movement*) alvás

ROI: értékelési terület *(region of interest*)

RR: ismételt (*repeated*) restraint stressz

RT-PCR: reverz transzkripció-polimeráz láncreakció (*reverse transcription-polymerase chain reaction*)

SA: streptavidin

SK: saját ketrecben tartott állat

SKR: saját ketrecben tartott állat, KPR-rel egyidejű leölés

SON: nucleus supraopticus (*supraopticus nucleus*)

ST: sóterhelt, 2% NaCl oldattal itatott állat

TH: tirozin-hidroxiláz

TNF alfa: tumor nekrózis faktor alfa

TRH: thyreotropin-felszabadító (*releasing*) hormon

TSA: tiramid szignál amplifikáció

ttg/ttkg: testsúly g/testsúly kg

TTX: tetrodotoxin

vHéj: a Nac ventrális Héj régiója

vs.: *versus*

VT: genetikailag vad típusú

ZI: zona incetra

ZsT: zsírdús táp

2. BEVEZETÉS

2.1. A hipotalamusz szerepe a homeosztázis szabályozásában

A homeosztázis, a szervezet belső paramétereinek (vércukorszint, testhőmérséklet, etc.) fenntartása a változó külső környezet ellenében, aktív szabályozó folyamatok révén valósul meg. E paraméterek szabályozása magában foglalja a szenzoros, érzelmi és tanult információk összegzését majd a megfelelő autonóm, endokrin és viselkedési válaszok kialakítását. Az egyes paraméterek szabályozása így végeredményben különböző élettani folyamatok (például táplálékfelvétel, folyadékháztartás, hőszabályozás, alvás-ébrenlét, reprodukció, illetve a stressz reakció) szabályozásában nyilvánul meg. E szabályozási feladatok összetettségét fokozza, hogy az egyes folyamatok nem függetlenek, hiszen a túlélés érdekében az egyik szükséglet kielégítése adott esetben felülírja a másikét (például stressz *kontra* táplálékfelvétel). Így a homeosztázis összességében egy igen jelentős integráció eredményeként jön létre. Nem véletlen, hogy számos kórképben a homeosztatikus szabályozás elemeinek működése együttesen borul fel, az étkezési zavarok például sokszor alvási zavarokkal járnak (Allison, Spaeth et al. 2016), a nemi hormonok zavarai hőszabályozási gondokkal kapcsolódnak össze (Charkoudian és Stachenfeld 2016), illetve mentális stresszbetegségekben a hangulat szélsőséges irányú eltolódása mellett jellemzően alvási és étkezési zavarok lépnek fel (Goldstein és Walker 2014, Bao és Swaab 2019).

A szervezetben a homeosztatikus integráció fő agyi központja a hipotalamusz, ami nagymértékben alkalmazkodott e funkció betöltéséhez. Először is, elhelyezkedése alapján egyedülállóan alkalmas arra, hogy közvetlen kapcsolatot tartson fenn a szubkortikális (limbikus) agyterületekkel, az agytörzsi és gerincvelői autonóm központokkal, és az endokrin rendszerrel is (Levine 2000). Másodszor, számos kis magot tartalmaz, mely lehetővé teszi a munkafolyamatok hatékony szervezését. Ez nem jelent szigorú funkcionális elkülönülést az egyes magok részéről (Goldstein, Levine et al. 2018), annál inkább lehetőséget a magas szintű finomszabályozásra, a hipotalamusz magjainak intenzív egymás közti kommunikációja révén (Ulrich-Lai és Ryan 2014) (1. ábra). Az integráció harmadik szintjét, a hipotalamusz jelátviteli folyamataiban fontos szerepet játszó neuromodulátorok, a neuropeptidek jelentik (Hokfelt, Broberger et al. 2000). A neuropeptidek nagyméretű és sűrűségű (*dense-core*) vezikulákban raktározódnak az axonterminálisokban, illetve dendritekben. Az axonokból jellegzetes módon extraszinaptikusan, a kis molekulájú neurotranszmitterekkel egyidőben szabadulnak fel (*corelease*), amikor a neuronok nagy frekvenciával, vagy sorozatban (*burst*) tüzelnek. Erre

különösen akkor van szükség, amikor az idegrendszer kihívásoknak van kitéve, például sérülés, fájdalom vagy stressz miatt (Hökfelt, Barde et al. 2018). A neuropeptidek mennyisége a terminálisok területén a kismolekulájú transzmitterekhez képes igen csekély, mégis nagy hatótávolságban képesek hatást kifejteni, mivel az extracelluláris folyadéktérben, illetve a liquorral nagy távolságba is eljutnak (*volume transmission*) és receptoraik affinitása az igen alacsony, nanomoláris tartományba esik (Taber és Hurley 2014, Hökfelt, Barde et al. 2018). Hátrányuk, hogy a peptidszintézis a sejttestben zajlik és mivel a felszabadult neuropeptidek esetében visszavételi mechanizmusok nem játszanak közre, a raktárak feltöltődése a terminálisban az axonális transzport, illetve a szintézis sebességének függvénye (Hokfelt, Broberger et al. 2000). Egy sejtben többféle neuropeptid is termelődhet (koexpresszió) (Skrapits, Borsay et al. 2015), egy neuropeptid ugyanakkor többféle működés szabályozásában is részt vehet. A kortikotropin-felszabadító hormon (CRH) például, klasszikus stressz hormonként ismert és anorexigén (Tsigos és Chrousos 2002), a melanin koncentráló hormon (*melanin concentrating hormone*, MCH) pedig orexigén, és meghatározó szereppel bír az elalvásban és az alvás fenntartásában (1. ábra) (Torterolo, Scorza et al. 2015).

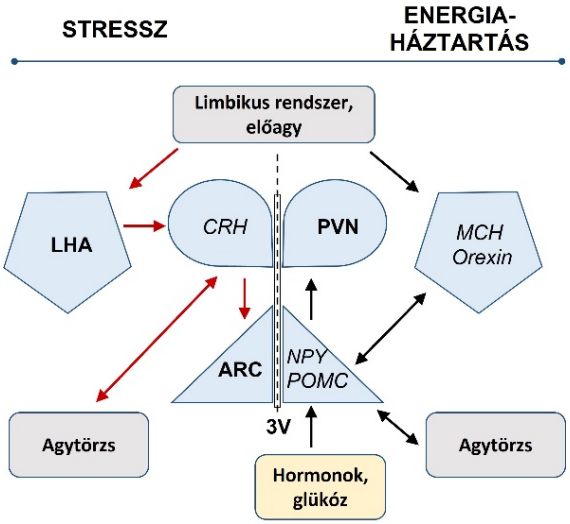

1. ábra. Homeosztatikus integráció a hipotalamuszban (kék) a stresszválasz (bal) és az energiaháztartás szabályozás (jobb) példáján. Stressz: elsődleges központ a nucleus paraventricularis hypothalami (PVN), mely integrálja a perifériáról beérkező információt, majd a hipofízisen keresztül aktiválja a mellékvesekérget és szervezi az endokrin és autonóm válaszokat. Energiaháztartás: elsődleges központ a nucleus arcuatus (ARC), mely neurális és humorális bemenetek összegzése után a hipotalamusz másodlagos központjaival kommunikál. Ugyanazok a neuropeptidek többféle funkcióval is bírnak, az egyes feladatok különböző aspektusait dolgozzák fel. CRH: stresszválasz, anorexigén; MCH és orexin: orexigén, alvás-ébrenlét szabályozás, stresszválasz; neuropeptid Y (NPY): orexigén, pro-opiomelanokortin (POMC): anorexigén. LHA: laterális hipotalamikus area, 3V: 3. agykamra. Ulrich-Lai munkája alapján (Ulrich-Lai és Ryan 2014).

2.2. A nyúltvelői noradrenerg felszálló pálya

A homeosztázis fenntartásának fontos eleme a homeosztázist veszélyeztető ingerekre, másnéven stresszorokra adott megfelelő válasz kialakítása, amit stresszválasznak nevezünk. A stresszválasz koordinációját a hipotalamusz végzi, melynek során a szimpatikus idegrendszer és a hipotalamusz-hipofízis-mellékvese (HPA) tengely működése is fokozódik. A szimpatikus aktiváció révén a mellékvesevelőből adrenalin kerül a vérbe, a HPA tengely stimulációjának első lépese pedig a tengely központját képező nucleus paraventricularis hypothalami (*hypothalamic paraventricular nucleus,* PVN) kissejtes CRH-termelő neuronjainak ingerlése. A hipofízis portális keringésébe jutó CRH hatására az adenohipofízisből adrenokortikotrop hormon (ACTH) szabadul fel, ami fokozza a mellékvesekéreg kortikoszteron szekrécióját, mely végül negatív visszacsatolással szabályozza a tengely működését. Mindezek a folyamatok a Cannon-féle vészreakciót indítják el, ami biztosítja a szervezet vészhelyzetre való felkészülését (üss, vagy fuss reakció), valamint változások történnek a viselkedés, a hangulat és kognitív funkciók terén is.

A testet érő behatásokat különböző receptorok érzékelik. A szomatoszenzoros rendszer által érzékelt fájdalmi ingerület a spinotalamikus, spinoreticuláris és trigeminotalamikus pályák kollaterálisanak közvetítésével eljut a nyúltvelőbe, a nucleus tractus solitarii kaudális részébe (NTS) és a kaudalis ventrolaterális medullába (cVLM), melyek területek egymással is kapcsolatban állnak, valamint a hídba, a locus ceruleusba (Kvetnansky, Sabban et al. 2009, Taylor és Westlund 2017). A visceroszenzoros információk, mint a baro- és kemoreceptorok ingerületei, a zsigeri fájdalom, a gastrointestinális rendszer feszülése-telítettsége, illetve a gyulladás okozta ingerületek, az agyidegek közvetítésével elsődlegesen az kaudális NTS-be kerülnek (Kvetnansky, Sabban et al. 2009). Az area postrema szintjében és attól kaudálisan az NTS és cVLM területén noradrenerg sejtcsoportok helyezkednek el, melyek a konvencionális nevezéktan alapján az A2, illetve az A1 sejtcsoportot alkotják. Az A2 sejtcsoporthoz összességében az NTS, a cirkumventrikuláris szervként működő area postrema és a nucleus dorsalis nervi vagi (DMX) noradrenerg neuronjai tartoznak (2. ábra) (Kvetnansky, Sabban et al. 2009). Az A1 neuronok axonjai, és az A2 sejtcsoport NTS területére eső neuronjainak (A2-NTS) axonjai képezik a stressz információ továbbítása szempontjából legjelentősebb pályát, a ventrális noradrenerg köteget, melynek fő végállomása a hipotalamusz. A pálya sérülése 90%-ban gátolja a stressz-tengely, vagyis HPA tengely aktiválását homeosztatikus stressz esetén (Pacak, Palkovits et al. 1995). Emiatt, és mivel IX. és X. agyidegek az NTS noradrenerg sejtjeivel közvetlen szinapszisokat képeznek (Appleyard, Marks et al. 2007), a nyúltvelői

noradrenerg neuronok a periféria felől a központi idegrendszerbe jutó stressz információ kapuőreinek tekinthetők. A HPA tengely kiindulópontját képező CRH neuronok katekolaminerg beidegzése 94%-ban az A1, A2 sejtcsoportokból ered, nagyobb részt az A2 neuronokból (Sawchenko és Swanson 1981, Sawchenko és Swanson 1982). Az A1, és elenyésző mértékben az A2 sejtcsoport látja el kizárólagosan excitatoros noradrenerg beidegzéssel az ozmoregulációért felelős magnocelluláris sejteket a PVN területén és szupraoptikus magban (*supraopticus nucleus,* SON), valamint a velük funkcionálisan szoros kapcsolatban álló anteroventrális periventricularis areat (Sawchenko és Swanson 1982, Pedrino, Rosa et al. 2014). Az A1 és A2 sejtcsoportok hipotalamuszon kívüli célterületei közül kiemelendő a locus ceruleus és amygdala, melyek szerepe a stresszel kapcsolatos érzelmi és viselkedési reakciókban ismert (Daviu, Bruchas et al. 2019). A felsőbb agyi központok az A1, A2 sejtcsoportok működését efferenseik révén befolyásolják (Tóth, Gallatz et al. 1999, Kvetnansky, Sabban et al. 2009).

2.3. A prolaktin-felszabadító peptid (PrRP)

Az A1 sejtcsoport idegsejtjei, és A2-NTS neuronok a noradrenalint mellett PrRP-t (*alias* PRLH) is expresszálnak (2. ábra) (Roland, Sutton et al. 1999, Maruyama, Matsumoto et al. 2001).

A PrRP-t human GR3 árva receptor ligandjaként azonosították 1998-ban (Hinuma, Habata et al. 1998). Elnevezése elhamarkodottnak bizonyult, mivel fiziológiás szerepét a prolaktin felszabadításban rágcsálóban és emberben is megcáfolták (Yamakawa, Kudo et al. 1999, Jarry, Heuer et al. 2000, Morales, Hinuma et al. 2000). A PrRP két izoformáját írták le; a PrRP31-et és a PrRP20-at, ez utóbbi a PrRP31 N-terminális peptid-fragmense. A PrRP csoport az úgynevezett RF-amid peptid családba tartozik (Hinuma, Habata et al. 1998). A család tagjainak közös jellemzője a C-terminálisan megjelenő arginin (R) és -amidált fenilalanin (F) szekvencia jelenléte, ide sorolható többek között a kisspeptin és a neuropeptid FF is.

PrRP-t szintetizáló sejtek az agyban a nyúltvelői két sejtcsoporton kívül csak a hipotalamusz nucleus dorzomedialisának (DM) poszteroventrális részében találhatók elszórtan, mely terület megnevezése az irodalomban nem egységes (Minami, Nakata et al. 1999, Roland, Sutton et al. 1999, Yamakawa, Kudo et al. 1999, Holt és Rinaman 2022). Fontos kiemelni, hogy a hipotalamusz PrRP-termelő sejtjei nem tartalmaznak noradrenalint (Dodd, Worth et al. 2014), mely kettős immunfestés révén lehetővé teszi a beidegzett területeken a nyúltvelői és DM eredetű PrRP sejtcsoportok axonjainak elkülönítését. Egy másik különbség, hogy nyúltvelőben a PrRP expresszió gonadalis szabályozás alatt áll. Nőstény patkányokban az A1 és A2-NTS

sejtcsoportok területén a proösztrusz idején magas, míg a hipotalamuszban termelődése független a nemi hormonoktól. Az A2-NTS területén a PrRP-immunpozitív sejtekben ösztrogén alfa receptor jelenlétét mutatták ki (Kataoka, Iijima et al. 2001).

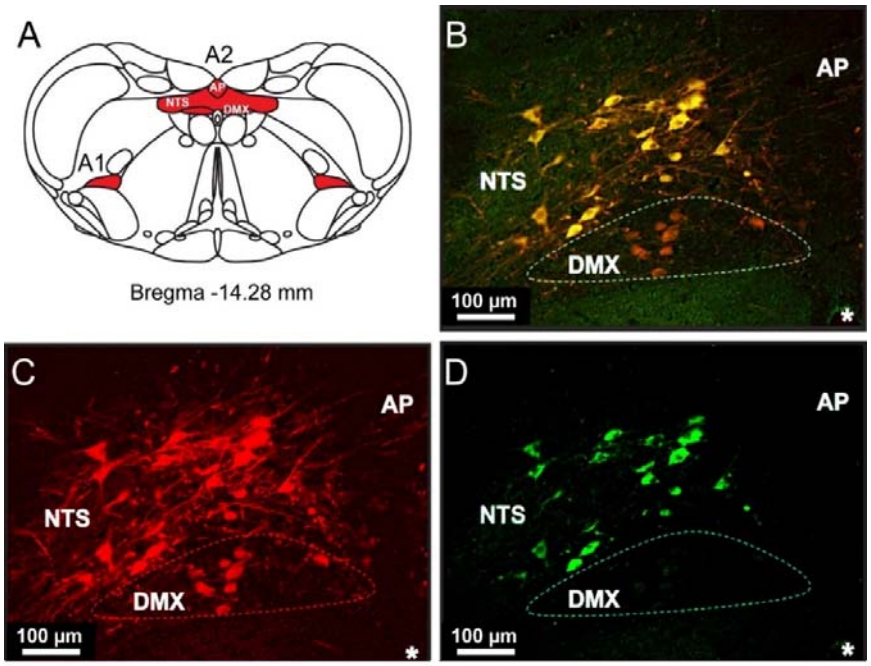

2. ábra. PrRP koexpresszió a nyúltvelői noradrenerg sejtcsoportokban. A Az A1 és A2 noradrenerg sejtcsoportok (piros) elhelyezkedése a patkány nyúltvelőben. Koronális metszet sémás ábrája a terület elülső határáról (Paxinos és Watson 2007). **B-D** Kettős, PrRP (zöld) és tirozin-hidroxiláz (piros, a noradrenerg sejtek markere) immunhisztokémiai festés a bal A2 területéről. A sárga neuronok (B) az NTS területén noradrenalint (C) és PrRP-t (D) is termelnek. AP: area postrema, DMX: nucleus dorsalis nervi vagi, NTS: nucleus tractus solitarii, *: canalis centralis.

A PrRP neuronok egérben, patkányban és emberben is főleg a hipotalamuszba vetítenek (Takahashi, Yoshinoya et al. 2000, Dodd és Luckman 2013). A legsűrűbben innervált területek közé tartozik a PVN, de jelentős beidegzést kap a peroptikus area, a DM és a laterális hipotalamikus area (LHA) is (Dodd és Luckman 2013). A PrRP rostok eredetét a beidegzett területeken nem vizsgálták.

A PrRP saját receptora a PrRPR (*alias* human GR3, GPR10) egy G-fehérje-kapcsolt receptor (GPCR) (Hinuma, Habata et al. 1998). Legnagyobb mennyiségben a nucleus reticularis thalamiban mutatták ki, ahol viszont PrRP-pozitív axonok nincsenek. Magas, illetve mérsékelt PrRPR expresszió jellemzi a hipotalamusz különböző magjait (PVN, DM), valamint a locus ceruleust, az NTS-t és az area postremát (Roland, Sutton et al. 1999). A PrRP sejtek célterületei és a PrRPR agyi eloszlása tehát csak részben átfedő. Kiderült azonban, hogy a PrRP jelentős affinitással kötődik a neuropeptid FF 2-es típusú receptorához (NPFF2R) is (Engström,

Brandt et al. 2003). Az NPFF2R patkány agyban legfőképp a talamuszban, valamint a presubiculumban fordul elő (Gouardères, Quelven et al. 2002).

A PrRP funkciói közül leginkább az energia egyensúlyra gyakorolt hatását és a stressz reakcióban betöltött szerepét vizsgálták. Anorexigén molekulaként az energiaháztartás rövid- és hosszútávú szabályozását is befolyásolja (Dodd és Luckman 2013). Fontos szerepet tölt be ugyanis a jóllakottsági szignálként ismert kolecisztokinin (Lawrence, Ellacott et al. 2002, Bechtold és Luckman 2006, Wall, Olivos et al. 2020) és a zsírraktárak mennyiségét tükröző leptin centrális hatásainak közvetítésében is (Takayanagi, Matsumoto et al. 2008, Dodd, Worth et al. 2014). Rágcsálókban az oldalkamrába intracerebroventrikulárisan (icv) beadott PrRP csökkenti az éjszakai táplálékfelvételt, növeli az oxigénfogyasztást és hosszabb távon a testhőmérsékletet (Lawrence, Liu et al. 2004, Dodd, Worth et al. 2014). Ezzel szemben, mind a PrRP gén, mind a PrRPR gén hiánya (KO egerek) a táplálékfogyasztás növekedésével jár, így ezek a KO állatok elhízásra és cukorbetegségre hajlamosak (Gu, Geddes et al. 2004, Takayanagi, Matsumoto et al. 2008). A fentieknek megfelelően a negatív energiaegyensúly (éhezés, laktáció) a PrRP mRNS expressziót mindhárom agyi PrRP sejtpopulációban csökkenti (Lawrence, Celsi et al. 2000).

A PrRP a stresszválasz kialakításában kulcsfontosságú molekula (Holt és Rinaman 2022). Rágcsálókban a PrRP-termelő sejtek a legkülönfélébb fizikai és pszichés stresszre aktiválódnak, és fokozott PrRP expresszióval reagálnak (Dodd és Luckman 2013). Ilyen stressz például az agytörzsi PrRP sejtek esetében az akut vérveszteség, a talpat ért áramütés (Morales és Sawchenko 2003), a formalin okozta fájdalom (Mera, Fujihara et al. 2006), az akut restraint (Adachi, Mochiduki et al. 2005, Mera, Fujihara et al. 2006), a vízbemerítéses-restraint (Maruyama, Matsumoto et al. 2001), az erőltetett fizikai aktivitás (Ohiwa, Chang et al. 2007), vagy a bakteriális lipopoliszacharid (LPS) által kiváltott gyulladás akut fázisa (Mera, Fujihara et al. 2006). A hipotalamusz PrRP neuronjait kevésbé vizsgálták, de azok is stressz érzékenyek, amit vízbe merítéses restraint stressz, illetve kondicionált félelem esetében mutattak ki (Maruyama, Matsumoto et al. 2001, Zhu és Onaka 2003). A centrálisan alkalmazott PrRP a CRH sejtek ingerlése révén aktiválja a HPA tengelyt (Matsumoto, Maruyama et al. 2000, Mera, Fujihara et al. 2006), ennek megfelelően a vérplazma ACTH (Matsumoto, Maruyama et al. 2000) és kortikoszteron (Seal, Small et al. 2002, Mera, Fujihara et al. 2006) szintjét is növeli. Azon túlmenően, hogy a PrRP önmagában a HPA tengely fokozott működését váltja ki, jelentősen potencírozza noradrenalin HPA tengelyt stimuláló hatását (Maruyama, Matsumoto et al. 2001, Uchida, Kobayashi et al. 2010), ami a nyúltvelői PrRP és noradrenalin koexpresszió fényében fontos tényező.

A PrRP egyéb endokrin hatásai között érdemes megemlíteni, hogy fokozza az oxitocin és a vazopresszin (AVP) elválasztást (Maruyama, Matsumoto et al. 1999, Uchida, Kobayashi et al. 2010, Yamashita, Takayanagi et al. 2013). Lényeges szimpatikus hatása ezenkívül, hogy emeli a vérnyomást és fokozza a szívfrekvenciát (Samson, Resch et al. 2000, Ma, MacTavish et al. 2009). A kardiovaszkuláris rendszert az NPFF2R közvetítésével, semmint saját receptorán keresztül befolyásolja (Ma, MacTavish et al. 2009). Két korábbi munka tanulmányozta a PrRP alvás-ébrenlét ciklusra gyakorolt hatását, melynek adatai, valószínűleg módszertani eltérések miatt ellentmondóak. Alvó állatban az egyszeri icv PrRP kezelés ébredést váltott ki (Lin, Arai et al. 2002), míg az aktív fázisban folyamatos infúzió formájában alkalmazott PrRP az alvást fokozta (Zhang, Inoué et al. 2001).

2.4. A nesfatin-1

Oh-I és munkatársai 2006-ban egy új neuropeptidet fedeztek fel a hipotalamuszban, mely egyszeri icv alkalmazást követően a patkányok éjszakai táplálékfelvételét 6 órán át erőteljesen gátolta, és hatását leptin független módon fejtette ki. Testsúlycsökkenést csak hosszú távú adagolása okozott. A peptidet nesfatin-1-nek nevezték el, munkájukat a Nature című folyóiratban publikálták (Oh, Shimizu et al. 2006). A 82 aminosavból álló nesfatin-1 egy korábban ismert prekurzor fehérje, a nucleobindin'2-encoded satiety- and fat-influencing protein, más néven NUCB2 fehérje, N-terminális szekretábilis peptid-fragmense. A NUCB2 szekvenciában azonosított prohormon konvertáz helyek alapján másik két peptid-fragmens, a nesfatin-2 és nesfatin-3 is keletkezhet, ezek biológiai funkciója ismeretlen (Johansson és Löfberg 2015, Schalla és Stengel 2018). A fehérjéket és az mRNS kimutatását célzó módszerek nesfatin-1 és NUCB2 molekulákat nem különítik el, ezért ilyen módszerek használatakor a két molekulát együttesen nesfatin-1/NUCB2-ként, röviden nesfatinként említik/említjük. Az állatok icv kezeléshez viszont a nesfatin-1 peptid rendelkezésre áll.

A NUCB2 erősen konzervatív fehérje, a patkány és az emberi NUCB2 között 87,4%-os a homológia (Oh, Shimizu et al. 2006). A nesfatin-1 jelentőségét hangsúlyozza, hogy az emberi NUCB2 génben a testtömeg indexszel összefüggő genetikai variációkat találtak (Zegers, Beckers et al. 2011). Farmakoterápiás előnye lehet, hogy intranazális beadása mellékhatások nélkül lehetséges (Shimizu, Oh et al. 2009). Ezenkívül telítődés nélkül képes átjutni a vér-agy gáton (Pan, Hsuchou et al. 2007), és a liquorban és a vérplazmában mért szintje korrelál (Tan, Hallschmid et al. 2011). Fenti tulajdonságai alapján a nesfatin-1 az elhízás kezelésében ígéretes gyógyszeripari célpontnak minősült és a további kutatások középpontjába került (Schalla és Stengel 2018).

A nesfatin a periférián és a központi idegrendszerben is rendkívül elterjedt. Az agyban a hipotalamuszban termelődik a legnagyobb mennyiségben. Számos neuropeptiddel koexpresszál, például CRH-val és thyreotropin-felszabadító hormonnal (TRH) a PVN területén, pro-opiomelanokortinnal (POMC) és kokain- és amfetamin-szabályozott transzkriptettel az ARC magban, MCH-val az dorzolaterális hipotalamuszban (DLH), valamint az oxitocinnal és az AVP-vel a magnocelluláris neuronokban (Brailoiu, Dun et al. 2007, Foo, Brismar et al. 2008, Fort, Salvert et al. 2008, Kohno, Nakata et al. 2008). Ugyanakkor nesfatin-pozitív neuronok jelentős populációi találhatóak az agytörzsben is (Edinger-Westphal mag, raphe magok, locus ceruleus, NTS, DMX, cVLM) (Brailoiu, Dun et al. 2007, Goebel, Stengel et al. 2009). A nesfatin. Kisebb mennyiségben azonban számos egyéb agyterületen is kimutatható (Stengel 2015).

A nesfatin-pozitív neuronok expressziós mintázata, és egyéb kísérleti adatok alapján nesfatin-1 táplálékfelvétel csökkentő hatásáért elsősorban a hipotalamusz nesfatin neuronjait teszik felelőssé (Oh, Shimizu et al. 2006, Sedbazar, Maejima et al. 2013, Zhang, Wang et al. 2019). Éhezést követő újraetetés során a PVN és SON nesfatin tartalmú neuronjai aktiválódnak (Kohno, Nakata et al. 2008). A nesfatin expresszió a PVN területén éhezésre csökken, az expresszió szelektív csendesítése pedig a táplálékfelvételt növeli (Sedbazar, Maejima et al. 2013, Nakata, Gantulga et al. 2016). A bizonyítékok szerint a nesfatin-1 táplálékfelvételre gyakorolt hatásait elsősorban a melanokortin (melanokortin 3/4 receptor) (Oh, Shimizu et al. 2006, Tanida és Mori 2011) és az oxitocin rendszer közvetíti (Maejima, Sedbazar et al. 2009), de felmerült a CRH (Stengel, Goebel et al. 2009), a TRH, és a hisztamin rendszer közreműködése is (Gotoh, Masaki et al. 2013). Említésre méltó, hogy *ex vivo* a nesfatin-1 az ARC neuropeptid Y (NPY) tartalmú orexinerg sejtjeit gátolja (Price, Samson et al. 2008).

Mivel a táplálékfelvétel és a vércukorszint centrális szabályozásának agyi területei átfednek, a nesfatin további lehetséges szerepei közt felvetődött a glükóz homeosztázis központi szabályozása is. A magas zsírtatalmú táplálék fogyasztása valóban hátrányosabban érinti a NUCB2 génkiütött egereket, mint a vad típust, mivel súlyos inzulinrezisztencia alakul náluk. Bár szerzők a makrofágokban termelődő nesfatin szerepét emelik ki a patomechanizmusban (Ravussin, Youm et al. 2018), egyéb adatok az agyi nesfatin központi szerepére utalnak. A hipoglikémia például mind a hipotalamuszban található (ARC, PVN, LHA), mind a nyúltvelői (NTS) nesfatin-termelő neuronokat jelentős mértékben aktiválja (Bonnet, Djelloul et al. 2013). A máj és a perifériás szövetek inzulin érzékenysége icv nesfatin- 1 infúziót követően nő, a májban csökkent glükóztermelés, a vázizomzatban emelkedett glükózfelvétel jelentkezik (Yang, Zhang et al. 2012, Guo, Liao et al. 2013).

Ellentétesen, amennyiben NUCB2 géncsendesítés történik a hipotalamuszban, a máj glükóz leadása nő, és a perifériás szövetek glükózfelvétele csökken (Wu, Yang et al. 2014).

A fentieken kívül a nesfatin számos egyéb működésben is vesz részt. Adatok láttak napvilágot többek között a nesfatin folyadékháztartásban (Yosten, Redlinger et al. 2012, Yoshimura, Matsuura et al. 2014, Nakata, Gantulga et al. 2016), reproduktív tengely szabályozásában, szimpatikus aktivitás szabályozásában, valamint a szorongás és a depresszió patomechanizmusában betöltött szerepéről is (Schalla és Stengel 2018).

Bár a nesfatin számos neuropeptid jelátvitelét befolyásolja, hatásámechanizmusában nem tartozik a klasszikus neuropeptidek közé, ugyanis az axonokba nem transzportálódik. Jelenlétét a dendrititek szekréciós vezikuláiban mutatták ki (Maejima, Sedbazar et al. 2009), ezért dendritikus felszabadulását és helyi, autokrin/parakrin hatásmechanizmusát feltételezik (Schalla és Stengel 2018). Receptora mindeddig azonosítatlan, de az *in vitro* kísérleti adatok saját Gi/Go-fehérje-kapcsolt receptor létezésére utalnak (Rupp, Wölk et al. 2021). Változatos biológiai hatásai valószínűleg intracelluláris jelátviteli folyamatainak rendkívüli sokszínűségével magyarázhatóak (Brailoiu, Dun et al. 2007, Rupp, Wölk et al. 2021).

3. MÓDSZEREK

A fejezet áttekintést nyújt a munkában felhasznált módszertani eszköztárról. A kísérleti módszerek részletes leírása a csatolt publikációkban szerepel. Gyakran található rövid ismertető a módszerekről az eredmények leírásánál is, amennyiben ez a megértéshez szükséges.

A kísérleteket patkányokon és egereken végeztük, a csatolt publikációkban fellelhető állatkísérleti engedélyek birtokában.

3.1. Nem-invazív állatkísérletek

- Testsúly, táplálék- és folyadékfogyasztás rendszeres mérése
- Intrauterin alultáplálás; az utódok táplálékmegvonása az időzítetten terhes patkány anyák fehérjecsökkentett (50%) táppal való etetését jelentette, amit terhesség első napjától a szülésig kaptak
- Echo mágneses rezonacia képalkotás (EchoMRI); testösszetétel meghatározása
- Hedonikus táplálékfelvétel mérése; cukrozott sűrített tej fogyasztása alapján
- Zsírpreferencia teszt; *ad libitum* hozzáférhető patkány eledel és zsírdús eledel közötti választás preferenciájának mérése
- Stressz kísérletek; akut, illetve krónikus (ismételt) restraint stressz, krónikus sóterhelés, akut hideg stressz
- Depresszió modellek; erőltetett úszás, tanult tehetetlenség
- Alváskísérletek; gyors szemmozgásos (*rapid eye movement*) alvás (REM) megvonás, illetve azt követő REM alvás pótlás (*rebound*), megfelelő kontroll csoportokkal

3.2. Beavatkozást igénylő állatkísérletek

- Csontvelőirtás, majd donor csontvelő transzplantálása egerekben
- Az arteria cerebri media féloldali elzárása egerekben
- Elektroenkefalográfia/elektromiográfia (EEG/EMG), beültetetett elektródák segítségével
- Biotelemetria; a testbe ültetett jeladók (szívfrekvencia, testhőmérséklet, mozgás mérése) és telemetriás ketrec (táp- és vízfogyasztással töltött idő mérése) segítségével
- Szerv-, vagy szövetirtás; bilaterális PVN lézió, ovariektómia, adrenalektómia

- Kanülbeültetés; az agy oldalkamrájába (műanyag kanül és Alzet minipumpa), véna jugularisba, azokon keresztül anyagok beadása
- Vérvétel; farok vénából, vena jugularisból
- Intraperitoneális injekciók; glükóz (IP-GTT) és inzulin (IP-ITT) tolerancia teszt, bróm-dezoxiuridin kezelés (*birth dating*), LPS kezelés
- Szervkivétel; frissen, dekaptitálás után, valamint fixáltan, transzkardiális formaldehid perfúzió után
- Hipofízis sejttenyészet készítése
- Patch clamp mérések szövetszeleten

3.3. Analitikai módszerek

- Metszetkészítés; friss fagyasztott és fixált szövetblokkokból
- Mikrodisszekció; mintavétel human és patkány agyszeletek meghatározott területeiről
- Mikrohullámmú kezelés (*microwave treatment,* MWT); szövettani metszetek előkezelése mikrosütőben
- Immunhisztokémia (IHC); a fénymikroszkópos, az immunoautoradiográfiás, illetve a fluoreszcens detektálás különböző módozatai
- *In situ* hibridizáció (ISH); radioaktív (kvantitatív) ISH, kettős ISH radioakívan jelölt és digoxigeninnel jelölt ribopróbákkal, ISH és IHC kombinációja
- Fehérje- és hormonmérések; radioimmunoassay, western blot, ELISA, IHC kvantitatív analízise
- RNS mérések; reverz transzkripció-polimeráz láncreakció (*reverse transcription-polymerase chain reaction*, RT-PCR), radioaktív ISH kvantitatív értékelése
- EEG adatok műszeres analízise
- Képalkotó eljárások; videofelvételek készítése, fény- és konfokális mikroszkópia
- Videofelvételek analízise; viselkedés vizsgálatok (alvás, cukrozott hedonikus tápfogyasztás mikrostruktúrájának analízise, erőltetett úszás értékelése)
- Statisztikai elemzések

4. CÉLKITŰZÉSEK

A neuroendokrinológia tudományát Magyarországon kiváló tudósok alapozták meg és vitték tovább. Szentágothai János és tanítványai úttörő munkát végeztek hipotalamo-adenohipofizeális rendszer tanulmányozásával kapcsolatban. Pályám elindítója Palkovits Miklós jelentősen hozzájárult az agyi neuropeptid-termelő sejtek feltérképezéséhez, és az agytörzsi katekolamin rendszer és a HPA tengely kapcsolatának feltárásához. (Palkovits 1982, Palkovits 1984). A neuromoduláció és a neuropeptid koexpresszió jelentőségének felismerése a jelátviteli folyamatok komplexitásában és flexibilitásában újabb szintre emelte az agyi szabályozó folyamatok, így a hipotalamusz integratív működésének és megértését (Nusbaum, Blitz et al. 2017). További előrelépést jelentett a felfedezés, miszerint egyes patológiák kialakulása, mint például a felnőttkori metabolikus szindróma, vagy stresszbetegségek, gyakran intrauterin és perinatális környezeti hatásokra vezethetőek vissza, melyben a homeosztázis centrális szabályozásának megváltozása meghatározó (Bouret 2009, McGowan és Matthews 2018). A folyamatosan bővülő, de korántsem teljes kép kialakításához a korszerű neuromorfológiai, elektrofiziológiai és molekuláris biológiai eszköztár elengedhetetlen. Az ismert neuropeptidek száma meghaladja a százat, receptoraiké a dupláját (Hökfelt, Barde et al. 2018). A módszerek tárháza egyre bővül, a vizsgálandó molekulák immunhisztokémiai módszerekkel történő megfelelő érzékenységű, együttes vizualizálása a szövetben mégis egyik legalapvetőbb kutatási eszköz maradt.

Mindezek figyelembevételével bemutatott munkámban a következő célokat tűztem ki:

I. Az immunhisztokémia alkalmazásának továbbfejlesztése

II. Az energiaháztartás szabályozás vizsgálata

a. A nesfatin funkcióinak feltárása az energiaháztartás, és azzal összefüggően a cirkadián ritmus szabályozásával kapcsolatban.

b. Az intrauterin alultáplált fenotípus kialakulásának hátterében álló agyi mechanizmusok vizsgálata.

III. A stresszválasz finomhangolásának tanulmányozása

a. A koexpresszió jelentősége akut és krónikus stresszben, két neuromodulátor, a nesfatin és a PrRP szerepének tanulmányozásán keresztül.

b. A PrRP jelátvitel jelentőségének feltárása a krónikus stressz okozta mentális stresszbetegségekben.

5. EREDMÉNYEK

5.1. Az immunhisztokémia alkalmazásának továbbfejlesztése

A fejezet a következő közleményeken alapszik:

1. Zsuzsanna E. Tóth* and Eva Mezey, *J. Histochem Cytochem* 2007, 55(6):545-554.
2. Zsuzsanna E. Toth et al**.,** *Exp Cell Res* 2007, 313(9):1943-1950.

*: levelező szerző

Az immunhisztokémia, gyakorlati alkalmazásának 1941-es megjelenése óta, az agykutatás módszertani eszköztárának alapvető eleme (Palkovits 1984, Ortiz Hidalgo 2022). Munkám során számos immunhisztokémiai módszert alkalmaztam, és a munka folytatását több esetben az immunfestésekkel kapcsolatos módszertani probléma akadályozta. Egyes problémák megoldása kapcsán született eredményeimet metodikai közleményekben foglaltam össze.

5.1.1. Az immunhisztkokémiai keresztreakciók megakadályozásának új módszere

1. Közlemény: *Simultaneous visualization of multiple antigens with tyramide signal amplification using antibodies from the same species*

A többes immunfluoreszcens festés használatával nagy felbontású képet kaphatunk a különböző antigének egymáshoz való térbeli viszonyáról (koexpresszió, szinaptikus kapcsolatok, sejten belüli molekuláris kölcsönhatások), ezért a többes immunfluoreszcens festés információ tartalma messze magasabb, mint a különböző egyedi festések összegéé. Mindennek a kutatásban és a szövettani patológiai diagnózisok felállításában is kiemelkedő szerepe van. Egyrészt, a patológiás szövettani mintával sok esetben gazdaságosan kell bánni korlátozott mennyisége miatt. Másrészt, a molekuláris patológiai differenciál diagnosztika fejlődése elengedhetetlenné teszi többféle biológiai marker jelenlétének egyidejű tesztelését, például tumorok alosztályok szerinti besorolásának kérdésében (Wharton, Wood et al. 2021). A multiplex immunfluoreszcens technikának mindemellett egyre nagyobb jelentősége van a tumor immunoterápiák hatékonyságának előrejelzésében is (Tan, Nerurkar et al. 2020).

A többes immunfluoreszcens festési eljárások kivitelezésének nagymértékben gátat szabott, hogy a kereskedelmi forgalomban kapható elsődleges antitestek korlátozott számú gazdaállatban készülnek. Ezért, ha például két különböző antigénre specifikus elsődleges antitest nyúl szérumból származik, ami a leggyakoribb, kettős immunfestés során a másodlagos, nyúl elleni antitest mindkettőt felismeri, ezért a két antigént nem tudjuk elkülöníteni. Nem specifikus keresztreakció a másodlagos antitestek között is kialakulhat, például a kecskében

termelt anti-nyúl IgG-t a szamárban termelt anti-kecske IgG felismeri. A probléma megoldására született korábbi megoldások (például, az elsődleges antitest fluorokrómmal történő közvetlen megjelölése, Fab fragmens használata, a második festésnél jelerősítés használata, izotipikus antitestek alkalmazása) kis érzékenységű, drága, bizonytalan kimenetelű, vagy hosszabb metodikai beállítást igénylő módszerek voltak. Ezért fejlesztettem ki egy egyszerű, olcsó és reprodukálható eljárást, mely nagy érzékenységű, így egyszerre több, kis mennyiségben jelenlévő antigén kimutatására alkalmas. Az eljárás alapját a mikrohullámú sütőben (700-800 W) történő hőkezelés képezi (MWT). A módszert az teszi lehetővé, hogy kísérleteink alapján a fluoreszcens jel erőssége az MWT következtében nem gyengül, ha tiramid szignál amplifikációt (TSA) használunk (3. ábra). A TSA lényege, hogy a jelet enzimhisztokémia révén teszi láthatóvá. A reakció során a fluorokrómhoz kapcsolt tiramidot a másodlagos antitesthez kapcsolt tormaperoxidáz (*horseradish peroxidase,* HRP) enzim hidrogén-peroxid jelenlétében

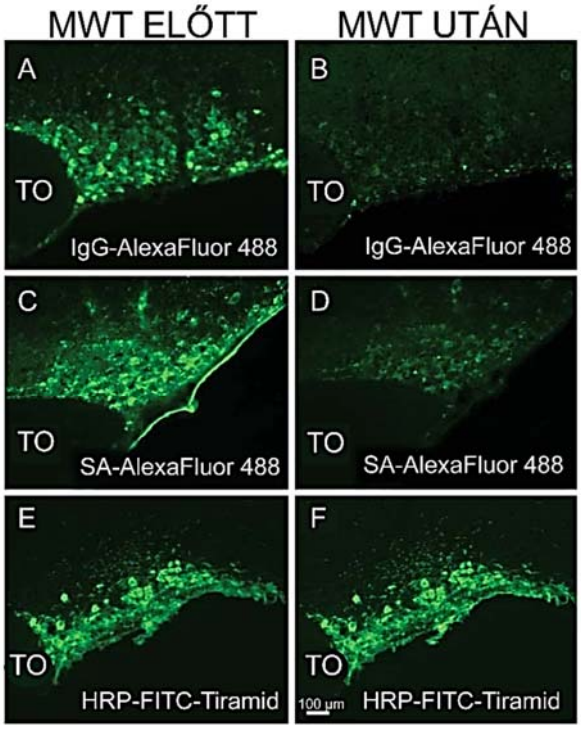

3. ábra. A mikrohullámú hőkezelés hatása a különböző fluoreszcens immunfestési eljárásokra. AVP immunfestés (PS41, 1:50, monoklonális egér antitest, H. Gainer, NIH, ajándéka) egér SON koronális metszetein. **A, B** Detektálás AlexaFluor 488 fluorokrómmal (zöld) konjugált egér elleni másodlagos ellenanyaggal (szamár IgG, 1:1000, Invitrogen, Carlsbad, CA, Cat. #: R37114). **C, D** Detektálás biotinilált másodlagos antitest (szamár IgG, 1:1000, Jackson ImmunoResearch Laboratories, West Grove, PA, Cat. #715-065-151) majd AlexaFluor 488 fluorokrómmal konjugált streptavidin (SA, 1:1000, Invitrogen, Cat. #S11223) alkalmazásával. **E, F** Detektálás TSA jelerősítéssel. A másodlagos ellenanyag HRP enzimmel konjugált nyúl elleni polimer IgG volt (higítatlan, kecskében termelt, 30 perc, SuperPicture, Zymed Laboratories Inc., South San Francisco, CA. Cat. #87-9263), melyet FITC-tiramid (zöld) reakció követett (TSA Fluorescein Tyramide Reagent Pack, PerkinElmer Life and Analytical Sciences, Boston, MA, Cat. #SAT701B001EA). TO: tractus opticus. A fenti kivételtől eltekintve az inkubációs idő az anitestekkel 1h volt.

kovalens kötésekkel a közvetlen környezetben megtalálható peptidek tirozin oldalláncaihoz köti. A reakció gyors (10 perc), és a fluorokróm feldúsulása miatt nagyfokú jelerősítéshez vezet (Adams 1992). Az MWT során a metszeteket 10 mM citrát puffert (pH 6,0) tartalmazó edénybe helyezzük és 100%-os teljesítmény mellett a puffert felforraljuk. Ezután a mikrosütő teljesítményét 50%-ra állítjuk és a metszeteket további 5 percig hőkezeljük. Az elpárolgott folyadékot desztillált vízzel pótoljuk és a metszeteket 30 percig szobahőn hűlni hagyjuk. A citrát puffert 0,1 M foszfát pufferre (PBS, pH 7,4) cseréljük, miután az immunfestést tovább folytatható. A kereszterakciók kivédésén túl a technika előnye, hogy az MWT egyben antigén feltárásra (Werner, Von Wasielewski et al. 1996) és adataink alapján a peroxidáz enzim aktivitás eliminálására is alkalmas, akár másodlagos antitesthez kapcsolt, HRP enzimről, akár az endogén peroxidáz aktivitásáról van szó.

Az TSA és az MWT ciklus ismételt alkalmazásával bebizonyítottam, hogy azonos gazdaállatból származó elsődleges antitestekkel és ugyanannak a másodlagos antitestnek a többszöri felhasználásával a többszörös fluoreszcens immunfestés nagy érzékenységgel és specifikusan elvégezhető (4. ábra).

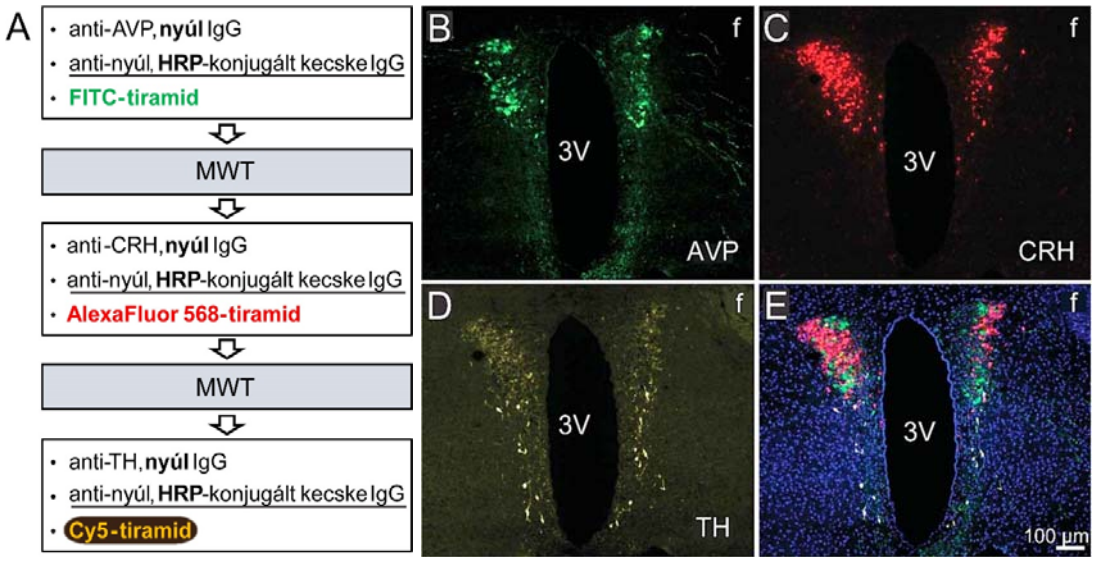

4. ábra. Tripla fluoreszcens immunfestés azonos gazdaállatban (nyúl) különböző antigének ellen termelt elsődleges antitestek és egyazon másodlagos antitest (aláhúzva) felhasználásával egér hipotalamusz metszeten. **A** Az immunfestés folyamatábrája. **B** AVP immunfestés (zöld), **C** CRH immunfestés (piros), **D** TH immunfestés (sárga), **E** a három imunfestés együtt, a sejtmagokat megjelenítő DAPI (kék) háttérfestéssel. MWT nélkül keresztreakciók jönnének létre az azonos gazdaállatból származó elsődleges antitestek és a HRP enzim többszöri alkalmazása miatt (vastag betű). f: fornix, HRP: tormaperoxidáz enzim, 3V: 3. agykamra.

Az módszer gyakorlati haszna, hogy a közleményben közölt eljárás képezi az egyik alapját a Perkin-Elmer Inc (Waltham, MA, USA), Akoya Biosciences (Marlborough, MA, USA) és más cégek által is forgalmazott „Opal Multiplex IHC” KIT-eknek. A KIT-ek

segítségével akár 7 biomarker szimultán kimutatása is lehetséges egy metszetben. A KIT-ek megvásárolhatók saját elsődleges antitestekkel való immunfestések, illetve az Opal tumor immunológiai IHC panelekben összeállított (Opal Cancer Immunology IHC Panels) elsődleges antitestekkel való immunfestések céljára (lásd Csatolmányok). A Leica cég által kínált BOND RX automata immunfestő készülék magában foglalja a technikát, és az Akoya partenerként 30 metszet egyszerre 7 különböző biomarkerrel történő immunfluoreszcens festését kínálja 14 h alatt (https://www.leicabiosystems.com/ihc-ish/ihc-ish-instruments/bond-rx/).

5.1.2. Zöld fluoreszcens fehérjét (GFP) kifejező transzplantált sejtek nyomonkövetése

2. Közlemény: ***Sensitive detection of GFP utilizing tyramide signal amplification to overcome gene silencing***

A GFP felfedezése (Shimomura 2005) számos téren forradalmasította a kutatást, így a fejlődéstanban (sorskövetés), az elektrofiziológiában (sejtek azonosítása), a molekuláris biológiában (bioszenzorok fejlesztése), a tumorkutatásban (rákos sejtek nyomonkövetése) és az őssejterápiában (transzplantált sejtek nyomonkövetése) is (Nakano, Migita et al. 2001, Abedi, Greer et al. 2004, Yagi, McMahon et al. 2004, Hoffman 2015, Tian, Xu et al. 2023). A GFP-t expresszáló csontvelői őssejtek sorsának nyomonkövetése a nem GFP-transzgén akkceptor szervezetben kezdetben több ellentmondó adatot eredményezett. Egyesek úgy találták, hogy a csontvelői őssejtek számos szövetben szövetspecifikus sejtekké differenciálódnak, mások viszont az ellenkezőjét állították (Jackson, Majka et al. 2002, Moore és Lemischka 2006). Mint kiderült, a kísérleti felállás (sérülés/betegség, vagy hiánya) nagyban befolyásolja a keringő őssejtek hozzájárulását a regenerációhoz (Abedi, Greer et al. 2004). A GFP detektálásában az is gondot okozott, hogy a natív GFP jel akkoriban még elég gyenge volt, ráadásul bebizonyosodott, hogy, az „idegen” gén kifejeződését az utódsejtekben szabályozó mechanizmusok csillapítják (McTaggart és Feng 2004, Brazelton és Blau 2005).

Kísérleteink bebizonyították, hogy a szignál erősítése szükséges és gyakorlatilag elégséges a GFP jel megfelelő kimutatásához. A vizsgálathoz hím transzgén egereket használtunk, melyek minden sejtjében egyenletesen fejeződött ki a GFP (Novak, Guo et al. 2000). A kísérlet során vad típusú nőstény egerekben radioaktív besugárzással kiirtottuk a csontvelőt, majd az egereket hím GFP-transzgén egerekből izolált csontvelő sejtekkel transzplantáltuk a farokvénán át. Felgyógyulás után a transzplantált egerekben elzártuk a jobb oldali arteria cerebri mediát, az agyban így kialakult féloldali sztrók a csontvelői őssejteket a sérülés/regeneráció helyére vonzotta. Az állatokat két hónappal a műtét után transzkardiális perfúzióval formaldehiddel fixáltuk. Az GFP jelet a striatumból származó 10 μm vastag

kriosztáttal készült metszeteken három különböző eljárással vizsgáltuk (5. ábra, A). Ugyanazokat a sejteket a szövetben először natívan néztük meg Leica DMR6000B invertált mikroszkóp segítségével. Ehhez a metszeteket átmenetileg fedőlemezzel lefedtük, médiumként Tris puffert (0,1 M, pH 7,4) használtunk. A sejtek ily módon kis nagyítással alig látszottak, és nagy nagyítással is nehezen értékelhető képet adtak (5. ábra, B). Fotózás után a metszetekről a fedőlemezeket Tris pufferben leáztattuk, majd szérumos blokkolást és sejt permeabilizást követően (Powerblock, Biogenex, San Ramon, CA, Cat. #HK083-5K), a metszeteket nyúlban termelt anti-GFP elsődleges antitesttel (1:2000, Molecular Probes, OR; Cat. #ab13970) egy éjszakán át inkubáltuk 4°C-on. Másnap a metszeteket kecskében termelt, AlexaFluor 594 fluorokrómmal konjugált, anti-nyúl IgG másodlagos antitesttel inkubáltuk (1:1000, Molecular Probes Cat. #A-11012), így határozottan felismerhető sejteket kaptunk (5. ábra, C). Ezután endogén peroxidáz blokkolást végeztünk, majd a jelet tovább erősítettük. A kecskében termelt másodlagos antitesthez lóban termelt, HRP enzimmel konjugált, anti-kecske IgG harmadlagos antitestet kötöttünk (1:500, Vector Laboratories, Burlingham, CA Cat. #PI-9500-1). A metszeteket egy éjszakán át inkubáltuk 4°C-on, majd a jelet TSA reakcióval, AlexaFluor 350 fluorokrómmal konjugált tiramid felhasználásával mutattuk ki (1:100, 10 perc, Molecular Probes, Cat. #T20937) (5. ábra, D).

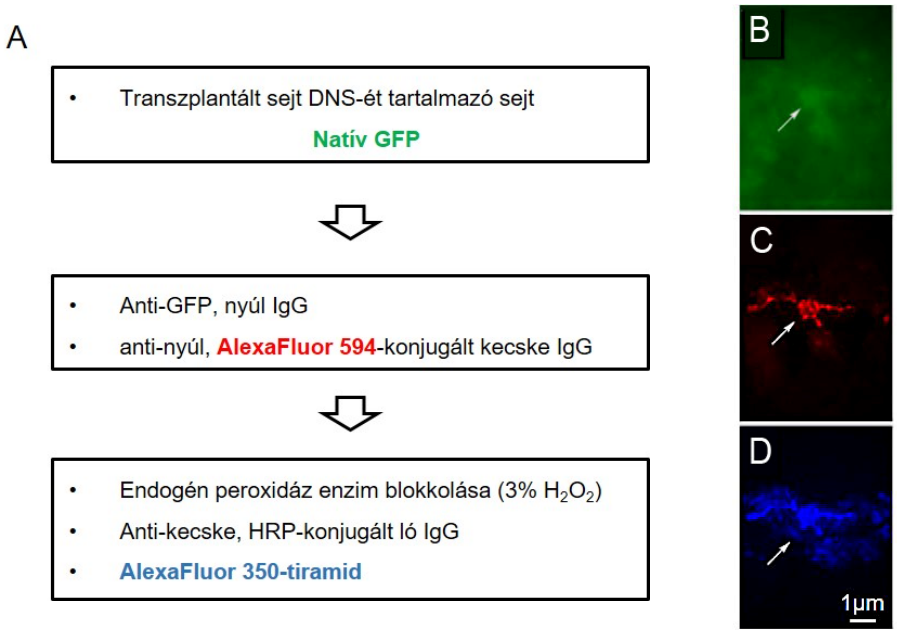

5. ábra. A donorból származó GFP jel immunhisztokémiai erősítése a transzplantált egér striatumában. A Az immunfestés folyamatábrája. **B** Natív GFP-t (zöld) expresszáló sejt. **C** A GFP közvetlen immunfluoreszcens detektálása piros fluorokrómmal konjugált másodlagos antitesttel. **D** Harmadik lépésben ugyanazt a sejtet TSA jelerősítés alkalmazásával is megfestettük (kék). Megjegyzés: a natív kép háttere világosabb, mint a többié, mert a sejt láthatóvá tételéhez hosszabb expozícióra volt szükség.

Kontrollként, párhuzamos sorozatmetszeteken hasonló immunfestéseket végeztünk, ahol eltérő márkájú másod-, és harmadlagos antitesteket, illetve más fluorokrómokat használtunk. A különböző kísérletek eredménye egybehangzó volt. Az egylépéses immunfluoreszcens festés, de leginkább a TSA amplifikálás jelentősen javította a GFP-t expresszáló sejtek megfelelő detektálását. A TSA használata látványosan gazdagabb morfológiai részletekkel is szolgált, bizonyítva, hogy a kerek csontvelői őssejtekből finom nyúlványokkal rendelkező morfológiailag mikrogliaként azonosítható sejtek keletkeztek az agyban (5. ábra, D).

További kontroll kísérletként egy független, érzékeny módszert, fluoreszcens ISH-t (FISH) alkalmaztunk, mellyel a hím donorokból származó Y kromoszómát mutattuk ki. A FISH-t aztán a GFP jelenlétének immunfluoreszcens (TSA) detektálásával kombináltuk (6. ábra, A). Először az immunfestést végeztük el, az elsődleges antitest a korábban használt nyúlban termelt anti-GFP (1:40 000) IgG volt. Másodlagos antitestként HRP enzimmel konjugált nyúl elleni polimer IgG-t (higítatlan, kecskében termelt, SuperPicture, Zymed Laboratories Inc., South San Francisco, CA Cat. #87-9263), majd FITC-tiramid reakciót alkalmaztunk (saját gyártmány, 1:10 000) (6. ábra, A, B, C). Ezután a metszeteket a peroxidáz enzim aktivitásának megszüntetése és a sejtmag feltárása céljából mikrohullámú kezelésnek vetettük alá. Az elpárolgott folyadékot pótoltuk és a metszeteket 2 órán keresztül hűlni hagytuk. A FISH-hez egy 1,5 kilobázis nagyságú digoxigeninnel jelölt (Digoxigenin RNA Labeling Kit,

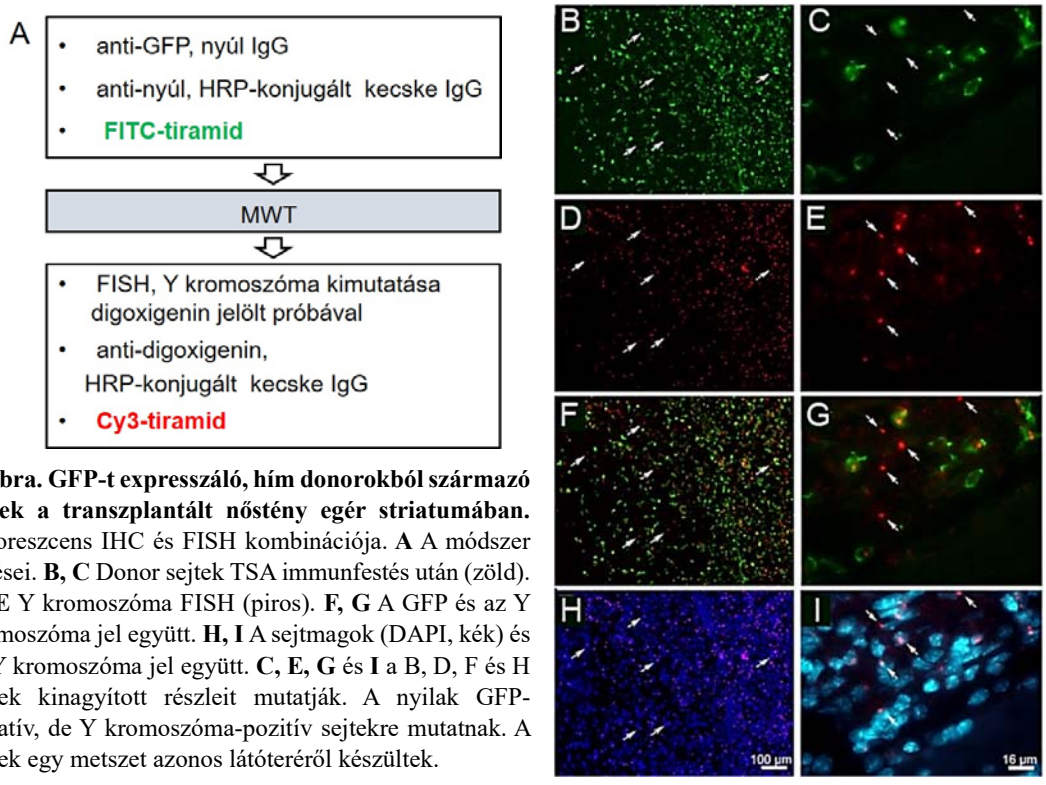

6. ábra. GFP-t expresszáló, hím donorokból származó sejtek a transzplantált nőstény egér striatumában. Fluoreszcens IHC és FISH kombinációja. **A** A módszer lépései. **B, C** Donor sejtek TSA immunfestés után (zöld). **D, E** Y kromoszóma FISH (piros). **F, G** A GFP és az Y kromoszóma jel együtt. **H, I** A sejtmagok (DAPI, kék) és az Y kromoszóma jel együtt. **C, E, G** és **I** a B, D, F és H képek kinagyított részleit mutatják. A nyilak GFP-negatív, de Y kromoszóma-pozitív sejtekre mutatnak. A képek egy metszet azonos látóteréről készültek.

Roche Applied Sciences, Indianapolis, IN Cat. #1 175 025) próbát használtunk, mely az egér Y kromoszómájának ismétlődő szekvenciáját ismerte fel (pY3531B). A hibridizációt követően a metszeteket HRP-konjugált anti-digoxigenin antitesttel inkubáltuk (1:600, Roche Applied Sciences,Indianapolis, IN, Cat. #1120773391). A jelölést Cy3-tiramid reakcióval vizualizáltuk (1:600, Cat. #NEL744001KT, TSA-Plus CY3 System KIT, PerkinElmer Life Sciences, Boston, MA) (6. ábra, A, D-G). A sejtmagokat DAPI háttérfestéssel jelenítettük meg (6. ábra, H, I).

Eredményeinket mennyiségileg is kiértékeltük (7. ábra). A különböző módszerekkel kimutatott donor sejtek mennyiségét azonos koronális szintről származó egész metszetekben számoltuk meg. A natív GFP jelhez képest az egylépéses immunfluoreszcens detektálás ugrásszerű mennyiségi változást okozott. Ehhez a TSA módszer további 40%-os növekedéssel járult hozzá. A TSA erősítés a FISH módszerrel jelölt donor sejtek 90%-át mutatta ki.

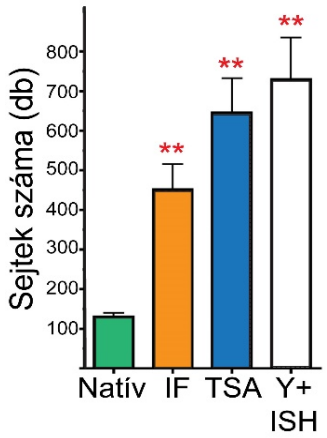

7. ábra. A GFP-t expresszáló, hím donorokból származó sejtek kimutatásának érzékenysége transzplantált nőstény egérek striatumában különböző módszerekkel. A grafikon a donor eredetű sejtek metszetenkénti számát mutatja, natív, fluorokrómmal jelölt másodlagos antitesttel történő immunfluoreszcens festés (IF), TSA erősítéses immunfestés és Y kromoszóma FISH alapján. Az analízis azonos koronális szintekből készült metszeteken, a kísérleti felállásra vak értékelő közreműködésével történt. Nem-parametrikus Friedman teszt, átlag ± standard hiba, p**<0,0001, n = 5 állat/módszer.

5.2. Az energiaháztartás szabályozás vizsgálata

A fejezet a következő közleményeken alapszik:

3. Katalin Könczöl et al., *International Journal of Obesity (Lond)* 2012, 36:1514-1521. *#
4. Szilvia Vas et al**.,** *PLoS One* 2013, 8(4):e59809. *#
5. Máté Durst et al**.,** *Frontiers in Neuroscience* 2022, 16:828571. *#
6. Máté Durst et al**.,** *International Journal of Obesity (Lond)* 2019, 43(4):917-927. *#

*: levelező szerző, #: utolsó szerző

Az elhízás és a 2-es típusú cukorbetegség (2TDM) szövődményei világszerte emberek ezreinek halálát okozzák. Az energiaháztartás zavarának számos oka lehet, ezek közé tartozik a túlzott ételfogyasztás, a mozgásszegény életmód, genetikai tényezők, különböző betegségek, illetve környezeti hatások. A környezeti hatások rendkívül széleskörűek lehetnek. A bemutatott

tanulmányok szempontjából két tényezőt emelek ki: 1, a felnőttkori táplálkozási szokásokat befolyásolja a méhen belüli tápanyagellátás 2, szoros kapcsolat áll fenn az energiaháztartás és az alvás-ébrenléti ciklus között. Az étkezések a napi ritmusnak megfelelően történnek, amihez a szervek működése és a metabolizmus is alkalmazkodik. Ezért az alvás-ébrenléti ciklus felborulása rendkívül káros hatással van az anyagcserére, és igen megnöveli a 2TDM és a metabolikus szindróma kialakulásának kockázatát (Challet 2019).

A szervezet energiaegyensúlya a táplálékfelvétel és az energialeadás arányának függvénye. A táplálékfelvételt rövidtávon a szervezetből érkező éhségi és jóllakottsági szignálok, hosszútávon a szervezet energia raktárainak állapota határozza meg. A gyomor-bél traktus állapotáról (mechano- és kemoreceptorok) a nyúltvelőben az NTS kap elsődleges információt főleg a nervus vaguson keresztül, amit a felsőbb agyi központok, kiemelten a hipotalamusz felé továbbít. A cirkumventrikuláris szervek közvetítésével érkeznek az agyba azok a humorális szignálok, melyek az éhségről (ghrelin), jóllakottságról (például kolecisztokinin), illetve a zsírraktárak állapotáról (leptin, inzulin), referálnak az agynak. A legfontosabb ilyen cirkumventrikuláris szerv a nyúltvelőben az area postrema, a hipotalamusz ventrális részén pedig az eminentia mediana és az ARC mag területe. A homeosztatikus táplálékfelvétel szabályozás elsődleges központja hipotalamuszban az ARC, ahol két ellentétes hatású sejtpopuláció, az orexigén NPY/aguti-kapcsolt peptid (AGRP) tartalmú neuronok és az anorexigén POMC/kokain és amfetamin regulált transzkript (CART) tartalmú neuronok egymást gátló sejtcsoportjai helyezkednek el. Az ARC idegi kapcsolatban áll a hipotalamusz másodlagos szabályozó központjaival, mint például a PVN és a LHA (Cifuentes és Acosta 2022).

Az energialeadást nagymértékben az alapanyagcsere határozza meg, melynek központi szabályozása a hipotalamusz-hipofízis pajzsmirigy tengely feladata. A tengely kiindulópontját a PVN TRH-termelő neuronjai képzik. Az energiaháztartás központi eleme a hőszabályozás is, melynek elsődleges integratív központja a hipotalamusz preoptikus areaja. A szabályozás kimeneti szárát a hipotalamusz autonóm efferensei jelentik, melyek a bőr vérkeringését és a barna zsírszövet hőtermelését befolyásolják (Cifuentes és Acosta 2022).

Ahogy a bevezetésben is említettem, a homeosztatikus funkciók állapotfüggő finomszabályozásában nagy szerepük van a neuropeptideknek, ezért az új neuropeptidek felfedezése és neuropeptidek különböző funkcióinak feltárása elengedhetetlenül fontos feladat. Ebben, és részben a következő fejezetben, a munkánk idején nemrégiben felfedezett nesfatin szerepkörét karakterizáltuk. A fejezet végén két tanulmány szól annak vizsgálatáról, hogy vajon

az intrauterin környezet milyen hatásmechanizmussal befolyásolhatja a felnőttkori táplálékfelvételt.

5.2.1. A nesfatin anorexigén hatásainak jellemzése

3. Közlemény: ***Nesfatin-1 exerts long-term effect on food intake and body temperature***

Mivel számos, a táplálékfelvétel szabályozásban fontos neuropeptid a hőszabályozásban is részt vesz (Pereira-da-Silva, Torsoni et al. 2003, Fan, Voss-Andreae et al. 2005, Lechan és Fekete 2006, Solinas, Summermatter et al. 2006, Kasahara, Takayanagi et al. 2007), feltételeztük, hogy a táplálékfelvételt csökkentő nesfatinról ugyanez bizonyítható. Feltételezésünket alátámasztotta, hogy a nesfatin több, a hőszabályozásban ismert szerepet játszó neuropeptiddel koexpressziót mutat (Pereira-da-Silva, Torsoni et al. 2003, Lechan és Fekete 2006, Brailoiu, Deliu et al. 2013). Ezenkívül szerettük volna részletesen jellemezni a nesfatin-1 táplálékfelvételre kifejtett hatását. Célunk az egyszeri icv nesfatin-1 kezelés által kiváltott hatások időbeli lefutásának tanulmányozása, a hatások napszaki ritmussal való összefüggésének vizsgálata, valamint a hőszabályozásban esetleg részvevő, nesfatin-termelő neuronok azonosítása volt. Kísérleteinkhez biotelemetriás készüléket használtunk, ami a táplálkozással eltöltött időt, a testhőmérsékletet, a szívfrekvenciát, és a patkányok mozgási aktivitását automatikusan detektálta 48 órán keresztül. Manuálisan mértük az állatok napi táp- és vízfogyasztását, amit az egy nappal korábban mért mennyiség különbségeként fejeztük ki. Az aktív (sötét) periódus elején az állatok jobb oldalkamrájába juttatott nesfatin- 1 hatására (25 pmol) az éjszaka első felében a táplálékfelvétellel töltött idő csökkent (8. ábra, A). Az állatok a következő aktív periódus elején is szignifikánsan kevesebb időt töltöttek táplálékfelvétellel, mint a kontrollok (8. ábra, A). Amikor a nesfatin-1 kezelést a passzív fázis elején végeztük el, az éjszakai táplálékfelvétellel töltött idő a következő két aktív fázisban is nagymértékben csökkent (8. ábra, B). A nappali táplálékfogyasztást ugyanakkor a nesfatin-1 kezelés a mérések szerint egyik kísérletben sem befolyásolta. A táplálékfelvétel időtartamának cirkadián görbéje mindkét fajta beadás mellett megmaradt, de amplitúdója ellaposodott (8. ábra A, B). Az elfogyasztott táp mennyiségét tekintve, a kezelés első napján a nesfatin-1 (aktív fázis elején adva) táplálékfelvételt csökkentő hatása nem érte el a szignifikancia szintet (8. ábra, C). A második nap a nesfatin-1 kezelt állatok az első naphoz képest mégis többet ettek, míg a kontrollok tápfogyasztása egyenletes volt (8. ábra, C). Az elfogyasztott táp napi mennyisége a passzív fázis elején végzett nesfatin-1 kezelés hatására nem változott, bár az előzőekben megfigyelt tendencia itt is látható volt. A nesfatin-1 a beadás napszakjától függetlenül, jelentősen befolyásolta a vízfogyasztást. A nesfatin-1 kezelt csoport kevesebbet ivott az első

napon, amit a második nap az állatok pótoltak (8. ábra, C). A testsúlyok napi változása tükrözte a táp- és vízfogyasztásban tapasztalt tendenciákat, de nem mutatott szignifikáns eltérést egyik kísérletben sem (8. ábra, C).

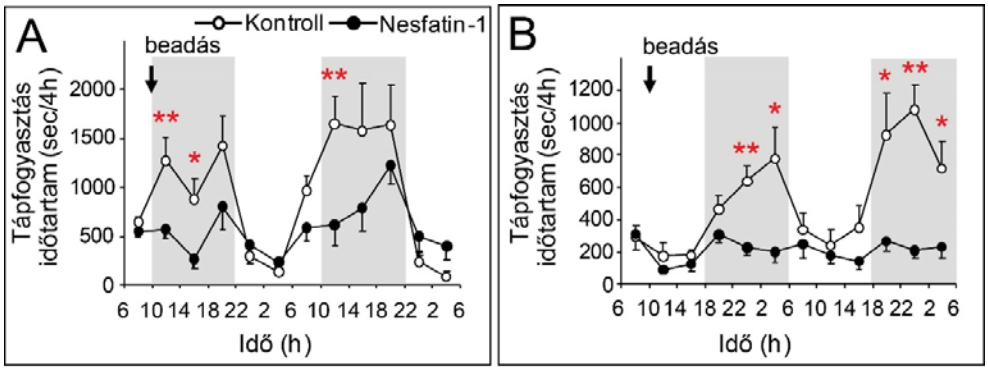

C

Beadás időpontja:		aktív fázis			passzív fázis		
	kezelés	0-24h	24-48h	n	0-24h	24-48h	n
Tápfelvétel változása (g)	kontroll	2,0 ± 1,0	1,6 ± 1,0	5,6	3,5 ± 1,1	2,3 ± 0,8	6
	nesfatin-1	- 1,0 ± 0,9	5,0 ± 1,8$^{\#}$	6	1,0 ± 0,9	3,2 ± 1,0	6
Vízivás változása (g)	kontroll	1,8 ± 2,0	2,2 ± 2,4	5	1,5 ± 3,1	3,0 ± 1,4	6
	nesfatin-1	- 12,2 ± 4,5*	8,2 ± 4,8$^{\#}$	5	- 8,0 ± 3,7*	8,7 ± 3,8$^{\#}$	6
Testsúly változása (g)	kontroll	3,4 ± 2,0	1,6 ± 1,6	5	6,2 ± 1,7	5,3 ± 1,9	6
	nesfatin-1	- 1,4 ± 2,8	3,0 ± 1,5	5	1,8 ± 0,9	4,7 ± 1,4	6

8. ábra. A nesfatin-1 (25 pmól) hatása a patkányok táplálkozására, vízfogyasztására és testsúlyára. A, B Táplálékfelvétellel töltött idő nesfatin-1-gyel, illetve fiziológiás sóoldattal való icv kezelés után. A telemetriás mérés 48 órán keresztül történt, a görbék 4 órás periódusok állatonként összegzett méréseinek átlagait mutatják esti (A) és nappali (B) beadást (nyilak) követően. Az állatok aktív fázisát (sötétség) szürke sávok jelzik. **C** A táp- és vízfogyasztás, illetve a testsúly napi változása az állatok előző nap mért egyéni adatához képest. Kétutas ismételt méréses ANOVA, Holm-Sidak post hoc teszt, átlag ± standard hiba, telemetria: p*<0,05, p**<0,01 *versus* kontroll, n = 5-6 állat/csoport (A), n = 10-12 állat/csoport (B), táblázat: p*<0,05 a kezelésre nézve, és p$^{\#}$<0,05 az időbeliségre nézve.

A dózisfüggés vizsgálatára a kezelést a passzív fázis elején 100 pmol nesfatin-1 beadásával megismételtük. A telemetriával mért táplálékfelvételi görbe az első mérési napon a kisebb dózishoz hasonlan alakult (9. ábra, A). A második nap passzív fázisának kezdetén csökkenés, majd egy átmeneti kompenzációs evésnek megfelelő növekedés volt mérhető, de a táplálékfelvétel időtartamát ez a dózis is csökkentette a második aktív fázis végén is. A cirkadián ritmus görbéje a kontrollhoz képest itt is ellapult maradt (9. ábra, A). A nagyobb nesfatin-1 dózis a fogyasztott táp mennyiségét a kezelés napján szignifikánsan csökkentette, másnap az állatok viszont többet ettek (kompenzáció). A nagyobb nappali dózis tehát a kis dózisnál megfigyelt tendenciákat felerősítette. Mindez a második napi testsúlyváltozás növekedésében is megnyilvánult. A nesfatin-1 kezelt állatok 24 órás folyadékfogyasztásának mérése a kis dózissal azonos eredményt hozott (9. ábra, B).

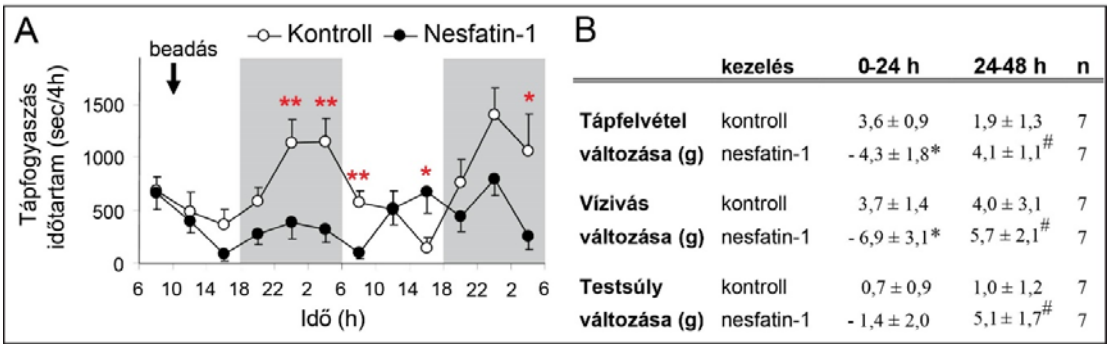

	kezelés	0-24 h	24-48 h	n
Tápfelvétel változása (g)	kontroll	3,6 ± 0,9	1,9 ± 1,3	7
	nesfatin-1	- 4,3 ± 1,8*	4,1 ± 1,1#	7
Vízivás változása (g)	kontroll	3,7 ± 1,4	4,0 ± 3,1	7
	nesfatin-1	- 6,9 ± 3,1*	5,7 ± 2,1#	7
Testsúly változása (g)	kontroll	0,7 ± 0,9	1,0 ± 1,2	7
	nesfatin-1	- 1,4 ± 2,0	5,1 ± 1,7#	7

9. ábra. A nesfatin-1 (100 pmól) hatása a patkányok táplálkozására, vízfogyasztására és testsúlyára. **A** Táplálékfelvétellel töltött idő nesfatin-1-gyel, illetve fiziológiás sóoldattal való icv kezelés után. A telemetriás mérés 48 órán keresztül történt, a görbe 4 órás periódusok állatonként összegzett méréseinek átlagait mutatja nappali beadást (nyíl) követően. Az állatok aktív fázisát (sötétség) szürke sávok jelzik. **B** A táp- és vízfogyasztás, illetve a testsúly napi változása az állatok előző nap mért egyéni adatához képest. Kétutas ismételt méréses ANOVA, Holm-Sidak post hoc teszt, átlag ± standard hiba, telemetria: p*<0,05, p**<0,01 versus kontroll, n = 7 állat/csoport, táblázat: p*<0,05 a kezelésre nézve, és p#<0,05 az időbeliségre nézve.

A nesfatin-1 már kis dózisban is a testhőmérséklet emelkedését váltotta ki (10. ábra). Amikor a beadás az aktív fázis elején történt, amikor a cirkadián ritmusnak megfelelően az állatok testhőmérséklete emelkedik, a nesfatin-1 a hőmérséklet emelkedését közvetlenül a kezelést követő időszakban számottevően fokozta (10. ábra, A, B). A passzív fázisokban a hatás még feltűnőbbé vált, mivel nesfatin-1 kezelt csoportban az állatok testhőmérséklete nem csökkent le a nappal mérhető normális szintre. A passzív fázisban alkalmazott nesfatin-1 akut hőmérséklet emelő hatása kisebb mértékű volt, mint az előző kísérletben (10. ábra, C, D). A

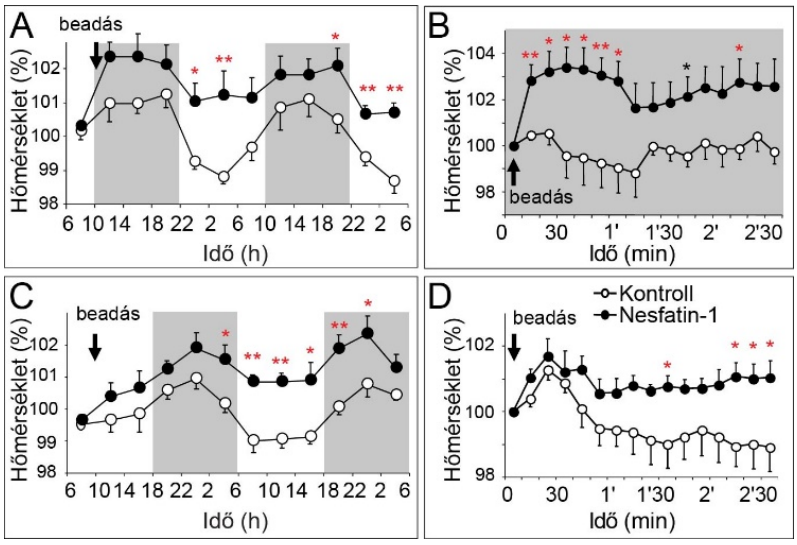

10. ábra. A nesfatin-1 (25 pmól) hatása a patkányok testhőmérsékletére. Az értékeket állatonként, a beadás előtti 6:00 és 7:00 óra között mért testhőmérsékletek átlagához (100%) viszonyítottuk. **A, C** A görbék 4 órás periódusok állatonként összegzett telemetriás méréseinek átlagait mutatják esti (A) és nappali (C) beadást (nyilak) követő 48 órában. Az állatok aktív fázisát (sötétség) szürke sávok jelzik. **B, D** A kezelést közvetlenül követő 2,5 óra részletes elemzése esti (B) és nappali (D) beadást követően. Kétutas ismételt méréses ANOVA, Holm-Sidak post hoc teszt, átlag ± standard hiba, p*<0,05, p**<0,01 *versus* kontroll, n = 5-6 állat/csoport (A, C), n = 8 állat/csoport (B, D).

következő passzív fázisban azonban itt is jelentős különbség látszott a kontrollok testhőmérsékletéhez képest, és a nesfatin-1 kezelt állatok magasabb testhőmérséklete a második aktív fázis elején is megfigyelhető volt (10. ábra, C, D). A nagyobb dózis erősebb akut hatást váltott ki, de a válasz jellege lényegében a kis dózishoz hasonló maradt. Jellemző volt tehát a nesfatin-1 testhőmérsékletre gyakorolt elnyújtott hatása, mely minden esetben szignifikáns volt a beadást követő világos periódusokban, és hőmérsékletgörbe cirkadián ritmusának ellapulását idézte elő (10. ábra, A, C).

Az állatok mozgási aktivitásában nem találtunk eltérést a csoportok között egyik típusú nesfatin-1 kezelésnél sem. A passzív fázis kezdetén alkalmazott nesfatin-1 (mindkét dózis) a beadást követő időszakban átmenetileg (30 percig) és enyhén fokozta a szívfrekvenciát, amikor a kezelés az aktív fázis elején történt ezt nem észlelhetük.

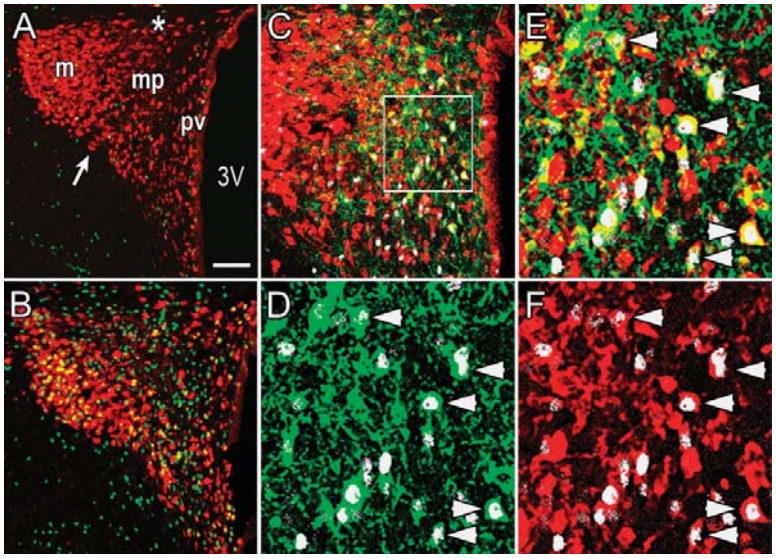

11. ábra. A hideg stressz hatása a PVN nesfatin-termelő sejtjeinek aktivitására. A kontroll**,** és **B** stresszelt állatok koronális metszetei a bal PVN területéről. Kettős, cFos (zöld) és nesfatin (piros) immunfluoreszcens festés, a kettősen jelölt sejtek magjai sárgák. **C** A mediális parvocelluláris PVN. Háromszoros, prepro-TRH (zöld), cFos (fehér) és nesfatin (piros) immunfluoreszcens festés. A triplán jelölt neuronok sárgák, fehér sejtmaggal. **D-F** A C panel bekeretezett részének kinagyított képei, ahol a háromszorosan jelölt (E), a cFos és prepro-TRH kettősen jelölt (D), illetve a cFos és nesfatin (F) kettősen jelölt sejtek látszanak. A nyílhegyek azonos sejtekre mutatnak. A PVN almagjai: m: magnocelluláris, mp: mediális parvocelluláris, pv: periventrikuláris parvocelluláris, csillag: dorzális parvocelluláris, nyíl: ventrális parvocelluláris szubdivízió. 3V: 3. agykamra. Mérték: 100 μm (A, B), 250 μm (C), 50 μm (D, E, F).

A hőháztartásra gyakorolt hatás lehetséges mechanizmusainak feltárására, feltérképeztük az agyban a hideg stresszre (4°C, 2 h) aktiválódó (cFos-pozitív) nesfatin neuronok elhelyezkedését. Erőteljes sejtaktivációt figyeltünk meg a hipotalamuszban az SON, a PVN, és az ARC nesfatin tartalmú idegsejtjeiben, a preoptikus areaban viszont a hideg-aktivált sejtek nesfatin-negatívnak bizonyultak. Mivel a PVN és ARC is befolyásolja a barna zsírszövet hőtermelését (Labbé, Caron et al. 2015), és a PVN részt vesz a bőr beidegzésében is

(Morrison és Nakamura 2019), adataink alapján az itt található nesfatin-termelő neuronok szerepet játszhatnak ezekben a hőszabályozó mechanizmusokban.

A hideg-aktivált nesfatin neuronok további jellemzésére a PVN szintjéből vett metszeteken háromszoros immunfestést végeztünk. A kissejtes PVN területén számos triplán jelölt, cFos-, nesfatin- és TRH-immunoreaktív neuront mutattunk ki (11. ábra). Ez felveti, hogy a nesfatin a hipotalamo-hipofízis-pajzsmirigy tengelyre, és ezen keresztül a metabolikus rátára is hathat. A nyúltvelői raphe obscurus és pallidus hidegre aktiválódó nesfatin neuronjai szintén TRH-t tartalmaztak, mely az itt található autonóm premotoros neuronok jellemzője. Ezek a neuronok közvetlenül részt vesznek a didergés és a barna zsírszövet szabályozásában, valamint a bőr ereinek szimpatikus beidegzésében (Johnson, Ulfhake et al. 1993, Morrison és Nakamura 2019), vagyis a nesfatin a termoreguláció több szintjén is bekapcsolódhat a hőszabályozásba.

5.2.2. A nesfatin és az alvás-ébrenléti ciklus kapcsolatának vizsgálata

4. Közlemény: ***Nesfatin-1/NUCB2 as a potential new element of sleep regulation in rats***

Fenti eredményeink alapján nesfatin-1 hatásai hosszútávúak és kapcsolatban állnak cirkadian ritmussal. Ennek jelentősége sokrétű. Mint már említettem, a nem megfelelő minőségű, mennyiségű, vagy rosszul időzített (többműszakos munkaidő) alvás kiemelt kockázati tényező az elhízás és a 2TDM szövődményeinek kialakulásában (Papatriantafyllou, Efthymiou et al. 2022). Ezen túlmenően közismert az alvás és a hangulati betegségek, például major depresszió (Riemann, Krone et al. 2020), valamint a táplálkozási zavarok és a hangulati betegségek szoros kapcsolata is (Donofry, Roecklein et al. 2016). Ezért a különböző homeosztatikus paraméterek szabályozásában fellelhető kapcsolódási pontok feltárása többféle kórkép etiológiájának tisztázásában is segíthet.

A legnagyobb nesfatint intenzíven termelő agyi sejtpopuláció agyban a zona incertában (ZI) és a DLH területén helyezkedik el, utóbbin belül a perifornikális areában (PFA) és a laterális hipotalamuszban (LH) nagy a nesfatin-pozitív sejtek sűrűsége. Ez a terület ad otthont az orexin- és az MCH-termelő neuronoknak is, melyek fontos szerepet játszanak az alvás-ébrenlét ciklus, az energiaháztartás és a hangulat szabályozásában (Valassi, Scacchi et al. 2008, Torterolo, Scorza et al. 2015, Yamashita és Yamanaka 2017, Han, Yuan et al. 2020). Az alapvetően csendes MCH-pozitív sejtek a nem-REM alvás alatt elkezdenek tüzelni, maximális aktivitásukat a REM alvás alatt érik el (Verret, Goutagny et al. 2003, Hassani, Lee et al. 2009). A területen található MCH-termelő sejtek nesfatint is koexpresszálnak, kis csoport MCH-negatív és nesfatin-pozitív neuron is található itt, melyekről annyit tudunk, hogy nem tartalmaznak orexint (Brailoiu, Dun et al. 2007, Fort, Salvert et al. 2008). A nesfatin anorexigén,

az alvás elősegítésében kritikus szerepű MCH pedig orexigén molekula (Torterolo, Scorza et al. 2015), ezért különösen érdekesnek találtuk a nesfatin alvás-ébrenlét ciklus szabályozásában betöltött esetleges szerepének feltárását. Számos kérdésre kerestünk választ: 1, befolyásolja-e a nesfatin-1 az alvás-ébrenlét ciklus architektúráját 2, miként hat a REM alvásmegvonás a DLH nesfatin expressziójára 3, REM alvás során eltér-e az MCH-pozitív és -negatív nesfatin neuronpopulációk aktivációja?

A patkányok agyába 25 pmol nesfatin-1-et injektáltunk icv a passzív fázis kezdetén, és EEG/EMG mérés segítségével követtük nyomon a vigilancia stádiumokat. A nesfatin-1 a REM alvást a beadás utáni 6 órán keresztül minimálisra redukálta (12 ábra, A). A kezelés mind a REM epizódok számát (12 ábra, B), mind a REM epizódok hosszát csökkentette (12 ábra, C). Kisebb mértékben a rágcsálókban ismert pre-REM (intermedier alvási stádium) alvást is gátolta (12 ábra, D-F). Növekedett viszont a passzív ébrenlét mennyisége (időtartam és epizódok száma), és átmeneti emelkedést tapasztaltunk a nem-REM alvás SWS1 stádiumában is.

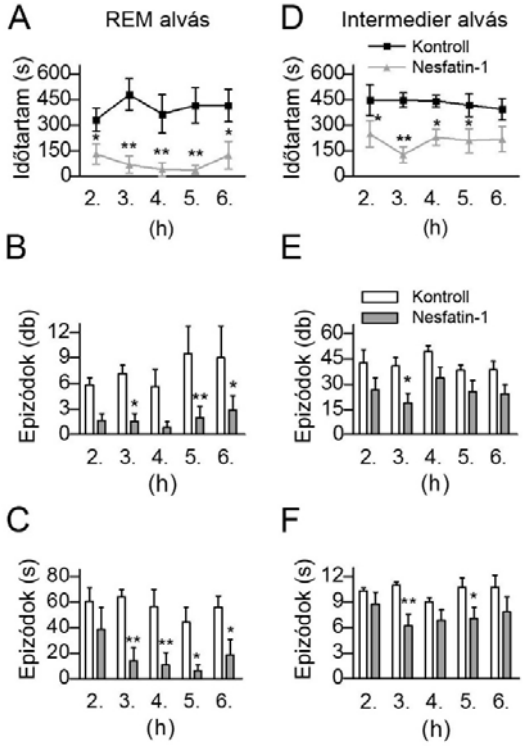

12. ábra. A centrális (icv) nesfatin-1 kezelés hatása a REM és az intermedier alvásra a passzív (világos) fázis 2.-6. órájában. A-C A REM alvás paraméterei; óránkénti REM idő (A), az epizódok óránkénti száma (B) és az epizódok átlagos időtartama (C). **D-F** Az intermedier alvás paraméterei; óránkénti intermedier alvással töltött idő (D), az epizódok óránkénti száma (E) és az epizódok átlagos időtartama (F). A kezelés a 0. órában történt, a kontroll állatok fiziológiás sóoldatot kaptak. Kétutas ismételt méréses ANOVA, Tukey post hoc teszt, átlag ± standard hiba, p*<0,05, p**<0,01 *versus* kontroll, n = 6 állat/csoport.

A következő kísérletben az úgynevezett virágcserép módszerrel az állatokat REM alvásmegvonásnak vetettük alá (Verret, Goutagny et al. 2003). A patkányokat egy kis platformra (KP) helyeztük 72 órára, ahol a helyhiány miatt nem tudnak REM alvásba merülni, ugyanis amint ezt megteszik, a fellépő izomatónia miatt a platformot övező vízbe pottyannak és felébrednek. Az állatok egy részét alvásmegvonás után leöltük, másik csoportjukat leölés előtt saját ketrecükbe (SK) helyeztük 3 órára. A REM megvont állatok ilyenkor szinte azonnal elalszanak, és a teljes időszakot a REM alvás pótlásával töltik (*rebound*, KPR csoport). Két csoport kontroll állat a kísérlet idejét háborítatlanul a saját ketrecében tölthette (SK és SKR csoportok), őket a KP és KPR csoportoknak megfelelő időben öltük le. További két stressz-kontroll csoport is használatos az alkalmazott paradigmában. Az ide sorolt állatok a KP állatokkal azonos körülmények között tartózkodtak, de egy nagy platformon (NP) helyezkedhettek el, ahol a REM alvás lehetséges. Így REM hiány nem lép fel, de a kísérleti stressz a KP csoportéval azonos lesz. A KPR csoportnak megfelelően, az ebbe a csoportba tartozó állatok egy része is ezt követően 3 órát a saját ketrecében tölthetett (NPR csoport).

A REM alvás megszüntetése a nesfatin mRNS- (kvantitatív ISH) és fehérjeszintjének (ELISA) nagymértékű csökkenését eredményezte. Az ezt követő REM pótlás, a nesfatin mRNS és fehérje expresszió normalizálódásához vezetett (13. ábra).

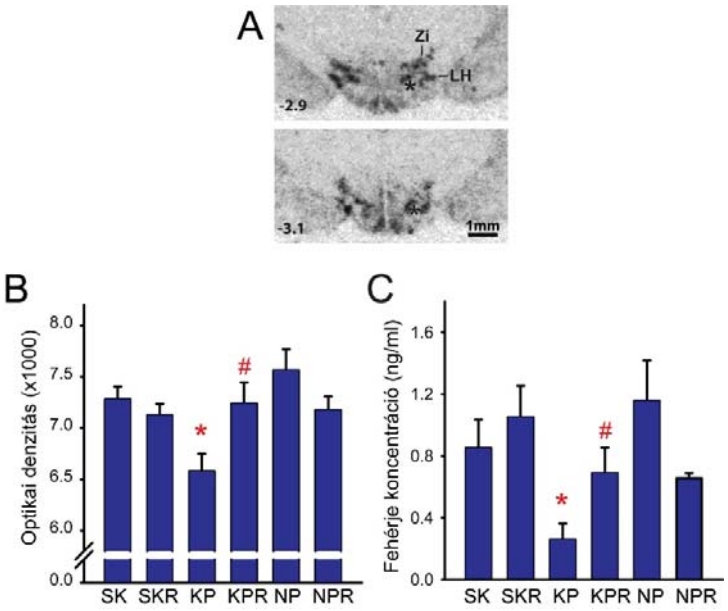

13. ábra. A nesfatin expresszió és a REM alvás kapcsolata. **A** Radioaktív nesfatin ISH szignál a DLH szintjén. Koronális metszetek autoradiográfiás képei, a bal alsó sarokban a bregmától való rosztro-kaudális távolság látszik mm-ben. A sötétedés mértéke a nesfatin mRNS mennyiségével arányos. LH: laterális hipotalamusz, ZI: zona incerta, csillag: fornix. **B, C** A ZI és DLH területén együtt mért Nesfatin mRNS- és fehérjeszintek a különböző kísérleti csoportokban. SK: saját ketrec, a KP kontrollja, SKR: saját ketrec,a KPR kontrollja, KP: kis platform alvásmegvonás, KPR: KP + 3 h REM pótlás saját ketrecben, NP: nagy platform, NPR: NP + 3 h saját ketrecben. Kétutas ANOVA, Student-Newman-Keuls post hoc teszt, $p^{*}<0,05$ *versus* többi csoport, $p^{\#}<0,05$ *versus* KP, n = 5-9 állat/csoport (B), illetve n = 4-7 állat/csoport (C).

A kísérletek eredményei a REM alvás és a vizsgált nesfatin sejtpopuláció szoros kapcsolatára utaltak. Ezért a REM alvás szabályozásban résztvevő nesfatin neuronok további vizsgálatához először hiánypótló munkaként meghatároztuk az MCH és nesfatin koexpresszió mértékét. A nesfatin-pozitív neuronok jelentős része MCH-t tartalmazott, a legnagyobb MCH-negatív nesfatin-termelő sejtpopulációt a PFA területén találtuk (MCH és nesfatin kettősen jelölt sejtek/nesfatin-pozitív neuronok: ZI: 81,9 ± 1,7%, PFA: 66,2 ± 4,8%, LH: 75,4 ± 2,1%, n = 5 állat/csoport). Az MCH-immunoreaktív neuronok gyakorlatilag mindegyike nesfatin-pozitív volt. A koexpresszió mértékét a kísérleti felállás (alvás csoportok) nem befolyásolta. Ezután a REM alvásmegmegvonás és a REM alvás pótlás során aktivált neuronokat háromszoros, nesfatin, MCH és cFos immunfestés segítségével azonosítottuk. Megállapítottuk, hogy az MCH és nesfatin kettősjelölt neuronok nagymértékben aktiválódtak a REM pótlás során mindhárom vizsgált területen (14. ábra).

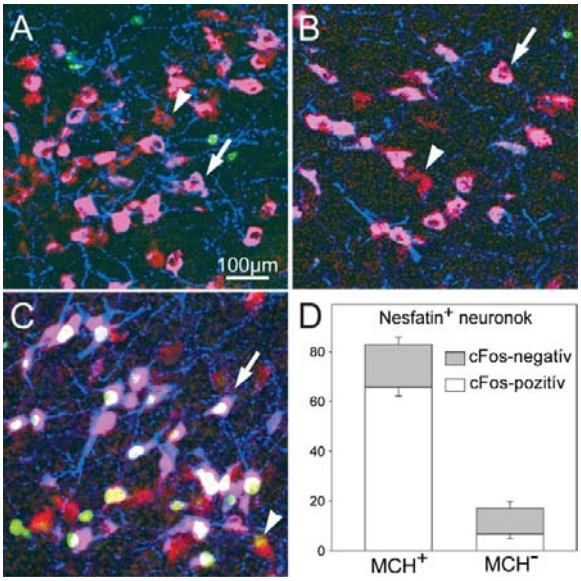

14. ábra. Az A nesfatin-termelő neuronok aktivitása az MCH koexpresszió függvényében a REM alvás pótlása során. A-C Háromszoros, nesfatin (piros), MCH (kék) és cFos (zöld) fluoreszcens immunfestés az LH területéről, egy SK (A), egy KP (B), és egy KPR (C) csoporthoz tartozó állatban. A nesfatin és MCH kettősjelölt neuronok rózsaszínűek (nyilak), az MCH-negatív nesfatin neuronok pirosak.(nyílhegyek). Az aktivált nesfatin-MCH kettősjelölt neuronok magjai fehérek, az aktivált nesfatin-pozitív, de MCH-negatív neuronok magja sárga. **D** Az REM alvás pótlásának hatása a különböző nesfatin sejtpopulációk aktiválódására (cFos). Átlag ± standard hiba, n = 5 állat.

Az MCH-negatív nesfatin neuronok nem reagáltak a REM pótlásra, kivéve a LH területén található sejtek egy kis hányadát (KPR: 37,6 ± 4,8%, $p<0,01$ *versus* SK (6,0 ± 2,4%) és KP: 15,0 ± 3,1%, n = 5 állat/csoport). A REM alvás szabályozásában tehát alapvetően az MCH-t és nesfatint koexpresszáló neuronok vettek részt.

Bár a nesfatin-1 receptora még nem ismert, többszörösen bizonyított táplálékfelvételt csökkentő hatása miatt az elhízás elleni küzdelemben potenciális gyógyszertani célpont (Finelli, Martelli et al. 2014, Schalla, Unniappan et al. 2020), ezért a hatások és lehetséges mellékhatások feltárása sürgető feladat. Munkánk jelentősége, hogy részletes jellemzést adtunk a nesfatin-1 hatásainak farmakodinamikájáról, korábban nem ismert hatásait tártuk fel, betekintést nyújtottunk ezek lehetséges hatásmechanizmusaiba, más hatásokat pedig az alkalmazott dózisok mellett kizártunk. Adataink arra hívják fel a figyelmet, hogy a nesfatin energiaháztartásra gyakorolt hatása összetett, mivel a táplálékfelvétel mellett az energialeadást is befolyásolja, és részt vesz az alvás-ébrenléti ciklus szabályozásában is. A centrális beadás ugyan nem teszi lehetővé a pontos támadáspontok meghatározását, de az alvásmegvonásos kísérletek révén a DLH-ZI területén egy a REM alvás szabályozásában részt vevő nesfatin sejtpopulációt sikerült azonosítanunk. Tekintve e terület jelentőségét a homeosztázis érintő információk komplex feldolgozásában (Bonnavion, Mickelsen et al. 2016), eredményeink felvetik a nesfatin lehetséges integratív szerepét a cirkadián ritmus és az energiaháztartás szabályozás összehangolásában.

5.2.3. Az intrauterin fehérje alultáplált fenotípus vizsgálata

A fejlődő magzat anyagcseréjét a hozzáférhető tápanyag mennyisége életre szólóan meghatározza. Akár túl kevés, akár túl sok a méhen belüli energia-ellátottság, az egyén elhízásra, metabolikus szindrómára és 2TDM-re való hajlammal születik (Gonzalez-Bulnes és Ovilo 2012). A fenotípus megnyilvánulását a későbbi életmód és táplálkozás szabja meg. A jelenség magyarázata mindkét esetben a fejlődő szervezet adott környezethez való prediktív alkalmazkodása, amit magzati programozásnak neveznek.

Az alacsony születési súllyal kombinált intrauterin növekedési retardáció (IUGR) a terhességi komplikációk egyik leggyakoribb szövődménye (Giouleka, Tsakiridis et al. 2023). A táplálékszegény méhen belüli körülmények az úgynevezett „takarékos” fenotípus („*thrifty” phenotype*) kifejlődését idézik elő. A takarékos fenotípus szervezete arra „számít”, hogy bármikor beköszönthet a „hét szűk esztendő”, ezért a későbbi életszakaszban a tápanyag lehetőség szerinti felhamozására rendezkedik be. Ennek első jele a születést követő intenzív felzárkózó növekedés (*catch-up growth*), melynek következtében az érintettek utolérik, illetve le is hagyják normál körülmények között született társaikat (Coupé, Grit et al. 2009, Kesavan és Devaskar 2019).

Mivel az energiaháztartás központi idegrendszeri szabályozó körei a kora magzati fejlődés során alakulnak ki, a központi idegrendszeri szabályozás elváltozásai elsődleges

jelentőségűek az IUGR fenotípus létrejöttében (Levin 2006, Pedroso, Souza et al. 2017). Ezek az elváltozások a hipotalamuszt érintik elsősorban, és epigenetikusan jönnek létre (Gali Ramamoorthy, Begum et al. 2015). Az IUGR okozta fenotípus hátterében álló agyi mechanizmusokat nem ismerjük teljességében, ezért a fenotípus kialakulását kétirányú megközelítéssel, a táplálékfelvétel szabályozás homeosztatikus és nem-homeosztatikus (jutalmi) oldaláról is tanulmányoztuk.

5.2.3.1. A 2-es típusú cukorbetegségre való hajlam kialakulásának vizsgálata

5. Közlemény: ***Hypothalamic nesfatin-1 resistance may underlie the development of type 2 diabetes mellitus in maternally undernourished non-obese rats***

A 2TDM patomechanizmusát leggyakrabban a túlsúlyhoz kötik, pedig a betegek legalább egyötödének testsúlya a normál tartományba esik (Vaag és Lund 2007). Ezekben a betegekben a 2TDM a zsírszöveti leptin mennyiségétől függetlenül alakul ki (Wang, Chandrasekera et al. 2014). Mint kiderült, a normál testsúly mellett fellépő 2TDM elsődleges kiváltó oka az IUGR (Vaag és Lund 2007), melyben a magzati programozás jelentős szerepet játszik (Gonzalez-Bulnes és Ovilo 2012).

Leptin független hatásmechanizmusa és a glükózháztartás központi szabályozásában kimutatott szerepe alapján (lásd Bevezetés) feltételeztük, hogy a hipotalamikus nesfatin sejtek magzati programozása hozzájárulhat az IUGR által kiváltott 2TDM kialakulásához. Kísérleteinkben a méhen belüli alultápláltságot a fehérje bevitel korlátozásával váltottuk ki, ugyanis ez a leginkább használt 2TDM rágcsálómodell (Martin-Gronert és Ozanne 2007), és jól tükrözi a human IUGR következményeit (Saleem, Sajjad et al. 2011). A terhes anyákat a terhesség első napjától a szülésig 50% fehérje csökkentett táppal etettük, a kísérletekhez a hím utódokat használtuk (protein-redukált, PR csoport). Modellünk jellemzésére az állatok fejlődését felnőttkorig (12. hét) követtük nyomon. A PR kölykök testsúly lemaradásukat a születés utáni első két hónapban behozták. Ezután a normál táplált (NT) és a PR csoport hetente mért testsúlya nem tért el (15. ábra, A). Ezt támasztotta alá a 12. héten EchoMRI módszerrel elvégzett testösszetétel vizsgálat is, mely szerint nem volt különbség a két csoport között, tehát az elhízás jelei a PR csoportban ekkor még nem mutatkoztak. A táplálkozási szokásokat felmérendő, az állatok kalóriabevitelét és zsírpreferenciáját (10 napos kísérlet) is tanulmányoztuk. Az PR állatok a felzárkózási periódus végén (6. hét) és a 12. héten is azonos

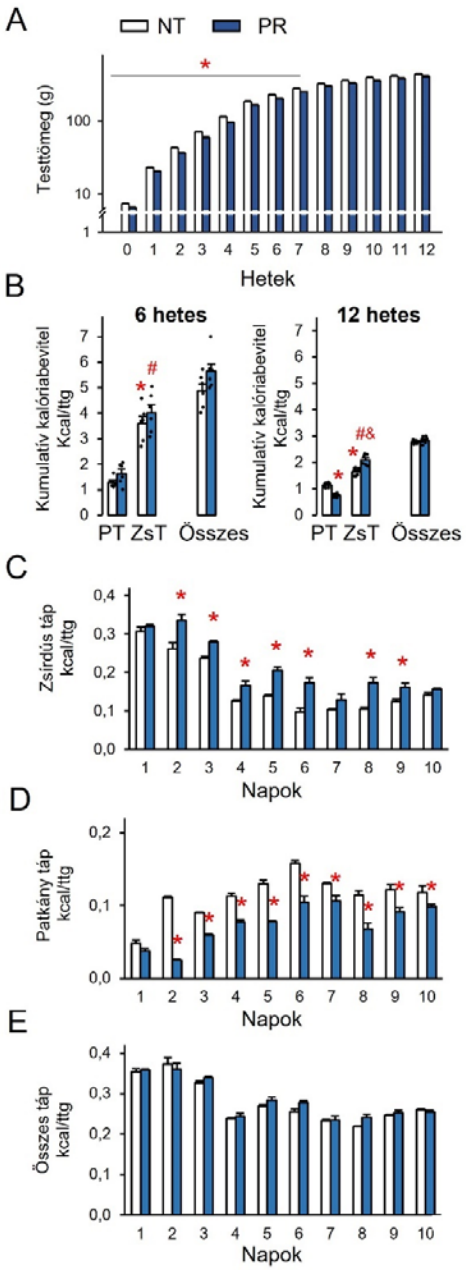

15. ábra. Az intrauterin fehérje alultápláltság hatása a fejlődésre, a kalória bevitelre és a zsírpreferenciára. **A** Hetente mért testtömeg az intrauterin normál- (NT) és alultáplált (PR) patkányokban. Student féle t-teszt, vagy Mann-Whitney U-teszt, NT *versus* PR p*<0,05. **B** Kumulatív kalóriabevitel a tíz napon át tartó zsírpreferencia teszt során. Az állatok szabadon választhattak a patkány táp (PT) és a zsírdús táp (ZsT) között. A PT és ZsT adatok összehasonlítása: kétutas ANOVA, Tukey post hoc teszt, p*<0,001 *versus* NT-PT, $p^{\#}$<0,001 *versus* PR-PT, $p^{\&}$<0,001 *versus* NT-ZsT csoportok. **C-E** Testtömegre viszonyított napi kalóriabevitelek a 12. posztnatális héten végzett zsírpreferencia teszt során zsírdús tápból (C), patkány tápból (D) és összesen (E). Kétutas ismételt méréses ANOVA, Tukey post hoc teszt, NT *versus* PR adott napon belül p*<0,01. Átlag ± standard hiba, n = 6 állat/csoport.

mennyiségű kalóriát fogyasztottak, mint a kontroll csoport. Természetesen a mennyiség fiatalabb korban abszolút értékben magasabb volt, mint felnőtt korban (15. ábra, B). Nem találtunk eltérést a 6 hetes állatok zsírdús táp iránti érdeklődésében sem, amit mindkét csoport szívesebben fogyasztott a normál patkány eledelnél. A felnőtt PR állatok viszont már kimondottan szívesebben választották a zsírdús tápot, mint a kontrollok (15. ábra, B), ezért a felnőtteknél a preferencia teszt tíz napját részletesen is megvizsgáltuk. Az PR állatok a mérési időszak második napjától kezdve kalóriaigényük nagyobb részét fedezték zsírdús tápból, mint NT társaik (15. ábra, C). Mivel ennek megfelelően kevesebb kalóriát fogyasztottak a patkány tápból (15. ábra, D), az összkalória bevitel a két csoportban azonos maradt (15. ábra, E). A zsír preferencia alakulásának dinamikája is azonos volt, a kezdeti lelkesedés a zsírdús táp iránt mindkét csoportban egy alacsonyabb, állandó szintre állt be a kísérlet 4.-5. napjától kezdődően (15. ábra, C-E).

Eredményeink alapján a PR fenotípusban az energiaegyensúly szabályozása az állatok életkorával változott. A felzárkózási periódusban a PR állatok a tápanyagot valószínűleg jobban hasznosították, mint a kontrollok, a később kialakult zsírpreferenciát pedig a patkány táp fogyasztásának csökkentésével kompenzálták. Mindemellett, amikor megvizsgáltuk az állatok

cukorháztartását, a PR állatok 6 hetes korban még egészségesek voltak(16. ábra, A, B), de 12 hetes korban már prediabeteses tüneteket mutattak (16. ábra, C, D).

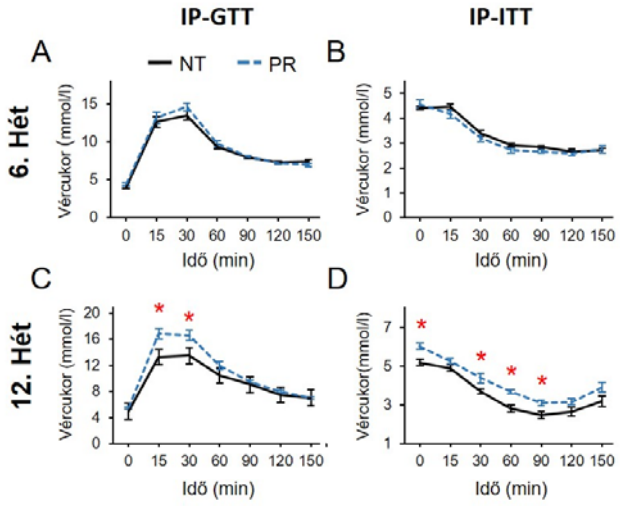

16. ábra. Glükóz- és inzulintolerancia az intrauterin tápláltság és az életkor függvényében. A, B Hat hetes és **C, D** 12 hetes NT és PR patkányok IP-GTT (A, C) és IP-ITT (B, D) tesztjének adatai. Kétutas ismételt méréses ANOVA, Tukey post hoc teszt, átlag ± standard hiba, p*<0,05 *versus* NT egy adott időpontban, n = 8 állat/csoport.

Rendellenesnek találtuk a PR csoport hipotalamikus nesfatin neuronjainak embrionális fejlődését is. Az osztódó sejtek jelölése bróm-dezoxiuridinnal kimutatta, hogy az embrionális fejlődés 13. napján kevesebb új nesfatin neuron jött létre a PR, mint az NT embriókban. A nesfatin-pozitív neuronok száma a felnőtt hipotalamuszban viszont már nem tért el a két csoportban.

A nesfatin mRNS expresszió mértéke (kvantitatív ISH) születéskor a hipotalamuszban a kontrollokéval egyezett, de a felnőttekben a PVN, az ARC és a LHA területén emelkedett volt. Mivel a két csoport testsúlya megegyezett, nesfatin rezisztenciára gyanakodtunk. Ezért megvizsgáltuk az akut icv nesfatin kezelés (25 pmol) éjszakai táplálék- és vízfogyasztásra gyakorolt hatását, valamint, hogy a kezelés befolyásolja-e az éhségre aktiválódó neuronok számát a hipotalamuszban. Korábbi adatainkkal összhangban, a nesfatin-1 hosszú távon, nyolc órán át gátolta a táplálék- (17. ábra, A-C) és a vízfogyasztást (17. ábra, D-F) az NT állatokban, de a PR állatokban nem hatott. Egy éjszaki éheztetés után, a nesfatin-1 csökkentette a cFos-pozitív neuronok számát az NT állatok ARC magjában. Azonban ez a hatás sem jelentkezett a PR állatokban (17. ábra, G, H). A kis és nagysejtes PVN, az SON és az LHA területén a cFos-pozitív sejtek száma nem változott a kezeléstől (17. ábra, I-L).

Eredményeink alátámasztották a PR állatok nesfatin-1 rezisztenciáját, ezért végezetül megvizsgáltuk a nesfatin-1 hatását a cukorháztartásra. Krónikus kezelést alkalmaztunk (70 pmol/nap, 7 napig), mivel az egyszeri akut kezelés korábban hatástalannak bizonyult (Su, Zhang et al. 2010). A táplálékfelvétel alapján a kezelés nem váltott ki nesfatin-1 rezisztenciát az NT állatokban (18. ábra, A), viszont javította a glükóz toleranciát és az inzulin érzékenységet (18. ábra, B, C). Ezzel szemben a PR állatokban a nesfatin-1 kezelés nem hatott a glükózháztartásra, bár az 1. és 4. napon a táplálékfelvételt csökkentette (18. ábra, D-F).

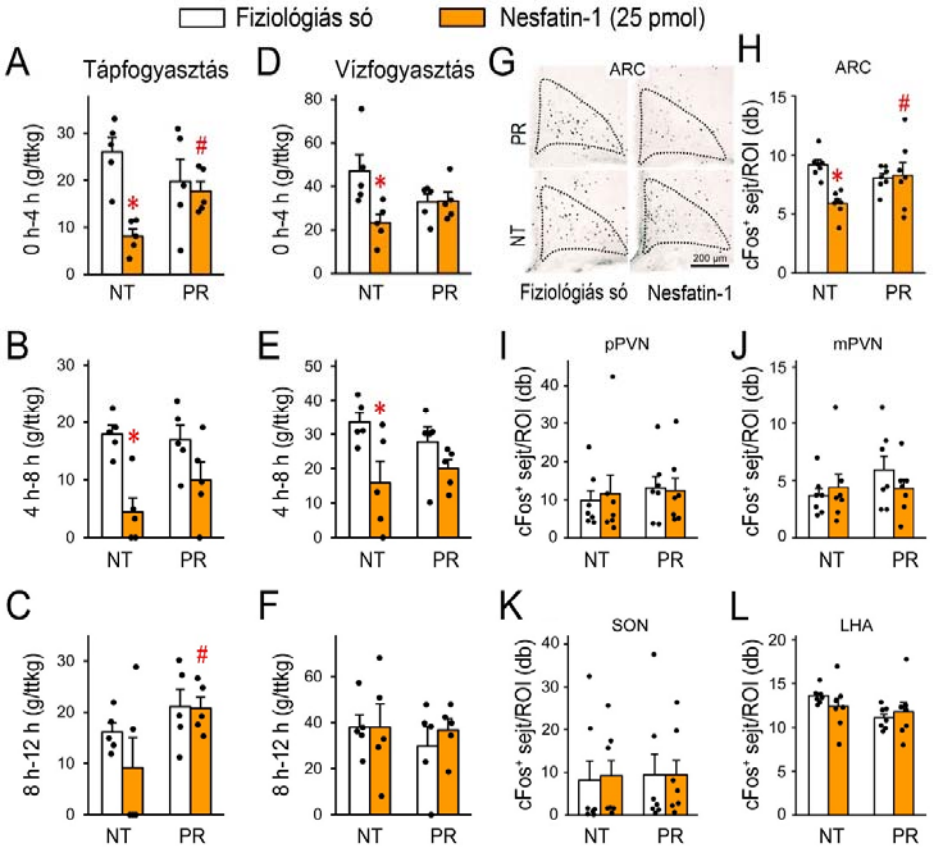

17. ábra. Az icv nesfatin-1 kezelés hatása a 12 hetes patkányok éjszakai táp- és vízfogyasztására, valamint az éhség okozta sejtaktivációra (cFos pozitivitás) az intrauterin tápláltság függvényében. **A-C** Relatív táplálékfelvétel **B-F** Relatív vízfogyasztás. Az A-C és D-E grafikonok a beadástól (0. időpont) 12 órán át, négy órás periódusokban mért adatokat ábrázolják. **G** Reprezentatív fénymikroszkópos felvételek, az ARC (szaggatott vonalon belül) szintjéről, a cFos-pozitiv sejtek sötétek. **H-L** A cFos-pozitív sejtek átlagos száma. A számolás a vizsgált területeken belül elhelyezett négyszögekben (*region of interest*, ROI) bilaterálisan történt. pPVN és mPVN: parvocelluláris és magnocelluláris PVN. Kétutas ANOVA, Tukey post hoc teszt, átlag ± standard hiba, p*<0,05 *versus*. NT-fiziológiás só; p$^{\#}$<0,05 *versus* NT-nesfatin-1, n = 5 állat/csoport (A-F), n = 7 állat/csoport (G-K).

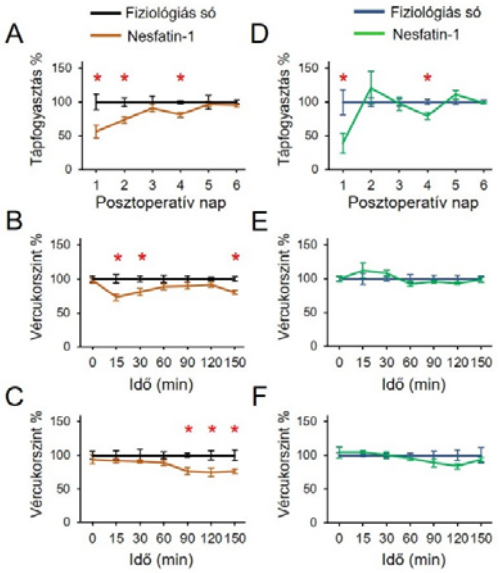

18. ábra. A krónikus icv nesfatin-1 infúzió (70 pmól/nap) hatása a 12 hetes patkányok táplálékfelvételére és glükóz homeosztázisára, az intrauterin tápláltság függvényében. A nulladik nap a műtétek és a kezelések kezdetének napja. A teszteket a kezelési időszak végén végeztük el. Az adatok viszonyítása a vivőanyagal kezelt csoport megfelelő adataihoz történt. **A-C** Az NT patkányok táplálékfelvételének (A), IP-GTT (B) és IP-ITT (C) tesztjének adatai. **D-E** A PR patkányok táplálékfelvételének (D), IP-GTT (E) és IP-ITT (F) tesztjének adatai. Student-féle t-tesztek (A, D), kétutas ismételt méréses ANOVA, Tukey post hoc teszt (B, C és E, F), átlag ± standard hiba, p*<0,05 fiziológiás só *versus* nesfatin-1 egy időponton belül, n = 6 állat/csoport.

5.2.3.2. A jutalmi táplálékfelvétel vizsgálata

6. Közlemény: ***Reward-representing D1-type neurons in the medial shell of the accumbens nucleus regulate palatable food intake***

A táplálkozást nemcsak a szükséglet kielégítése motiválhatja. Többet eszünk, ha az étel ízlik, és megkívánhatjuk kedvenc ételünket, akkor is, ha nem vagyunk éhesek, de rágondolunk. Az ilyen, úgynevezett jutalmi táplálkozás elemei ennek megfelelően az ízletesség (kedveltség,'*liking*'), az étvágy ('*wanting*') és az ehhez kapcsolódó asszociatív tanulás (Berridge és Kringelbach 2008). Hosszútávon az éhség nélküli, pusztán az élvezet kedvéért történő, evés pozitív energiaegyensúlyhoz vezet, és az elhízás vezető okai között szerepel (Sutton, L'Insalata et al. 2022).

A jutalmi táplálékfelvétel ellenőrzését számos hedonikus „forró" központ, „hideg" központ, illetve motivációért felelős agyterület végzi (például orbitofrontális kéreg, inzula, ventrális pallidum). Ezek közül a ventrális striatumhoz tartozó nucleus accumbens (Nac) vezető szerepet játszik az ízletességre adott reakciók ('*liking*') szabályozásában, és az ízletes ételek keresésére valamint fogyasztására irányuló motiváció szabályozásában is (Saper, Chou et al. 2002, Morales és Berridge 2020). Túlsúlyos egyénekben úgy találták, hogy a striatumban, mely a ventralis tegmentális areaból kiinduló mezolimbikus dopaminerg pálya végállomása, alacsony a 2-es típusú dopamin receptor (D2R) expressziója (Guo, Simmons et al. 2014). Ezért a striatum alulműködését okolták a kóros mértékű élvezeti táplálkozásért, ami az úgynevezett „jutalom hiány" elmélet felállításához a vezetett. Eszerint a túlevő betegek jutalom érzetének kielégítéséhez nagyobb mennyiségű étel szükséges, mint másoknak. Későbbi kutatások bebizonyították, hogy a D2R csökkent mennyisége, az elhízás miatt a megemelkedett leptinszint következménye, nem pedig a túlzott táplálékfogyasztás kiváltó oka (Billes, Simonds et al. 2012, Morales és Berridge 2020), így ez az elmélet megbukott.

O'Connor és munkatársai kimutatták, hogy a Nac Héj (*shell*) régiójában található, 1-es típusú dopamin receptort (D1R) hordozó GABAerg neuronok aktiválása a homeosztatikus táplálékfelvétel leállításához, gátlásuk pedig táplálékfelvétel meghosszabításához vezet, mivel ezek sejtek a laterális hipotalamikus area rosztrális részének közvetlen beidegzésén keresztül szabályozzák a táplálkozással eltöltött időt (O'Connor, Kremer et al. 2015). Ismert, hogy a D1R expresszió leptin független (Billes, Simonds et al. 2012), és az intrauterin alultápláltság a jutalmi táplálékfelvételt is megváltoztatja (Tonkiss, Shukitt-Hale et al. 1990, Gonzalez-Bulnes és Ovilo 2012). A kialakuló elhízás elsődleges oka pedig ilyenkor a hiperfágia (Vickers, Breier

et al. 2000). Ezért feltételeztük, hogy a háttérben a jutalmi táplálékfelvétel leállításának zavara áll. A vizsgálatokhoz a PR patkánymodellt használtuk.

A PR állatok testsúlyra viszonyított heti tápfogyasztása az elválasztástól (3. hét) 11 hetes korig nem tért el NT társaikétól. Ezután azonban egészen a kísérleti periódus végéig (14. hét) mérhetően magasabb lett. A hiperfágia a vizsgált időszakban nem okozott eltérést a két csoport testtömegében. Kísérleteinket azonos testtömegű, 14 hetes állatokon végeztük.

A jutalmi táplálékfogyasztást az éjszakai táplálkozás befejeztével jóllakott állatokon tanulmányoztuk. A kísérleti körülményekhez előzőleg hozzászoktatott állatok cukrozott sűrített tejet kaptak, amit 10 percig fogyaszthattak. A PR csoport jutalmi tápfogyasztása szignifikánsan magasabb volt, mint a kontroll csoporté. A kísérlet után videofelvételekről elemeztük a táplálkozási viselkedés finommotorikáját (Davis és Smith 1992). Az ízletességet (’*liking*’) tükröző markerekben (lefetyelés paraméterei) a két csoport egyáltalán nem tért el, de a táplálkozással töltött idő a PR és kontroll viszonylatában szignifikancia-közeli értéket mutatott (Student-féle t-teszt, NT *versus* PR, p = 0,071, n= 7-8 állat/csoport), a PR állatok mintha több időt töltöttek volna táplálkozással. Ezután a legfontosabb Nac alrégiókban megvizsgáltuk cukrozott tej fogyasztásának hatására aktiválódott sejtek mennyiségét. A következő területeket elemeztük: a ’*liking*’ és ’*wanting*’ centrumként egyaránt nyilvántartott hedonikus „forrópont” a Nac mediális Héjának rosztrális részén, és a tisztán ’wanting’ asszociált Mag (*Core*). Kontroll területként az egyik funkcióhoz sem köthető a ventrális Héj aktivációját is analizáltuk (19. ábra, A) (Záborszky, Alheid et al. 1985, Peciña és Berridge 2005, Peciña és Berridge 2013).

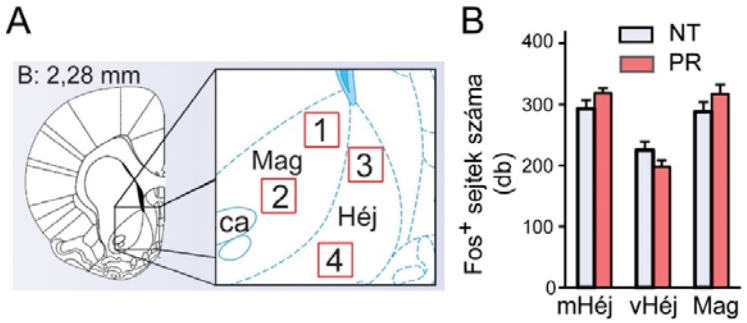

19. ábra. A neuronális aktiváció mértéke a nucleus accumbensben cukrozott sűritett tej fogyasztása után az intrauterin alultápláltság függvényében. A Sémás rajz az elemzett területről. Frontális metszet a bregmától 2,28 mm-re rosztrálisan (Paxinos és Watson 2007). A sejtaktiváció (cFos-pozitivitás) mértékét az accumbens magon belül elhelyezett azonos méretű ROI négyszögekben bilaterálisan számolva határoztuk meg. A következő ROI négyszögeket helyeztük el: 1+2, Mag; 3, mediális Héj, hedonikus forrópont; 4, kontroll terület a ventrális Héjban. **B** A cFos-pozitív sejtek területenkénti száma, Student-féle t-próba, átlag ± standard hiba, n = 8-9 állat/csoport. ca: commissura anterior, mHéj: mediális Héj, vHéj: ventrális Héj.

A cukrozott tej fogyasztása a Nac számos neuronját stimulálta (cFos^{+}), de összehasonlítva a kísérleti csoportokat nem volt különbség egyik Nac alrégióban sem (19. ábra, A, B). Kérdéses

volt ezek után, hogy az Nac hedonikus forrópontjának aktivitása tükrözi-e a táplálék jutalmi értékét? A kérdés megválaszolására megnéztük, korrelál-e az aktivált sejtek száma és az elfogyasztott édes tej mennyisége a csoportokon belül? Szoros pozitív korrelációt találtunk a mediális Héjban az NT és PR állatok esetében is, tehát kérdésünkre igennel tudtunk válaszolni (20. ábra). A PR állatokban azonban hasonló mértékű sejtaktivációhoz több cukros tej elfogyasztása párosult, mint az NT állatokban, ami a sejtaktiválásához szükséges küszöbérték emelkedésére utalt. Az elfogyasztott jutalmi táp mennyisége és az aktivált sejtek száma között szoros pozitív korreláció volt a motivációs aspektussal asszociált Mag alrégióban is a PR állatokban, ami az NT csoportnál nem állt fenn. A kontroll területen egyik csoportban sem korreláltak a mért adatok (20. ábra).

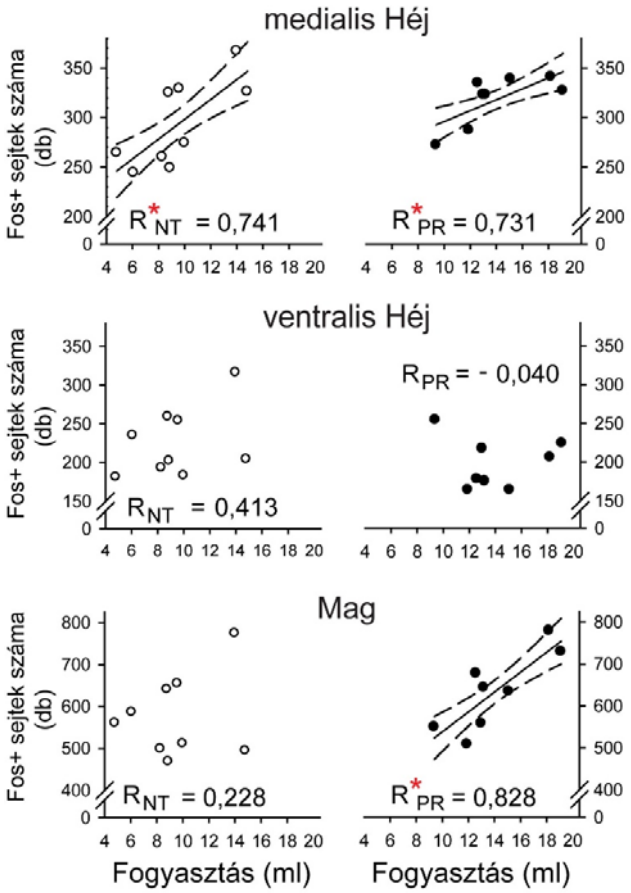

20. ábra. Az elfogyasztott édes tej mennyiségének és a sejtaktiválódás mértékének korrelációja az Nac alrégiókban az intrauterin alultápláltság függvényében. Fehér kör: NT, fekete kör PR állatok adatai. A grafikonon a folytonos vonal a lineáris regressziót, a szaggatott vonalak a 95%-os konfidencia intervallumokat mutatják, 'R' a korrelációs együttható. Pearson korreláció, p* <0,05, n = 8-9 állat/csoport.

A következőkben a laterális hipotalamikus area rosztrális részének sejtaktivációját vizsgáltuk meg. Közvetlenül a tractus opticus felett, az LH területén, nem volt különbség a

csoportok között. A fornix laterális szomszédságában viszont az aktivált sejtek száma nagyobb volt a PR, mint az NT állatokban. Ezek a sejtek az irodalomban bemutatott, a táplálékfelvétel leállításáért felelős sejteknek megfelelően (O'Connor, Kremer et al. 2015), sem orexint, sem MCH-t nem termeltek. Mivel a táplálékfelvétel időtartamának szabályozása a hipotalamusz ezen területén az Nac Héjból irányított, D1R mediált módon történik (O'Connor, Kremer et al. 2015), kvantitatív ISH módszerrel megmértük a D1R és a D2R mRNS expresszió mértékét az Nac különböző alrégióiban. A D2R expresszió mértéke azonos volt a két csoportban, de a mediális Héj régióban a D1R mRNS-szintje a PR állatokban alacsonyabb volt, mint az NT patkányokban (21. ábra, A, B). A D1R mennyiségének csökkenését a PR állatokban fehérjeszinten is igazoltuk (21. ábra, C). Annak kiderítésére, hogy a csökkenés esetleg fokozott dopamin transzmisszió eredménye-e, megmértük a mezolimbikus pálya kiindulópontját képező ventralis tegmentalis areaban a TH (dopamin szintézis sebesség meghatározó enzime) prekurzor mRNS expresszió mértékét, amit az intrauterin körülmények nem befolyásoltak (21. ábra, D). A dopamin szintézis mértéke tehát nem igazolt fokozott jelátvitelt a PR állatokban.

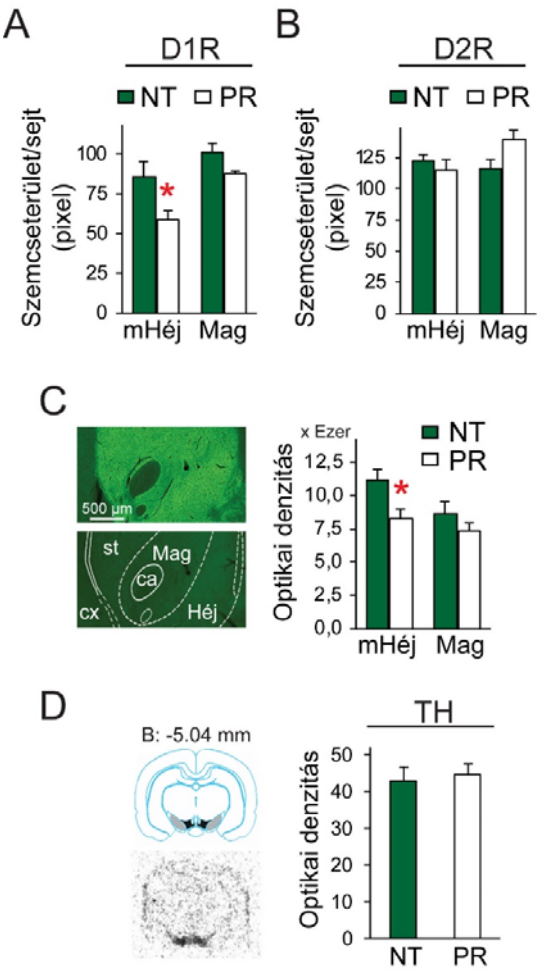

21. ábra. A mezolimbikus dopaminerg pálya kulcsmolekuláinak expressziója az intrauterin alultápláltság függvényében. A D1R és **B** D2R mRNS expresszió mértéke az Nac alrégióiban. Az mRNS kimutatása radioaktív ISH módszer segítségével történt. A metszeteken a jelölt sejtek felett megjelenő ezüstszemcsék (autoradiográfiás jel) által elfoglalt terület nagyságát mértük, mely arányos az mRNS expresszió mértékével. **C** A bal felső képen egy NT állat koronális agyi metszetén elvégzett D1R immunfestés eredménye látható, alatta ugyanazon állat szomszédos metszete, de az immunfestés során az elsődleges antitestet kihagytuk. Jobb oldalon a jelintenzitás mérésének eredményét ábrázoltuk. **D** A TH prekurzor mRNS expressziója középagyban radioaktív ISH detektálással, és a ventralis tegmentalis areaban mért autoradiográfiás jel intenzitásának adatai. Bal felső kép: A terület sémás ábrája. Frontális metszet, a bregmától kaudálisan, -5.04 mm-re (Paxinos és Watson 2007). A szürke szín a substantia nigrát, a fekete szín a ventralis tegmentalis areat jelöli, mely területek dopamin sejteket tartalmaznak. Bal alsó kép: Ugyanazon szintből készült koronális metszet autoradiográfiás képe egy NT állatból, melyen a rajznak megfelelő magokban, sötéten látszik az ISH szignál. A sötétedés mértéke a TH prekurzor mRNS mennyiségével arányos. Student-féle t-teszt, átlag ± standard hiba, NT *versus* PR p*<0,05, n = 6 állat/csoport. ca: commissura anterior, cx: kortex, mHéj: mediális Héj, st: striatum.

Következő kísérletünk egyértelműen bebizonyította, hogy a Nac mediális Héjában a jutalmi tápfogyasztásra adott válasz a D1R pozitív neuronokhoz kötött. Az NT állatokban a cukros tej fogyasztása javarészt a mediális Héj D1R-pozitív sejtjeinek aktiválódását idézte elő (22. ábra, A). A cFos-pozitív sejtek száma ebben a kísérletben is pozitívan korrelált az elfogyasztott tej mennyiségével (22. ábra, B). A részletesebb elemzés kimutatta, hogy a fenti a korreláció csak a D1R és cFos kettősen jelölt sejtekre áll fenn, a D1R-negatív aktivált sejtekre nem igaz (22. ábra, B). A jutalmi tápfogyasztás mértékét a Nac mediális Héj régiójába injektált D1R agonista (SKF-82958) drasztikusan csökkentette (22. ábra, C, D), ezzel együtt a laterális

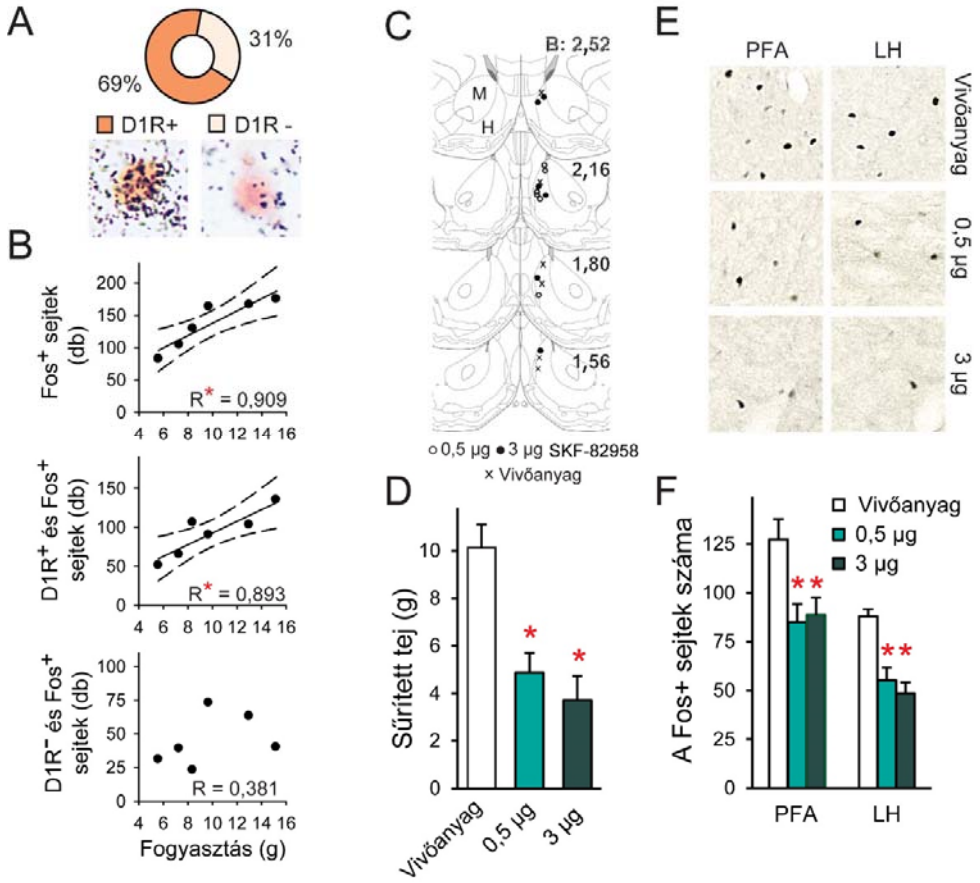

22. ábra. A D1R jelátvitel szerepe nomál táplált állatok jutalmi táplálékfelvételében. A D1R-pozitív és D1R-negatív, aktivált sejtek mennyiségi megoszlása a Nac mediális Héj régiójában cukros tej elfogyasztása után. Az illusztratív képek két cFos-immunpozitív (barna sejtmagok) sejtet ábrázolnak, melyek közül a bal oldali D1R mRNS-t termel (pozitív ISH jel, fekete ezüstszemcsék tömörülése a sejt körül), a jobb oldali D1R-negatív. **B** Az elfogyasztott cukros tej mennyisége és az aktivált összes sejt, $D1R^+$ sejt és $D1R^-$ sejt száma közötti korrelációk. A folytonos vonal a lineáris regressziót, a szaggatott vonalak a 95%-os konfidencia intervallumokat mutatják, 'R' a korrelációs együttható. Pearson korreláció, p*<0,05, n = 6 állat/csoport. **C** Sémás ábra, az injektált anyagok beadási helyeinek jelölésével a mediális Héjban (Paxinos és Watson 2007). A D1R agonistát (SKF-82958) két dózisban (0,5 µg és 3 µg) alkalmaztuk, a vivőanyag fiziológiás só volt. A bregmától való rosztrális távolságokat mm-ben tüntettük fel. **D** A mediális Héjba injektált D1R agonista hatása a jutalmi táplálékfelvételre. **E** A cFos immunfestés (fekete sejmagok) eredményét bemutató illusztratív mikrofotók a rosztrális PFA és LH területéről. **F** A cFos-pozitív sejtek száma az elemzett területeken. Egyutas ANOVA, Student-Newman-Keuls post-hoc teszt, átlag ± standard hiba, p*<0,05 *versus* vivőanyag, n = 6 állat/csoport. M: Nac Mag régió, H: Nac mediális Héj régió.

hipotalamikus area rosztrális részében aktiválódott neuronok száma is kevesebb lett (22. ábra, E, F). A tejfogyasztás csökkenését a táplálkozás leállítása okozta, mivel a videofelvételek tanúsága szerint csökkent a táplálkozással töltött idő. A lefetyelés finommotorikájának ízletességre vonatkozó paraméterei a D1R agonista kezeléstől nem függtek.

A PR modell felhasználásával a homeosztatikus és a nem-homeosztatikus szabályozás eddig nem ismert zavarait mutattuk ki, melyek még az elhízást megelőzően jelennek meg a 2TDM-re és metabolikus szindrómára hajlamos fenotípusban. Adataink alapján a hipotalamikus nesfatin-1-rezisztencia kialakulása fontos tényező a T2DM kialakulásában fehérjehiány okozta IUGR esetén. Megállapítottuk, hogy nesfatin táplálékfelvételre gyakorolt hatásának fontos célterülete az ARC mag, melyben a prediabeteses PR fenotípusban nesfatin-1 rezisztencia lép fel.

Azonosítottunk továbbá egy D1R-pozitív sejtcsoportot a Nac mediális Héj régiójában, melynek aktivációja tükrözi a táplálék jutalmi értékét. A jutalmi táplálékfelvétel megnövekedésének oka a PR állatokban elsősorban a megnövekedett étvágy volt. A folyamat mechanizmusában valószínűleg a Nac mediális Héj régiójában található sejtek csökkent D1R expressziója és nehezebb ingerelhetősége játszik közre, mely a táplálékfelvétel leállításának késleltetéshez vezet a laterális hipotalamuszon keresztül. Mivel az elégtelen intrauterin környezet a terhességi szövődmények egyik legyakoribb oka (Saleem, Sajjad et al. 2011), eredményeinknek klinikai jelentősége lehet.

5.3. A stresszválasz finomhangolásának tanulmányozása

A fejezet a következő közleményeken alapszik:

7. Katalin Könczöl et al., *Neurochemistry International* 2010, 57:189–197. *#

8. Zsuzsanna E. Toth* et al., *Journal of Neurochemistry* 2008, 104(3):653-66.

9. Rita Matuska et al., *Brain Structure and Function* 2020, 225:969–984. *#

10. Szilvia Vas et al., *The Journal of Neuroscience* 2023, 43(5):846–862. * #

*: levelező szerző, #: utolsó szerző

A mentális stresszbetegségek; a szorongás, a poszttraumás stresszbetegség és a major depresszió kialakulásának fő rizikó faktora a krónikus stressz (Bao és Swaab 2019). Míg a társadalom számára a megfelelő ellátás az emelkedő esetszámok miatt egyre nagyobb gazdasági teher, a betegek vállát a gyötrő lelki szenvedés nyomja, amit főként a major depressziós és bipoláris páciensek magas öngyilkossági rátája tükröz (Bachmann 2018).

Ahogy a bevezetésben említettem, a HPA tengely kiindulási pontját képező CRH neuronok stimulálásában az agytörzsi ventrális noradrenerg pálya működése meghatározó. A stresszválasz kialakításában azonban a CRH-n kívül számos egyéb neuropeptid is részt vesz (Rana, Behl et al. 2022). A PVN mediális parvocelluláris (mpPVN) részében elhelyezkedő CRH sejtekben AVP is termelődik, ami potencírozza a CRH hatását a hipofízis ACTH termelésére (Watanabe és Orth 1987). Különböző stresszhelyzetekben többek között ez teszi lehetővé a HPA tengely működésének plasztikus változását. Egymást követő, eltérő jellegű stresszorok esetén a stresszválasz facilitációja következik be, amiben közrejátszik, hogy az AVP gén kifejeződése kevésbé érzékeny a negatív glükokortikoid visszacsatolásra, mint a CRH gén expressziója (Dallman 1993). Ismételt, azonos stresszor által kiváltott válaszreakció során viszont a szervezet habituációja történik. Patkányokban a restraint ismétlésének gyakoriságával a CRH és a kortikoszteron válasz is látványosan csökken (Ma és Lightman 1998), míg az adaptáció során a kissejtes AVP génexpresszió a stresszor ismétlődésének gyakoriságával fokozatosan emelkedik (Dallman 1993, Ma és Lightman 1998).

Mindezek alapján feltételeztük, hogy a neuropeptid koexpressziónak a stresszhez való adaptáció mechanizmusában fontos szerepe lehet. Stresszel kapcsolatos munkáimban ezért a nesfatin és a PrRP szerepkörére koncentráltam. A munka jelentősége, hogy napjainkban a mentális stresszbetegségek kezelésében alternatív terápiás célpontokként előtérbe kerültek a neuropeptidek (Hökfelt, Barde et al. 2018, Mantas, Saarinen et al. 2021), mivel a betegek jelentős részében a klasszikus szerotonin és noradrenalin visszavétel gátló gyógyszerek hatástalanoknak bizonyultak (Voineskos, Daskalakis et al. 2020).

5.3.1. A nesfatin szerepének vizsgálata a HPA tengely szabályozásában

7. Közlemény: ***Nesfatin-1/NUCB2 may participate in the activation of the hypothalamic-pituitary-adrenal axis in rats.***

A nesfatinról felfedezése után néhány éven belül számos olyan új adat látott napvilágot, melyek alapján körvonalazódott, hogy szerepet játszhat a stresszválaszban. Kimutatták például, hogy a stresszválasz szempontjából meghatározó sejtcsoportok, például a PVN CRH neuronjai, az A2 sejtcsoport, és az Edinger-Wesfal mag sejtjei tartalmaznak nesfatint is (Brailoiu, Dun et al. 2007, Foo, Brismar et al. 2008). A PVN, az NTS és a ventrolaterális medulla területén elhelyezkedő nesfatin-termelő neuronok számos stresszor hatására aktiválódnak (Goebel, Stengel et al. 2009), és a centrálisan alkalmazott nesfatin-1 fokozza a szorongást és félelmet (Merali, Cayer et al. 2008). Mindezek alapján a nesfatin és a HPA tengely kapcsolatát behatóbban kívántuk tanulmányozni.

Legelőször megvizsgáltuk, hogy a HPA tengely aktivitását befolyásolja-e az exogén nesfatin-1? A kísérletek során icv kanülön keresztül nesfatin-1-et (25 pmol és 100 pmol), illetve vivőanyagot juttatunk a patkányok oldalkamrájába. Ezután, a szabadon mozgó állatokból a véna jugularisba előzőleg beültetett kanülön át adott időközönként hormonmeghatározásra vérmintát vettünk. A nesfatin-1 harminc perccel a kezelést követően jelentősen megemelte a vérplazma ACTH szintjét, ami szignifikáns maradt még a 60. percben is (23. ábra, A). A vérplazma kortikoszteron koncentrációja kis késéssel követte az ACTH szint növekedését, és a nesfatin-1 kezelt állatokban utolsó mért időpontban, a beadás utáni 100. percben is magasabb volt, mint a kontrollokban (23. ábra, B).

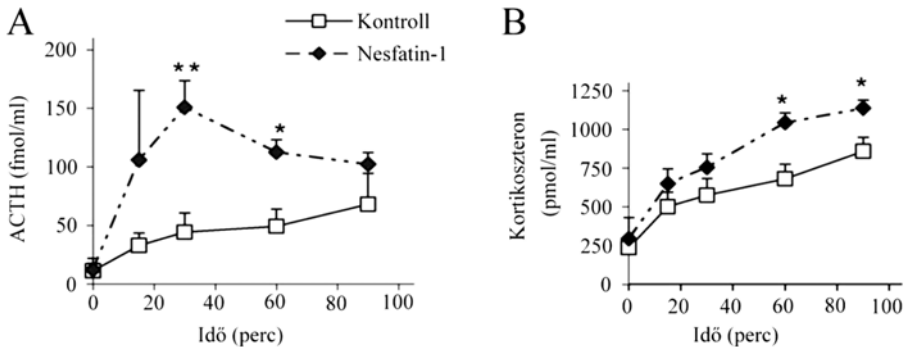

23. ábra. Az icv injektált nesfatin-1 hatása a HPA tengelyre. **A** A vérplazma ACTH és **B** kortikoszteron szintjének időbeli alakulása 25 pmól nesfatin-1, illetve fiziológiás só (kontroll) icv beadását követően (0. perc). Student-féle t-próba, átlag ± standard hiba, kontroll *versus* nesfatin-1 p*<0,05, p**<0,01, n = 3- 5 állat/csoport.

További kérdés volt, vajon a nesfatin-1 képes-e a hipofízis sejtek ACTH szekrécióját közvetlenül stimulálni? Felnőtt patkányok hipofíziséből készített sejttenyészeten a nesfatin-1 két különböző dózisban (25 pmol és 100 pmol) alkalmazva sem hatott, ezt a mechanizmust tehát kizártuk. Ezzel párhuzamosan kimutattuk, hogy a hipofizeotróp CRH sejtek elhelyezkedésének megfelelő mpPVN alrégióban a nesfatin-termelő neuronok stressz érzékenyek. A restraint stressz (4 h) ugyanis, a területen belüli nesfatin-pozitív neuronok közel felét aktiválta ($cFos^+$) (24. ábra), és ugyanitt megemelkedett a nesfatin mRNS expressziója is.

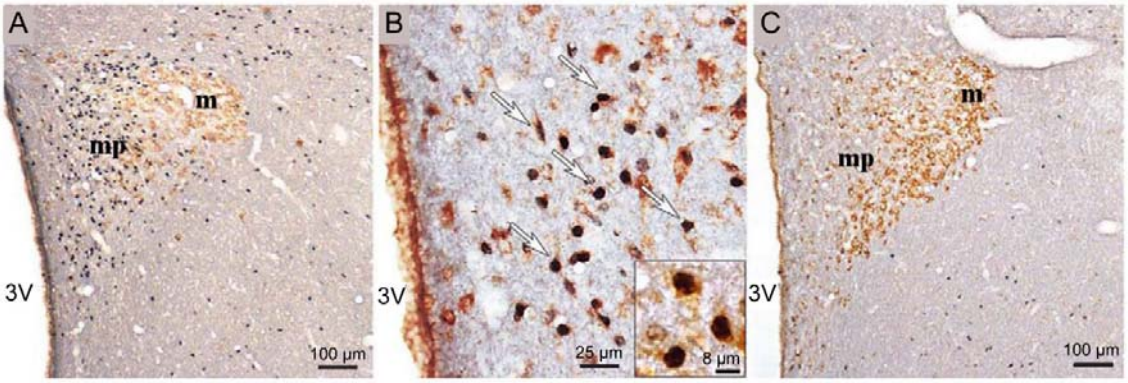

24. ábra. A PVN nesfatin-termelő sejtjeinek részvétele a stresszválaszban. Kettős, cFos (sötét sejtmagok) és nesfatin (barna sejtek) immunfestés a PVN szintjéből készült koronális metszeteken. **A** Áttekintő kép stresszelt (4 h restraint) állatból. **B** A mpPVN nagyobb nagyítással stresszelt állatból. A nyilak nesfatin és cFos kettősen jelölt neuronokra mutatnak. További nagyítás az inzertben látható. **C** Áttekintő kép kontroll, nem stresszelt állatból. PVN alrégiók: m: magnocelluláris, mp: mediális parvocelluláris, 3V: 3. agykamra.

Következő gondolatunk az volt, hogy amennyiben az mpPVN nesfatin neuronjai valódi elemei a HPA tengelynek, a nesfatin expressziót a glükokortikoidok ezen a területen feltehetően negatív visszacsatolással szabályozzák. Bilaterális adrenalektómia után egy héttel kvantitatív ISH módszerrel valóban detektálni tudtuk a nesfatin mRNS expresszió fokozódását az mpPVN területén (25. ábra).

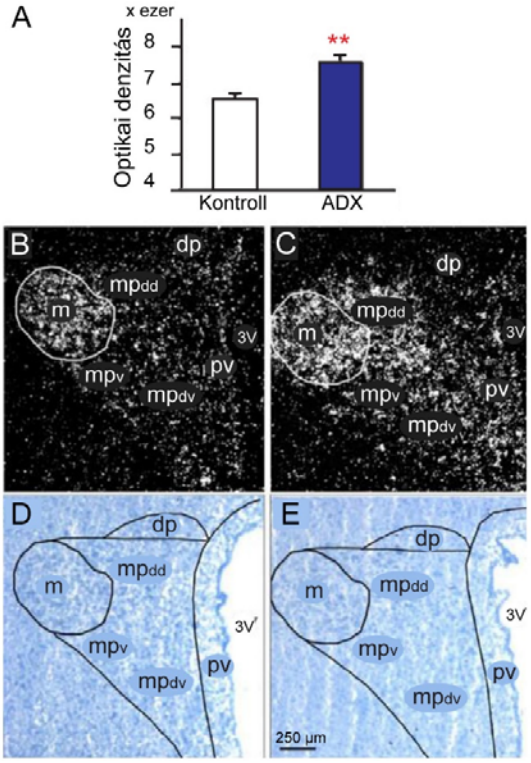

25. ábra. Az adrenalektómia (ADX) hatása a mpPVN nesfatin mRNS expressziójára. **A** A kvantitatív nesfatin ISH mérési adatai. Az értékelés során a metszetek autoradiográfiás képeiről az optikai denzitást mértük. Student-féle t-teszt, átlag ± standard hiba, álműtött kontroll *versus* ADX p**<0,01, n = 6- 7 állat/csoport. **B, C** A nesfatin mRNS expresszió helyének és erősségének megfelelő ISH jel a PVN területén, álműtött kontroll (B) és ADX állatból (C). Sötét látóteres felvételek, az autoradiográfiás jel (ezüstszemcsék a sejtek felett) fehér foltok gyanánt látszanak. **C, D** Világos látóteres képek a B és C képeken látható területről Giemsa (kék) háttérfestéssel. A PVN almagjai: dp: dorzális parvocelluláris, pv: periventrikularis, m: magnocelluláris, mp: mediális parvocelluláris, és annak további tagozódása: mpv: pre-autonóm régió, mpdd: dorzális preautonóm régió, mpdv: ventrális régió.

Vizsgálatainkat a nyúltvelőben folytattuk. Mivel az A2 sejtcsoport neuronjaiban a nesfatin és a noradrenalin koexpresszióját kimutatták (Brailoiu, Dun et al. 2007) és nesfatin-termelő sejtek jelenlétét írták le az A1 noradrenerg sejtcsoport elhelyezkedésének megfelelő cVLM területén is (Goebel, Stengel et al. 2009), a restraint stressz hatását ezeken a területeken is megvizsgáltuk. Az A2 sejtcsoportban nem, de a cVLM területén emelkedett nesfatin mRNS expressziót detektáltunk a stresszelt csoportban. A nyúltvelői nesfatin sejtek további kémiai karakterizálása bebizonyította, hogy a cVLM nesfatin-pozitív neuronjainak többsége az A1 sejtcsoport része. Kimutattuk továbbá a PrRP, a TH és a nesfatin nagymértékű koexpresszióját is mindkét sejtcsoportban (26. ábra).

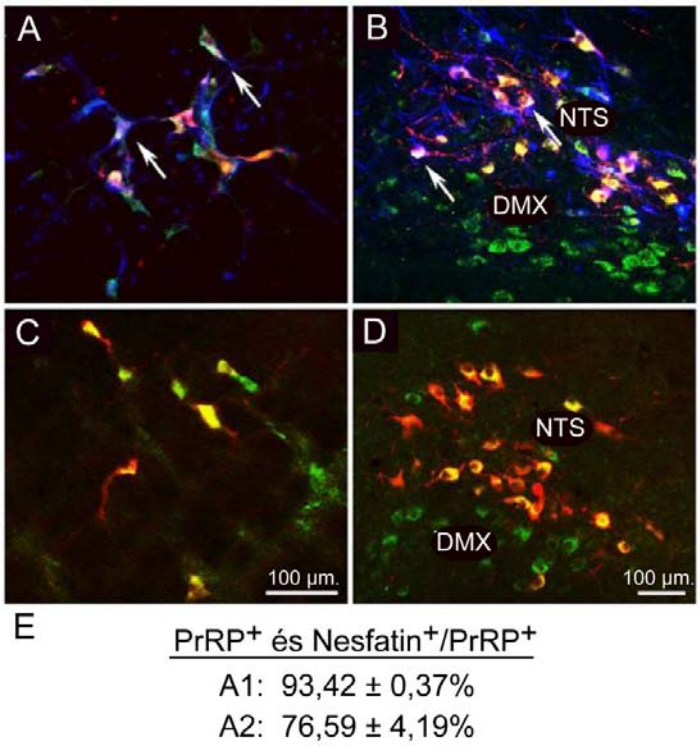

26. ábra. A nesfatin és a PrRP koexpressziója az A1 és A2 nyúltvelői sejtcsoportokban. A, B Háromszoros, nesfatin (zöld), PrRP (piros) és TH (kék) immunfluoreszcens festés az A1 (A) és az A2 (B) sejtcsoportok területéről. A nyilak hármasan jelölt sejtekre mutatnak. **C, D** Kettős, PrRP (piros) és nesfatin (zöld) immunfluoreszcens festés az A1 (C) és A2 (D) sejtcsoportok területéről. A duplán jelölt sejtek sárgák.

Eredményeink igazolták, hogy a nesfatin a HPA tengely szabályozó eleme, és az endogén nesfatin már a nyúltvelői katekolaminerg sejtcsoportok szintjén is szerepet játszhat a stresszválasz kialakításában. További kísérleteinkben a krónikus stresszhez való adaptáció és a mentális stresszbetegségek kialakulásának mechanizmusait vizsgáltuk.

5.3.2. A PrRP jelentősége a krónikus stresszhez való alkalmazkodásban

8. Közlemény: ***Chronic repeated restraint stress increases prolactin-releasing peptide/tyrosine-hydroxylase ratio with gender-related differences in the rat brain***

A PrRP akut stresszben betöltött szerepével kapcsolatban számos publikáció jelent meg (Sun, Fujiwara et al. 2005). A nyúltvelői PrRP és noradrenalin koexpresszió (Chen, Dun et al. 1999), és PrRP noradrenalin hatását potencírozó képessége (Maruyama, Matsumoto et al. 2001) miatt felvetődött, hogy a CRH/AVP együttműködéshez hasonlóan (Ma és Lightman 1998), a PrRP szerepe is előtérbe kerülhet a krónikus stresszhez való adaptációban. A hipotézis ellenőrzéséhez a patkányokat krónikus ismételt restraint stressznek (*repeated restraint*, RR) vetettünk alá, melyet a reggeli órákban 1 órán át végeztünk egy héten keresztül. Mivel a krónikus stresszre adott válaszban nemek közti különbségek észlelhetőek, és a PrRP működése és termelődése is függ a nemi hormonoktól (Dodd és Luckman 2013), hímeket és nőstényeket (metösztrusz és diösztrusz stádiumokban) is összehasonlítottunk. Munkánk harmadik célkitűzéseként arra kerestünk választ, hogy a PVN léziója befolyásolja-e a PrRP neuronok krónikus stresszre adott reakcióját, mivel Dayas és munkatársai szerint akut restraint során a nyúltvelői A1 és A2 sejtek aktivitását a PVN efferensei szabályozzák (Dayas, Buller et al. 2004).

A hím állatokban a krónikus stressz tipikus testi tünetei (testsúlygyarapodás csökkenése, mellékvese hipertrófia, tímusz involúció) klasszikusan megfigyelhetőek voltak. A nőstényeknél csak a testsúlynövekedés lassú ütemét észleltük. A kontroll nőstények plazma kortikoszteron szintje magasabb volt, mint a hímeké. A stresszhez való adaptáció mindkét nemben a kortikoszteron koncentráció enyhe megemelkedésével járt, az emelkedés mértéke a nőstényekben a hímekéhez viszonyítva kisebb volt A plazma prolaktin szintje nem változott (1. táblázat).

1. táblázat. A krónikus ismételt restraint stressz (RR) hatása a testi paraméterekre és a stresszhormon szintekre. Student-féle t-teszt, átlag ± standard hiba, $p^{*}<0,05$ *versus* kontroll hím, $p^{\#}<0,05$ *verus* kontroll nőstény, súlyadatok n = 5-8 állat/csoport, hormonmérések n = 7-12 állat/csoport.

	Testsúlygyarapodás (g)	Relatív mellékvese súly (mg/ttkg)	Relatív tímusz súly (mg/ttkg)	Kortikoszteron (pmol/ml)	Prolaktin (ng/ml)
Kontroll-hím	45,6 ± 2,5	145,8 ± 5,0	2002,6 ± 105,7	74,4 ± 17,4	2,7 ± 0,5
RR-hím	22,3 ± 3,1*	181,6 ± 10,0*	1460,8 ± 16,4*	636,2 ± 56,4*	4,7 ± 1,1
Kontroll-nőstény	10,8 ± 1,8	322,2 ± 12,2	2011,7 ± 309,9	234,4 ± 71,6	2,2 ± 0,7
RR-nőstény	4,0 ± 1,3$^{\#}$	319,4 ± 17,3	2088,5 ± 115,5	682,8 ± 118,3$^{\#}$	2,4 ± 0,6

A szövettani vizsgálatok első lépéseként kettős ISH módszerrel megerősítettük azt a korábban kettős immunhisztokémiával kimutatott tényt (Chen, Dun et al. 1999, Sun, Fujiwara et al. 2005), hogy a nyúltvelői A1 sejtcsoport neuronjainak mindegyike és az A2 sejtcsoport NTS területére eső neuronjainak többsége TH és PrRP mRNS-t is tartalmaz. A PrRP-termelő neuronok tehát gyakorlatilag e katekolaminerg sejtcsoportok részét képezik. Ezután, rádioaktív ISH módszerrel elemeztük az egyes sejtekben az mRNS expresszió mértékét és megszámoltuk a PrRP-pozitív sejteket. A PrRP mRNS expressziója nőstényekben az A1 és A2 sejtcsoportban is magasabb volt, mint a hímekben, az egyes sejtek PrRP mRNS-szintjét tekintve (27. ábra, A, B), és az A1 sejtcsoportban a pozitív sejtek számát nézve is. Ez új adatnak számított, hiszen korábban, csak proösztruszos nőstényeknél mutattak ki magas PrRP expressziót (Kataoka, Iijima et al. 2001). A DM nem-katekolaminerg PrRP neuronjainak esetében a PrRP expresszióban nem találtunk nemi különbséget (27. ábra, C). A krónikus stressz fokozta a PrRP mRNS expressziót az A1 sejtcsoport és a DM területén mindkét nemben (27. ábra, A, C), ami

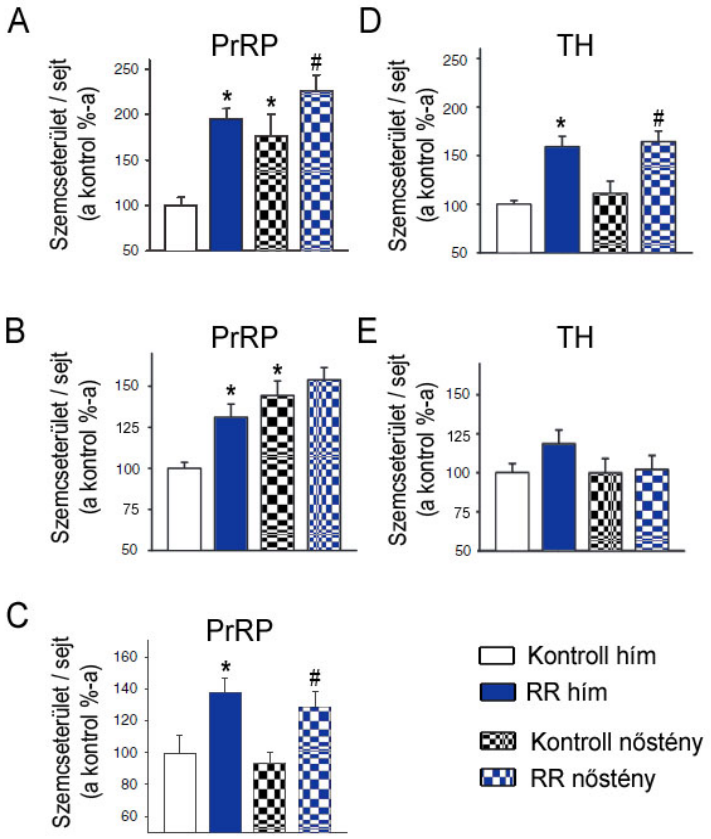

27. ábra. A krónikus ismételt restraint stressz (RR) hatása a hím és nőstény patkányok PrRP és TH mRNS expressziójára. Az mRNS kimutatása radioaktív ISH módszer segítségével történt, a metszeteken a jelölt sejtek felett megjelenő ezüstszemcsék (autoradiográfiás jel) által elfoglalt terület nagyságát mértük, mely arányos az mRNS expresszió mértékével. **A-C** PrRP mRNS expresszió az A1 sejtcsoportban (A), az A2-NTS sejtekben (B) és a DM magban (C). **D, E** TH mRNS expresszió az A1 sejtcsoportban (D) és az A2-NTS sejtekben (E). Kétutas ANOVA, Student-Newman-Keuls post hoc teszt, átlag ± standard hiba, $p^{*}<0,05$ *versus* kontroll hím és $p^{\#}<0,05$ *versus* kontroll nőstény, n = 9-17 állat/csoport.

az A1 sejtcsoportban ismételten a pozitív sejtek számának emelkedésében is megnyilvánult. Az A2-NTS sejtekben viszont, ahol nőstényekben eleve magasabb volt a PrRP mRNS mennyisége a hímekénél, a stressz csak a hímekben okozott PrRP mRNS-szint emelkedést (27. ábra, B). A TH mRNS expresszióban, amit párhuzamos (szomszédos) metszeteken mértük, a nemek között nem volt különbség. A krónikus stressz az A1 sejtcsoportban mindkét nemben fokozta a TH mRNS expressziót a sejtekben (27. ábra, D) és a detektálható TH-pozitív sejtek számát is. Az A2-NTS (27. ábra, E) és az A2-DMX területén azonban nem okozott változást. Eredményeinket immunoautoradiográfiás módszerrel fehérjeszinten is megerősítettük.

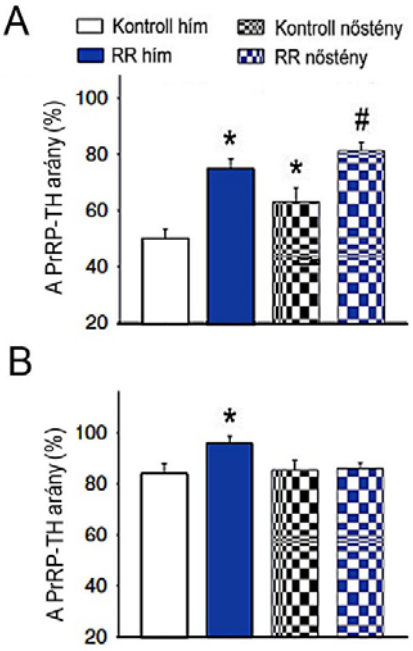

28. ábra. A PrRP és TH mRNS expresszió arányának változása RR hatására különböző nemű patkányokban. A A1 sejtcsoport. **B** A2-NTS. A számolás a sejtszám adatok alapján történt. Kétutas ANOVA, Student-Newman-Keuls post hoc teszt, átlag ± standard hiba, $p^{*}<0,05$ *verus* kontroll hím, $p^{\#}<0,01$ *versus* kontroll nőstény, n = 9-16 állat/csoport.

A PrRP-TH mRNS arány az A1 sejtcsoportban a nőstényekben magasabb volt, mint hímekben (28. ábra, A). A krónikus stresszre adott válaszreakció során a PrRP és TH mRNS expresszió aránya a PrRP javára tolódott A1 sejtcsoport területén mindkét nemben (28. ábra, A), az A2-NTS területén pedig a stresszreakciót mutató hímekben (28. ábra, B). A PrRP-TH expresszió arány változását kettős ISH módszerrel is igazoltuk.

A bilaterális PVN lézió következtében az A2-NTS neuronok PrRP és TH mRNS expressziója is erősen lecsökkent (sejtekben mért mennyiség és sejtszám), de a krónikus stressz okozta génexpressziós válaszok megmaradtak, tehát ezek a válaszok elsősorban a perifériás bemenenetektől függtek, illetve más agyterületek szabályozó hatása alatt állhattak.

A PrRP expresszióban tapasztalt nemi különbségek további vizsgálatokra sarkalltak. Ismert volt, hogy nőstény patkányokban immunhisztokémiai módszerrel ösztrogén alfa receptor jelenlétét mutatták ki az NTS PrRP-pozitív neuronjaiban, valamint, hogy az ovariektómiát követő hormonpótlás a PrRP mRNS-szint növekedését idézi elő (Kataoka, Iijima et al. 2001). Kettős immunofluoreszcens festéssel, melynek során antigén feltárást és jelerősítést alkalmaztunk, sikerült az A1 sejtcsoport PrRP neuronjaiban is ösztrogén alfa receptor immunpozitivitást kimutatnunk (29. ábra, A), viszont mind az A1, mind A2 sejtcsoport PrRP neuronjai negatívnak mutatkoztak az ösztrogén béta receptor immunoreaktivitást tekintve. Az ováriumok eltávolítása után a PrRP mRNS expresszió

az álműtött nőstényekhez és a hímekhez képest is jelentősen csökkent mindkét nyúltvelői sejtcsoportban (29. ábra, B). A PrRP expresszió női nemi hormon függését a fehérje mennyiségi meghatározásával is megerősítettük (29. ábra, C).

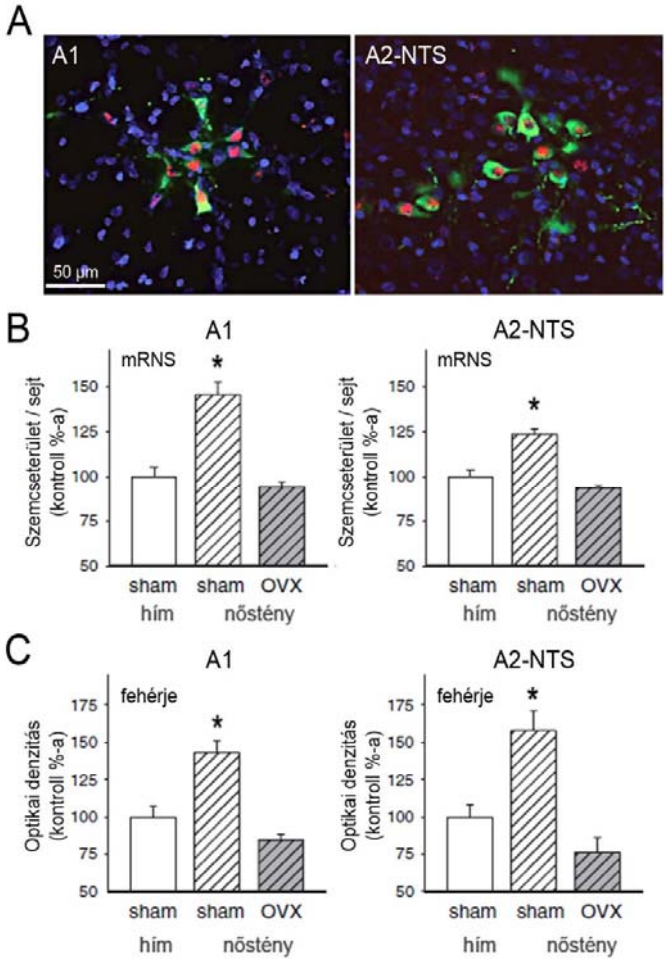

29. ábra. A nyúltvelői PrRP expresszió női nemi hormon függése. A Kettős, ösztrogén alfa receptor (piros magok) és a PrRP (zöld citoplazma) fluoreszcens immunfestés az A1 és A2-NTS sejtcsoport neuronjaiban. A metszeteken DAPI (kék) háttérfestés jelöli a sejtmagokat. **B** PrRP mRNS (rádioaktív IHS jel mérése) és **C** fehérjeszintek (immunautoradiográfiai jel mérése) hímekben, álműtött nőstényekben és ovariektomizált nőstényekben az A1 és az A2-NTS sejtcsoportokban. Az adatokat a hímek átlagához viszonyítottuk. Egyutas ANOVA, átlag ± standard hiba, álműtött nőstény *versus* többi csoport p*<0,001, n = 5-7 állat/csoport.

5.3.3. Krónikus ozmotikus stressz modellek összehasonlító vizsgálata

9. Közlemény: *Colocalized neurotransmitters in the hindbrain cooperate in adaptation to chronic hypernatremia*

A nyúltvelői A1 és A2 sejtcsoportok tanulmányozásával kapcsolatos eredményeink (PrRP szerepe a krónikus stresszben, PrRP, noradrenalin és nesfatin koexpresszió ezekben a sejtcsoportokban) a kotranszmitterek szerepének jelentőségére hívták fel a figyelmet a krónikus stresszhez való alkalmazkodásban. Következő kísérleteinkben e három neurotranszmitter

szerepét krónikus ozmotikus stressz (hipernatrémia) modellekben vizsgáltuk. A hipernatrémia az ozmoregulációban résztvevő agyterületeket és a HPA tengelyt is mozgósítja, és az akut restraint stresszre adott HPA választ gátolja (Krause, Pati et al. 2017). A nyúltvelői noradrenalin sejtek hipernatrémiára specifikusan aktiválódnak, hiponatrémiára nem reagálnak (Hochstenbach és Ciriello 1995). A noradrenerg beidegzés a hipotalamusz hipernatrémiára adott válaszainak kialakításában főszerepet játszik. A szabályozás szempontjából legfontosabb agyterületek noradrenalin tartalmú beidegzést főleg az A1 és kisebb mértékben az A2 sejtcsoportokból kapnak (Sawchenko és Swanson 1981, Cunningham és Sawchenko 1988, Bourque 2008, Pedrino, Rosa et al. 2014), tehát gyakorlatilag a PrRP tartalmú sejtekből (Maruyama, Matsumoto et al. 2001). A hipernatrémiához való adaptációban legfontosabb hipotalamikus területek a stresszválasz szempontjából a kissejtes PVN, az ozmotikus kihívásra adott autonóm, endokrin és viselkedési válaszok szabályozásának szempontjából pedig a magnocelluláris magok (mPVN, SON), valamint az anteroventrális periventrikuláris area (AV3V) (Bourque 2008).

A PrRP és a nesfatin ozmoregulációban betöltött szerepét korábban nem vizsgálták. A PrRP fokozza az AVP és az oxitocin felszabadulását, ezenkívül részt vesz a kardiovaszkuláris szabályozásban és a vértérfogat szabályozásában is, mely hatások kapcsolódhatnak a krónikus hipernatrémiához való alkalmazkodáshoz. A kardiovaszkuláris szabályozásban az agytörzsi nesfatin részvételét is kimutatták (Mimee, Smith et al. 2012).

Mindezek alapján a következők kérdéseket foglalmaztuk meg:

1. Vajon az állatokban a stresszhormonok szintje függ-e a krónikus hipernatrémia típusától (eu- vagy hypervolémiás, veleszületett vagy szerzett)? A kérdés megválaszolásához kétféle hipernatrémia modellt hasonlítottunk össze. Az egyik modellben vad típusú (VT), és genetikailag AVP hiányos örökletes diabetes insipidusban szenvedő euvolémiás Brattleboro patkányokat (DI) használtunk. A másik modellben az állatok egy csoportjában krónikus sóterheléssel (ST csoport: 2% NaCl víz helyett 6 napig) hipervolémiás hipernatrémiát idéztünk elő, a kontrollok csapvizet kaptak.
2. A krónikus hipernatrémia különböző típusai eltérően befolyásolják-e az akut restraint stresszre adott hormonális és nyúltvelői génexpressziós válaszokat?
3. A TH, PrRP és nesfatin expresszió mértéke a nyúltvelőben tükrözi-e a HPA tengely érzékenységét az akut (3 h) restraint stresszre krónikus hipernatrémiában szenvedő állatokban?
4. Kimutatható-e a PrRP jelátvitel szerepe és ennek megfelelően a PrRP-noradrenalin interakció lehetséges szerepe a krónikus hipernatrémiához történő adaptációban a hipotalamuszban?

Modelljeinket a plazma ozmolalitásának mérésével validáltuk, mely mindkét modellben megemelkedett (2. és 3. táblázat). A DI állatok testsúlya kissé alacsonyabb volt, mint a vad típusúaké, és folyadékháztartásuk alapján diabetes insipidusban szenvedtek, de a veleszületett körülményekhez nagymértékben alkalmazkodtak. A krónikus stressz tipikus tünetei (mellékvese megnagyobbodás, tímusz involúció) nem látszottak (2. táblázat) és a plazma ACTH és kortikoszteron szintjük is a normális tartományba esett (30. ábra, A, B). A sóterhelés jobban igénybe vette az állatok szervezetét. A testsúly nagymértékben csökkent, és megjelentek a krónikus stressz tipikus testi tünetei (3. táblázat), melyet enyhén emelkedett plazma ACTH és kortikoszteron koncentráció kísért (30. ábra, C, D). A sóterhelt állatok tápálékfelvétele a kísérlet során folyamatosan csökkent, folyadékfogyasztásuk folyamatosan emelkedett.

2. táblázat. A Brattleboro állatok testi paraméterei, napi táplálék- és vízfogyasztása. A mérések 5 egymást követő napon keresztül történtek. Student-féle t-teszt, átlag ± standard hiba, p*<0,05, p**<0,01 p**<0,001 *versus* VT, n = 7 állat/csoport. DI: homozigóta AVP deficiens, VT: homozigóta vad típusú

	testsúly (g)	plazma ozmolalitás (mOsm/l)	relatív mellékvese súly (g/ttkg)	relatív tímusz súly (g/ttkg)	táp (g)	relatív táp (g/ttkg)	víz (g)	relatív víz (g/ttkg)
VT	408 ± 9	305 ± 4	97 ± 5	923 ± 82	24 ± 1	66 ± 3	31 ± 1	76 ± 3
DI	356* ± 15	335*** ± 2	95 ± 9	815 ± 78	21** ± 1	63 ± 3	147*** ± 6	415*** ± 16

3. táblázat. A magas sótartalmú (ST) folyadék itatásának hatása a Wistar patkányok testi paramétereire. A kontroll állatok csapvizet ittak (nem-sós, NS). Az ST csoport 2%-os NaCl oldatot kapott inni 6 egymást követő napon keresztül. Student-féle t-teszt, átlag ± standard hiba, p*<0,05, p**<0,001 *versus* NS, n = 8 állat/csoport.

	testsúly változás (g)	plazma ozmolalitás (mOsm/l)	relatív mellékvese súly (g/ttkg)	relatív tímusz súly (g/ttkg)
NS	49 ± 2	304 ± 1	166 ± 8	2349 ± 139
ST	-46*** ± 5	363*** ± 7	219* ± 17	944*** ± 102

Az akut restraint mindkét modell kontroll állataiban erősen stimulálta a HPA tengelyt (30. ábra). A hipernatrémia az akut restraintre adott ACTH választ a DI állatokban nem befolyásolta szignifikánsan, de a kortikoszteron választ enyhén gátolta (30. ábra, A B). A sóterhelt állatok HPA válasza az akut stresszre erősen sérült volt (30. ábra, C, D).

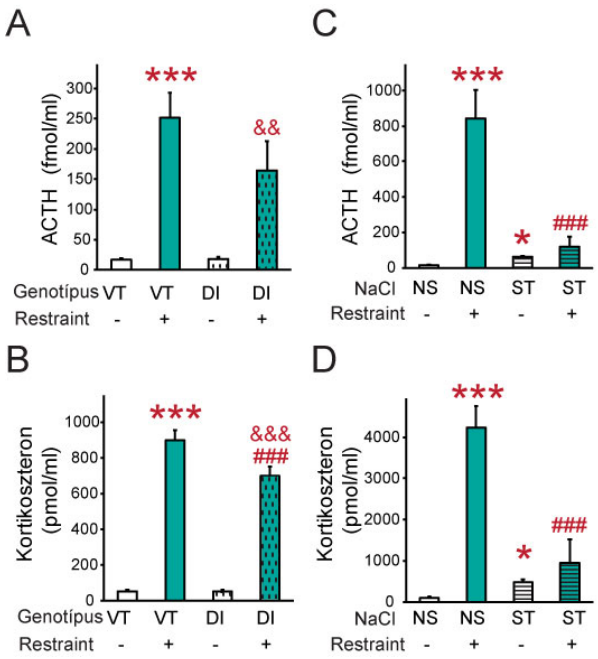

30. ábra. A HPA tengely aktivitása a vizsgált krónikus hipernatrémia modellekben alapállapotban és akut restraint stressz elszenvedése után. A, **B** Genetikailag AVP deficiens és kontroll Brattleboro állatok plazma ACTH (A) és kortikoszteron szintjei (B). **C, D** Sóterhelt és kontroll Wistar patkányok plazma ACTH (C) és kortikoszteron szintjei (D). Student-féle t-teszt, ST *versus* NS $p^{*}\leq 0{,}001$. Kétutas ANOVA, Student-Newman-Keuls post hoc teszt, $p^{***}\leq 0{,}001$ *versus* VT-kontroll, illetve NS-kontroll (nem stresszelt) $p^{\#\#\#}\leq 0{,}001$ *versus* VT-restraint, illetve NS-restraint, $p^{\&\&\&} \leq 0{,}001$ és $p^{\&\&}\leq 0{,}01$ *versus* DI-kontroll (nem stresszelt), DI modell: n = 7 állat/csoport, HS modell: n = 7-8 állat/csoport. Állatmodellek: DI: homozigóta AVP hiányos, NS: nem-sóterhelt, ST: 2% NaCl itatott (6 nap), VT: homozigóta Brattleboro vad típus.

A krónikus stresszhez való adaptáció megnyilvánulása a naiv (nem stresszelt) DI állatokban a megemelkedett PrRP és nesfatin mRNS expresszió volt az A1 és A2 sejtcsoportok területén (4. táblázat). A krónikus sóterhelésre adott adaptációs válasz az A1 sejtcsoportban hasonlóan alakult, de ebben a modellben a TH mRNS expresszió is megemelkedett a kontrollhoz képest. Az A2 sejtcsoportban viszont a Brattleboro modellel szemben csapvízet ivó naiv állatokhoz képesti alacsony PrRP mRNS expresszió jelentette a különbséget (4. táblázat).

4. táblázat. A TH, PrRP és nesfatin mRNS-szintek változásainak összefoglalása a vizsgált hipernatrémia modellekben. Állatmodellek: Brattleboro DI: homozigóta AVP hiányos, VT: homozigóta vad típus; Wistar: NS: nem-sóterhelt, ST: 2% NaCl itatott (6 nap).

A1	TH	PrRP	Nesfatin	A2	TH	PrRP	Nesfatin
VT - naiv	normál	normál	normál	normál	normál	normál	normál
VT - restraint	**nő**	**nő**	**nő**	**VT + restraint**	nem nő	nem nő	nem nő
DI - naiv	normál	magas	magas	**DI + naiv**	normál	magas	magas
DI - restraint	**nő**	**nő**	nem nő	**DI + restraint**	nem nő	nem nő	nem nő
NS - naiv	normál	normál	normál	normál	normál	normál	normál
NS - restraint	**nő**	**nő**	**nő**	**NS + restraint**	**nem nő**	**nem nő**	**nem nő**
ST - naiv	magas	magas	magas	**ST + naiv**	normál	csökken	magas
ST - restraint	nem nő	nem nő	nem nő	**ST + restraint**	nem nő	nem nő	nem nő

Az akut restraintre csak az A1 sejtcsoport reagált, a csapvizet ivó állatokban mindhárom gén expressziója fokozódott mindkét modellben. A DI állatokban a restraintre adott génexpressziós válaszok megtartottak voltak, de a nesfatin mRNS emelkedés elmaradt. A sóterhelés mellett viszont a restraintre adott génexpressziós válaszok egyike sem alakult ki (4. táblázat).

Összességében megállapítottuk, hogy a Brattleboro modell kísérleti csoportjait tekintve a TH mRNS expresszió az A1 sejtcsoportban tükrözte a HPA aktiváció mértékékét (pozitív korreláció az ACTH és kortikoszteron szintekkel) (31. ábra, A, B). A sóterhelés jobban igénybe vette a HPA tengelyt (emelkedett hormonszintek) és az A1 sejtcsoport TH kapacitását (emelkedett TH expresszió). Ezek állatok így nem tudtak megfelelő választ kialakítani az újabb akut stresszre, a HPA tengely és az A1 terület aktiválódása is elmaradt, a hormon és TH mRNS értékek nem korreláltak (31. ábra, C, D). A HPA tengely aktiválhatósága tehát összefüggést mutatott az A1 sejtcsoport TH kapacitásával. A koexpresszió révén a neuromodulátorként ható neuropeptidek a noradrenerg kapacitás megőrzésében valószínűleg fontos szerepet játszanak, így krónikus stresszhez való adaptáció alapkövei.

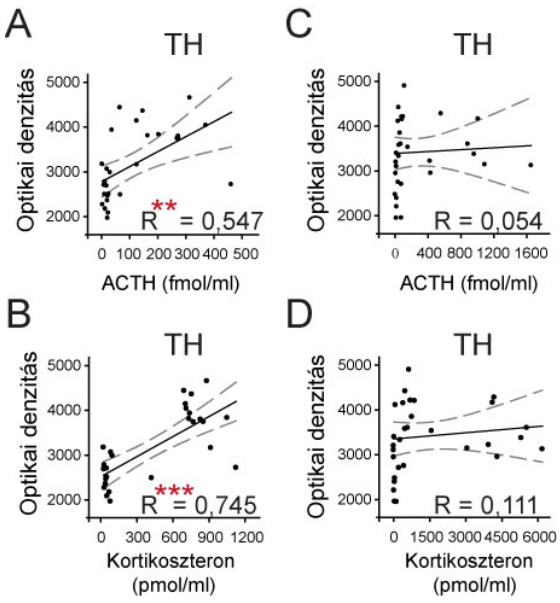

31. ábra. Az A1 sejtcsoport TH mRNS expressziójának kapcsolata a HPA tengely aktivitásával. A A TH mRNS expresszió és az ACTH szint (A), valamint a kortikoszteron szint (B) közötti korreláció a Brattleboro modellben. **C, D** A TH mRNS expresszió és az ACTH szint (C), valamint a kortikoszteron szint (D) közötti korreláció a sóterheléses Wistar hipernatrémia modellben. Pearson korreláció. A folytonos vonal a lineáris regressziót, a szaggatott vonalak a 95%-os konfidencia intervallumokat mutatják, 'R' a korrelációs együttható, p***<0,001, p**<0,01, DI modell: n = 28 állat, sóterhelés modell: n = 31 állat.

A krónikus hipernatrémiához való alkalmazkodást a hipotalamusz szintjén vizsgáltuk tovább a sóterheléses modellben. Az elemzett területek a hipotalamusz ozmoregulációs és

stressz központjai voltak: az AV3V, a PVN, és az SON. A PrRP-tartalmú beidegzés jellemzéséhez, konfokális mikroszkópia segítségével tanulmányoztuk a varikozitások TH tartalmát. Az AV3V és a PVN területén a PrRP-pozitív varikozitások kétharmada TH-immunpozitívnak bizonyult, és szinte kizárólag kettősen jelölt varikozitásokat találtunk az SON területén. A számolások tehát a PrRP beidegzés javarészt nyúltvelői eredetét igazolták a vizsgált magokban, melyek közül az AV3V és a mediális parvocelluláris PVN területén jelentős mértékű PrRPR (GPR10) expressziót is kimutattunk. A krónikus sóterhelés hatására a PrRP-immunpozitív rostok denzitása mindhárom vizsgált területen megnövekedett (5. táblázat). Ezzel párhuzamosan a PrRPR fehérje mennyisége a legsűrűbben beidegzett PVN területén csökkent (western blot mérések).

5. táblázat. A PrRP-immunopozitív rostok denzitásának változása krónikus sóterhelés hatására. A rostok denzitását konfokális mikroszkópos felvételek alapján azonos méretű ROI négyszögekben mértük, és a rostok által elfoglalt terület arányában fejeztük ki ($\mu m^2/100\ \mu m^2$). Student-féle t teszt, átlag ± standard hiba, Sóterhelt (ST) *versus* normál só (NS) csoportok p*<0,05, n = 4 állat/csoport.

	AV3V	SON	PVN
NS	1,2 ± 0,2	1,0 ± 0,1	4,2 ± 0,2
ST	3,0* ± 0,2	1,4* ± 0,1	10,2* ± 1,6

A sóterhelés következtében mindhárom területen fokozódott a TH enzim aktivitása, amit a TH enzim 31-es szerin aminosavának emelkedett foszforilációja (pTH-Ser31) jelzett (western blot mérések). Ez egyúttal a katekolamin felszabadulás mértékének növekedésére is utalt (Dunkley, Bobrovskaya et al. 2004). Az eredmények alapján tehát a krónikusan sóterhelt állatokban megfigyelt nyúltvelői TH és PrRP mRNS expresszió változást a hipotalamuszban megemelkedett TH és PrRP transzmisszió magyarázhatja.

Összefoglalva a fenti eredményeket (8. és 9. közlemény), többféle modellben bizonyítottuk a PrRP kiemelkedő szerepét a krónikus stresszhez való adaptációban. Az adaptáció egyik mechanizmusa a nyúltvelői PrRP/noradrenalin arány eltolódása a PrRP javára, ami akut stressz esetén nem történik meg (Maruyama, Matsumoto et al. 2001). A nyúltvelői PrRP expresszió ösztrogén érzékenysége ezenkívül a nemek eltérő stressz reakciójának egyik alapja lehet.

Megállapítottuk továbbá, hogy a krónikus hipernatrémia típusa meghatározza a HPA tengely aktivitását, és az akut restraint stresszre adott hormonális és nyúltvelői génexpressziós válaszokat. A hipervolémiás hipernatrémia a kardiovaszkulásris regulációt és a vértérfogat szabályozást is jobban igénybe veszi, mint az euvolémiás hipernatrémia, ennek megfelelően a sóterhelt modellben erőteljesebb eltéréseket tapasztaltunk a vizsgált paraméterekben. Másrészt,

az AVP hiányos Blattreboro állatok már embrionális koruktól kezdve alkalmazkodhattak az állapotukhoz, így kompenzációs mechanizmusok révén csökkenthetik a központi idegrendszeri szabályozó rendszereket érintő terhelést.

Munkánk fontos eredménye, hogy kimutattuk a TH, PrRP és nesfatin expresszió mértéke a nyúltvelőben tükrözi HPA tengely akut stresszre való érzékenységét a krónikus hipernatrémiában szenvedő állatokban. Adataink alapján a HPA tengely homeosztatikus stresszre történő aktiválásában a nyúltvelői A1 sejtcsoport noradrenalin kapacitása valószínűleg meghatározó. A TH, PrRP és a nesfatin gének összehangolt szabályozás alatt állnak. A PrRP és a nesfatin (Brailoiu, Deliu et al. 2013) gazdaságosabbá teheti a katekolaminerg sejtek működését azáltal, hogy segíthet fenntartani a noradrenalin kapacitást, és így biztosítani a HPA tengely megfelelő reakciókészségének megőrzését.

Nemutolsó sorban bizonyítékot találtunk a PrRP és noradrenalin neurotranszmisszióra és annak jelentőségére a hipotalamuszban krónikus hipervolémiás hipernatrémiában. Tekintve a nyúltvelői eredetű noreadrenalin tartalmú beidegzés elsődleges szerepét az ozmotikus regulációban (Sawchenko és Swanson 1981, Bourque 2008), és azt, hogy a vizsgált területeken a PrRP beidegzés zömében nyúltvelői eredetű volt (PrRP és noradrenalin tartalmú axonok), felvetődik a két transzmitter interakciójának fontossága a szabályozásban. Ezen felül, a PrRP hatás eddig fel nem ismert helyeként azonosítottuk az AV3V területét, ami kulcsfontosságú központ a folyadékháztartás szabályozás endokrin és autonóm aspektusainak összeszervezésében (McKinley, Pennington et al. 2021).

5.3.4. Új, PrRP tartalmú pálya azonosítása

10. Közlemény: *Prolactin-releasing peptide contributes to stress-related mood disorders and inhibits sleep/mood regulatory melanin-concentrating hormone neurons in rats*

A mentális stresszbetegségek hangulati és alvászavarokban nyilvánulnak meg, melyek kialakulásának hátterében a HPA tengely diszfunkciója áll, de pontos mechanizmusok feltáratlanok (Goldstein és Walker 2014, Bao és Swaab 2019). Krónikus stresszmodellekel végzett fenti kísérleteink eredményei alapján felmerült, hogy a PrRP szerepet játszhat e betegségek patomechanizmusában. Ezt a feltételezésünket alátámasztotta, hogy a PrRP génkiütött egerek krónikus kontextuális félelmi ACTH válasza elégtelen (Yoshida, Takayanagi et al. 2014). Bizonyítékot találtak a PrRP és az alvás-ébrenlét szabályozás a kapcsolatára is, bár a hozzáférhető irodalmi adatok ellentmondóak voltak (Zhang, Inoué et al. 2001, Lin, Arai et al. 2002).

Mivel a PrRP neuronok fő beidegzési célterülete a hipotalamusz, valószínűnek tűnt, hogy a mentális stresszbetegségekben feltételezett hatását is a hipotalamuszon keresztül érheti el. Morfológiai megfigyeléseink során a DLH, ezen belül az MCH neuronok kerülte látótérbe mint a hatás lehetséges közvetítői. Patkányokban ugyanis fénymikroszkóppal a PrRP-immunoreaktív axonok sűrű hálózatát figyeltük meg a PFA és az LH területén, ahol a PrRP rostok az MCH-pozitív sejtek perikarionjain számos szoros kontaktust hoztak létre.

Az MCH-termelő neuronok az alvás, a hangulat a stressz és a táplálékfelvétel szabályozás központi integrátorai, amit a hálózatkutatásban csomópontként (*hub*) emlegetnek. Az MCH alvás-ébrenléti ciklus szabályozásban betöltött kritikus szerepét már bemutattam. Az MCH jelátvitel zavara és a szorongás, depresszió, illetve poszttraumás stresszbetegség patofiziológiája közti szoros összefüggés tekintetében is gazdag az irodalom (Chaki, Funakoshi et al. 2005, Chung, Parks et al. 2011, Torterolo, Scorza et al. 2015, Concetti, Bracey et al. 2020). Számos erőfeszítés történt a depresszió kezelésére alkalmas, mellékhatások nélkül alkalmazható human MCH1 receptor antagonisták kifejlesztésre, amit azonban még nem sikerült megvalósítani (Chung, Parks et al. 2011, Johansson és Löfberg 2015)**.**

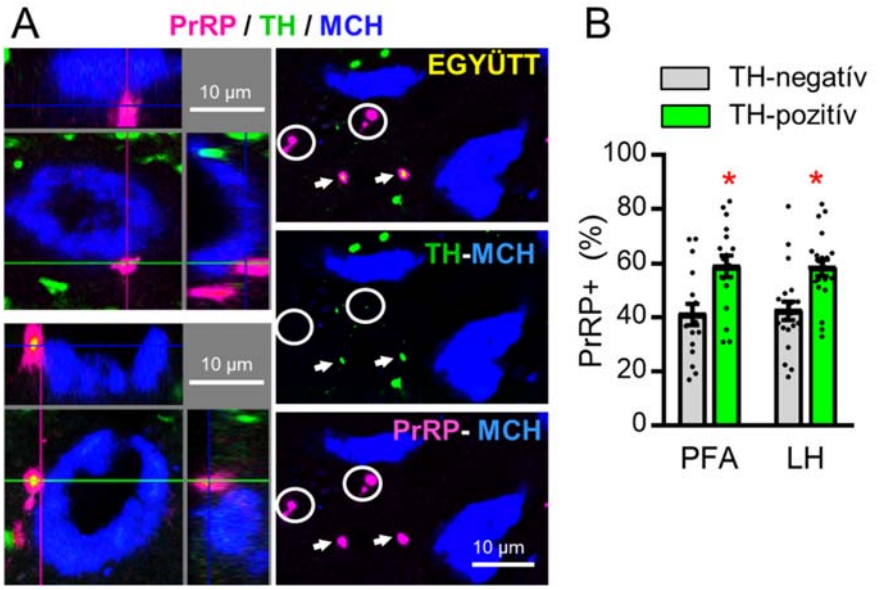

32. ábra. A PFA és az LH PrRP beidegzésének vizsgálata. A Illusztratív, egy optikai szeletetet bemutató konfokális felvételek. Háromszoros, PrRP (magenta), TH (zöld) és MCH (kék) immunfestés. Bal; TH-negatív (fent), és TH-pozitív (lent) $PrRP^+$ terminálisok szoros kapcsolata az MCH^+ neuronokkal. Jobb, TH-negatív (körök) és TH-pozitív (nyílhegyek) $PrRP^+$ axonális varikozitások az MCH^+ neuronok szomszédságában. **B** A $PrRP^+$ varikozitások megoszlása a TH tartalom alapján a PFA és az LH területén. Kétutas ANOVA, Student-Newman-Keuls post hoc teszt, átlag standard ± hiba, TH-pozitív *versus* TH-negatív PrRP-tartalmú varikozitások száma p*<0,05, n = 20 (PFA) és n = 17 (LH) felvétel elemzése alapján.

A PrRP-MCH neuronális kapcsolat tehát ígéretesnek látszott, ezért részletesebben is megvizsgáltuk. A PrRP-pozitív terminálisok TH tartalmát konfokális mikroszkópia segítségével elemeztük (32. ábra, A). Kiderült, hogy a TH-pozitív, tehát A1, A2 sejtcsoportokból eredető beidegzés közel 60%-ot, a TH-negatív, vagyis DM eredetű PrRP beidegzés közel 40%-ot tesz ki a PFA és az LH területén is (32. ábra, B). Ugyanakkor, bár mind PrRPR, mind NPFF2R mRNS-t tartalmazó sejtek voltak a DLH területén, a kettős ISH egyértelműen kizárta az MCH sejtek közvetlen PrRP beidegzését, mivel az MCH neuronok nem expresszálták egyik receptort sem. Az receptorokat kifejező sejtek a területen nagy számban megtalálható orexin-termelő neuronokkal sem mutattak egyezést, kevés nesfatin-pozitív neuron azonban expresszált PrRPR-t.

A morfológiai adatok hátterében álló funkcionalitás vizsgálatára a következőkben elektrofiziológiai (patch clamp) méréseket végeztünk. A mérések 30 napos patkányok agy szeletein, a PFA területén elhelyezkedő MCH sejteken történtek. A PrRP-vel bolus formájában történő (3,5 μM) ingerlés az MCH sejtekben kifelé irányuló áramot gerjesztett (33. ábra, A), és hiperpolarizációt váltott ki (33. ábra, B), amit azonban a nátrium csatorna blokkoló tetrodotoxin (660 nM) jelenléte az inkubációs oldatban megakadályozott (33. ábra, C). A mérések tehát igazolták a morfológiai megfigyeléseket, és a PrRP MCH neuronokra kifejtett preszinaptikus gátló hatásról tanúskodtak. Ezek után természetesen a PrRP és a noradrenalin együttes hatását is megvizsgáltuk. A noradrenalin az MCH neuronok ismert gátlószere (van den Pol, Acuna-Goycolea et al. 2004), amit a nyugalmi membrán potenciálok változásának mérésével reprodukálhatóan bizonyítottunk (33. ábra, D). Amikor kétszeri ismételt noradrenalin ingerlés után harmadszorra közvetlenül a noradrenalin előtt PrRP-t adtunk a sejtekhez, az MCH neuronokra kifejtett gátló hatás mértéke majdnem megduplázódott, időtartama azonban nem változott az előző, csak noradrenalinnal történő ingerléshez képest (33. ábra, D, E). TTX jelenlétében csak a noradrenalin hatása érvényesült (33. ábra, D, E). A noradrenalin hatása specifikus volt, hiszen az irodalmi adatoknak megfelelően, az alfa2-adrenerg receptor antagonista yohimbine (2 μM) a hatást kivédte (33. ábra, F). A PrRP presznaptikus hatásának mechanizmusát tisztázandó, az előző kísérletet a GABA-A receptor antagonista pikrotoxin (100 μM) jelenlétében és TTX hiányában is megismételtük. A pikrotoxin a PrRP hiperpolarizáló hatását megszüntette, míg a noradrenalin válasz megmaradt (33. ábra, G, H). Végeredményben tehát elmondhattuk, hogy a PrRP preszinaptikusan, GABA-A receptorokon keresztül gátolta az MCH neuronokat, ami jelentősen növelte a noradrenalin ismert posztszinaptikus gátló hatását.

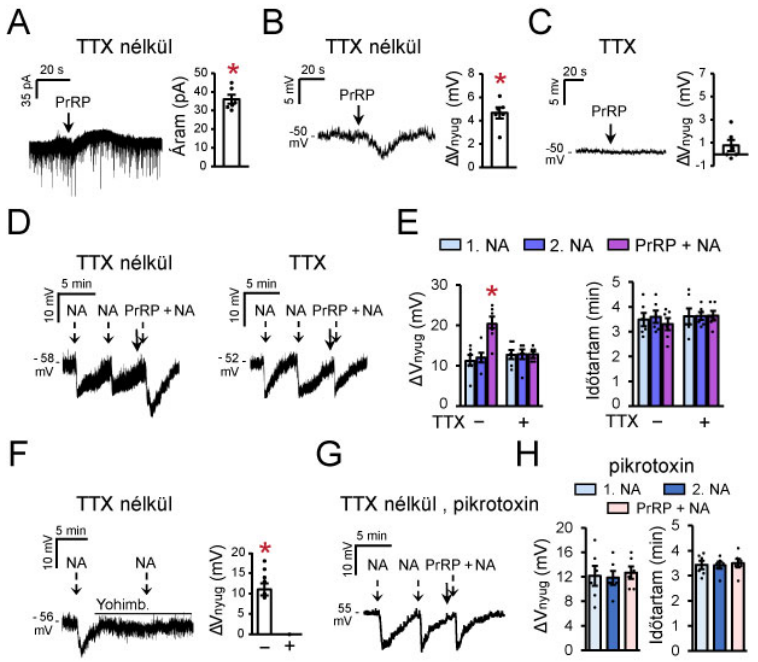

33. ábra. A PrRP hatása az MCH neuronokra *ex vivo*. **A** PrRP (3,5 µM) ingerlés hatása az MCH sejtekben mérhető ionáramra tetrodotoxin (TTX) hiányában **B, C** A PrRP ingerlés hatása az MCH neuronok nyugalmi membrán potenciál változására (ΔVnyug) TTX hiányában (B) és TTX (inkubációs oldatban) mellett (C) **D** ΔVnyug válaszok ismételt noradrenalin (NA, 10 mM) ingerlés, illetve PrRP+NA ingerlés során, TTX hiányában és mellett. **E** A D ábrán bemutatott ΔVnyug hatások (feszültség és időtartam) összesített adatai. **F** NA ingerlésre adott ΔVnyug válaszok az alfa2-adrenerg receptor antagonista yohimbin hiányában és jelenlétében (2 mM, vízszintes vonal), TTX hiányában. **G**, ΔVnyug válaszok ismételt NA ingerlés, illetve PrRP+NA ingerlés során a GABA-A receptor antagonista pikrotoxin (100 mM, inkubációs oldatban) jelenlétében és TTX hiányában. **H** A G ábrán bemutatott hatások összesített adatai. A-C és F: Student-féle t-teszt, p*<0,0001 *versus* stimulálatlan sejt. E, H: Egyutas ismételt méréses ANOVA, Holm-Sidak post hoc teszt, PrRP+NA *versus* első és második NA, p*<0,0001. Átlag ± standard hiba, n = 6 sejt, kivéve C ahol n = 4 sejt, 1-2 sejt/állat. A nyilak a drogok bolus alkalmazásának időpontját jelzik.

Tekintettel az MCH alapvető szerepére a REM és kisebb mértékben a nem-REM alvás előidézésében (Torterolo, Scorza et al. 2015), valamint az alvási és hangulati zavarok szoros kapcsolatára (Riemann, Krone et al. 2020), tanulmányoztuk a PrRP expresszió és az alvás kapcsolatát is. A passzív fázis kezdetén icv alkalmazott PrRP dózis függően (nmol: 1,6; 4,0; 10,0) csökkentette a nem-REM alvás látenciáját, és az ébrenlét rovására növelte a nem-REM alvással töltött időt. A PrRP hatása rövid (30 perc) volt, mely alatt az állatok nem jutottak el a REM alvásig, így a REM alvásra kifejtett hatást nem tudtuk értékelni. A REM nyomás növelésére, ezért REM alvásmegvonást (72 óra) alkalmaztunk a már korábban használt virágcserép módszer szerint (lásd 4. közlemény). Az alvásmegvonás a PrRP mRNS mennyiségének és a PrRP-immunoreaktív sejtek számának fokozódását vonta maga után az A1 sejtcsoportban és a DM területén. A REM alvás pótlásával (3 óra) a DM területén a PrRP expressziója (mRNS, immunoreaktív sejtek száma) normalizálódott. A stressz-kontroll

csoportok a PrRP expresszió emelkedés és a kísérleti stressz szoros kapcsolatát sugallták az A1 sejtcsoportban (emelkedett mRNS mennyiség és sejtszámok az NP és NPR csoportokban). Az A2 sejtcsoportban PrRP expresszió nem változott egyik kísérleti csoportban sem.

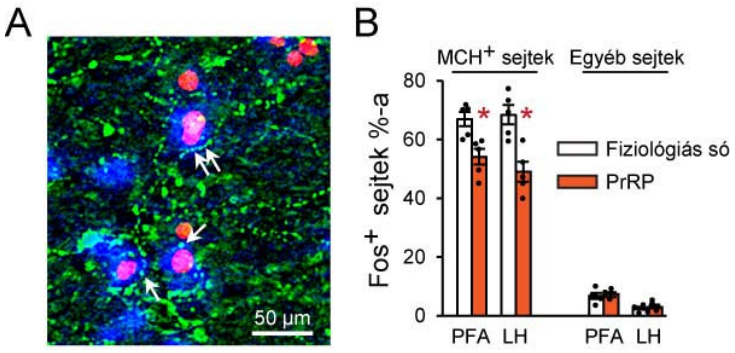

34. ábra. A PrRP hatása az MCH neuronokra *in vivo*. A REM alvásmegvonást követően (virágcserép módszer) PrRP-t (4 nmól), vagy fiziológiás sóoldatot (5 µl) adtunk be icv a patkányoknak, majd hagytuk őket aludni (KPR csoport) a leölés előtt. A hipotalamusz koronális metszetein háromszoros, MCH (kék), cFos (piros) és PrRP (zöld) fluoreszcens immunfestést végeztünk. A nyilak a REM-aktivált MCH$^+$ sejtekkel szoros kontaktusokat képező PrRP-pozitív axon varikozitásokra mutatnak. **B** A Fos$^+$ aktivált, MCH-pozitív és MCH-negatív neuronok százalékos aránya a PFA és az LH területén. A számolás bilaterálisan, ROI négyzeteken belül történt. Kétutas ANOVA, Student-Newman-Keuls post hoc teszt, PrRP *versus* fiziológiás sóoldat p*<0,01, átlag ± standard hiba, n = 5 állat/csoport.

A következő kísérletben, a REM pótlás előtt az állatokat PrRP-vel (4 nmól), illetve fiziológiás sóval kezeltük, amit icv adtunk be. A PrRP tartalmú axon varikozitások a REM-aktív, MCH és cFos kettősjelölt neuronokon is szoros kontaktusokkat képeztek (34. ábra, A), melyek számát az exogén alkalmazott PrRP mintegy 20%-ban csökkentette a PFA és az LH területén is (34. ábra, B). Fontos megjegyezni, hogy az MCH-negatív neuronok aktivitását nem befolyásolta a kezelés. Mivel a visszaalvás során a REM epizódok száma egyenesen arányos az MCH és cFos kettősen jelölt neuronok mennyiségével (Kitka, Adori et al. 2011), kísérletünkkel feltártuk a PrRP és a REM alvás kapcsolatát, és egyúttal bizonyítottuk, hogy a PrRP *in vivo* is gátolja az MCH neuronokat.

A PrRP szerepét a mentális stresszbetegségekben különböző „depresszió” állatmodellekben vizsgáltuk tovább. Az első modell az erőltetett úszási teszt volt. A teszt az adott időtartamra vízbe helyezett állatok stresszel való megbírkózási képességét értékeli az úszással, lebegéssel és a medence szélénél való küzdéssel töltött viselkedés alapján. A lebegés időarányos növekedése passzív viselkedésnek minősül, és a stresszel való megbírkózás sikertelenségének a jele. Az állatokat 30 perccel a teszt előtt kezeltük icv injekciók formájában. Ez az idő a saját (EEG mérés), és mások (Seal, Small et al. 2002) adatai szerint is, elég a PrRP akut hatásának megszűnéséhez, a receptorok pedig ekkora deszenzitizálódnak (Luttrell és Lefkowitz 2002, Scherrer, Tryoen-Tóth et al. 2006, Madsen, Thorsen et al. 2012). A PrRP ilyen

körülmények között a passzív viselkedést fokozta, így ez a kísérlet a PrRP jelátvitel és a „depressziószerű” viselkedés közvetlen kapcsolatát bizonyította.

Második modellünk a depresszió gyulladásos modellje volt (Frenois, Moreau et al. 2007, Dantzer 2009). Az intraperitoneálisan alkalmazott LPS által (1 mg/ttkg) kiváltott gyulladás akut fázisát (3 óra túlélés), és a 24 óra múlva, az akut gyulladás lezajlásával kialakuló „depressziószerű” állapotot is tanulmányoztuk. A korai fázisban az LPS a nyúltvelői PrRP-pozitív sejteket nagymértékben aktiválta, ami a 3 órás túlélés mellett, figyelembe véve, hogy a cFos transzkripciós faktor egy korai válasz gén, tartósan fennálló aktivitásnak tekinthető. Ezzel egyidőben a tumor nekrózis faktor alfa (pro-inflammatorikus citokin) relatív mRNS mennyisége (RT-PCR, A2 sejtcsoportban mért adatok) megemelkedett, megerősítve a gyulladás fennállását (35. ábra, A). Ugyanakkor, a kezeletlen csoporthoz képest a PrRP mRNS relatív mennyisége is magas volt, az összes PrRP-termelő sejtpopulációban (35. ábra, B). Ezzel szemben a DLH mintákban a PrRP receptorok (35. ábra, C), és a pro-MCH relatív mRNS mennyisége (35. ábra, D) csökkent az LPS kezelés után. Az eredmények tehát arra utaltak, hogy a gyulladás hatására megnövekedett a PrRP igény, és a DLH területén fokozott volt PrRP felszabadulás, ami receptor alulszabályozódást és az MCH expresszió gátlását idézte elő.

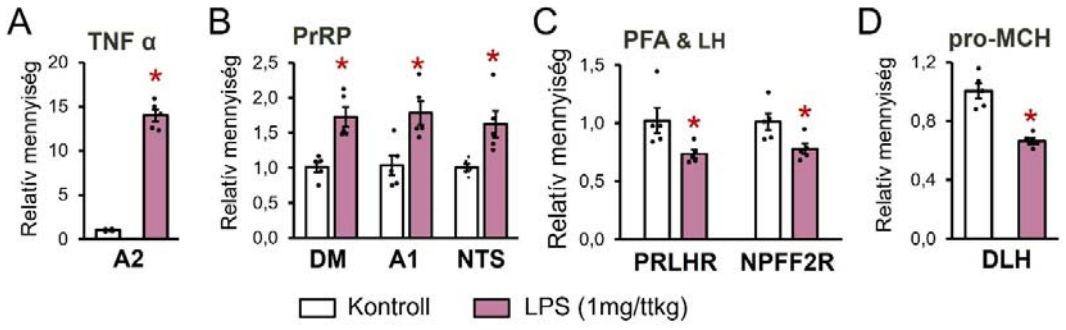

35. ábra. Akut gyulladás következtében fellépő génexpressziós változások intraperitonealis LPS kezelést követően 3 órával. A A tumor nekrózis faktor alfa (TNF alfa, gyulladás marker) relatív mRNS-szintjei az A2 sejtcsoportból vett mintákban **B** Relatív PrRP mRNS-szintek a PrRP-termelő sejtpopulációkban. **C** A PrRP receptorainak relatív mRNS-szintjei a DLH mintákban.**D** A pro-MCH relatív mRNS-szintjei a DLH mintákban. A mérések RT-PCR módszerrel történtek. Student-féle t-teszt, LPS *versus* fiziológiás só p*<0,01, kivéve C, ahol p*<0,05, n = 5 állat/csoport.

A „depressziószerű” viselkedés megjelenését az LPS-kezelt állatokban, a kezelések után egy nappal, erőltetett úszás teszttel igazoltuk. Immunfestéssel értékeltük ki PrRP és MCH fehérjék expressziójában bekövetkezett változásokat a DLH területéről készített szövettani metszetekben. Az LPS-kezelt állatokban a kontrollhoz képest dramatikusan lecsökkent a PrRP-immunoreaktív rostok sűrűsége a PFA és az LH területén is (36. ábra, A, B). Az MCH-pozitív neuronok sejttestjeiben a fluoreszcencia intenzitása viszont emelkedett (36. ábra, C, D).

Összességében arra következtettünk, hogy a hosszan elhúzódó stressz túlterheli a PrRP rendszert, ami a DLH területén a PrRP raktárak kimerüléséhez vezet, és a stresszel való megbírkózási képesség romlásával, valamint az MCH megváltozott expressziójával jár együtt.

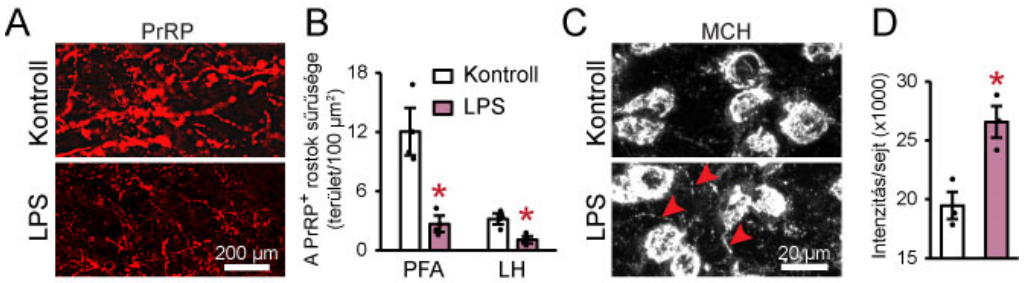

36. ábra. A PrRP és MCH immunpozitivitás változása a hipotalamuszban az LPS kezelést követően 24 órával. A PrRP-immunpozitív axonok (piros) a PFA területén. Illusztratív konfokális felvételek kontroll (fiziológiás só injekció) és intraperitoneálisan LPS (1mg/ttkg) kezelt állatokból. **B** A PrRP-pozitív rostok sűrűsége a PFA és az LH területén a kezelt állatokban. A rostsűrűséget konfokális mikroszkópos képek felhasználásával bilaterálisan, azonos méretű ROI négyszögekben mértük, és a rostok által elfoglalt terület arányában fejeztük ki. **C** MCH-immunpozitív sejtekről (fehér) készült illusztratív konfokális felvétel a PFA területéről. A nyílhegyek axonokra mutatnak. **D** Az MCH^+ neuronok sejttestjeiben mért immunfluoreszcenciás jel intenzitása. A jelintenzitást konfokális mikroszkópos felvételekről mértük, csak fókuszsíkba eső sejteket értékeltük. Student-féle t-teszt, átlag ± standard hiba, kontroll *versus* LPS p*<0,05, n = 3 állat/csoport.

Utolsóként a tanult tehetetlenség modellt alkalmaztuk, amit jelenleg patomechanizmusa és tünetei alapján az emberi depresszió szempontjából a legrelevánsabb modellnek tartanak (Wang, Timberlake et al. 2017). A modell három kísérleti csoportot különít el. Az úgynevezett tréning során az állatokat egyesével egy kétkamrás kísérleti ketrec egyik kamrájába helyezik. A stresszelt csoport itt egy enyhe, a tappancsokra mért áramütés sorozatot szenved el, ami elől az állatok nem tudnak elmenekülni. A kontroll állatokat nem éri trauma. A későbbi teszt során, az összes állat az előzőhöz hasonló áramütés sorozatnak van kitéve, és az egyes áramütéseket előre hang és fény jelzi. Mivel most a kamra ajtaja nyitva áll, az áramütések elől az állatok átmenekülhetnek a másik, biztonságos kamrába. Ez a kísérleti felállás a korábban stresszelt csoportot a menekülési viselkedés alapján két további csoportra különíti el. Azok az állatok, amelyek nem nagyon igyekeznek elmenekülni a náluk kialakult tanult tehetelenség miatt, a “depresszióra” hajlamos csoportot alkotják. Azok viszont, amelyek hasonló fürgeséggel menekülnek, mint a kontrollok, vagyis a korábbi stressz ellenére a tanult tehetetlenség nem fejlődik ki náluk, az ellenálló csoportot képezik. Kísérletünkben a tréning és a teszt között egy hét telt el. Adataink alapján (széklet bogyók mennyisége) a tréning azonos mértékben, és erősen stresszelte a későbbi “hajlamos” és “ellenálló” állatokat, míg a teszt nem okozott különösebb stresszt egyik csoportnak sem. Az állatokat egy nappal a teszt után öltük le, amikor is a vérplazmából mért kortikoszteron szintek a “hajlamos” és “ellenálló” csoportokban egyforma

mértékben emelkedettek voltak a kontrollokéhoz képest. A tréning tehát krónikus stresszt váltott ki ezekben az állatokban, mely a kortikoszteron értékek alapján enyhe mértékű volt. A mérsékelt stresszhatást támasztotta alá az is, hogy a tréning és teszt közt eltelt időszakban az állatok tápfogyasztása és testsúlyváltozása a kontrollokéval megegyezett.

Az állatok agymintáiból a PrRP, a PrRP receptorok és a pro-MCH mRNS relatív mennyiségét határoztuk meg. A "hajlamos" csoportra specifikus PrRP mRNS expresszió emelkedést mutattunk ki a DM területén (37. ábra, A). Az A1 sejtcsoportban a PrRP mRNS expresszió a "hajlamos" és az "ellenálló" csoportban is magasabb volt, mint a kontrollokban, a két csoport közötti különbség a szignifikancia szint határát súrolta. Az A2-NTS területén nem volt változása PrRP expresszióban. A PFA és az LH együttes mintáiban a PrRP receptorok relatív mRNS mennyisége a "hajlamos" csoportban specifikusan csökkent (37. ábra, B), amit a PrRP felszabadulásra adott válaszreakció jeleként értelmezhetünk. A krónikus stresszre a pro-MCH mRNS relatív mennyiségének csökkenése volt az "ellenálló" csoportban a válasz, a "hajlamos" csoportban ez nem következett be (37. ábra, C).

A kísérlet alapján elmondhatjuk, hogy a megfelelő PrRP jelátvitel megőrzése a DLH területén védelmet nyújtott a tanult tehetetlenség kialakulásával szemben.

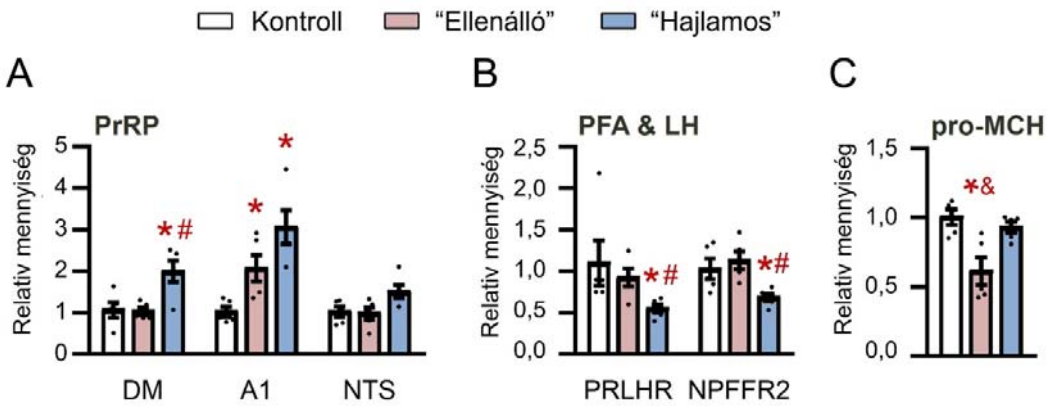

37. ábra. Génexpressziós változások a depresszió tanult tehetetlenség állatmodelljében. A Relatív PrRP mRNS-szintek a PrRP-termelő sejtpopulációkban. **B** A PrRP receptorainak relatív mRNS-szintjei a DLH mintákban. **C** A pro-MCH relatív mRNS-szintjei a DLH mintákban. A mérések RT-PCR módszerrel történtek. Egyutas ANOVA, Student-Newman-Keuls post hoc teszt, átlag ± standard hiba, $p^{*}<0,05$ a kontrollhoz képest, $p^{\#}<0,05$ az „ellenálló" csoporthoz képest, $p^{\&} = 0,006$ a „hajlamos" csoporthoz képest, „ellenálló" v*ersus* „hajlamos" $p = 0,053$ az A ábra A1 sejtcsoport esetében, n = 5 állat/csoport.

Eredményeinket *post mortem* human agymintákban történt mérésekkel egészítettük ki, melynek keretében kontroll és öngyilkos férfiak mintáit hasonlítottuk össze. Az analízist dorzális (DHA) és laterális (LHA) hipotalamikus area mintákon végeztük (38. ábra, A), melyek a patkány PFA, illetve LH agyterületeinek felelnek meg, és nagy sűrűségben tartalmaznak

MCH-termelő neuronokat (Krolewski, Medina et al. 2010). Az öngyilkosok mintáiban mind a PrRPR, mind az NPFF2R mRNS relatív mennyisége alacsonyabb volt, mint a természetes halált elszenvedett alanyok mintáiban (38. ábra, B, C). A human és az állatkísérletes adatok tehát megerősítették egymást. Bár az öngyilkosság etiológiája összetett, az egyik leggyakoribb oka a depresszió (Bachmann 2018), ami kiemeli eredményeink transzlációs jelentőségét.

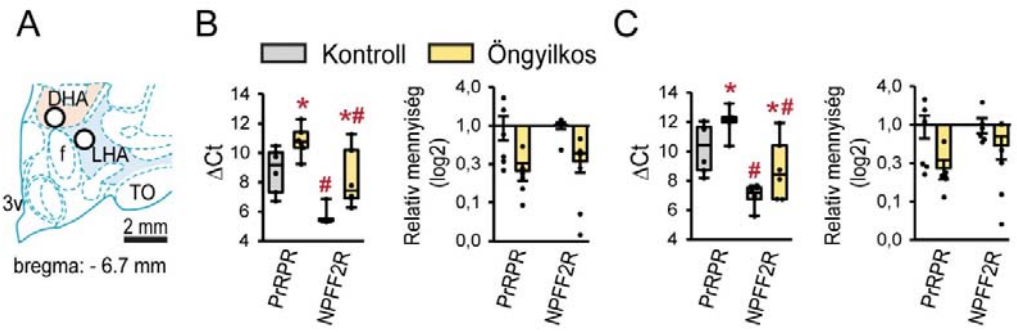

38. ábra. A PrRP receptorok expressziója kontroll és öngyilkos férfiak *post mortem* hipotalamusz mintáiban. **A** Sémás ábra a Humán agy atlasz alapján (Mai, Majtanik et al. 2015), mely a mikordisszekciós mintavételek helyét és méretét (fehér körök) mutatja. DHA: dorzális hipotalamikus area, f: fornix, LHA: laterális hipotalamikus area, TO: tractus opticus. **B** Az LHA, és **C** a DHA területén mért PrRPR és NPFF2R mRNS adatok. A mérések RT-PCR módszerrel történtek. A ΔCt értékeket dobozdiagrammok (a doboz a felső és alsó kvartiliseket jelzi, a bajszok a minimális és maximális adatpontokig terjednek), a relatív mRNS mennyiségeket oszlopdiagrammok (átlag ± standard hiba) mutatják. Kétutas ismételt méréses ANOVA, Student-Newman-Keuls post hoc teszt, $p^{*}<0,05$ *versus* nem öngyilkos kontroll receptoron belül, $p^{\#}<0,05$ *versus* PrRPR halálnemen belül, n = 6 minta /csoport.

Összefoglalva, egy új PrRP-MCH pályát azonosítottunk, melynek elégtelen működése szerepet játszhat a mentális stresszbetegségek kialakulásában. Adataink szerint a krónikus stressz túlterheli a PrRP rendszert, ami a DLH területén a PrRP receptorok alulszabályozása és a PrRP raktárak kimerülése miatt a jelátvitel elégtelenségéhez vezet. A hangulati stresszbetegségek kialakulása közben az MCH rendszer működési zavara is fellép, amihez feltehetően hozzájárul a károsodott PrRP jelátvitel. A hipotézis teljes igazolása további munkát kíván.

A szerotonin és noradrenalin visszavétel gátló antidepresszánsokat széles körben alkalmazzák a stresszel összefüggő mentális zavarok kezelésére, bár a mellékhatások gyakoriak és az esetek 30%-ában a gyógyszerek hatástalanok (Voineskos, Daskalakis et al. 2020). A kombinált monoaminerg és peptiderg rendszerekre is ható antidepresszáns gyógyszerek kifejlesztése új irányokat nyithat a kezelésben, melyek egyik célpontja a jövőben a PrRP rendszer lehet.

6. ÖSSZEGZÉS, KITEKINTÉS

A táplálkozási zavarok (i.e. anorexia nervosa, bulimia nervosa), valamint az elhízás és szövődményei világszerte milliókat sújtó betegségek. Kialakulásukban genetikai, epigenetikai és környezeti/társadalmi tényezők összessége játszik szerepet. Hasonló tömegeket érintenek a szintén multifaktoriális etiológiájú mentális stresszbetegségek is. A kétféle betegség típus közötti szoros kapcsolat vitathatatlan. A környezeti stresszel való elégtelen megbírkózás gyakran nyilvánul meg testsúlyváltozásban, ami a táplálkozási szokások és a homeosztatikus szabályozás diszharmóniájának következménye. Ezenkívül, mind a táplálkozási mind a hangulati betegségek tipikusan alvászavarokkal is járnak (Reutrakul és Van Cauter 2018, Steiger és Pawlowski 2019).

Mivel a hipotalamusz létfontosságú struktúra a különböző homeosztatikus funkciók szabályozásában, kommunikációs útvonalai kulcsfontosságúak a fent említett élettani és pszihológiai működések szempontjából is. Bár az alapvető pályák korábbról ismertek (lásd Bevezetés), a kommunikáció módozataiban mindig születnek meghatározóan új felfedezések. Az egyik ilyen felfedezés a bélflóra (mikrobiom) és az agy közötti kommunikáció, az úgynevezett bél-agy tengely, melynek jelentőségére az elmúlt évtized alatt derült fény (Chang, Wei et al. 2022). A vastagbelet kolonizáló mikrobiom összetételét jelentősen befolyásolja a táplálék minősége és a stressz, a mikrobiom egészsége pedig meghatározza az immunrendszer állapotát. Adott esetben a mikrobiom változásai gyulladásos folyamatokat indítanak el. A gyulladásról szóló információ humorálisan (citokinek), és a nervus vagus közvetítésével a nyúltvelői noradrenerg rendszeren keresztül a hipotalamuszba jut, ahol ennek hatására aktiválódik a HPA tengely, és egyéb endokrin és autonóm válaszok születnek (Appleton 2018).

A működésbeli változások egyik bizonyítéka az agy funkcionális kapcsolatrendszerében fennálló hangsúlyok eltolódása, melynek kimutatása a 90-es évektől vált vizsgálhatóvá az fMRI elterjedésével. Ily módon derült ki, hogy a hipotalamusz nyugalmi állapot funkcionális kapcsolatrendszere neurológiai és pszichiátriai betegségekben, valamit a jóllakottsági szinttel összefüggésben is megváltozik. Éhes, különösen elhízott személyeknél például a kommunikáció a jutalommal kapcsolatos agyi régiók felé erősödik (Kullmann és Veit 2021). A kapcsolatrendszer plaszticitásának fontos tényezője a neuronális jelátvitel sokszínűsége, melynek alapja a neuropeptid koexpresszió. Ez egyben az integratív működés lényegi eleme is, tekintve, hogy számos neuropeptid többféle funkcióban is részt vesz (Hokfelt, Broberger et al. 2000).

Bemutatott munkám jelentősége, hogy új adatokat szolgáltat a fent körvonalazott hipotalamikus integratív működés mechanizmusairól. Mind a nesfatin-1, mind a PrRP ígéretes gyógyszertani célpontok, a PrRP analógok fejlesztése és terápiás potenciáljuk feltérképezése intenzíven folyik (Schalla és Stengel 2018, Pražienková, Popelová et al. 2019, Xu és Chen 2020). További kutatásokat igényel azonban a nesfatin-1 pontos hatásmechanizmusának és receptorának feltárása. Érdekes kérdés az is, hogy mi az oka a nesfatin a központi idegrendszerben való széleskörű elterjedtségének, szemben a PrRP expresszió igen korlátozott voltával. Az integrációs működés megértésében a koexpressziós mintázatok különböző állapotokban történő egy sejt szintű analízise segíthet, és valószínűleg újabb neuropeptidek felfedezése is várható. Nélkülözhetetlenek a folyamatos kutatásmódszertani fejlesztések is, mivel a népesség jelentős részét érintő metabolikus, cirkadián és stressz eredetű betegségek jövőbeni eredményes kezeléséhez a homeosztatikus szabályozás vizsgálatának komplex megközelítése szükséges.

7. ÚJ TUDOMÁNYOS EREDMÉNYEK

I. Célkitűzés: Az immunhisztokémia alkalmazásának továbbfejlesztése

1. Új, könnyen reprodukálható, egyszerű és érzékeny immunhisztokémiai festési eljárást vezettem be az azonos gazda állatból származó antitestek használatából fakadó keresztreakciók kivédésére, amivel hozzájárultam a kereskedelemben kapható KIT-ek és automatizált immunfestő berendezések gyártásához.
2. Bebizonyítottuk, hogy a donor eredetű GFP-t expresszáló csontvelői őssejtek transzplantáció utáni nyomonkövetése TSA amplifikálással kombinált immunhisztokémiai festéssel végezhető el kielégítően.

II. Célkitűzés: Az energiaháztartás szabályozás vizsgálata

3. Kimutattuk, hogy az icv alkalmazott nesfatin-1 táplálék- és vízfelvételre gyakorolt hatásai a hosszútávúak, és összefüggnek a cirkadián ritmussal.
4. Kimutattuk, hogy az icv alkalmazott nesfatin-1 növeli a testhőmérsékletet, és feltártunk egyes szóbajövő mechanizmusokat.
5. Leírtuk az icv nesfatin-1 alvás-ébrenléti ciklusra gyakorolt hatását, és az MCH és nesfatin koexpresszáló sejtek és a REM alvás szoros kapcsolatát. Adataink alapján a nesfatin a REM alvásszabályozás fontos tényezője.
6. Patkány modellben kimutattuk, hogy az intrauterin alultápláltság következtében felnőttkorra kialakuló prediabeteses állapot hátterében a hipotalamusz, főleg a nucleus arcuatus nesfatin-1 rezisztenciája áll. A nesfatin-1 rezisztencia elsődlegesen, normál testsúly mellett alakul ki. A nesfatin-1 rezisztens állatokban a hipotalamusz nesfatin neuronjainak fejlődése zavart szenved.
7. Megállapítottuk, hogy nem-rezisztens állatokban a krónikus icv nesfatin-1 kezelés javítja a glükóztoleranciát és az inzulinérzékenységet.
8. A nucleus accumbens mediális Héj régiójában egy a táplálék jutalmi értékét tükröző sejtcsoportot azonosítottunk, ami D1R-mediált módon szabályozza a táplálékfogyasztás leállítását, valószínűleg a laterális hipotalamikus areán keresztül. Kimutattuk, hogy az intrauterin alultáplált, de még nem-elhízott patkányok hiperfágiásak, jutalmi táplálkozásuk fokozott, aminek hátterében a nucleus accumbens mediális Héj régiójában a D1R jelátvitel károsodása áll.

III. Célkitűzés: A stresszválasz finomhangolásának tanulmányozása

9. Elsőként azonosítottuk a HPA tengely szabályozásában új elemként a nesfatint, mely az agytörzs és a PVN szintjén is részt vehet a stresszválasz szervezésében.
10. Kimutattuk, hogy a HPA tengely aktiválásában elsődleges szerepű nyúltvelői noradrenerg neuronokban a PrRP és TH koexpresszió aránya krónikus restraint stressz hatására a PrRP irányába tolódik el. Mivel a TH a noradrenalin szintézis sebesség meghatározó enzime, ez a PrRP és noradrenalin arány elolódását jelenti. A jelenség nemi különbséget mutat, a háttérben a nyúltvelői PrRP sejtcsoportok ösztrogén alfa receptor-pozitivitása húzódik meg.
11. Megállapítottuk, hogy nyúltvelői A1 sejtcsoportban és az A2-NTS területén nagyfokú a TH, PrRP és nesfatin koexpresszió. Hipernatrémiás állatokban az akut restraint stresszre adott válasz a fenti transzmitterek össszehangolt működésének eredménye, melyben az A1 sejtcsoport noradrenalin kapacitásának megőrzése mérvadó.
12. Kimutattuk a PrRP szerepét a krónikus a hipernatrémiához való adaptációban. A hatás egyik helyeként az anteroventrális periventrikuláris areát jelöltük meg, mely a folyadékháztartás szabályozás endokrin és autonóm aspektusainak fő organizátor központja.
13. Leírtunk és funkcionálisan jellemeztünk egy új agypályát, melyen keresztül a PrRP a hipotalamusz MCH tartalmú neuronjait gátolja.
14. Kimutattuk, hogy a PrRP fokozza noradrenalin MCH-termelő neuronokra kifejtett gátló hatását.
15. Patkány modellek felhasználásával bebizonyítottuk, hogy a PrRP jelátvitel károsodása a dorzolaterális hipotalamuszban „depressziószerű” viselkedéssel társul, míg normál PrRP jelátvitel esetén nem alakul ki ez a viselkedés. Kimutattuk a PrRP jelátvitel károsodását öngyilkosok megfelelő agymintáiban is.

8. HIVATKOZÁSOK JEGYZÉKE

Abedi, M., D. A. Greer, G. A. Colvin, D. A. Demers, M. S. Dooner, J. A. Harpel, J. Pimentel, M. K. Menon and P. J. Quesenberry (2004). "Tissue injury in marrow transdifferentiation." Blood Cells Mol Dis **32**(1): 42-46.

Adachi, S., A. Mochiduki, H. Nemoto, B. Sun, K. Fujiwara, H. Matsumoto and K. Inoue (2005). "Estrogen suppresses the stress response of prolactin-releasing peptide-producing cells." Neurosci Lett **380**(3): 311-315.

Adams, J. C. (1992). "Biotin amplification of biotin and horseradish peroxidase signals in histochemical stains." J Histochem Cytochem **40**(10): 1457-1463.

Allison, K. C., A. Spaeth and C. M. Hopkins (2016). "Sleep and Eating Disorders." Curr Psychiatry Rep **18**(10): 92.

Appleton, J. (2018). "The Gut-Brain Axis: Influence of Microbiota on Mood and Mental Health." Integr Med (Encinitas) **17**(4): 28-32.

Appleyard, S. M., D. Marks, K. Kobayashi, H. Okano, M. J. Low and M. C. Andresen (2007). "Visceral afferents directly activate catecholamine neurons in the solitary tract nucleus." J Neurosci **27**(48): 13292-13302.

Bachmann, S. (2018). "Epidemiology of Suicide and the Psychiatric Perspective." Int J Environ Res Public Health **15**(7).

Bao, A. M. and D. F. Swaab (2019). "The human hypothalamus in mood disorders: The HPA axis in the center." IBRO Rep **6**: 45-53.

Bechtold, D. A. and S. M. Luckman (2006). "Prolactin-releasing Peptide mediates cholecystokinin-induced satiety in mice." Endocrinology **147**(10): 4723-4729.

Berridge, K. C. and M. L. Kringelbach (2008). "Affective neuroscience of pleasure: reward in humans and animals." Psychopharmacology (Berl) **199**(3): 457-480.

Billes, S. K., S. E. Simonds and M. A. Cowley (2012). "Leptin reduces food intake via a dopamine D2 receptor-dependent mechanism." Mol Metab **1**(1-2): 86-93.

Bonnavion, P., L. E. Mickelsen, A. Fujita, L. de Lecea and A. C. Jackson (2016). "Hubs and spokes of the lateral hypothalamus: cell types, circuits and behaviour." J Physiol **594**(22): 6443-6462.

Bonnet, M. S., M. Djelloul, V. Tillement, C. Tardivel, L. Mounien, J. Trouslard, J. D. Troadec and M. Dallaporta (2013). "Central NUCB2/Nesfatin-1-expressing neurones belong to the hypothalamic-brainstem circuitry activated by hypoglycaemia." J Neuroendocrinol **25**(1): 1-13.

Bouret, S. G. (2009). "Early life origins of obesity: role of hypothalamic programming." J Pediatr Gastroenterol Nutr **48 Suppl 1**: S31-38.

Bourque, C. W. (2008). "Central mechanisms of osmosensation and systemic osmoregulation." Nat Rev Neurosci **9**(7): 519-531.

Brailoiu, G. C., E. Deliu, A. A. Tica, J. E. Rabinowitz, D. G. Tilley, K. Benamar, W. J. Koch and E. Brailoiu (2013). "Nesfatin-1 activates cardiac vagal neurons of nucleus ambiguus and elicits bradycardia in conscious rats." J Neurochem **126**(6): 739-748.

Brailoiu, G. C., S. L. Dun, E. Brailoiu, S. Inan, J. Yang, J. K. Chang and N. J. Dun (2007). "Nesfatin-1: distribution and interaction with a G protein-coupled receptor in the rat brain." Endocrinology **148**(10): 5088-5094.

Brazelton, T. R. and H. M. Blau (2005). "Optimizing techniques for tracking transplanted stem cells in vivo." Stem Cells **23**(9): 1251-1265.

Chaki, S., T. Funakoshi, S. Hirota-Okuno, M. Nishiguchi, T. Shimazaki, M. Iijima, A. J. Grottick, K. Kanuma, K. Omodera, Y. Sekiguchi, S. Okuyama, T. A. Tran, G. Semple and W. Thomsen (2005). "Anxiolytic- and antidepressant-like profile of ATC0065 and ATC0175: nonpeptidic and orally active melanin-concentrating hormone receptor 1 antagonists." J Pharmacol Exp Ther **313**(2): 831-839.

Challet, E. (2019). "The circadian regulation of food intake." Nat Rev Endocrinol **15**(7): 393-405.

Chang, L., Y. Wei and K. Hashimoto (2022). "Brain-gut-microbiota axis in depression: A historical overview and future directions." Brain Res Bull **182**: 44-56.

Charkoudian, N. and N. Stachenfeld (2016). "Sex hormone effects on autonomic mechanisms of thermoregulation in humans." Auton Neurosci **196**: 75-80.

Chen, C., S. L. Dun, N. J. Dun and J. K. Chang (1999). "Prolactin-releasing peptide-immunoreactivity in A1 and A2 noradrenergic neurons of the rat medulla." Brain Res **822**(1-2): 276-279.

Chung, S., G. S. Parks, C. Lee and O. Civelli (2011). "Recent updates on the melanin-concentrating hormone (MCH) and its receptor system: lessons from MCH1R antagonists." J Mol Neurosci **43**(1): 115-121.

Cifuentes, L. and A. Acosta (2022). "Homeostatic regulation of food intake." Clin Res Hepatol Gastroenterol **46**(2): 101794.

Concetti, C., E. F. Bracey, D. Peleg-Raibstein and D. Burdakov (2020). "Control of fear extinction by hypothalamic melanin-concentrating hormone-expressing neurons." Proc Natl Acad Sci U S A **117**(36): 22514-22521.

Coupé, B., I. Grit, D. Darmaun and P. Parnet (2009). "The timing of "catch-up growth" affects metabolism and appetite regulation in male rats born with intrauterine growth restriction." Am J Physiol Regul Integr Comp Physiol **297**(3): R813-824.

Cunningham, E. T., Jr. and P. E. Sawchenko (1988). "Anatomical specificity of noradrenergic inputs to the paraventricular and supraoptic nuclei of the rat hypothalamus." J Comp Neurol **274**(1): 60-76.

Dallman, M. F. (1993). "Stress update Adaptation of the hypothalamic-pituitary-adrenal axis to chronic stress." Trends Endocrinol Metab **4**(2): 62-69.

Dantzer, R. (2009). "Cytokine, sickness behavior, and depression." Immunol Allergy Clin North Am **29**(2): 247-264.

Davis, J. D. and G. P. Smith (1992). "Analysis of the microstructure of the rhythmic tongue movements of rats ingesting maltose and sucrose solutions." Behav Neurosci **106**(1): 217-228.

Daviu, N., M. R. Bruchas, B. Moghaddam, C. Sandi and A. Beyeler (2019). "Neurobiological links between stress and anxiety." Neurobiol Stress **11**: 100191.

Dayas, C. V., K. M. Buller and T. A. Day (2004). "Hypothalamic paraventricular nucleus neurons regulate medullary catecholamine cell responses to restraint stress." J Comp Neurol **478**(1): 22-34.

Dodd, G. T. and S. M. Luckman (2013). "Physiological Roles of GPR10 and PrRP Signaling." Front Endocrinol (Lausanne) **4**: 20.

Dodd, G. T., A. A. Worth, N. Nunn, A. K. Korpal, D. A. Bechtold, M. B. Allison, M. G. Myers, Jr., M. A. Statnick and S. M. Luckman (2014). "The thermogenic effect of leptin is dependent on a distinct population of prolactin-releasing peptide neurons in the dorsomedial hypothalamus." Cell Metab **20**(4): 639-649.

Donofry, S. D., K. A. Roecklein, J. E. Wildes, M. A. Miller and K. I. Erickson (2016). "Alterations in emotion generation and regulation neurocircuitry in depression and eating disorders: A comparative review of structural and functional neuroimaging studies." Neurosci Biobehav Rev **68**: 911-927.

Dunkley, P. R., L. Bobrovskaya, M. E. Graham, E. I. von Nagy-Felsobuki and P. W. Dickson (2004). "Tyrosine hydroxylase phosphorylation: regulation and consequences." J Neurochem **91**(5): 1025-1043.

Engström, M., A. Brandt, S. Wurster, J. M. Savola and P. Panula (2003). "Prolactin releasing peptide has high affinity and efficacy at neuropeptide FF2 receptors." J Pharmacol Exp Ther **305**(3): 825-832.

Fan, W., A. Voss-Andreae, W. H. Cao and S. F. Morrison (2005). "Regulation of thermogenesis by the central melanocortin system." Peptides **26**(10): 1800-1813.

Finelli, C., G. Martelli, R. Rossano, M. C. Padula, N. La Sala, L. Sommella and G. Tarantino (2014). "Nesfatin-1: role as possible new anti-obesity treatment." Excli j **13**: 586-591.

Foo, K. S., H. Brismar and C. Broberger (2008). "Distribution and neuropeptide coexistence of nucleobindin-2 mRNA/nesfatin-like immunoreactivity in the rat CNS." Neuroscience **156**(3): 563-579.

Fort, P., D. Salvert, L. Hanriot, S. Jego, H. Shimizu, K. Hashimoto, M. Mori and P. H. Luppi (2008). "The satiety molecule nesfatin-1 is co-expressed with melanin concentrating hormone in tuberal hypothalamic neurons of the rat." Neuroscience **155**(1): 174-181.

Frenois, F., M. Moreau, J. O'Connor, M. Lawson, C. Micon, J. Lestage, K. W. Kelley, R. Dantzer and N. Castanon (2007). "Lipopolysaccharide induces delayed FosB/DeltaFosB immunostaining within the mouse extended amygdala, hippocampus and hypothalamus, that parallel the expression of depressive-like behavior." Psychoneuroendocrinology **32**(5): 516-531.

Gali Ramamoorthy, T., G. Begum, E. Harno and A. White (2015). "Developmental programming of hypothalamic neuronal circuits: impact on energy balance control." Front Neurosci **9**: 126.

Giouleka, S., I. Tsakiridis, A. Mamopoulos, I. Kalogiannidis, A. Athanasiadis and T. Dagklis (2023). "Fetal Growth Restriction: A Comprehensive Review of Major Guidelines." Obstet Gynecol Surv **78**(11): 690-708.

Goebel, M., A. Stengel, L. Wang, N. W. Lambrecht and Y. Taché (2009). "Nesfatin-1 immunoreactivity in rat brain and spinal cord autonomic nuclei." Neurosci Lett **452**(3): 241-246.

Goebel, M., A. Stengel, L. Wang and Y. Taché (2009). "Restraint stress activates nesfatin-1-immunoreactive brain nuclei in rats." Brain Res **1300**: 114-124.

Goldstein, A. N. and M. P. Walker (2014). "The role of sleep in emotional brain function." Annu Rev Clin Psychol **10**: 679-708.

Goldstein, N., B. J. Levine, K. A. Loy, W. L. Duke, O. S. Meyerson, A. A. Jamnik and M. E. Carter (2018). "Hypothalamic Neurons that Regulate Feeding Can Influence Sleep/Wake States Based on Homeostatic Need." Curr Biol **28**(23): 3736-3747.e3733.

Gonzalez-Bulnes, A. and C. Ovilo (2012). "Genetic basis, nutritional challenges and adaptive responses in the prenatal origin of obesity and type-2 diabetes." Curr Diabetes Rev **8**(2): 144-154.

Gotoh, K., T. Masaki, S. Chiba, H. Ando, T. Shimasaki, K. Mitsutomi, K. Fujiwara, I. Katsuragi, T. Kakuma, T. Sakata and H. Yoshimatsu (2013). "Nesfatin-1, corticotropin-releasing hormone, thyrotropin-releasing hormone, and neuronal histamine interact in the hypothalamus to regulate feeding behavior." J Neurochem **124**(1): 90-99.

Gouardères, C., I. Quelven, C. Mollereau, H. Mazarguil, S. Q. Rice and J. M. Zajac (2002). "Quantitative autoradiographic distribution of NPFF1 neuropeptide FF receptor in the rat brain and comparison with NPFF2 receptor by using [125I]YVP and [(125I]EYF as selective radioligands." Neuroscience **115**(2): 349-361.

Gu, W., B. J. Geddes, C. Zhang, K. P. Foley and A. Stricker-Krongrad (2004). "The prolactin-releasing peptide receptor (GPR10) regulates body weight homeostasis in mice." J Mol Neurosci **22**(1-2): 93-103.

Guo, J., W. K. Simmons, P. Herscovitch, A. Martin and K. D. Hall (2014). "Striatal dopamine D2-like receptor correlation patterns with human obesity and opportunistic eating behavior." Mol Psychiatry **19**(10): 1078-1084.

Guo, Y., Y. Liao, G. Fang, J. Dong and Z. Li (2013). "Increased nucleobindin-2 (NUCB2) transcriptional activity links the regulation of insulin sensitivity in Type 2 diabetes mellitus." J Endocrinol Invest **36**(10): 883-888.

Han, Y., K. Yuan, Y. Zheng and L. Lu (2020). "Orexin Receptor Antagonists as Emerging Treatments for Psychiatric Disorders." Neurosci Bull **36**(4): 432-448.

Hassani, O. K., M. G. Lee and B. E. Jones (2009). "Melanin-concentrating hormone neurons discharge in a reciprocal manner to orexin neurons across the sleep-wake cycle." Proc Natl Acad Sci U S A **106**(7): 2418-2422.

Hinuma, S., Y. Habata, R. Fujii, Y. Kawamata, M. Hosoya, S. Fukusumi, C. Kitada, Y. Masuo, T. Asano, H. Matsumoto, M. Sekiguchi, T. Kurokawa, O. Nishimura, H. Onda and M. Fujino (1998). "A prolactin-releasing peptide in the brain." Nature **393**(6682): 272-276.

Hochstenbach, S. L. and J. Ciriello (1995). "Plasma hypernatremia induces c-fos activity in medullary catecholaminergic neurons." Brain Res **674**(1): 46-54.

Hoffman, R. M. (2015). "Application of GFP imaging in cancer." Lab Invest **95**(4): 432-452.

Hökfelt, T., S. Barde, Z. D. Xu, E. Kuteeva, J. Rüegg, E. Le Maitre, M. Risling, J. Kehr, R. Ihnatko, E. Theodorsson, M. Palkovits, W. Deakin, G. Bagdy, G. Juhasz, H. J. Prud'homme, N. Mechawar, R. Diaz-Heijtz and S. O. Ögren (2018). "Neuropeptide and Small Transmitter Coexistence: Fundamental Studies and Relevance to Mental Illness." Front Neural Circuits **12**: 106.

Hokfelt, T., C. Broberger, Z. Q. Xu, V. Sergeyev, R. Ubink and M. Diez (2000). "Neuropeptides--an overview." Neuropharmacology **39**(8): 1337-1356.

Holt, M. K. and L. Rinaman (2022). "The role of nucleus of the solitary tract glucagon-like peptide-1 and prolactin-releasing peptide neurons in stress: anatomy, physiology and cellular interactions." Br J Pharmacol **179**(4): 642-658.

Jackson, K. A., S. M. Majka, G. G. Wulf and M. A. Goodell (2002). "Stem cells: a minireview." J Cell Biochem Suppl **38**: 1-6.

Jarry, H., H. Heuer, L. Schomburg and K. Bauer (2000). "Prolactin-releasing peptides do not stimulate prolactin release in vivo." Neuroendocrinology **71**(4): 262-267.

Johansson, A. and C. Löfberg (2015). "Novel MCH1 receptor antagonists: a patent review." Expert Opin Ther Pat **25**(2): 193-207.

Johnson, H., B. Ulfhake, A. Dagerlind, G. W. Bennett, K. C. Fone and T. Hökfelt (1993). "The serotoninergic bulbospinal system and brainstem-spinal cord content of serotonin-, TRH-, and substance P-like immunoreactivity in the aged rat with special reference to the spinal cord motor nucleus." Synapse **15**(1): 63-89.

Kasahara, Y., Y. Takayanagi, T. Kawada, K. Itoi and K. Nishimori (2007). "Impaired thermoregulatory ability of oxytocin-deficient mice during cold-exposure." Biosci Biotechnol Biochem **71**(12): 3122-3126.

Kataoka, Y., N. Iijima, T. Yano, K. Kakihara, S. Hayashi, S. Hinuma, H. Honjo, S. Hayashi, M. Tanaka and Y. Ibata (2001). "Gonadal regulation of PrRP mRNA expression in the nucleus tractus solitarius and ventral and lateral reticular nuclei of the rat." Brain Res Mol Brain Res **87**(1): 42-47.

Kesavan, K. and S. U. Devaskar (2019). "Intrauterine Growth Restriction: Postnatal Monitoring and Outcomes." Pediatr Clin North Am **66**(2): 403-423.

Kitka, T., C. Adori, Z. Katai, S. Vas, E. Molnar, R. S. Papp, Z. E. Toth and G. Bagdy (2011). "Association between the activation of MCH and orexin immunorective neurons and REM sleep architecture during REM rebound after a three day long REM deprivation." Neurochem Int **59**(5): 686-694.

Kohno, D., M. Nakata, Y. Maejima, H. Shimizu, U. Sedbazar, N. Yoshida, K. Dezaki, T. Onaka, M. Mori and T. Yada (2008). "Nesfatin-1 neurons in paraventricular and supraoptic nuclei of the rat hypothalamus coexpress oxytocin and vasopressin and are activated by refeeding." Endocrinology **149**(3): 1295-1301.

Krause, E. G., D. Pati and C. J. Frazier (2017). "Chronic salt-loading reduces basal excitatory input to CRH neurons in the paraventricular nucleus and accelerates recovery from restraint stress in male mice." Physiol Behav **176**: 189-194.

Krolewski, D. M., A. Medina, I. A. Kerman, R. Bernard, S. Burke, R. C. Thompson, W. E. Bunney, Jr., A. F. Schatzberg, R. M. Myers, H. Akil, E. G. Jones and S. J. Watson (2010). "Expression patterns of corticotropin-releasing factor, arginine vasopressin, histidine decarboxylase, melanin-concentrating hormone, and orexin genes in the human hypothalamus." J Comp Neurol **518**(22): 4591-4611.

Kullmann, S. and R. Veit (2021). "Resting-state functional connectivity of the human hypothalamus." Handb Clin Neurol **179**: 113-124.

Kvetnansky, R., E. L. Sabban and M. Palkovits (2009). "Catecholaminergic systems in stress: structural and molecular genetic approaches." Physiol Rev **89**(2): 535-606.

Labbé, S. M., A. Caron, D. Lanfray, B. Monge-Rofarello, T. J. Bartness and D. Richard (2015). "Hypothalamic control of brown adipose tissue thermogenesis." Front Syst Neurosci **9**: 150.

Lawrence, C. B., F. Celsi, J. Brennand and S. M. Luckman (2000). "Alternative role for prolactin-releasing peptide in the regulation of food intake." Nat Neurosci **3**(7): 645-646.

Lawrence, C. B., K. L. Ellacott and S. M. Luckman (2002). "PRL-releasing peptide reduces food intake and may mediate satiety signaling." Endocrinology **143**(2): 360-367.

Lawrence, C. B., Y. L. Liu, M. J. Stock and S. M. Luckman (2004). "Anorectic actions of prolactin-releasing peptide are mediated by corticotropin-releasing hormone receptors." Am J Physiol Regul Integr Comp Physiol **286**(1): R101-107.

Lechan, R. M. and C. Fekete (2006). "The TRH neuron: a hypothalamic integrator of energy metabolism." Prog Brain Res **153**: 209-235.

Levin, B. E. (2006). "Metabolic imprinting: critical impact of the perinatal environment on the regulation of energy homeostasis." Philos Trans R Soc Lond B Biol Sci **361**(1471): 1107-1121.

Levine, J. E. (2000). The Hypothalamus as a Major Integrating Center. Neuroendocrinology in Physiology and Medicine. P. M. Conn and M. E. Freeman. Totowa, NJ, Humana Press**:** 75-93.

Lin, S. H., A. C. Arai, R. A. España, C. W. Berridge, F. M. Leslie, J. R. Huguenard, M. Vergnes and O. Civelli (2002). "Prolactin-releasing peptide (PrRP) promotes awakening and suppresses absence seizures." Neuroscience **114**(1): 229-238.

Luttrell, L. M. and R. J. Lefkowitz (2002). "The role of beta-arrestins in the termination and transduction of G-protein-coupled receptor signals." J Cell Sci **115**(Pt 3): 455-465.

Ma, L., D. MacTavish, F. Simonin, J. J. Bourguignon, T. Watanabe and J. H. Jhamandas (2009). "Prolactin-releasing peptide effects in the rat brain are mediated through the Neuropeptide FF receptor." Eur J Neurosci **30**(8): 1585-1593.

Ma, X. M. and S. L. Lightman (1998). "The arginine vasopressin and corticotrophin-releasing hormone gene transcription responses to varied frequencies of repeated stress in rats." J Physiol **510 (Pt 2)**(Pt 2): 605-614.

Madsen, K. L., T. S. Thorsen, T. Rahbek-Clemmensen, J. Eriksen and U. Gether (2012). "Protein interacting with C kinase 1 (PICK1) reduces reinsertion rates of interaction partners sorted to Rab11-dependent slow recycling pathway." J Biol Chem **287**(15): 12293-12308.

Maejima, Y., U. Sedbazar, S. Suyama, D. Kohno, T. Onaka, E. Takano, N. Yoshida, M. Koike, Y. Uchiyama, K. Fujiwara, T. Yashiro, T. L. Horvath, M. O. Dietrich, S. Tanaka, K. Dezaki, I. S. Oh, K. Hashimoto, H. Shimizu, M. Nakata, M. Mori and T. Yada (2009). "Nesfatin-1-regulated oxytocinergic signaling in the paraventricular nucleus causes anorexia through a leptin-independent melanocortin pathway." Cell Metab **10**(5): 355-365.

Mai, J. K., M. Majtanik and G. Paxinos (2015). Atlas of the Human Brain, Elsevier Science.

Mantas, I., M. Saarinen, Z. D. Xu and P. Svenningsson (2021). "Update on GPCR-based targets for the development of novel antidepressants." Mol Psychiatry.

Martin-Gronert, M. S. and S. E. Ozanne (2007). "Experimental IUGR and later diabetes." J Intern Med **261**(5): 437-452.

Maruyama, M., H. Matsumoto, K. Fujiwara, J. Noguchi, C. Kitada, M. Fujino and K. Inoue (2001). "Prolactin-releasing peptide as a novel stress mediator in the central nervous system." Endocrinology **142**(5): 2032-2038.

Maruyama, M., H. Matsumoto, K. Fujiwara, J. Noguchi, C. Kitada, S. Hinuma, H. Onda, O. Nishimura, M. Fujino, T. Higuchi and K. Inoue (1999). "Central administration of prolactin-releasing peptide stimulates oxytocin release in rats." Neurosci Lett **276**(3): 193-196.

Matsumoto, H., M. Maruyama, J. Noguchi, Y. Horikoshi, K. Fujiwara, C. Kitada, S. Hinuma, H. Onda, O. Nishimura, K. Inoue and M. Fujino (2000). "Stimulation of corticotropin-releasing hormone-mediated adrenocorticotropin secretion by central administration of prolactin-releasing peptide in rats." Neurosci Lett **285**(3): 234-238.

McGowan, P. O. and S. G. Matthews (2018). "Prenatal Stress, Glucocorticoids, and Developmental Programming of the Stress Response." Endocrinology **159**(1): 69-82.

McKinley, M. J., G. L. Pennington and P. J. Ryan (2021). "The median preoptic nucleus: A major regulator of fluid, temperature, sleep, and cardiovascular homeostasis." Handb Clin Neurol **179**: 435-454.

McTaggart, R. A. and S. Feng (2004). "An uncomfortable silence em leader while we all search for a better reporter gene in adult stem cell biology." Hepatology **39**(4): 1143-1146.

Mera, T., H. Fujihara, M. Kawasaki, H. Hashimoto, T. Saito, M. Shibata, J. Saito, T. Oka, S. Tsuji, T. Onaka and Y. Ueta (2006). "Prolactin-releasing peptide is a potent mediator of stress responses in the brain through the hypothalamic paraventricular nucleus." Neuroscience **141**(2): 1069-1086.

Merali, Z., C. Cayer, P. Kent and H. Anisman (2008). "Nesfatin-1 increases anxiety- and fear-related behaviors in the rat." Psychopharmacology (Berl) **201**(1): 115-123.

Mimee, A., P. M. Smith and A. V. Ferguson (2012). "Nesfatin-1 influences the excitability of neurons in the nucleus of the solitary tract and regulates cardiovascular function." Am J Physiol Regul Integr Comp Physiol **302**(11): R1297-1304.

Minami, S., T. Nakata, R. Tokita, H. Onodera and J. Imaki (1999). "Cellular localization of prolactin-releasing peptide messenger RNA in the rat brain." Neurosci Lett **266**(1): 73-75.

Moore, K. A. and I. R. Lemischka (2006). "Stem cells and their niches." Science **311**(5769): 1880-1885.

Morales, I. and K. C. Berridge (2020). "'Liking' and 'wanting' in eating and food reward: Brain mechanisms and clinical implications." Physiol Behav **227**: 113152.

Morales, T., S. Hinuma and P. E. Sawchenko (2000). "Prolactin-releasing peptide is expressed in afferents to the endocrine hypothalamus, but not in neurosecretory neurones." J Neuroendocrinol **12**(2): 131-140.

Morales, T. and P. E. Sawchenko (2003). "Brainstem prolactin-releasing peptide neurons are sensitive to stress and lactation." Neuroscience **121**(3): 771-778.

Morrison, S. F. and K. Nakamura (2019). "Central Mechanisms for Thermoregulation." Annu Rev Physiol **81**: 285-308.

Nakano, K., M. Migita, H. Mochizuki and T. Shimada (2001). "Differentiation of transplanted bone marrow cells in the adult mouse brain." Transplantation **71**(12): 1735-1740.

Nakata, M., D. Gantulga, P. Santoso, B. Zhang, C. Masuda, M. Mori, T. Okada and T. Yada (2016). "Paraventricular NUCB2/Nesfatin-1 Supports Oxytocin and Vasopressin Neurons to Control Feeding Behavior and Fluid Balance in Male Mice." Endocrinology **157**(6): 2322-2332.

Novak, A., C. Guo, W. Yang, A. Nagy and C. G. Lobe (2000). "Z/EG, a double reporter mouse line that expresses enhanced green fluorescent protein upon Cre-mediated excision." Genesis **28**(3-4): 147-155.

Nusbaum, M. P., D. M. Blitz and E. Marder (2017). "Functional consequences of neuropeptide and small-molecule co-transmission." Nat Rev Neurosci **18**(7): 389-403.

O'Connor, E. C., Y. Kremer, S. Lefort, M. Harada, V. Pascoli, C. Rohner and C. Lüscher (2015). "Accumbal D1R Neurons Projecting to Lateral Hypothalamus Authorize Feeding." Neuron **88**(3): 553-564.

Oh, I. S., H. Shimizu, T. Satoh, S. Okada, S. Adachi, K. Inoue, H. Eguchi, M. Yamamoto, T. Imaki, K. Hashimoto, T. Tsuchiya, T. Monden, K. Horiguchi, M. Yamada and M. Mori (2006). "Identification of nesfatin-1 as a satiety molecule in the hypothalamus." Nature **443**(7112): 709-712.

Ohiwa, N., H. Chang, T. Saito, T. Onaka, T. Fujikawa and H. Soya (2007). "Possible inhibitory role of prolactin-releasing peptide for ACTH release associated with running stress." Am J Physiol Regul Integr Comp Physiol **292**(1): R497-504.

Ortiz Hidalgo, C. (2022). "Immunohistochemistry in Historical Perspective: Knowing the Past to Understand the Present." Methods Mol Biol **2422**: 17-31.

Pacak, K., M. Palkovits, I. J. Kopin and D. S. Goldstein (1995). "Stress-induced norepinephrine release in the hypothalamic paraventricular nucleus and pituitary-adrenocortical and sympathoadrenal activity: in vivo microdialysis studies." Front Neuroendocrinol **16**(2): 89-150.

Palkovits, M. (1982). "Neuropeptides in the median eminence: their sources and destinations." Peptides **3**(3): 299-303.

Palkovits, M. (1984). "Distribution of neuropeptides in the central nervous system: a review of biochemical mapping studies." Prog Neurobiol **23**(3): 151-189.

Pan, W., H. Hsuchou and A. J. Kastin (2007). "Nesfatin-1 crosses the blood-brain barrier without saturation." Peptides **28**(11): 2223-2228.

Papatriantafyllou, E., D. Efthymiou, E. Zoumbaneas, C. A. Popescu and E. Vassilopoulou (2022). "Sleep Deprivation: Effects on Weight Loss and Weight Loss Maintenance." Nutrients **14**(8).

Paxinos, G. and C. Watson (2007). The Rat Brain in Stereotaxic Coordinates. London, Amsterdam, Elsevier.

Peciña, S. and K. C. Berridge (2005). "Hedonic hot spot in nucleus accumbens shell: where do mu-opioids cause increased hedonic impact of sweetness?" J Neurosci **25**(50): 11777-11786.

Peciña, S. and K. C. Berridge (2013). "Dopamine or opioid stimulation of nucleus accumbens similarly amplify cue-triggered 'wanting' for reward: entire core and medial shell mapped as substrates for PIT enhancement." Eur J Neurosci **37**(9): 1529-1540.

Pedrino, G. R., D. A. Rosa, O. U. Lopes and S. L. Cravo (2014). Frontiers in Neuroscience Catecholaminergic Medullary Pathways and Cardiovascular Responses to Expanded Circulating Volume and Increased Osmolarity. Neurobiology of Body Fluid Homeostasis: Transduction and Integration. L. A. De Luca, Jr., J. V. Menani and A. K. Johnson. Boca Raton (FL), CRC Press/Taylor & Francis

Pedroso, A. P., A. P. Souza, A. P. Dornellas, L. M. Oyama, C. M. Nascimento, G. M. Santos, J. C. Rosa, R. P. Bertolla, J. Klawitter, U. Christians, A. K. Tashima and E. B. Ribeiro (2017). "Intrauterine Growth Restriction Programs the Hypothalamus of Adult Male Rats: Integrated Analysis of Proteomic and Metabolomic Data." J Proteome Res **16**(4): 1515-1525.

Pereira-da-Silva, M., M. A. Torsoni, H. V. Nourani, V. D. Augusto, C. T. Souza, A. L. Gasparetti, J. B. Carvalheira, G. Ventrucci, M. C. Marcondes, A. P. Cruz-Neto, M. J. Saad, A. C. Boschero, E. M. Carneiro and L. A. Velloso (2003). "Hypothalamic melanin-concentrating hormone is induced by cold exposure and participates in the control of energy expenditure in rats." Endocrinology **144**(11): 4831-4840.

Pražienková, V., A. Popelová, J. Kuneš and L. Maletínská (2019). "Prolactin-Releasing Peptide: Physiological and Pharmacological Properties." Int J Mol Sci **20**(21).

Price, C. J., W. K. Samson and A. V. Ferguson (2008). "Nesfatin-1 inhibits NPY neurons in the arcuate nucleus." Brain Res **1230**: 99-106.

Rana, T., T. Behl, A. Sehgal, S. Singh, N. Sharma, A. Abdeen, S. F. Ibrahim, V. Mani, M. S. Iqbal, S. Bhatia, M. M. Abdel Daim and S. Bungau (2022). "Exploring the role of neuropeptides in depression and anxiety." Prog Neuropsychopharmacol Biol Psychiatry **114**: 110478.

Ravussin, A., Y. H. Youm, J. Sander, S. Ryu, K. Nguyen, L. Varela, G. I. Shulman, S. Sidorov, T. L. Horvath, J. L. Schultze and V. D. Dixit (2018). "Loss of Nucleobindin-2 Causes Insulin Resistance in Obesity without Impacting Satiety or Adiposity." Cell Rep **24**(5): 1085-1092.e1086.

Reutrakul, S. and E. Van Cauter (2018). "Sleep influences on obesity, insulin resistance, and risk of type 2 diabetes." Metabolism **84**: 56-66.

Riemann, D., L. B. Krone, K. Wulff and C. Nissen (2020). "Sleep, insomnia, and depression." Neuropsychopharmacology **45**(1): 74-89.

Roland, B. L., S. W. Sutton, S. J. Wilson, L. Luo, J. Pyati, R. Huvar, M. G. Erlander and T. W. Lovenberg (1999). "Anatomical distribution of prolactin-releasing peptide and its receptor suggests additional functions in the central nervous system and periphery." Endocrinology **140**(12): 5736-5745.

Rupp, S. K., E. Wölk and A. Stengel (2021). "Nesfatin-1 Receptor: Distribution, Signaling and Increasing Evidence for a G Protein-Coupled Receptor - A Systematic Review." Front Endocrinol (Lausanne) **12**: 740174.

Saleem, T., N. Sajjad, S. Fatima, N. Habib, S. R. Ali and M. Qadir (2011). "Intrauterine growth retardation--small events, big consequences." Ital J Pediatr **37**: 41.

Samson, W. K., Z. T. Resch and T. C. Murphy (2000). "A novel action of the newly described prolactin-releasing peptides: cardiovascular regulation." Brain Res **858**(1): 19-25.

Saper, C. B., T. C. Chou and J. K. Elmquist (2002). "The need to feed: homeostatic and hedonic control of eating." Neuron **36**(2): 199-211.

Sawchenko, P. E. and L. W. Swanson (1981). "Central noradrenergic pathways for the integration of hypothalamic neuroendocrine and autonomic responses." Science **214**(4521): 685-687.

Sawchenko, P. E. and L. W. Swanson (1982). "The organization of noradrenergic pathways from the brainstem to the paraventricular and supraoptic nuclei in the rat." Brain Res **257**(3): 275-325.

Schalla, M. A. and A. Stengel (2018). "Current Understanding of the Role of Nesfatin-1." J Endocr Soc **2**(10): 1188-1206.

Schalla, M. A., S. Unniappan, N. W. G. Lambrecht, M. Mori, Y. Taché and A. Stengel (2020). "NUCB2/nesfatin-1 - Inhibitory effects on food intake, body weight and metabolism." Peptides **128**: 170308.

Scherrer, G., P. Tryoen-Tóth, D. Filliol, A. Matifas, D. Laustriat, Y. Q. Cao, A. I. Basbaum, A. Dierich, J. L. Vonesh, C. Gavériaux-Ruff and B. L. Kieffer (2006). "Knockin mice expressing fluorescent delta-opioid receptors uncover G protein-coupled receptor dynamics in vivo." Proc Natl Acad Sci U S A **103**(25): 9691-9696.

Seal, L. J., C. J. Small, W. S. Dhillo, A. R. Kennedy, M. A. Ghatei and S. R. Bloom (2002). "Prolactin-releasing peptide releases corticotropin-releasing hormone and increases plasma adrenocorticotropin via the paraventricular nucleus of the hypothalamus." Neuroendocrinology **76**(2): 70-78.

Sedbazar, U., Y. Maejima, M. Nakata, M. Mori and T. Yada (2013). "Paraventricular NUCB2/nesfatin-1 rises in synchrony with feeding suppression during early light phase in rats." Biochem Biophys Res Commun **434**(3): 434-438.

Shimizu, H., I. S. Oh, S. Okada and M. Mori (2009). "Nesfatin-1: an overview and future clinical application." Endocr J **56**(4): 537-543.

Shimomura, O. (2005). "The discovery of aequorin and green fluorescent protein." J Microsc **217**(Pt 1): 1-15.

Skrapits, K., B. Borsay, L. Herczeg, P. Ciofi, Z. Liposits and E. Hrabovszky (2015). "Neuropeptide co-expression in hypothalamic kisspeptin neurons of laboratory animals and the human." Front Neurosci **9**: 29.

Solinas, G., S. Summermatter, D. Mainieri, M. Gubler, J. P. Montani, J. Seydoux, S. R. Smith and A. G. Dulloo (2006). "Corticotropin-releasing hormone directly stimulates thermogenesis in skeletal muscle possibly through substrate cycling between de novo lipogenesis and lipid oxidation." Endocrinology **147**(1): 31-38.

Steiger, A. and M. Pawlowski (2019). "Depression and Sleep." Int J Mol Sci **20**(3).

Stengel, A. (2015). "Nesfatin-1 - More than a food intake regulatory peptide." Peptides **72**: 175-183.

Stengel, A., M. Goebel, L. Wang, J. Rivier, P. Kobelt, H. Mönnikes, N. W. Lambrecht and Y. Taché (2009). "Central nesfatin-1 reduces dark-phase food intake and gastric emptying in rats: differential role of corticotropin-releasing factor2 receptor." Endocrinology **150**(11): 4911-4919.

Su, Y., J. Zhang, Y. Tang, F. Bi and J. N. Liu (2010). "The novel function of nesfatin-1: anti-hyperglycemia." Biochem Biophys Res Commun **391**(1): 1039-1042.

Sun, B., K. Fujiwara, S. Adachi and K. Inoue (2005). "Physiological roles of prolactin-releasing peptide." Regul Pept **126**(1-2): 27-33.

Sutton, C. A., A. M. L'Insalata and T. L. Fazzino (2022). "Reward sensitivity, eating behavior, and obesity-related outcomes: A systematic review." Physiol Behav **252**: 113843.

Taber, K. H. and R. A. Hurley (2014). "Volume transmission in the brain: beyond the synapse." J Neuropsychiatry Clin Neurosci **26**(1): iv, 1-4.

Takahashi, K., A. Yoshinoya, Z. Arihara, O. Murakami, K. Totsune, M. Sone, H. Sasano and S. Shibahara (2000). "Regional distribution of immunoreactive prolactin-releasing peptide in the human brain." Peptides **21**(10): 1551-1555.

Takayanagi, Y., H. Matsumoto, M. Nakata, T. Mera, S. Fukusumi, S. Hinuma, Y. Ueta, T. Yada, G. Leng and T. Onaka (2008). "Endogenous prolactin-releasing peptide regulates food intake in rodents." J Clin Invest **118**(12): 4014-4024.

Tan, B. K., M. Hallschmid, W. Kern, H. Lehnert and H. S. Randeva (2011). "Decreased cerebrospinal fluid/plasma ratio of the novel satiety molecule, nesfatin-1/NUCB-2, in obese humans: evidence of nesfatin-1/NUCB-2 resistance and implications for obesity treatment." J Clin Endocrinol Metab **96**(4): E669-673.

Tan, W. C. C., S. N. Nerurkar, H. Y. Cai, H. H. M. Ng, D. Wu, Y. T. F. Wee, J. C. T. Lim, J. Yeong and T. K. H. Lim (2020). "Overview of multiplex immunohistochemistry/ immunofluorescence techniques in the era of cancer immunotherapy." Cancer Commun (Lond) **40**(4): 135-153.

Tanida, M. and M. Mori (2011). "Nesfatin-1 stimulates renal sympathetic nerve activity in rats." Neuroreport **22**(6): 309-312.

Taylor, B. K. and K. N. Westlund (2017). "The noradrenergic locus coeruleus as a chronic pain generator." J Neurosci Res **95**(6): 1336-1346.

Tian, F., G. Xu, S. Zhou, S. Chen and D. He (2023). "Principles and applications of green fluorescent protein-based biosensors: a mini-review." Analyst **148**(13): 2882-2891.

Tonkiss, J., B. Shukitt-Hale, R. N. Formica, F. J. Rocco and J. R. Galler (1990). "Prenatal protein malnutrition alters response to reward in adult rats." Physiol Behav **48**(5): 675-680.

Torterolo, P., C. Scorza, P. Lagos, J. Urbanavicius, L. Benedetto, C. Pascovich, X. López-Hill, M. H. Chase and J. M. Monti (2015). "Melanin-Concentrating Hormone (MCH): Role in REM Sleep and Depression." Front Neurosci **9**: 475.

Tóth, Z. E., K. Gallatz, M. Fodor and M. Palkovits (1999). "Decussations of the descending paraventricular pathways to the brainstem and spinal cord autonomic centers." J Comp Neurol **414**(2): 255-266.

Tsigos, C. and G. P. Chrousos (2002). "Hypothalamic-pituitary-adrenal axis, neuroendocrine factors and stress." J Psychosom Res **53**(4): 865-871.

Uchida, K., D. Kobayashi, G. Das, T. Onaka, K. Inoue and K. Itoi (2010). "Participation of the prolactin-releasing peptide-containing neurones in caudal medulla in conveying haemorrhagic stress-induced signals to the paraventricular nucleus of the hypothalamus." J Neuroendocrinol **22**(1): 33-42.

Ulrich-Lai, Y. M. and K. K. Ryan (2014). "Neuroendocrine circuits governing energy balance and stress regulation: functional overlap and therapeutic implications." Cell Metab **19**(6): 910-925.

Vaag, A. and S. S. Lund (2007). "Non-obese patients with type 2 diabetes and prediabetic subjects: distinct phenotypes requiring special diabetes treatment and (or) prevention?" Appl Physiol Nutr Metab **32**(5): 912-920.

Valassi, E., M. Scacchi and F. Cavagnini (2008). "Neuroendocrine control of food intake." Nutr Metab Cardiovasc Dis **18**(2): 158-168.

van den Pol, A. N., C. Acuna-Goycolea, K. R. Clark and P. K. Ghosh (2004). "Physiological properties of hypothalamic MCH neurons identified with selective expression of reporter gene after recombinant virus infection." Neuron **42**(4): 635-652.

Verret, L., R. Goutagny, P. Fort, L. Cagnon, D. Salvert, L. Léger, R. Boissard, P. Salin, C. Peyron and P. H. Luppi (2003). "A role of melanin-concentrating hormone producing neurons in the central regulation of paradoxical sleep." BMC Neurosci **4**: 19.

Vickers, M. H., B. H. Breier, W. S. Cutfield, P. L. Hofman and P. D. Gluckman (2000). "Fetal origins of hyperphagia, obesity, and hypertension and postnatal amplification by hypercaloric nutrition." Am J Physiol Endocrinol Metab **279**(1): E83-87.

Voineskos, D., Z. J. Daskalakis and D. M. Blumberger (2020). "Management of Treatment-Resistant Depression: Challenges and Strategies." Neuropsychiatr Dis Treat **16**: 221-234.

Wall, K. D., D. R. Olivos and L. Rinaman (2020). "High Fat Diet Attenuates Cholecystokinin-Induced cFos Activation of Prolactin-Releasing Peptide-Expressing A2 Noradrenergic Neurons in the Caudal Nucleus of the Solitary Tract." Neuroscience **447**: 113-121.

Wang, B., P. C. Chandrasekera and J. J. Pippin (2014). "Leptin- and leptin receptor-deficient rodent models: relevance for human type 2 diabetes." Curr Diabetes Rev **10**(2): 131-145.

Wang, Q., M. A. Timberlake, 2nd, K. Prall and Y. Dwivedi (2017). "The recent progress in animal models of depression." Prog Neuropsychopharmacol Biol Psychiatry **77**: 99-109.

Watanabe, T. and D. N. Orth (1987). "Detailed kinetic analysis of adrenocorticotropin secretion by dispersed rat anterior pituitary cells in a microperifusion system: effects of ovine corticotropin-releasing factor and arginine vasopressin." Endocrinology **121**(3): 1133-1145.

Werner, M., R. Von Wasielewski and P. Komminoth (1996). "Antigen retrieval, signal amplification and intensification in immunohistochemistry." Histochem Cell Biol **105**(4): 253-260.

Wharton, K. A., Jr., D. Wood, M. Manesse, K. H. Maclean, F. Leiss and A. Zuraw (2021). "Tissue Multiplex Analyte Detection in Anatomic Pathology - Pathways to Clinical Implementation." Front Mol Biosci **8**: 672531.

Wu, D., M. Yang, Y. Chen, Y. Jia, Z. A. Ma, G. Boden, L. Li and G. Yang (2014). "Hypothalamic nesfatin-1/NUCB2 knockdown augments hepatic gluconeogenesis that is correlated with inhibition of mTOR-STAT3 signaling pathway in rats." Diabetes **63**(4): 1234-1247.

Xu, Y. and F. Chen (2020). "Antioxidant, Anti-Inflammatory and Anti-Apoptotic Activities of Nesfatin-1: A Review." J Inflamm Res **13**: 607-617.

Yagi, T., E. J. McMahon, S. Takikita, I. Mohri, G. K. Matsushima and K. Suzuki (2004). "Fate of donor hematopoietic cells in demyelinating mutant mouse, twitcher, following transplantation of GFP+ bone marrow cells." Neurobiol Dis **16**(1): 98-109.

Yamakawa, K., K. Kudo, S. Kanba and J. Arita (1999). "Distribution of prolactin-releasing peptide-immunoreactive neurons in the rat hypothalamus." Neurosci Lett **267**(2): 113-116.

Yamashita, M., Y. Takayanagi, M. Yoshida, K. Nishimori, M. Kusama and T. Onaka (2013). "Involvement of prolactin-releasing peptide in the activation of oxytocin neurones in response to food intake." J Neuroendocrinol **25**(5): 455-465.

Yamashita, T. and A. Yamanaka (2017). "Lateral hypothalamic circuits for sleep-wake control." Curr Opin Neurobiol **44**: 94-100.

Yang, M., Z. Zhang, C. Wang, K. Li, S. Li, G. Boden, L. Li and G. Yang (2012). "Nesfatin-1 action in the brain increases insulin sensitivity through Akt/AMPK/TORC2 pathway in diet-induced insulin resistance." Diabetes **61**(8): 1959-1968.

Yoshida, M., Y. Takayanagi and T. Onaka (2014). "The medial amygdala-medullary PrRP-synthesizing neuron pathway mediates neuroendocrine responses to contextual conditioned fear in male rodents." Endocrinology **155**(8): 2996-3004.

Yoshimura, M., T. Matsuura, J. Ohkubo, T. Maruyama, T. Ishikura, H. Hashimoto, T. Kakuma, M. Mori and Y. Ueta (2014). "A role of nesfatin-1/NucB2 in dehydration-induced anorexia." Am J Physiol Regul Integr Comp Physiol **307**(2): R225-236.

Yosten, G. L., L. Redlinger and W. K. Samson (2012). "Evidence for a role of endogenous nesfatin-1 in the control of water drinking." J Neuroendocrinol **24**(7): 1078-1084.

Záborszky, L., G. F. Alheid, M. C. Beinfeld, L. E. Eiden, L. Heimer and M. Palkovits (1985). "Cholecystokinin innervation of the ventral striatum: a morphological and radioimmunological study." Neuroscience **14**(2): 427-453.

Zegers, D., S. Beckers, I. L. Mertens, L. F. Van Gaal and W. Van Hul (2011). "Association between polymorphisms of the Nesfatin gene, NUCB2, and obesity in men." Mol Genet Metab **103**(3): 282-286.

Zhang, S. Q., S. Inoué and M. Kimura (2001). "Sleep-promoting activity of prolactin-releasing peptide (PrRP) in the rat." Neuroreport **12**(15): 3173-3176.

Zhang, T., M. Wang, L. Liu, B. He, J. Hu and Y. Wang (2019). "Hypothalamic nesfatin-1 mediates feeding behavior via MC3/4R-ERK signaling pathway after weight loss in obese Sprague-Dawley rats." Peptides **119**: 170080.

Zhu, L. L. and T. Onaka (2003). "Facilitative role of prolactin-releasing peptide neurons in oxytocin cell activation after conditioned-fear stimuli." Neuroscience **118**(4): 1045-1053.

9. KÖSZÖNETNYILVÁNÍTÁS

Szeretnék köszönetet nyilvánítani egykori PhD témavezetőmnek, professzor Palkovits Miklósnak, akitől a kutatómunka alapjait megtanultam. Neki köszönhetem külföldi tanulmányutaimat is, melyek nagy lendületet adtak további fejlődésemnek.

Hálás vagyok dr. Mezei Évának, aki az NIH-ben mentorom volt, és akivel számos eredményes munkát és egy életre szóló barátságot tudhatunk magunk mögött. Ki szeretném emelni dr. Harold Gainert, aki rengeteget segített tudományos gondolkodásom fejlődésében.

Köszönetet szeretnék mondani PhD hallgatóimnak, dr. Könczöl Katalinnak, dr. Durst Máténak, dr. Vas Szilviának és Sípos Klaudiának lelkes munkájukért, fiatalos szellemiségükért, mely a laboratórium légkörét frissítette, és nemutolsó sorban barátságukért.

Ugyancsak köszönet illeti a volt Neuromorfológiai Laboratórium alapkövét képező munkatársnőimet, dr. Gallatz Katalint és Helfferich Frigyesné, Juditot. Gallatz Katalinhoz bármikor fordulhatok ma is, szakmai és egyéb kérdésekben is. Helfferichné, Judit vezetett be asszisztensnőként a laboratóriumi munka alapjaiba, szigorúsága, erkölcsi tartása meghatározta számomra a mércét. Hasonló alapkövét képezi jelenlegi munkacsoportomnak Kerti Judit, az asszisztensnőm, akinek technikai tudása nélkül a bemutatott munkák kivitelezése nem valósulhatott volna meg.

Számos további jelenlegi és volt intézeti munkatársam például dr. Papp Rege Sugárka, dr. Bodnár Ibolya és néhai professzor Nagy György járult hozzá jelentősen az elvégzett munkákhoz, mindezt köszönöm nekik és elnézést kérek, amiért a felsorolás hiányos. A laboratóriumi állatokkal végzett munkáért Deák Szilviát, Gróti Zoltánt illeti köszönet.

Fel sem tudom sorolni az összes kollaborátort, akiknek hozzájárulása a munkákhoz nélkülözhetetlen volt. Mindenképp meg kell említenem közülük a KOKI-ból dr. Kovács Krisztinát, dr. Ferenczi Szilamért, dr. Zelena Dórát (ma már PTE AOK Élettani Intézet), dr. Fekete Csabát és dr. Gereben Balázst. Dr. Bagdy Györgynek (SE Gyógyszerhatástani Intézet) köszönöm, hogy segített az alvásmegvonásos állatkísérletek megvalósításában, amit az Intézet keretei között nem tudtam volna megcsinálni.

Hálás vagyok az Anatómiai, Szövet- és Fejlődéstani Intézet volt és jelenlegi intézetvezetőinek hogy támogatták munkámat az Intézetben.

Végezetül köszönöm családomnak az áldozatvállalást, ami lehetővé tette, hogy a család és munka közti egyensúly olykor a munka javára tolódjon el.

10. AZ ÉRTEKEZÉS ALAPJÁUL SZOLGÁLÓ KÖZLEMÉNYEK

1. **Tóth ZE**, Mezey E., *Simultaneous visualization of multiple antigens with tyramide signal amplification using antibodies from the same species*
   J Histochem Cytochem, 55(6):545-54. (2007)
   doi: 10.1369/jhc.6A7134.2007.
   IF: 2,335 Független idéző: 145

2. **Tóth ZE**, Shahar T, Leker R, Szalayova I, Bratincsák A, Key S, Lonyai A, Németh K, Mezey E., *Sensitive detection of GFP utilizing tyramide signal amplification to overcome gene silencing*
   Exp Cell Res, 15;313(9):1943-50. (2007)
   doi: 10.1016/j.yexcr.2007.02.024.
   IF: 3,695 Független idéző: 18

3. Könczöl K, Pintér O, Ferenczi S, Varga J, Kovács K, Palkovits M, Zelena D, **Tóth ZE**., *Nesfatin-1 exerts long-term effect on food intake and body temperature*
   Int J Obes (Lond), 36(12):1514-21. (2012)
   doi: 10.1038/ijo.2012.2.
   IF: 5,221 Független idéző: 93

4. Vas S, Ádori C, Könczöl K, Kátai Z, Pap D, Papp RS, Bagdy G, Palkovits M, **Tóth ZE**., *Nesfatin-1/NUCB2 as a potential new element of sleep regulation in rats*
   Plos One, 8(4):e59809. (2013)
   doi: 10.1371/journal.pone.0059809.
   IF: 3,534 Független idéző: 54

5. Durst M, Könczöl K, Ocskay K, Sípos K, Várnai P, Szilvásy-Szabó A, Fekete C, **Tóth ZE**., *Hypothalamic Nesfatin-1 Resistance May Underlie the Development of Type 2 Diabetes Mellitus in Maternally Undernourished Non-obese Rats*
   Front Neurosci, 16:828571. (2022)
   doi: 10.3389/fnins.2022.828571.
   IF: 4,300 Független idéző: 3

6. Durst M, Könczöl K, Balázsa T, Eyre MD, **Tóth ZE**., *Reward-representing D1-type neurons in the medial shell of the accumbens nucleus regulate palatable food intake*
   Int J Obes (Lond), 43(4):917-927. (2019)
   doi: 10.1038/s41366-018-0133-y.
   IF: 4,419 Független idéző: 27

7. Könczöl K, Bodnár I, Zelena D, Pintér O, Papp RS, Palkovits M, Nagy GM, **Tóth ZE**., *Nesfatin-1/NUCB2 may participate in the activation of the hypothalamic-pituitary-adrenal axis in rats*
   Neurochem Int, 57(3):189-97. (2010)
   doi: 10.1016/j.neuint.2010.04.012.
   IF: 3,601 Független idéző: 89

8. **Tóth ZE**, Zelena D, Mergl Z, Kirilly E, Várnai P, Mezey E, Makara GB, Palkovits M., *Chronic repeated restraint stress increases prolactin-releasing peptide/tyrosine-hydroxylase ratio with gender-related differences in the rat brain*
   J Neurochem, 104(3):653-66. (2008)
   doi: 10.1111/j.1471-4159.2007.05069.x.
   IF: 4,500 Független idéző: 15

9. Matuska R, Zelena D, Könczöl K, Papp RS, Durst M, Guba D, Török B, Varnai P, **Tóth ZE**., *Colocalized neurotransmitters in the hindbrain cooperate in adaptation to chronic hypernatremia*
   Brain Struct Funct, 225(3):969–984. (2020)
   doi: 10.1007/s00429-020-02049-y.
   IF: 3,270 Független idéző: 1

10. Vas S, Papp RS, Könczöl K, Bogáthy E, Papp N, Ádori C, Durst M, Sípos K, Ocskay K, Farkas I, Bálint F, Ferenci S, Török B, Kovács A, Szabó E, Zelena D, Kovács KJ, Földes A, Kató E, Köles L, Bagdy G, Palkovits M, **Tóth ZE**., *Prolactin-Releasing Peptide Contributes to Stress-Related Mood Disorders and Inhibits Sleep/Mood Regulatory Melanin-Concentrating Hormone Neurons in Rats*
    J Neurosci, 43(5):846-862. (2023)
    doi: 10.1523/JNEUROSCI.2139-21.2022.
    IF: 5,300 (2022) Független idéző: 1

11. FÜGGELÉK: AZ ÉRTEKEZÉS ALAPJÁT KÉPEZŐ KÖZLEMÉNYEK ÉS CSATOLMÁNYOK

Volume 55(6): 545–554, 2007
Journal of Histochemistry & Cytochemistry
http://www.jhc.org

ARTICLE

Simultaneous Visualization of Multiple Antigens With Tyramide Signal Amplification Using Antibodies From the Same Species

Zsuzsanna E. Tóth and Éva Mezey

Craniofacial and Skeletal Diseases Branch, National Institute of Dental and Craniofacial Research, National Institutes of Health, Bethesda, Maryland (ZET,EM), and Laboratory of Neuromorphology, Department of Anatomy, Histology and Embryology, Semmelweis University and the Hungarian Academy of Sciences, Budapest, Hungary (ZET)

SUMMARY After immunohistochemistry (IHC) began to be used routinely, a number of investigators worked on methods for staining multiple molecules in the same tissue sections or cells. Achieving this goal was not easy, however. One reason for this is that the majority of primary antibodies used in IHC reactions are raised in rabbits, and recognizing signals from two different rabbit antibodies is not trivial. Thus, all of the protocols described to date have serious limitations. Here we report a simple, quick, and inexpensive solution to the problem. It has two major advantages over existing methods. First, by using antibodies from the same host, two or more antigens can be visualized in the same section with commercially available fluorescent dyes. Second, because the technique relies on signal amplification, both rare and abundant antigens can be detected. **(J Histochem Cytochem 55:545–554, 2007)**

KEY WORDS
immunohistochemistry
multiple antigens
multiplex detection
tyramide signal amplification

During the last three decades, immunohistochemistry (IHC) has been an invaluable tool for localizing different proteins in cells and cellular compartments. Antibodies are also used routinely to visualize specific DNA and RNA species in cells without the need for preparing radioactive probes. Currently available techniques are quite sensitive, and reagents now marketed potentially allow one to detect multiple molecules in the same section (see Mayer and Bendayan 2001). Multiplex detection, however, typically requires primary antibodies raised in two or more different species, and the majority of commercial antibodies are made in rabbits because this is easy and cost effective. When tyramide signal amplification (TSA) was introduced, it increased the sensitivity of IHC and also made it possible to use two antibodies from the same species to stain two separate molecules (Hunyady et al. 1996). The method that we described in that paper for double staining is reliable, but when both antigens are rare and both signals need to be enhanced it could not be used. Thus, we looked for an easy, inexpensive, and reproducible way to detect as many different rare target molecules as one can separate by fluorescent spectra in tissue sections. Microwaving the sections before each procedure allowed us to achieve this goal.

Correspondence to: Zsuzsanna E. Tóth, CSDB, NIDCR, NIH, Bethesda, MD 20892-2190. E-mail: tothzs@ana.sote.hu

Received for publication October 27, 2006; accepted January 5, 2007 [DOI: 10.1369/jhc.6A7134.2007].

Materials and Methods

Animals

Adult male mice and rats were terminally anesthetized and perfused transcardially with 4% paraformaldehyde. Ileums and brains were removed and submerged in 10% and then 20% sucrose solutions (15–18 hr each). This served to cryoprotect the tissues, which were next quickly frozen on dry ice, wrapped in aluminum foil, and stored at −80C until they were sectioned. Ten-μm-thick sections were cut in a cryostat, thaw mounted on Super Colorfrost/Plus slides (Fisher Scientific; Pittsburgh, PA), and kept at −80C until they were stained.

Microwave Treatment (MWT) and IHC

MWT for Double IHC. Slides were placed flat on the bottom of a plastic container (12 × 9 × 6 cm) filled with 200 ml of 10 mM citric acid buffer, pH 6.0. An 800-W household microwave oven was used to first bring the liquid to the boiling point (~2.5 min) at 100% power, and then the sections were microwaved for an additional 5 min at 50% power. Slides were allowed to cool in the citric acid buffer for 30 min at room temperature and then rinsed with 1X PBS.

Endogenous Peroxidase Activity. Because TSA is based on a chemical reaction catalyzed by peroxidase (HRP) enzyme, it is essential to be sure that there is no tissue-derived (endogenous)

0022-1554/07/$3.30

HRP activity that would result in a nonspecific reaction. To make sure that we could visualize and eliminate such activity, we used rat small intestine as a test tissue because white blood cells in the lamina propria are well known for exhibiting HRP activity that is very hard to block (Hunyady et al. 2000). Sections of perfused rat ileum were washed three times for 3 min each in PBS and then one time in Tris–HCl, pH 8.0. Endogenous peroxidase activity was visualized with a DAB reaction using reagents from the SuperPicture HRP Polymer conjugate rabbit primary (DAB) kit (cat. #87-9263; Zymed Laboratories, South San Francisco, CA). HRP activity in the tissue could be eliminated by microwaving sections for ~2.5 min in 10 mM citric acid buffer, pH 6.0, at 100% power (until the liquid starts to boil) and then letting the slides cool in the same buffer for 30 min at room temperature.

IHC. Coronal sections at the levels of the hypothalamus and striatum of mouse and rat brains were stained. Slides were washed three times (for 3 min each) in PBS and subsequently incubated for 10 min in a 1X Universal Blocking Reagent (Biogenex; San Ramon, CA). They were then rinsed with distilled water and incubated in the primary antibody. All antibodies were diluted to working concentrations in PBS containing 1% BSA and 0.25% Triton X-100. When the TSA reaction was performed later, endogenous peroxidase activity was blocked by traditional 15-min incubation in a 3% hydrogen peroxide solution for comparison purposes with sections that underwent MWT. For detection we used a variety of reagents described below. Between incubations we washed the sections three times in PBS (3 min per wash). The following staining methods were used.

Testing the Effect of MWT on Fluorescence Intensity of a Previous Staining (Vasopressin Neurophysin IHC). The primary antibody, PS 41, diluted to 1:50 (mouse monoclonal provided by H. Gainer; NIH, Bethesda, MD) was applied for 1 hr at room temperature and developed using three different techniques. In the first two techniques, an affinity-purified anti-mouse IgG antibody was used that was conjugated to either an AlexaFluor 488 (1:1000, donkey; Invitrogen, Carlsbad, CA) or to a biotin-SP (1:1000, donkey; Jackson ImmunoResearch Laboratories, West Grove, PA). The latter was then visualized with AlexaFluor 488 conjugated to streptavidin (1:1000; Invitrogen). All incubations were performed for 1 hr at room temperature. A third technique utilized the SuperPicture HRP Polymer conjugate for mouse primary antibodies (Zymed Laboratories). The conjugate was applied to sections undiluted for 30 min at room temperature, followed by a Tyramide-FITC (cat. #SAT701B001EA, TSA Fluorescein Tyramide Reagent Pack; PerkinElmer Life and Analytical Sciences, Boston, MA) reaction according to the manufacturer's instructions.

Testing the Ability of MWT to Eliminate Cross-reactivity Between IgGs Raised in the Same Host. For these tests, double IHC was used with a microglia-specific antibody (Iba) in combination with either tyrosine hydroxylase (TH) or orexin (Figure 1). Duplicate slides were prepared for primary incubations to compare treatments. Sections were incubated first in anti-Iba (1:1000, rabbit; Chemicon, Temecula, CA) overnight at 4C, then in biotin-SP-conjugated anti-rabbit IgG raised either in donkey (1:1000; Jackson ImmunoResearch Laboratories) for the double staining with TH (1:500, rabbit;

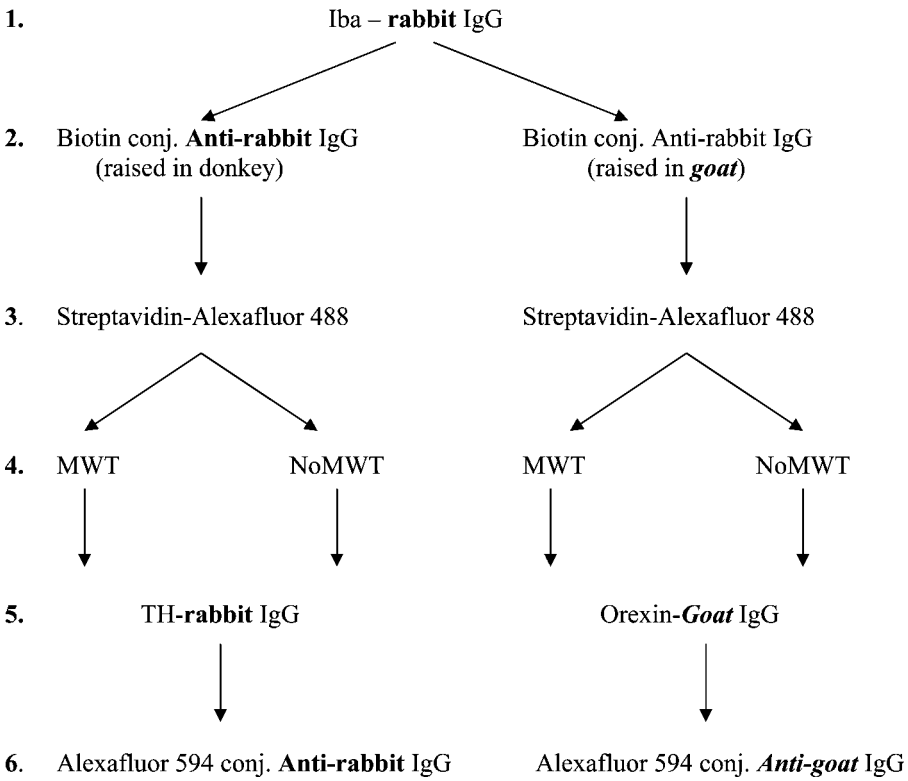

Figure 1 Step by step illustration of the method applied to test the effect of microwave treatment (MWT) on fluorescent double immunostainings performed using antibodies raised in the same species. The potential cross-reactivity problems that might result in false colocalization signals are indicated by bold characters. Iba: microglial marker, TH: tyrosine hydroxilase.

Chemicon) or in goat (1:1000; Vector Laboratories, Burlingame, CA) for double staining with orexin (1:50, goat; Santa Cruz Biotechnology, Santa Cruz, CA) for 1 hr at room temperature. Next, slides were incubated in AlexaFluor 488-conjugated streptavidin (1:1000; Invitrogen) for 1 hr at room temperature. One group of slides was microwave treated before applying the anti-TH or the anti-orexin primary antibodies overnight at 4C. The second stainings were visualized by AlexaFluor 594-conjugated anti-rabbit IgG (1:1000, goat; Invitrogen) and anti-goat IgG (1:500, donkey; Invitrogen) secondary antibodies for 1 hr at room temperature, respectively.

Testing the Effect of MWT When Amplifying Both Signals and Using Antibodies From the Same Host. Double IHC was performed using a combination of a neuronal-specific nuclear antibody, NeuN, and a TH antibody (Figure 2). The anti-NeuN (1:200, mouse; Chemicon) was applied for 1 hr at room temperature, followed by incubation in SuperPicture HRP Polymer conjugate for mouse primary antibodies (Zymed Laboratories) and AlexaFluor 594-Tyramide (Invitrogen). After the first immunostaining, one group of slides was microwave treated. Slides were then incubated in anti-TH primary antibody (1:1000, mouse; Incstar Corporation, Stillwater, MN) for 1 hr at room temperature. The second immunostaining was developed again using the SuperPicture HRP Polymer conjugate for mouse primary antibodies, and FITC-Tyramide (PerkinElmer) was used as the fluorochrome for visualization.

A combination of TH, the rate-limiting enzyme in catecholamine biosynthesis (an accepted marker of dopaminergic neurons) and GFAP (an astrocyte-specific marker) was used to perform double IHC (Figure 3). For the first immunostaining, an anti-TH antibody was used here that was raised in rabbit (1:500; Chemicon) and an HRP-conjugated anti-rabbit IgG (1:100, goat; Vector Laboratories) was used as a secondary antibody (1 hr and 2 hr incubations at room temperature, respectively). Staining was then developed by FITC-Tyramide according to the manufacturer's instructions. After MWT, an anti-GFAP antibody (1:500; Dako, Carpinteria, CA) that was also raised in rabbit was applied for 1 hr at room temperature. Secondary detection was the same as for the TH immunostaining, except that AlexaFluor 594-Tyramide (Invitrogen) was used for the visualization.

To demonstrate the power of the technique, we performed a triple immunostaining using same host (rabbit) antibodies. Vasopressin, CRF, and TH immunostaining were performed on the same section from colchicine-treated mouse (Figure 4). Vasopressin antibody (VA4, rabbit) (Alstein et al. 1988) was used at a 1:1000 dilution for 2 hr, the anti-TH antibody (rabbit, cat. #AB 151; Chemicon) was used at 1:500 for 1 hr, and the anti-CRF (a gift from Wylie Vale) (Sawchenko and Swanson 1981) was used at 1:5000 for 3 hr, all at room temperature. Endogenous peroxidase blocking was performed after the incubation with the first primary (vasopressin) antibody. Immunostainings were developed using SuperPicture HRP Polymer conjugate for rabbit primary antibodies (Zymed Laboratories), FITC-Tyramide (PerkinElmer) for the vasopressin, AlexaFluor 568-Tyramide for the CRF, and CY5-Tyramide for the TH (all from PerkinElmer). We applied a MWT step after each immunostaining.

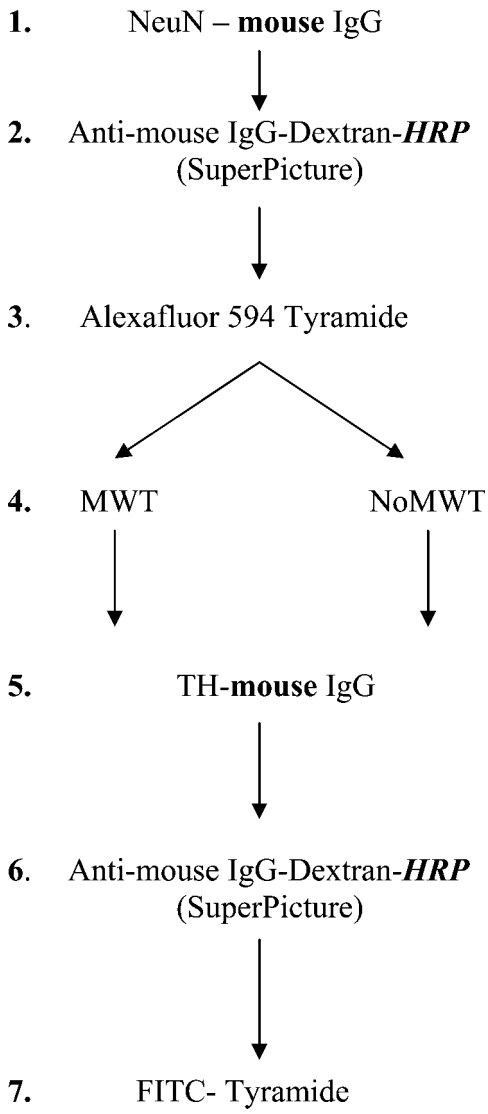

Figure 2 Step by step illustration of the method applied to test the effect of MWT on NeuN (neuronal cell marker) and TH fluorescent double immunostaining performed using primary antibodies from the same host animals (mouse) and amplification of the signals. We used the same anti-mouse HRP Polymer conjugate (SuperPicture) as secondary antibody for both stainings. The potential species and peroxidase enzyme (HRP) cross-reactivity problems that might result in false colocalization signals are indicated by bold characters.

All immunostainings were evaluated using a conventional inverted Leica microscope (DMI 6000B; Leica, Wetzlar, Germany) equipped with the appropriate fluorescent filter cubes (A4, TX2, and L5) using an EXFO illumination system (EXFO; Mississauga, Ontario). The microscope is driven by an Apple computer (G4; Apple, Cupertino, CA) using Volocity software (Improvision Inc.; Lexington, MA) for image capturing.

Results

MWT as described above completely eliminates endogenous peroxidase activity in the rat ileum (Figure 5).

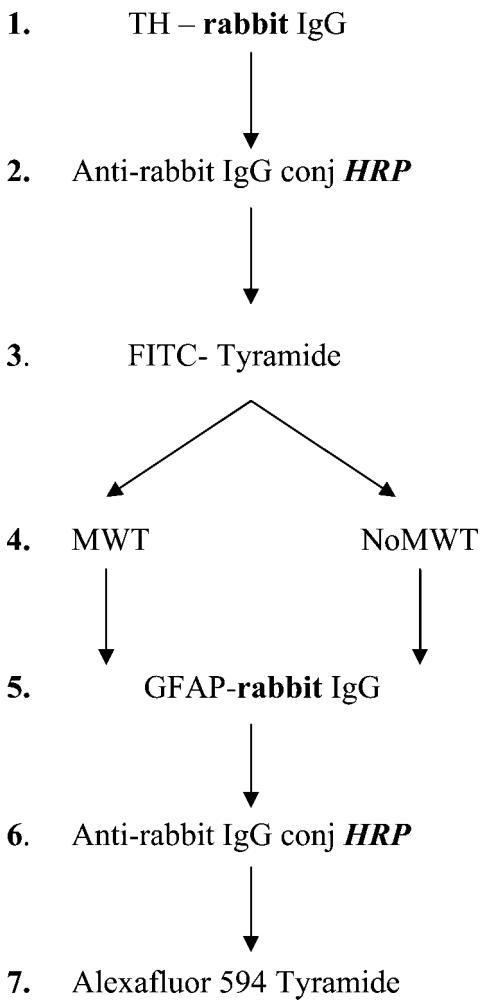

Figure 3 Step by step illustration of the method applied to test the effect of MWT on TH and GFAP (astrocyte-specific marker) fluorescent double immunostaining performed by using primary antibodies from the same host animals (rabbit) and amplification of the signals. We used the same HRP-conjugated anti-rabbit IgG as secondary antibody for both stainings. The potential species and peroxidase enzyme (HRP) cross-reactivity problems that might result in false colocalization signals are indicated by bold characters.

Without MWT, many cells (shown by arrows) are stained by DAB (Figure 5A). After the section has been microwaved, there is no remaining HRP activity as demonstrated by the complete lack of reactive cells in Figure 5B.

When using fluorescent secondary antibodies, we found that subsequent MWT significantly reduces the intensity of the fluorochrome conjugates. The effect of MWT on different kinds of fluorescent conjugates is shown in Figures 6A–6F. Vasopressin-associated neurophysin immunostaining was performed in mouse supraoptic nuclei using different dyes. In coronal brain sections, vasopressin–neurophysin gives a bright green signal when AlexaFluor 488-conjugated secondary anti-

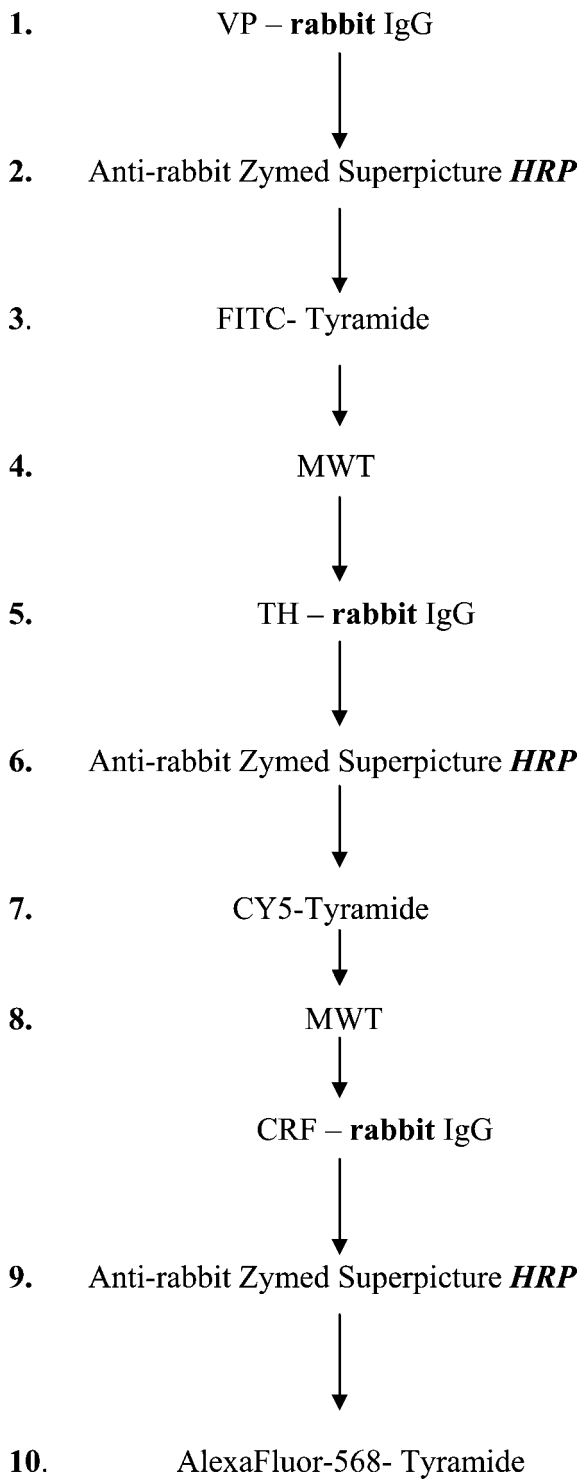

Figure 4 Step by step illustration of the method applied to test the effect of MWT on a fluorescent triple immunostaining performed by using primary antibodies from the same host animals (rabbit) and amplification of the signals by using the same HRP-conjugated anti-rabbit IgG as secondary antibody. The potential species and peroxidase enzyme (HRP) cross-reactivity problems that might result in false colocalization signals are indicated by bold characters.

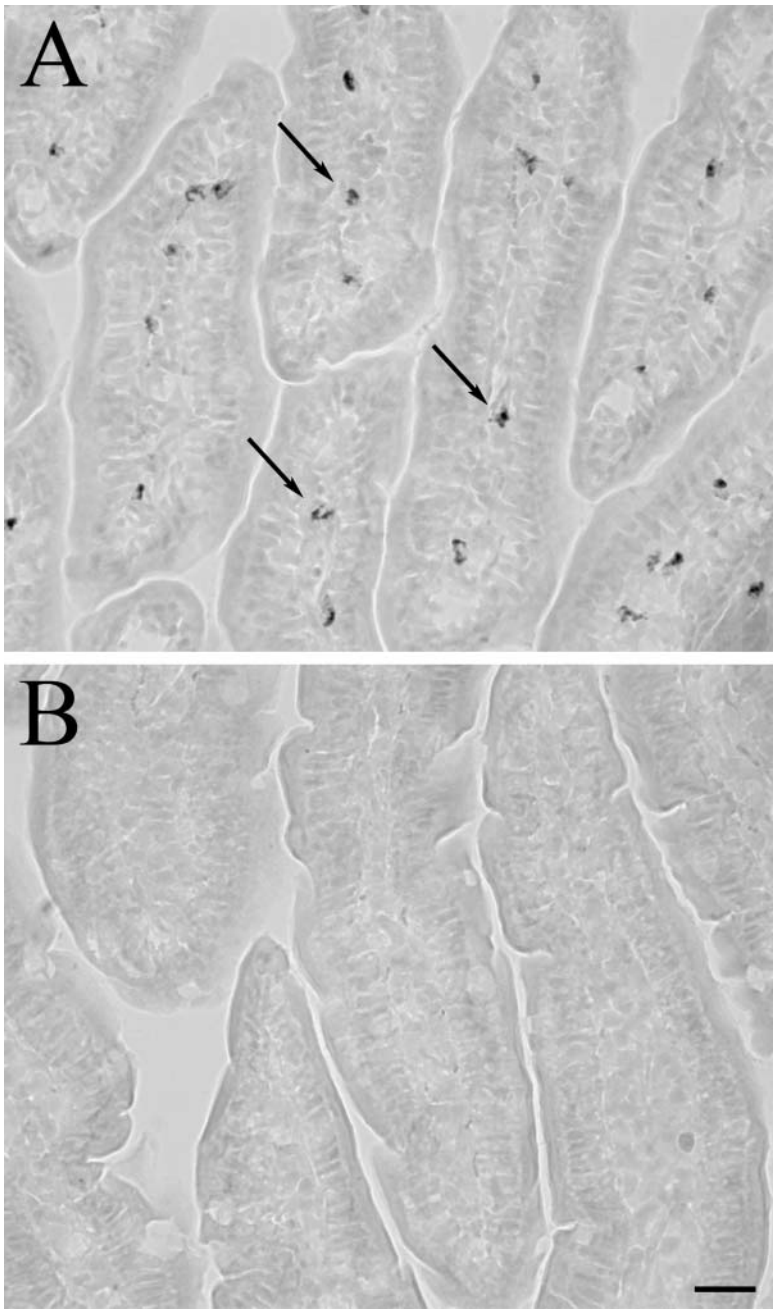

Figure 5 MWT eliminates endogenous peroxidase activity. (**A**) DAB reaction products on a rat ileum section without blocking endogenous peroxidase activity. Many cells (arrows) expressing peroxide–enzyme are stained. (**B**) DAB reaction performed on a section previously microwave treated in 10 mM citric acid buffer. No reaction product can be seen. Bar = 25 μm.

body is used (Figure 6A). Intensity of the fluorescent staining, however, is not preserved following MWT (Figure 6B). Staining with the same primary antibody as in Figure 6A and using biotinylated secondary antibody followed by an AlexaFluor 488-conjugated streptavidin results in a bright staining (Figure 6C) that is significantly diminished, but still clearly visible after MWT (Figure 6D). In Figure 6E, the vasopressin–neurophysin immunostaining is detected by a HRP-conjugated secondary antibody, and FITC-conjugated tyramide is then used as a substrate. In this case, the MWT (Figure 6F) does not affect the intensity of the fluorescence signal.

In a double-immunostaining procedure, a coronal section across the rat striatum was first stained with a microglial marker (Iba), and the staining was developed with streptavidin AlexaFluor 488 (green). The second primary antibody was directed against TH and visualized with anti-rabbit AlexaFluor 594 (red). Both primary antibodies were raised in rabbit. As shown in Figure 7A, the anti-rabbit AlexaFluor 594 antibody recognizes both the rabbit anti-Iba and the rabbit anti-TH

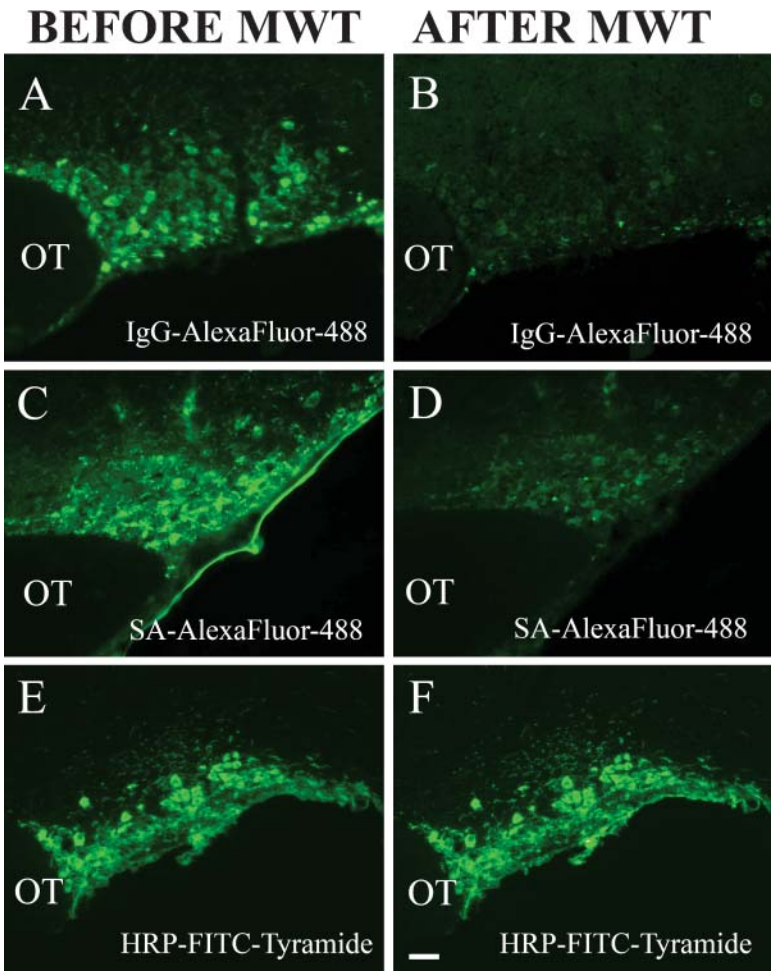

Figure 6 Effect of MWT on different types of fluorescent conjugates. (**A–F**) Vasopressin immunostaining of mouse supraoptic nuclei. Coronal brain sections. Intensity of the fluorescent staining is differently preserved following MWT depending on the detection system used. (**A,B**) Vasopressin immunofluorescence staining using AlexaFluor 488-conjugated secondary antibody, before (**A**) and after (**B**) microwaving. Most of the signal disappears. (**C,D**) Staining with the same primary antibody as in **A** detected by using biotinylated secondary antibody and AlexaFluor 488-conjugated streptavidin. MWT (**D**) reduces the signal compared with the control (**C**) but is still clearly visible. (**E,F**) Vasopressin immunostaining detected by HRP-conjugated secondary antibody and FITC-conjugated tyramide. MWT (**F**) does not affect the intensity of the fluorescence signal. OT, optic tract. Bar = 100 μm.

antibodies. If MWT is used after the Iba staining reactions are performed (Figure 7B), there is no false Iba/TH colocalization signal, and the green microglia (Iba positive) is clearly separated from the red dopaminergic (TH-positive) labeling. In our experience, swapping the order of the antibodies does not affect the staining intensity for either antigen (data not shown). Next, a double staining was performed with two primary antibodies raised in different species (Iba raised in rabbit and developed with a biotinylated secondary antibody followed by streptavidin AlexaFluor 488 and orexin raised in goat and developed using an anti-goat IgG conjugated to AlexaFluor 594). Even though the two primary antibodies were made in different species, we still saw a false double labeling of cells (arrows in Figure 7C). The false staining in this case is caused by the secondary goat antibody used for the detection of Iba, which is bound by the anti-goat AlexaFluor 594 that is meant to visualize orexin. If MWT is used after the first staining sequence, the Iba (green) and orexin (red) dyes give separate signals; thus, MWT prevents the nonspecific labeling (Figure 7D).

In the third series of double immunostainings, we used a mouse monoclonal antibody that recognizes a neuronal-specific nuclear antigen (NeuN) and a rabbit anti-TH antibody (TH is the rate-limiting enzyme in catecholamine biosynthesis and is an accepted marker of dopamine-making cells). After the primary NeuN incubation, an anti-mouse SuperPicture was used to introduce HRP enzyme at the antigenic site. This was followed by the addition of AlexaFluor 594-Tyramide as a substrate. Next, the second primary incubation (TH) was performed followed again by the same anti-mouse SuperPicture as for the NeuN, and the reaction was finished by the addition of FITC-Tyramide as a substrate. The TH staining gives false colocalization signal with the NeuN staining (yellow cell nuclei) in Figure 8A, because the HRP enzyme that catalyzed the first tyramide reaction (red) was still capable of binding the second tyramide substrate (green) and because of the species crossreactivity. The MWT after the first sequence of reactions inactivated the HRP enzyme in the SuperPicture reagent and made it possible to perform a second consecutive peroxidase reaction without any

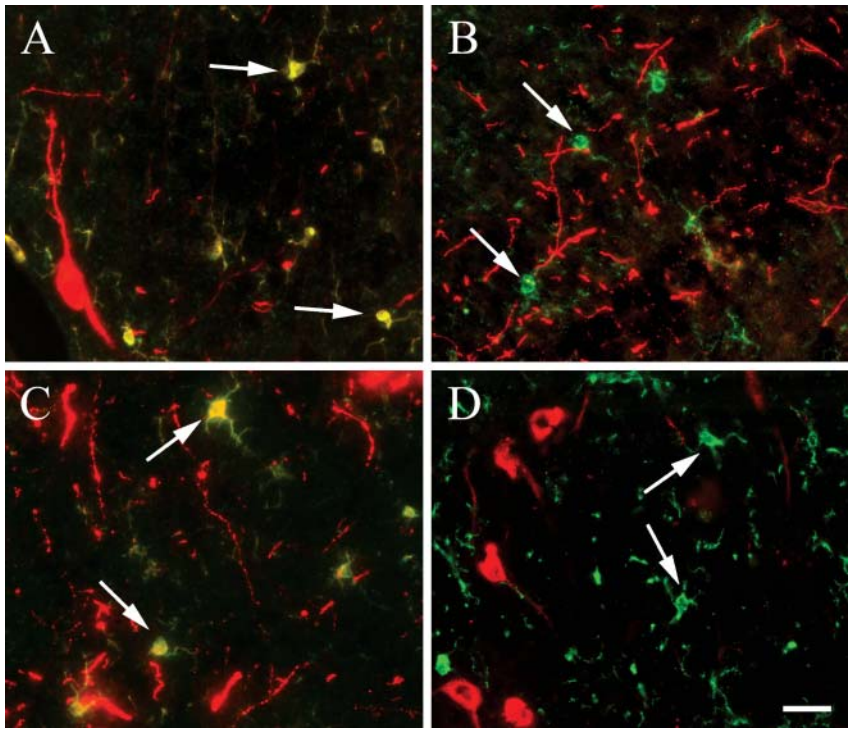

Figure 7 Double fluorescence immunostaining using antibodies from same host. (**A**) Double immunostaining for microglial marker (Iba) (green, streptavidin AlexaFluor 488) and TH (red, anti-rabbit AlexaFluor 594). Both primary antibodies were raised in rabbit. The anti-rabbit antibody used for detecting the second staining binds to the free sites of the first primary antibody giving a false (yellow) colocalization signal (arrows). (**B**) Same staining as in **A**, using MWT after the first staining. There is no false colocalization signal; microglia is green (arrows) and dopamine fibers are red. (**C**) Double immunostaining for microglial marker (Iba), (green, streptavidin AlexaFluor 488) and orexin (red, anti-goat AlexaFluor 594). For the Iba detection biotinylated anti-rabbit secondary antibody was used that was made in goat. The second staining gives false positive signal because the anti-goat antibody binds to the secondary antibody of the first staining (yellow cells, arrows). (**D**) Iba (green cells, arrows) and orexin (red) double staining give separate labelings when MWT was used between the two stainings. Coronal brain sections from rat. Bar = 100 μm.

sign of cross-reactivity. There is a nice separation of red nuclei (neurons) and green fibers (TH) in the striatum (Figure 8B). When two anti-rabbit antibodies were used (GFAP and TH) in the same section, and both stainings were amplified using different color tyramide substrates, the MWT following the first staining completely eliminated the cross-reactivity between the two detection sequences (Figure 8C). Dopaminergic neuronal fibers are shown in green (TH staining, FITC-Tyramide), and astroglia are shown in red (GFAP staining, AlexaFluor 594-Tyramide). Finally, to demonstrate the efficiency of the technique we performed a triple immunolabeling in the mouse hypothalamus where all three antibodies were made in rabbit, and HRP-based amplification was used three times – all in the same section and all done in 1 day. All three stainings show a distinct individual pattern characteristic to vasopressin (Figure 9A), CRF (Figure 9B), and TH (Figure 9C).

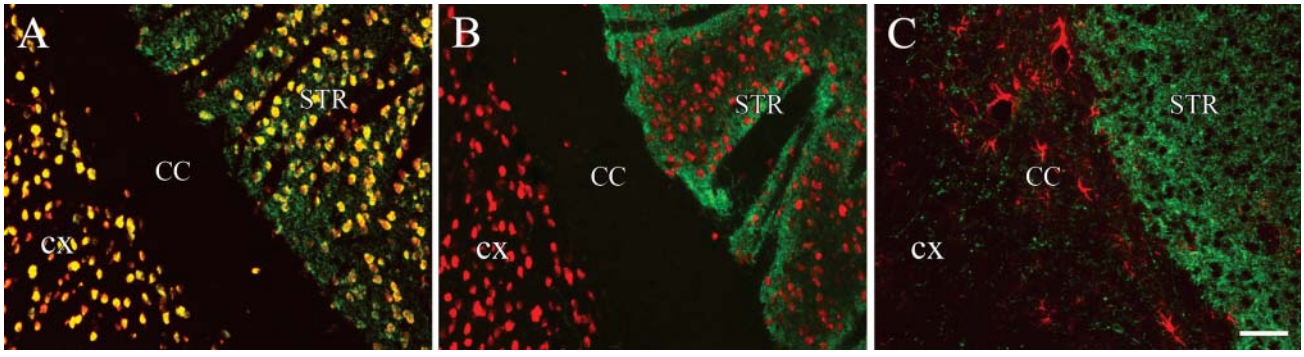

Figure 8 MWT for double stainings with amplification of the signals. (**A,B**) Double staining for neuronal marker, NeuN, red, AlexaFluor 594-Tyramide and TH, green, FITC-Tyramide. TH staining gives false colocalization signal with the NeuN staining (yellow cell nuclei) in **A** because the HRP enzyme that catalyzed the first tyramide reaction also worked for the second tyramide reaction and because of the species cross-reactivity. MWT inactivates the HRP enzyme and makes it possible to perform a second peroxidase reaction without getting any cross-reaction (**B**). (**C**) Double staining using two primary antibodies raised both in rabbit and double amplification (anti-rabbit-HRP and tyramide reaction). Dopaminergic neuronal fibers are shown in green (TH staining, FITC-Tyramide), astroglia are shown in red (GFAP staining, AlexaFluor 594-Tyramide). MWT was used between the stainings. No cross-reaction is present. Coronal (**A,B**) or sagittal (**C**) sections from mouse brain. CX, cortex; CC, corpus callosum; STR, striatum. Bar = 100 μm.

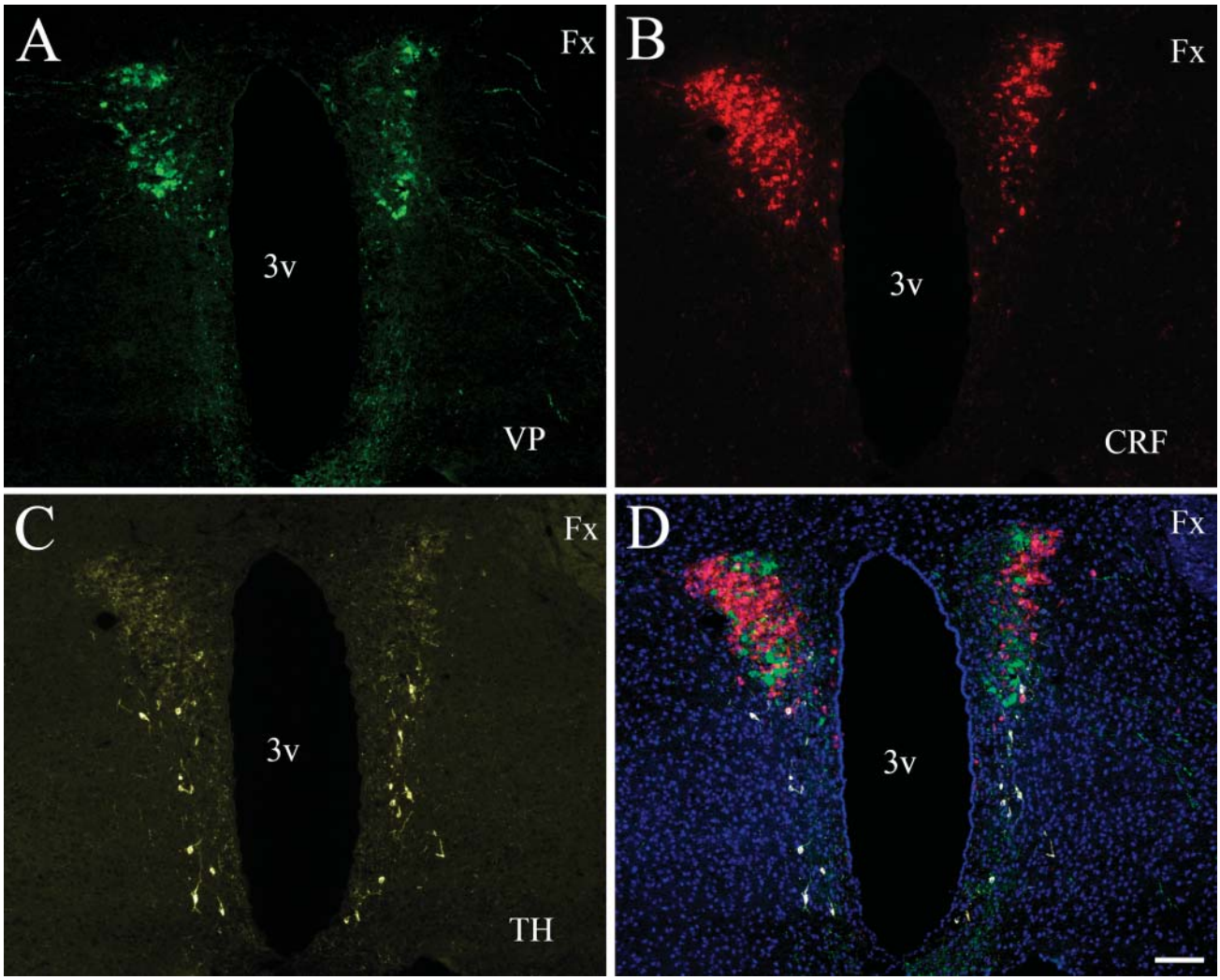

Figure 9 Triple immunostaining using same host antibodies. A section of the mouse hypothalamic paraventricular nucleus is shown where cells were immunostained for vasopressin (**A**) visualized with FITC (green), for CRF (**B**) visualized with AlexaFluor 568 (red) and for TH (**C**) visualized with CY5 colorized in yellow. The overlay of the three stainings is demonstrated in (**D**) where all cell nuclei are stained with DAPI, a chromosomal stain. Bar = 100 μm. Fx, fornix; 3v, third ventricle.

There is no nonspecific staining observed when the three labels are overlaid (Figure 9D).

Discussion

Use of the microwave oven as a histological tool was introduced in the early 1990s (Leong 1996; Shin et al. 2002) and involved many histological procedures such as tissue fixation, demineralization, in situ hybridization, and immunocytochemistry (Shin et al. 2002; Emerson et al. 2006; Tesch et al. 2006). Many antibodies and conditions were tested, and the major advantage of the use of microwave technology seemed to be the speed of the procedures enabling significantly faster results in human diagnostics during surgical procedures or routine laboratory work (Cuevas et al. 1994; Brown and Chirala 1995; McMahon and McQuaid 1996; Sperry et al. 1996; Munoz et al. 2004; Ridderstrale et al. 2005). A special advantage of the microwave antigen retrieval that seemed to be very useful in human pathology was the ability of using archived paraffin sections from autopsy cases. These tissues were usually very hard to work with because of the significant loss of antigenicity due to high temperatures of the paraffin-embedding procedure as well as the overfixation of these tissues by immersion in high percentage of formaldehyde (for months to years) in routine pathology (Cuevas et al. 1994; Leong 1996; Bohle et al. 1997; Bull and Harnden 1999; Relf et al. 2002; Kitayama 2005; Tesch et al. 2006). Microwave pretreatment was not only useful for immunocytochemistry but also for tissue pretreatment prior to

in situ hybridization histochemistry (McMahon and McQuaid 1996; Sperry et al. 1996; Bull and Harnden 1999; Relf et al. 2002; Ridderstrale et al. 2005). We wondered if MWT could also be used to help us perform double labeling of the same sections with two (or more) antibodies that were raised in the same host. Several methods have been used to achieve this goal. The first such technique used elution of the first antibody–peroxidase complex after the water-insoluble DAB precipitate has formed (Nakane 1968). This technique includes an acid wash to remove the first antibody and is likely to cause deterioration in the quality of the tissue. Another method used immunostaining of two thin adjacent sections with the respective antibodies to try to superimpose the images to find the cells that reacted with both antibodies (Weber et al. 1982; Wolter 1985). This technique is not easy to perform and has a limitation based on section thickness and cell size (the smaller the cells the more difficult to find matching cells). Another technique was to use a secondary polyclonal monovalent F(ab) antibody after the first staining to block the excess sites from the first primary antibody. This would prevent the second secondary antibody from binding to the first primary antibody (that is from the same host). Then one can proceed to incubate with the second primary antibody followed by a secondary antibody (Negoescu et al. 1994). This technique requires very careful control experiments and is difficult and time-consuming.

Heat treatment was also suggested to denature immunoglobulins, even before MWT became available (Kolodziejczyk and Baertschi 1986). This protocol used excessive heat (130C) to remove the immunoglobulins after pictures of a staining were taken. Then a new staining was performed and new pictures were taken and compared with the first set of images. Although the technique worked reliably, there were several drawbacks. Five to seven days of tissue protection (to preserve structure in the face of excessive heat) were needed between the different stainings. Another difficulty is that it is not always easy to predict where pictures should be taken from for colocalization with a subsequent antigen. When the TSA technique became widely used in IHC, we published a protocol that utilized the sensitivity of the TSA technique to double label in the same section with two antibodies from the same host. This protocol uses a very dilute primary antibody that is not recognized by a simple secondary antibody, but can be visualized using TSA. The other primary antibody is then used at regular working dilution and is detected by a secondary antibody—without amplification (Hunyady et al. 1996). This method also needs very careful design; the optimal dilution for the first primary antibody needs to be titrated accurately and will be different for every unique antibody. Furthermore, if both antigens are rare and both need to be amplified, the technique cannot be used.

Lan et al. (1995) suggested the use of microwave to denature already bound antibody molecules to use two primary antibodies and detect nuclear and cytoplasmic antigens using alkaline phosphatase and HRP enzymatic visualization. Tornehave et al. (2000) suggested the use of microwave for double labeling and suggested that moderate microwaving does not elute antibodies that bind, but rather prevents them from binding to subsequently applied reagents. These authors suggested microwaving between the first and second staining cycles to enable double-indirect immunofluorescence staining when the antibodies used are raised in the same species. Later, however, serious questions were raised about the ability of MWT to completely abolish contaminating staining (Bauer et al. 2001). Furthermore, the loss of fluorescence due to the MWT was also not addressed in the above studies. Our protocol takes advantage of the TSA technique at several levels. First, using TSA enables detection of very rare antigens. Second, due to the very high amounts of fluorochrome binding to the peroxidase enzyme, fluorescent intensity is not affected by the MWT. Because the tyramide–fluorochrome complex is insoluble in water, once the deposit forms, the product is very stable and the tissue can be microwaved long enough to disrupt all protein bonds as well as to block endogenous and also intentional (i.e., included in the reagents that we use intentionally) peroxidase activity in the tissue. The technique is fast and easy to perform, and using the SuperPicture complex significantly increases sensitivity. The procedure is fast, can be repeated as many times as needed, and only the tyramide–fluorochrome complex will remain at the antigenic site. Several spectrally non-overlapping fluorochromes could be used in the same section for conventional or confocal fluorescent analysis. This protocol eliminates the problems with double-staining techniques used currently and due to its sensitivity can be used in fluorescent staining procedures to detect a variety of rare antigens.

Acknowledgments

This research was supported by the Division of Intramural Research, National Institute of Dental and Craniofacial Research, Intramural Research Programs, National Institutes of Health. Z.E.T. is supported by OTKA T-043169.

Literature Cited

Alstein M, Whitnall MH, House S, Key S, Gainer H (1988) An immunochemical analysis of oxytocin and vasopressin prohormone processing in vivo. Peptides 9:87–105

Bauer M, Schilling N, Spanel-Borowski K (2001) Limitation of microwave treatment for double immunolabelling with antibodies of the same species and isotype. Histochem Cell Biol 116:227–232

Bohle RM, Bonczkowitz M, Altmannsberger HM, Schulz A (1997) Immunohistochemical double staining of microwave enhanced and nonenhanced nuclear and cytoplasmic antigens. Biotech Histochem 72:10–15

Brown RW, Chirala R (1995) Utility of microwave-citrate antigen retrieval in diagnostic immunohistochemistry. Mod Pathol 8:515–520

Bull JH, Harnden P (1999) Efficient nuclear FISH on paraffin-embedded tissue sections using microwave pretreatment. Biotechniques 26:416–418, 422

Cuevas EC, Bateman AC, Wilkins BS, Johnson PA, Williams JH, Lee AH, Jones DB, et al. (1994) Microwave antigen retrieval in immunocytochemistry: a study of 80 antibodies. J Clin Pathol 47: 448–452

Emerson LL, Tripp SR, Baird BC, Layfield LJ, Rohr LR (2006) A comparison of immunohistochemical stain quality in conventional and rapid microwave processed tissues. Am J Clin Pathol 125:176–183

Hunyady B, Krempels K, Harta G, Mezey E (1996) Immunohistochemical signal amplification by catalyzed reporter deposition and its application in double immunostaining. J Histochem Cytochem 44:1353–1362

Hunyady B, Mezey E, Palkovits M (2000) Gastrointestinal immunology: cell types in the lamina propria—a morphological review. Acta Physiol Hung 87:305–328

Kitayama Y (2005) Modified fluorescence in situ hybridization methods using pathology archives. Neuropathology 25:269–273

Kolodziejczyk E, Baertschi AJ (1986) Multiple immunolabeling in histology: a new method using thermo-inactivation of immunoglobulins. J Histochem Cytochem 34:1725–1729

Lan HY, Mu W, Nikolic-Paterson DJ, Atkins RC (1995) A novel, simple, reliable, and sensitive method for multiple immunoenzyme staining: use of microwave oven heating to block antibody cross-reactivity and retrieve antigens. J Histochem Cytochem 43:97–102

Leong AS (1996) Microwaves in diagnostic immunohistochemistry. Eur J Morphol 34:381–383

Mayer G, Bendayan M (2001) Amplification methods for the immunolocalization of rare molecules in cells and tissues. Prog Histochem Cytochem 36:3–85

McMahon J, McQuaid S (1996) The use of microwave irradiation as a pretreatment to in situ hybridization for the detection of measles virus and chicken anaemia virus in formalin-fixed paraffin-embedded tissue. Histochem J 28:157–164

Munoz TE, Giberson RT, Demaree R, Day JR (2004) Microwave-assisted immunostaining: a new approach yields fast and consistent results. J Neurosci Methods 137:133–139

Nakane PK (1968) Simultaneous localization of multiple tissue antigens using the peroxidase-labeled antibody method: a study on pituitary glands of the rat. J Histochem Cytochem 16:557–560

Negoescu A, Labat-Moleur F, Lorimier P, Lamarcq L, Guillermet C, Chambaz E, Brambilla E (1994) F(ab) secondary antibodies: a general method for double immunolabeling with primary antisera from the same species. Efficiency control by chemiluminescence. J Histochem Cytochem 42:433–437

Relf BL, Machaalani R, Waters KA (2002) Retrieval of mRNA from paraffin-embedded human infant brain tissue for non-radioactive in situ hybridization using oligonucleotides. J Neurosci Methods 115:129–136

Ridderstrale KK, Grushko TA, Kim HJ, Olopade OI (2005) Single-day FISH procedure for paraffin-embedded tissue sections using a microwave oven. Biotechniques 39:316,318,320

Sawchenko PE, Swanson LW (1981) A method for tracing biochemically defined pathways in the central nervous system using combined fluorescence retrograde transport and immunohistochemical techniques. Brain Res 210:31–51

Shin M, Hishikawa Y, Izumi S, Koji T (2002) Southwestern histochemistry as a molecular histochemical tool for analysis of expression of transcription factors: application to paraffin-embedded tissue sections. Med Electron Microsc 35:217–224

Sperry A, Jin L, Lloyd RV (1996) Microwave treatment enhances detection of RNA and DNA by in situ hybridization. Diagn Mol Pathol 5:291–296

Tesch GH, Lan HY, Nikolic-Paterson DJ (2006) Treatment of tissue sections for in situ hybridization. Methods Mol Biol 326:1–7

Tornehave D, Hougaard DM, Larsson L (2000) Microwaving for double indirect immunofluorescence with primary antibodies from the same species and for staining of mouse tissues with mouse monoclonal antibodies. Histochem Cell Biol 113:19–23

Weber E, Roth KA, Barchas JD (1982) Immunohistochemical distribution of alpha-neo-endorphin/dynorphin neuronal systems in rat brain: evidence for colocalization. Proc Natl Acad Sci USA 79: 3062–3066

Wolter HJ (1985) Corticotropin-releasing factor: immunohistochemical colocalization with adrenocorticotropin and beta-endorphin, but not with Met-enkephalin, in subpopulations of duodenal perikarya of rat. Biochem Biophys Res Commun 128:402–410

The Journal of Histochemistry & Cytochemistry

available at www.sciencedirect.com

ScienceDirect

www.elsevier.com/locate/yexcr

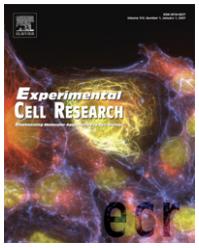

Research Article

Sensitive detection of GFP utilizing tyramide signal amplification to overcome gene silencing

Zsuzsanna E. Toth[a,b], *Tal Shahar*[c], *Ronen Leker*[c,e], *Ildiko Szalayova*[a], *András Bratincsák*[d], *Sharon Key*[a], *Anna Lonyai*[c], *Krisztián Németh*[a,f], *Éva Mezey*[a,*]

[a]*CSDB, NIH, NIDCR, Building 49, Room 5A-76, 49 Convent Drive, Bethesda, MD 20892, USA*
[b]*Laboratory of Neuromorphology of the Semmelweis University and the Hungarian Academy of Sciences, H-1094 Budapest, Hungary*
[c]*NINDS, NIH, Bethesda, MD, USA*
[d]*NIMH, NIH, Bethesda, MD, USA*
[e]*Stroke Service and The Cerebrovascular Disease Research Laboratory, Hebrew University Hadassah Medical Center, Jersusalem, Israel*
[f]*Department of Dermato-Venereology and -Oncology, Semmelweis University, H-1085 Budapest, Maria u. 41., Hungary*

ARTICLE INFORMATION

Article Chronology:
Received 11 December 2006
Revised version received
24 February 2007
Accepted 28 February 2007
Available online 12 March 2007

Keywords:
Hematopoetic stem cell
Stem cell transplantation
Lineage tracking
Green fluorescent protein
Immunohistochemistry
Cell fate

ABSTRACT

The green fluorescent protein (GFP) is among the most commonly used expression markers in biology. GFP-tagged cells have played a particularly important role in studies of cell lineage. Sensitive detection of GFP is crucially important for such studies to be successful, and problems with detection may account for discrepancies in the literature regarding the possible fate choices of stem cells. Here we describe a very sensitive technique for visualization of GFP. Using it we can detect about 90% of cells of donor origin while we could only see about 50% of these cells when we employ the methods that are in general use in other laboratories. In addition, we provide evidence that some cells permanently silence GFP expression. In the case of the progeny of bone marrow stem cells, it appears that the more distantly related they are to their precursors, the more likely it is that they will turn off the lineage marker.

Published by Elsevier Inc.

Introduction

The green fluorescent protein (GFP) was discovered as a by product of isolating aequorin from jelly fish by Shimomura et al. [2] in 1962. The importance of the discovery was not obvious until much later; GFP proved to be an excellent protein marker molecule for gene expression (see [2]). Gradually, immunohistochemical (IHC) detection techniques have become more and more sensitive. We can measure and visualize proteins in amounts that were unimaginable 10 years ago. Numerous studies utilized GFP to track cell fate following bone marrow transplantation, local injection or promoter specific expression [3–10]. While a variety of groups showed that GFP-expressing bone marrow cells are able to seed many tissues and differentiate into tissue specific cells, an equal number of papers failed to confirm those results and

* *Corresponding author*. Fax: +1 301 496 1339.
E-mail addresses: ztoth@mail.nih.gov (Zs.E. Toth), mezeye@mail.nih.gov (É. Mezey).

0014-4827/$ – see front matter. Published by Elsevier Inc.
doi:10.1016/j.yexcr.2007.02.024

stated the opposite [11,12]. One of the factors that seem to affect chimerism is the presence or absence of tissue injury/disease. In normal, healthy tissue circulating bone marrow cells do not seem to contribute to regeneration as much as when the tissue is in "need" [4]. Furthermore, it was noted by several studies that the expression of GFP is variable; in many instances the expression weakens with time or in some cases GFP becomes undetectable [13]. The possibility that the GFP transgene can be silenced has also been raised [14–20]. The field has been plagued by controversy mostly due to differences in techniques used by the different groups to follow cell fate as summarized in [21]. In the last decade a new, very sensitive technique became available utilizing tyramide signal amplification [22,23] and its application to immunohistochemistry was reported [1] describing dilutions of primary antibodies for optimal immunohistochemistry [24] as well as its use in dual immunostaining techniques [25]. Since we also noticed very faint green fluorescent cells in our experimental samples, we decided to apply this technique to attempt to visualize most of the GFP expressing cells. The use of this newly designed, sensitive method might help to clarify the confusion in the literature.

Materials and methods

Animal experiments

Female C57B mice were irradiated using 900 rad in two equal doses (irradiation time was 4 min 15 s each time) 8 h apart. Following the second irradiation, the animals were transplanted with bone marrow from male Z/EG (lacZ/EGFP) double reporter transgenic mice [26] that had previously been crossed with a Cre-actin mouse to result in an animal which ubiquitously and stably express the green fluorescent protein. Donor mice were euthanized by decapitation under anesthesia and the bodies were dipped in 70% ethanol. The skin and lower limb muscles were removed for the exposure and isolation of the femurs. In a sterile tissue culture hood, a cut was made on both ends of the bone and the marrow was flushed out with a 20-G needle filled with 4 ml sterile DMEM. The cells were dissociated by sequentially passing them through 18, 20 and 25 G needles until getting a single cell suspension. For further purification, the cells were spun at 1000 RPM for 8 min and the supernatant was discarded. Cells were resuspended in 2 ml of DMEM and were kept on 4 °C until transplantation (within hours). The irradiated mice received a sterile bone marrow injection through the tail vein with a sterile 27-gauge needle immediately after the second irradiation; an infrared lamp was used to visualize the tail vein accurately. Each mouse received 5×10^6 cells in 0.5 ml of sterile DMEM.

After full recovery, the mice underwent middle cerebral artery occlusion (MCAO) to induce stroke. The distal MCA was electrocoagulated and cut with a technique [27] modified for mouse from Tamamura [28,29]. This procedure causes a large infarct involving cortical zones [30]. Two months after the MCAO, the animals were terminally anesthetized and perfused by 4% buffered paraformaldehyde. The brains were removed and cryoprotected by immersion into sucrose solutions of increasing concentrations (5%, 10% and 20%). Finally, the brains were quickly frozen on powdered dry ice and kept in aluminum foil at −80 °C until they were sectioned.

Immunohistochemistry (IHC) to detect GFP

Ten-micrometer-thin sections of perfused mouse brains were cut and placed on positively charged microscope slides (Fisher Scientific, Pittsburg, PA Cat#12-550-15). The slides were kept at −80 °C until they were processed. At first the slides were coverslipped with Tris buffer and pictures were taken to record the native GFP fluorescence using a Leica DMR6000B inverted microscope with an FITC filter (L cube). The coverslips were then removed and the sections were treated with Powerblock (Biogenex, San Ramon, CA, Cat #: HK083-5K) containing 0.25% Triton X for 10 min at RT and incubated overnight at 4 °C in the primary anti-GFP rabbit antibody at 1:2000 dilution (Molecular Probes, OR; Cat#ab13970). Following incubation with the primary antibody, we blocked endogenous peroxidase activity by incubating the slides in 3% H_2O_2 in 1xPBS for 20 min. Next, GFP immunostaining and amplification were carried out in two different ways: (a) The primary antibody was detected using a goat anti-rabbit IgG conjugated to Alexa Fluor 594 (1:1000, for 1 h at RT). This was followed by an anti-goat IgG conjugated to HRP (overnight at 4 °C) visualized with a Tyramide–Alexa Fluor 350 conjugate (Molecular Probes–Invitrogen, Cat # T20937) at a dilution of 1:100 for 10 min. This way, the original fluorescence stayed green, the immunostained GFP was red and the amplified immunostained GFP was blue.

1.	GFP–rabbit IgG
	↓
2.	Goat–anti-rabbit Alexa Fluor 594
	↓
3.	Anti–Goat IgG–HRP
	↓
4.	Alexa Fluor 350–tyramide

(b) In another set of sections, the primary antibody was detected with anti-rabbit IgG conjugated to FITC (Jackson Immunologicals) applied for 1 h at RT at a dilution of 1:100. Next an anti-FITC-conjugated HRP antibody (1:500, Roche Applied Bioscience, Indianapolis, IN #1426346) was applied overnight at 4 °C followed by a tyramide–Alexa Fluor 594 conjugate (Molecular Probes–Invitrogen, Cat # T20935) at a dilution of 1:200 for 10 min.

1.	GFP–rabbit IgG
	↓
2.	Goat–anti-rabbit IgG–FITC
	↓
3.	Anti-FITC Rabbit IgG–HRP
	↓
4.	Alexa Fluor 594–tyramide

Combined detection of GFP by IHC and the Y chromosome by in situ hybridization (FISH)

To colocalize GFP and the Y chromosome in the same cells, sections were washed in PBS (pH 7.4) three times for 3 min,

rinsed with distilled water and incubated in 1× Powerblock for 10 min. The sections were rinsed again with distilled water and incubated in rabbit anti-GFP antibody (1:40,000, Molecular Probes, Eugene, OR) for 1 h at room temperature. The endogenous peroxidase activity was blocked with a 3% hydrogen peroxide solution for 15 min followed by 4 PBS washes lasting 3 min each. The secondary antibody – an anti-rabbit HRP polymer conjugate (SuperPicture, Zymed Laboratories Inc., South San Francisco, CA) – was applied undiluted for 30 min, and the staining was subsequently visualized using a custom-made FITC-conjugated tyramide at 1:10000 for 10 min at RT. To perform Y chromosomal FISH, the same sections were immersed in 10 mM citric acid (pH 6.0) and microwaved in a kitchen microwave (GE, 700W) for 5 min at 50% power after the liquid started to boil. The water that evaporated was replaced with distilled water, and the sections were left in the solution to cool for 2 h at RT. Microwave treatment inactivates any HRP activity that is present in the tissue—i.e., endogenous HRP and/or HRP incorporated in reagents used in previous steps [31]. The Y chromosomal hybridization was performed as described earlier [7] using a 1.5-kb RNA probe (pY3531B) generated against a repeat sequence of the mouse Y chromosome and labeled with digoxigenin–uridine 5′-triphosphate using the digoxigenin labeling kit (Digoxigenin RNA Labeling Kit, Cat. # 1 175 02; Roche Applied Sciences, Indianapolis, IN). After the

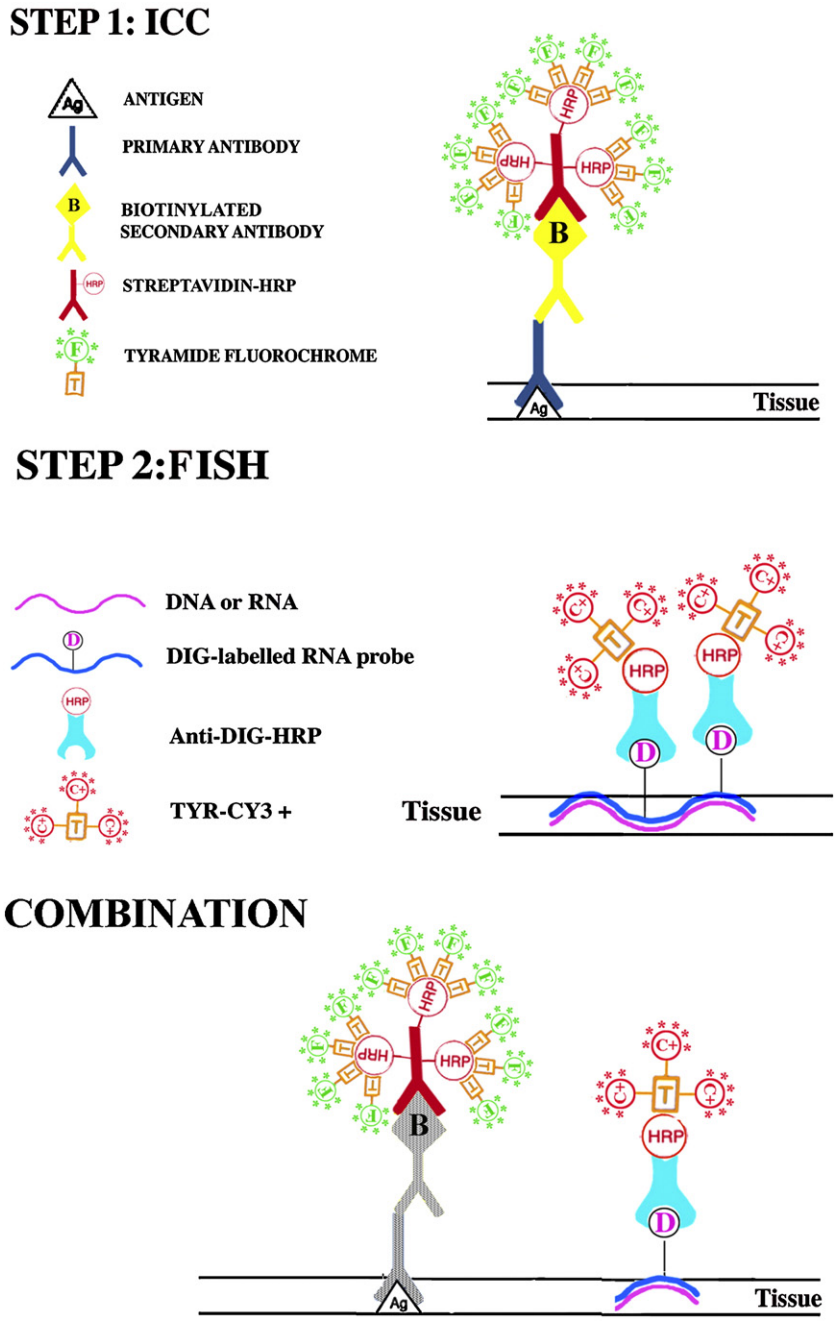

Fig. 1 – A schematic drawing to demonstrate the staining procedure when combining immunohistochemistry with non-radioactive in situ hybridization histochemistry (ISHH).

hybridization step and several washes in SSC (for details see our Web site: http://intramural.nimh.nih.gov/lcmr/snge/), the digoxigenin was detected with an anti-digoxigenin antibody that was conjugated to horseradish peroxidase (1:600, Roche Applied Sciences, Indianapolis, IN, Cat No: 1120773391) visualized using the TSA-Plus CY3 System (1:600, PerkinElmer Life Sciences, Boston, MA (now Invitrogen)) (Fig. 1).

1.	GFP–rabbit IgG
	↓
2.	Anti-rabbit IgG–dextran–HRP (SuperPicture)
	↓
3.	FITC–tyramide
	↓
4.	Microwave treatment
	↓
5.	(F)ISH (DIG-labeled Y probe)
	↓
6.	Rabbit–anti-digoxigenin–HRP
	↓
7.	CY3–tyramide+

Finally, all sections were stained with the chromosomal stain, DAPI (1:50000; 1 min, RT) to visualize nuclei. The sections were viewed in a Leica DMR6000 fluorescence microscope and pictures were taken using a Hamamatsu camera and Volocity software (Improvision, Lexington, MA) and high resolution images were analyzed using NIH Image software, Version 1.35.

Controls for specificity and sensitivity of the immunostaining procedures

To ensure the specificity of the immunostaining, we performed the same procedures after omitting the primary and/or secondary antibodies in each step. We used secondary antibodies that were cross absorbed with IgGs of any species that were used to raise previous secondary antibodies to make sure that non-specific binding will not occur at any step during the staining procedure. We have used the GFP amplification sequence, including all the reagents, in brains that were not transplanted with GFP bone marrow and did not observe any staining. We have used several GFP antibodies that were raised against different antigenic sites of the protein and observed similar results. We also used several different dilutions and combinations of tyramide reagents that all resulted in similar staining patterns. We have used the technique in 20 mice brains with similar results—5 of which were used to do the quantitative studies.

Quantitative evaluation

Sections cut at the same level of 5 mouse brains were used to count the number of GFP positive cells following the different staining protocols. The whole section was scanned and cells counted by two independent investigators. The number of GFP positive or Y positive cells in a section was expressed as a percentage of all cells determined by the number of all DAPI-positive cell nuclei counted. Statistical analysis was performed using the Friedman non-parametric test and Prism (GraphPad) software.

Results

A one-step immunostaining protocol (using the primary antibody and a fluorochrome-conjugated secondary antibody) for GFP cells (Fig. 2B) yielded higher signal intensity and a crisper image than was seen by imaging native fluorescence (Fig. 2A). The difference between the two images, however, was more qualitative than quantitative. Due to the increase in staining intensity with IHC (depositing more fluorochrome at the antigen site), more cells were readily detectable even with low magnification. On the other hand, the TSA signal amplification procedure using Alexa Fluor 594–Tyramide conjugate (Figs. 2C and D) revealed "new" structures; i.e., cells that were not detected before and many fine processes of cells and cell bodies vs. cell bodies alone (Figs. 2C and D and Fig. 3). When we performed amplified immunostaining for GFP in combination with the Y chromosome in situ hybridization (Fig. 4), we found a number of Y chromosome positive (i.e., donor origin) cells that were not GFP positive even when the most sensitive staining procedure was used. When we compared the number of cells that were visible under low magnification, 40% more cells were detected with amplified IHC than unamplified IHC (Fig. 5). ISH detected an additional 10% of cells that were Y chromosome positive but were negative for GFP immunostaining even after amplification (Fig. 5). The difference between the cell numbers by the different

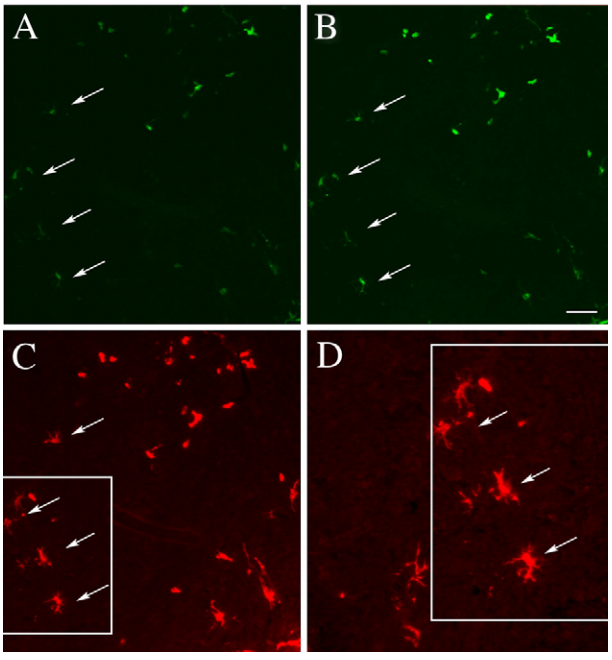

Fig. 2 – Comparison of native GFP fluorescence (A) with one-step antibody staining using a GFP primary and an anti-rabbit–FITC-conjugated secondary antibody (B) and then an antibody to FITC that is preconjugated with HRP and subsequently adding the high affinity substrate tyramide that is conjugated to Alexa Fluor 594 (C). (D) is an area enlarged from A, B and C to demonstrate cells that were not visible before amplification. Scale bars: 50 μm (A–C) and 25 μm (D).

techniques was statistically significant (difference between means $p<0.0001$).

Discussion

The first transgenic mouse was produced by Gordon in 1980 [32]. By constructing transgenes that contained GFP cDNA driven by specific promoter sequences the target proteins could now be identified by detecting the green fluorescence [33]. The use of green fluorescence protein revolutionized the monitoring of gene expression. Many techniques were used and compared to optimize the immunohistochemical detection of GFP using conventional [34] and confocal microscope [35] even in paraffin embedded tissue. As more and more studies relying on GFP appeared, there were hints that the transgenes might be silenced depending on age, tissue, differentiation and many other factors. Mothe et al. [36] compared detection of GFP in transgenic mice and rats and found that sometimes GFP has to be immunostained to be seen and suggested the possibility of a partial silencing of the transgene after cell transplantation. This could potentially occur because of genetic changes in the DNA or alterations in transcription or translation. DNA methylation is the best known mechanism for silencing a transgene at the level of DNA [37]. There are also many examples of RNAi-mediated inhibition of translation and non-methylation-mediated transcriptional gene silencing including the silencing of the green fluorescent protein. It is not yet known why GFP expression diminishes or completely shuts down in transgenic animals. It is possible that as cells proliferate and differentiate the GFP sequence will be noticed at a checkpoint during the cell cycle and marked to be shut down [38]. Since the expression of GFP varies among cells, it is likely that using traditional detection methods we miss many GFP+ cells. The methods and problems of GFP detection have been nicely summarized in a recent review [21]. The fact that GFP turns off may account for many publications in the literature that state that no donor cells were detected when using GFP as a reporter gene to label bone marrow [39–41]. This might be a reason why the literature is so confusing in regards to the question of plasticity and transdifferentiation.

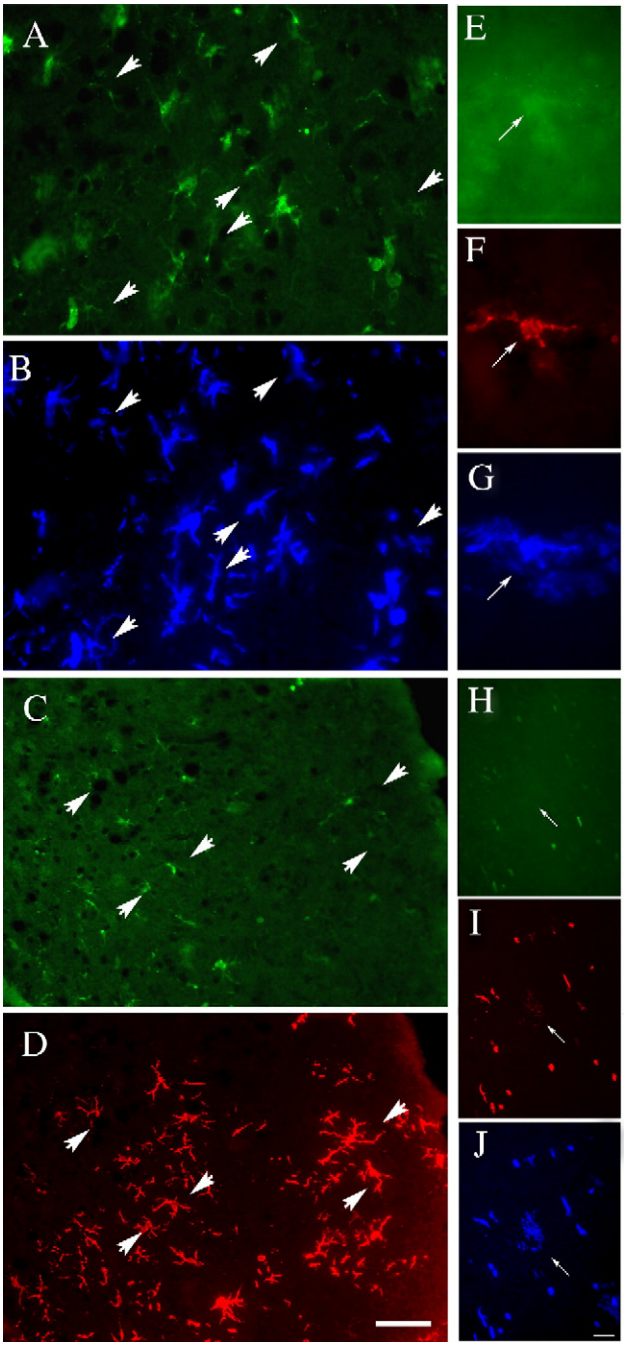

Fig. 3 – Examples of GFP amplification in the brains of mice that underwent GFP bone marrow transplantation and MCAO ligation. Panel A is a field of striatum following immunostaining for GFP using a primary antibody raised in rabbit. A biotinylated anti-rabbit IgG was then followed by the ABC reagent and then a tyramide-conjugated Alexa-350 was added as a substrate (B). Arrows point at cells that became visible following the amplification procedure. In another section, a similar procedure was used, but after the first immunostaining using a rabbit anti-GFP, the staining was developed with anti-rabbit IgG-Alexa Fluor 488 raised in goat (C). Then a biotinylated anti-goat IgG was added followed by the ABC reagent. Finally, an Alexa-594–tyramide was used as a substrate that resulted in a red fluorescent deposit (D). High magnification image of a cell is shown in native green fluorescence (E), following a one-step immunostaining with Alexa Fluor 594 (F) and then amplified using tyramide-350. Note the fine arborization of the cell that was not visible in green (G). (H) Native GFP fluorescence followed by an immunostaining in red (I) and it is only after the amplification using 350-tyramide that the whole cell is recognized (J). Scale bars: 25 μm A–D and 12 μm (E–J).

Conclusion

Our experiments demonstrate that on the average we fail to detect half of the cells that express GFP if we use only traditional immunostaining. It is interesting to note that the cells that are still strongly fluorescent are microglia—which

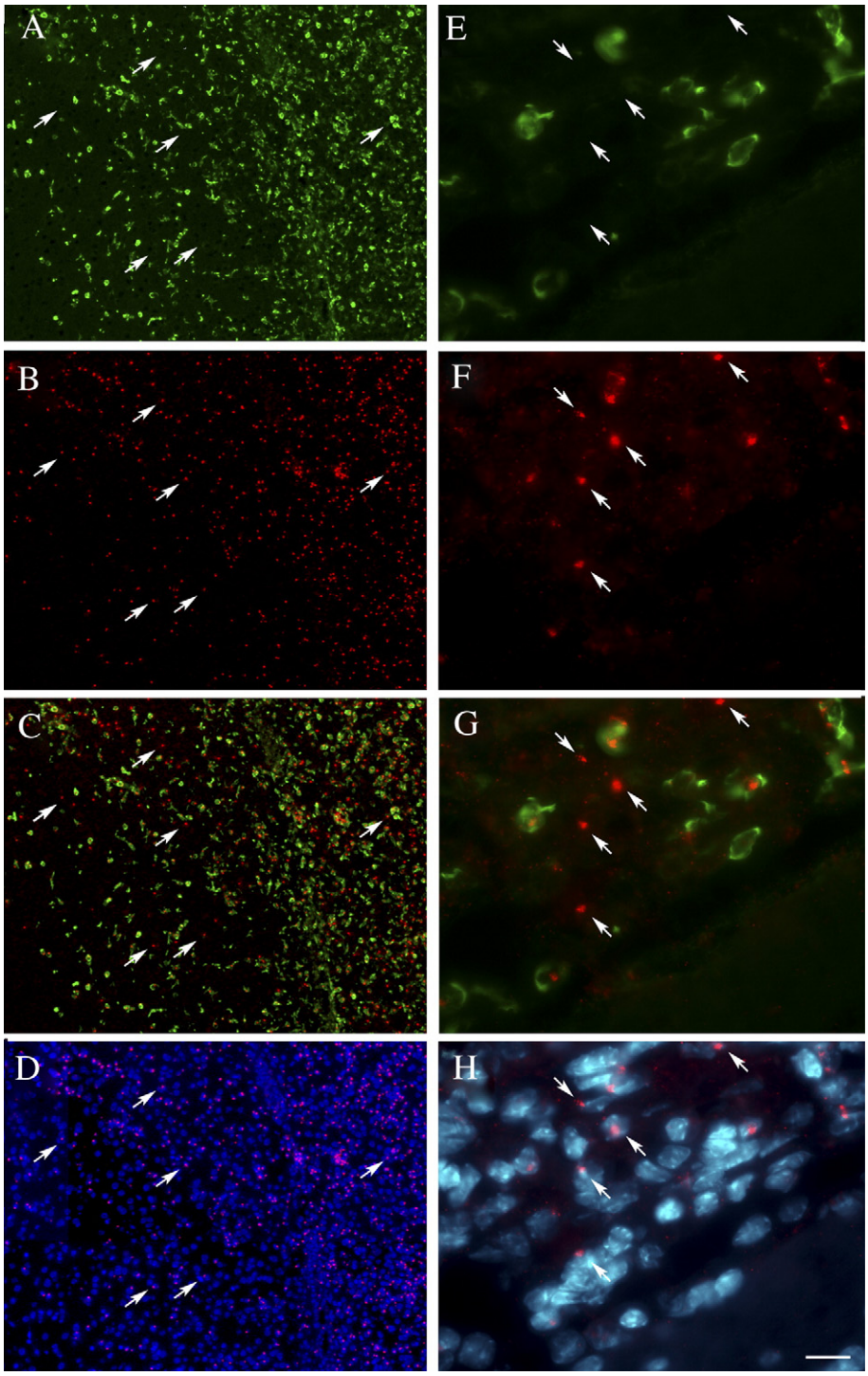

Fig. 4 – Amplified GFP immunostaining (green) was performed in the same sections where the Y chromosome was visualized with FISH (red) (A–D, low magnification and E–H, high magnification). Panels C and G show an image taken through a dual filter to reveal colocalization of Y and GFP. Panels D and H are overlaid images through the UV (DAPI) and the red (Y chromosome) filter to demonstrate the nuclear localization of the Y chromosome. Arrows point at Y chromosomes that belong to cells with no GFP staining. Scale bars: 100 μm (A–D) and 16 μm (E–H).

are known to be of bone marrow origin. We suggest that the loss of GFP may be a function of differentiation, i.e., the less cells resemble their bone marrow precursors, the less GFP is expressed. Based on our results, the maximal GFP sensitivity can be achieved by simply using a dextran backbone secondary antibody (such as Zymed's SuperPicture™), which deposits multiple peroxidase sites at the antigenic site and then visualize using a Tyramide–fluorochrome (Invitrogen). This technique enables one to detect about 90% of all donor cells present using GFP immunostaining—as shown by the Y

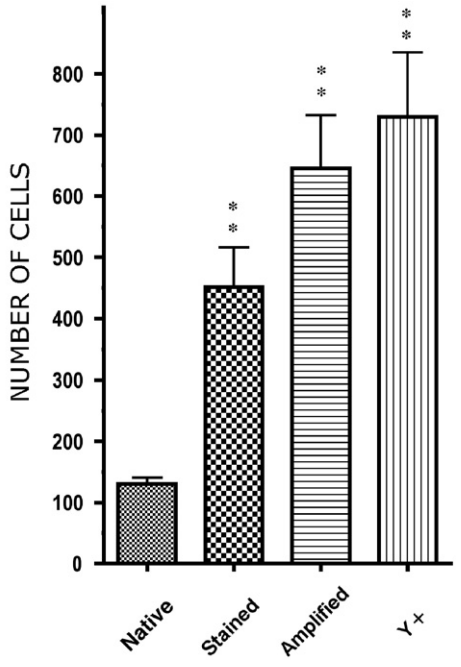

Fig. 5 – Comparison of the number of donor derived cells in the brain counted based on native fluorescence, immunostained fluorescence, following signal amplification and the number of Y chromosome containing nuclei. Each column represents the average of five animals; sections were taken at the same coronal level. Median values are significantly different at $p<0.0001$ using the Friedman non-parametric test.

chromosome hybridization of gender mismatched transplants. The technique can also be used to detect any other marker protein in the cells (using the water insoluble tyramide) and then performing the Y chromosome hybridization to detect all donor cells. Even the number of Y chromosome positive cells would underestimate the number of all donor-derived cells since there is a portion of donor cells that will not have the Y chromosome (or even the nucleus) in the section. Increasing our detection sensitivity in such a way will hopefully result in settling many presently unanswered questions and might help resolve the contradictions in the literature regarding (trans)differentiation of different cell types in a variety of tissues.

Acknowledgments

This research was supported by the DIR, NIDCR, NINDS and NIMH of the Intramural Research Program, NIH. Zs.E.T. is also supported by OTKA T 043169. The authors want to acknowledge the help of Joanne Severe with the statistics.

Appendix A. Supplementary data

Supplementary data associated with this article can be found, in the online version, at doi:10.1016/j.yexcr.2007.02.024.

REFERENCES

[1] R.P. van Gijlswijk, H.J. Zijlmans, J. Wiegant, M.N. Bobrow, T.J. Erickson, K.E. Adler, H.J. Tanke, A.K. Raap, Fluorochrome-labeled tyramides: use in immunocytochemistry and fluorescence in situ hybridization, J. Histochem. Cytochem. 45 (1997) 375–382.
[2] O. Shimomura, The discovery of aequorin and green fluorescent protein, J. Microsc. 217 (2005) 1–15.
[3] G.F. Beilhack, Y.C. Scheffold, I.L. Weissman, C. Taylor, L. Jerabek, M.J. Burge, M.A. Masek, J.A. Shizuru, Purified allogeneic hematopoietic stem cell transplantation blocks diabetes pathogenesis in NOD mice, Diabetes 52 (2003) 59–68.
[4] M. Abedi, D.A. Greer, G.A. Colvin, D.A. Demers, M.S. Dooner, J.A. Harpel, J. Pimentel, M.K. Menon, P.J. Quesenberry, Tissue injury in marrow transdifferentiation, Blood Cells Mol. Diseases 32 (2004) 42–46.
[5] T. Yagi, E.J. McMahon, S. Takikita, I. Mohri, G.K. Matsushima, K. Suzuki, Fate of donor hematopoietic cells in demyelinating mutant mouse, twitcher, following transplantation of GFP+ bone marrow cells, Neurobiol. Dis. 16 (2004) 98–109.
[6] T. Ito, A. Suzuki, M. Okabe, E. Imai, M. Hori, Application of bone marrow-derived stem cells in experimental nephrology, Exp. Nephrol. 9 (2001) 444–450.
[7] E. Mezey, K.J. Chandross, G. Harta, R.A. Maki, S.R. McKercher, Turning blood into brain: cells bearing neuronal antigens generated in vivo from bone marrow, Science 290 (2000) 1779–1782.
[8] H. Shichinohe, S. Kuroda, J.B. Lee, G. Nishimura, S. Yano, T. Seki, J. Ikeda, M. Tamura, Y. Iwasaki, In vivo tracking of bone marrow stromal cells transplanted into mice cerebral infarct by fluorescence optical imaging, Brain Res. Brain Res. Protoc. 13 (2004) 166–175.
[9] K. Nakano, M. Migita, H. Mochizuki, T. Shimada, Differentiation of transplanted bone marrow cells in the adult mouse brain, Transplantation 71 (2001) 1735–1740.
[10] C.P. Hofstetter, E.J. Schwarz, D. Hess, J. Widenfalk, A. El Manira, D.J. Prockop, L. Olson, Marrow stromal cells form guiding strands in the injured spinal cord and promote recovery, Proc. Natl. Acad. Sci. U. S. A. 99 (2002) 2199–2204.
[11] K.A. Moore, I.R. Lemischka, Stem cells and their niches, Science 311 (2006) 1880–1885.
[12] K.A. Jackson, S.M. Majka, G.G. Wulf, M.A. Goodell, Stem cells: a minireview, J. Cell Biochem. Suppl. 38 (2002) 1–6.
[13] R.A. McTaggart, S. Feng, An uncomfortable silence em leader while we all search for a better reporter gene in adult stem cell biology, Hepatology 39 (2004) 1143–1146.
[14] H. Xia, Q. Mao, H.L. Paulson, B.L. Davidson, siRNA-mediated gene silencing in vitro and in vivo, Nat. Biotechnol. 20 (2002) 1006–1010.
[15] G. Tiscornia, O. Singer, M. Ikawa, I.M. Verma, A general method for gene knockdown in mice by using lentiviral vectors expressing small interfering RNA, Proc. Natl. Acad. Sci. U. S. A. 100 (2003) 1844–1848.
[16] T. Takada, K. Nemoto, A. Yamashita, M. Kato, Y. Kondo, R. Torii, Efficient gene silencing and cell differentiation using siRNA in mouse and monkey ES cells, Biochem. Biophys. Res. Commun. 331 (2005) 1039–1044.
[17] M.C. Siomi, H. Tsukumo, A. Ishizuka, T. Nagami, H. Siomi, A potential link between transgene silencing and poly(A) tails, Rna 11 (2005) 1004–1011.
[18] A. Rinne, C. Littwitz, M.C. Kienitz, A. Gmerek, L.I. Bosche, L. Pott, K. Bender, Gene silencing in adult rat cardiac myocytes in vitro by adenovirus-mediated RNA interference, J. Muscle Res. Cell Motil. (2006).
[19] N.J. Caplen, S. Parrish, F. Imani, A. Fire, R.A. Morgan, Specific inhibition of gene expression by small double-stranded RNAs

in invertebrate and vertebrate systems, Proc. Natl. Acad. Sci. U. S. A. 98 (2001) 9742–9747.
[20] M. Amarzguioui, J.J. Rossi, D. Kim, Approaches for chemically synthesized siRNA and vector-mediated RNAi, FEBS Lett. 579 (2005) 5974–5981.
[21] T.R. Brazelton, H.M. Blau, Optimizing techniques for tracking transplanted stem cells in vivo, Stem Cells 23 (2005) 1251–1265.
[22] M.N. Bobrow, T.D. Harris, K.J. Shaughnessy, G.J. Litt, Catalyzed reporter deposition, a novel method of signal amplification. Application to immunoassays, J. Immunol. Methods 125 (1989) 279–285.
[23] J.C. Adams, Biotin amplification of biotin and horseradish peroxidase signals in histochemical stains, J. Histochem. Cytochem. 40 (1992) 1457–1463.
[24] R. von Wasielewski, M. Mengel, S. Gignac, L. Wilkens, M. Werner, A. Georgii, Tyramine amplification technique in routine immunohistochemistry, J. Histochem. Cytochem. 45 (1997) 1455–1459.
[25] B. Hunyady, K. Krempels, G. Harta, E. Mezey, Immunohistochemical signal amplification by catalyzed reporter deposition and its application in double immunostaining, J. Histochem. Cytochem. 44 (1996) 1353–1362.
[26] A. Novak, C. Guo, W. Yang, A. Nagy, C.G. Lobe, Z/EG, a double reporter mouse line that expresses enhanced green fluorescent protein upon Cre-mediated excision, Genesis 28 (2000) 147–155.
[27] R.R. Leker, M. Aharonowiz, N.H. Greig, H. Ovadia, The role of p53-induced apoptosis in cerebral ischemia: effects of the p53 inhibitor pifithrin alpha, Exp. Neurol. 187 (2004) 478–486.
[28] A. Tamura, D.I. Graham, J. McCulloch, G.M. Teasdale, Focal cerebral ischaemia in the rat: 2. Regional cerebral blood flow determined by [^{14}C]iodoantipyrine autoradiography following middle cerebral artery occlusion, J. Cereb. Blood Flow Metab. 1 (1981) 61–69.
[29] A. Tamura, Middle cerebral artery occlusion in the young rat, Stroke 14 (1983) 831–832.
[30] L. Belayev, R. Busto, W. Zhao, G. Fernandez, M.D. Ginsberg, Middle cerebral artery occlusion in the mouse by intraluminal suture coated with poly-L-lysine: neurological and histological validation, Brain Res. 833 (1999) 181–190.
[31] Zs.E. Toth, E. Mezey, Simultaneous visualization of multiple antigens with tyramide signal amplification using antibodies from the same species, J. Histochem. Cytochem. doi: 10.1369/jhc.6A7134.2007.
[32] J.W. Gordon, G.A. Scangos, D.J. Plotkin, J.A. Barbosa, F.H. Ruddle, Genetic transformation of mouse embryos by microinjection of purified DNA, Proc. Natl. Acad. Sci. U. S. A. 77 (1980) 7380–7384.
[33] A.K. Hadjantonakis, M. Gertsenstein, M. Ikawa, M. Okabe, A. Nagy, Generating green fluorescent mice by germline transmission of green fluorescent ES cells, Mech. Dev. 76 (1998) 79–90.
[34] R. Shariatmadari, P.P. Sipila, I.T. Huhtaniemi, M. Poutanen, Improved technique for detection of enhanced green fluorescent protein in transgenic mice, Biotechniques 30 (2001) 1282–1285.
[35] I. Walter, M. Fleischmann, D. Klein, M. Muller, B. Salmons, W.H. Gunzburg, M. Renner, W. Gelbmann, Rapid and sensitive detection of enhanced green fluorescent protein expression in paraffin sections by confocal laser scanning microscopy, Histochem. J. 32 (2000) 99–103.
[36] A.J. Mothe, I. Kulbatski, R.L. van Bendegem, L. Lee, E. Kobayashi, A. Keating, C.H. Tator, Analysis of green fluorescent protein expression in transgenic rats for tracking transplanted neural stem/progenitor cells, J. Histochem. Cytochem. 53 (2005) 1215–1226.
[37] L. Jones, A.J. Hamilton, O. Voinnet, C.L. Thomas, A.J. Maule, D.C. Baulcombe, RNA–DNA interactions and DNA methylation in post-transcriptional gene silencing, Plant Cell 11 (1999) 2291–2301.
[38] J.F. Lambert, M. Liu, G.A. Colvin, M. Dooner, C.I. McAuliffe, P.S. Becker, B.G. Forget, S.M. Weissman, P.J. Quesenberry, Marrow stem cells shift gene expression and engraftment phenotype with cell cycle transit, J. Exp. Med. 197 (2003) 1563–1572.
[39] L.B. Balsam, A.J. Wagers, J.L. Christensen, T. Kofidis, I.L. Weissman, R.C. Robbins, Haematopoietic stem cells adopt mature haematopoietic fates in ischaemic myocardium, Nature 428 (2004) 668–673.
[40] M. Massengale, A.J. Wagers, H. Vogel, I.L. Weissman, Hematopoietic cells maintain hematopoietic fates upon entering the brain, J. Exp. Med. 201 (2005) 1579–1589.
[41] A.J. Wagers, R.I. Sherwood, J.L. Christensen, I.L. Weissman, Little evidence for developmental plasticity of adult hematopoietic stem cells, Science 297 (2002) 2256–2259.

International Journal of Obesity (2012) **36,** 1514 – 1521

www.nature.com/ijo

ORIGINAL ARTICLE

Nesfatin-1 exerts long-term effect on food intake and body temperature

K Könczöl[1], O Pintér[2], S Ferenczi[3], J Varga[2], K Kovács[3], M Palkovits[1], D Zelena[2,4] and ZE Tóth[1,4]

OBJECTIVE: To determine whether the anorexigenic peptide, nesfatin-1 affects energy expenditure, and to follow the time course of its effects.
DESIGN: Food intake duration, core body temperature, locomotor activity and heart rate of rats were measured by telemetry for 48 h after a single intracerebroventricular injection of 25 or 100 pmol nesfatin-1 applied in the dark or the light phase of the day. Body weight, food and water intake changes were measured daily. Furthermore, cold-responsive nesfatin-1/NUCB2 neurons were mapped in the brain.
RESULTS: Nesfatin-1 reduced duration of nocturnal food intake for 2 days independently of circadian time injected, and raised body temperature immediately, or with little delay depending on the dose and circadian time applied. The body temperature remained higher during the next light phases of the 48 h observation period, and the circadian curve of temperature flattened. After light phase application, the heart rate was elevated transiently. Locomotion did not change. Daily food and water intake, as well as body weight measurements point to a potential decrease in all parameters on the first day and some degree of compensation on the second day. Cold-activated (Fos positive) nesfatin-1/NUCB2 neurones have been revealed in several brain nuclei involved in cold adaptation. Nesfatin-1 co-localised with prepro-thyrotropin-releasing hormone in cold responsive neurones of the hypothalamic paraventricular nucleus, and in neurones of the nucleus raphe pallidus and obscurus that are premotor neurones regulating brown adipose tissue thermogenesis and skin blood flow.
CONCLUSION: Nesfatin-1 has a remarkably prolonged effect on food intake and body temperature. Time course of nesfatin-1's effects may be varied depending on the time applied. Many of the nesfatin-1/NUCB2 neurones are cold sensitive, and are positioned in key centres of thermoregulation. Nesfatin-1 regulates energy expenditure a far more potent way than it was recognised before making it a preferable candidate anti-obesity drug.

International Journal of Obesity (2012) **36,** 1514–1521; doi:10.1038/ijo.2012.2; published online 31 January 2012

Keywords: circadian rhythm; cold stress; rat; telemetry; thermoregulation

INTRODUCTION

Obesity and its complications cause death of thousands of people every year worldwide, therefore research for possible therapeutic targets is intensively continued. Nesfatin-1 was discovered a few years ago as a new agent in the regulation of the food intake.[1] It is the N-terminal fragment of the nucleobindin 2 protein (NUCB2) named after nucleobindin2-encoded satiety- and fat-influencing protein. Other fragments like nesfatin-2 and nesfatin-3 have DNA-binding domains and unknown function.[1] Intracerebroventricular (icv) administration of nesfatin-1 decreases nocturnal food intake in a dose-dependent manner.[1] Injected into fasted rats, nesfatin-1 activates food intake regulatory autonomic centres in the brain, such as the neurons of the hypothalamic paraventricular nucleus (PVN), and the nucleus of the solitary tract (NTS).[2] Moreover, fasting results in depletion of nesfatin-1 /NUCB2 mRNA and peptide in the supraoptic nucleus and in the PVN, whereas icv administration of an antisense oligonucleotide prepared against nesfatin-1 /NUCB2 induces an increase in food intake and body weight gain.[1,3]

Localisation and wide distribution of nesfatin-1-producing neurons in the brain predispose its involvement in many other functions. As it has been already shown, nesfatin-1 decreases water intake, increases the mean arterial pressure, evokes anxiety-related behaviour, and participates in the stress reaction.[4–6] Recently, a relationship between nesfatin-1 level and occurrence of epileptic seizures has also been established in human patients.[7]

Long-term energy balance is determined both by the regulation of the food intake and by the energy expenditure. This is supported by the fact that many anorexigenic and orexigenic neuropeptides are also involved in the central control of thermogenesis, like corticotropin-releasing hormone, thyrotropin-releasing hormone (TRH) and oxytocin in the PVN, proopiomelanocortin and cocaine- and amphetamine-regulated transcript in the arcuate nucleus (ARC), prolactin-releasing peptide in the NTS and in the caudal ventrolateral medulla and melanin-concentrating hormone in the tuberohypothalamic area.[6,8–11] Nesfatin-1 is co-expressed with all of the above-mentioned neuropeptides suggesting a possible association with thermoregulation that had not been investigated, yet.[11–17] Besides, both body temperature and food intake have a diurnal rhythm, and there are no data in the literature about longer than 24 h observations on nesfatin-1's effect. Considering these, the present

[1]Neuromorphological and Neuroendocrine Research Laboratory, Department of Anatomy, Histology and Embryology, Semmelweis University and the Hungarian Academy of Sciences, Budapest, Hungary; [2]Laboratory of Behavioural and Stress Studies, Budapest, Hungary and [3]Laboratory of Molecular Neuroendocrinology, Institute of Experimental Medicine, Hungarian Academy of Sciences, Budapest, Hungary. Correspondence: Mrs K Könczöl or Dr ZE Tóth, Neuromorphological and Neuroendocrine Research Laboratory, Department of Anatomy, Histology and Embryology, Semmelweis University and the Hungarian Academy of Sciences, 1094 Tűzoltó utca 58, Budapest, Hungary.
E-mails: konkat6@gmail.com (KK) or tothzs@ana.sote.hu (ZET)
[4]These authors contributed equally to this work.
Received 22 July 2011; revised 12 December 2011; accepted 17 December 2011; published online 31 January 2012

work aimed to investigate (1) whether any prolonged visceral consequences of a single icv nesfatin-1 injection exist, (2) whether actions of nesfatin-1 interact with the diurnal cycle of the animals, and (3) whether certain nesfatin-1/NUCB2 neurons in the central nervous system are functionally involved in thermoregulation. To determine this, we injected nesfatin-1 or vehicle icv into the lateral ventricle of rats either at the beginning of the light phase, or at the beginning of the dark phase, and used a telemetric device to follow the core body temperature, heart rate and locomotion for 48 h. Additionally, in another experiment, we subjected rats to cold and activation of subsets of nesfatin-1/NUCB2 immunopositive neurons in the brain was examined.

MATERIALS AND METHODS

Animals

Male Wistar rats (TOXI-COOP Ltd., Budapest, Hungary) weighing 250–300 g were used for the studies ($n = 37$). Animals were kept with light–dark cycle of 12:12 h at room temperature (21 ± 1 °C), and had free access to standard rodent chow and tap water except otherwise indicated. Experiments were performed according to the European Communities Council Directive of 24 November 1986 (86/609/EEC) and were supervised by the Animal Welfare Committee of the Institute of Experimental Medicine, Hungarian Academy of Sciences, Budapest, Hungary.

Biotelemetry

The biotelemetric recordings were made by means of a 12-channel VitalView system (Minimitters.Co., Bend, OR, USA) in every minute for 48 h.[18]

Feeding duration was determined by infrared feeding monitor belonging to the Vital View system designed for use with the Nalgene food chambers. When the subject places its head in the feeding chamber, a beam of infrared light is broken. At the same time, a clock starts and continues to run as long as the beam is interrupted. This equipment allows ad libitum feeding without restriction, but it is narrow enough not to be convenient to be in there, unless feeding.

In case of light phase experiments, lights were on at 06:00 h and off at 18:00 h. In case of dark phase injections, rats were housed in opposite diurnal cycle (light on at 22:00 h and off at 10:00 h) for three weeks before the injections. A polyethylene guide cannula was inserted into the right lateral ventricle (stereotaxic coordinates: 0.8 mm caudal to the Bregma, 2 mm from the midline, 4 mm ventrally) under deep anaesthesia with ketamine (50 mg kg^{-1}, Richter Gedeon Nyrt, Budapest, Hungary) and xylazine (15 mg kg^{-1}, CP-Pharma, Bönsensell, Germany). The cannula was fixed to the skull with acrylic dental cement. At the same time, VitalView biotelemetry emitters were implanted into the abdominal cavity. The negative and positive heart rate leads were attached to the anterior right side of the chest (near the clavicle) and to the posterior chest wall (left to the sternum and anterior to the last rib), respectively. Animals were allowed to recover for one week, whereas handled daily to reduce future experimental stress. Once recovered, they have received either 5 μl of nesfatin-1 dissolved in physiological saline, (25 pmol, $n = 10–12$, light phase injections and $n = 5–6$, dark phase injections, or 100 pmol, $n = 7$, light phase injections) or 5 μl of saline icv. The icv injections were always made between 10:00 and 10:30 h applying it through a 26-guage needle, which was connected by polyethylene tubing to a 10 μl Hamilton syringe. Telemetric data were calculated as sum ± s.e.m. (food intake duration and locomotion) or mean ± s.e.m. (core temperature and heart rate) in each 4 h (2 days measurement), or 10-min (short time observations) time bin. Temperature data were normalised to the average temperature between 6 h and 7 h on the day of the injection (2 days measurements), or to the average temperature of 10 min before the injection (short-term observations). Heart rate data for short-term observations were expressed in percentage of average values measured 10 min before the injections. Body weight, food and water intake were measured daily, data were calculated as differences between the consecutive days for each individual, and expressed as mean ± s.e.m. Evaluation of the data was performed by using two ways repeated measure ANOVA with the help of the STATISTICA 9.0 software (StatSoft, Tulsa, OK, USA).

Cold exposure

Rats were kept one per cage for 3 days before the experiment. On the experimental day, animals were placed to cages without bedding, and were exposed to 4 °C in a cold room ($n = 3$), or were kept at room temperature ($n = 3$). After 2 h, the animals were anaesthetised (see above) and transcardially perfused with 4% paraformaldehyde.

Immunohistochemistry (IHC)

Brains were cryoprotected in 20% sucrose overnight, and cut into 50 μm thick serial coronal sections on a frigomobil (Frigomobil, Reichter-Jung, Vienna, Austria). Immunostainings always started with blocking the endogenous peroxidase activity, using a 3% H_2O_2 solution for 15 min. Then, the sections were blocked in 1% BSA and 0.5% TritonX-100/PBS for 1 h. The same solution was used to dilute the antibodies. Incubations were made for 2 days at 4 °C in the primary antibodies and for 1 h at room temperature, when secondary or tertiary antibodies were used. The sections were washed three times for 5 min in PBS following each incubation step. As multiple labellings were performed with primary antibodies raised in the same hosts, sections were microwave-treated in 0.1 M citric-acid (pH 6.0) for 5 min after each immunostaining to block the peroxidase enzyme used for visualisation in the previous step, and to prevent crossreactions.[19]

Fos and nesfatin-1/NUCB2 double and Fos, nesfatin-1/NUCB2 and prepro-TRH triple immunostainings

Sections of cold exposed and control animals were incubated first in rabbit anti-Fos (1:30 000, Santa Cruz Biotechnology, Inc., Santa Cruz, CA, USA), in biotinylated anti rabbit IgG (1:1000, Vector Laboratories, Inc., Burlingame, CA, USA), and in extravidine-peroxidase (1:1000, Sigma, Budapest, Hungary). The immunostaining was visualised by FITC-conjugated tyramide (Invitrogen, Budapest, Hungary). After this, the sections were incubated in rabbit anti-nesfatin-1/NUCB2 (1:12 000, Phoenix Pharmaceuticals, Inc., Burlingame, CA, USA) and in anti-rabbit IgG polymer-HRP (Millipore, Budapest, Hungary). The second immunostaining was developed by tyramide-conjugated Alexa Fluor 568 (Invitrogen).

In case of triple labelling, the Fos IHC was performed first, as described. Sections were then incubated in rabbit anti-prepro-TRH (1:5000, kindly provided by Eva Redei), and in anti-rabbit IgG polymer-HRP (Millipore). The prepro-TRH antigen was visualised by tyramide-conjugated Alexa Fluor 568 (Invitrogen). The third IHC was performed using a rabbit anti-nesfatin-1/NUCB2 (1:12 000), a goat anti-rabbit IgG polymer-HRP (Millipore), and Alexa Fluor 405-tyramide (Invitrogen).

Colocalisation of prepro-TRH and nesfatin-1/NUCB2 in the brainstem

As previous report suggested that TRH immunoreactivity in brainstem raphe neurons can be revealed only after colchicine treatment,[20] sections from control and from colchicine-treated animals were also used. Colchicine (200 μg/20 μl) was injected under deep anaesthesia and stereotaxic control to the right lateral ventricle of rats by a Hamilton syringe. After 2 days, the animals were anaesthetised again, and transcardially perfused with 4% paraformaldehyde. Nesfatin-1/NUCB2 immunostaining was performed first, using anti-rabbit IgG polymer-HRP (Millipore) and tyramide-conjugated Alexa Fluor 568 (Invitrogen). The rabbit anti-prepro-TRH was applied next, followed by anti rabbit IgG polymer-HRP secondary antibody (Millipore), and FITC-conjugated tyramide (Invitrogen) for visualisation. Sections were counterstained with DAPI (Invitrogen).

Sections were mounted on non-coated slides, air dried and coverslipped with DPX (Sigma). Images were captured by a Nikon Eclipse E800 microscope attached to a Bio-Rad Radiance 2100 Rainbow confocal scanning system (Bio-Rad Microscience Ltd, Hemel Hempstead, England, UK).

RESULTS

Effects of icv nesfatin-1 on physiological parameters

Nesfatin-1 (25 pmol), added at the onset of the dark phase, diminished the duration of nocturnal food intake in the first 6 h and also decreased it at the beginning of the next dark phase (Figure 1a) (effect of treatment: $F_{(1,9)} = 4.\ 63$, $P = 0.05$). Additionally, nesfatin-1 blunted the duration of nocturnal food intake for 48 h, when it was applied during the beginning of the light phase, too (Figure 1b) (effect of treatment: $F_{(1,\ 11)} = 11.9$, $P < 0.01$). A circadian rhythm of food intake was observable in both cases (effect of time: $F_{(11,99)} = 10.5$, $P < 0.01$ for dark and $F_{(11,121)} = 5.83$, $P < 0.01$ for light phase application), but with much smaller amplitude than that of the controls (Figure 1) (treatment × time interaction: $F_{(11,99)} = 3.06$, $P < 0.01$ for dark and $F_{(11,121)} = 4.41$, $P < 0.01$ for light phase application). Light phase injections had no significant effect on the daily amount of food consumed, indicating that animals either may have eaten more during the shortened durations at night, or made up for food intake during the day. However, dark phase application showed a clear reduction in food consumption on the first day and a compensation on the second day (effect of time: $F_{(1,21)} = 4.66$, $P < 0.05$, treatment × time interaction: $F_{(1,21)} = 6.09$, $P < 0.05$), (Figure 1c). Nesfatin-1 treatment reduced water intake on the first day, that was followed by a compensatory increase on the second day in both cases (effect of treatment: $F_{(1,9)} = 6.1$, $P < 0.05$, effect of time: $F_{(1,21)} = 5.2$, $P < 0.05$, tendency for treatment × time interaction: $F_{(1,21)} = 4.8$, $P = 0.056$ for dark phase, and treatment within the first day $P < 0.05$ (*post hoc* comparison Holm–Sidak method), effect of time: $F_{(1,23)} = 7.02$, $P < 0.05$, tendency for treatment × time interaction: $F_{(1,23)} = 4.89$, $P = 0.05$ for light phase injections) (Figure 1c). Body weight changes reflected the tendencies observed with food and water intake, but they did not reach the level of significance in any cases (Figure 1c).

Nesfatin-1 (25 pmol) also affected the core body temperature of rats. When it was applied at the onset of the dark phase, the temperature started to elevate immediately (Figures 2a and b) (effect of treatment: $F_{(1,9)} = 7.85$, $P < 0.05$). The difference between the groups was not so pronounced during the dark phases, but it was markedly significant during the light phases of the 48 h observation period (Figure 2a). In case of light phase injections, core body temperature started to elevate slightly approximately 1.5 h after the injection (Figures 2c and d) (effect of treatment: $F_{(1,14)} = 14.2$, $P < 0.01$). Body temperature of control and treated rats converged during the dark phase, but next day the temperature of the treated animals remained higher resulting in a maximal difference between the groups. The temperature difference between the groups existed also the second night (Figure 2c). Both dark phase and light phase injections resulted in a flattened circadian curve (effect of time: $F_{(11,99)} = 10.4$, $P < 0.01$ for dark and $F_{(11,154)} = 8.25$, $P < 0.01$ for light phase application), mainly as a consequence of the higher daytime temperature.

There was no notable influence of 25 pmol of nesfatin-1 on the heart rate, except a short interim elevation approximately 1.5 h after the light phase injection (Figures 3a-d) (effect of time: $F_{(11,88)} = 19.7$, $P < 0.01$ for dark and $F_{(11,198)} = 16.7$, $P < 0.01$ for light phase application). To elucidate whether changes in the locomotion may be responsible for the alterations in the heart rate and the core body temperature, locomotion data were evaluated through the 48 h observation period and also in more detail regarding a 2.5 h long period immediately after the injections. Significant changes were found in neither case (Figures 3e and f, Supplementary Figures 1A and B).

Effects of higher dose of nesfatin-1 (100 pmol) administered during the light phase showed the same tendencies observed with that of 25 pmol (food intake duration: effect of treatment: $F_{(1,154)} = 9.07$, $P < 0.01$, effect of time: $F_{(11,154)} = 4.24$, $P < 0.01$, treatment × time interaction: $F_{(11,154)} = 3.12$, $P < 0.01$; body temperature: effect of treatment: $F_{(1,132)} = 6.45$, $P < 0.05$, effect of time: $F_{(11,132)} = 9.98$, $P < 0.01$, treatment × time interaction: $F_{(11,132)} = 5.75$, $P < 0.01$; heart rate: effect of time: $F_{(11,380)} = 4.74$, $P < 0.01$), (Supplementary Figure 2). Temperature and heart rate changes were enhanced immediately after the injection, compared with

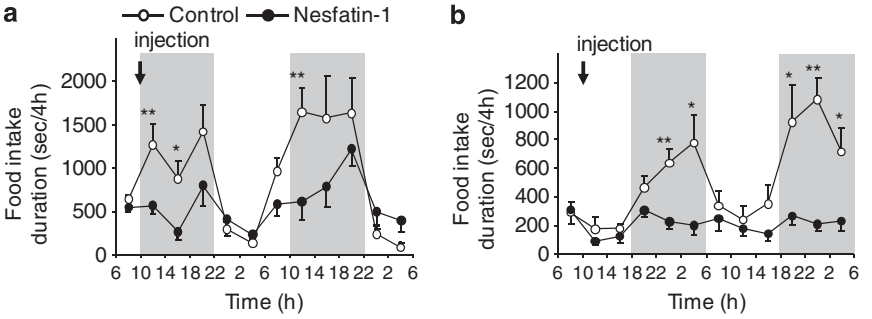

c

		dark phase injections			light phase injections		
	treatment	0-24h	24-48h	n	0-24h	24-48h	n
Food intake	control	2.0 ± 1.0	1.6 ± 1.0	5,6	3.5 ± 1.1	2.3 ± 0.8	6
change (g)	nesfatin	-1.0 ± 0.9	5.0 ± 1.8$^{\#}$	6	1.0 ± 0.9	3.2 ± 1.0	6
Water intake	control	1.8 ± 2.0	2.2 ± 2.4	5	1.5 ± 3.1	3.0 ± 1.4	6
change (g)	nesfatin	-12.2 ± 4.5*	8.2 ± 4.8$^{\#}$	5	-8.0 ± 3.7*	8.7 ± 3.8$^{\#}$	6
Body weight	control	3.4 ± 2.0	1.6 ± 1.6	5	6.2 ± 1.7	5.3 ± 1.9	6
change (g)	nesfatin	-1.4 ± 2.8	3.0 ± 1.5	5	1.8 ± 0.9	4.7 ± 1.4	6

Figure 1. Food intake and related parameters in rats after icv administration of 25 pmol of nesfatin-1. (**a**, **b**) Time spent with food intake in case of dark ($n = 5$–6) and light phase ($n = 10$–12) injections (arrows) of nesfatin-1 or saline, respectively. Data were recorded continuously, summarised at 4 h intervals and plotted over a 48 h period. Dark phases are labelled by grey shadows. Sum ± s.e.m., *$P < 0.05$, **$P < 0.01$. (**c**) Daily changes in food and water intake, as well as in the body weight in case of dark ($n = 5$–6) and light phase ($n = 6$) injections of nesfatin-1, or saline. Mean ± s.e.m., *$P < 0.05$ for treatment, $^{\#}P < 0.05$ for time effect. See text for details of statistical analysis.

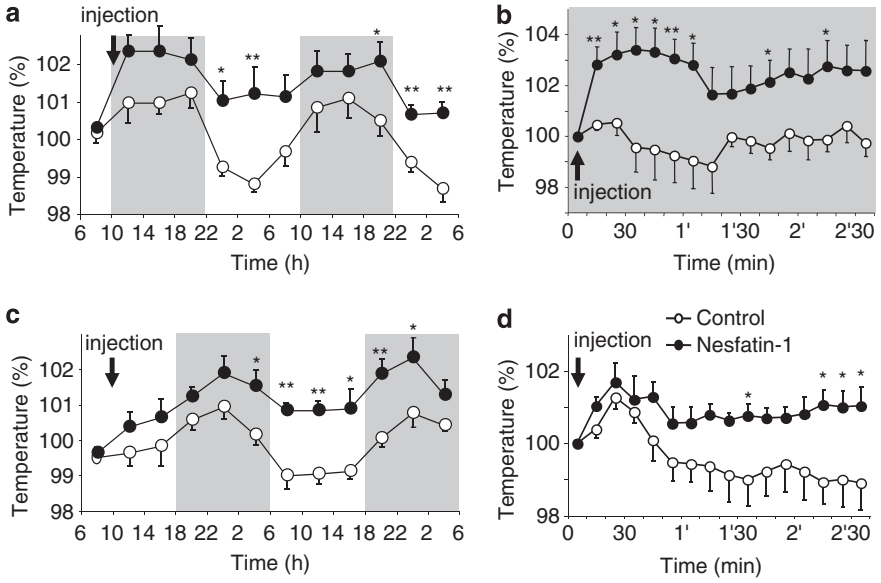

Figure 2. Effect of nesfatin-1 (25 pmol) on core body temperature of rats. Nesfatin-1 or saline were injected intracerebroventricularly (arrows) and core body temperature was recorded in every minute by remote radio telemetry. (**a**, **c**) Results after dark and light phase injections, respectively, averaged at 4 h intervals and plotted over a 48 h period. Data of each animal were normalised to the mean temperature value of the same animal measured between 6–7 h, at the beginning of the recording (100%). (**b**, **d**) Detailed analysis of (**a**, **c**), respectively, showing the mean values calculated at 10 min intervals over a 2.5 h period immediately after the injection. Data were normalised to the average temperature of 10 min before the injection. Dark phases are labelled by grey shadows. Mean ± s.e.m., $n = 5–6$ (**a**, **c**) or 8 (**b**, **d**) per group, $^*P < 0.05$, $^{**}P < 0.01$. See text for details of statistical analysis.

the lower dose applied (Supplementary Figures 2B and C). Again, there was no change in locomotion either immediately after the injections (Supplementary Figure 1C), or all along the observation period (not shown). A definite reduction in the amount of consumed food was observed on the first day after the injections, followed by compensatory eating next day, that probably happened mainly during the second light phase (effect of treatment: $F_{(1,12)} = 8.55$, $P < 0.05$, tendency for time effect: $F_{(1,27)} = 4.33$, $P = 0.06$, treatment × time interaction: $F_{(1,27)} = 9.88$, $P < 0.01$), (Supplementary Table 1 and Supplementary Figure 2A). Changes in water intake were comparable in groups treated with 25 or 100 pmol nesfatin-1 (tendency for treatment effect: $F_{(1,12)} = 3.89$, $P = 0.07$, treatment within first day (*post hoc* comparison Holm–Sidak method): $P < 0.05$, time: $F_{(1,27)} = 5.29$, $P < 0.05$, treatment × time interaction: $F_{(1,27)} = 4.83$, $P < 0.05$) (Supplementary Table 1). Higher dose of nesfatin- 1 enhanced tendencies observed previously on body weight (effect of time: $F_{(1,27)} = 5.15$, $P < 0.05$, tendency for treatment × time effect: $F_{(1,27)} = 4.33$, $P = 0.06$), (Supplementary Table 1).

Effect of cold stress on activation of nesfatin-1/NUCB2 expressing neurons

Exposure of rats to cold induced strong Fos activation in neurons at several brain nuclei, as previously described.[21] Control rats showed only minimal labelling (Figures 4a, c, e, g; 5a and 6a-c). In the preoptic region, most of the Fos-positive cells were located in the medial preoptic area lacking nesfatin-1/NUCB2 labelling (Figures 4a and b). Cold activated only few nesfatin-1/NUCB2 neurons in the periventricular preoptic nucleus (Figures 4a-d). Here, a group of double-labelled cells was seen, in the close vicinity of the third ventricle (Figure 4d, arrow). Nesfatin-1/NUCB2 and Fos double IHC revealed heavy labelling of the magnocellular cells in the supraoptic nucleus (Figures 4e and f), and less extensive activation in the medial and lateral parts of the ARC (Figures 4g and h). Activated nesfatin-1/NUCB2 immunopositive neurons were present in high number also in the magno-, and parvocellular subdivisions of the PVN (Figures 5a and b). Within the parvocellular PVN, Fos and nesfatin-1/NUCB2 double positive neurons were observed both in the hypophysiotropic (Figures 5a and b, mp and p) and in the autonomic projecting subdivisions (Figures 5a and b, arrow and asterisk). Triple IHC demonstrated that many cold-activated nesfatin-1/NUCB2 cells in the parvocellular PVN were prepro-TRH positive (Figures 5c-f).

In the lower brainstem, cold exposure induced a very strong Fos labelling in all of the nesfatin-1/NUCB2 expressing neurons in the nucleus raphe pallidus (Figures 6a and d) and raphe obscurus (Figures 6b and e), scattered double-labelled cells were found in the NTS (Figures 6c and f). Almost all of the nesfatin-1/NUCB2 immunoreactive cells in the nucleus raphe pallidus and obscurus contained prepro-TRH, too (Figures 6g-i).

DISCUSSION

Although nesfatin-1 is a potent anorexigen that may have therapeutic significance, long-term effects of a single injection have not been investigated yet. In the present paper, we report for the first time that icv-administered nesfatin-1 influences nocturnal food intake, as well as core body temperature over a 48 h period, modifies the circadian amplitude of these two parameters, and its effects interact with the circadian rhythm. We also provide new data on functional relevance of certain nesfatin-1/NUCB2 neurons located at thermoregulatory key centres in response to cold, further confirming its involvement in regulation of energy expenditure.

The 25 pmol dose of icv nesfatin-1 for rats was chosen according to Oh-I *et al.*[1], who applied this dose as a maximal one, establishing that 5 pmol is already effective. Most of the

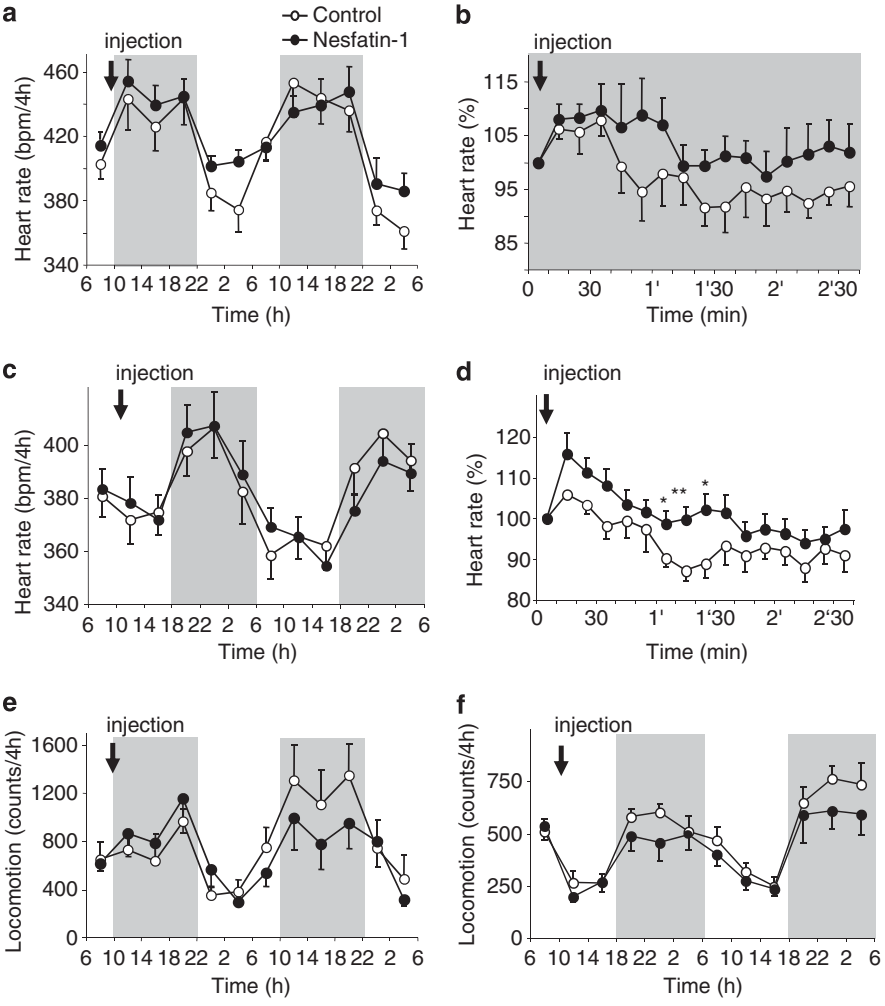

Figure 3. Effect of nesfatin-1 (25 pmol) on heart rate (**a**–**d**) and locomotion (**e**, **f**) of rats. Nesfatin-1 or saline were injected intracerebroventricularly (arrows) and parameters were recorded in every minute by remote radio telemetry. (**a**, **c**) Heart rate results after dark and light phase injections, respectively, averaged at 4 h intervals and plotted over a 48 h period. (**b**, **d**) Detailed analysis of (**a**, **c**) respectively, showing the mean values calculated at 10 min intervals over a 2.5 h period immediately after the drug applications, and expressed in percentage of average values measured 10 min before the injections. (**e**, **f**) Locomotion after dark and light phase injections, respectively, recorded in every minute, summarised at 4 h intervals and plotted over a 48 h period. Dark phases are labelled by grey shadows. Dark phase injections ($n = 5$–6), light phase injections ($n = 10$). Mean ± s.e.m. (heart rate) or sum ± s.e.m. (locomotion). *$P < 0.05$. See text for details of statistical analysis.

authors working on rats and using icv injections investigating different aspects of nesfatin-1's actions have also found the 5–20 pmol dose range effective, higher doses only caused earlier timing of the effect, and/or enhanced the tendencies observed with lower dose.[5,22,23] We also found the 25 pmol dose as an adequate one, increasing the dose to 100 pmol did not lead to any substantially new observations.

Long-lasting effects and interference with the diurnal rhythm are not exclusive among the peptides regulating energy balance. Orexin initiates daytime food intake only, and NPY's action on body temperature is maintained for at least 24 h.[24,25] Earlier data showed that nesfatin-1 reduced nocturnal food intake in the first 6 h after icv injections or given intranasally at the beginning of the dark phase.[1,3] Report about longer than 24 h observations is not published so far. In our experiments, duration of food intake was also decreased in the first 6 h after injection of the drug at the beginning of the dark phase. In addition, nesfatin-1 decreased nocturnal food intake duration at the beginning of the second night, too. Nesfatin-1's long-time nocturnal food intake-reducing capability was evident even when it was given during the light phase of the day, supposing a possible interaction with the circadian rhythm. So far, food intake duration after nesfatin-1 treatment was measured in mice only, where it also had a tendency to reduce total mealtime and time spent with food consumption.[26] Daily food and water intake, as well as body weight measurements point to a potential decrease in all parameters on the first day and some degree of compensation on the second day. Therefore, as it seems, chronic treatment is necessary for developing a permanent body weight-reducing effect.[1]

Anorexigenic compounds, like prolactin-releasing peptide, corticotropin-releasing hormone, cocaine- and amphetamine-regulated transcript and TRH often affect not only the food intake, but–through the energy expenditure–also the thermoregulation.[12,27–29] To reveal whether nesfatin-1 may alter the body temperature, we injected it during the light phase when the body temperature of the nocturnal animals is naturally lower. Lower dose of nesfatin-1 caused only a transient 1% elevation in body temperature within the first 3 h. Nonetheless, the main effect was seen during the next light phase when the body temperature of

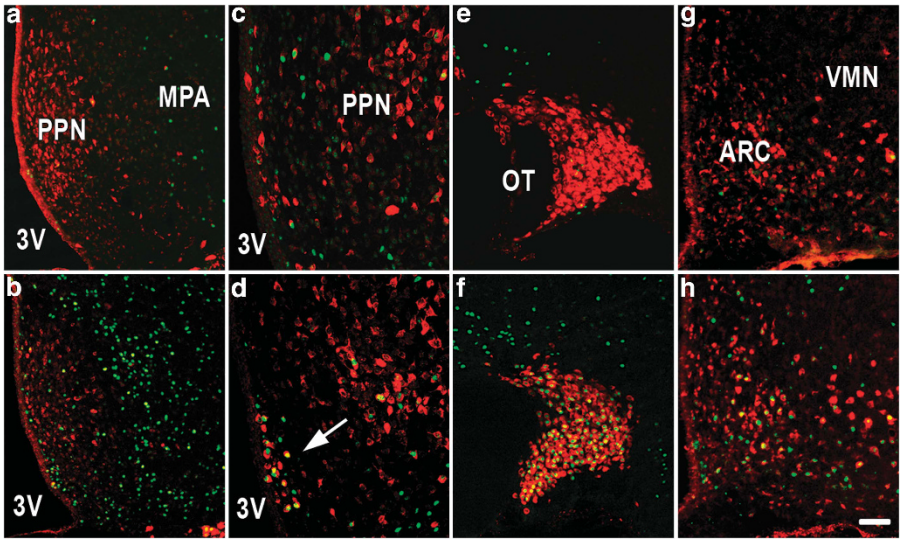

Figure 4. Cold stress activated nesfatin-1/NUCB2 immunopositive neurons in the hypothalamus. Activated, Fos-positive neuronal cell nuclei are green, nesfatin-1/NUCB2 labelled neurons are red, double labelled cells are yellow. Top (**a**, **c**, **e**, **g**); control, bottom (**b**, **d**, **f**, **h**); cold exposed animals. (**a**, **b**) Strong Fos activation without nesfatin-1/NUCB2 labelling in the medial preoptic area. (**c**, **d**) Scattered double-labelled cells in the periventricular preoptic nucleus. A group of neurons located at the vicinity of the 3rd ventricle is strongly activated by cold (**d**, arrow). (**e**, **f**) Heavy Fos activation in the supraoptic nucleus. (**g**, **h**) Double-labelled neurons in the ARC. MPA, medial preoptic area, OT, optic tract, PPN, periventricular preoptic nucleus, 3V, third ventricle, VMN, ventromedial nucleus. Scale bar: 100 μm for **a**, **b**, **e**, **f**, and 50 μm for **c**, **d**, **g**, **h**.

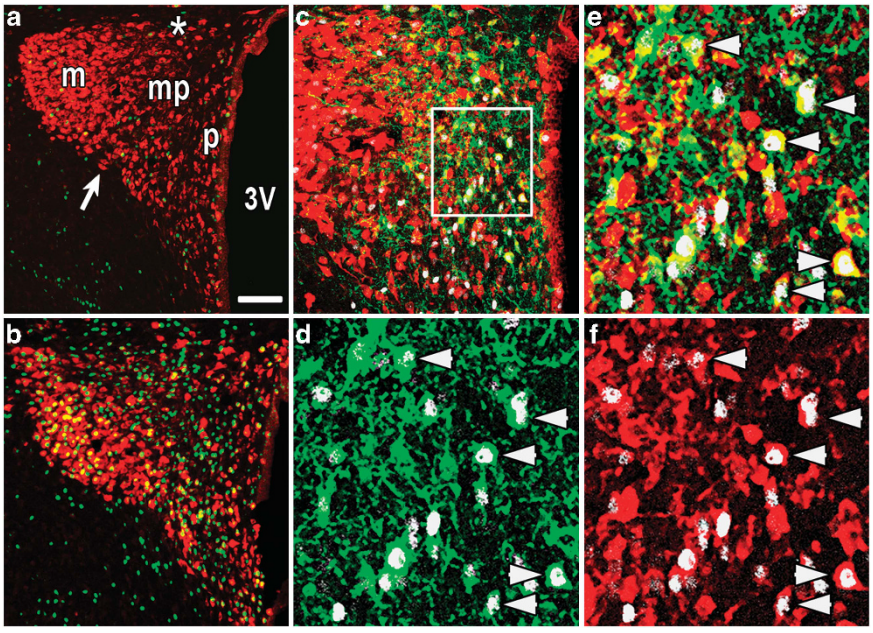

Figure 5. Cold stress activated nesfatin-1/NUCB2 immunopositive neurons in the hypothalamic PVN. (**a**, **b**) Control and cold-exposed animals, respectively. Activated, Fos-positive neuronal cell nuclei are green, nesfatin-1/NUCB2-labelled neurons are red, double-labelled cells are yellow. Double-labelled cells are seen in all subdivisions. (**c**–**f**) Cold stress activated prepro-TRH / nesfatin1/NUCB2-positive neurons in the medial parvocellular PVN. Fos is shown in white, prepro-TRH in green, and nesfatin1/NUCB2 in red. Triple-labelled cells are yellow with white nucleus. (**c**) Triple labelling, smaller magnification. (**e**) Enlarged picture of the framed area in (**c**). (**d**) The same area as in (**e**) showing the Fos and prepro-TRH labelling separately. (**f**) The same area as in (**e**) showing the Fos and nesfatin-1/NUCB2 labelling separately. The arrows on (**d**, **e**) and (**f**) point to identical cells immunopositive for all the three peptides. Hypophyseotropic subdivisions: m, magnocellular; mp, medial parvocellular; p, periventricular parvocellular. Autonom projecting subdivisions: asterisk and arrow; dorsal and ventral parvocellular components, respectively. 3V, third ventricle, Scale bar: 100 μm for **a**, **b**, 250 μm for **c**, 50 μm for **e, f**.

the rats failed to decrease to the level of the controls and remained higher during the second night too. In contrast, nesfatin-1 injected at the beginning of the dark phase elevated body temperature immediately for 1 h, indicating that there may be a potentiating action on the increased sympathetic activity characteristic to the animals at this time of the day.[30–32] The temperature of the treated rats practically did not differ at nights, but again it failed to fall during the next two light phases. Higher dose of nesfatin-1 one applied during the light phase caused somehow similar effect then the lower dose applied at dark,

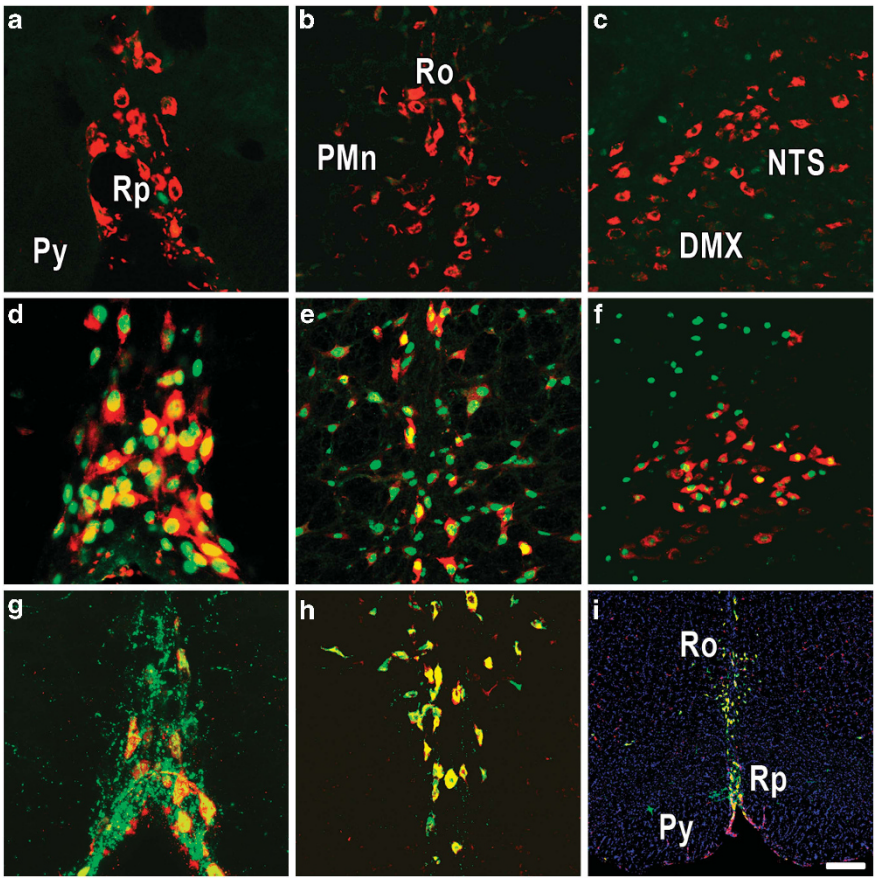

Figure 6. Cold sensitivity and characterisation of nesfatin-1/NUCB2 immunopositive neurons in the brainstem. (**a**–**f**) Effect of cold stress. Activated, Fos-positive neuronal cell nuclei are green, nesfatin-1/NUCB2-labelled neurons are red, double-labelled cells are yellow. Pictures of control (**a**–**c**) and cold exposed (**d**–**f**) animals are under each other, respectively. All nesfatin-1/NUCB2 neurons are activated in the nucleus raphe pallidus (**a**, **d**) and in the nucleus raphe obscurus (**b**, **e**). Many double-labelled cells are observed in the NTS, commissural part (**c**, **f**). (**g**–**i**) Colocalisation of nesfatin-1/NUCB2 and prepro-TRH in the nucleus raphe pallidus and obscurus. Prepro-TRH-positivity is seen as green, nesfatin-1/NUCB2 neurons are red, double-labelled cells are yellow. DAPI counterstaining on I is blue. Colchicine treatment (**h**, **i**) eliminates immunostaining of the fibres that partly mask the cells (**g**). DMX, dorsal vagal nucleus, PMn, paramedian reticular nucleus, Py, pyramidal tract, Ro, nucleus raphe obscurus, Rp, nucleus raphe pallidus. Scale bar: 30 μm for **a**, **d**, **g**; 50 μm for **b**, **c**, **e**, **f**, **h** and 220 μm for **i**.

indicating that the elevated concentration may compensate for the reduced daytime sensitivity. There is a general consensus in the literature that nesfatin-1 itself is able to increase sympathetic activity, therefore such interaction is not surprising.[4,23] It is interesting, however, that there was no effect of nesfatin-1 on the heart rate applied at night, meanwhile a limited and belated (starting more than 1 h after injection) heart rate elevation was observed, when it was given during the light phase. This became more definite using higher dose of nesfatin-1. Yosten *et al*.[4] did not find any change in heart rate after nesfatin-1 treatment during the light phase, but they measured it only for 1 h after injection.

The mechanism through nesfatin-1 is able to modify the core temperature of the animals is not yet clear. Participation of nesfatin-1/NUCB2 in several autonomic functions is proposed, as nesfatin-1/NUCB2 neurons are present in high number in the hypothalamus and the lower brainstem autonomic centres.[9,33] Many of these neurons were activated by cold, suggesting that nesfatin-1/NUCB2 may mediate thermoregulatory, as well as other responses to cold. Regulation of heat loss and thermogenesis are the two main effectors to maintain body temperature.[34] Setting heat loss includes adjusting thermoregulatory behaviour and skin blood flow, whereas controlling thermogenesis is realized through regulation of the skeletal muscle (shivering) and/or the brown adipose tissue (BAT) heat production (non shivering).[34] Although importance of BAT was earlier recognised only in mammals, it had recently been demonstrated that humans also possess essential amounts of functioning BAT.[35] Retrograde, transsynaptic virus labelling of the BAT is a good tool to reveal areas in the brain connected directly or indirectly to the BAT. By this way, it has been shown that the PVN, the ARC, the nucleus raphe pallidus and raphe obscurus, and the NTS, where cold stress activated a number of nesfatin1/NUCB2-positive cells, are all among the elements of the polysynaptic pathways toward the BAT.[36,37] Moreover, many effects of nesfatin-1 are mediated through melanocortin-3/4 receptors, and the melanocortin-3/4 receptor antagonist SHU9119 significantly decreases BAT temperature.[4,23,38] In addition, prepro-TRH, precursor of TRH, a key factor regulating basal metabolic rate and thermogenesis, co-localised in the cold responsive nesfatin-1/NUCB2 cells in the PVN and in the brainstem raphe nuclei.[12] Although Johnson *et al*.[20] suggested colchicine treatment for TRH immunostaining, the prepro-TRH antibody we used worked without it. Colchicine treatment was still helpful, as it reduced the number of immunopositive fibres that might otherwise mask the cells (see Figures 6g and h for comparison). Nesfatin-1/NUCB2 has previously been colocalised with serotonin in the caudal raphe nuclei,[9] and serotonin-containing neurons here are TRH positive.[20] Therefore, TRH, serotonin and nesfatin-1/NUCB2 are probably co-expressed in these nuclei. Serotonin expressing raphe pallidus and obscurus neurons exert their actions as preganglionic premotor neurons

regulating skin blood flow.[34] Thus, nesfatin-1 expressed in these cells is in a position to modify also heat dissipation.

In conclusion, our observations provide a new insight on nesfatin-1 function, and on neurocircuitry that may mediate its actions. As nesfatin-1 is expressed in human, acts as anorexigen, and its role has recently been suggested in many other functions such as, epilepsy and puberty onset, our data may be relevant regarding nesfatin-1, as a potential pharmacotherapeutical target.[7,39,40]

CONFLICT OF INTEREST

The authors declare no conflict of interest.

ACKNOWLEDGEMENTS

We would like to thank Éva Rédei (Northwestern University, Chicago, IL, USA) for kindly providing the prepro-TRH antibody and for Szilvia Deák and Judit Kerti for the technical assistance. The study was sponsored by ETT–2009/ 495 (ZE Toth) and by OTKA CK-80180 (M Palkovits, ZE Toth, K Könczöl) and OTKA NK-71629 (D Zelena) and TÁMOP-4.2.1.B-09/1/KMR-2010-0001. ZE Toth is supported by the Bolyai fellowship.

REFERENCES

1 Oh-I S, Shimizu H, Satoh T, Okada S, Adachi S, Inoue K *et al.* Identification of nesfatin-1 as a satiety molecule in the hypothalamus. *Nature* 2006; **443**: 709 - 712.
2 Maejima Y, Sedbazar U, Suyama S, Kohno D, Onaka T, Takano E *et al.* Nesfatin-1-regulated oxytocinergic signaling in the paraventricular nucleus causes anorexia through a leptin-independent melanocortin pathway. *Cell Metab* 2009; **10**: 355 - 365.
3 Shimizu H, Oh IS, Okada S, Mori M. Nesfatin-1: an overview and future clinical application. *Endocr J* 2009; **56**: 537 - 543.
4 Yosten GL, Samson WK. Nesfatin-1 exerts cardiovascular actions in brain: possible interaction with the central melanocortin system. *Am J Physiol Regul Integr Comp Physiol* 2009; **297**: R330 - R336.
5 Merali Z, Cayer C, Kent P, Anisman H. Nesfatin-1 increases anxiety- and fear-related behaviors in the rat. *Psychopharmacology (Berl)* 2008; **201**: 115 - 123.
6 Konczol K, Bodnar I, Zelena D, Pinter O, Papp RS, Palkovits M *et al.* Nesfatin-1/NUCB2 may participate in the activation of the hypothalamic-pituitary-adrenal axis in rats. *Neurochem Int* 2010; **57**: 189 - 197.
7 Aydin S, Dag E, Ozkan Y, Erman F, Dagli AF, Kilic N *et al.* Nesfatin-1 and ghrelin levels in serum and saliva of epileptic patients: hormonal changes can have a major effect on seizure disorders. *Mol Cell Biochem* 2009; **328**: 49 - 56.
8 Kohno D, Nakata M, Maejima Y, Shimizu H, Sedbazar U, Yoshida N *et al.* Nesfatin-1 neurons in paraventricular and supraoptic nuclei of the rat hypothalamus coexpress oxytocin and vasopressin and are activated by refeeding. *Endocrinology* 2008; **149**: 1295 - 1301.
9 Brailoiu GC, Dun SL, Brailoiu E, Inan S, Yang J, Chang JK *et al.* Nesfatin-1: distribution and interaction with a G protein-coupled receptor in the rat brain. *Endocrinology* 2007; **148**: 5088 - 5094.
10 Fort P, Salvert D, Hanriot L, Jego S, Shimizu H, Hashimoto K *et al.* The satiety molecule nesfatin-1 is co-expressed with melanin concentrating hormone in tuberal hypothalamic neurons of the rat. *Neuroscience* 2008; **155**: 174 - 181.
11 Pereira-da-Silva M, Torsoni MA, Nourani HV, Augusto VD, Souza CT, Gasparetti AL *et al.* Hypothalamic melanin-concentrating hormone is induced by cold exposure and participates in the control of energy expenditure in rats. *Endocrinology* 2003; **144**: 4831 - 4840.
12 Lechan RM, Fekete C. The TRH neuron: a hypothalamic integrator of energy metabolism. *Prog Brain Res* 2006; **153**: 209 - 235.
13 Masaki T, Yoshimichi G, Chiba S, Yasuda T, Noguchi H, Kakuma T *et al.* Corticotropin-releasing hormone-mediated pathway of leptin to regulate feeding, adiposity, and uncoupling protein expression in mice. *Endocrinology* 2003; **144**: 3547 - 3554.
14 Solinas G, Summermatter S, Mainieri D, Gubler M, Montani JP, Seydoux J *et al.* Corticotropin-releasing hormone directly stimulates thermogenesis in skeletal muscle possibly through substrate cycling between *de novo* lipogenesis and lipid oxidation. *Endocrinology* 2006; **147**: 31 - 38.
15 Fan W, Voss-Andreae A, Cao WH, Morrison SF. Regulation of thermogenesis by the central melanocortin system. *Peptides* 2005; **26**: 1800 - 1813.
16 Kong WM, Stanley S, Gardiner J, Abbott C, Murphy K, Seth A *et al.* A role for arcuate cocaine and amphetamine-regulated transcript in hyperphagia, thermogenesis, and cold adaptation. *FASEB J* 2003; **17**: 1688 - 1690.
17 Ellacott KL, Lawrence CB, Rothwell NJ, Luckman SM. PRL-releasing peptide interacts with leptin to reduce food intake and body weight. *Endocrinology* 2002; **143**: 368 - 374.
18 Mikics E, Baranyi J, Haller J. Rats exposed to traumatic stress bury unfamiliar objects--a novel measure of hyper-vigilance in PTSD models? *Physiol Behav* 2008; **94**: 341 - 348.
19 Toth ZE, Mezey E. Simultaneous visualization of multiple antigens with tyramide signal amplification using antibodies from the same species. *J Histochem Cytochem* 2007; **55**: 545 - 554.
20 Johnson H, Ulfhake B, Dagerlind A, Bennett GW, Fone KC, Hokfelt T. The serotoninergic bulbospinal system and brainstem-spinal cord content of serotonin-, TRH-, and substance P-like immunoreactivity in the aged rat with special reference to the spinal cord motor nucleus. *Synapse* 1993; **15**: 63 - 89.
21 Bratincsak A, Palkovits M. Activation of brain areas in rat following warm and cold ambient exposure. *Neuroscience* 2004; **127**: 385 - 397.
22 Stengel A, Goebel M, Wang L, Rivier J, Kobelt P, Monnikes H *et al.* Central nesfatin-1 reduces dark-phase food intake and gastric emptying in rats: differential role of corticotropin-releasing factor2 receptor. *Endocrinology* 2009; **150**: 4911 - 4919.
23 Tanida M, Mori M. Nesfatin-1 stimulates renal sympathetic nerve activity in rats. *Neuroreport* 2011; **22**: 309 - 312.
24 Berthoud HR, Patterson LM, Sutton GM, Morrison C, Zheng H. Orexin inputs to caudal raphe neurons involved in thermal, cardiovascular, and gastrointestinal regulation. *Histochem Cell Biol* 2005; **123**: 147 - 156.
25 Szekely M, Petervari E, Pakai E, Hummel Z, Szelenyi Z. Acute, subacute and chronic effects of central neuropeptide Y on energy balance in rats. *Neuropeptides* 2005; **39**: 103 - 115.
26 Goebel M, Stengel A, Wang L, Tache Y. Central nesfatin-1 reduces the nocturnal food intake in mice by reducing meal size and increasing inter-meal intervals. *Peptides* 2011; **32**: 36 - 43.
27 Ellacott KL, Lawrence CB, Pritchard LE, Luckman SM. Repeated administration of the anorectic factor prolactin-releasing peptide leads to tolerance to its effects on energy homeostasis. *Am J Physiol Regul Integr Comp Physiol* 2003; **285**: R1005 - R1010.
28 Buwalda B, de Boer SF, Van Kalkeren AA, Koolhaas JM. Physiological and behavioral effects of chronic intracerebroventricular infusion of corticotropin-releasing factor in the rat. *Psychoneuroendocrinology* 1997; **22**: 297 - 309.
29 Skibicka KP, Alhadeff AL, Grill HJ. Hindbrain cocaine- and amphetamine-regulated transcript induces hypothermia mediated by GLP-1 receptors. *J Neurosci* 2009; **29**: 6973 - 6981.
30 Cahill AL, Ehret CF. Alpha-methyl-p-tyrosine shifts circadian temperature rhythms. *Am J Physiol* 1982; **243**: R218 - R222.
31 Aguzzi J, Bullock NM, Tosini G. Spontaneous internal desynchronization of locomotor activity and body temperature rhythms from plasma melatonin rhythm in rats exposed to constant dim light. *J Circadian Rhythms* 2006; **4**: 6.
32 Makino M, Hayashi H, Takezawa H, Hirai M, Saito H, Ebihara S. Circadian rhythms of cardiovascular functions are modulated by the baroreflex and the autonomic nervous system in the rat. *Circulation* 1997; **96**: 1667 - 1674.
33 Foo KS, Brismar H, Broberger C. Distribution and neuropeptide coexistence of nucleobindin-2 mRNA/nesfatin-like immunoreactivity in the rat CNS. *Neuroscience* 2008; **156**: 563 - 579.
34 Morrison SF, Nakamura K. Central neural pathways for thermoregulation. *Front Biosci* 2011; **16**: 74 - 104.
35 Seale P, Kajimura S, Spiegelman BM. Transcriptional control of brown adipocyte development and physiological function--of mice and men. *Genes Dev* 2009; **23**: 788 - 797.
36 Oldfield BJ, Giles ME, Watson A, Anderson C, Colvill LM, McKinley MJ. The neurochemical characterisation of hypothalamic pathways projecting polysynaptically to brown adipose tissue in the rat. *Neuroscience* 2002; **110**: 515 - 526.
37 Cano G, Passerin AM, Schiltz JC, Card JP, Morrison SF, Sved AF. Anatomical substrates for the central control of sympathetic outflow to interscapular adipose tissue during cold exposure. *J Comp Neurol* 2003; **460**: 303 - 326.
38 Verty AN, Allen AM, Oldfield BJ. The endogenous actions of hypothalamic peptides on brown adipose tissue thermogenesis in the rat. *Endocrinology* 2010; **151**: 4236 - 4246.
39 Garcia-Galiano D, Navarro VM, Roa J, Ruiz-Pino F, Sanchez-Garrido MA, Pineda R *et al.* The anorexigenic neuropeptide, nesfatin-1, is indispensable for normal puberty onset in the female rat. *J Neurosci* 2010; **30**: 7783 - 7792.
40 Tan BK, Hallschmid M, Kern W, Lehnert H, Randeva HS. Decreased cerebrospinal fluid/plasma ratio of the novel satiety molecule, nesfatin-1/NUCB-2, in obese humans: evidence of nesfatin-1/NUCB-2 resistance and implications for obesity treatment. *J Clin Endocrinol Metab* 2011; **96**: E669 - E673.

Supplementary Information accompanies the paper on International Journal of Obesity website (http://www.nature.com/ijo)

OPEN ACCESS Freely available online

Nesfatin-1/NUCB2 as a Potential New Element of Sleep Regulation in Rats

Szilvia Vas[1], Csaba Ádori[1,2], Katalin Könczöl[3], Zita Kátai[1], Dorottya Pap[1], Rege S. Papp[3], György Bagdy[1,4,5], Miklós Palkovits[3], Zsuzsanna E. Tóth[3]*

1 Department of Pharmacodynamics, Semmelweis University, Budapest, Hungary, **2** Department of Neuroscience, Karolinska Institute, Stockholm, Sweden, **3** Neuromorphological and Neuroendocrine Research Laboratory, Department of Anatomy, Histology and Embryology, Semmelweis University and the Hungarian Academy of Sciences, Budapest, Hungary, **4** Group of Neurochemistry, Hungarian Academy of Sciences, Budapest, Hungary, **5** Group of Neuropsychopharmacology, Hungarian Academy of Sciences, Budapest, Hungary

Abstract

Study Objectives: Millions suffer from sleep disorders that often accompany severe illnesses such as major depression; a leading psychiatric disorder characterized by appetite and rapid eye movement sleep (REMS) abnormalities. Melanin-concentrating hormone (MCH) and nesfatin-1/NUCB2 (nesfatin) are strongly co - expressed in the hypothalamus and are involved both in food intake regulation and depression. Since MCH was recognized earlier as a hypnogenic factor, we analyzed the potential role of nesfatin on vigilance.

Design: We subjected rats to a 72 h-long REMS deprivation using the classic flower pot method, followed by a 3 h-long 'rebound sleep'. Nesfatin mRNA and protein expressions as well as neuronal activity (Fos) were measured by quantitative *in situ* hybridization technique, ELISA and immunohistochemistry, respectively, in 'deprived' and 'rebound' groups, relative to controls sacrificed at the same time. We also analyzed electroencephalogram of rats treated by intracerebroventricularly administered nesfatin-1, or saline.

Results: REMS deprivation downregulated the expression of nesfatin (mRNA and protein), however, enhanced REMS during 'rebound' reversed this to control levels. Additionally, increased transcriptional activity (Fos) was demonstrated in nesfatin neurons during 'rebound'. Centrally administered nesfatin-1 at light on reduced REMS and intermediate stage of sleep, while increased passive wake for several hours and also caused a short-term increase in light slow wave sleep.

Conclusions: The data designate nesfatin as a potential new factor in sleep regulation, which fact can also be relevant in the better understanding of the role of nesfatin in the pathomechanism of depression.

Citation: Vas S, Ádori C, Könczöl K, Kátai Z, Pap D, et al. (2013) Nesfatin-1/NUCB2 as a Potential New Element of Sleep Regulation in Rats. PLoS ONE 8(4): e59809. doi:10.1371/journal.pone.0059809

Editor: Gilberto Fisone, Karolinska Institutet, Sweden

Received December 12, 2012; **Accepted** February 18, 2013; **Published** April 1, 2013

Funding: This work was supported by the 6th Framework Program of the European Community (LSHM-CT-2004-503474), Hungarian Research Fund Grant (T020500), Ministry of Welfare Research Grant 460/2006, TAMOP-4.2.1. B-09/1/KMR-2010-0001 (http://www.tamop-palyazat.hu, G.B.), OTKA-CK-80180 (www.otka.hu, M.P.) and ETT495/05 (http://www.ett.hu, Z.E.T.). The funders had no role in study design, data collection and analysis, decision to publish, or preparation of the manuscript.

Competing Interests: The authors have declared that no competing interests exist.

* E-mail: tothzs@ana.sote.hu

Introduction

Nesfatin-1, the N-terminal fragment of the nucleobindin2 protein (NUCB2) is a potent anorexigen decreasing nocturnal food intake in rodents in a dose-dependent manner [1]. Higher plasma nesfatin-1/NUCB2 (nesfatin) levels in overweight patients point to its role in food intake regulation also in humans [2]. In addition, nesfatin has been associated with further functions too, like processing emotional states, such as anxiety and stress [3,4]. Since depression, a major cause of morbidity worldwide is also characterized by marked alterations in emotional states and feeding, initial research on the role of nesfatin regarding this field may have high relevance. As already has been established, patients with major depressive disorder possess high plasma level of nesfatin [5]. For plasma and cerebrospinal fluid nesfatin levels positively correlate, CNS problems related to alterations in nesfatin expression may underlie this elevation [2]. This is also supported by the fact that nesfatin mRNA content is elevated in the Edinger-Westphal nucleus of depressed male suicide victims [6]. Besides emotional and feeding disturbances, sleep-wake regulation is another function typically affected in depression [7]. Impaired sleep continuity, decreased rapid eye movement sleep (REMS) latency and elevated time spent in REMS are characteristic sleep-EEG changes in depressed patients [8,9] moreover, antidepressant medication also alters sleep. As a consequence, the existence of a relationship between nesfatin and sleep regulation can be assumed [10].

The largest population of nesfatin neurons in the CNS can be found in the perifornical and lateral hypothalamic (LH) areas that belong to the dorsolateral hypothalamus (DLH) and in the zona incerta (ZI) [11,12]. These areas are closely associated with sleep-wake regulation [13], and are also related to both control of

feeding and depression [14–17]. Two main types of neurons forming intermingled, but separate populations were identified in this region before; the orexin and the melanin-concentrating hormone (MCH) producing cell groups, both increasing food intake, but acting oppositely on vigilance [18,19]. Nesfatin is highly co - expressed with MCH, although a smaller portion of nesfatin neurons is MCH - negative [10]. Since MCH increases REMS [20], but unlike nesfatin, it is an orexigenic peptide, the possible role of nesfatin-1 in the regulation of sleep has a special interest.

Based on the facts above, in this study, we aimed to investigate the effect of intracerebroventricularly (icv) administered nesfatin-1 on vigilance stages, like wakefulness, REMS and non-REMS. We also raised the questions, whether selective REMS pressure impacts expression of nesfatin, and alters activation of the nesfatin - immunoreactive neurons in the DLH and the ZI.

To elucidate this, we performed REMS deprivation using the classic flower pot method [20], followed or not by rebound sleep, and determined nesfatin protein and mRNA expressions by ELISA and quantitative *in situ* hybridization (ISH) method. Finally, we analyzed the activation pattern of MCH - positive and - negative nesfatin cell populations under the different experimental conditions using Fos/nesfatin/MCH triple immunostainings.

Materials and Methods

Ethics Statement

Experiments were performed according to the European Communities Council Directive of 24 November 1986 (86/609/EEC) and the National Institutes of Health "Principles of Laboratory Animal Care" (NIH Publications No. 85-23, revised 1985), as well as specific national laws (the Hungarian Governmental Regulations on animal studies, December 31, 1998). All experiments were approved by the National Scientific Ethical Committee on Animal Experimentation, and permitted by the governement (Food Chain Safety and Animal Health Directorate of the Central Agricultural Office, Permit Number: 22.1/1375/7/2010). All surgery was performed under anesthesia, and all efforts were made to minimize suffering.

Animals. Male Wistar rats (Semmelweis University, Budapest, Hungary) weighing 300–350 g were used for the studies. Animals were kept with light-dark cycle of 12:12 h (light on at 10:00 and off at 22:00, daylight type fluorescent tubes, 18 W, approximately 300 lx) at room temperature (21±1°C), and had free access to standard rodent chow and tap water. Animals were habituated to the conditions in the experimental room at least for two weeks.

Experiment 1. Effects of REMS Deprivation and the 'Rebound Sleep' on the Expression of Nesfatin mRNA and Protein

REMS deprivation. REMS deprivation was performed using the flower pot method, as described earlier [20,21]. Briefly, animals were placed on round platforms situated in the middle of a round water tank with a surface 0.5 cm above the water level at lights on (10:00) for 72 h. The diameter of the platforms was either small (6.5 cm) or large (13 cm). As muscle atony is typical for REMS, animals on the small pots fall into the water immediately after entering REMS. Contrarily, rats on the large pots fit better on the surface and may sleep REMS, therefore they are used as stress controls. According to this, animals were randomly divided into six groups. The 1st group; small (SP), and the 2nd group; large pot (LP) kept rats, that were sacrificed after spent 72 h on the platforms. The 3rd group; SP plus rebound (SPR), and the 4th group; LP plus rebound (LPR) rats that, after spending 72 h on SP or LP platforms, respectively, were transferred to their home cages at lights on for 3h rebound sleep after which they were killed. The 5th group; home cage (HC) and the 6th group; HCR animals were controls, kept undisturbed in their home cages, and killed at the end of the experiment either at lights on (HC) or 3 h later (HCR), respectively. Rats were sacrificed by decapitation (n = 7 for ELISA, n = 9 for ISH) or perfused with 4% paraformaldehyde in 0.1 M phosphate buffered saline, pH = 7.4 (PBS) for immunohistochemistry (n = 5). The brains were removed and frozen on dry ice. Fixed tissue was cryoprotected in 20% sucrose overnight before freezing.

Rats on the platforms were fed *ad libitum* without restriction using a waterproof food supplier unit at a distance easy to approach. Body weight change and food intake of rats during the time spent on the platforms were measured.

***In situ* hybridization technique.** The rat nesfatin-1 cDNA (246 bp) was purchased from Invitrogen (Budapest, Hungary, GenBank Acc: DY314804), cloned into a pBC KS+ vector and verified by sequencing. The rat corticotropin - releasing hormone (CRH) cDNA (468 bp) was kindly provided by W.S. Young 3rd, and used as earlier described [22]. The [35S]UTP-labeled sense and antisense riboprobes were prepared by *in vitro* transcription (Maxiscript KIT), according to the manufacturer's protocol.

Hypothalamic regions of fresh frozen brains were cut into 12 μm thick serial coronal sections in a cryostat (Leica Microsystems GmbH, Wetzlar, Germany). The sections were thaw-mounted and air-dried at 37°C onto positively charged Superfrost Plus slides (Thermo Scientific, Budapest, Hungary). Slides were stored at −80°C until used. Hybridizations were performed overnight in humid chambers at 55°C with 10^6 cpm/slide of the [35S]UTP-labeled probes, as described earlier [4]. After this step, sections were apposed to a BAS-MS imaging plate (Fuji Photo Film Co., LTD., Kanagawa, Japan, NJ) for 3 days, and then data were read out by a Fujifilm FLA-8000 Image Analyzer. Expression levels were evaluated from the images recorded on the phosphor imager. Mean grey values of the area of interest were measured by using the Image J 1.32j software (Wayne Rasband; NIH, Bethesda, MD, USA) on both sides of 4–6 sections in each animal. Background values measured in parallel were subtracted. The average/animal data were used for statistical evaluation.

ELISA measurements. Hypothalamic regions of fresh frozen brains were cut into 300 μm thick serial coronal sections in a cryostat (Leica). DLH with ZI was dissected by micropunch technique [23], using a special punching needle (inner diameter of 500 μm). Tissue pellets were stored at −80°C until further processing. Samples were homogenized in 200 μl of 0.1 M HCl/0.3 μM aprotinin solution (Sigma-Aldrich, Budapest, Hungary) by ultrasound sonication for 3×15 seconds on ice. Then, samples were centrifuged for 20 min at 15,300 rpm at 4°C. The supernatants were divided into two portions and dried by a vacuum concentrator (Savant Instruments Inc, Holbrook, NY, USA). The first portion was reconstituted in 40 μl 0.1 M Tris buffer (pH = 8.0) and the total protein concentration was determined by using a Lowry-based assay. The second portion was reconstituted in 400 μl 1x sample buffer provided in the ELISA kit and used for determining nesfatin protein concentrations, by a commercially available ELISA kit (Phonix Europe GmbH, Karlsruhe, Germany) according to the manufacturer's protocol.

Immunohistochemistry. Hypothalami were cut into 50 μm thick serial coronal sections on a frigomobil (Frigomobil, Reichter-Jung, Vienna, Austria). Immunostaining started with blocking the endogenous peroxidase activity, using a 3% H_2O_2 solution

(Sigma-Aldrich) for 15 min. Then, sections were blocked in 1% BSA and 0.5% TritonX-100/PBS all from Sigma-Aldrich for 1 h. The same solution was used to dilute the antibodies. Incubations were made for 2 days at 4°C in primary antibodies and for 1 h at room temperature, in secondary or tertiary antibodies. Sections were washed 3 times for 5 min in PBS following each incubation step. To block peroxidase enzyme used for visualization previously, and to prevent species cross-reactions caused by primary antibodies raised in the same hosts, sections were microwave-treated in 0.1 M citric-acid (pH = 6.0) for 5 min after each immunostaining [24].

Fos immunostaining was performed using rabbit anti-Fos primary antibody (1:30,000, Santa Cruz Biotechnology, Inc., Santa Cruz, CA, USA) and anti-rabbit IgG polymer-HRP (Millipore, Budapest, Hungary) secondary antibody. The immunostaining was visualized by FITC-conjugated tyramide (Invitrogen, Budapest, Hungary). Next, sections were incubated in rabbit anti-nesfatin (1:24,000, Phoenix Pharmaceuticals, Inc., Burlingame, CA, USA) and again in anti-rabbit IgG polymer-HRP (Millipore). The second immunostaining was developed by tyramide-conjugated Alexa Fluor 568 (Invitrogen). In case of triple immunostainings, rabbit anti-MCH was applied (1:10,000, Phoenix Europe GmbH), followed by incubation in biotinylated anti-rabbit IgG as secondary antibody (1:1,000, Vector Laboratories, Inc., Burlingame, CA, USA) and in extravidine-peroxidase (1:1,000, Sigma). The MCH antigen was visualized by tyramide-conjugated biotin (Invitrogen) and Streptavidin-Cy5 (1:1000, Jackson ImmunoResearch Europe Ltd, Newmarket, Suffolk, UK). Sections were mounted on non-coated slides, air - dried and coverslipped with DPX (Sigma).

Image analysis. Nesfatin - positive cell populations were analyzed in three areas: 1) ZI, 2) LH, 3) perifornical area, including the perifornical nucleus itself [25]. Images were captured bilaterally using a 20X objective (S Fluor 20X/0.75, ∞/0.17, WD1.0) on 3–5 sections per animal by a Nicon Eclipse E800 microscope attached to a Bio-Rad Radiance 2100 Rainbow confocal scanning system by sequential scanning. Cell counts and determination of co - localization were made using the AnalySIS Pro 3.2 program (Olympus, Soft Imaging Solutions GmbH, Münster, Germany), by simultaneous examination of the greyscale images of the separated channels and the colored overlay picture. To identify neurons in the pictures, a numbered grid of the same size was placed over the overlay picture and the greyscale pictures of the separated channels. Only neurons with visible cell nuclei were counted. Percentages of nesfatin/MCH double labeled neurons among the nesfatin positive ones, the percentages of Fos/nesfatin within the single nesfatin and Fos/nesfatin/MCH within the nesfatin/MCH double positive subpopulations were calculated per animal. Data are presented as the average of the results from 5 animals per group.

Experiment 2. Effects of Exogenously Administered Nesfatin-1 on Vigilance

EEG measurements. Rats (n = 6) were equipped with electroencephalographic (EEG) and electromyographic (EMG) electrodes for EEG recordings, as described earlier [26,27]. Stereotaxic surgery was performed under 2% halothane anesthesia (using Fluotec 3 halothane vaporizer). All efforts were made to minimize suffering of the animals. Briefly, stainless steel screw electrodes were implanted epidurally over the left frontal motor cortex (coordinates: anterior-posterior (A-P): 2.0 mm from bregma, lateral (L): 2.0 mm to the midline, [25] the left parietal cortex (A-P: 2.0 mm from lambda, L: 2.0 mm) for fronto-parietal EEG recordings, and a ground electrode was placed over the cerebellum. In addition, EMG electrodes (stainless steel spring electrodes embedded in silicon rubber, Plastics One Inc., Roanoke, VA, USA) were placed into the muscles of the neck. At the same time, a plastic cannula was implanted into the right lateral ventricle (coordinates: A-P: −0.8 mm to the bregma level, L: 2.0 mm, and ventral: 4.0 mm below the skull surface). The cannula and the EEG electrodes were anchored to the skull with dental cement (SpofaDental a.s., Markova, Czeh Republic). A stainless steel obturator was inserted into the guide cannula and was kept patent until use. After surgery, rats were kept in single cages in the recording chamber, and were allowed to recover for 7 days. Animals were then habituated to the recording conditions for five days before experiment started by attaching them to the polygraph using a flexible recording cable and an electric swivel, fixed above the cages, permitting free movements. During the recovery and the habituation period to the recording conditions, animals were also handled daily to minimize future experimental stress, as described earlier [28]. On the day of the experiment, 25 pmol/5 µl of nesfatin-1 dissolved in physiological saline was injected into the lateral ventricle of rats at light onset [29]. Control rats received 5 µl physiological saline icv. After injections, animals returned to their home cages and vigilance was recorded for 24 h. The placement of the cannula was verified at the end of the study by injecting 10 nM/3 µl of angiotensin II icv. Only animals reacting with an intensive drinking response were included in the study.

Sleep scoring. The vigilance states were classified by SleepSign for Animal sleep analysis software (Kissei Comtec America, Inc., USA) for 4 sec periods using conventional criteria [27,30] followed by visual supervision of an expert scorer who was blind to experimental treatment.

The differentiated vigilance states were the following: 1) wakefulness; EEG is characterized by low amplitude activity at beta (14–30 Hz), alpha (8–13 Hz) and theta (5–9 Hz) frequencies accompanied by high or low EMG and motor activity, 2) REMS; low amplitude and high frequency EEG activity with regular theta waves (5–9 Hz) accompanied by silent EMG and motor activity with occasional twitching, 3) intermediate stage of sleep (IS); a brief stage just prior to REMS and sometimes just after it, characterized by unusual association of high amplitude spindles (mean 12.5 Hz) and low-frequency (mean 5.4 Hz) theta rhythm; 4) non-REMS; slow cortical waves (0.5–4 Hz) accompanied by reduced EMG and motor activity [27]. In sleep analysis after icv nesfatin-1 treatment, the following vigilance parameters were calculated: time spent in active (AW) and passive (PW) wake, REMS, IS, as well as in light slow wave sleep (SWS1) and deep slow wave sleep (SWS2), per hour. Additionally, specific parameters were calculated, namely, the number and the average duration of episodes in REMS, IS, SWS1 and SWS2. An episode of any vigilance stages was defined as an item lasting at least 4 sec and not interrupted by any other vigilance stages for longer than 4 sec. Sleep fragmentation was defined as the number of wake epochs (AW, PW) after a sleep stage (SWS1, SWS2, REM, IS). Since despite the habituation procedure that minimized stress, the process of icv administration disturbed daily rhythm of the animals, the 1st h of all EEG recordings had been omitted from the evaluation and sleep scoring, and the analysis was performed from the beginning of the 2nd h to the end of the 6th h of passive phase.

Statistics. We used STATISTICA 7.0 program (Statsoft Inc., Tulsa, OK, USA) to statistical analysis. Two-Way ANOVA followed by all pairwise comparisons with Student-Newman-Keuls Method was used for determining significance in nesfatin-1 mRNA and protein expressions and CRH mRNA expression. One Way ANOVA and One Way ANOVA on Ranks followed by

all pairwise comparisons with Tukey or Dunn's Method was applied to analyze morphological data as well as cumulative food intake and body weight change. Sleep data of different vigilance stages, summarized hourly, were evaluated by Two Way ANOVA for repeated measures (repeated factor: time). In case of inhomogeneous variances of the experimental groups, repeated measures ANOVA on Ranks was performed. For *post hoc* analysis, all pairwise comparisons with Tukey HSD were used. The results are presented as mean ± standard error of mean (SEM).

Results

Changes in Nesfatin mRNA and Protein Levels after REMS Deprivation and Rebound

The DLH with the ZI hosts the most prominent nesfatin - expressing cell population in the hypothalamus regarding the number of the cells and the expression level of the peptide (Fig. 1A). Nesfatin mRNA and protein expressions have responded for the experimental paradigms with parallel changes. There was no difference between HC and HCR groups, indicating that there is little or no spontaneous switch in nesfatin expression within three hours after the lights on (Fig. 1B,C). Nevertheless, a significant interaction was seen between the type of the platform and level of the rebound (nesfatin mRNA and protein measurements, pot x rebound interaction: $F_{(2,39)} = 4.90$, $p<0.05$ and $F_{(2,28)} = 4.10$, $p<0.05$, respectively). Both nesfatin mRNA and protein levels decreased exclusively in REMS - deprived small pot kept animals, followed by a relative increase after the three hour rebound sleep (Fig. 1B,C). Large pot conditions (with or without rebound) did not affect nesfatin expression (Fig. 1B,C).

Stress - Related Changes in Rats following REMS Deprivation

CRH mRNA level in the hypothalamic paraventricular nucleus, the centre of the stress response in the central nervous system, as well as body weight changes and cumulative food intake, during the 72 h spent on the platforms, were measured. Both SP and LP kept animals showed elevated CRH mRNA levels and a negative energy balance, compared to HC controls, indicating stress evoked by the experimental conditions. However, there was no significant difference between the LP and SP kept rats regarding these parameters (Fig. 2A,B). Cumulative food intake did not change between the groups (Fig. 2C), confirming that negative energy balance observed was not caused by fasting on platforms. However, animals on either type of platform spent considerable amount of time with swimming (unpublished data), thus fur of the animals are often wet, and this fact can also contribute to the increased energy expenditure of LP and SP kept rats.

Activation of Nesfatin - Positive Neuronal Cell Population

Since REMS deprivation evoked very specific changes in nesfatin level demonstrated by ISH and ELISA measurements, morphological studies were performed on hypothalamic sections of HC, SP and SPR animals. Rebound evoked a robust activation in nesfatin - positive cells in each investigated area (Fig. 3). In order to further characterize the nesfatin - producing cell population, we used triple fluorescent immunostaining for the visualization of nesfatin, MCH and Fos.

Co - localization of MHC and nesfatin. In home cage controls, most of the nesfatin-immunoreactive cells co - localized with MCH, with slight differences in the investigated areas (rate of MCH/nesfatin co - localization: ZI: 81.9±1.7%, perifornical area: 66.2±4.8%, LH: 75.4±2.1%, n = 5). The experimental conditions did not affect the percentage of nesfatin/MCH co - localization.

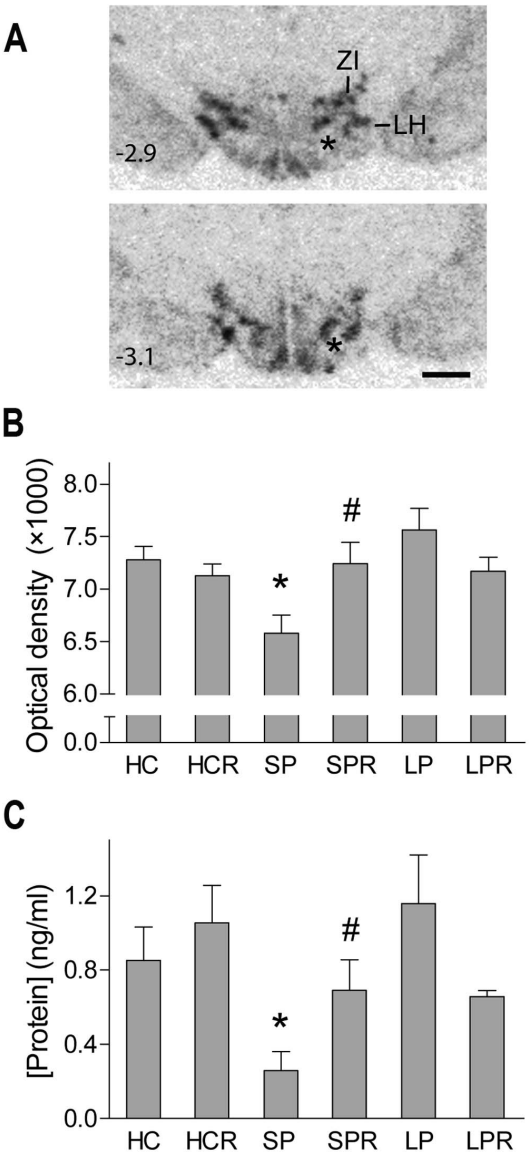

Figure 1. Nesfatin-1/NUCB2 expression as controlled by rapid eye movement sleep stage. A. Autoradiographic images of coronal sections through the middle portion of the hypothalamus showing the area of interest hybridized against nesfatin-1/NUCB2 mRNA in control animals. The upper and the lower panels show two different rostro - caudal levels. Distance from the bregma is indicated at bottom left in millimeters. Asterix: fornix, LH: lateral hypothalamic area, ZI: zona incerta, scale: 1 mm. **B**,**C**. Nesfatin-1/NUCB2 mRNA and protein levels in the different experimental groups determined by quantitative ISH and ELISA measurements, respectively. HC: home cage control, sacrificed with the animals kept on platforms, HCR: home cage control "rebound", sacrificed at the same time as rebound groups, SP: small pot, SPR: small pot plus sleep rebound, LP: large pot, LPR: large pot plus sleep rebound groups. $p^*<0.05$ *vs.* all other groups, $p\# <0.05$ *vs.* SP group, n = 5–9 for **B** and n = 4–7 for **C**.
doi:10.1371/journal.pone.0059809.g001

Neuronal activation due to the experimental conditions. Fos positivity in the HC and SP groups did not differ significantly from each other in any areas, although there was a difference between the MCH - negative and positive nesfatin populations. Nesfatin/MCH double positive neurons exhibited minimal activation (less than 0.5%). MCH - negative nesfatin neurons showed a substantial activity in the perifornical area,

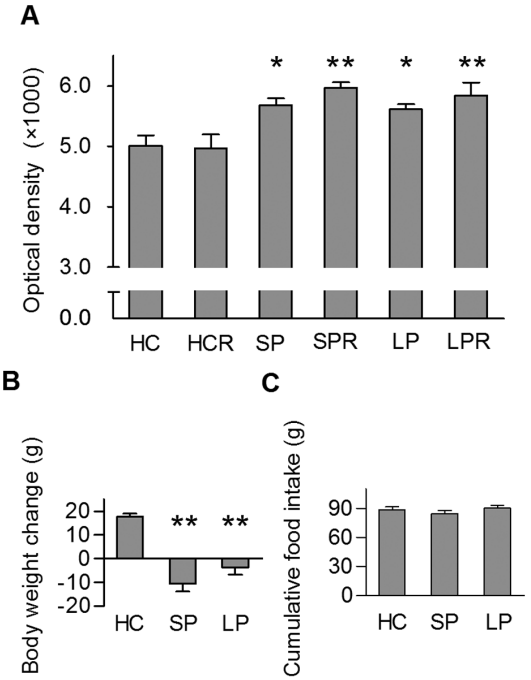

Figure 2. Stress-related changes and energy balance of the experimental animals. Data show significantly increased levels of CRH mRNA in the hypothalamic paraventricular nucleus (**A**) and decreased body weights (**B**) both in the SP and LP kept animals, compared to HC, without difference between the above mentioned groups. **C**. Cumulative food intake shows no alterations. HC: home cage control, sacrificed with the animals kept on platforms, HCR: home cage control ''rebound'', sacrificed at the same time as rebound groups, SP: small pot, SPR: small pot plus sleep rebound, LP: large pot, LPR: large pot plus sleep rebound groups. Data are shown as mean ± SEM, n = 10–11, p*<0.05, p**<0.01 *vs*. HC.
doi:10.1371/journal.pone.0059809.g002

(24.4±8.1% and 39.4±7.4% in HC and SP groups, respectively), while in the ZI and the LH, the activity of the MCH - negative nesfatin neurons was less than 20% in both groups.

Sleep rebound strongly activated the nesfatin/MCH double positive neurons regardless of the area examined (ZI: 86.9±2.9%, perifornical area: 78.3±2.7%, LH: 79.0±1.8%, Fig. 4). MCH - negative nesfatin neurons were not activated by rebound sleep in the ZI and the perifornical area, however, some activation was detected in the LH (Fig. 4C arrowhead), (SPR: 37.6±4.8%, $p<0.01$ *vs*. HC: 6.0±2.4% and SP: 15.0±3.1% groups, n = 5).

Effects of icv Administered Nesfatin-1 on Vigilance from the 2nd to the End of the 6th Hours of Passive Phase

According to our results, icv administered nesfatin-1 significantly increased sleep fragmentation ($F_{(1,10)} = 5.1046$, $p<0.05$) and caused a trend-level decrease in total sleep time ($p = 0.0587$) during the five investigated hours of passive phase. Regarding the different sleep stages, nesfatin-1 markedly diminished the time spent in REMS ($F_{(1,10)} = 18.99$, $p<0.001$), compared to controls. This decrease was ca. 60% in the 2nd h, however, in the next three hours of sleep, the fall in REMS time approached an approximate value of 90%, while in the 6th h it was ca. 70% (Fig. 5A). Similarly, the amount of IS showed a significant decrease being the lowest in the 3rd h ($F_{(1,10)} = 11.04$, $p<0.01$, Fig. 5B). The REMS and IS - declining effect in sleep time was also apparent in the number and the average duration of the episodes both in REMS ($F_{(1,10)} = 10.45$, $p<0.01$ and $F_{(1,10)} = 12.81$, $p<0.01$, respectively, Fig. 5C,E) and IS ($F_{(1,10)} = 7.18$, $p<0.05$ and $F_{(1,10)} = 6.99$, $p<0.05$, respectively, Fig. 5D,F). Considering the time spent in NREM sleep, a significant time × treatment interaction ($F_{(2,20)} = 4.092$, $p<0.05$) was revealed in SWS1, when repeated measure ANOVA was performed including the 2nd, 3rd and 4th hours only. The following *post hoc* test resulted in significant increase of SWS1 regarding the 3rd and 4th h (Fig. 6A). The time spent in SWS2 showed no alteration in any investigated hours (Fig. 6B).

The amount of PW elevated markedly ($F_{(1,10)} = 8.955$, $p<0.05$, Fig. 6C), in contrast to AW, which was unchanged (data not shown). Noteworthy, that the increase of SWS1 and PW was parallel to the elevation of episode-numbers generally ($F_{(1,10)} = 9.87$, $p<0.05$, Fig. 6D and ($F_{(1,10)} = 6.46$, $p<0.05$, Fig. 6F, respectively), although average episode-durations of these stages were unaffected. However, SWS2 showed no alteration despite an increase in the number of episodes in the 4th h (Fig. 6E).

Discussion

In this study we provide evidence for the implication of the recently identified anorexigenic molecule, nesfatin in the regulation of sleep of rat. According to our results, abolishment of REMS decreased nesfatin mRNA and protein expression in the DLH, a prominent site of nesfatin expression implicated in vigilance, feeding and depression [13,18,31,32], while the subsequent REMS rebound restored these levels. We found that central administration of nesfatin-1 diminished the time spent in REMS and IS, while increased PW and SWS1, further reinforcing its impact in the regulation of vigilance. Very recently Jego et al. have also established the effect of icv nesfatin-1 on sleep architecture, although demonstrating different results [33]. The discrepancy may be explained by the different doses they used as well as the different timing of the icv nesfatin administration.

To abolish REMS completely, rats were kept on single platforms surrounded by water for 72 h [20,21]. As muscle atony is typical of REMS, animals fall into the water and awake as they switch to REMS. Classic (one rat per cage on a single pot) and modified (several rats per cage on multiple pots) platform methods are widely used to abolish REMS [20,21,34,35]. Multiple platforms were originally introduced as an alternate of single one to reduce stress caused by mobile restriction and social isolation [35–37]. However, even if rats are kept together from an early age to establish social stability and avoid stress caused by rearrangement of the social hierarchy when placed on multiple platforms, they show the same adrenocorticotropic hormone (ACTH), and just minimally higher corticosterone levels than rats on single platforms [38]. Because of these reasons, and since unique activity of MCH neurons during REMS recovery was demonstrated firstly with the classical flowerpot method [20], we adopted this technique.

To isolate effects of stress, LP kept animals were used as controls. The likewise elevated CRH levels in the hypothalamic paraventricular nucleus, the similar plasma ACTH and corticosterone concentrations [35] and the negative energy balance in both groups confirm that LP and SP animals are exposed to the same stress conditions with comparable activity of the hypothalamo - pituitary - adrenal axis. Another aspect of importance is thermogenesis due to wet fur. SP animals get wet when fall asleep, but LP animals also spend considerable amount of time in the water with swimming during the deprivation procedure. Thus, differences either in thermoregulation due to the wet fur and in the amount of the restraint stress, are not considered as major factors regarding the results detected only in SP animals. Furthermore,

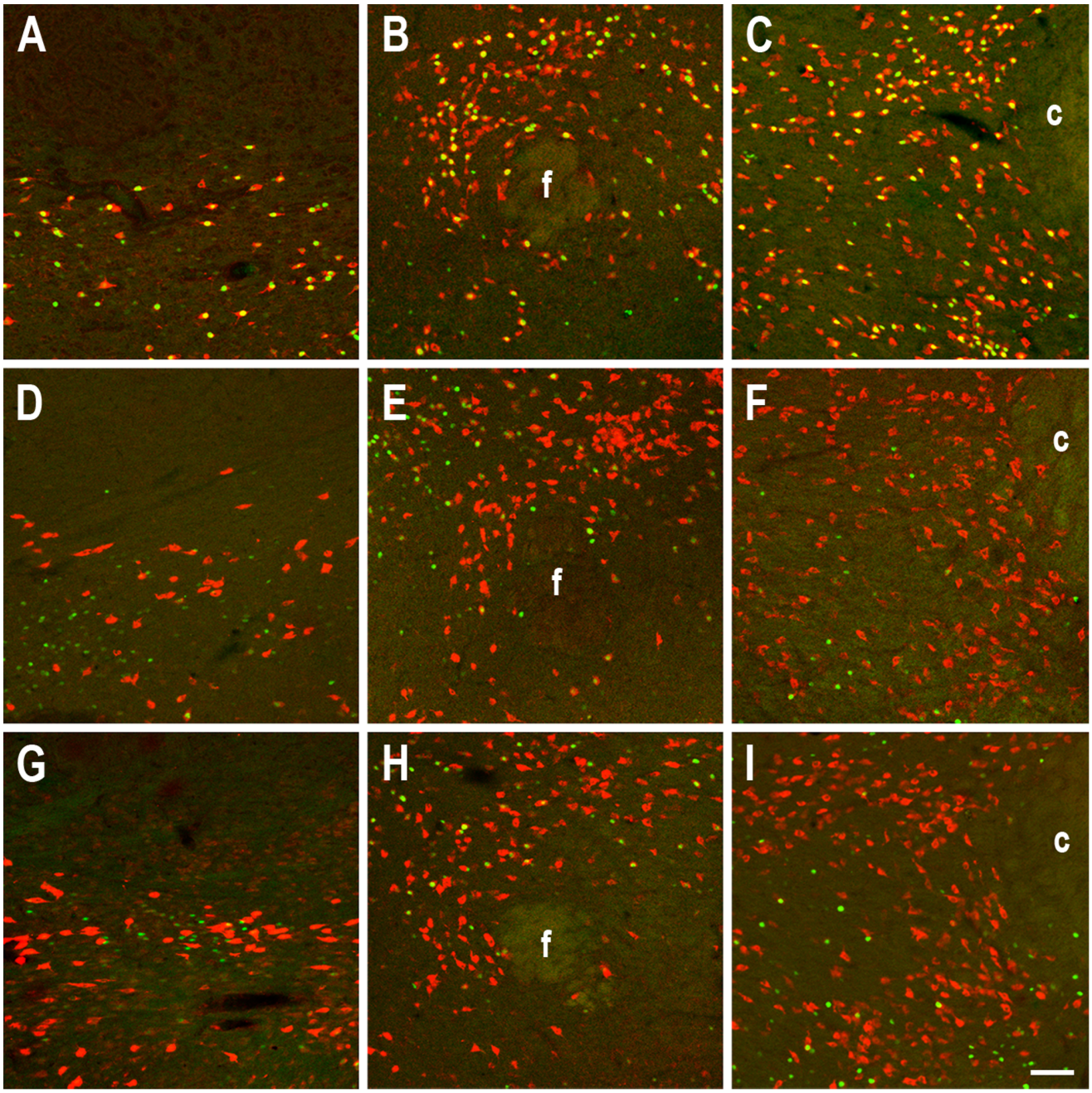

Figure 3. Effect of rebound sleep on the activity of nesfatin1/NUCB2 (nesfatin) - positive cell population. Fos (green) and nesfatin (red) double fluorescent immunostainings showing the three investigated areas arranged in columns (left: zona incerta, middle: perifornical area, right: lateral hypothalamic area) in rapid eye movement sleep (REMS) - deprived - sleep rebound (**A–C**), REMS - deprived without rebound (**D–F**) and home cage kept (**G–I**) animals. c: capsula interna, f: fornix, scale: 100 μm.
doi:10.1371/journal.pone.0059809.g003

changes in the sleep architecture also designate large pot kept animals as useful controls. Both LP and SP rats have been reported to reduce SWS [37] in line with our paradigm, as some degree of SWS1 rebound was also observed in these groups [21]. The existence of REMS rebound in LPR animals and data of Machado et al. [21,37] suggest that LP animals were subjected to REMS deprivation due to stress [39], but in the SP rats, REMS ceased totally, creating an elemental difference between LP and SP conditions [37]. This substantial contrast is reflected in the marked alterations of REMS architecture and connected Fos activity in the DLH of LPR rats, compared to SPR ones [21,40]. As a consequence, any small pot - specific observation is likely due to the lack of REMS.

Our data suggest a striking link between nesfatin expression and REMS. Animals in the SP group reacted with an exclusive and remarkable decrease in nesfatin mRNA and protein levels to the lack of REMS, while nesfatin expression of animals in the HC and LP groups was alike. On the other hand, a significantly higher amount of REMS rebound with longer average duration of episodes compared to LPR and HCR groups [21] returned these

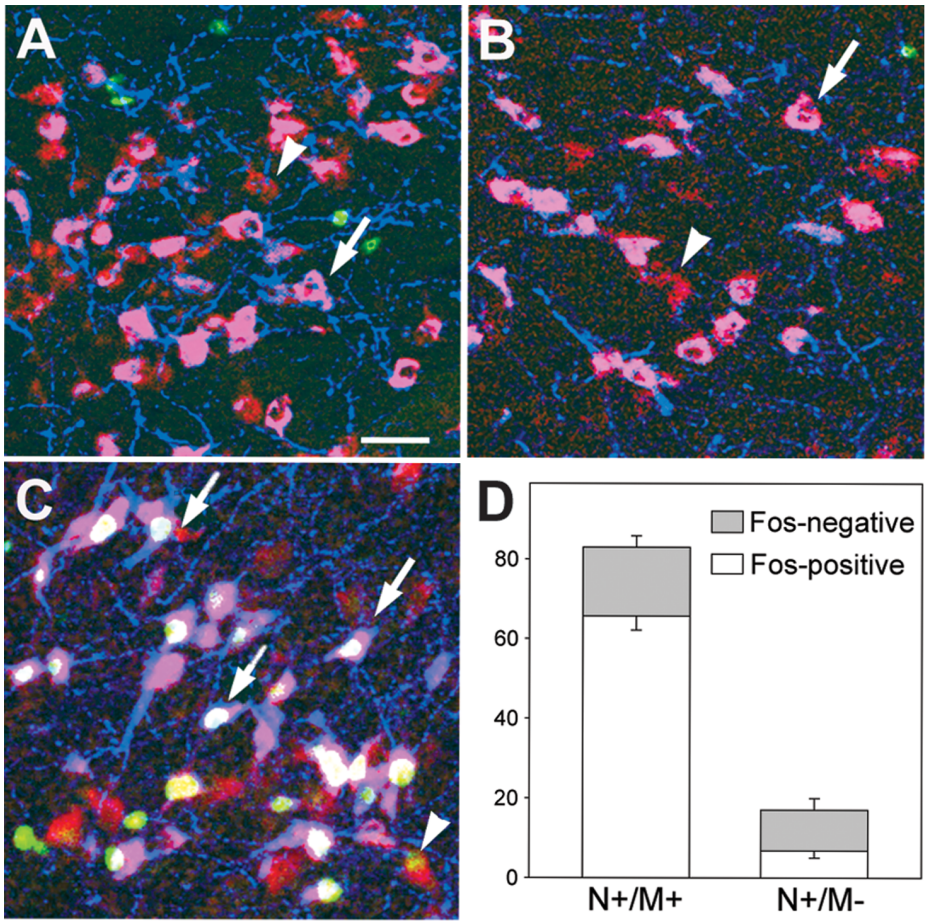

Figure 4. Participation of melanin-concentrating hormone (MCH)-positive and MCH - negative nesfatin-1/NUCB2 (nesfatin) neurons in the sleep - wake cycle. A–C. Illustrative pictures of the lateral hypothalamic area demonstrating the results of the triple fluorescent immunostainings for nesfatin (red), MCH (blue) and Fos (green) in a home cage kept (**A**), a rapid eye movement sleep (REMS) - deprived (**B**) and a REMS - deprived - sleep rebound (**C**) animal. Nesfatin/MCH double-positive neurons are pink (arrows), MCH - negative nesfatin neurons are red (arrowheads). Activated nesfatin/MCH neurons show white nuclei, activated nesfatin - positive, but MCH - negative neurons show yellow nuclei. Note that majority of the MCH - positive nesfatin neurons are activated (Fos - positive, arrows) by rebound, while only a few of the MCH - negative neurons showed Fos - positivity (arrowhead). Scale bar: 100 μm. **D**. Distribution of MCH - positive (N^+/M^+) and MCH - negative (N^+/M) neurons within the nesfatin producing cell population and percentage of activated (Fos - positive) cells after REMS deprivation followed by rebound. Data are shown as mean ± SEM, n = 5.
doi:10.1371/journal.pone.0059809.g004

values to the control levels. There was no difference between the HC and HCR groups indicating that circadian rhythm does not influence nesfatin expression in the first three hours of sleep after lights on.

Since nesfatin is an anorexigen and decrease of nesfatin mRNA level in certain hypothalamic nuclei, like the paraventricular and the supraoptic nuclei (but not in the DLH - unpublished observations), was established after fasting [41,42], it is important to clarify whether negative energy balance of animals may, or may not be responsible for the reduction of nesfatin expression. It is noteworthy to mention that animals were not food - deprived during the 72 h on platforms. The cumulative food intake of rats was identical in all groups. In spite of this, both SP and LP animals had a decreased body weight, indicating elevated energy expenditure. However, they did not differ significantly in this respect, and there was no change in nesfatin mRNA expression in LP rats. Therefore, we can exclude the idea that the changes in the nesfatin expression in the SP animals may be related to the disturbed energy homeostasis.

To characterize both neurochemically and neuromorphologically the nesfatin - positive cell population responsible for the observed results, we applied multiple immunostainings. Majority of the nesfatin - expressing neurons co - expressed MCH, and practically all MCH cells co - expressed nesfatin, in agreement with earlier findings [10]. REMS rebound evoked Fos expression in large percent of nesfatin neurons. Most of these nesfatin neurons were MCH - positive confirming previous reports [20,40], revealing a strong activation in all investigated areas. MCH - negative nesfatin cells showed little activation in the LH and no activation in both the ZI and the perifornical area. Since Fos is a transcription factor, indicating ongoing transcriptional activity [43], the appearance of Fos signal in the nesfatin - immunoreactive neurons is also in line with our findings showing an elevation of nesfatin mRNA and protein levels during REM rebound. The potential role of nesfatin in REMS regulation was further examined by analyzing the effect of the peptide administered centrally on vigilance stages in control rats. The applied 25 pmol dose was established according to previous studies [1,4,44]. As animals were presumably disturbed by the icv procedure, despite

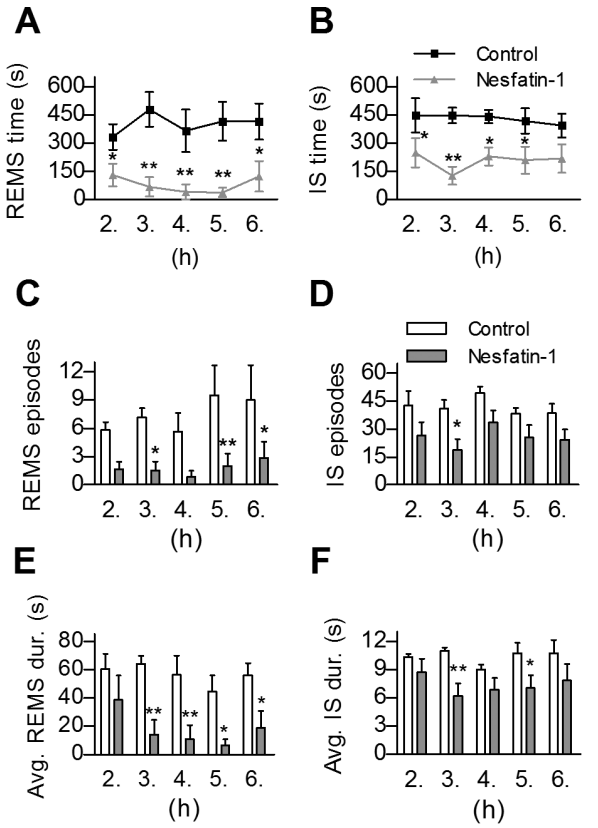

Figure 5. Effects of intracerebroventricularly administered nesfatin-1 on rapid eye movement sleep (REMS) and intermediate stage of sleep (IS). A,B. The time spent in REMS and IS per hour, respectively in the 2nd–6th hours of passive (light) phase. **C,D**. The number and -E,F- the average duration of REMS and IS episodes per hour, respectively. Data are presented as mean ± SEM, n = 6 per group, p*<0.05, p**<0.01.
doi:10.1371/journal.pone.0059809.g005

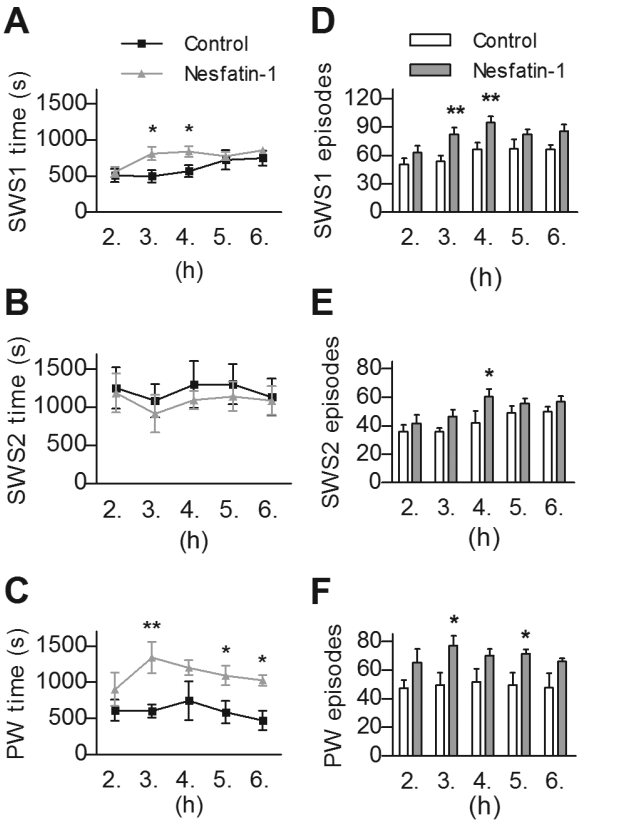

Figure 6. Effects of intracerebroventricularly administered nesfatin-1 on slow wave sleep and passive wake (PW) vigilance stages. The time spent and the number of episodes in light slow wave sleep (SWS1, **A** and **D**, respectively), deep slow wave sleep (SWS2, **B** and **E**, respectively) as well as in PW (**C** and **F**, respectively), per hour in the 2nd–6th hours of passive (light) phase. Data are presented as mean ± SEM, n = 6 per group, p*<0.05, p**<0.01.
doi:10.1371/journal.pone.0059809.g006

previous habituation [4,21], moreover, increased plasma ACTH and corticosterone levels have been reported after icv nesfatin-1 injection in the first 30 and 60 min, respectively [4,45], we omitted the first hour and evaluated vigilance from the beginning of the 2nd to the end of the 6th hours of passive phase.

Centrally injected nesfatin-1 had an IS-REMS decreasing effect lasting 5–6 hours following administration. Decrease in the number of REMS and IS as well as the average duration of REMS episodes seem to be involved in this effect, suggesting that neurons both in onset and maintenance of IS-REMS may be affected. The decline of REMS and IS was presumably compensated by a short-lived elevation of SWS1, and we also found a parallel increase in the amount of passive wake, and it was prolonged. There was a tendency for decrease of total sleep time.

The mechanism of nesfatin-1's action on vigilance stages needs to be clarified in the future. Increase in the activity of the ascending arousal system and/or decrease in midbrain reticular arousal threshold by nesfatin-1 directly or indirectly, may be one explanation. Indeed, Yoshida et al. have reported that centrally administered nesfatin-1 induced Fos expression in noradrenergic neurons of the locus coeruleus and serotonergic cells of the dorsal and median raphe nuclei [45], structures known to be parts of the brainstem arousal system [46]. However, we should not ignore that icv nesfatin-1 has been demonstrated to cause Fos expression also in the PVN, the nucleus of the solitary tract and the nucleus supraopticus [45], all being related to stress and therefore, may potentially alter sleep architecture [39,47,48].

In relationship with MCH, it is interesting to notice a consequent opposite effect of nesfatin-1. Unlike nesfatin-1, MCH has been shown to induce a dose-dependent increase of REMS when centrally injected [20]. Ahnaou et al. have demonstrated that MCH_1 receptor antagonist compounds decreased REMS, IS and SWS2, while wake stages increased [49]. Moreover, on food intake and energy expenditure, MCH and nesfatin act also oppositely [1,15,44]. Co - localization of MCH with other neuropeptides having opposite effect is not unique. A high percent of orexigenic MCH neurons co - localize with the anorexigenic cocaine and amphetamine regulated transcript [50].

Additionally, as for synaptic action of MCH, it has a predominantly inhibitory effect pre- and postsynaptically and attenuates the activation of N-, L- and P/Q-type calcium channels, while nesfatin-1 has been found to rise intracellular Ca^{2+} concentrations, by stimulating Ca^{2+} entry *via* N-, L- and P/Q-type calcium channels [12,51]. At the same time, the receptor or receptors for nesfatin-1 have not been identified yet; therefore the precise mechanism of nesfatin's action remains to be elucidated.

In summary, we revealed a close association between REMS architecture and nesfatin expression in the DLH and the ZI, as well as a possible negative feedback effect of nesfatin-1 on REMS, inasmuch as there is a disinhibition of nesfatin expression by

REMS rebound in the DLH and ZI, and an inhibition of REMS by icv nesfatin-1. Further data are needed about the role of other nesfatin - expressing brain areas in this process that theoretically can be related to the sleep-wake regulation. Our results confirm earlier findings implicating the integrative role of the DLH and ZI in the control of a wide variety of functions, like energy homeostasis, vigilance, regulation of motor activity and reward, as well as more recently, in mood and depression [13,14,52,53]. Sleep architecture of humans is strongly affected by several illnesses, like narcolepsy, anorexia and depression [7,54–56]. Hence, the present findings may be relevant not only in sleep research, but also in other studies regarding sleep related disorders. Depression and anorexia are among those affecting the population worldwide. Thus, the possibility that nesfatin, the anorexigenic peptide, recently been related also to depression [5,6] may emerge as a potential new link between these diseases and sleep disturbances, calls for further investigation.

Acknowledgments

We would like to thank to Szilvia Deák and Judit Kerti for their excellent technical support.

Author Contributions

Conceived and designed the experiments: ZET SV CÁ KK GB MP. Performed the experiments: SV CÁ KK ZK DP RSP ZET. Analyzed the data: SV CÁ KK GB MP ZET. Contributed reagents/materials/analysis tools: GB MP ZET. Wrote the paper: SV CÁ KK MP RSP ZET.

References

1. Oh-I S, Shimizu H, Satoh T, Okada S, Adachi S, et al. (2006) Identification of nesfatin-1 as a satiety molecule in the hypothalamus. Nature 443: 709–712.
2. Tan BK, Hallschmid M, Kern W, Lehnert H, Randeva HS (2011) Decreased cerebrospinal fluid/plasma ratio of the novel satiety molecule, nesfatin-1/NUCB-2, in obese humans: evidence of nesfatin-1/NUCB-2 resistance and implications for obesity treatment. J Clin Endocrinol Metab 96: E669–673.
3. Merali Z, Cayer C, Kent P, Anisman H (2008) Nesfatin-1 increases anxiety- and fear-related behaviors in the rat. Psychopharmacology (Berl) 201: 115–123.
4. Konczol K, Bodnar I, Zelena D, Pinter O, Papp RS, et al. (2010) Nesfatin-1/NUCB2 may participate in the activation of the hypothalamic-pituitary-adrenal axis in rats. Neurochem Int 57: 189–197.
5. Ari M, Ozturk OH, Bez Y, Oktar S, Erduran D (2011) High plasma nesfatin-1 level in patients with major depressive disorder. Prog Neuropsychopharmacol Biol Psychiatry 35: 497–500.
6. Bloem B, Xu L, Morava E, Faludi G, Palkovits M, et al. (2012) Sex-specific differences in the dynamics of cocaine- and amphetamine-regulated transcript and nesfatin-1 expressions in the midbrain of depressed suicide victims vs. controls. Neuropharmacology 62: 297–303.
7. Holshoe JM (2009) Antidepressants and sleep: a review. Perspect Psychiatr Care 45: 191–197.
8. Steiger A, Kimura M (2010) Wake and sleep EEG provide biomarkers in depression. J Psychiatr Res 44: 242–252.
9. Landolt HP, Gillin JC (2002) Different effects of phenelzine treatment on EEG topography in waking and sleep in depressed patients. Neuropsychopharmacology 27: 462–469.
10. Fort P, Salvert D, Hanriot L, Jego S, Shimizu H, et al. (2008) The satiety molecule nesfatin-1 is co-expressed with melanin concentrating hormone in tuberal hypothalamic neurons of the rat. Neuroscience 155: 174–181.
11. Goebel-Stengel M, Wang L, Stengel A, Tache Y (2011) Localization of nesfatin-1 neurons in the mouse brain and functional implication. Brain Res 1396: 20–34.
12. Brailoiu GC, Dun SL, Brailoiu E, Inan S, Yang J, et al. (2007) Nesfatin-1: distribution and interaction with a G protein-coupled receptor in the rat brain. Endocrinology 148: 5088–5094.
13. Alam MN, Gong H, Alam T, Jaganath R, McGinty D, et al. (2002) Sleep-waking discharge patterns of neurons recorded in the rat perifornical lateral hypothalamic area. J Physiol 538: 619–631.
14. Nollet M, Gaillard P, Minier F, Tanti A, Belzung C, et al. (2011) Activation of orexin neurons in dorsomedial/perifornical hypothalamus and antidepressant reversal in a rodent model of depression. Neuropharmacology 61: 336–346.
15. Qu D, Ludwig DS, Gammeltoft S, Piper M, Pelleymounter MA, et al. (1996) A role for melanin-concentrating hormone in the central regulation of feeding behaviour. Nature 380: 243–247.
16. Shimazaki T, Yoshimizu T, Chaki S (2006) Melanin-concentrating hormone MCH1 receptor antagonists: a potential new approach to the treatment of depression and anxiety disorders. CNS Drugs 20: 801–811.
17. Torterolo P, Lagos P, Monti JM (2011) Melanin-concentrating hormone: a new sleep factor? Front Neurol 2: 14.
18. Hassani OK, Lee MG, Jones BE (2009) Melanin-concentrating hormone neurons discharge in a reciprocal manner to orexin neurons across the sleep-wake cycle. Proc Natl Acad Sci U S A 106: 2418–2422.
19. Fenzl T, Romanowski CP, Flachskamm C, Deussing JM, Kimura M (2011) Wake-promoting effects of orexin: Its independent actions against the background of an impaired corticotropine-releasing hormone receptor system. Behav Brain Res 222: 43–50.
20. Verret L, Goutagny R, Fort P, Cagnon L, Salvert D, et al. (2003) A role of melanin-concentrating hormone producing neurons in the central regulation of paradoxical sleep. BMC Neurosci 4: 19.
21. Kitka T, Katai Z, Pap D, Molnar E, Adori C, et al. (2009) Small platform sleep deprivation selectively increases the average duration of rapid eye movement sleep episodes during sleep rebound. Behav Brain Res 205: 482–487.
22. Zelena D, Mergl Z, Foldes A, Kovacs KJ, Toth Z, et al. (2003) Role of hypothalamic inputs in maintaining pituitary-adrenal responsiveness in repeated restraint. Am J Physiol Endocrinol Metab 285: E1110–1117.
23. Palkovits M (1973) Isolated removal of hypothalamic or other brain nuclei of the rat. Brain Res 59: 449–450.
24. Toth ZE, Mezey E (2007) Simultaneous visualization of multiple antigens with tyramide signal amplification using antibodies from the same species. J Histochem Cytochem 55: 545–554.
25. Paxinos G, Watson C, editors (2007) The Rat Brain in Stereotaxic Coordinates. 6th ed. San Diego: Academic Press.
26. Filakovszky J, Gerber K, Bagdy G (1999) A serotonin-1A receptor agonist and an N-methyl-D-aspartate receptor antagonist oppose each others effects in a genetic rat epilepsy model. Neurosci Lett 261: 89–92.
27. Kantor S, Jakus R, Balogh B, Benko A, Bagdy G (2004) Increased wakefulness, motor activity and decreased theta activity after blockade of the 5-HT2B receptor by the subtype-selective antagonist SB-215505. Br J Pharmacol 142: 1332–1342.
28. Graf M, Jakus R, Kantor S, Levay G, Bagdy G (2004) Selective 5-HT1A and 5-HT7 antagonists decrease epileptic activity in the WAG/Rij rat model of absence epilepsy. Neurosci Lett 359: 45–48.
29. To CT, Bagdy G (1999) Anxiogenic effect of central CCK administration is attenuated by chronic fluoxetine or ipsapirone treatment. Neuropharmacology 38: 279–282.
30. Kantor S, Jakus R, Bodizs R, Halasz P, Bagdy G (2002) Acute and long-term effects of the 5-HT2 receptor antagonist ritanserin on EEG power spectra, motor activity, and sleep: changes at the light-dark phase shift. Brain Res 943: 105–111.
31. Valassi E, Scacchi M, Cavagnini F (2008) Neuroendocrine control of food intake. Nutr Metab Cardiovasc Dis 18: 158–168.
32. Foo KS, Brismar H, Broberger C (2008) Distribution and neuropeptide coexistence of nucleobindin-2 mRNA/nesfatin-like immunoreactivity in the rat CNS. Neuroscience 156: 563–579.
33. Jego S, Salvert D, Renouard L, Mori M, Goutagny R, et al. Tuberal Hypothalamic Neurons Secreting the Satiety Molecule Nesfatin-1 Are Critically Involved in Paradoxical (REM) Sleep Homeostasis. PLoS One 7: e52525.
34. Maloney KJ, Mainville L, Jones BE (2000) c-Fos expression in GABAergic, serotonergic, and other neurons of the pontomedullary reticular formation and raphe after paradoxical sleep deprivation and recovery. J Neurosci 20: 4669–4679.
35. Suchecki D, Lobo LL, Hipolide DC, Tufik S (1998) Increased ACTH and corticosterone secretion induced by different methods of paradoxical sleep deprivation. J Sleep Res 7: 276–281.
36. van Hulzen ZJ, Coenen AM (1981) Paradoxical sleep deprivation and locomotor activity in rats. Physiol Behav 27: 741–744.
37. Machado RB, Hipolide DC, Benedito-Silva AA, Tufik S (2004) Sleep deprivation induced by the modified multiple platform technique: quantification of sleep loss and recovery. Brain Res 1004: 45–51.
38. Suchecki D, Tiba PA, Tufik S (2002) Hormonal and behavioural responses of paradoxical sleep-deprived rats to the elevated plus maze. J Neuroendocrinol 14: 549–554.
39. Cheeta S, Ruigt G, van Proosdij J, Willner P (1997) Changes in sleep architecture following chronic mild stress. Biol Psychiatry 41: 419–427.
40. Kitka T, Adori C, Katai Z, Vas S, Molnar E, et al. (2011) Association between the activation of MCH and orexin immunorective neurons and REM sleep architecture during REM rebound after a three day long REM deprivation. Neurochem Int 59: 686–694.
41. Shimizu H, Oh IS, Okada S, Mori M (2009) Nesfatin-1: an overview and future clinical application. Endocr J 56: 537–543.
42. Kohno D, Nakata M, Maejima Y, Shimizu H, Sedbazar U, et al. (2008) Nesfatin-1 neurons in paraventricular and supraoptic nuclei of the rat hypothalamus coexpress oxytocin and vasopressin and are activated by refeeding. Endocrinology 149: 1295–1301.

43. Franza BR Jr, Rauscher FJ 3rd, Josephs SF, Curran T (1988) The Fos complex and Fos-related antigens recognize sequence elements that contain AP-1 binding sites. Science 239: 1150–1153.
44. Konczol K, Pinter O, Ferenczi S, Varga J, Kovacs K, et al. (2012) Nesfatin-1 exerts long-term effect on food intake and body temperature. Int J Obes (Lond).
45. Yoshida N, Maejima Y, Sedbazar U, Ando A, Kurita H, et al. (2010) Stressor-responsive central nesfatin-1 activates corticotropin-releasing hormone, noradrenaline and serotonin neurons and evokes hypothalamic-pituitary-adrenal axis. Aging (Albany NY) 2: 775–784.
46. Saper CB, Fuller PM, Pedersen NP, Lu J, Scammell TE (2010) Sleep state switching. Neuron 68: 1023–1042.
47. Romanowski CP, Fenzl T, Flachskamm C, Wurst W, Holsboer F, et al. (2010) Central deficiency of corticotropin-releasing hormone receptor type 1 (CRH-R1) abolishes effects of CRH on NREM but not on REM sleep in mice. Sleep 33: 427–436.
48. Rachalski A, Alexandre C, Bernard JF, Saurini F, Lesch KP, et al. (2009) Altered sleep homeostasis after restraint stress in 5-HTT knock-out male mice: a role for hypocretins. J Neurosci 29: 15575–15585.
49. Ahnaou A, Drinkenburg WH, Bouwknecht JA, Alcazar J, Steckler T, et al. (2008) Blocking melanin-concentrating hormone MCH1 receptor affects rat sleep-wake architecture. Eur J Pharmacol 579: 177–188.
50. Hillebrand JJ, de Wied D, Adan RA (2002) Neuropeptides, food intake and body weight regulation: a hypothalamic focus. Peptides 23: 2283–2306.
51. Gao XB, van den Pol AN (2002) Melanin-concentrating hormone depresses L-, N-, and P/Q-type voltage-dependent calcium channels in rat lateral hypothalamic neurons. J Physiol 542: 273–286.
52. Harris GC, Wimmer M, Aston-Jones G (2005) A role for lateral hypothalamic orexin neurons in reward seeking. Nature 437: 556–559.
53. Bernardis LL, Bellinger LL (1996) The lateral hypothalamic area revisited: ingestive behavior. Neurosci Biobehav Rev 20: 189–287.
54. Cinosi E, Di Iorio G, Acciavatti T, Cornelio M, Vellante F, et al. (2011) Sleep disturbances in eating disorders: a review. Clin Ter 162: e195–202.
55. de Lecea L, Sutcliffe JG, Fabre V (2002) Hypocretins/orexins as integrators of physiological information: lessons from mutant animals. Neuropeptides 36: 85–95.
56. Sehgal A, Mignot E (2011) Genetics of sleep and sleep disorders. Cell 146: 194–207.

frontiers in Neuroscience

toth.zsuzsanna.emese_174_24

ORIGINAL RESEARCH
published: 21 March 2022
doi: 10.3389/fnins.2022.828571

Hypothalamic Nesfatin-1 Resistance May Underlie the Development of Type 2 Diabetes Mellitus in Maternally Undernourished Non-obese Rats

Máté Durst[1†], Katalin Könczöl[1†], Klementina Ocskay[1], Klaudia Sípos[1], Péter Várnai[2], Anett Szilvásy-Szabó[3], Csaba Fekete[3] and Zsuzsanna E. Tóth[1]*

[1] Laboratory of Neuroendocrinology and in situ Hybridization, Department of Anatomy, Histology and Embryology, Semmelweis University, Budapest, Hungary, [2] Department of Physiology, Semmelweis University, Budapest, Hungary, [3] Laboratory of Integrative Neuroendocrinology, Institute of Experimental Medicine, Budapest, Hungary

Intrauterine growth retardation (IUGR) poses a high risk for developing late-onset, non-obese type 2 diabetes (T2DM). The exact mechanism underlying this phenomenon is unknown, although the contribution of the central nervous system is recognized. The main hypothalamic nuclei involved in the homeostatic regulation express nesfatin-1, an anorexigenic neuropeptide and identified regulator of blood glucose level. Using intrauterine protein restricted rat model (PR) of IUGR, we investigated, whether IUGR alters the function of nesfatin-1. We show that PR rats develop fat preference and impaired glucose homeostasis by adulthood, while the body composition and caloric intake of normal nourished (NN) and PR rats are similar. Plasma nesfatin-1 levels are unaffected by IUGR in both neonates and adults, but pro-nesfatin-1 mRNA expression is upregulated in the hypothalamus of adult PR animals. We find that centrally injected nesfatin-1 inhibits the fasting induced neuronal activation in the hypothalamic arcuate nucleus in adult NN rats. This effect of nesfatin-1 is not seen in PR rats. The anorexigenic effect of centrally injected nesfatin-1 is also reduced in adult PR rats. Moreover, chronic central nesfatin-1 administration improves the glucose tolerance and insulin sensitivity in NN rats but not in PR animals. Birth dating of nesfatin-1 cells by bromodeoxyuridine (BrDU) reveals that formation of nesfatin-1 cells in the hypothalamus of PR rats is disturbed. Our results suggest that adult PR rats acquire hypothalamic nesfatin-1-resistance, probably due to the altered development of the hypothalamic nesfatin-1 cells. Hypothalamic nesfatin-1-resistance, in turn, may contribute to the development of non-obese type T2DM.

Keywords: IP-ITT, IP-GTT, neuronal birth dating, cFos, arcuate nucleus, nesfatin-1

OPEN ACCESS

Edited by:
Lee E. Eiden, National Institutes of Health (NIH), United States

Reviewed by:
Johan Ruud, University of Gothenburg, Sweden
Andreas Stengel, Charité Universitätsmedizin Berlin, Germany

***Correspondence:**
Zsuzsanna E. Tóth
toth.zsuzsanna.emese@med.semmelweis-univ.hu

† These authors have contributed equally to this work and share first authorship

Specialty section:
This article was submitted to Neuroendocrine Science, a section of the journal Frontiers in Neuroscience

Received: *06 December 2021*
Accepted: *08 February 2022*
Published: *21 March 2022*

Citation:
Durst M, Könczöl K, Ocskay K, Sípos K, Várnai P, Szilvásy-Szabó A, Fekete C and Tóth ZE (2022) Hypothalamic Nesfatin-1 Resistance May Underlie the Development of Type 2 Diabetes Mellitus in Maternally Undernourished Non-obese Rats. Front. Neurosci. 16:828571. doi: 10.3389/fnins.2022.828571

INTRODUCTION

Type 2 diabetes (T2DM) is a global health concern. Besides causing serious complications, T2DM has recently been associated with increased odds of in-hospital death with COVID-19 (Barron et al., 2020). Although obesity is a major risk factor for T2DM, relatively large proportion of T2DM patients (around 20% in Europe, and much higher in Asia) are non-obese (Vaag and Lund, 2007), and the disease develops independently of the amount of the adipose tissue hormone, leptin (Wang et al., 2014). The etiology and pathophysiology of non-obese T2DM are unclear. However, intrauterine growth retardation (IUGR) combined with low birthweight is a primary contributor to the development of the disease (Vaag and Lund, 2007). This condition is usually attributed to a poor intrauterine environment, one of the most common complications of pregnancy (Saleem et al., 2011).

Intrauterine undernourishment induced by protein restriction (PR) is a widely used rodent model in T2DM research (Martin-Gronert and Ozanne, 2007; Pinney, 2013). This model reproduces well the consequences of human IUGR (Saleem et al., 2011). The adverse fetal environment induces a predictive adaptive response (fetal programing) in the organism (Barker et al., 1993), and permanently alters the function of the hypothalamic circuits regulating food intake, energy expenditure and glucose homeostasis. Metabolic syndrome develops depending on the genetic predisposition of the individual and the quality of the postnatal environment (Levin, 2006; Carey et al., 2013; Pedroso et al., 2017; Timper and Brüning, 2017; Durst et al., 2019).

Nesfatin-1, the N-terminal fragment of the nucleobindin-2 protein (NUCB2) is an anorexigenic neuropeptide (Oh-I et al., 2006; Maejima et al., 2009; Shimizu et al., 2009), although its production has also been demonstrated in several peripheral organs (Wei et al., 2018). It is highly expressed in the arcuate (ARC), paraventricular (PVN), and supraoptic (SON) nuclei of the hypothalamus and in the lateral hypothalamic area (LHA) (Brailoiu et al., 2007; Foo et al., 2008). All these areas are considered hypothalamic feeding centers (Schwartz et al., 2000; Maejima et al., 2018). Acute intracerebroventricular (icv) administration of nesfatin-1 reduces food intake and increases energy expenditure in a leptin independent way (Oh-I et al., 2006; Könczöl et al., 2012). Chronic nesfatin-1 treatment leads to weight loss (Oh-I et al., 2006).

Nesfatin-1 is also an important factor in the central control of glucose homeostasis. Autonomic control of the pancreas and the liver arises mainly from the hypothalamic ARC and PVN nuclei as well as the LHA (Uyama et al., 2004; Sandoval et al., 2009; Pozo and Claret, 2018), which contain a high density of nesfatin-1 neurons. Insulin sensitivity in the liver and peripheral tissues increases upon icv infusion of nesfatin-1 in rats during euglycemic-hyperinsulinemic clamps (Guo et al., 2013). Nesfatin-1 delivered into the hypothalamus *via* the third ventricle inhibits hepatic glucose production and promotes glucose uptake in skeletal muscle (Gantulga et al., 2012; Yang et al., 2012; Guo et al., 2013; Nakata and Yada, 2013). Based on collective data, NUCB2/nesfatin-1 with its associated regulatory processes are recognized as promising targets for treating type 2 diabetes, obesity and metabolic syndrome (Nakata and Yada, 2013).

Considering that (1) IUGR is one of the main risk factors for developing non-obese T2DM, (2) fetal programing of the central nervous system contributes primarily to the development of the IUGR phenotype, (3) the role of hypothalamic NUCB2/nesfatin-1 in the regulation of food intake and glucose homeostasis is established and that (4) nesfatin-1 acts in a leptin independent manner, the role of NUCB2/nesfatin-1 in the development of the non-obese type T2DM in the IUGR phenotype can be assumed. To investigate this, we used a PR rat model of IUGR and characterized the development, food preference, glucose homeostasis as well as the hypothalamic nesfatin-1 system of these animals. We also examined the effect of acute and chronic nesfatin-1 treatment on glucose homeostasis in our model.

MATERIALS AND METHODS

Animals and Tissue Handling

Rats (Wistar, Toxi-Coop Toxicological Research Center Zrt, Dunakeszi, Hungary) were housed under standard laboratory conditions (22 ± 1°C, 12-h day cycle) and had free access to food and water. Experiments were performed using males, except otherwise indicated. During brain surgeries and transcardial perfusions, anesthesia was applied using a mixture of ketamine (75 mg/bwkg) (Richter Gedeon Nyrt, Budapest, Hungary) and xylazine (15 mg/bwkg) (CP-Pharma, Burgdorf, Germany) given intramuscularly. Animals were handled daily for two weeks before experiments to avoid experimental stress. Tissues were stored at −80°C until used.

Experiments conformed to the European Communities Council Directive (2010/63/EU) and were approved by the Semmelweis University Employment and Animal Welfare Committee (XIV-I-001/2262-4/2012). The approval numbers of the Research Ethics Committee are PE/EA/1563-7/2017, PE/EA/1122-2-7/2020.

PR Rat Model

PR and normal nourished (NN) rats were generated as we earlier described (Durst et al., 2019). Briefly, the cycle of the females was monitored by daily examination of the vaginal smear. Females were selected for mating in proestrus or estrus. Females were considered timed-pregnant, if sperm cells appeared in the vaginal smear the following morning. This day was considered the embryonic day zero (E0). Pregnant female rats were then housed individually and kept either on a standard diet (Maintenance diet, Altromin Spezialfutter GmbH, Lage, Germany, catalog# 1324), or a low protein (42% protein relative to standard) diet (Protein deficient diet I, Altromin Spezialfutter GmbH, Lage, Germany, catalog# C1003) during pregnancy (**Table 1**). After delivery, all dams received standard rat chow (Desai et al., 2007) and litter sizes were adjusted to eight male pups. Bodyweight (bw) of the offsprings were measured weekly. To avoid the confounding effects of any inter-litter differences or bias subjects of three different litters were selected into each experimental

group. Experiments were performed using neonates (maximum 4 days old), 6 weeks old and adult, 12 weeks old animals.

Magnetic Resonance Imaging

Body-composition analysis (fat content, lean body weight, free and total water content) was performed in adult (12-week-old), awake NN and PR rats (n = 5/group) using an EchoMRI 700 Whole Body Composition Analyzer (Zinsser Analytic GmbH, Frankfurt am Main, Germany).

Food Preference Test

Fat preference of NN and PR rats (n = 6/group) was tested at 6 and 12 weeks of age. Rats were kept individually, and offered by both standard and high fat diet (HFD) on an *ad libitum* basis for 10 days. The diet of each rat was measured manually at the beginning and at the end of the experiment and the individual food consumption was calculated. HFD contained standard rat chow supplemented with 50% extra lard (**Table 1**) (Tesco, Budaörs, Hungary) (Polyak et al., 2016). The left and right positions of the diets in the hoppers of the cages were changed daily. The food preference test of 12-week-old animals was repeated using another cohort of rats to obtain daily data. The caloric intake/bwg values were calculated and used for statistical analyses.

Intraperitoneal Glucose (IP-GTT) and Insulin (IP-ITT) Tolerance Tests

IP-GTT was performed to assess the ability of animals to metabolize glucose. IP-ITT was performed to assess the sensitivity of insulin-responsive tissues. We used untreated 6 week-old and adult NN and PR rats (n = 8/group), as well as adults with previous chronic nesfatin-1 or vehicle treatment (see below). After overnight fasting, rats were given ip injections of 2 g/bwkg glucose (Merck Kft., Budapest, Hungary) or 0.75 IU/bwkg insulin (Humulin R, Eli Lilly, Utrecht, Netherlands) diluted in saline. Glucose concentration was measured in blood samples collected from the tip of the tail just before (0 min), as well as 15, 30, 60, 90, 120, and 150 min after glucose (IP-GTT) or insulin (IP-ITT) challenges using a D-cont® Trend Blood Glucose Meter (77 Elektronika Kft., Budapest, HU).

Birth Dating of Hypothalamic Cells by Bromodeoxyuridine Labeling

Timed-pregnant rats were given a single dose (160 mg/bw kg) of intraperitoneal (ip) bromodeoxyuridine (BrDU) (Merck) injection on the gestational day 13 (Markakis, 2002). NN and PR male offsprings (n = 4/group) of different dams were perfusion-fixed with 4% paraformaldehyde dissolved in PBS (Merck) at 12 weeks of age. The brains were removed and processed for BrDU and nesfatin-1 immunohistochemistry (see below). Two animals/group was omitted from the colocalization study, as they failed to show any BrDU labeling in the brain.

TABLE 1 | Composition of the diets used in the study.

	Standard diet		High fat diet		Low protein diet	
	(g%)	(kcal %)	(g%)	(kcal %)	(g%)	(kcal %)
Protein	19.2	23.9	12.8	10	8.1	9.2
Carbohydrate	53.4	64.8	35.6	27.3	70.5	78
Fat	4.1	11.3	36.07	62.7	5.1	12.8
Energy (kcal/g)	3.23		5.35		3.56	

Acute Intracerebroventricular Nesfatin-1 Administrations

Cannulation and nesfatin-1 administration was performed as described earlier (Konczol et al., 2010). Briefly, a polyethylene guide cannula (Smiths Medical ASD, Inc., NH, United States) was inserted stereotaxically into the right lateral ventricle (0.8 mm caudal to the bregma, 2.0 mm lateral to the sagittal suture and 4.0 mm below the skull surface) of adult rats. The placement of the cannulas was verified by injecting 10 nM/3 μl of angiotensin II into the brains 1 day after surgery. Only animals reacting with an intensive drinking response were included in the study. Following surgery, rats were kept individually and allowed to recover for one week. On the day of the experiment, the rats were randomly divided into four groups: NN-Nesfatin-1, PR-Nesfatin-1, NN-Saline, PR-Saline. Nesfatin-1 (Phoenix Pharmaceuticals Inc., Burlingame, CA, United States) was dissolved in saline at a concentration of 5 pmol/μl. Each rat received 5 μl of nesfatin-1 (25 pmol), or saline icv at the beginning of the dark cycle. Two different experiments were performed.

1. To measure the effect of nesfatin-1 on food and water intakes, food was withdrawn from the animals (n = 5/group) 1 h before the injections. Immediately after the injections (zero timepoint) food was returned to rats and their food and water intakes were measured manually at certain intervals of time (0–4, 4–8, and 8–12 h).
2. To understand the effect of nesfatin-1 on fasting-induced neuronal activation, the animals (n = 7/group) were fasted for 24 h. Rats were perfusion-fixed with 4% paraformaldehyde 90 min after the icv injections. The brains were removed and processed for cFos immunohistochemistry (see below).

Chronic Intracerebroventricular Nesfatin-1 Treatment

A catheter (Alzet® brain-infusion kit 2) connected to an osmotic minipump (Alzet® Model 2001, Durect Corporation, Cupertino, CA, United States) was implanted into the right cerebral ventricle of rats according to the manufacturer's instructions. The minipump delivered nesfatin-1 (70 pmol/day) or vehicle [sterile artificial cerebrospinal fluid (ACSF), composition in mmol/l: NaCl: 140, KCl: 3.35, $MgCl_2$: 1.15, $CaCl_2$: 1.26, Na_2HPO_4:1.2, NaH_2PO_4: 0.3] icv to rats with 1 μl/h pumping rate for 7 days (cohort 1: NN-nesfatin-1 and NN-aCSF, n = 6/group; cohort 2: PR-nesfatin-1 and PR-aCSF, n = 6/group). Food intake and bodyweight of rats were measured daily. At the end of the infusion period, rats were tested for glucose and insulin tolerance (see below). After the experiments the animals were sacrificed by

decapitation. The accuracy of the placement of the cannulas was verified later histologically.

Quantitative *in situ* Hybridization

NUCB2 mRNA levels in the different hypothalamic nuclei were determined by radioactive *in situ* hybridization (ISH) providing a linear relationship between the signal intensity and the mRNA expression level (Chen C. C. et al., 2012). Hybridizations were performed using fresh frozen coronal sections as earlier described by [^{35}S]UTP-labeled (Per-Form Hungária Kft, Budapest, Hungary) antisense riboprobes (Tóth et al., 2008; Konczol et al., 2010). Riboprobes were generated by *in vitro* transcription according to the manufacturer instructions (MAXIscript Kit, Thermo Fisher Scientific, Budapest, Hungary). The cDNA template for the *in vitro* transcription corresponded to the 286–531 bs of the rat NUCB2 sequences. Specificity of cDNA was verified by sequencing and assessed by BLAST screening[1] of the rat genome. Fresh-frozen 12 μm thick serial coronal sections from the brains of NN and PR rats (neonates on postnatal day 0) (n = 4–6/group) and adults (n = 6/group) were hybridized overnight with 10^6 DPM/slide of radioactively labeled riboprobe. Next day, after washing and dehydrating steps (Tóth et al., 2008; Konczol et al., 2010), sections were apposed to an imaging plate (Fuji Photo Film Co., Ltd., Kanagawa, Japan, NJ) for a week. Data were read out by a Fujifilm FLA-8000 Image Analyzer. Optical densities (mean gray values) of the individual nuclei were measured from the storage phosphor recordings with the help of the ImageJ 1.32j software (Wayne Rasband; NIH, Bethesda, MD, United States). The same nuclei were evaluated by applying the same settings both across the sections and across the animals. Background values were measured in parallel and subtracted. Data were assessed bilaterally from at least two sections per animal selected from the centers of the investigated areas (SON, PVN, LHA, ARC). The average/animal data were compared statistically.

Enzyme-Linked Immunosorbent Assay

Peripheral nesfatin-1 protein levels were determined from plasma samples of PR and NN neonates (4-day old) and adults (12-week-old) using a Nesfatin-1 (1–82) (Rat) EIA kit (EK-003-22) (Phoenix) according to the manufacturer's instructions (n = 3/group). All samples were measured in one assay, the intraassay coefficient of variability was 2.52.

Immunohistochemistry

The perfusion-fixed brains were cryoprotected in 20% sucrose (Merck) solution and then frozen in dry ice-cold methyl-butane (Merck). Free-floating 50 μm thick serial coronal sections of the hypothalamus were cut by a frigomobil (Frigomobil, Reichter-Jung, Vienna, Austria). Immunohistochemistry was performed using standard protocols. For cFos immunostaining we used a rabbit anti-cFos (1:20,000, Cat. # ABE 457, Merck) primary antibody. The cFos signal was developed by using the standard ABC method and nickel-diaminobenzidine as chromogen. For BrDU and nesfatin-1 double fluorescence immunostaining, the sections were treated with 2N HCl at 37°C for 30 min to perform antigen retrieval. The following primary antibodies were used: mouse anti-BrDU (1:1,000, Cat. # B8434, Merck) and rabbit anti-nesfatin-1 (1:6,000, Cat. # H-003-22, Phoenix, recognizes also NUCB2 protein). The BrDU and nesfatin-1 immunostainings were visualized sequentially by using TSA Kits containing Alexa Fluor 488 and 568 fluorophores, respectively (Cat. # T20912, T20924, Thermo Fisher Scientific). Microwave treatment in 0.1 M citric acid at pH 6 was used to eliminate the activity of the secondary antibody conjugated peroxidase enzyme between the two detection steps (Toth and Mezey, 2007).

Cell Counting

The number of cFos-labeled cells was counted in light microscopic pictures (see imaging) within regions of interests (ROIs). ROIs were placed within the centers of the relevant hypothalamic nuclei at the same rostro-caudal level across the animals determined by using the Rat Brain Atlas (Paxinos and Watson, 2007). The size of the ROI was 100 × 100 μm (SON, parvocellular PVN, magnocellular PVN, ARC), or 200 × 200 μm (LHA). The SON and subnuclei of PVN were evaluated using one ROI/nucleus. Two and three ROIs were placed over different regions of the ARC and LHA, respectively. Data of 4 (SON, PVN) or 7 (ARC, LHA) sections per animal were assessed bilaterally with the help of the cell counter tool (manual counting) in the ImageJ application. The cells were counted by a person skilled in the evaluation of immunohistochemical stainings. The average count per ROI/animal data were compared statistically.

The number of nesfatin-1 cells in adults (n = 4/group) and the BrDU and nesfatin-1 double immunostaining (n = 2/group) was evaluated in two non-consecutive sections at 2.9 mm and 3.1 mm caudal to the bregma. The hypothalami were outlined on tile-scanned confocal images (see imaging) with the help of the Rat Brain Atlas (Paxinos and Watson, 2007). Nesfatin-1$^+$ and BrDU$^+$ cells in the different channels were labeled and counted bilaterally with the help of the ImageJ program. The number of nesfatin-1 cells/section/animal and the percentage of BrDU$^+$ nesfatin-1 cells/section/animal were compared statistically.

Imaging

Light microscopic pictures of cFos immunostained sections were taken by an Olympus BX60 microscope (objectives: UPlanFLN 10×/0.30) interfaced with a SPOT Xplorer 17.4 camera (Diagnostic Instruments Inc., Sterling Heights, MI, United States). Confocal tile scans of BrDU and nesfatin-1 double-labeled sections were acquired on a LSM 780 confocal laser-scanning microscope (Zeiss, Jena, Germany) using a 20×/0.8 M27 objective with a resolution of 2.4 pixel/micron and pinhole diameter 0.00057. The images were stitched using the ZEN 2010 program. Contrast and sharpness of the illustrative images were adjusted in Adobe Photoshop CS 8.0. Multi-panel figures were assembled in PowerPoint 2016.

Statistics

Data analyses were performed by investigators blinded to experimental groups. The size of the experimental groups was determined based our previous experience (Könczöl et al., 2012;

[1] https://blast.ncbi.nlm.nih.gov/Blast.cgi

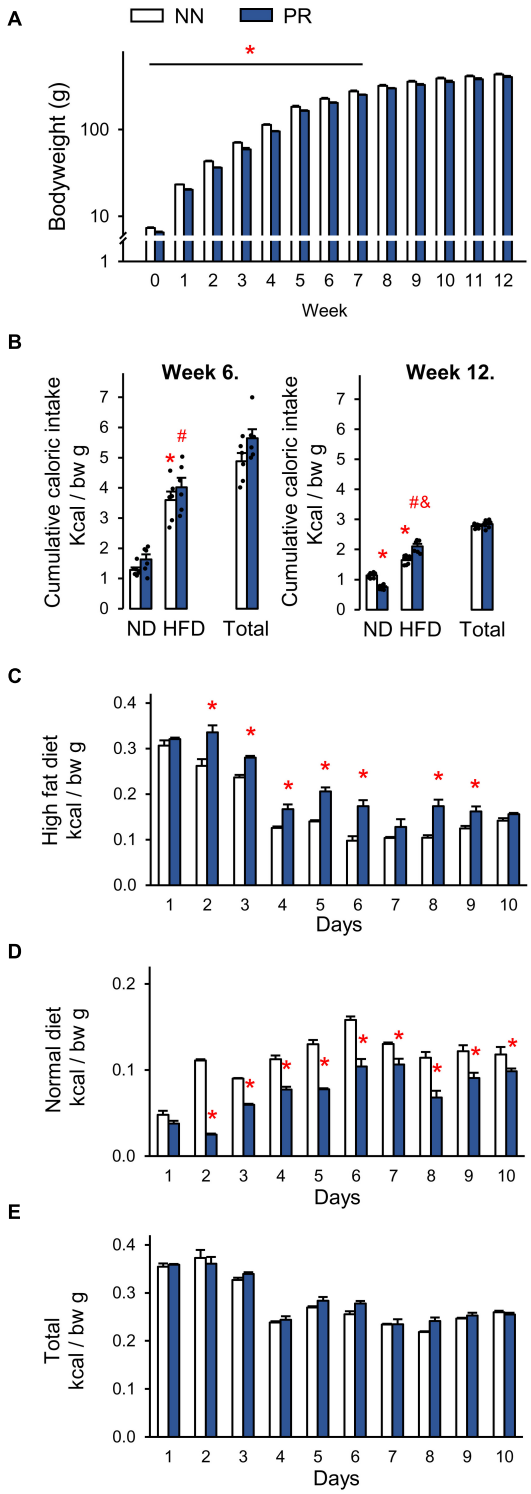

FIGURE 1 | Postnatal development of normal nourished (NN) and intrauterine protein restricted (PR) rats as well as relative caloric intakes of normal (ND) and high fat (HFD) diets. **(A)** Weekly bodyweights. PR rats had lower than normal bodyweight at birth (week 0) and until week 8. Student's *t*-test, or Mann-Whitney *U*-test, NN vs. PR $^{*}p < 0.05$, $n = 6$. Note the logarithmic scale on the y axis. **(B)** Caloric intakes of ND and HFD. Both diets were offered for *(Continued)*

FIGURE 1 | 10 days as a free choice. Both NN and PR rats prefer HFD over ND at postnatal week 6 (left, catch up growth period) and postnatal week 12 (right, catch up growth completed). At postnatal week 12 PR rats consume relatively more of HFD and less of ND than NN rats. The total caloric intake of PR rats is normal. ND—HFD bars: Two-way ANOVA, week 6: effect of diet: $F_{(1,\ 20)} = 101.87$, $p < 0.001$, week 12: phenotype × diet: $F_{(1,\ 20)} = 49.01$, $p < 0.001$.Tukey multiple comparison test, $^{*}p < 0.001$ vs. NN-ND, $^{\#}p < 0.001$ vs. PR-ND, $^{\&}p < 0.001$ vs. NN-HFD. **(C–E)** Relative daily caloric intakes during the fat preference test performed at postnatal week 12. **(C)** HFD. Two-way RM ANOVA, effect of time: $F_{(9,\ 90)} = 286.90$, $p < 0.001$, effect of phenotype: $F_{(1,\ 90)} = 19{,}28$, $p < 0.001$, phenotype × time: $F_{(9,\ 90)} = 8.48$, $p < 0.001$. **(D)** ND. Two-way RM ANOVA, effect of time: $F_{(9,\ 90)} = 107.81$, $p < 0.001$, effect of phenotype: $F_{(1,\ 90)} = 51.06$, $p < 0.001$, phenotype × time: $F_{(9,\ 90)} = 20.03$, $p < 0.001$. **(E)** HFD + ND as total. Two-way RM ANOVA, effect of time: $F_{(9,\ 90)} = 168.83$, $p < 0.001$. Tukey multiple comparison tests, NN vs. PR within day $^{*}p < 0.01$. Means ± SEM, $n = 6$ for all graphs. bw: bodyweight.

TABLE 2 | Body composition of the adult (12 week-old) experimental animals.

	Total body mass (g)	Fat content (%)	Lean body mass (%)	Total water content (%)	Free water content (%)
Control	446 ±17	14.3 ± 0.69	80.2 ± 0.73	67.0 ± 0.70	0.32 ± 0.02
PR	494 ± 9	16.3 ± 0.94	77.5 ± 0.95	64.6 ± 0.70	0.34 ± 0.04
p	0.176	0.251	0.232	0.24	0.591

Mean ± SEM as well as p-values calculated by Student's t-test, n = 5.

Durst et al., 2019). Statistical significances were calculated employing the Sigmastat 3.5 application (Systat Software Inc., Chicago, IL). Student's *t*-test (two-tailed) was used for comparing two groups with normal distribution of data, otherwise Mann-Whitney *U*-test was applied. When comparing the effects of two factors, two-way ANOVA, or for consecutive measurements two-way RM ANOVA was applied followed by Tukey *post hoc* analysis. The statistics were performed using the original data values. Differences between groups were considered statistically significant, when $p < 0.05$. Results are expressed as means ± SEM values.

RESULTS

PR Animals Exhibit Fast Catch-Up Growth, Enhanced Fat Preference and Impaired Glucose Homeostasis

PR animals were born with a lower body weight than NN animals and this difference was maintained until the eighth week after birth. This time can be considered the end of the catch-up growth period (**Figure 1A**). From week 8 until the end of the experiment (week 12), the bodyweights of the PR and NN rats were similar. Analysis of body composition by EchoMRI also confirmed that the fat content, lean and total body masses, as well as total and free water content of PR rats at 12 weeks of age were similar to those of NN rats (**Table 2**).

In another experiment, we measured the caloric intake of rats and examined their fat preference. During the catch-up growth period, at 6 weeks of age (**Figure 1B**, left), rats in both groups

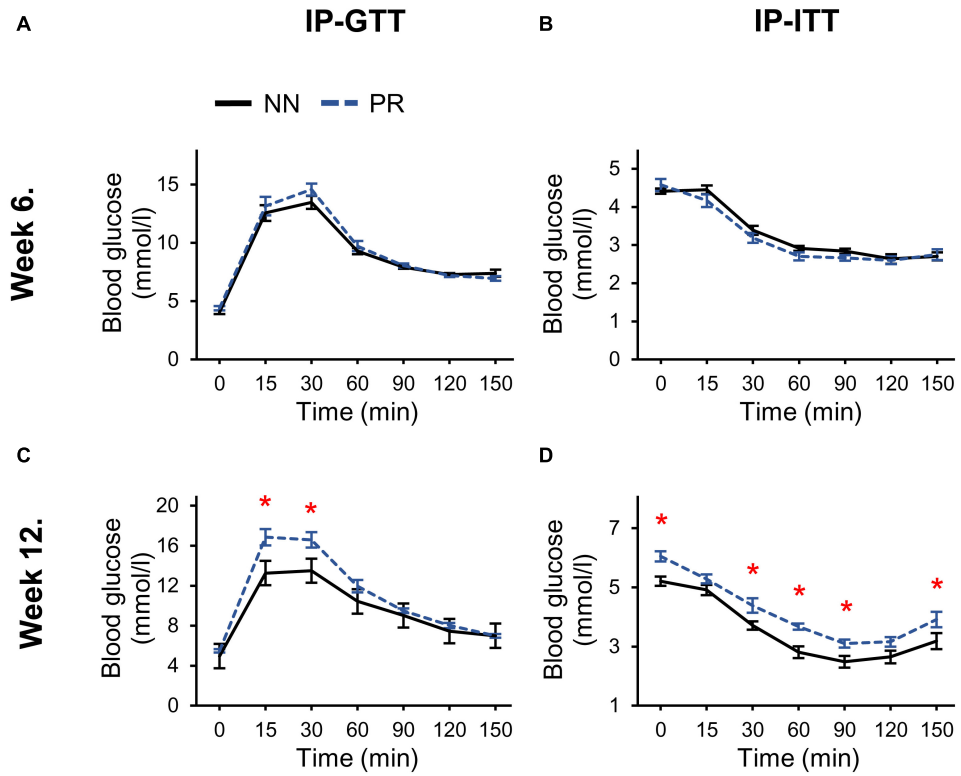

FIGURE 2 | Glucose and insulin tolerances of NN and PR rats. **(A)** Intraperitoneal glucose (IP-GTT) and **(B)** intraperitoneal insulin tolerance tests (IP-ITT) performed at postnatal week 6 show similar responses to glucose and insulin in both groups. **(C)** IP-GTT performed at postnatal week 12 shows decreased glucose tolerance of PR rats. Two-way RM ANOVA, effect of phenotype: $F_{(1,\ 78)} = 6.494$, $p = 0.023$, effect of time: $F_{(6,\ 78)} = 87.342$, $p < 0.001$, effect of phenotype × time: $F_{(6,\ 78)} = 2.972$, $p = 0.011$. **(D)** IP-ITT shows decreased insulin sensitivity of PR rats compared to NN controls. Two-way RM ANOVA, effect of phenotype: $F_{(1,\ 81)} = 18.714$, $p < 0.001$, effect of time: $F_{(6,\ 81)} = 93.725$, $p < 0.001$. Tukey multiple comparison tests, NN vs. PR within one time point, $^*p < 0.05$. Means ± SEM, $n = 8$ for all graphs.

showed a similar preference for HFD over ND. The total caloric intake per bodyweight was therefore not different between the groups (**Figure 1B**, left). After the catch-up growth period, at 12 weeks of age, rats continued to prefer HFD over ND, but to a different extent depending on phenotype (**Figure 1B**, right). PR rats consumed more calories from HFD, than NN rats. Since they consumed correspondingly less calories from ND, the total caloric intake per bodyweight remained the same in the two groups (**Figure 1B** right).

Daily analysis of the preference test of adults revealed that calorie consumption from HFD was initially very high (**Figure 1C**). It then decreased over time in both groups, and remained more or less constant after day 6. The increased fat preference of PR rats relative to controls was observed from day 2 and lasted practically until the end of the observation period (**Figure 1C**). Calorie consumption of ND showed an opposite dynamics (**Figure 1D**). It increased over time in both groups until about day 6, and did not change dramatically thereafter. From day 2 of the testing period, PR rats consumed fewer calories from ND, than NN rats (**Figure 1D**). The caloric intake from HFD was extremely high in both groups at the beginning of the testing period, and no compensation was made at the expense of ND. Therefore, the daily total caloric intakes were higher on the first 3 days compared to the other days (**Figure 1E**). However, there was no difference between the phenotypes on any of the experimental days (**Figure 1E**).

The response to the intraperitoneal glucose and insulin treatment at week 6 was similar in PR and NN rats (**Figures 2A,B**). However, by week 12, both glucose tolerance and insulin sensitivity of PR rats were reduced (**Figures 2C,D**). In addition, fasting blood glucose levels (zero timepoint) of PR rats were elevated at week 12 (cohorts$_{1+2}$ PR: 5.77 ± 0.14 mmol/l, NN: 5.09 ± 0.12 mmol/l, Student's t-test, $p < 0.001$).

Alterations in the Hypothalamic NUCB2/Nesfatin-1 System Characterize the PR Rats

To assess whether fetal programming affected the development of hypothalamic nesfatin-1 neurons, we performed birth dating of cells by BrDU on the embryonic day 13 (E13) (**Figure 3A**). E13 was chosen based on data from previous studies (Altman and Bayer, 1986; Markakis, 2002). Our data suggest, that fewer nesfatin-1 cells were generated on E13 in PR rats than in NN rats (**Figure 3B**). However, the number of nesfatin-1 positive cells in adulthood was similar between groups (**Figure 3C**).

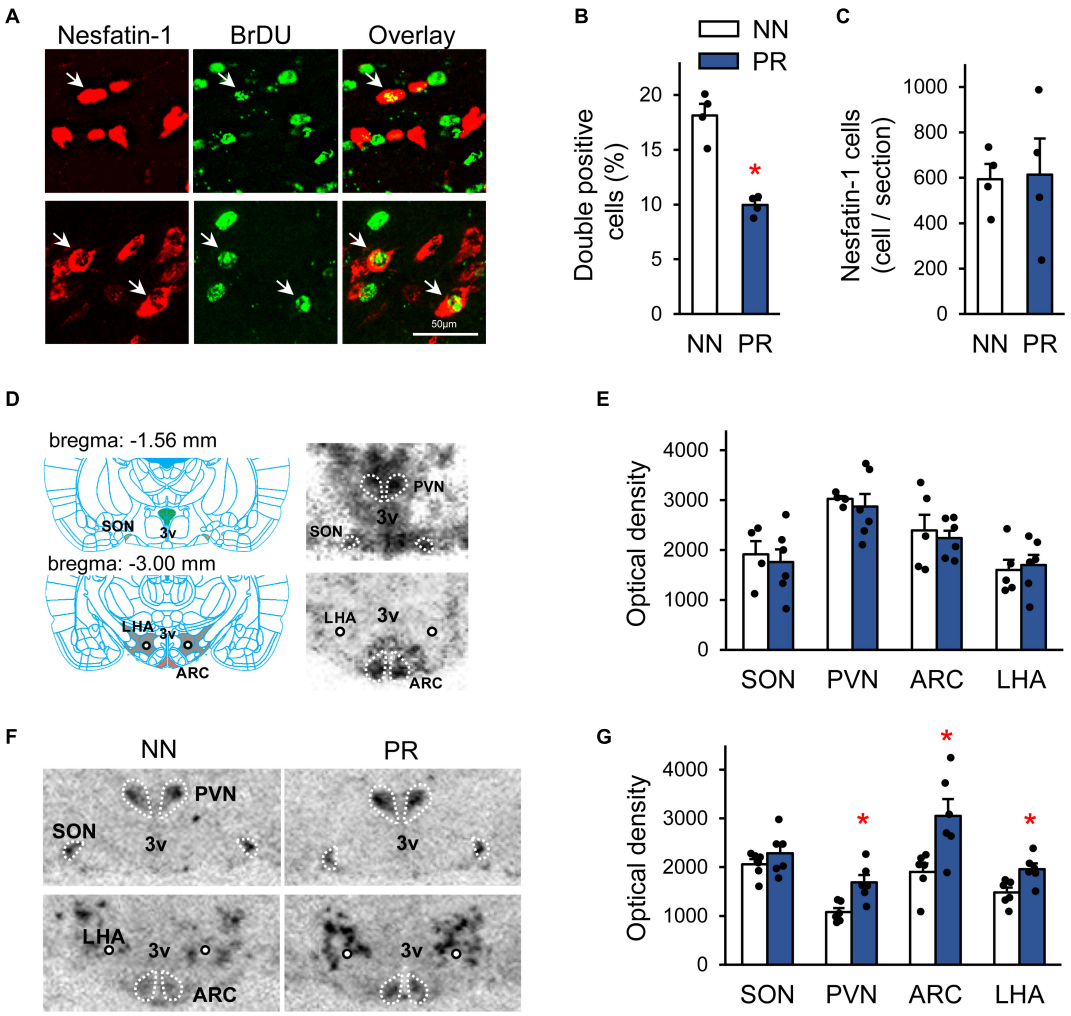

FIGURE 3 | Characterization of the peripheral and central nesfatin-1 system. **(A)** Birth dating of nesfatin-1 neurons by bromodeoxyuridine (BrDU) at the embryonic day 13 (E13). Confocal microscopic images showing nesfatin-1 and BrDU double-labeled cells (arrows) in the hypothalamus of a NN rat. The immunostaining was performed using coronal hypothalamic sections of adult offspring. **(B)** Percentage of nesfatin-1 cells generated at E13 (BrDU and nesfatin-1 double-labeled cells) in the hypothalamus. Two-way RM-ANOVA, effect of phenotype $F_{(1,\ 2)} = 71.83$, $^*p = 0.014$, $n = 2$ animals and 4 sections/group. **(C)** The number of hypothalamic nesfatin-1 positive cells in adults. $n = 4$ animals/group. **(D)** Left: Schematic (Paxinos and Watson, 2007) showing the location of the investigated hypothalamic nuclei in coronal brain sections. The rostro-caudal distance from the bregma level is indicated for each section. ARC, arcuate nucleus; PVN, paraventricular nucleus; SON, supraoptic nucleus; LHA, lateral hypothalamic area; 3V, 3rd ventricle; circle, fornix. Right: Detection of NUCB2/nesfatin-1 mRNA by radioactive *in situ* hybridization technique in the investigated areas in neonatal rats. Autoradiographic images (NN rat) of coronal sections. The darker the shades of gray, the stronger the signal. **(E)** Bar graph showing NUCB2/nesfatin-1 mRNA levels in the investigated nuclei in neonates, $n = 4$–6. **(F)** Autoradiographic images showing NUCB2/nesfatin-1 mRNA expression in adult NN and PR rats. Note the enhanced signal intensity in most of the measured nuclei in the PR rat. **(G)** Bar graph showing NUCB2/nesfatin-1 mRNA levels in the investigated areas in adults. Student's *t*-test, or Mann-Whitney *U*-test, NN vs. PR $^*p < 0.05$, $n = 6$. Bar graphs show means ± SEM.

Next, we examined the expression of NUCB2/nesfatin-1 mRNA in the SON, PVN, ARC and LHA by ISH (**Figure 3D**). NUCB2/nesfatin-1 mRNA was detectable at birth in all investigated areas, and the expression levels in PR animals were not different from those observed in NN rats (**Figures 3D,E**). In contrast, in adult, 12 week-old PR rats NUCB2/nesfatin-1 mRNA expression was markedly upregulated in the PVN, ARC and LHA (**Figures 3F,G**). However, blood concentrations of nesfatin-1 were similar between groups in both neonates (5.0 ± 0.6 and 6.2 ± 1.0 ng/μl in NN and PR groups, respectively, Student's *t*-test, $p = 0.329$, $n = 3$/group) and adults (11.1 ± 1.7 and 7.7 ± 0.7 ng/μl in NN and PR groups, respectively, Student's *t*-test, $p = 0.139$, $n = 3$/group).

PR Animals Develop Hypothalamic Nesfatin-1 Resistance by Adulthood

To investigate the functional significance of the alterations found in the hypothalamic nesfatin-1 system of PR rats, we administered nesfatin-1 icv to the rats and measured their food

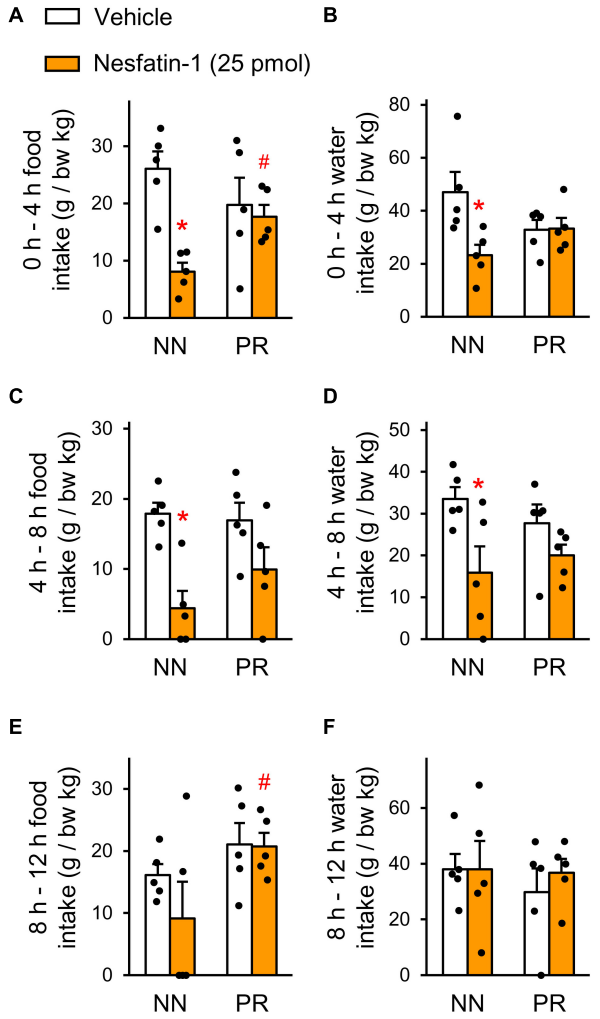

FIGURE 4 | Effect of acute intracerebroventricular (icv) injection of nesfatin-1 (25 pmol), or vehicle on nocturnal food and water intakes of NN and PR rats. Food **(A,C,E)** and water **(B,D,F)** intakes of 12 week-old NN and PR rats were measured at 4 h intervals. Zero is the timepoint of treatments. **(A,B)** 0–4 h. Two-way ANOVA, food intake, effect of treatment $F_{(1,\ 16)} = 10.43$, $p = 0.005$ treatment × phenotype: $F_{(1,\ 16)} = 6.530$, $p = 0.021$, water intake, treatment × phenotype: $F_{(1,\ 16)} = 5.66$, $p = 0.030$. **(C,D)** 4–8 h. Two-way ANOVA food intake, effect of treatment: $F_{(1,\ 16)} = 16.85$, $p < 0.001$, water intake, effect of treatment: $F_{(1,\ 16)} = 8.51$, $p < 0.010$. **(E,F)** 8–12 h. Two-way ANOVA, effect of phenotype: $F_{(1,\ 16)} = 5.04$, $p = 0.039$; NN vs. PR within nesfatin-1, $p = 0.041$. Effects of nesfatin-1 are impaired in PR rats. Tukey multiple comparison tests, $^{*}p < 0.05$ vs. NN-vehicle, $^{\#}p < 0.05$ vs. NN-nesfatin-1. Means ± SEM, $n = 5$ for all graphs.

and water intakes. Nesfatin-1 significantly reduced the relative food and water intake of NN rats in the first 4 h after treatment (**Figures 4A,B**). Food and water consumption of the PR group was not affected by nesfatin-1 during this period. Similar observations were made between 4 and 8 h post-treatment (**Figures 4C,D**). The effect of nesfatin-1 on the food intake continued to differ between NN and PR rats for the remainder of the dark phase (**Figure 4E**). Water consumption was no longer affected by nesfatin-1 during this period (**Figure 4F**).

In order to identify hypothalamic nuclei, where nesfatin-1 resistance develops in PR rats, we measured the effect of icv nesfatin-1 on the number of fasting-activated neurons in the SON, PVN, ARC, and LHA (**Figure 5**). Treatment with nesfatin-1 significantly reduced the number of cFos-positive cells in the ARC of NN animals, but did not have this effect in PR rats (**Figures 5A,B**). No differences were found between the groups in the other nuclei investigated (**Figures 5C–F**).

Chronic Intracerebroventricular Nesfatin-1 Treatment Improves the Glucose Homeostasis Only in Normal Nourished Rats

Finally, we assessed the effect of nesfatin-1 on glucose homeostasis. Since acute icv injection of 25 pmol nesfatin-1 was reported to have no effect on blood glucose levels in mice (Su et al., 2010), we applied chronic icv nesfatin-1 treatment (70 pmol/day, for 7 days). In NN rats, the treatment hindered the recovery from the surgery (bodyweight change$_{\text{days } 0-6}$: −1 ± 3.2 g and −14.8 ± 2.4 g in the vehicle and nesfatin-1 treated groups, respectively, Student's *t*-test, $p = 0.034$). Nesfatin-1 also reduced the food intake of NN animals (**Figure 6A**). The IP-GTT (**Figure 6B**) and IP-ITT (**Figure 6C**) performed at the end of the treatments showed an improved glucose tolerance and insulin sensitivity of nesfatin-1 treated NN rats relative to the vehicle-treated NN group.

Chronic treatment with nesfatin-1 did not induce nesfatin-1 resistance in NN animals, and even had a beneficial effect on their glucose homeostasis. We, therefore tested PR animals in a separate experiment. Treatment with nesfatin-1 did not affect the recovery of PR rats (bodyweight change$_{\text{days } 0-6}$: 2.2 ± 2.1 and 5.3 ± 4.8 g in the vehicle and nesfatin-1 treated groups, respectively, Student's *t*-test, $p = 0.557$), although slightly reduced their food intake (**Figure 6D**). Glucose homeostasis of PR rats was not affected by the treatment (**Figures 6E,F**).

DISCUSSION

The present study shows that in non-obese PR rats, central nesfatin-1 resistance probably contributes to the development of T2DM. Dysfunction of nesfatin-1 signaling in the ARC seems to play an important role in this process.

Insulin resistance and elevated hepatic glucose production are the main characteristics in T2DM. Impaired glucose tolerance and fasting hyperglycemia, which developed in PR rats with normal body composition between the 6th and 12th postnatal weeks, are among the early signs of the disease (Al-Goblan et al., 2014). Therefore, fetal programming by intrauterine protein restriction, predisposes development of T2DM as a primary effect, not secondarily to obesity.

According to the thrifty phenotype hypothesis (Barker et al., 1993), PR induces a predictive adaptive response of the organism by alternative metabolic programming of the organs to use the nutritional supply with a maximal effectiveness. In nutrient-rich environment, PR rats exhibited the typical signs of the thrifty

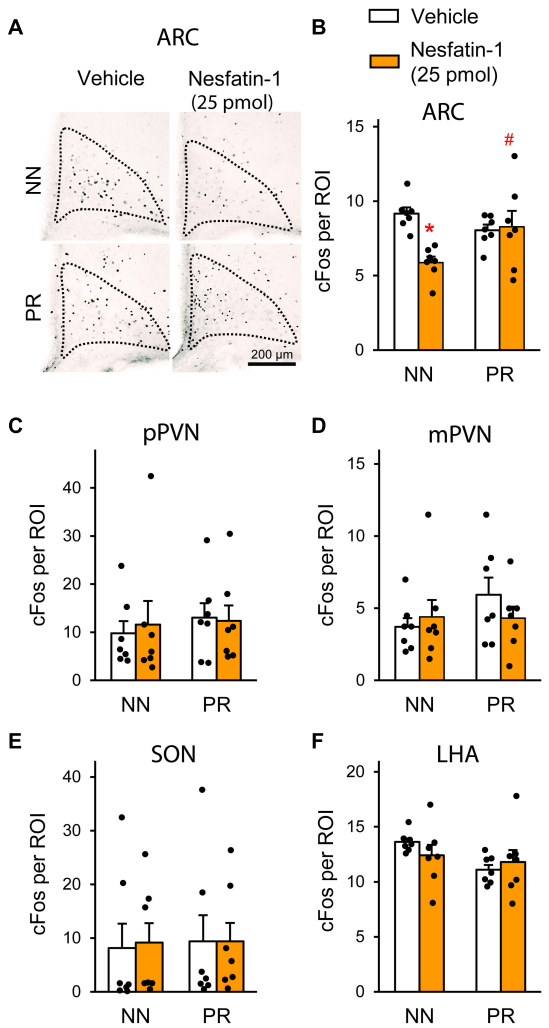

FIGURE 5 | Neuronal activation (cFos) in the hypothalamus following acute icv nesfatin-1 injection (25 pmol) into NN and PR rats subjected to overnight fasting. **(A)** Representative light microscopic images showing cFos-immunoreactive cell nuclei (black dots) mainly within the medial ARC of the different experimental groups. **(B–F)** Bar graphs showing the quantitative data on the number of cFos-positive cells per region of interest (ROI). **(B)** ARC. Nesfatin-1 reduced the number of fasting activated neurons in the NN rats. Two-way ANOVA, effect of treatment: $F_{(1,\ 24)} = 5.743$, $p = 0.025$; treatment × phenotype: $F_{(1,\ 24)} = 7.671$, $p = 0.011$. Tukey multiple comparison test, $^{*}p < 0.05$ vs. NN-vehicle; $^{\#}p < 0.05$ vs. NN-nesfatin-1. **(C)** Parvocellular PVN (pPVN). **(D)** Magnocellular PVN (mPVN). **(E)** SON. **(F)** LHA. Two-way ANOVA, Means ± SEM, $n = 7$.

phenotype; intense catch-up growth and preference for HFD relative to control peers (Langley-Evans et al., 2005). Importantly, preference for HFD developed after the completion of the catch up growth. This suggests that during the manifestation of the PR phenotype different mechanisms are turned on sequentially to modify the energy homeostasis.

Both adult PR and NN rats preferred HFD over ND, and caloric overconsumption was counter-regulated in both phenotypes with similar dynamics (after 3 days). However, PR animals consequently (from the 2nd day of the preference test) covered more of their daily caloric needs from HFD compared to control rats. In turn, they consumed less of ND to keep their daily caloric intake at normal level. Thus, energy balance regulation was functional in PR rats, but worked with different settings compared to NN animals.

Although the mRNA expression of NUCB2/nesfatin-1 was similar in the hypothalamus of PR and NN rats at birth, it was upregulated in the PVN, LHA and ARC in adult PR rats. Peripheral (blood) nesfatin-1 levels were unaltered. Despite chronic icv nesfatin-1 treatment causes weight loss (Oh-I et al., 2006), and acute injection of nesfatin-1 into the PVN or LHA reduces the cumulative food intake of rats (Chen X. et al., 2012), the increased nesfatin-1 production in PR rats was without a negative effect on food intake and bodyweight. Additionally, when we injected nesfatin-1 icv to rats, the treatment was not effective in reducing the nocturnal food intake of PR animals. Thus, adult PR rats were resistant to centrally added nesfatin-1, and NUCB2/nesfatin-1 mRNA was upregulated in the measured nuclei as compensation. Our data indicate that nesfatin-1 has an essential role in the regulation of the energy homeostasis *via* the PVN, LHA and ARC.

Nesfatin-1 reduced the number of fasting activated ARC neurons in NN rats, when it was applied icv at the time of the expected meal. Nesfatin-1 applied icv also reduces the food intake in previously fasted rats (Yosten and Samson, 2009). The phenotype of non-responding cells would be hard to identify. However, the neuronal activity in two key cell populations of the ARC correlates with energy status in rodents. Orexigenic, neuropeptide Y (NPY) producing ARC neurons are activated by fasting, while anorexigenic, melanocortin expressing neurons are activated by refeeding (Fekete et al., 2012; Betley et al., 2013). Almost all (∼94%) of activated, i.e., cFos-immunoreactive neurons are NPY cells in the ARC of fasted mice (Becskei et al., 2009). Therefore, one explanation is that nesfatin-1 reduced the number of cFos-immunopositive cells by acting on NPY neurons. This would be consistent with *ex vivo* data showing that nesfatin-1 hyperpolarizes NPY cells (Price et al., 2008). Regardless of this, fasting triggers an extensive orexigenic drive primarily *via* the activation of the NPY cells in the ARC. Nesfatin-1 reduced the orexigenic drive (i.e., food intake) in NN, but not in PR animals, and our cFos data point to the ARC as a site of action. The ARC plays a master role in the control of food intake, energy expenditure and glucose homeostasis by integrating both central and peripheral/ neuronal and humoral (leptin, insulin, glucose, ghrelin) inputs (Timper and Brüning, 2017). The inhibition of the orexigenic drive in the ARC by nesfatin-1 and the impairment of this function in PR animals is therefore of great relevance for understanding the role of nesfatin-1 in the regulation of the energy homeostasis. It also identifies the ARC as a site, where nesfatin-1 resistance in PR animals most probably has functional consequences.

The hypothalamic centers for food intake and blood glucose level regulation overlap (Kleinridders et al., 2009; Sandoval et al., 2009). We provided a direct evidence that hypothalamic nesfatin-1 resistance affects food intake, and may contribute to deterioration of the glucose homeostasis in PR rats. Hepatic

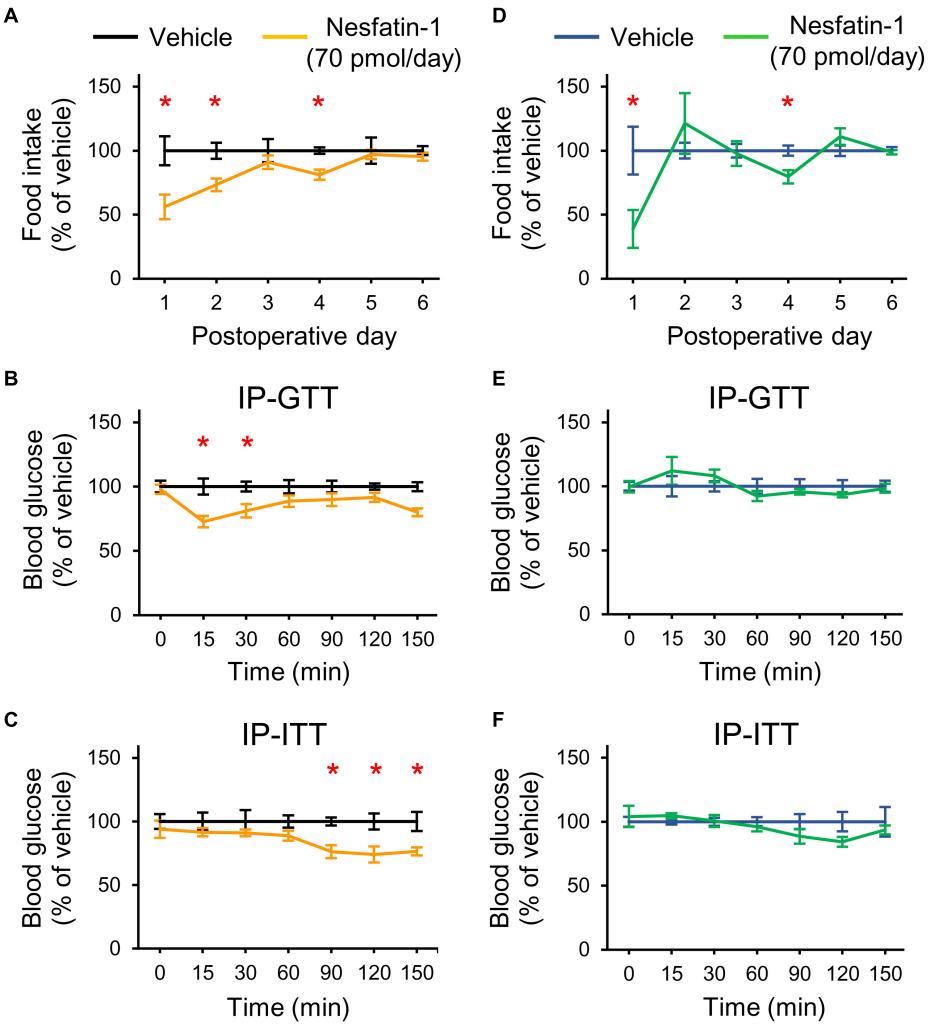

FIGURE 6 | Effects of chronic icv nesfatin-1 (70 pmol/day) or vehicle infusions on the food intake and glucose homeostasis of NN and PR rats. Day zero was the day of cannula and infusion pump implantations as well as the beginning of the treatments. The tests were performed at the end of the treatment period (7 days). **(A)** Relative food intake of NN rats. Student's *t*-test, vehicle vs. nesfatin-1, day 1: $^*p = 0.013$, day 2: $^*p = 0.007$, day 4: $^*p = 0.003$. **(B)** IP-GTT shows increased glucose tolerance of NN-nesfatin-1 rats. Two-way RM ANOVA, effect of phenotype: $F_{(1,\ 60)} = 17.554$, $p = 0.002$, effect of time: $F_{(6,\ 60)} = 81.649$, $p < 0.001$, effect of phenotype × time: $F_{(6,\ 60)} = 3.760$, $p = 0.003$. **(C)** IP-ITT shows increased insulin sensitivity. Two-way RM ANOVA, effect of phenotype: $F_{(1,\ 60)} = 19.324$, $p = 0.001$, effect of time: $F_{(6,\ 60)} = 23.382$, $p < 0.001$. Tukey multiple comparison tests, vehicle vs. nesfatin-1 within day $^*p < 0.05$ for **(B,C)**. **(D)** Relative food intake of PR rats. Student's *t*-test, vehicle vs. nesfatin-1, day1: $^*p = 0.029$, day4: $^*p = 0.011$ **(E,F)** IP-GTT and IP-ITT data of PR rats, respectively. No significant differences were seen. Means ± SEM, $n = 6$ for all graphs.

glucose flux increases, while glucose uptake of peripheral tissues decreases in mice with hypothalamic knockdown of NUCB2/nesfatin-1 (Wu et al., 2014). Nesfatin-1 injected icv increases muscle glucose absorption and inhibits hepatic glucose production in rats during euglycemic-hyperinsulinemic clamping (Yang et al., 2012). Now, we showed that chronic icv nesfatin-1 treatment improves the performance of NN rats in IP-GTT and IP-ITT tests. The treatment at the dose and timing used here was ineffective in PR rats.

The limitation of our study is that the exact mechanism of how T2DM develops in hypothalamic nesfatin-1 resistance remains to be elucidated. Unfortunately, nesfatin-1 agonists and antagonists are not available, since the receptor of nesfatin-1 is unidentified. Transgenic mouse models may help future studies. As nesfatin-1 is not transported to axons, local, auto/paracrine mechanisms of nesfatin-1's action are assumed *via* dendritic release (Brailoiu et al., 2007; Foo et al., 2008). Indeed, neurogenesis of nesfatin-1 cells was complete, but the time course of cell formation was disturbed in PR rats, suggesting that hypothalamic nesfatin-1 resistance in PR rats may have developed due to alternative fetal programming of hypothalamic nesfatin-1 neurons. The importance of the ARC is stressed, since both POMC and NPY neurons in the ARC were shown to regulate glucose production of the liver (Könner et al., 2007; Dodd et al., 2018). Nesfatin-1 is abundandly expressed in the ARC (Brailoiu et al., 2007), thus, it may act on the glucose homeostasis by influencing the

function of these neurons. Indeed, most of the nesfatin-1's action requires melanocortin 3/4 receptor, and nesfatin-1 inhibits the NPY neurons *in vitro* (Schalla et al., 2020).

In summary, we demonstrated the existence of hypothalamic nesfatin-1 resistance in PR rats by using two different approaches. Our data suggest that hypothalamic nesfatin-1 resistance may be a substantial factor in development of non-obese T2DM induced by IUGR. Our finding, that treatment with nesfatin-1 may improve the glucose homeostasis and that nesfatin-1 acts independently of leptin (Shimizu et al., 2009), makes the hypothalamic nesfatin-1 system a potential therapeutic target for the treatment of T2DM.

DATA AVAILABILITY STATEMENT

The raw data supporting the conclusions of this article will be made available by the authors, without undue reservation.

ETHICS STATEMENT

The animal study was reviewed and approved by the Semmelweis University Workplace Animal Welfare Body Committee Semmelweis University, Budapest, Üllői út 26., Hungary.

AUTHOR CONTRIBUTIONS

ZT designed the research. MD, KK, KO, KS, and ZT performed the experiments and analyzed the data. PV performed molecular biology. AS-S performed MRI. MD, KK, CF, and ZT wrote the manuscript. All authors contributed to the article and approved the submitted version.

FUNDING

This work was funded by the Hungarian National Research, Development and Innovation Fund (Grant Nos. NKFI K115422 and TKP2021-EGA-25) to ZT and (Grant No. NKFI K134357) to PV. Project No. TKP2021-EGA-25 has been implemented with the support provided by the Ministry of Innovation and Technology of Hungary from the National Research, Development and Innovation Fund, financed under the TKP2021-EGA funding scheme.

ACKNOWLEDGMENTS

We would like to express our most honest gratitude for Judit Kerti, Szilvia Deák, and Zoltán Gróti for their indispensable technical assistance.

REFERENCES

Al-Goblan, A. S., Al-Alfi, M. A., and Khan, M. Z. (2014). Mechanism linking diabetes mellitus and obesity. *Diabetes Metab. Syndr. Obes.* 7, 587–591. doi: 10.2147/dmso.S67400

Altman, J., and Bayer, S. A. (1986). The development of the rat hypothalamus. *Adv. Anat. Embryol. Cell Biol.* 100, 1–178.

Barker, D. J., Gluckman, P. D., Godfrey, K. M., Harding, J. E., Owens, J. A., and Robinson, J. S. (1993). Fetal nutrition and cardiovascular disease in adult life. *Lancet* 341, 938–941. doi: 10.1016/0140-6736(93)91224-a

Barron, E., Bakhai, C., Kar, P., Weaver, A., Bradley, D., Ismail, H., et al. (2020). Associations of type 1 and type 2 diabetes with COVID-19-related mortality in England: a whole-population study. *Lancet Diabetes Endocrinol.* 8, 813–822. doi: 10.1016/s2213-8587(20)30272-2

Becskei, C., Lutz, T. A., and Riediger, T. (2009). Blunted fasting-induced hypothalamic activation and refeeding hyperphagia in late-onset obesity. *Neuroendocrinology* 90, 371–382. doi: 10.1159/000251723

Betley, J. N., Cao, Z. F., Ritola, K. D., and Sternson, S. M. (2013). Parallel, redundant circuit organization for homeostatic control of feeding behavior. *Cell* 155, 1337–1350. doi: 10.1016/j.cell.2013.11.002

Brailoiu, G. C., Dun, S. L., Brailoiu, E., Inan, S., Yang, J., Chang, J. K., et al. (2007). Nesfatin-1: distribution and interaction with a G protein-coupled receptor in the rat brain. *Endocrinology* 148, 5088–5094. doi: 10.1210/en.2007-0701

Carey, M., Kehlenbrink, S., and Hawkins, M. (2013). Evidence for central regulation of glucose metabolism. *J. Biol. Chem.* 288, 34981–34988. doi: 10.1074/jbc.R113.506782

Chen, C. C., Wada, K., and Jarvis, E. D. (2012). Radioactive *in situ* hybridization for detecting diverse gene expression patterns in tissue. *J. Vis. Exp.* 62:3764. doi: 10.3791/3764

Chen, X., Dong, J., and Jiang, Z. Y. (2012). Nesfatin-1 influences the excitability of glucosensing neurons in the hypothalamic nuclei and inhibits the food intake. *Regul. Pept.* 177, 21–26. doi: 10.1016/j.regpep.2012.04.003

Desai, M., Gayle, D., Babu, J., and Ross, M. G. (2007). The timing of nutrient restriction during rat pregnancy/lactation alters metabolic syndrome phenotype. *Am. J. Obstet. Gynecol.* 196(6) 555, e551–e557, 555.e1–555.e7. doi: 10.1016/j.ajog.2006.11.036

Dodd, G. T., Michael, N. J., Lee-Young, R. S., Mangiafico, S. P., Pryor, J. T., Munder, A. C., et al. (2018). Insulin regulates POMC neuronal plasticity to control glucose metabolism. *eLife* 7:e38704. doi: 10.7554/eLife.38704

Durst, M., Könczöl, K., Balázsa, T., Eyre, M. D., and Tóth, Z. E. (2019). Reward-representing D1-type neurons in the medial shell of the accumbens nucleus regulate palatable food intake. *Int. J. Obes.* 43, 917–927. doi: 10.1038/s41366-018-0133-y

Fekete, C., Zséli, G., Singru, P. S., Kádár, A., Wittmann, G., Füzesi, T., et al. (2012). Activation of anorexigenic pro-opiomelanocortin neurones during refeeding is independent of vagal and brainstem inputs. *J. Neuroendocrinol.* 24, 1423–1431. doi: 10.1111/j.1365-2826.2012.02354.x

Foo, K. S., Brismar, H., and Broberger, C. (2008). Distribution and neuropeptide coexistence of nucleobindin-2 mRNA/nesfatin-like immunoreactivity in the rat CNS. *Neuroscience* 156, 563–579. doi: 10.1016/j.neuroscience.2008.07.054

Gantulga, D., Maejima, Y., Nakata, M., and Yada, T. (2012). Glucose and insulin induce Ca2+ signaling in nesfatin-1 neurons in the hypothalamic paraventricular nucleus. *Biochem. Biophys. Res. Commun.* 420, 811–815. doi: 10.1016/j.bbrc.2012.03.079

Guo, Y., Liao, Y., Fang, G., Dong, J., and Li, Z. (2013). Increased nucleobindin-2 (NUCB2) transcriptional activity links the regulation of insulin sensitivity in Type 2 diabetes mellitus. *J. Endocrinol. Invest.* 36, 883–888. doi: 10.3275/9000

Kleinridders, A., Könner, A. C., and Brüning, J. C. (2009). CNS-targets in control of energy and glucose homeostasis. *Curr. Opin. Pharmacol.* 9, 794–804. doi: 10.1016/j.coph.2009.10.006

Konczol, K., Bodnar, I., Zelena, D., Pinter, O., Papp, R. S., Palkovits, M., et al. (2010). Nesfatin-1/NUCB2 may participate in the activation of the hypothalamic-pituitary-adrenal axis in rats. *Neurochem. Int.* 57, 189–197. doi: 10.1016/j.neuint.2010.04.012

Könczöl, K., Pintér, O., Ferenczi, S., Varga, J., Kovács, K., Palkovits, M., et al. (2012). Nesfatin-1 exerts long-term effect on food intake and body temperature. *Int. J. Obes.* 36, 1514–1521. doi: 10.1038/ijo.2012.2

Könner, A. C., Janoschek, R., Plum, L., Jordan, S. D., Rother, E., Ma, X., et al. (2007). Insulin action in AgRP-expressing neurons is required for suppression of hepatic glucose production. *Cell Metab.* 5, 438–449. doi: 10.1016/j.cmet.2007.05.004

Langley-Evans, S. C., Bellinger, L., and McMullen, S. (2005). Animal models of programming: early life influences on appetite and feeding behaviour. *Matern Child Nutr.* 1, 142–148. doi: 10.1111/j.1740-8709.2005.00015.x

Levin, B. E. (2006). Metabolic imprinting: critical impact of the perinatal environment on the regulation of energy homeostasis. *Philos. Trans. R. Soc. Lond. B Biol. Sci.* 361, 1107–1121. doi: 10.1098/rstb.2006.1851

Maejima, Y., Sedbazar, U., Suyama, S., Kohno, D., Onaka, T., Takano, E., et al. (2009). Nesfatin-1-regulated oxytocinergic signaling in the paraventricular nucleus causes anorexia through a leptin-independent melanocortin pathway. *Cell Metab.* 10, 355–365. doi: 10.1016/j.cmet.2009.09.002

Maejima, Y., Yokota, S., Nishimori, K., and Shimomura, K. (2018). The anorexigenic neural pathways of oxytocin and their clinical implication. *Neuroendocrinology* 107, 91–104. doi: 10.1159/000489263

Markakis, E. A. (2002). Development of the neuroendocrine hypothalamus. *Front. Neuroendocrinol.* 23, 257–291. doi: 10.1016/s0091-3022(02)00003-1

Martin-Gronert, M. S., and Ozanne, S. E. (2007). Experimental IUGR and later diabetes. *J. Intern. Med.* 261, 437–452. doi: 10.1111/j.1365-2796.2007.01800.x

Nakata, M., and Yada, T. (2013). Role of NUCB2/nesfatin-1 in glucose control: diverse functions in islets, adipocytes and brain. *Curr. Pharm. Des.* 19, 6960–6965. doi: 10.2174/13816128193913112713011 2

Oh-I, S., Shimizu, H., Satoh, T., Okada, S., Adachi, S., Inoue, K., et al. (2006). Identification of nesfatin-1 as a satiety molecule in the hypothalamus. *Nature* 443, 709–712. doi: 10.1038/nature05162

Paxinos, G., and Watson, C. (2007). *The Rat Brain in Stereotaxic Coordinates*, 6th Edn. San Diego, CA: Academic Press.

Pedroso, A. P., Souza, A. P., Dornellas, A. P. S., Oyama, L. M., Nascimento, C. M. O., Santos, G. M. S., et al. (2017). Intrauterine growth restriction programs the hypothalamus of adult male rats: integrated analysis of proteomic and metabolomic data. *J. Proteome Res.* 16, 1515–1525. doi: 10.1021/acs.jproteome.6b00923

Pinney, S. E. (2013). Intrauterine growth retardation - A developmental model of type 2 diabetes. *Drug Discov. Today Dis. Models* 10, e71–e77. doi: 10.1016/j.ddmod.2013.01.003

Polyak, A., Winkler, Z., Kuti, D., Ferenczi, S., and Kovacs, K. J. (2016). Brown adipose tissue in obesity: Fractalkine-receptor dependent immune cell recruitment affects metabolic-related gene expression. *Biochim. Biophys. Acta* 1861, 1614–1622. doi: 10.1016/j.bbalip.2016.07.002

Pozo, M., and Claret, M. (2018). Hypothalamic control of systemic glucose homeostasis: the pancreas connection. *Trends Endocrinol. Metab.* 29, 581–594. doi: 10.1016/j.tem.2018.05.001

Price, C. J., Samson, W. K., and Ferguson, A. V. (2008). Nesfatin-1 inhibits NPY neurons in the arcuate nucleus. *Brain Res.* 1230, 99–106. doi: 10.1016/j.brainres.2008.06.084

Saleem, T., Sajjad, N., Fatima, S., Habib, N., Ali, S. R., and Qadir, M. (2011). Intrauterine growth retardation–small events, big consequences. *Ital. J. Pediatr.* 37:41. doi: 10.1186/1824-7288-37-41

Sandoval, D. A., Obici, S., and Seeley, R. J. (2009). Targeting the CNS to treat type 2 diabetes. *Nat. Rev. Drug Discov.* 8, 386–398. doi: 10.1038/nrd2874

Schalla, M. A., Unniappan, S., Lambrecht, N. W. G., Mori, M., Tache, Y., and Stengel, A. (2020). NUCB2/nesfatin-1-Inhibitory effects on food intake, body weight and metabolism. *Peptides* 128:170308. doi: 10.1016/j.peptides.2020.170308

Schwartz, M. W., Woods, S. C., Porte, D. Jr., Seeley, R. J., and Baskin, D. G. (2000). Central nervous system control of food intake. *Nature* 404, 661–671. doi: 10.1038/35007534

Shimizu, H., Oh, I. S., Hashimoto, K., Nakata, M., Yamamoto, S., Yoshida, N., et al. (2009). Peripheral administration of nesfatin-1 reduces food intake in mice: the leptin-independent mechanism. *Endocrinology* 150, 662–671. doi: 10.1210/en.2008-0598

Su, Y., Zhang, J., Tang, Y., Bi, F., and Liu, J. N. (2010). The novel function of nesfatin-1: anti-hyperglycemia. *Biochem. Biophys. Res. Commun.* 391, 1039–1042. doi: 10.1016/j.bbrc.2009.12.014

Timper, K., and Brüning, J. C. (2017). Hypothalamic circuits regulating appetite and energy homeostasis: pathways to obesity. *Dis. Model. Mech.* 10, 679–689. doi: 10.1242/dmm.026609

Toth, Z. E., and Mezey, E. (2007). Simultaneous visualization of multiple antigens with tyramide signal amplification using antibodies from the same species. *J. Histochem. Cytochem.* 55, 545–554. doi: 10.1369/jhc.6A7134.2007

Tóth, Z. E., Zelena, D., Mergl, Z., Kirilly, E., Várnai, P., Mezey, E., et al. (2008). Chronic repeated restraint stress increases prolactin-releasing peptide/tyrosine-hydroxylase ratio with gender-related differences in the rat brain. *J. Neurochem.* 104, 653–666. doi: 10.1111/j.1471-4159.2007.05069.x

Uyama, N., Geerts, A., and Reynaert, H. (2004). Neural connections between the hypothalamus and the liver. *Anat. Rec. A Discov. Mol. Cell. Evol. Biol.* 280, 808–820. doi: 10.1002/ar.a.20086

Vaag, A., and Lund, S. S. (2007). Non-obese patients with type 2 diabetes and prediabetic subjects: distinct phenotypes requiring special diabetes treatment and (or) prevention? *Appl. Physiol. Nutr. Metab.* 32, 912–920. doi: 10.1139/h07-100

Wang, B., Chandrasekera, P. C., and Pippin, J. J. (2014). Leptin- and leptin receptor-deficient rodent models: relevance for human type 2 diabetes. *Curr. Diabetes Rev.* 10, 131–145. doi: 10.2174/1573399810666140508121012

Wei, Y., Li, J., Wang, H., and Wang, G. (2018). NUCB2/nesfatin-1: expression and functions in the regulation of emotion and stress. *Prog. Neuropsychopharmacol. Biol. Psychiatry* 81, 221–227. doi: 10.1016/j.pnpbp.2017.09.024

Wu, D., Yang, M., Chen, Y., Jia, Y., Ma, Z. A., Boden, G., et al. (2014). Hypothalamic nesfatin-1/NUCB2 knockdown augments hepatic gluconeogenesis that is correlated with inhibition of mTOR-STAT3 signaling pathway in rats. *Diabetes* 63, 1234–1247. doi: 10.2337/db13-0899

Yang, M., Zhang, Z., Wang, C., Li, K., Li, S., Boden, G., et al. (2012). Nesfatin-1 action in the brain increases insulin sensitivity through Akt/AMPK/TORC2 pathway in diet-induced insulin resistance. *Diabetes* 61, 1959–1968. doi: 10.2337/db11-1755

Yosten, G. L., and Samson, W. K. (2009). Nesfatin-1 exerts cardiovascular actions in brain: possible interaction with the central melanocortin system. *Am. J. Physiol. Regul. Integr. Comp. Physiol.* 297, R330–R336. doi: 10.1152/ajpregu.90867.2008

Conflict of Interest: The authors declare that the research was conducted in the absence of any commercial or financial relationships that could be construed as a potential conflict of interest.

Publisher's Note: All claims expressed in this article are solely those of the authors and do not necessarily represent those of their affiliated organizations, or those of the publisher, the editors and the reviewers. Any product that may be evaluated in this article, or claim that may be made by its manufacturer, is not guaranteed or endorsed by the publisher.

International Journal of Obesity (2019) 43:917–927
https://doi.org/10.1038/s41366-018-0133-y

ARTICLE

Animal models

Reward-representing D1-type neurons in the medial shell of the accumbens nucleus regulate palatable food intake

Máté Durst[1] · Katalin Könczöl[1] · Tamás Balázsa[1] · Mark D. Eyre[2] · Zsuzsanna E. Tóth[1]

Received: 17 January 2018 / Revised: 6 April 2018 / Accepted: 10 May 2018 / Published online: 15 June 2018

Abstract

Background/objectives Dysfunction in reward-related aspects of feeding, and consequent overeating in humans, is a major contributor to obesity. Intrauterine undernutrition and overnutrition are among the predisposing factors, but the exact mechanism of how overeating develops is still unclear. Consummatory behavior is regulated by the medial shell (mSh) of the accumbens nucleus (Nac) through direct connections with the rostral part of the lateral hypothalamic area (LHA). Our aim was to investigate whether an altered Nac-LHA circuit may underlie hyperphagic behavior.

Subjects/methods Intrauterine protein-restricted (PR) male Wistar rats were used as models for hyperphagia. The experiments were performed using young adult control (normally nourished) and PR animals. Sweet condensed milk (SCM) served as a reward to test consumption and subsequent activation (Fos+) of Nac and LHA neurons. Expression levels of type 1 and 2 dopamine receptors (D1R, D2R) in the Nac, as well as tyrosine hydroxylase (TH) levels in the ventral tegmental area, were determined. The D1R agonist SKF82958 was injected into the mSh-Nac of control rats to test the effect of D1R signaling on SCM intake and neuronal cell activation in the LHA.

Results A group of food reward-representing D1R+ neurons was identified in the mSh-Nac. Activation (Fos+) of these neurons was highly proportional to the consumed palatable food. D1R agonist treatment attenuated SCM intake and diminished the number of SCM-activated cells in the LHA. Hyperphagic PR rats showed increased intake of SCM, reduced D1R expression, and an impaired response to SCM-evoked neuronal activation in the mSh-Nac, accompanied by an elevated number of Fos+ neurons in the LHA compared to controls.

Conclusions Sensitivity of food reward-representing neurons in the mSh-Nac determines the level of satisfaction that governs cessation of consumption, probably through connections with the LHA. D1R signaling is a key element in this function, and is impaired in obesity-prone rats.

Introduction

Feeding reward dysregulation is a basic factor in overeating and consequent obesity [1]. The central process leading to reward dysregulation is still unknown, but both low and high birth weights are implicated as risk factors [2, 3]. Rats prenatally exposed to scarcity regarding overall nutrition, or merely protein restriction, show profound hyperphagia [4, 5] and an altered behavioral response to feeding reward [6, 7]. Reward deficit — reduced reward from eating and continued food intake to reach satisfaction — has been suggested as an underlying factor in both humans and rodents, which was connected to striatal type 2 dopamine receptor (D2R) downregulation and hypofunction [8–10]. However, according to other data, D2R downregulation cannot be a primary factor in hyperphagia, but instead is a consequence of overconsumption, increased body mass index and leptin levels [8, 11, 12].

Palatable food intake is regulated mainly by the accumbens nucleus (Nac) circuits [13]. Most of the neurons in the Nac (95%) are medium spiny neurons (MSNs) primarily

Electronic supplementary material The online version of this article (https://doi.org/10.1038/s41366-018-0133-y) contains supplementary material, which is available to authorized users.

✉ Zsuzsanna E. Tóth
toth.zsuzsanna.emese@med.semmelweis-univ.hu

[1] Laboratory of Neuroendocrinology and In Situ Hybridization, Department of Anatomy, Histology and Embryology, Semmelweis University, Tűzoltó utca 58, Budapest, Hungary

[2] Department of Physiology I, University of Freiburg, Hermann-Herder-Str. 7, Freiburg 79104, Germany

bearing D1Rs and/or D2Rs, and receiving dopaminergic input from the ventral tegmental area (VTA) [14]. Subregions of the Nac are distinguished as the shell and the core [15], which participate in different aspects of feeding reward in rats. Using Fos protein induction it was shown that the actual pleasure (palatability or 'liking') of food consumption is represented within the cells of the rostral dorsomedial portion of the shell (i.e. medial shell (mSh)) [16], while the motivation to eat, or incentive salience ('wanting'), is represented within the mSh, as well as in the entire core [17]. The mSh has been implicated in the intimate control of feeding behavior, as blockade of glutamate receptors exclusively here, but not in the core, elicits pronounced feeding [18]. Stopping feeding, which is crucial to prevent overeating, is also realized via a pathway originating from the mSh [19, 20]. The pathway includes D1R-expressing MSNs that, upon activation, stop ongoing eating in mice [19]. These D1R+ neurons target the rostral part of the lateral hypothalamus (LH) [20, 21], an area known to be engaged in reward-related food intake regulation [13]. The lateral hypothalamic area (LHA) target neurons increase their calcium activity during the eating of palatable food, and are distinct from the mostly more caudally located melanin-concentrating hormone (MCH) and orexin producing neurons [21, 22].

We hypothesized that a low protein diet during fetal development leads to long-term changes in Nac-circuits and affects mechanisms involved in the cessation of eating. To test this, we compared the hedonic food intake of satiated rats with or without prenatal protein restriction. We evaluated the microstructure of reward-related consummatory behavior and analyzed the Fos expression elicited by palatable food in the Nac and the LHA. We found that the activation pattern of D1R+ MSNs in the mSh reflects the reward value of food, and that altered D1R signaling probably plays a decisive role in hyperphagic behavior.

Materials and methods

Animals

Rats (Wistar, Toxi-Coop Toxicological Research Center Zrt, Dunakeszi, Hungary) were housed under standard laboratory conditions (22 ± 1 °C, 12-hour day cycle) and had free access to standard rodent chow and tap water except when otherwise indicated. When anesthesia was needed, a mixture of ketamine (75 mg/bwkg) (Richter Gedeon Nyrt, Budapest, Hungary) and xylasine (15 mg/bwkg) (CP-Pharma, Burgdorf, Germany) was injected intramuscularly. Experiments were performed according to the European Communities Council Directive (86/609/EEC/2 and 2010/63/EU) and were supervised by the Animal Care and Use Committee of the Institute of Experimental Medicine, Hungarian Academy of Sciences, Budapest, Hungary (XIV-I-001/2262-4/2012).

Experimental design and sample sizes are shown in Supplemental Table (ST) 1. Experiments were performed once, except otherwise indicated.

Intrauterine feeding protocol

Timed pregnant female rats were housed individually and kept on a low protein diet (8.8% crude protein, 8.1% crude fat, 5.0% crude fiber, 5.3% crude ash, 69.7% nitrogen-free extracts (Ssniff Spezialdiäten GmbH, Soest, Germany, catalog# E15202-24)) only during pregnancy. Control timed pregnant female rats received standard laboratory chow (19.2% crude protein, 4.1% crude fat, 6.1% crude fiber, 6.9% crude ash, 53.4% nitrogen-free extracts (Altromin Spezialfutter GmbH, Lage, Germany, catalog# 1324)). Energy in the low protein diet was made up with additional carbohydrate and lipid. More details on diets are provided in ST2, and the full compositions can be downloaded from the relevant Company home page (http://www.ssniff.com and https://altromin.com). After delivery, protein-restricted (PR) dams were returned to the standard laboratory chow diet. To standardize nursing conditions all litter sizes were adjusted to eight male pups (no females). Control and intrauterine PR dams nursed control and intrauterine PR pups, respectively. Bodyweight and food intake after weaning were measured weekly for each animal. Experiments were carried out using these male offspring at 14 weeks of age. Experimental groups (control and PR) consisted of subjects of three different litters to avoid any intra-litter effects or bias.

Assessment of palatable food intake

The influence of palatable food was examined by presenting sweetened condensed milk (SCM; Sole-Mizo Zrt, Csorna, Hungary) (diluted 1:2 in tap water) to control and intrauterine PR animals, according to the protocol of Brand et al. [23]. Briefly, this protocol was in three stages. Firstly, the evening prior to the training day, rats in their home cage were presented with a water bottle containing SCM and allowed a few licks in order to familiarize the animals to the taste of SCM. Next morning, at the beginning of the passive phase, when animals were sated after nocturnal food intake, rats were transferred to the experimental room suitable for behavioral recordings. They were placed into a clean "experimental" cage, to familiarize them with the behavioral recording environment for 5 min. SCM was then presented for a further 10 min, and consumption was measured. Finally, the next (experimental) day, rats were assigned into experimental sessions. For every session, one

pair of rats was investigated, selected randomly from different experimental groups. The experimental protocol was the same as the previous training day, but the behavior was also video recorded, and used for analysis. Animals were placed back to their home cages for 90 min, and then anaesthetized and transcardially perfused with 4% paraformaldehyde in 0.1 M phosphate buffered saline. Brains were removed, post-fixed for 1 h in the same fixative, immersed in 20% sucrose solution overnight, and then frozen and stored at −80 °C until processed.

D1R-agonist treatment

Normally nourished animals were handled daily for 3 weeks before experiments. One week before the experiments they were implanted with a chronically indwelling guide cannula (Plastics One Inc, Roanoke, VA) (22 ga) directed 0.5 mm above the right Nac mSh (1.48 mm rostral to bregma, 0.82 mm lateral to midline, 6.47 mm ventral from the skull) [24]. Rats were kept individually after operation. Reward-driven behavior was assessed after recovery, using the same training schedule as described above, except that 10 min before SCM was provided, rats received intra-accumbal drug injections. The different treatment groups received 0.5 or 3 µg of the selective D1 receptor agonist SKF-82958 (Sigma-Aldrich Kft.; Budapest, HU) dissolved in 1 µl of physiological saline, or vehicle alone, through internal cannulas with 0.5 mm extensions beyond the guide cannulas. Cannula placements were evaluated after perfusion fixation on histological brain sections. Only animals with correct cannula positions and uninjured lateral ventricles were included for further analysis.

Microstructure analysis of feeding behavior

Behavioral video recordings were slowed down to 0.25 times normal speed (VLC media player, VideoLAN, Paris, France) during analysis to achieve sufficient resolution in time. Meal duration, mean size and duration of lick clusters, and initial & mean rates of licking were determined for each group. The effective time spent licking during the 10 min experimental period was regarded as meal duration. By definition, continuous segments of licking separated by pauses longer than 500 ms were regarded as lick clusters [25]. The number of lick clusters was determined and used to calculate mean cluster duration (meal duration/cluster number) and cluster size (cluster duration × mean licking rate). Mean licking rates were determined by counting the number of licks during six periods (6 × 10 sec) of continuous licking that were selected equally across the whole drinking process. Initial licking rates were calculated based on data from the first period chosen at the beginning of the drinking process.

Immunohistochemistry

Single Fos, Fos–orexin, and Fos–MCH double immunostainings, as well as D1R immunofluorescence staining, were applied on sections from different experiments (see ST1). Standard immunohistochemical reactions were performed using 50 µm thick, perfused-fixed, free-floating sections as described previously [26], except for the following reactions: (1) for Fos immunostaining prior to in situ hybridization, a modified serum-free protocol was applied using 20 µm-thick sections. Solutions were treated with 0.1% diethylpirocarbonate, and 1000 U/ml heparin was added to inhibit RNases (Sigma), (2) for D1R protein visualization we used 50% ethanol application for 30 min instead of our standard permeabilization with 1% Triton X-100 (Sigma). For more details on antibodies and detection, see ST3.

In situ hybridization

Sections mounted on Superfrost Ultra Plus slides (Thermo Fisher Scientific, Waltham, MA, USA) were hybridized using S35-UTP-labeled riboprobes to detect D1-2R mRNAs in the Nac, and tyrosine hydroxylase (TH) precursor mRNA in the VTA, as described previously [27]. Riboprobes were prepared using D1R (GenBank Acc: NM_012546.3, 981–1393 bps) and D2R (NM_012547.1, 981–1393 bps) cDNA fragments subcloned into Bluescript KSII + vectors as templates. Specificity of cDNAs was verified by sequencing and assessed by BLAST screening (https://blast.ncbi.nlm.nih.gov/Blast.cgi) of the rat genome. The rat tyrosine hydroxylase (TH) intronic cDNA was provided by Harold Gainer (NIH, Bethesda, MD) [28]. After hybridizations, sections were apposed to a BAS-MS imaging plate (Fuji Photo Film Co., Ltd., Kanagawa, Japan, NJ) for 2 (DRs) and 7 (TH) days, and then data were read out by a Fujifilm FLA-8000 Image Analyzer. Sections with D1R and D2R labeling were dipped in Kodak NTB nuclear emulsion (Carestream Health Inc., Rochester, NY) for 5 days according to the manufacturer's instructions and developed using Kodak developer and fixer (Sigma) [29, 30].The sections were stained with Giemsa (Sigma) except those with prior Fos immunohistochemistry.

Quantitative analyses of immunostained sections

Evaluations were performed using microphotographs taken by an Olympus BX60 microscope (objective: UPlan FL 4×/0.13) interfaced with a SPOT Xplorer 17.4 camera (Diagnostic Instruments Inc., Sterling Heights, MI) and with the help of the ImageJ 1.46r (Wayne Rasband NIH, Bethesda, MD) application.

Fos-labeled cells in Nac and in the LHA were counted within regions of interest bilaterally (ROI sizes: 200 µm ×

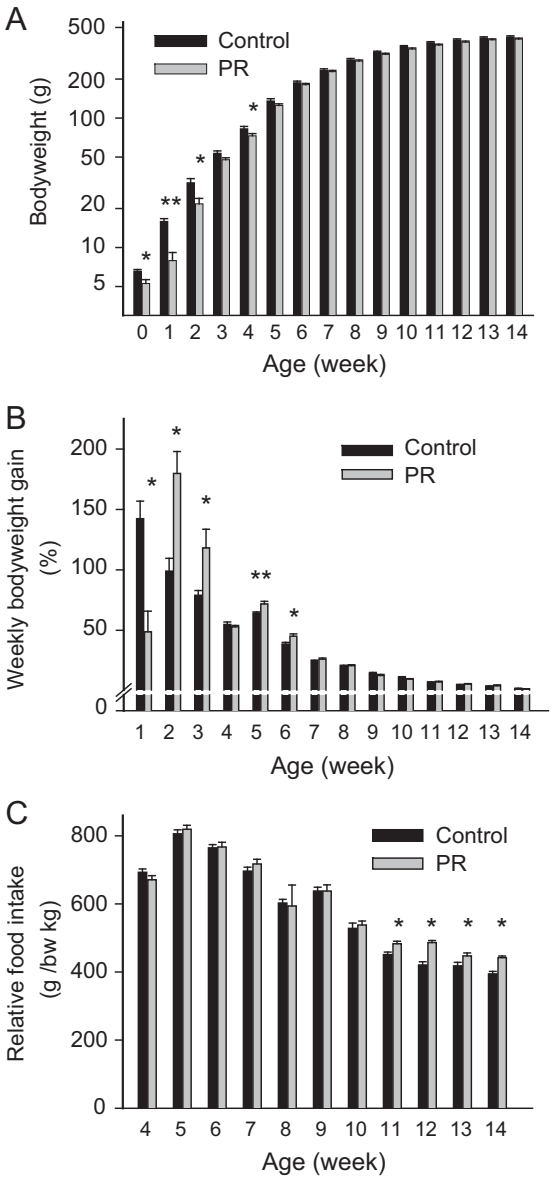

Fig. 1 Bodyweight and food intake during postnatal development. **a** Weekly bodyweight measurements. PR pups were born smaller. The difference between groups diminished by the 6th week. **b** Weekly bodyweight gain relative to the bodyweight measured on the previous week. There was a decrease with age in both groups ($p < 0.001$). PR pups gained poorly during the 1st week. They gained relatively more weight than controls in the next few weeks (catch up growth). **c** Food consumption relative to bodyweight, measured weekly after weaning. PR rats consumed relatively more of chow than controls starting from the 11th week. Data are presented as means ± SEM. $n = 9$-8, $^{**}p < 0.01$, $^{*}p < 0.05$ vs. controls

200 µm and 400 µm × 400 µm for Nac and LHA, respectively). The Nac was evaluated in three sections/animal representing the rostral part of the Nac between [1.7–2.2 mm] rostral to Bregma [24]. The core was evaluated as the sum of two regions (ROI 1 and 2), ROI 3 was superimposed over the mSh (hedonic hot spot [16]), ROI 4 was placed ventrally to the mSh. The LHA was evaluated in five sections/animal representing the area [1.8–2.4 mm] caudal from Bregma [20]. ROI 5 was superimposed lateral to the fornix (referred as "perifornical" region, PF), ROI 6 was overlaid dorsal to the optic tract representing the lateral hypothalamus (LH) (see illustrations in the Results section). The number of cells/animal was used for statistics.

The optical densities of D1R immunostained sections were measured according to Sato et al. [31] in the mSh and core on gray scale unmodified images in three sections/animal using the same ROIs as above. The average/animal data were used for statistics.

Quantification of in situ hybridization data

Radioactive in situ hybridization provides a linear relationship between the signal intensity and the mRNA expression level [32]. D1-2R mRNA expressions were determined from images of autoradiographic emulsion-coated sections, as earlier described [33, 34]. Microphotographs were taken by an Olympus BX51 microscope (objective: UPlan FLN 10×/0.30) attached to a QImaging QCam system (Quantitative Imaging Corporation, Surrey, Canada). Two images were taken/area. The darkfield image was superimposed on the brightfield image. The brightfield images were used to identify cells. Measurements were performed on the darkfield images. The labeled cellular profiles were selected using the threshold tool in the ImageJ software. The area covered by silver grains was measured and expressed as pixels/cell [34, 35]. Expression level of TH precursor mRNA in the VTA was evaluated from the image recorded by the phosphoimager as earlier described [36]. Mean gray values were measured bilaterally with ImageJ, in three sections/animal (D1R) between [1.7–2.2 mm] rostral to Bregma, and in six sections/animal (TH) between [5.0–5.4 mm] caudal from Bregma. In all cases, the average/animal data were compared statistically.

Fos immunoreactivity and D1R-mRNA labeling in the Nac mSh were counted similarly as described above using microphotographs (taken using an Olympus BX60 microscope (objective: UPlan 20×/0.50 Ph1). Percentages of single-labeled and double-labeled cells were calculated.

Statistics

Data analyses were performed by investigators blinded to treatments. Statistical significances were calculated employing Sigmastat 3.5 application (Systat Software, Inc., Chicago, IL). Studies were designed to reach the desired power of 0.8 with alpha = 0.05. For comparing control and PR groups Student's *t*-tests (two-tailed) were used. When treatment (intrauterine conditions) and time interaction was also evaluated, repeated measures ANOVA was used. For evaluating effects of different doses of D1 agonist

Table 1 Palatable food intake and microstructure of consummatory behavior of control and intrauterine protein-restricted (PR) rats

	SCM intake (g)	Meal duration (s)	Initial licking rate (1/s)	Mean licking rate (1/s)	Mean cluster size (licks)	Mean cluster duration (s)
Control	9.5 ± 1.1	342 ± 40	6.3 ± 0.1	6.2 ± 0.1	59.3 ± 5.6	9.6 ± 1.0
PR	14.1 ± 1.2*	441 ± 28	6.2 ± 0.0	6.0 ± 0.1	61.6 ± 7.3	10.2 ± 1.2

Data are presented as means ± SEM, $n = 8$–9 for sweet condensed milk (SCM) intake and $n = 7$–8 for all other parameters

*$p < 0.05$

treatment, a one-way ANOVA test followed by Student–Newman–Keuls post-hoc analysis was applied. Correlations were calculated by the Pearson method. When normality or equal variance tests failed, non-parametric equivalents of the above methods (Mann–Whitney test, Kruskal–Wallis test, Spearman method, respectively) were used. Differences between groups were considered statistically significant when $*p < 0.05$. Results are expressed as means ± SEM values.

Results

Development of intrauterine PR animals

The low protein diet did not influence the duration of pregnancy (control: 22.6 ± 0.2 days vs. PR: 22.3 ± 0.3 days) or the litter size (control: 15.1 ± 0.9 vs. PR: 14.6 ± 0.6 pups). It resulted, however, in a significant reduction in the birthweights of offspring (Fig. 1a, $p < 0.05$). The bodyweight of PR pups was markedly lower compared to controls, especially on the first ($p < 0.01$), but also on the second postnatal week ($p < 0.05$). Subsequently, the PR animals started to catch up controls and the bodyweights were comparable from the 5th week onward. From the 11th week to the time of the experiments (14th week), bodyweights of PR and control peers did not differ significantly (Fig. 1a). The weekly body weight gain decreased with age in both groups ($p < 0.01$) (Fig. 1b). During the 1st postnatal week PR pups fell behind controls in weight gain ($p < 0.05$). They then exhibited a period of accelerated weight gain from the 2nd to the 6th week to catch up controls (2nd, 3rd, 6th weeks $p < 0.05$, 5th week $p < 0.01$). The relative bodyweight gain of groups was similar later on. Food intake of rats did not differ in the first 10 weeks, but from the 11th week PR animals became hyperphagic (Fig. 1c, $p < 0.05$)

Palatable food consumption

In order to study feeding reward, a highly palatable food, sweetened condensed milk solution, was offered to satiated animals. PR subjects consumed more SCM during the training day (6.16 ± 0.9 and 15.11 ± 1.3 g for control and PR groups, respectively; $p < 0.001$), and also on the experimental day ($p < 0.05$) (Table 1). Microstructure analysis of eating behavior showed a slight, non-significant increase in meal duration ($p = 0.071$), and no difference in initial and mean licking rates, mean duration or size of lick clusters compared to controls (Table 1). As lick cluster size and initial licking rate measure hedonic response to palatability ('liking') [25, 37], we concluded that PR rats did not exhibit a heightened hedonic response.

Impact of feeding reward on Fos induction in the Nac and rostral LHA

Neuronal activation elicited by SCM consumption in the Nac was measured by counting the number of Fos+ neurons in the core (associated with 'motivation') (Fig. 2a, ROIs 1. and 2.), in the mSh hot spot (associated both with 'motivation' and 'liking') (Fig. 2a, ROI 3.) and ventral to this area within the shell (no currently known association) (Fig. 2a, ROI 4.) identified according to coordinates given by Pecina and Berridge [16]. The average Fos-count was similar between groups in all of the investigated areas (Fig. 2a, bottom). To see how reward-related consumption is reflected in cell activation in Nac, relationships between the volumes of consumed SCM and the Fos-counts were examined *within* groups. Both controls and PRs produced strong, linear, positive correlations within the mSh ($R_{Control} = 0.741$, $p < 0.05$; $R_{PR} = 0.731$, $p < 0.05$). However, we noticed a right shift toward higher amounts of SCM consumption in PR rats compared to controls (Fig. 2b top). No correlations were found in the control area, in the ventral shell ($R_{Control} = 0.413$, $p = 0.269$; $R_{PR} = -0.040$, $p = 0.925$) (Fig. 2b middle), and Fos-count and SCM intake correlated positively in the core in PR rats only ($R_{Control} = 0.228$, $p = 0.556$; $R_{PR} = 0.828$, $p < 0.05$) (Fig. 2b bottom). Thus, (1) reward valence of food is strictly encoded as a "Fos-print" within the mSh; (2) mSh neurons in PR rats have a heightened activation threshold for palatable food intake; (3) there is a difference between PR and control rats in the reaction for reward-related food consumption in the core.

Neuronal activation in response to SCM intake was also determined in the target area of mSh neurons in the *rostral* part of the LHA. Based on earlier findings, ROI analysis was performed in two regions [20]; lateral to the fornix

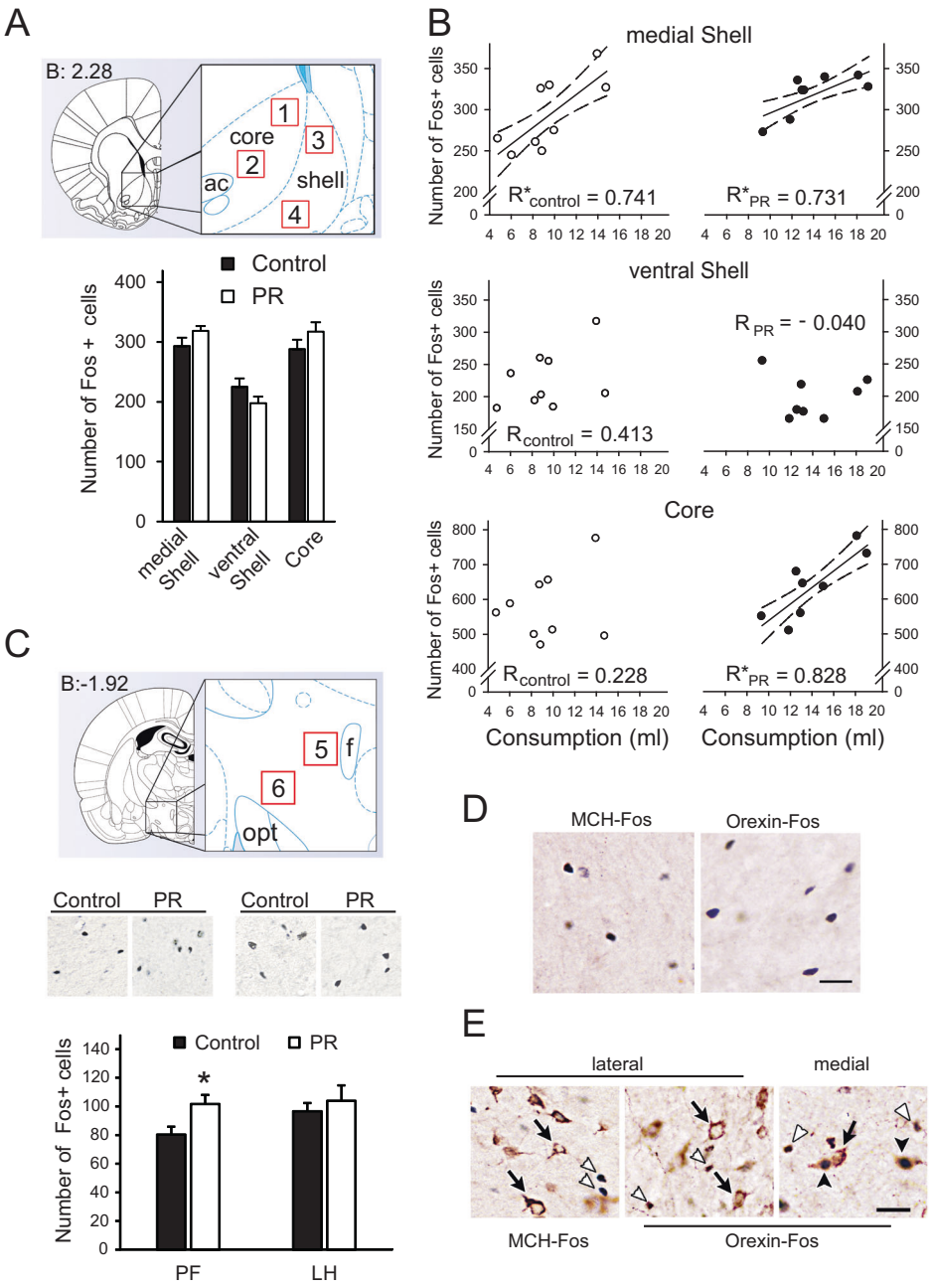

(perifornically, PF) (Fig. 2c top, ROI 5.) and in the lateral hypothalamus (LH) (Fig. 2c top, ROI 6.). PR animals with higher SCM intake exhibited more Fos+ cells than the controls in the PF region (ROI 5, $p < 0.05$) (Fig. 2c, bottom left). The LH area (ROI 6) responded to the challenge similarly in both groups (Fig. 2c, bottom right). MCH-producing and orexin-producing cells were not present at this rostro-caudal level (Fig. 2d). MCH and orexin neurons caudal to the analyzed area were not Fos+ lateral to the fornix, while many orexin cells were Fos+ medial to the fornix (Fig. 2e).

Evaluation of the main components of the dopaminergic transmission to the Nac

Substantially less D1R mRNA was expressed in the neuronal somata in the mSh in PR animals ($p < 0.05$), but expression in the core was similar to controls (Fig. 3a). Unlike the D1R, expression of D2R mRNA was not significantly different between groups (Fig. 3b). Immunohistochemistry showed intense expression of D1Rs in the striatum and the Nac compared to the cortex (Fig. 3c left, top). D1R immunostaining appeared as seemingly

◀ **Fig. 2** Fos activation pattern of accumbal and lateral hypothalamic neurons following intake of highly rewarding food. **a** Top: Brain regions of interest (ROIs) for counting Fos-labeled cell nuclei in the accumbens nucleus. The diagram was adopted from the Atlas of Paxinos and Watson [24] and illustrates a sampling frontal section level of 2.28 mm to Bregma. ROIs (200 µm × 200 µm) were overlaid on microphotographs in the different areas: 1–2, core; 3, medial shell hedonic hot spot; 4, control area in the ventral part of the shell. Bottom: The number of Fos-positive cells per area/animal. No significant difference existed between the experimental groups, $n = 8$-9. **b** Fos activation in the accumbens nucleus in relation to the amount of consumed sweet milk. Strong correlations were found in the medial shell (top) in both control (left, open circle) and PR (right, filled circle) groups and in the core (bottom) in PR rats only. Note that Fos-counts are in the same range in the individual areas, but there is a shift toward higher quantities of consumed milk in PR rats. Solid and dashed lines show the regression lines and the 95% confidence intervals, respectively, see correlation coefficients (R) on the graphs, $*p < 0.05$, $n =$ 8–9. **c** Top: a similar diagram as in A, showing location of ROIs (400 µm × 400 µm) for counting Fos-labeled cell nuclei in the rostral lateral hypothalamic area at a sampling frontal section level of −1.92 mm caudal from Bregma. ROIs were placed: 5, laterally to fornix (PF), 6, on the lateral hypothalamus (LH). Bottom: The number of Fos+ cells per area/animal. A higher Fos-count was detected in the PF area in PR rats, but there was no significant difference in the LH region. Fos+ cell nuclei appear as black dots on the representative pictures (left the PF, right the LH regions, respectively, $n = 7$,$*p < 0.05$ vs. controls. : **d** Palatable food intake-activated neurons in the rostral LHA were non-MCH, non-orexin cells. Double immunostainings from control animals. Fos+ nuclei are seen as dark dots. Scale: 50 µm. **e** Fos induction in the caudal part of the hypothalamus. Many Fos+ cells were seen caudal to the analyzed area (white arrowheads). MCH cells were Fos-negative. Orexin cells lateral to the fornix were also Fos-negative. Many of orexin cells were double-labeled medial to the fornix. Black arrows: Fos-negative MCH or orexin cells, black arrowheads: orexin and Fos double-labeled cells. Control animals. Scale: 50 µm. Data are presented as means ± SEM. ac anterior commissure, f fornix, LH lateral hypothalamic, and PF perifornical regions of the lateral hypothalamic area (LHA), opt optic tract, PR intrauterine protein-restricted

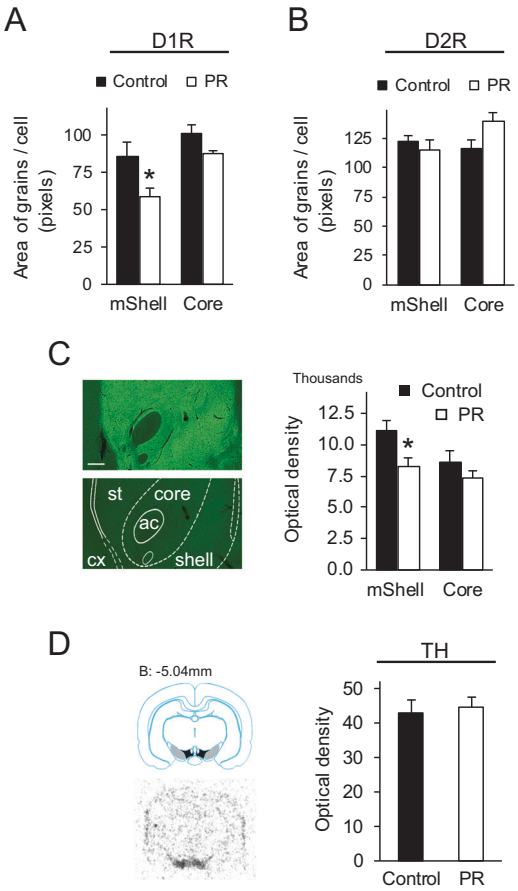

Fig. 3 Expression of key molecules of dopaminergic transmission in non-challenged rats. **a** D1R mRNA expression in the accumbens nucleus decreased significantly in the medial shell in PR rats. **b** D2R mRNA expression did not change significantly. **c** D1R protein expression. There was an intense labeling by immunohistochemistry in the striatum and the accumbens nucleus compared to the cortex (left, top). No signal was detected in sections when the primary antibody was omitted (left, bottom). Scale: 250 µm. Right: Intensity measurements of immunostainings confirmed the reduced D1R protein expression in the medial shell in PR rats. There was no significant difference in the core. **d** Expression of tyrosine hydroxylase precursor mRNA in ventral tegmental area (VTA). Left, top: A diagram adopted from the Atlas of Paxinos and Watson [24] illustrating a sampling frontal section level of 5.04 mm caudal from Bregma. At this level TH is expressed in the VTA (black) and the substantia nigra (gray). Left bottom: Autoradiographic image of a section from the corresponding level, showing intense precursor TH mRNA expession according to the labeled areas above. Only a background is seen in the other parts of the section. Optical density measurements in the VTA showed that TH gene expression was unaffected by prenatal nutritional conditions. Data are expressed as means ± SEM, $n = 6$, $*p < 0.05$ vs. controls. ac anterior commissure, cx cortex, mShell medial shell, PR intrauterine protein-restricted, st striatum, TH tyrosine hydroxylase

homogenous labeling; the cells, dendrites, and axons were indistinguishable, in accordance with earlier data [38]. There was no specific staining in the sections when the primary antibody was omitted from the reactions (Fig. 3c left, bottom). Optical density analysis confirmed the reduced D1R protein expression in the mSh ($p < 0.05$), a difference that was not apparent in the core (Fig. 3c, right).

To assess whether D1R density is related to altered dopamine production, we measured TH expression in the VTA, as this provides the main dopaminergic input to the Nac. Since there is a large pool of both TH mRNA and protein here, we detected TH precursor mRNA expression (Fig. 3d left), which reflects the rate of transcription directly. Based on our data, TH gene expression was unaffected by prenatal feeding conditions (Fig. 3d, right).

Role of mSh D1Rs in reward-driven consumption

As the relationship between the SCM-evoked Fos-activation and D1R expression of mSh neurons remained an open question, in a repeated experiment we challenged normally nourished rats with SCM, and assessed colocalization of D1R mRNA and Fos-immunoreactivity in the mSh. More than two-thirds of the Fos+ neurons (69 ± 4 %) expressed D1R mRNA (Fig. 4a). Again, a strong linear correlation was apparent between the quantity of SCM consumed and the number of Fos+ cells ($R = 0.909$; $p < 0.05$) (Fig. 4b).

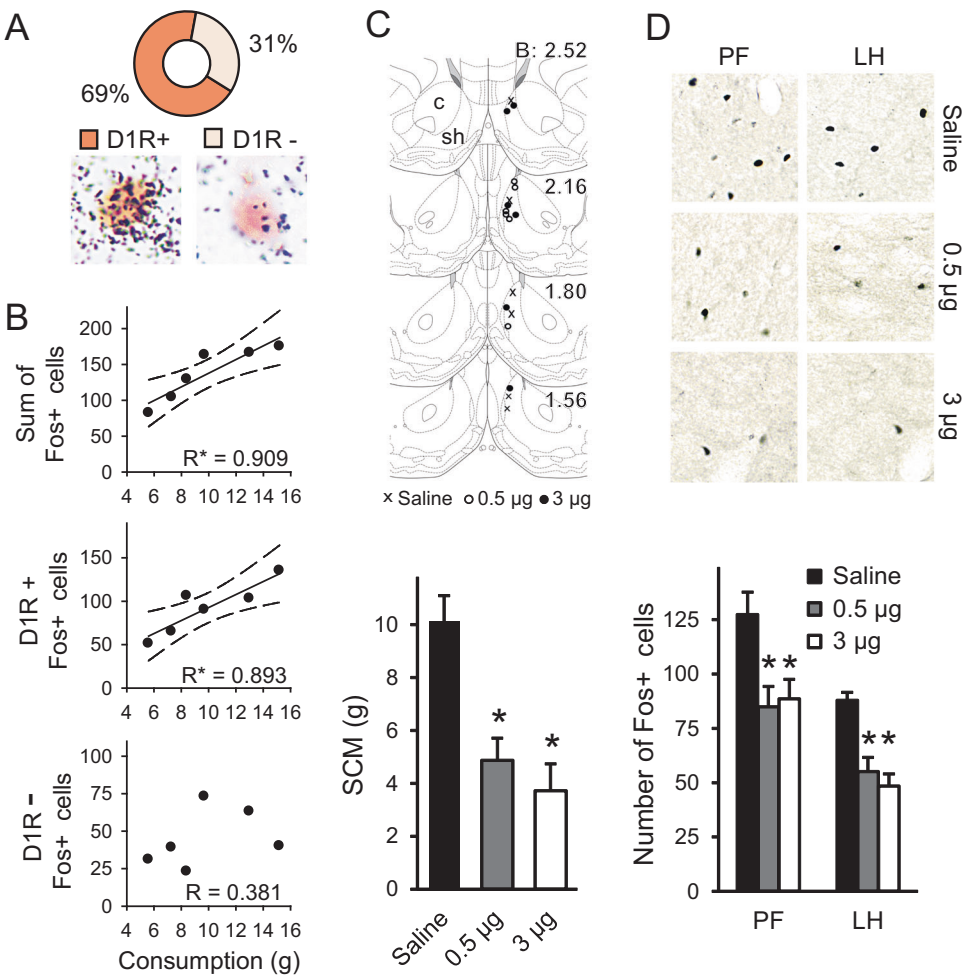

Fig. 4 Evaluation of role of medial shell D1R signaling in reward–related food intake. **a** Sweet milk intake elicited neuronal activation mostly in D1R+ and less in D1R− cells in the medial shell. The representative pictures show Fos-immunoreactive cells (brown nuclei) with positive (left, dense silver grain accumulation) and negative (right, few scattered grains at background level) D1R mRNA labeling. **b** Fos activation in the accumbens nucleus in relation to the amount of consumed sweet milk. As before (Fig. 2b), a strong correlation was established between the consumed quantity and the number of Fos+ neurons. Separate analysis of D1R-positive and D1R-negative Fos cells verified that only D1R-bearing neurons code reward-related information. Solid and dashed lines show linear regressions and 95% confidence intervals, respectively, see correlation coefficients on the graphs, $*p < 0.05$, $n = 6$. **c** Influence of local stimulation of medial shell neurons with D1 agonist SKF-82958 on SCM intake and neuronal activation in the LHA. Top: Illustration of microinjection sites for different doses of SKF-82958. The diagrams were adopted from the Atlas of Paxinos and Watson [24] and illustrate frontal section levels rostral to Bregma in mm as indicated. Bottom: SCM consumption was attenuated markedly by the treatment independently from doses applied. **d** The number of Fos+ cells in the lateral hypothalamic area after SCM intake. The different doses reduced cell activation in a similar manner in both investigated areas. Top: Fos+ cell nuclei appear as black dots on the representative pictures. Bottom: Results of the quantitative analyses, $n = 6$,$*p < 0.05$ vs. saline. Data are presented as means ± SEM. c core, sh shell, LH lateral hypothalamic, PF perifornical regions of the lateral hypothalamic area

However, when the D1R-positive and negative Fos populations were analyzed separately, it became clear that only the D1R-expressing neurons reflect reward-related food intake proportionally to consumed SCM quantity ($R_{D1Rpos} = 0.893$; $p < 0.05$ and $R_{D1Rneg} = 0.381$; $p = 0.456$) (Fig. 4b).

To address the function of D1Rs in feeding reward, a selective D1R agonist, SKF-82958, was infused into the right mSh of normally nourished rats (Fig. 4c, top), just before palatable food intake. The doses applied (0.5 and 3 µg) attenuated greatly the amount of consumed SCM ($p < 0.01$) (Fig. 4c, bottom) and duration of the meal ($p < 0.05$) (Table 2), without significant differences between the doses. In agreement with the reduced consumption, stimulation of mSh D1Rs also led to a decreased number of SCM-evoked Fos+ neurons in the LHA. The two doses acted similarly, and the response was obvious in both measured regions ($p < 0.05$ for PF and, $p < 0.001$ for LH) (Fig. 4d). However, the treatments did not influence liking-associated reactions during consumption, such as initial and mean licking rates, mean cluster size or duration (Table 2).

Table 2 Effect of D1R agonist (SKF-82958) infusion into the right medial shell on the microstructure of consummatory behavior

	Meal duration (s)	Initial licking rate (1/s)	Mean licking rate (1/s)	Mean cluster size (licks)	Mean cluster duration (s)
Saline	402 ± 29	6.6 ± 0.1	6.5 ± 0.1	68.3 ± 5.9	10.5 ± 0.8
0.5 µg SKF-82958	232* ± 42	7.0 ± 0.3	6.6 ± 0.2	59.9 ± 9.5	9.2 ± 1.4
3 µg SKF-82958	181* ± 50	7.3 ± 0.1	6.9 ± 0.1	52.4 ± 7.9	7.5 ± 1.0

Data are presented as means ± SEM, $n = 6$, $^*p < 0.05$ vs. saline

Discussion

The role of the Nac-LHA circuit has recently been emphasized in cessation of the eating behavior, which is crucial to prevent overeating [13, 20, 39]. Perturbation of function may cause abnormal eating behavior by an unknown mechanism.

We investigated this circuit in normal, as well as in PR rats, as it was shown earlier that prenatal protein or general food restriction leads to hyperphagia and an altered response to food reward [4–7]. The PR feeding model we used here is a good representation of the human situation for generating a late onset obese phenotype with metabolic syndrome [40], although development of the condition greatly depends on the postnatal nutritional supply [41, 42]. Generally, late catch-up growth and high caloric food exacerbate the manifestation of obesity [4, 41], while the lack of these factors delays it [42, 43]. Our subjects were young adults fed with standard rat chow from weaning. Catch-up growth started from the 2nd week, as the pups with intrauterine retardation become stronger, but definitive hyperphagia was observed only from the 11th week. We chose 14-week-old rats for the experiments because by that time a slight and constant hyperphagia has developed and the bodyweight of the animals was in the normal range. The intrauterine protein restriction during gestation only has been reported to produce rats with a normal lipid profile, glucose & insulin concentrations compared to those of controls up to the age of 9 months [41, 43]. The weights of fat depots are also comparable to controls in these young adults [44, 45]. This indicates that metabolic regulation has the capacity to keep the parameters in balance at young ages, and thus the alterations we found precede the metabolic changes, and do not happen along with them.

When we evaluated the attitude for food reward, PR rats licked significantly more SCM solution, even during the training period. PR rats in an operant conditioning task produced higher response rates compared to controls [6], suggesting an increased motivation. Since 'liking' and motivation together determine consumption, we assessed "liking" reactions [25, 46]. We failed to detect elevated "liking" reactions in PR rats. Thus, the increased motivational aspect of reward is probably the only reason behind the higher consumption.

Sweet taste represents a high reward valence and triggers a robust neuronal activation in the Nac [47]. Based on neuronal activation-induced Fos expression, we identified a reward-reflecting D1R-bearing neuronal population in the mSh both in control and PR rats. Quite remarkably, activation of these neurons is proportional to the quantity of SCM consumed. The amount of activated cells may depend on the amount of dopamine released, which may happen, as for example dopamine release occurs proportionally to the concentration of sucrose provided to rats [48, 49]. Higher SCM consumption, however, did not evoke a higher number of Fos+ cells in PRs, as it would be expected if intensified responsiveness for feeding reward was assumed. Instead, mSh reward-reflecting neurons displayed reduced sensitivity for reward. Additionally, D1R deficiency appeared in the mSh of PRs, suggesting that a shortfall of D1R signaling may be responsible for these findings. Since there was no sign of elevated dopamine synthesis in the VTA, D1R downregulation did not occur secondarily in response to augmented dopamine release. According to the revised reward deficiency hypothesis for overeating, dopamine deficiency is a primary factor in driving reward-seeking behavior [50], and both D1Rs and D2Rs in the Nac endorse addiction-related behaviors [51]. D2R expression was unaffected in PRs, as we expected, considering that PR rats were lean, and that the generation of striatal D2R deficiency is a leptin-dependent process [8, 9, 12]. On the other hand, D1R expression is independent from leptin [12] and negatively regulated by the satiety signal, ghrelin, a hormone potent in food reward reinforcement [52]. Elevated plasma ghrelin levels have been found perinatally in different intrauterine undernourished rat models [53, 54] and in newborn infants with intrauterine growth retardation [55].

D1R+ neurons in the mSh control feeding behavior. D1R stimulation inhibits GABAergic neurons in the rostral LHA through a direct projection, resulting in the cessation of feeding [20]. By using local D1R agonist injection into control rats, we showed that D1R stimulation enhances the attainment of reward satisfaction, and also reduces hedonic food consumption. There is an orexigenic GABAergic cell population in the rostral LHA that is immunonegative for both MCH and orexin, the stimulation of which enhances

both appetitive and consummatory behaviors [21, 22]. These are probably the targets of the mSh D1R+ cells, as in our experiments D1R stimulation suppressed the SCM-evoked activation of the rostral LHA non-MCH, non-orexin neurons in both measured regions. Conversely, in D1R-deficient PR animals, the control of LHA orexigenic neurons was impaired; they had an elevated number of Fos+ cells in the LHA, and consumed more SCM than their normally nourished peers. We observed a difference in reaction between the measured LHA regions, suggesting a difference in sensitivity between the lateral and perifornical populations, which confirms that LHA reward-responsive cells are heterogenous [22]. Interestingly, SCM drinking induced Fos in the orexin cells medial to the fornix. These cells probably reacted to dopamine released from VTA during SCM drinking. Medial orexin cells lack D1-2Rs, and are transsynaptically regulated by dopamine [56]. Since they are not innervated by the Nac, they were not in focus regarding the present study. However, the role of these cells was revealed in dopamine agonist-elicited arousal [56].

In summary, we propose that dopamine released upon SCM drinking proportionally builds up a stop signal in D1R-bearing mSh neurons that finally culminates as reward is satieted, and leads to the termination of food intake through the inhibition of LHA cells. A D1R deficiency induces an increased threshold of reward-reflecting neurons, shifting the level of termination. Future directions would include clarifying how exactly phenotypical changes occur, and particularly whether accumbal D1R deficiency could be connected to the development of striatal D2R down-regulation later on. A more challenging question is how prenatal programming could be reversed in order to maintain a healthy reward system.

Acknowledgements We thank Krisztina J. Kovács (Institute of Experimental Medicine, Budapest, Hungary) for helpful comments on the manuscript; Judit Kerti and Szilvia Deák for the excellent technical assistance. This work was supported by NKFI K 115422 (ZET); the EFOP-3.6.3-VEKOP-16-2017-00009 and the Excellence Program (Semmelweis University).

Conflict of interest The authors declare that they have no conflict of interest.

References

1. Stice E, Spoor S, Bohon C, Veldhuizen MG, Small DM. Relation of reward from food intake and anticipated food intake to obesity: a functional magnetic resonance imaging study. J Abnorm Psychol. 2008;117:924–35.
2. Perala MM, Mannisto S, Kaartinen NE, Kajantie E, Osmond C, Barker DJP, et al. Body size at birth is associated with food and nutrient intake in adulthood. PLoS ONE. 2012;7:6.
3. Gonzalez-Bulnes A, Ovilo C. Genetic basis, nutritional challenges and adaptive responses in the prenatal origin of obesity and type-2 diabetes. Curr Diabetes Rev. 2012;8:144–54.
4. Vickers MH, Breier BH, Cutfield WS, Hofman PL, Gluckman PD. Fetal origins of hyperphagia, obesity, and hypertension and postnatal amplification by hypercaloric nutrition. Am J Physiol Endocrinol Metab. 2000;279:E83–7.
5. Desai M, Gayle D, Babu J, Ross MG. Programmed obesity in intrauterine growth-restricted newborns: modulation by newborn nutrition. Am J Physiol Regul Integr Comp Physiol. 2005;288:R91–6.
6. Tonkiss J, Shukitt-Hale B, Formica RN, Rocco FJ, Galler JR. Prenatal protein malnutrition alters response to reward in adult rats. Physiol Behav. 1990;48:675–80.
7. Laureano DP, Dalle Molle R, Alves MB, Luft C, Desai M, Ross MG, et al. Intrauterine growth restriction modifies the hedonic response to sweet taste in newborn pups—role of the accumbal mu-opioid receptors. Neuroscience. 2016;322:500–8.
8. Wang GJ, Volkow ND, Logan J, Pappas NR, Wong CT, Zhu W, et al. Brain dopamine and obesity. Lancet (London, England). 2001;357:354–7.
9. Dalle Molle R, Laureano DP, Alves MB, Reis TM, Desai M, Ross MG, et al. Intrauterine growth restriction increases the preference for palatable foods and affects sensitivity to food rewards in male and female adult rats. Brain Res. 2015;1618:41–9.
10. Stice E, Spoor S, Bohon C, Small DM. Relation between obesity and blunted striatal response to food is moderated by TaqIA A1 allele. Science. 2008;322:449–52.
11. Johnson PM, Kenny PJ. Dopamine D2 receptors in addiction-like reward dysfunction and compulsive eating in obese rats. Nat Neurosci. 2010;13:635–41.
12. Billesa SK, Simonds SE, Cowley MA. Leptin reduces food intake via a dopamine D2 receptor-dependent mechanism. Mol Metab. 2012;1:86–93.
13. Saper CB, Chou TC, Elmquist JK. The need to feed: homeostatic and hedonic control of eating. Neuron. 2002;36:199–211.
14. Yager LM, Garcia AF, Wunsch AM, Ferguson SM. The ins and outs of the striatum: role in drug addiction. Neuroscience. 2015;301:529–41.
15. Zaborszky L, Alheid GF, Beinfeld MC, Eiden LE, Heimer L, Palkovits M. Cholecystokinin innervation of the ventral striatum: a morphological and radioimmunological study. Neuroscience. 1985;14:427–53.
16. Pecina S, Berridge KC. Hedonic hot spot in nucleus accumbens shell: where do mu-opioids cause increased hedonic impact of sweetness? J Neurosci. 2005;25:11777–86.
17. Pecina S, Berridge KC. Dopamine or opioid stimulation of nucleus accumbens similarly amplify cue-triggered 'wanting' for reward: entire core and medial shell mapped as substrates for PIT enhancement. Eur J Neurosci. 2013;37:1529–40.
18. Maldonado-Irizarry CS, Swanson CJ, Kelley AE. Glutamate receptors in the nucleus accumbens shell control feeding behavior via the lateral hypothalamus. J Neurosci. 1995;15:6779–88.
19. Prado L, Luis-Islas J, Sandoval OI, Puron L, Gil MM, Luna A, et al. Activation of glutamatergic fibers in the anterior NAc shell modulates reward activity in the aNAcSh, the lateral

hypothalamus, and medial prefrontal cortex and transiently stops feeding. J Neurosci. 2016;36:12511–29.
20. O'Connor EC, Kremer Y, Lefort S, Harada M, Pascoli V, Rohner C, et al. Accumbal D1R neurons projecting to lateral hypothalamus authorize feeding. Neuron. 2015;88:553–64.
21. Sano H, Yokoi M. Striatal medium spiny neurons terminate in a distinct region in the lateral hypothalamic area and do not directly innervate orexin/hypocretin- or melanin-concentrating hormone-containing neurons. J Neurosci. 2007;27:6948–55.
22. Jennings JH, Ung RL, Resendez SL, Stamatakis AM, Taylor JG, Huang J, et al. Visualizing hypothalamic network dynamics for appetitive and consummatory behaviors. Cell. 2015;160:516–27.
23. Brand T, Spanagel R, Schneider M. Decreased reward sensitivity in rats from the Fischer344 strain compared to Wistar rats is paralleled by differences in endocannabinoid signaling. PLoS ONE. 2012;7:e31169.
24. Paxinos G, Watson C. The rat brain in stereotaxic coordinates. 6th ed. Elsevier; 2007.
25. Davis JD, Smith GP. Analysis of the microstructure of the rhythmic tongue movements of rats ingesting maltose and sucrose solutions. Behav Neurosci. 1992;106:217–28.
26. Konczol K, Pinter O, Ferenczi S, Varga J, Kovacs K, Palkovits M, et al. Nesfatin-1 exerts long-term effect on food intake and body temperature. Int J Obes (London). 2012;36:1514–21.
27. Konczol K, Bodnar I, Zelena D, Pinter O, Papp RS, Palkovits M, et al. Nesfatin-1/NUCB2 may participate in the activation of the hypothalamic-pituitary-adrenal axis in rats. Neurochem Int. 2010;57:189–97.
28. Rusnak M, Gainer H. Differential effects of forskolin on tyrosine hydroxylase gene transcription in identified brainstem catecholaminergic neuronal subtypes in organotypic culture. Eur J Neurosci. 2005;21:889–98.
29. Toth ZE, Heinzlmann A, Hashimoto H, Koves K. Distribution of secretin receptors in the rat central nervous system: an in situ hybridization study. J Mol Neurosci. 2013;50:172–8.
30. Rusnak M, Toth ZE, House SB, Gainer H. Depolarization and neurotransmitter regulation of vasopressin gene expression in the rat suprachiasmatic nucleus in vitro. J Neurosci. 2007;27:141–51.
31. Sato K, Sumi-Ichinose C, Kaji R, Ikemoto K, Nomura T, Nagatsu I, et al. Differential involvement of striosome and matrix dopamine systems in a transgenic model of dopa-responsive dystonia. Proc Natl Acad Sci USA. 2008;105:12551–6.
32. Chen CC, Wada K, Jarvis ED. Radioactive in situ hybridization for detecting diverse gene expression patterns in tissue. J Visual Exp 2012;62:3764.
33. Toth ZE, Zelena D, Mergl Z, Kirilly E, Varnai P, Mezey E, et al. Chronic repeated restraint stress increases prolactin-releasing peptide/tyrosine-hydroxylase ratio with gender-related differences in the rat brain. J Neurochem. 2008;104:653–66.
34. Lanoue AC, Blatt GJ, Soghomonian JJ. Decreased parvalbumin mRNA expression in dorsolateral prefrontal cortex in Parkinson's disease. Brain Res. 2013;1531:37–47.
35. Wittmann G, Mohacsik P, Balkhi MY, Gereben B, Lechan RM. Endotoxin-induced inflammation down-regulates L-type amino acid transporter 1 (LAT1) expression at the blood-brain barrier of male rats and mice. Fluids Barriers CNS. 2015;12:21.
36. Vas S, Adori C, Konczol K, Katai Z, Pap D, Papp RS, et al. Nesfatin-1/NUCB2 as a potential new element of sleep regulation in rats. PLoS ONE. 2013;8:10.
37. Smith GP. John Davis and the meanings of licking. Appetite. 2001;36:84–92.
38. Levey AI, Hersch SM, Rye DB, Sunahara RK, Niznik HB, Kitt CA, et al. Localization of D1 and D2 dopamine receptors in brain with subtype-specific antibodies. Proc Natl Acad Sci USA. 1993;90:8861–5.
39. Ferrario CR, Labouebe G, Liu S, Nieh EH, Routh VH, Xu SJ, et al. Homeostasis meets motivation in the battle to control food intake. J Neurosci. 2016;36:11469–81.
40. Ozanne SE, Jensen CB, Tingey KJ, Storgaard H, Madsbad S, Vaag AA. Low birthweight is associated with specific changes in muscle insulin-signalling protein expression. Diabetologia. 2005;48:547–52.
41. Coupe B, Grit I, Darmaun D, Parnet P. The timing of "catch-up growth" affects metabolism and appetite regulation in male rats born with intrauterine growth restriction. Am J Physiol Regul Integr Comp Physiol. 2009;297:R813–24.
42. Lim JS, Lee JA, Hwang JS, Shin CH, Yang SW. Non-catch-up growth in intrauterine growth-retarded rats showed glucose intolerance and increased expression of PDX-1 mRNA. Pediatr Int. 2011;53:181–6.
43. Erhuma A, Salter AM, Sculley DV, Langley-Evans SC, Bennett AJ. Prenatal exposure to a low-protein diet programs disordered regulation of lipid metabolism in the aging rat. Am J Physiol Endocrinol Metab. 2007;292:E1702–14.
44. Bellinger L, Sculley DV, Langley-Evans SC. Exposure to undernutrition in fetal life determines fat distribution, locomotor activity and food intake in ageing rats. Int J Obes (London). 2006;30:729–38.
45. Bieswal F, Ahn MT, Reusens B, Holvoet P, Raes M, Rees WD, et al. The importance of catch-up growth after early malnutrition for the programming of obesity in male rat. Obesity (Silver Spring, MD). 2006;14:1330–43.
46. Dwyer DM. Licking and liking: The assessment of hedonic responses in rodents. Q J Exp Psychol. 2012;65:371–94.
47. Hajnal A, Norgren R, Kovacs P. Parabrachial coding of sapid sucrose: relevance to reward and obesity. In: Finger TE, (ed). International symposium on olfaction and taste. 1170. Malden: Wiley-Blackwell; 2009. p. 347–64.
48. Hajnal A, Smith GP, Norgren R. Oral sucrose stimulation increases accumbens dopamine in the rat. Am J Physiol Regul Integr Comp Physiol. 2004;286:R31–7.
49. Duong A, Weingarten HP. Dopamine antagonists act on central, but not peripheral, receptors to inhibit sham and real feeding. Physiol Behav. 1993;54:449–54.
50. Blum K, Gardner E, Oscar-Berman M, Gold M. "Liking" and "Wanting" linked to reward deficiency syndrome (RDS): hypothesizing differential responsivity in brain reward circuitry. Curr Pharm Des. 2012;18:113–8.
51. Schmidt HD, Pierce RC. Cooperative activation of D1-like and D2-like dopamine receptors in the nucleus accumbens shell is required for the reinstatement of cocaine-seeking bahavior in the rat. Neuroscience. 2006;142:451–61.
52. Skibicka KP, Hansson C, Egecioglu E, Dickson SL. Role of ghrelin in food reward: impact of ghrelin on sucrose self-administration and mesolimbic dopamine and acetylcholine receptor gene expression. Addict Biol. 2012;17:95–107.
53. Wang X, Liang L, Du L. The effects of intrauterine undernutrition on pancreas ghrelin and insulin expression in neonate rats. J Endocrinol. 2007;194:121–9.
54. Kyriakakou M, Malamitsi-Puchner A, Mastorakos G, Boutsikou T, Hassiakos D, Papassotiriou I, et al. The role of IGF-1 and ghrelin in the compensation of intrauterine growth restriction. Reprod Sci. 2009;16:1193–200.
55. Chiesa C, Osborn JF, Haass C, Natale F, Spinelli M, Scapillati E, et al. Ghrelin, leptin, IGF-1, IGFBP-3, and insulin concentrations at birth: is there a relationship with fetal growth and neonatal anthropometry? Clin Chem. 2008;54:550–8.
56. Bubser M, Fadel JR, Jackson LL, Meador-Woodruff JH, Jing D, Deutch AY. Dopaminergic regulation of orexin neurons. Eur J Neurosci. 2005;21:2993–3001.

Neurochemistry International 57 (2010) 189–197

Contents lists available at ScienceDirect

Neurochemistry International

journal homepage: www.elsevier.com/locate/neuint

Nesfatin-1/NUCB2 may participate in the activation of the hypothalamic–pituitary–adrenal axis in rats

Katalin Könczöl [a], Ibolya Bodnár [a,d], Dóra Zelena [b], Ottó Pintér [b], Rege Sugárka Papp [a], Miklós Palkovits [a], György M. Nagy [a,d], Zsuzsanna E. Tóth [a,c,*]

[a] Neuromorphological and Neuroendocrine Research Laboratory, Semmelweis University and the Hungarian Academy of Sciences, Budapest, Hungary
[b] Laboratory of Behavioural and Stress Studies, Institute of Experimental Medicine, Hungarian Academy of Sciences, Budapest, Hungary
[c] Department of Anatomy, Histology and Embryology, Semmelweis University, Budapest, Hungary
[d] Department of Human Morphology and Developmental Biology, Semmelweis University, Budapest, Hungary

ARTICLE INFO

Article history:
Received 29 March 2010
Received in revised form 21 April 2010
Accepted 22 April 2010
Available online 6 May 2010

Keywords:
ACTH
Adrenalectomy
Corticosterone
Fos
In situ hybridzation
Restraint

ABSTRACT

Nesfatin-1 is an anorexigenic peptide originating from nucleobinding-2 (NUCB2) protein. Nesfatin-1/NUCB2-immunoreactive neurons are present in the hypothalamic paraventricular nucleus, the center of the stress-axis, and in the medullary A1 and A2 catecholamine cell groups. The A1 and A2 cell groups mediate viscerosensory stress information toward the hypothalamic paraventricular nucleus. They contain noradrenaline, but subsets of these neurons also express prolactin-releasing peptide acting synergistically with noradrenaline in the activation of the hypothalamic paraventricular nucleus during stress. We investigated the possible role of nesfatin-1/NUCB2 in the stress response. Intracerebroventricular administration of nesfatin-1 elevated both plasma adrenocorticotropin and corticosterone levels, while *in vitro* stimulation of the hypophysis was ineffective. Single, long-duration restraint stress activated (Fos positivity) many of the nesfatin-1/NUCB2-immunoreactive neurons in the parvocellular part of the hypothalamic paraventricular nucleus, evoked nesfatin-1/NUCB2 mRNA expression in the parvocellular part of the paraventricular nucleus and in the A1, but not in the A2 cell group. Nesfatin-1/NUCB2 was shown to co-localize in a high percentage of prolactin-releasing peptide producing neurons, in both medullary catecholamine cell groups further supporting its involvement in the stress response. Finally, bilateral adrenalectomy evoked an increasing nesfatin-1/NUCB2 mRNA expression, indicating that it is under the negative feedback of adrenal steroids. These data provide the first evidence for possible participation of nesfatin-1/NUCB2 in the stress-axis regulation, both at the level of the brainstem and in the hypothalamus.

1. Introduction

Nesfatin-1 is a newly discovered anorexigenic peptide originating from precursor protein called nucleobinding-2 (NUCB2) (Oh et al., 2006). Its wide expression in the brain however, indicates implications in additional physiological functions (Foo et al., 2008). Nesfatin-1/NUCB2 is co-expressed with various neuropeptides in the brain, such as vasopressin, oxytocin in the magnocellular part of the hypothalamic paraventricular (PVN) and supraoptic nuclei, corticotropin-releasing hormone (CRH) in the parvocellular part of the PVN, and tyrosine-hydroxilase (TH; rate limiting enzyme of the catecholamine synthesis) in the arcuate nucleus and in the medullary A2 catecholamine cell group [cells are dispersed in the nucleus of the solitary tract (NTS) and dorsal motor nucleus of vagus (DMX) complex] (Brailoiu et al., 2007; Foo et al., 2008; Fort et al., 2008). Goebel et al. (2009a) identified nesfatin-1/NUCB2-like cells also in the caudal and rostral ventrolateral medulla, where the A1/C1 catecholamine cell groups are localized, but the catecholamine character of these cells were not documented. The A1 and A2 catecholamine cell groups are known to receive peripheral stress signals and relay them to the PVN, where through CRH/vasopressin-containing parvocellular PVN neurons activate the hypothalamic-pituitary–adrenal (HPA) axis, resulting in adrenocorticotropin (ACTH) release from the anterior pituitary and

Abbreviations: ACTH, adrenocorticotropin; ADX, adrenalectomy; CRH, corticotropin-releasing hormone; DMX, dorsal motor nucleus of the vagus nerve; HPA axis, hypothalamic–pituitary–adrenal axis; icv, intracerebroventricular; IHC, immunohistochemistry; ISH, *in situ* hybridization; NTS, nucleus of the solitary tract; NUCB2, nucleobinding-2 protein; PBS, 0.1 M phosphate buffered saline pH 7.4; PrRP, prolactin-releasing peptide; PVN, hypothalamic paraventricular nucleus; RT, room temperature; TH, tyrosine-hydroxilase.

* Corresponding author at: Neuromorphological and Neuroendocrine Research Laboratory, Department of Anatomy, Histology and Embryology, Semmelweis University and the Hungarian Academy of Sciences, 1094 Tűzoltó utca 58, Budapest, Hungary. Tel.: +361 215 6920x3686; fax: +361 215 1612.
E-mail address: tothzs@ana.sote.hu (Z.E. Tóth).

0197-0186/$ – see front matter © 2010 Elsevier Ltd. All rights reserved.
doi:10.1016/j.neuint.2010.04.012

stimulation of corticosterone secretion of the adrenal gland (Pacak et al., 1993; Petrov et al., 1993). As part of the regulation, corticosterone exerts a negative feedback on parvocellular PVN neurons, therefore CRH and vasopressin mRNA expression increases after adrenalectomy (ADX) (Aguilera, 1994; Sawchenko and Swanson, 1982; Young et al., 1986). The main transmitter from the medulla to the PVN is noradrenaline (measured by TH), but prolactin-releasing peptide (PrRP) co-expressed in a high percentage of A1 and A2 neurons is also able to activate CRH/vasopressin neurons in the PVN and to elevate ACTH and corticosterone levels (Maruyama et al., 2001; Sun et al., 2005). The presence of nesfatin-1/NUCB2 in the A2 catecholamine cell group and in the ventrolateral medulla, as well as in the CRH-positive parvocellular PVN neurons suggests that nesfatin-1/NUCB2 may also play a role in stress response. Actually, nesfatin-1/NUCB2 mRNA expression elevates after acute restraint stress in the Edinger–Wesphal nucleus (Okere et al., 2010). Restraint (30 min) and abdominal surgery-induced postoperative gastric ileus induce Fos expression in nesfatin-1/NUCB2-positive neurons of the supraoptic nucleus, the PVN, the locus ceruleus, the NTS and the ventrolateral medulla (Goebel et al., 2009b; Stengel et al., 2010). Since the stress response suppresses "unnecessary" bodily functions (digestion, reproduction etc.), it is very important for survival. The anorexigenic effect of repeated acute restraint is a leptin-independent process, like the effect of nesfatin-1/NUCB2 (Harris et al., 2002; Oh et al., 2006). It has already been shown, that restraint stress activates nesfatin-1/NUCB2-positive neurons in the PVN, the NTS and in the ventrolateral medulla (Goebel et al., 2009b). Additionally, nesfatin-1 induces stress-related behavior, like anxiety and fear (Merali et al., 2008). However, there is no direct evidence yet for the participation of nesfatin-1/NUCB2 in the activation of the HPA axis. Therefore, we administered nesfatin-1 peptide intracerebro-ventricularly (icv) and determined its effect on plasma ACTH and corticosterone levels *in vivo,* and on ACTH release from pituitary cell cultures *in vitro*. We performed a single, long-duration restraint stress on rats and examined nesfatin-1/NUCB2 mRNA expression by quantitative *in situ* hybridization (ISH), as well as activation of nesfatin-1/NUCB2 positive cells by Fos immunohistochemistry in the hypothalamus and the medulla. We also co-localized nesfatin-1/NUCB2 in the A1 and A2 cell groups with PrRP and TH. Using bilateral adrenalectomy, we investigated if nesfatin-1/NUCB2 mRNA expression in the PVN is sensitive to steroid feedback.

2. Experimental procedures

2.1. Animals

Male Wistar rats (Charles-Rivers, Gödöllő, Hungary) weighing 250–300 g were kept under standard laboratory conditions. Experiments were performed according to the regulations set up by the Hungarian Council for Animal Care, and were supervised by the Institutional Animal Care and Use Committee of the Institute of Experimental Medicine, Hungarian Academy of Sciences (animal protocol number: 1894/003/2004). All efforts were made to minimize animal suffering, to reduce the number of animals used, and to utilize alternatives to *in vivo* techniques, if available.

2.2. Experiment 1. Effect of exogenously administered nesfatin-1 on ACTH and corticosterone release in vivo

Animals ($n = 5$/group) were handled daily for 2 weeks before surgery to minimize stress caused by the experimental procedure. Intracerebro ventricular cannulation was performed under ketamine (50 mg/kg) and xylazine (15 mg/kg) anesthesia using polyethylene cannulas inserted stereotaxically into the lateral ventricle (0.8 mm caudal to the bregma, 2.0 mm lateral to the midline, and 4.0 mm below the surface of the skull) (Zelena et al., 1999). Placement of the cannulas was verified by injecting 10 nM/3 μl of angiotensin II into the brains 1 day after surgery. Only animals reacting with an intensive drinking response were included in the study. Rats were allowed to recover for 3 days, then they were anesthetised and a permanent cannula (silicon tubing, inner diameter 0.50 mm, external diameter 0.90 mm; Dow-Corning Corp., Midland, MI, USA and Beckton-Dickinson, Parsipparny, NY, USA) was implanted into the right jugular vein allowing frequent blood sampling from freely moving animals (Bodnar et al., 2009). After 3 days of recovery, 25 or 100 pmol/5 μl of nesfatin-1 dissolved in physiological saline was injected into the lateral ventricle between 08:00 and 09:00. In the same conditions, control rats received 5 μl physiological saline. Blood samples (400 μl) were collected on ice at 0 (before icv injection), 15, 30, 60 and 90 min after the injections and replaced immediately by physiological saline. The plasma was separated and stored at −20 °C until assayed for hormone content.

2.3. Experiment 2. Effect of exogenously administered nesfatin-1 on pituitary cell cultures in vitro

Cultures were made as described earlier (Raptis et al., 2004). Pituitary glands from 3 male rats were collected freshly. Cultures were maintained at 37 °C in a standard CO_2 incubator for 24 h. Next day, the plates were divided into 4 groups and the media were changed to control ($n = 4$), and treated with 5 nM ($n = 4$), 10 nM ($n = 4$) and 50 nM ($n = 3$) nesfatin-1, respectively. After 1 h, media were collected and stored at −20 °C until the ACTH levels were measured.

2.4. Experiment 3. Restraint stress

Single, long-duration restraint was performed as previously described (Zelena et al., 2003). Animals were placed into transparent plastic tubes (5–6 cm inner diameter) having a 4 cm long conical head part ending with a large breathing hole. Behind the body, the rear end of the tube was loosely packed with paper towels. This method allows restraint without any pain and minimizes temperature effects. Restraint lasted for 4 h in the morning (08:00–12:00) and was finished by transcardial perfusion of the animals with 4% paraformaldehyde in 0.1 M phosphate buffered saline (PBS). Non-stressed rats were used, as controls. Brains ($n = 6$ animals/group) were removed and cryoprotected. Caudal medullary and hypothalamic regions were cut into 20 μm thick coronal serial sections and stored at −20 °C in RNase free anti-freeze medium until used for quantitative *in situ* hybridization and immunohistochemistry.

2.5. Experiment 4. Adrenalectomy (ADX)

Bilateral adrenalectomy and sham operations were performed through a dorsal incision, under ketamine-xylasine anesthesia ($n = 7$ animals/group). After surgery, rats received 0.9% saline instead of drinking water. One week later, animals were killed by decapitation, brains were removed, frozen on dry ice and stored at −80 °C until processed for quantitative *in situ* hybridization. To confirm success of ADX, trunk blood was collected after decapitation and plasma corticosterone levels were measured. Only ADX animals with practically zero corticosterone levels were included in the further analysis.

2.6. Analytical methods

2.6.1. Hormone measurements

ACTH and corticosterone levels were measured from unextracted plasma with a radio-immunoassay, as described earlier

(Makara and Kovacs, 1997; Zelena et al., 2003). All samples were measured in duplicates. The intra-assay coefficient of variation was 10.4% and 6.3% for ACTH and corticosterone measurements, respectively. The sensitivity of the assays was 2.0 fmol/ml for ACTH and 2.7 pmol/ml for corticosterone, respectively. All samples from one experiment were measured in one assay.

2.6.2. Immunohistochemistry (IHC)

IHCs always started with blocking the endogenous peroxidase activity, using a 3% H_2O_2 solution for 15 min at room temperature (RT). Then, the sections were blocked in 1% BSA and 0.5% TritonX-100 for 1 h at RT. Primary, as well as secondary and tertiary antibodies were applied for 2 days at 4 °C (primaries) and for 1 h at RT, respectively. The sections were washed 3 times for 5 min in PBS following each incubation step.

1. For the Fos and nesfatin-1/NUCB2 double IHC, serial sections of brains (n = 4/group) from 2.4. were washed out from the anti-freeze medium 3 times for 10 min in PBS. Rabbit anti-Fos (1:15,000) was used as a primary antibody and the immunostaining was continued by applying the standard ABC method, using biotinylated anti-rabbit IgG (1:1000) and extravidine-peroxidase (1:1000). The reaction was visualized by nickel-intensified-DAB reaction. The second IHC was performed the same way, except this time rabbit anti-nesfatin-1/NUCB2 was used as a primary antibody (1:3000) and DAB reaction performed for colorisation. Sections were mounted on gelatin-coated slides, air-dried and coverslipped with DPX.
2. For the fluorescens immunostainings perfused-fixed brains from two control animals were immersed in 20% sucrose solution, and the caudal medullae were cut into 50 μm thick serial coronal sections. Sections from #1 rat were double immunostained for PrRP and nesfatin-1/NUCB2, while sections from #2 rat were triple immunostained for PrRP, nesfatin-1/NUCB2 and TH. The sections were incubated consecutively in rabbit anti-nesfatin-1/NUCB2 antibody (1:20,000), in biotinylated anti-rabbit IgG (1:1000) and in extravidin-peroxidase (1:1000). FITC-tyramide was used for visualization. Next, the sections were microwave-treated in 0.1 M citric-acid (pH 6.0) for 5 min to prevent cross-reaction with the second primary antibody made in rabbit and to block the peroxidase enzyme from the first immunostaining, as well as to perform antigen retrieval (Toth et al., 2008). The second IHC was performed using a rabbit anti-PrRP primary antibody (1:10,000), a goat anti-rabbit IgG polymer-HRP, and detected by Alexa Fluor 568-tyramide. The sections for the triple immunostaining were treated with 3% H_2O_2 solution containing 0.01% sodium azide to block peroxidase activity, and incubated in mouse anti-TH primary (1:1000), followed by a goat anti-mouse IgG polymer-HRP. Vizualization was performed by tyramide-conjugated Alexa Fluor 405. The sections were mounted on non-coated precleaned slides and coverslipped with Vectashield mounting medium.

2.6.3. In situ hybridizations

The 246 bp long cDNA according to the sequence of nesfatin-1 was cloned into a pBC KS+ vector. The [^{35}S]UTP-labeled antisense and sense riboprobes were prepared by *in vitro* transcription (Maxiscript KIT) with T3 and T7 RNA polymerases, respectively. In a preliminary experiment using hypothalamic rat brain sections, the antisense probe produced specific signal pattern according to literature, the sense probe did not give any signal.

Perfused-fixed sections from 2.4. were washed 3 times for 10 min in sterile PBS then mounted and air-dried at RT on positively charged Superfrost Plus slides (Menzel GmbH & Co KG, Braunschweig, Germany). Hypothalamic regions of fresh frozen brains from 2.5. were cut into 12 μm thick serial coronal sections in a cryostat (Leica Microsystems GmbH, Wetzlar, Germany). The sections were thaw-mounted and air-dried at 37 °C onto positively charged Superfrost Plus slides. All the slides were stored at −80 °C until used. Hybridizations were performed overnight in humid chambers at 55 °C with 10^6 cpm/slide of the [^{35}S]UTP-labeled probes. Next day, the sections were washed to get rid of the non-specifically bound probes, for details see Zelena et al. (2003). The sections were apposed to a BAS-MS imaging plate (Fuji Photo Film Co., LTD., Kanagawa, Japan, NJ) for 3 days in case of the hypothalamic and for 8 days in case of the medullae, then data were read out by a Fujifilm FLA-8000 Image Analyzer. Medullary sections were dipped into Kodak NTB nuclear track emulsion, and kept at 4 °C in dark. The emulsion-coated slides were developed after 6 weeks, using Kodak Dektol developer and fixer at 18 °C. The sections were counter-stained with 0.5% Giemsa solution, air-dried and coverslipped using DPX mounting medium.

2.7. Statistical analysis

Statistical significance of differences between groups was calculated by unpaired t-test, using the Sigmastat 3.5 program (Systat Software, Inc., Chicago, IL). Differences between groups were considered statistically significant when $^*p < 0.05$. Results are expressed as means ± SEM.

2.7.1. Quantification of the ISHs

Nesfatin-1/NUCB2 mRNA expression levels in the medial parvocellular PVN and in the A2 cell group were evaluated from the images recorded on the phosphor imager. Mean grey values were measured on both sides of two (PVN) or four (A2 area: at the level of the obex ± 0.12 mm) sections per animal, corresponding to the central region of the nuclei. Nesfatin-1/NUCB2 mRNA signal in the ventrolateral medulla was too weak to quantify it from the imaging plate, therefore here the quantification was performed using darkfield microscopical images taken from the emulsion-coated slides, as described previously (Zelena et al., 2003). Pictures taken from both sides of sections (4–5/animal) between the level of the obex and 0.6 mm caudal to it, were included in the analysis. Measurements were performed by using the Image J 1.32j software (Wayne Rasband; NIH, Bethesda, MD, USA). Results were expressed as pixels per labeled cells (i.e. cell surface covered by grains) occupied by the silver grains. The average/animal data were used for further statistical evaluation. In every case, parallel measurements were made outside the nuclei and background values were subtracted from the values measured in the nuclei. Darkfield and brightfield images of the same areas of the sections were used for demonstration in the figures. In case of the A1 region, the darkfield and brightfield pictures were overlayed in Adobe Photoshop CS (Adobe Systems Inc., McLean, VA, USA).

2.7.2. Calculating PrRP and nesfatin-1/NUCB2 co-localization

Confocal microscopy images of the A1 and A2 regions from the level of the area postrema to the beginning of the spinal cord were taken by a Nicon Eclipse E800 microscope attached to a Bio-Rad Radiance 2100 Rainbow confocal scanning system by sequential scanning. Cell counts were made with the help of the analySIS Pro 3.2 program (Soft Imaging system GmbH), by simultaneous examination of the greyscale images of the separated channels and the colored overlay picture. To identify neurons in the pictures a numbered grid of the same size was placed over the overlay picture and the greyscale pictures of the separated channels. PrRP and PrRP-nesfatin-1/NUCB2 double-labeled neurons were counted bilaterally on each section, summarized, and the percentage of double-positive cells among the PrRP-positive ones was calculated per animal. Data are presented as the average of the results received from the sections of the two animals used.

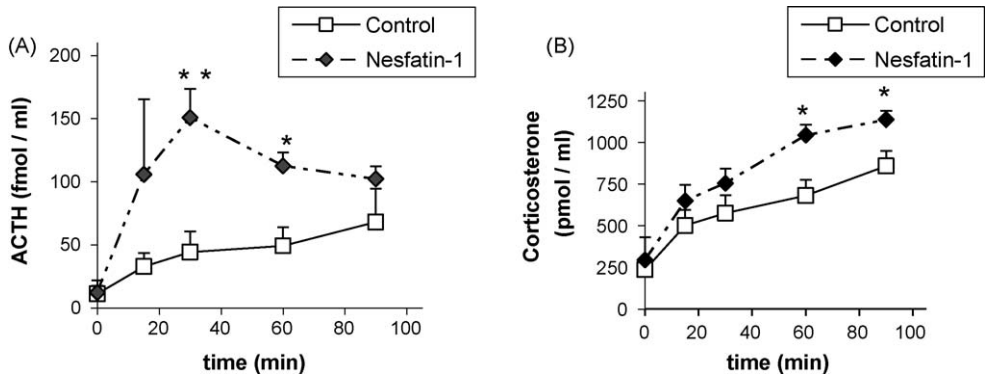

Fig. 1. Plasma ACTH and corticosterone concentrations after icv injection of 25 pmol nesfatin-1 peptide or vehicle. The effect of the experimental stress on the ACTH (A) and corticosterone (B) levels can be observed in the controls causing an elevation in time (not labeled). Nesfatin-1 treatment caused an additional, time dependent increase both in plasma ACTH and corticosterone concentrations. Significant effect of nesfatin-1 treatment compared to the vehicle treatment is labeled by stars. ACTH elevation preceded corticosterone elevation with a half an hour, and it ended by 90 min. Open squares: control animals, filled squares: Nesfatin-1-injected animals, $n = 3–5$, $^{*}p < 0.05$, $^{**}p < 0.01$.

2.7.3. Calculating the percentage of Fos and nesfatin-1/NUCB2 double-labeled neurons

The quantitative assessment of the Fos-nesfatin-1/NUCB2 double immunostained cells in the medial parvocellular part of the PVN was made by counting the total number of nesfatin-1/NUCB2-positive and double-labeled neurons using a Visopan projection microscope on 3 sections per animal. Average per animal data were used for calculating percentage values. Data are presented as the average per group.

3. Materials

Ketamine was obtained from Richter (Budapest, Hungary), xylazine was from CP-Pharma (Bönsensell, Germany). The rat nesfatin-1/NUCB2 (H-003-22) and the rat PrRP (H-008-52) antisera, as well as the rat nesfatin-1 (1–82) peptide were from Phoenix Pharmaceuticals Inc. (Burlingame, CA, USA). Nesfatin-1 peptide was dissolved in sterile physiological saline and a stock solution of 20 μM was prepared, aliquoted and kept at −20 °C. When it was necessary, the stock solution was further diluted with physiological saline on the day of the experiments. SMEM, DMEM, calf serum, tyramide-conjugated FITC, Alexa Fluor 568 and 405, and the nesfatin-1/NUCB2 cDNA (clone ID: IMAGE: 8363301) were obtained from Invitrogen GmbH (Lofer, Austria), BSA, extravidine-peroxidase, DAB, Giemsa solution, DPX, Kodak Dektol developer and fixer were from Sigma–Aldrich Kft. (Budapest, Hungary). Rabbit anti-Fos (Sc-52) was purchased from Santa Cruz Biotechnology, Inc. (Santa Cruz, USA), biotinylated anti-rabbit IgG (BA-1000) and Vectashield mounting medium were from Vector Laboratories, Inc. (Burlingame, CA, USA). The goat anti-rabbit and anti-mouse IgG polymer-HRPs (AP 342P and AP 340P, respectively) and the mouse TH primary antibody (MAB318) were obtained from Millipore (Temecula, CA, USA). The [^{35}S]UTP was purchased from Per-Form Hungaria Kft. (Budapest, Hungary), Maxiscript KIT was from Ambion (Austin, TX, USA), Kodak NTB nuclear track emulsion was from Molecular Imaging Systems (Carestream Health Inc., Rochester, NY, USA).

4. Results

4.1. Experiment 1

To eliminate the stress inducing effect of the experimental procedure hormonal changes in the nesfatin-1 administered group were compared to those ones in vehicle treated controls. Exogenously administered nesfatin-1 (25 pmol/animal) time dependently elevated the plasma ACTH and corticosterone levels. The increase was 240% of the control after 30 min in case of ACTH, and 50% of the control after 60 min in case of corticosterone. The ACTH and corticosterone elevations were still significant at 60 and 90 min, respectively (Fig. 1A and B). Increasing the dose of icv nesfatin-1 from 25 to 100 pmol did not result proportionally higher magnitude of ACTH response, indicating that a plato has been reached at dose of 25 pmol (not shown).

4.2. Experiment 2

Nesfatin-1 had no effect on ACTH release of the pituitary cell cultures *in vitro*, even when higher doses of nesfatin-1 were applied (5, 10 and 50 nM, data not shown).

4.3. Experiment 3

Efficacy of exogenously added nesfatin-1 to stimulate the HPA axis led us to investigate whether endogenous nesfatin-1/NUCB2

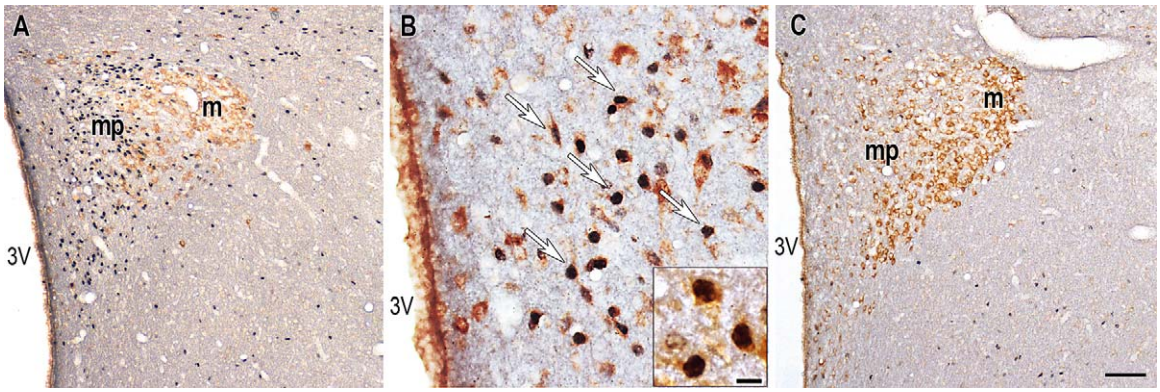

Fig. 2. Activation of nesfatin-1/NUCB2-positive neurons in the PVN after restraint. Nesfatin-1/NUCB2 labeling is brown, Fos-positive cell nuclei are dark bluish. (A) Restraint-induced strong cell activation in the medial parvocellular but not in the magnocellular part of the PVN. (B) High magnification picture of the medial parvocellular PVN in a restraint stressed animal. Many of the nesfatin-1/NUCB2 positive neurons are double labeled (arrows). Double-labeled cells are shown with an even higher magnification on the insert. (C) There is only minimal Fos positivity in the PVN of the control animals. 3 V: third ventricle, m: magnocellular, mp: medial parvocellular part of the PVN, respectively. Scale bars: 100 μm for (A and C), 25 μm for (B), 8 μm on the inset.

participates in the response to stress. We have found intensive neuronal cell activation in response to restraint stress in the medial parvocellular part of the PVN. In restraint stressed animals 47.0 ± 3.8%, while in control animals 3.9 ± 0.3% of the cells immunoreactive for nesfatin-1/NUCB2 were Fos positive, respectively (Fig. 2). However, nesfatin-1/NUCB2 producing neurons located in the magnocellular PVN were Fos negative (Fig. 2A). There were no Fos-nesfatin-1/NUCB2 double-labeled neurons observed in the caudal medulla 4 h after beginning of the restraint stress (not shown).

Besides provoking neuronal activations, restraint also induced nesfatin-1/NUCB2 mRNA expression in the medial parvocellular PVN. The mean grey values were 4688 ± 149 and 5353 ± 210 for the control and the restraint stressed groups, respectively, $n = 6$, $p < 0.05$ (Fig. 3, upper panel). Nesfatin-1/NUCB2 mRNA increase evoked by restraint was observed both in the hypophysiotropic and the pre-autonomic regions of the medial parvocellular subdivision (Fig. 3, lower panel) (Viau and Sawchenko, 2002). Additionally, nesfatin-1/NUCB2 mRNA expression was significantly elevated in the caudal

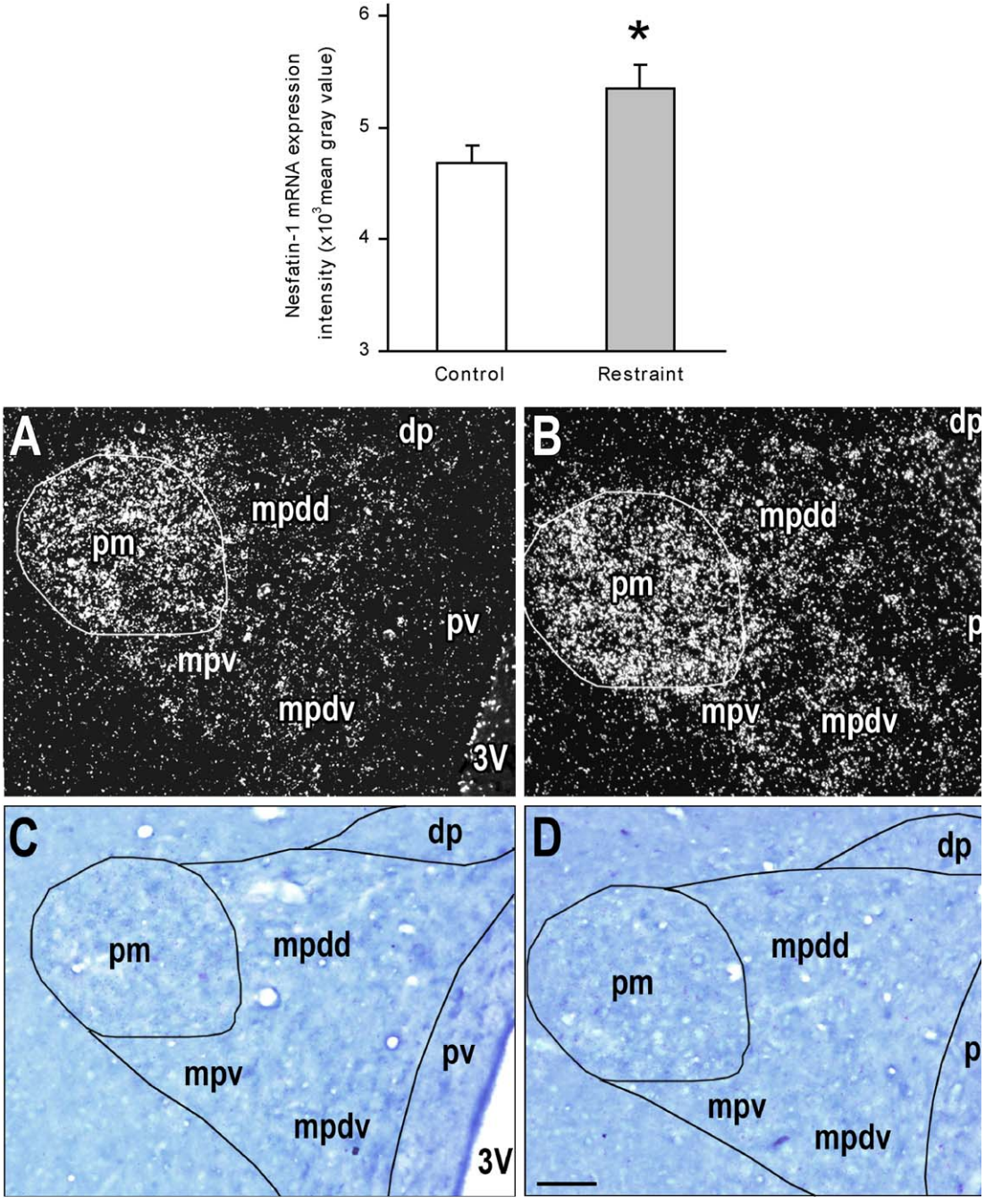

Fig. 3. Effect of restraint stress on nesfatin-1/NUCB2 mRNA expression in the PVN. (Upper panel) Bar graph showing quantitative data on the nesfatin-1/NUCB2 mRNA expression in control and restraint stressed animals. There is a significant increase for restraint, $n = 6$, $^{*}p < 0.05$. (Lower panel: A and B) Nesfatin-1/NUCB2 mRNA *in situ* hybridization signal (silver grains) in the PVN in a control and a restraint stressed animal, respectively. Darkfield pictures, the posterior magnocellular subdivision is outlined to separate it from the parvocellular PVN. More dense signal can be observed both in the hypophysiotropic (dorsal and ventral components) and in the pre-autonomic regions of the medial parvocellular PVN after restraint. (C and D) Brightfield pictures of the same sections, as in (A and B) stained by Giemsa, respectively, showing the subdivisions of the PVN. pm: posterior magnocellular, dp: dorsal parvocellular, mp: medial parvocellular, pv: periventricular subdivisions of the PVN, 3 V: third ventricle. Organization of the mp subdivision: mpdd: dorsal component, mpdv: ventral component, mpv: pre-autonomic region. Scale bar: 250 μm.

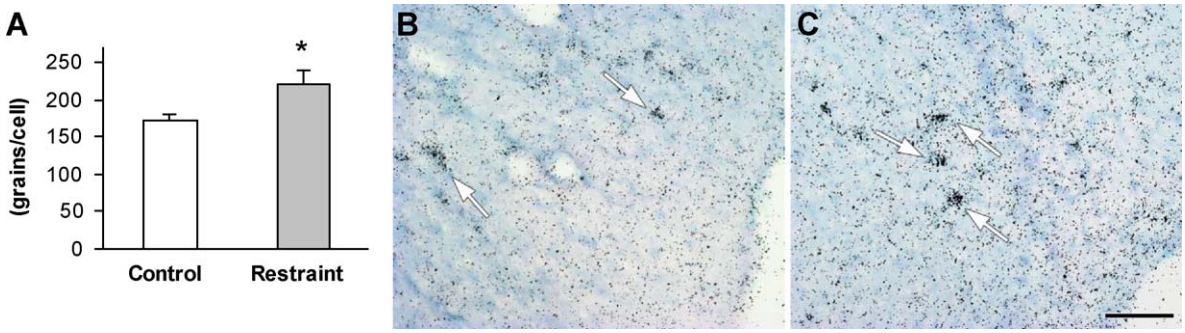

Fig. 4. Nesfatin-1/NUCB2 mRNA expression in the ventrolateral medulla. (A) Quantification of the *in situ* hybridization signal (grains/cell) indicates significantly increased mRNA expression in the restraint stressed group compared to the control. (B and C) Representative pictures from the ventrolateral medulla of a control (B) and a restraint stressed (C) animal after *in situ* hybridization (ISH) for nesfatin-1/NUCB2 mRNA. The labeling is more dense in (C). Arrows point to labeled cells. Scale bar: 100 μm, $n = 6$, $^{*}p < 0.05$.

ventrolateral medulla too, where the grains per cell values were 176.1 ± 14.0 and 223.9 ± 12.8 for the control and the restraint stressed groups, respectively, $n = 6$, $p < 0.05$ (Fig. 4A–C). However, there was no change in the A2 cell group [mean grey values of the control and the restraint stressed groups were 3067 ± 163 and 3062 ± 178, respectively ($n = 6$)].

Triple immunohistochemistry for nesfatin-1/NUCB2, TH and PrRP showed that many of the nesfatin-1/NUCB2 expressing neurons in the caudal ventrolateral medulla actually belonged to the A1 catecholamine cell group (TH-positive), and confirmed that many of the A2 noradrenergic neurons produce both nesfatin-1/NUCB2 and TH (Fig. 5A and B). Additionally, it was revealed that a high percentage of PrRP expressing neurons in the A1 and A2 cell groups co-localize with nesfatin-1/NUCB2 (Fig. 5A–D). In fact, $93.42 \pm 0.37\%$ and $76.59 \pm 4.19\%$ of PrRP neurons in the A1 and the A2 cell group co-localized with nesfatin-1/NUCB2, respectively.

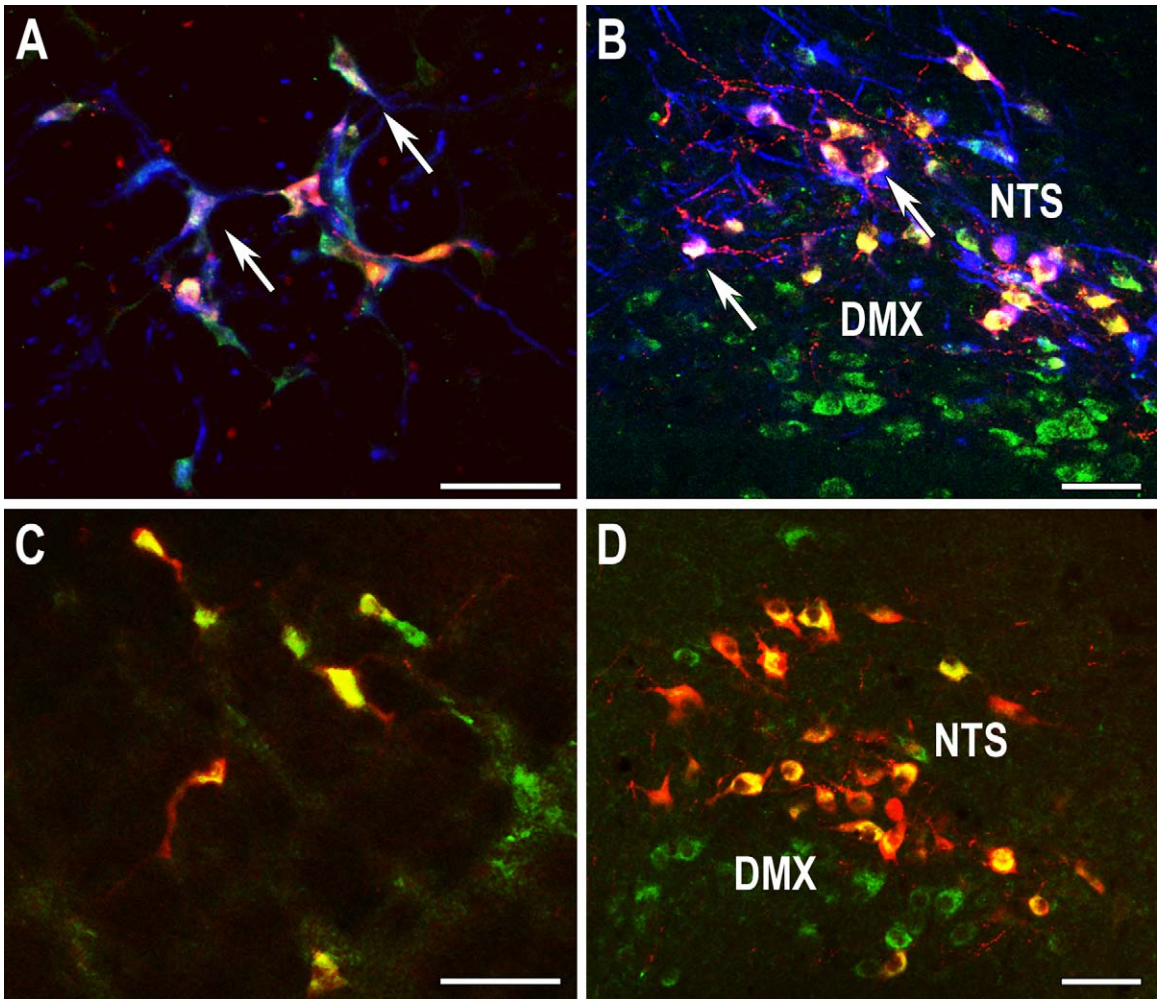

Fig. 5. Co-localization of nesfatin-1/NUCB2 (green), prolactin-releasing peptide (PrRP, red) and TH (blue) in the medulla. (A and B) Representative confocal images from the A1 and from the A2 cell groups, respectively. Triple labeled cells are whitish (arrows). (C and D) Co-localization of PrRP and nesfatin-1/NUCB2 in the A2 and A1 cell groups, respectively. Double-labeled neurons are in yellow. NTS: nucleus of the solitary tract, DMX: dorsal motor nucleus of the vagus nerve. Scale bars: 100 μm.

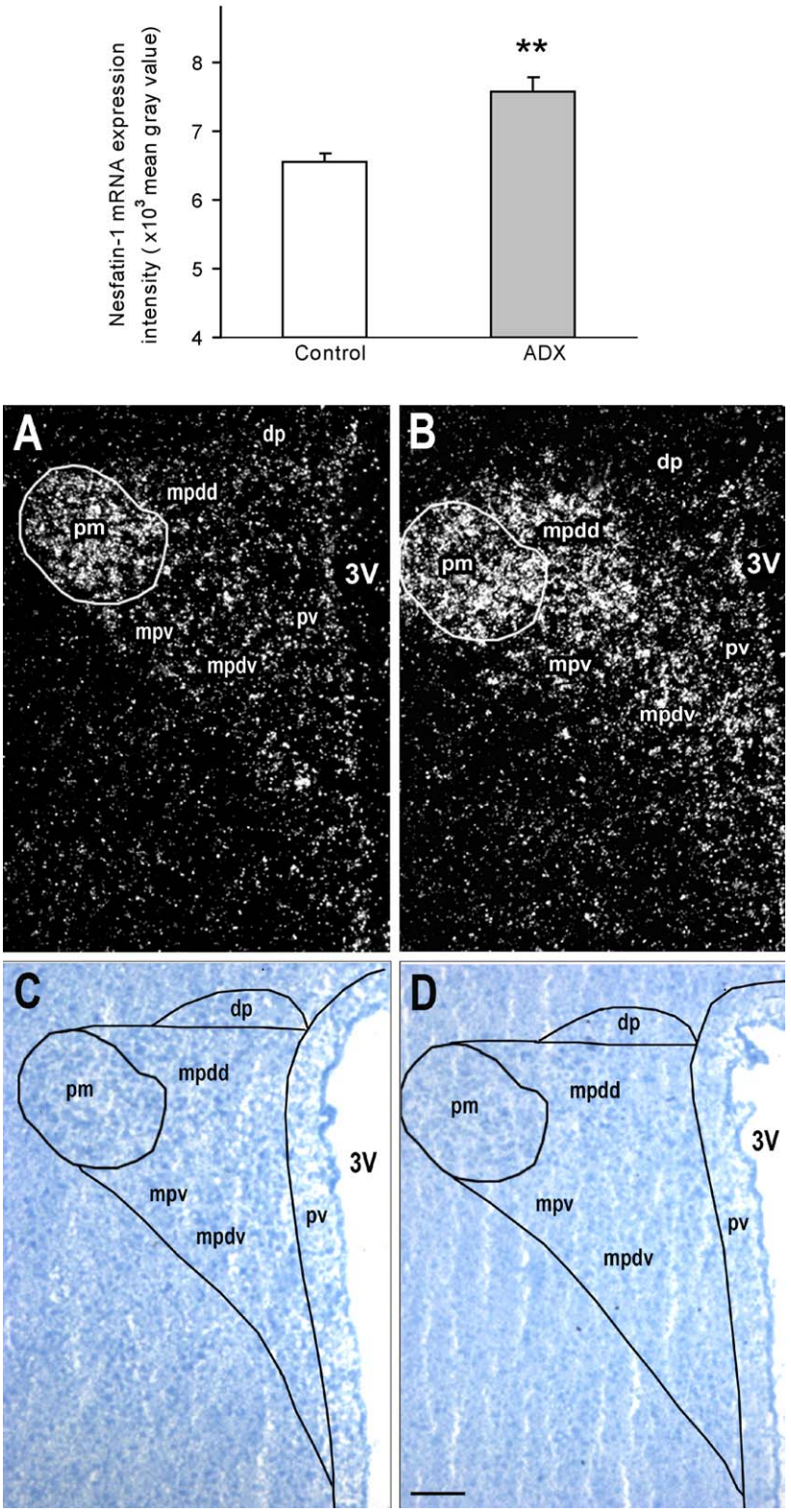

Fig. 6. Effect of adrenalectomy (ADX) on nesfatin-1/NUCB2 mRNA expression in the medial parvocellular part of the PVN. (Upper panel) Bar graph showing quantitative data on the nesfatin-1/NUCB2 mRNA expression in control and ADX animals. There is a significant increase for ADX, $n = 6–7$, $^{*}p < 0.01$. (Lower panel: A and B) Nesfatin-1/NUCB2 mRNA *in situ* hybridization signal (silver grains) in the PVN in a control and an ADX animal, respectively. Darkfield pictures, the posterior magnocellular subdivision is outlined to separate it from the parvocellular PVN. The density of silver grains in (B) is especially high in the dorsal component (mpdd), where most of the CRH containing hypophysiotropic neurons are located. (C and D) Brightfield pictures of the same sections, as in (A and B) stained by Giemsa, respectively, showing the subdivisions of the PVN. pm: posterior magnocellular, dp: dorsal parvocellular, mp: medial parvocellular, pv: periventricular subdivisions of the PVN, 3 V: third ventricle. Organization of the mp: mpdd: dorsal component, mpdv: ventral component, mpv: pre-auronomic region. Scale bar: 250 μm.

4.4. Experiment 4

Since according to our results, not only the exogenously administered, but also the endogenously produced nesfatin-1/NUCB2 was likely to participate in the regulation of the HPA axis activity, we finally examined the sensitivity of hypothalamic nesfatin-1/NUCB2 producing neurons to the negative steroid feedback. One week after bilateral adrenalectomy, nesfatin-1/NUCB2 mRNA expression significantly elevated in the medial parvocellular PVN. The mean grey values were 6551 ± 135 and 7569 ± 214 for the control and the ADX groups, respectively, $n = 6–7$, $p < 0.05$. Within the medial parvocellular subdivision the ISH signal was especially dense in the dorsal component (mpdd), where the hypophysiotropic CRH producing cell population is located (Fig. 6) (Viau and Sawchenko, 2002).

5. Discussion

Nesfatin-1 was originally described as an anorexigenic peptide (Oh et al., 2006). Control of energy balance is in a reciprocal relationship with the HPA axis activation, because both starvation and obesity lead to an increase in CRH expression, while hypophagia and body weight decrease is a typical syndrome in chronic stress (Cunningham et al., 1986; Dallman et al., 2006; Harris et al., 2002; Zelena et al., 2004). Additional data, like presence of nesfatin-1/NUCB2 in stress-responsive areas in the brain (PVN, NTS, ventrolateral medulla), co-localization of nesfatin-1/NUCB2 with CRH, and the fact, that 30 min restraint caused Fos activation of nesfatin-1/NUCB2 producing neurons of the PVN, NTS and in the ventrolateral medulla, all pointed out to the possible involvement of nesfatin-1/NUCB2 in the response to stress (Brailoiu et al., 2007; Foo et al., 2008; Goebel et al., 2009b). Our data confirm this hypothesis, since icv nesfatin-1 caused a significant elevation of plasma ACTH and corticosterone levels compared to the control. Nesfatin-1 (25 pmol/rat) was also effective to induce stress-related behavior in rats (Merali et al., 2008). In our experiments, icv nesfatin-1 resulted a 3-fold increase in the ACTH level 30 min after injection and had a short duration. In comparison, vasopressin co-localizing also with CRH in the PVN, has a maximal effect on ACTH release 10 min after application, indicating that nesfatin-1/NUCB2 plays role in the later phase of the stress response (Bernardini et al., 1994; Kovacs, 1998). Both CRH and vasopressin are released from paraventricular axon terminals into the hypophyseal portal system and act on pituitary cells to release ACTH (Lightman, 2008). We failed to prove a direct effect of nesfatin-1 on the ACTH release of pituitary cells (*in vitro*), even when high dose of the peptide was applied. This observation is in agreement with findings showing that nesfatin-1/NUCB2-immunoreactivity is lacking in the axon terminals, and confined exclusively to perikarya and primary dendrites (Foo et al., 2008). Immuno-electronmicroscopy revealed nesfatin-1/NUCB2-positive secretory vesicles in the PVN suggesting paracrin/autocrin mechanisms for nesfatin-1/NUCB2's actions (Maejima et al., 2009). This type of neuronal communication in the PVN had been reported previously (Landgraf and Neumann, 2004). Morphological evidence for action of nesfatin-1/NUCB2 inside the PVN is consistent with physiological evidence showing nesfatin-1/NUCB2 capability to influence excitability of PVN neurons (Price et al., 2008).

In order to investigate participation of endogenous nesfatin-1/NUCB2 in stress, we applied restraint and examined cell activation by nesfatin-1/NUCB2 and Fos double immunohistochemistry, as well as nesfatin-1/NUCB2 mRNA changes in the PVN and in the medulla. We applied restraint, because it is a strong, combined physical-psychological stress stimulus strongly elevating both the ACTH and the corticosterone levels (Zelena et al., 2003). We failed to observe cell activation in the nesfatin-1/NUCB2-expressing neurons of the A1 and A2 cell groups, unlike it was previously reported, probably due to the different experimental conditions (Goebel et al., 2009b). Fos is usually a short time expressing gene, therefore the Fos-reaction was probably over in medullary catecholamine neurons by the end of the 4th hour (Morgan and Curran, 1989). In contrast, we have found significant elevation in nesfatin-1/NUCB2 mRNA expression in the caudal ventrolateral medulla, in response to restraint. It should be mentioned, that a lower sensitivity of the A2 cell group (NTS-DMX complex) versus the A1 cell group (caudal ventrolateral medulla) to restraint has been reported previously (Toth et al., 2008).

To further characterize medullary nesfatin-1/NUCB2-positive neurons, we applied immunostainings for PrRP and TH. Similarly to nesfatin-1/NUCB2, PrRP is also an anorexigenic peptide produced by a subset of A1 and A2 catecholamine neurons, and plays a role in the stress response (Sun et al., 2005). Medullary and hypothalamic PrRP-positive neurons show increased accumulation of Fos protein in response to stress (Maruyama et al., 2001). Central administration of PrRP stimulates CRH-mediated ACTH secretion and PrRP potentiates the effect of noradrenaline in this respect (Maruyama et al., 2001). Additionally, PrRP applied icv elevates the number of Fos-immunoreactive nuclei in high percentage of the CRH-positive cells of the PVN, and PrRP mRNA expression in the medulla increases after acute and chronic restraint stress (Mera et al., 2006; Toth et al., 2008). We have found a high percent of co-localization of nesfatin-1/NUCB2, TH and PrRP especially in the A1 cell group, indicating that most of the A1 and A2 neurons co-express noradrenaline, PrRP and nesfatin-1/NUCB2. The A1 and A2 cell groups receive restraint-induced stress signals directly from the periphery, and are responsible for the stress-induced activation of the higher autonomic centers, like the PVN triggering the activation of the HPA axis (Pacak et al., 1993; Petrov et al., 1993). PrRP and noradrenaline, as neurotransmitters, act synergistically in this process (Maruyama et al., 2001). In turn, descending fibers directly from the PVN, and directly or indirectly from other areas of the hypothalamus and the limbic system also control the A1 and A2 cell groups (Saha, 2005; Toth et al., 1999). Since nesfatin-1/NUCB2 is not transported through axons, but probably acts locally, further examinations are needed to elucidate the exact mechanism of medullary nesfatin-1/NUCB2 action in response to stress.

Unlike the medulla, restraint evoked strong activation of nesfatin-1/NUCB2-positive medial parvocellular PVN neurons, as well as nesfatin-1/NUCB2 mRNA increase. The elevation was observed both in the hypophysiotropic and the pre-autonomic regions of the medial parvocellular PVN. (Viau and Sawchenko, 2002). Nesfatin-1/NUCB2 is co-expressed with CRH in the dorsal component of the medial parvocellular PVN, and CRH mRNA expression peaks 4 h after single stress, therefore we have chosen this timing (Foo et al., 2008; Ma et al., 1997). Four hour however, is also the time point when Fos protein expression peaks during single long-duration restraint in the PVN (Tan and Nagata, 2002).

Finally, we investigated the effect of bilateral adrenalectomy on the nesfatin-1/NUCB2 mRNA expression in the medial parvocellular PVN and detected a marked increase restricted to the area of hypophysiotropic CRH neurons, showing that the HPA regulatory system exerts a negative feedback on the nesfatin-1/NUCB2 gene expression.

Our data demonstrate for the first time a direct influence of nesfatin-1/NUCB2 on the stress system. However, since many agents are related to the stress response, a bystander response of nesfatin-1/NUCB2 cannot be entirely excluded under the present experimental conditions. According to our results, nesfatin-1/NUCB2 acts on the stress system both at the level of the medulla and in the parvocellular PVN, but not at the level of the pituitary

gland. Nesfatin-1/NUCB2 co-localizes with noradrenaline and PrRP in the medulla. An exciting question for the future is, how nesfatin-1/NUCB2 might functionally cooperate with the other co-expressed factors in these areas. Additionally, further studies using inhibition of the expression of nesfatin-1/NUCB2 are needed to clarify its exact role in the stress response.

Conflict of interest

The authors declare no conflicts of interest.

Acknowledgements

This work was supported by ETT 495/09 (Z.E. Tóth), ETT 458/09, OTKA-68170 (G.M. Nagy), NK-72929 (M. Palkovits), and OTKA NN-71629 (D. Zelena). Z.E. Tóth is supported by the Bolyai fellowship. The authors thank for Judit Kerti and Szilvia Deák for the technical assistance.

References

Aguilera, G., 1994. Regulation of pituitary ACTH secretion during chronic stress. Front. Neuroendocrinol. 15, 321–350.
Bernardini, R., Chiarenza, A., Kamilaris, T.C., Renaud, N., Lempereur, L., Demitrack, M., Gold, P.W., Chrousos, G.P., 1994. In vivo and in vitro effects of arginine-vasopressin receptor antagonists on the hypothalamic–pituitary–adrenal axis in the rat. Neuroendocrinology 60, 503–508.
Bodnar, I., Banky, Z., Zelena, D., Halasz, B., 2009. Glutamate receptor antagonist infused into the hypothalamic suprachiasmatic nuclei interferes with the diurnal fluctuations in plasma prolactin and corticosterone levels and injected into the mesencephalic dorsal raphe nucleus attenuates the suckling stimulus-induced release of prolactin of the rat. Brain Res. Bull. 80, 9–16.
Brailoiu, G.C., Dun, S.L., Brailoiu, E., Inan, S., Yang, J., Chang, J.K., Dun, N.J., 2007. Nesfatin-1: distribution and interaction with a G protein-coupled receptor in the rat brain. Endocrinology 148, 5088–5094.
Cunningham, J.J., Calles-Escandon, J., Garrido, F., Carr, D.B., Bode, H.H., 1986. Hypercorticosteronuria and diminished pituitary responsiveness to corticotropin-releasing factor in obese Zucker rats. Endocrinology 118, 98–101.
Dallman, M.F., Pecoraro, N.C., La Fleur, S.E., Warne, J.P., Ginsberg, A.B., Akana, S.F., Laugero, K.C., Houshyar, H., Strack, A.M., Bhatnagar, S., Bell, M.E., 2006. Glucocorticoids, chronic stress, and obesity. Prog. Brain Res. 153, 75–105.
Foo, K.S., Brismar, H., Broberger, C., 2008. Distribution and neuropeptide coexistence of nucleobindin-2 mRNA/nesfatin-like immunoreactivity in the rat CNS. Neuroscience 156, 563–579.
Fort, P., Salvert, D., Hanriot, L., Jego, S., Shimizu, H., Hashimoto, K., Mori, M., Luppi, P.H., 2008. The satiety molecule nesfatin-1 is co-expressed with melanin concentrating hormone in tuberal hypothalamic neurons of the rat. Neuroscience 155, 174–181.
Goebel, M., Stengel, A., Wang, L., Lambrecht, N.W., Tache, Y., 2009a. Nesfatin-1 immunoreactivity in rat brain and spinal cord autonomic nuclei. Neurosci. Lett. 452, 241–246.
Goebel, M., Stengel, A., Wang, L., Tache, Y., 2009b. Restraint stress activates nesfatin-1-immunoreactive brain nuclei in rats. Brain Res. 1300, 114–124.
Harris, R.B., Mitchell, T.D., Simpson, J., Redmann Jr., S.M., Youngblood, B.D., Ryan, D.H., 2002. Weight loss in rats exposed to repeated acute restraint stress is independent of energy or leptin status. Am. J. Physiol. Regul. Integr. Comp. Physiol. 282, R77–R88.
Kovacs, K.J., 1998. Functional neuroanatomy of the parvocellular vasopressinergic system: transcriptional responses to stress and glucocorticoid feedback. Prog. Brain Res. 119, 31–43.
Landgraf, R., Neumann, I.D., 2004. Vasopressin and oxytocin release within the brain: a dynamic concept of multiple and variable modes of neuropeptide communication. Front. Neuroendocrinol. 25, 150–176.
Lightman, S.L., 2008. The neuroendocrinology of stress: a never ending story. J. Neuroendocrinol. 20, 880–884.
Ma, X.M., Levy, A., Lightman, S.L., 1997. Rapid changes in heteronuclear RNA for corticotrophin-releasing hormone and arginine vasopressin in response to acute stress. J. Endocrinol. 152, 81–89.
Maejima, Y., Sedbazar, U., Suyama, S., Kohno, D., Onaka, T., Takano, E., Yoshida, N., Koike, M., Uchiyama, Y., Fujiwara, K., Yashiro, T., Horvath, T.L., Dietrich, M.O., Tanaka, S., Dezaki, K., Oh, I.S., Hashimoto, K., Shimizu, H., Nakata, M., Mori, M., Yada, T., 2009. Nesfatin-1-regulated oxytocinergic signaling in the paraventricular nucleus causes anorexia through a leptin-independent melanocortin pathway. Cell Metab. 10, 355–365.
Makara, G.B., Kovacs, K.J., 1997. Lesioning of the hypothalamic paraventricular nucleus inhibits ether-induced ACTH but not prolactin release. Neurobiology (Bp) 5, 403–411.
Maruyama, M., Matsumoto, H., Fujiwara, K., Noguchi, J., Kitada, C., Fujino, M., Inoue, K., 2001. Prolactin-releasing peptide as a novel stress mediator in the central nervous system. Endocrinology 142, 2032–2038.
Mera, T., Fujihara, H., Kawasaki, M., Hashimoto, H., Saito, T., Shibata, M., Saito, J., Oka, T., Tsuji, S., Onaka, T., Ueta, Y., 2006. Prolactin-releasing peptide is a potent mediator of stress responses in the brain through the hypothalamic paraventricular nucleus. Neuroscience 141, 1069–1086.
Merali, Z., Cayer, C., Kent, P., Anisman, H., 2008. Nesfatin-1 increases anxiety- and fear-related behaviors in the rat. Psychopharmacology (Berl.) 201, 115–123.
Morgan, J.I., Curran, T., 1989. Stimulus-transcription coupling in neurons: role of cellular immediate-early genes. Trends Neurosci. 12, 459–462.
Oh, I.S., Shimizu, H., Satoh, T., Okada, S., Adachi, S., Inoue, K., Eguchi, H., Yamamoto, M., Imaki, T., Hashimoto, K., Tsuchiya, T., Monden, T., Horiguchi, K., Yamada, M., Mori, M., 2006. Identification of nesfatin-1 as a satiety molecule in the hypothalamus. Nature 443, 709–712.
Okere, B., Xu, L., Roubos, E.W., Sonetti, D., Kozicz, T., 2010. Restraint stress alters the secretory activity of neurons co-expressing urocortin-1, cocaine- and amphetamine-regulated transcript peptide and nesfatin-1 in the mouse Edinger-Westphal nucleus. Brain Res. 1317, 92–99.
Pacak, K., Palkovits, M., Kvetnansky, R., Kopin, I.J., Goldstein, D.S., 1993. Stress-induced norepinephrine release in the paraventricular nucleus of rats with brainstem hemisections: a microdialysis study. Neuroendocrinology 58, 196–201.
Petrov, T., Krukoff, T.L., Jhamandas, J.H., 1993. Branching projections of catecholaminergic brainstem neurons to the paraventricular hypothalamic nucleus and the central nucleus of the amygdala in the rat. Brain Res. 609, 81–92.
Price, C.J., Hoyda, T.D., Samson, W.K., Ferguson, A.V., 2008. Nesfatin-1 influences the excitability of paraventricular nucleus neurones. J. Neuroendocrinol. 20, 245–250.
Raptis, S., Fekete, C., Sarkar, S., Rand, W.M., Emerson, C.H., Nagy, G.M., Lechan, R.M., 2004. Cocaine- and amphetamine-regulated transcript co-contained in thyrotropin-releasing hormone (TRH) neurons of the hypothalamic paraventricular nucleus modulates TRH-induced prolactin secretion. Endocrinology 145, 1695–1699.
Saha, S., 2005. Role of the central nucleus of the amygdala in the control of blood pressure: descending pathways to medullary cardiovascular nuclei. Clin. Exp. Pharmacol. Physiol. 32, 450–456.
Sawchenko, P.E., Swanson, L.W., 1982. The organization of noradrenergic pathways from the brainstem to the paraventricular and supraoptic nuclei in the rat. Brain Res. 257, 275–325.
Stengel, A., Goebel, M., Wang, L., Tache, Y., 2010. Abdominal surgery activates nesfatin-1 immunoreactive brain nuclei in rats. Peptides 31, 263–270.
Sun, B., Fujiwara, K., Adachi, S., Inoue, K., 2005. Physiological roles of prolactin-releasing peptide. Regul. Pept. 126, 27–33.
Tan, Z., Nagata, S., 2002. PVN c-fos expression, HPA axis response and immune cell distribution during restraint stress. J. UOEH 24, 131–149.
Toth, Z.E., Gallatz, K., Fodor, M., Palkovits, M., 1999. Decussations of the descending paraventricular pathways to the brainstem and spinal cord autonomic centers. J. Comp. Neurol. 414, 255–266.
Toth, Z.E., Zelena, D., Mergl, Z., Kirilly, E., Varnai, P., Mezey, E., Makara, G.B., Palkovits, M., 2008. Chronic repeated restraint stress increases prolactin-releasing peptide/tyrosine-hydroxylase ratio with gender-related differences in the rat brain. J. Neurochem. 104, 653–666.
Viau, V., Sawchenko, P.E., 2002. Hypophysiotropic neurons of the paraventricular nucleus respond in spatially, temporally, and phenotypically differentiated manners to acute vs. repeated restraint stress: rapid publication. J. Comp. Neurol. 445, 293–307.
Young 3rd, W.S., Mezey, E., Siegel, R.E., 1986. Quantitative in situ hybridization histochemistry reveals increased levels of corticotropin-releasing factor mRNA after adrenalectomy in rats. Neurosci. Lett. 70, 198–203.
Zelena, D., Foldes, A., Mergl, Z., Barna, I., Kovacs, K.J., Makara, G.B., 2004. Effects of repeated restraint stress on hypothalamo-pituitary-adrenocortical function in vasopressin deficient Brattleboro rats. Brain. Res. Bull. 63, 521–530.
Zelena, D., Kiem, D.T., Barna, I., Makara, G.B., 1999. Alpha 2-adrenoreceptor subtypes regulate ACTH and beta-endorphin secretions during stress in the rat. Psychoneuroendocrinology 24, 333–343.
Zelena, D., Mergl, Z., Foldes, A., Kovacs, K.J., Toth, Z., Makara, G.B., 2003. Role of hypothalamic inputs in maintaining pituitary–adrenal responsiveness in repeated restraint. Am. J. Physiol. Endocrinol. Metab. 285, E1110–E1117.

JOURNAL OF NEUROCHEMISTRY | 2008 | 104 | 653–666 doi: 10.1111/j.1471-4159.2007.05069.x

Chronic repeated restraint stress increases prolactin-releasing peptide/tyrosine-hydroxylase ratio with gender-related differences in the rat brain

Zsuzsanna E. Tóth,* Dóra Zelena,† Zsuzsa Mergl,† Eszter Kirilly,‡,§ Péter Várnai,¶ Éva Mezey,** Gábor B. Makara† and Miklós Palkovits*

*Neuromorphological and Neuroendocrine Research Laboratory, Department of Anatomy, Histology and Embryology of the Semmelweis University and the Hungarian Academy of Sciences, Budapest, Hungary

†Institute of Experimental Medicine, Hungarian Academy of Sciences, Budapest, Hungary

‡Department of Pharmacology and Pharmacotherapy, Faculty of Medicine, Semmelweis University, Budapest, Hungary

§Laboratory of Neurochemistry and Experimental Medicine, National Institute of Psychiatry and Neurology, Budapest, Hungary

¶Department of Physiology, Faculty of Medicine, Semmelweis University, Budapest, Hungary

**CSDB, NIDCR, NIH, Bethesda, Maryland, USA

Abstract

In this study, we investigated the effect of chronic repeated restraint (RR) on prolactin-releasing peptide (PrRP) expression. In the brainstem, where PrRP colocalize with norepinephrine in neurons of the A1 and A2 catecholaminergic cell groups, the expression of tyrosine hydroxylase (TH) has also been examined. In the brainstem, but not in the hypothalamus, the basal PrRP expression in female rats was higher than that in the males that was abolished by ovariectomy. RR evoked an elevation of PrRP expression in all areas investigated, with smaller reaction in the brainstems of females. There was no gender-related difference in the RR-evoked TH expression. Elevation of PrRP was relatively higher than elevation of TH, causing a shift in PrRP/TH ratio in the brainstem after RR. Estrogen α receptors were found in the PrRP neurons of the A1 and A2 cell groups, but not in the hypothalamus. Bilateral lesions of the hypothalamic paraventricular nucleus did not prevent RR-evoked changes. Elevated PrRP production parallel with increased PrRP/TH ratio in A1/A2 neurons indicate that: (i) there is a clear difference in the regulation of TH and PrRP expression after RR, and (ii) among other factors this may also contribute to the changed sensitivity of the hypothalamo-pituitary–adrenal axis during chronic stress.

Keywords: estrogen receptor alpha, gender-related difference, hypothalamic paraventricular nucleus lesion, *in situ* hybridization, rat.

J. Neurochem. (2008) **104**, 653–666.

Prolactin-releasing peptide (PrRP) was discovered in the last decade (Hinuma *et al.* 1998). It has been showed that PrRP- or PrRP mRNA-positive neurons are present only in three areas of the rat brain: in the hypothalamic dorsomedial nucleus (DM), in the nucleus of the solitary tract (NTS) and in the ventral and lateral reticular nuclei in the caudal ventrolateral medulla (Minami *et al.* 1999; Yamakawa *et al.* 1999).

Prolactin-releasing peptide plays a significant role in the regulation of the hypothalamo-pituitary–adrenal (HPA) axis (Matsumoto *et al.* 2000; Maruyama *et al.* 2001; Morales and Sawchenko 2003; Samson *et al.* 2003; Zhu and Onaka 2003; Adachi *et al.* 2005; Mera *et al.* 2006; Ohiwa *et al.* 2007) in

Received June 5, 2007; revised manuscript received August 13, 2007; accepted September 14, 2007.

Address correspondence and reprint requests to Zsuzsanna E. Tóth, Neuromorphological and Neuroendocrine Research Laboratory, Department of Anatomy, Histology and Embryology of the Semmelweis University and the Hungarian Academy of Sciences, Tüzoltó-utca 58, H-1094 Budapest, Hungary. E-mail: tothzs@ana.sote.hu

Abbreviations used: ACTH, adrenocorticotrophin; AVP, vasopressin; CRH, corticotrophin-releasing hormone; DIG, digoxigenin; DM, dorsomedial nucleus; DMX, dorsal motor nucleus of the vagus; ER, estrogen receptor; GRE, glucocorticoid responsive element; HPA, hypothalamo-pituitary–adrenal axis; ISH, *in situ* hybridization; NTS, nucleus of the solitary tract; OVX, ovariectomy; PBS, phosphate-buffered saline; PrRP, prolactin-releasing peptide; PVN, paraventricular nucleus; RR, repeated restraint; TH, tyrosine hydroxylase.

addition to influencing energy balance by acting as an anorexigen, it reduces food intake and body weight gain (Seal *et al.* 2001; Lawrence *et al.* 2002).

As chronic stress challenges both the endocrine regulation and the energy balance and is characterized by a decrease in body and thymus and increase in adrenal weights, consistent with the chronic activation of the HPA axis and elevated basal serum corticosterone levels (Du Ruisseau *et al.* 1977; Blanchard *et al.* 1993) we assumed that PrRP is involved in chronic stress. To test our hypothesis, we examined PrRP mRNA and protein expression in the brain following 7 days of daily restraint. It has been showed in our previous work that this procedure was effective to induce chronic stress symptoms in rats (Zelena *et al.* 2004).

Parvocelullar neurons of the hypothalamic paraventricular nucleus (PVN) coexpress corticotrophin-releasing hormone (CRH) and vasopressin (AVP) that elicit adrenocorticotrophin (ACTH) and glucocorticoid responses to stress by potentiating each other's actions (Kiss *et al.* 1984; Sawchenko *et al.* 1984). After adrenalectomy and in chronic stress, AVP expression is increased in the CRH neurons of the PVN, suggesting changes in regulatory mechanisms (Dallman 1993; Aguilera 1994). We wondered if a similar phenomenon exists between tyrosine hydroxylase (TH) (the rate limiting enzyme of the norepinephrine biosynthesis) and PrRP which are coexpressed in the brainstem A1 (caudal ventrolateral medulla) and A2 (NTS) catecholaminergic cell groups responsible for the stress-induced noradrenergic activation of the PVN (Pacak *et al.* 1993; Petrov *et al.* 1993; Chen *et al.* 1999; Sun *et al.* 2005a). Therefore, we examined if there was a correlation between changes in TH and PrRP mRNA and protein levels in the brainstem during chronic stress.

In response to acute as well as chronic stress gender-related differences have been found by several groups (Galea *et al.* 1997; Zelena *et al.* 2004; Serova *et al.* 2005). Effect of PrRP can be also dependent on sex; it stimulates AVP secretion only in female rats (Maruyama *et al.* 1999). Furthermore, estrogen suppressed c-*fos* activation of the PrRP neurons in the NTS after acute restraint stress (Adachi *et al.* 2005). In agreement with this finding estrogen receptor alpha (ERα) receptors were shown to be present in the NTS PrRP-expressing neurons (Kataoka *et al.* 2001). Thus, we decided to study if the PrRP reaction to the chronic stress is gender dependent. To test this, we performed our experiments both on male and female rats.

Finally, as in response to acute restraint the presence of intact efferents from the PVN was shown to be essential for c-*fos* activation of medullary catecholaminergic neurons (Dayas *et al.* 2004), we assumed that these fibers might also be able to influence the RR stress-induced activity of the medullary PrRP/TH neurons. To test the hypothesis, bilateral PVN lesions have been performed *prior* to restraint, in one group of male animals.

Materials and methods

Animals

We used male and female Wistar rats (Charles-Rivers, Gödöllő, Hungary) weighing 250–300 g. Rats were kept under standard laboratory conditions fed *ad libitum* and allowed to drink tap water. Experiments were performed according to the regulations set up by the Hungarian Council for Animal Care and were supervised by the Institutional Animal Care and Use Committee of the Institute of Experimental Medicine, Hungarian Academy of Sciences.

Repeated restraint

Repeated restraint is a combined psychological–physical stress stimulus. As was shown previously, 7 days of daily restraint is sufficient for the animals to develop symptoms of chronic stress (Zelena *et al.* 2004). Two independent experiments were performed. Rats were divided into four groups: control male, control female, chronic restraint stressed (RR) male, and RR female with total number of 12 animals per each group. The animals endured restraint stress every day at the same time for 1 h between 9:00 and 12:00 AM for 7 days as described previously (Zelena *et al.* 2003). Briefly, the animals were placed into transparent plastic tubes (5–6 cm inner diameter) having a 4 cm long conical head part ending with a large breathing hole. Behind the body, the rear end of the tube was loosely packed with paper towels. Body weights were measured before the first and (7 days later) after the last restraint. Twenty-four hours after the last restraint all animals were killed by decapitation. After decapitation trunk blood was collected for hormonal measurements, the adrenal and the thymus weights were determined, and the brains were removed quickly, frozen on dry ice and stored at −80°C until used for single and double *in situ* hybridization (ISH) histochemistry. The experiment was repeated for PrRP and TH autoimmunoradiography ($n = 5$ for control and $n = 7$ for RR groups). At the end of the experiment the animals were deeply anesthetized by i.p. injection of ketamine (50 mg/kg; SelBruHa Állatgyógyászati Kft, Budapest, Hungary), xylazine (20 mg/kg; Spofa, Prague, Czech Republic), promethazinium chloratum (0.2 mL/kg; EGIS, Budapest, Hungary), and perfused transcardically with 4% paraformaldehyde solution. The stage of the estrus cycle of females was determined by examining vaginal cytology, and only females in diestrus or metestrus were used for the study. The brains were removed and the brainstems were transferred into 10% and 20% sucrose then cut into 20 μm thick serial coronal sections in a cryostat.

Paraventricular nucleus lesions

Male rats were divided into four groups: sham operated ($n = 10$), bilateral PVN lesioned ($n = 12$), sham operated, and chronic restraint stressed ($n = 10$), and bilateral PVN lesioned and chronic restraint stressed ($n = 8$). The operated animals were housed individually after surgery. The lesions were performed in deep anesthesia and placed stereotaxically, as described previously, using wire knifes fashioned from the stainless steel mandrel of a 20-gauge spinal needle. The lesions destroyed all CRH-containing cell bodies in the PVN because of an inverted cone-shaped lesion (3.0–3.8 mm in diameter at its base) (Makara and Kovacs 1997). Control rats were subjected to sham operations consisting of opening the skull and introducing the knife into the midline in the brain to a position

5.0 mm below the brain surface, i.e. just above the hypothalamus. From the fifth day after surgery, one group of sham operated and one group of PVN-lesioned rats were subjected to the RR. To evaluate the PVN lesions histologically, the brains were removed and frozen on dry ice. The hypothalami were serially sectioned in a cryostat in the coronal plane. Every fifth 12 μm thick section was stained for hematoxilin–eosin and the location and the extent of the lesions were recorded. Only rats showing a distinct and complete lesion were retained for later analysis by single and double ISH histochemistry.

Ovariectomy

Rats were divided into three groups. Female rats were ovariectomized (n = 7) and at the same time sham operations were performed on control female (n = 5) and male rats (n = 5). The cycle of the females was followed and 2 weeks later, the rats were perfused with 4% paraformaldehyde. The perfusion was performed in three consecutive days, in a way that control females in met- or diestrus were performed together with control males and ovariectomy (OVX) females. The brains were removed and cryoprotected using 10% and 20% sucrose solution, cut into four 20 μm thick serial coronal sections under Rnase-free conditions in a cryostat, and stored in sterile anti-freeze medium at −20°C until used. One series of sections were used for PrRP immunoautoradiography, another series was mounted on Superfrost Plus slides (Fisher Scientific, Pittsburgh, PA, USA) and used for ISH for PrRP mRNA.

Determination of plasma prolactin and corticosterone levels

Trunk blood was collected in K-EDTA containing tubes on ice. After centrifugation, the plasma was stored at −20°C until measurements were performed. For prolactin radioimmunoassay, we used materials donated by the Pituitary Program (National Institute of Diabetes, Digestive and Kidney Diseases, Bethesda, MD, USA). The intra-assay and interassay coefficients of variation were 11.35% and 11.72%, respectively. Plasma corticosterone was measured from 10 μL unextracted plasma with a radio-immuno assay using a specific antiserum developed in the Institute of Experimental Medicine, Budapest, Hungary (Makara and Kovacs 1997; Zelena *et al.* 2003). The intra- and interassay coefficients of variation were 6.4% and 16.6%, respectively. The sensitivity of the prolactin and corticosterone radio-immuno assay were 2 ng/mL and 20 pmol/mL, respectively.

Probes for the *in situ* hybridizations

The probe for the PrRP ISH was generated by cloning a 230 bp long cDNA fragment of the prepro-PrRP cDNA (10–240 bp of the coding sequence, GenBank accession number AB015418) into a Bluescript II SK vector (Stratagene, La Jolla, CA, USA). The identity of the clone was confirmed by DNA sequence analysis. The radioactively-labeled [^{35}S]UTP (NEN, Boston, MA, USA) riboprobe for the ISH was prepared by *in vitro* transcription using a Maxiscript Kit (Ambion, Austin, TX, USA). For the TH ISH the cDNA probe, a fragment of the TH cDNA (GenBank accession number M23598) corresponding to nucleotides 684–1068 of the coding sequence was kindly provided by Dr W. S. Young (Young *et al.* 1987). The digoxigenin (DIG)-labeled riboprobe was prepared by *in vitro* transcription using the DIG RNA Labeling Kit (Roche, Budapest, Hungary).

In situ hybridization

Medullary and the caudal hypothalamic regions of the fresh frozen brains were cut into 12 μm thick coronal sections in a cryostat. The sections were thaw-mounted and air-dried at 37°C onto positively charged Superfrost Plus slides. The slides were then stored at −80°C until used. Six continuous series of sections were cut from the caudal medulla, and adjacent sections were placed on identical location of the slides. Perfused fixed sections from the OVX experiment were microwaved for antigen retrieval in 10 mmol/L citric acid buffer (pH 6.0) for 5 min after the liquid started to boil and then cooled at 25°C for 30 min. The slides were hybridized overnight in humid chambers at 55°C with 10^6 cpm/slide of the [^{35}S]UTP-labeled probes [for more details see (Zelena *et al.* 2003)]. For the double ISHs, we mixed 1 μL (350–400 ng/μL) of DIG-labeled TH probe with 10^6 cpm [^{35}S]UTP-labeled PrRP probe per slide. The sections were washed the next day and those for double ISH were processed for DIG immunohistochemistry according to the instructions of the DIG Nucleic Acid Detection Kit (Roche). The radioactive ISHs were exposed to Kodak Bio-Max MR films (Sigma, Budapest, Hungary) and later dipped into NTB3 nuclear track emulsion (Eastman Kodak Co., Rochester, NY, USA), or in case of double ISHs into Ilford G.5 Nuclear Research emulsion (Polysciences Inc., Warrington, PA, USA). After appropriate incubation times (as judged from the X-ray films) at 4°C in the dark, the emulsion-coated slides were developed using Kodak Dektol developer and fixer at 18°C (Kodak). The single ISH sections were counter-stained with 0.5% Giemsa solution (Sigma), air dried and coverslipped using Cytoseal 60 mounting medium (Stephens Scientific, Riverdale, NJ, USA). The double-labeled (DIG and radioactivity) sections were not counter-stained.

Quantitative analysis of the ISH signals

Quantitative analysis of ISH was performed only on undamaged sections showing clear signal using darkfield microscopical images and the Image J 1.32j software (Wayne Rasband; NIH, Bethesda, MD, USA), as previously reported (Zelena *et al.* 2003). Results were expressed as pixels per labeled cells (i.e. cell surface covered by grains) occupied by the silver grains and the number of labeled cells/section. For each cell, three background samples were taken over an equivalent area surrounding the cell, and the signal threshold was calculated as pixel value of background +3.0 SD. Only cells with pixel values above these criteria were included in the analysis. The analysis was made between the level of the obex and 0.6 mm caudal to it in case of the A1 cell group, and at the obex ± 0.12 mm in case of the A2 cell group, where the number and the signal intensity of PrRP-expressing neurons were the highest. At least data of 3–4 sections per animal on both sides were analyzed, taking care of matching the rostrocaudal level of the sections between the animals. The average/animal data were used for further statistical evaluation. Darkfield images of the sections were taken through red or green filters and then overlayed with the brightfield image of the same area in Adobe Photoshop 5.0 for demonstration in the figures (Adobe Systems Inc., McLean, VA, USA).

Determination of PrRP–TH ratio

To get the optimal sensitivity for both PrRP and TH ISH, neighboring (12 μm apart) sections were hybridized separately for TH or PrRP mRNAs with appropriate [^{35}S]UTP-labeled probes. As PrRP-positive cells are subsets of brainstem noradrenergic neurons

comprising the A1 and A2 catecholaminergic cell groups (Sun *et al.* 2005a), the percentage of PrRP-positive cells among the total number of TH-positive cells in an area was calculated for each pair of sections. To confirm the accuracy of the results, we also colocalized the PrRP and TH mRNAs by double ISH technique using DIG-labeled TH and [^{35}S]UTP-labeled PrRP probes.

Immunoautoradiography

The fixative was washed out from the sections with phosphate-buffered saline (PBS) then the endogenous peroxidase was blocked using 3% H_2O_2 for 15 min at 25°C. Next, the sections were immersed in 1% bovine serum albumin and 0.5% Triton-X100 in PBS for an hour to block non-specific binding. The sections were then incubated with primary antibodies to TH (1 : 1000; Chemicon, Temecula, CA, USA) or PrRP 31 (1 : 8000; Phoenix Pharmaceuticals Inc., Belmont, CA, USA) overnight at 4°C or at 25°C, respectively. The following day, biotinylated secondary anti-mouse (for TH) and anti-rabbit (for PrRP) antibodies (Vector Laboratories, Burlingame, CA, USA) were applied in a 1 : 1000 dilution for 1 h at 25°C. The PrRP immunostaining was amplified using the ABC kit (Vector) and biotinylated tyramide. The immunostainings were detected by [^{35}S]-labeled streptavidin (NEN) used in 1 : 2000 for the TH and 1 : 1000 for the PrRP. The sections were washed, mounted on pre-cleaned glass slides (Fisher), dehydrated in ethanol series and exposed to BAS-MS 2340 Imaging Plate (FujiPhotoFilm Co. Ltd, Tokyo, Japan) for 3 and 7 days for TH and PrRP, respectively. For quantification, the average densities in 2–4 representative sections from the central region of the nuclei recorded on the phosphorimager were measured using the IMAGE QUANT software version 5.2 (Amersham Biosciences, Piscataway, NJ, USA).

Double immunostaining for ERα or ERβ and PrRP

Brainstem and hypothalamic sections of female rats in met- or diestrus (n = 3) prepared the same way as for the immunoautoradiography were washed in PBS and treated with 1% sodium borohydride for 10 min. After thorough washing steps the sections were incubated in 1X Universal Blocking Reagent (Biogenex, San Ramon, CA, USA) for 30 min. Then, they were transferred to the ERα (1 : 30 000 rabbit; Upstate, Lake Placid, NY, USA) or ERβ (1 : 250, rabbit; Zymed Laboratories, San Francisco, CA, USA) antibodies for 3 days, at 4°C. The sections were exposed to a biotinylated anti-rabbit secondary antibody (1 : 1000; Vector) for 1 h, and incubated in ABC reagent (Vector) also for 1 h. The immunostaining was amplified by biotin–tyramide reaction and visualized by Streptavidin AlexaFluor 594 (1 : 1000; Invitrogen, Eugene, OR, USA). Then, the sections were microwave treated for 5 min in citric acid buffer (pH 6.0) and cooled for 30 min. For the second immunostaining the anti-PrRP-31 (1 : 8000; Phoenix) antibody was applied overnight, at 25°C. The PrRP immunostaining was developed using peroxidase-conjugated anti-rabbit secondary antibody for 2 h (1 : 100; Vector) followed by a 10 min incubation in FITC-tyramide (Invitrogen). Images were captured on a Leica DMI 6000 fluorescence microscope equipped with an Orca-AG camera (Leica, Bannockburn, IL, USA) and operated by the VOLOCITY 4.0 software (Improvision, Lexington, MA, USA). Fluorescence was detected using standard 4′,6-diamidino-2-phenylindole, FITC, Texas Red filter sets. Optical sections along the Z-axis were acquired with increments of 0.5 μm. The fluorescent data sets were deconvolved by VOLOCITY 4.0 program.

Statistical analysis

Two-way ANOVA was used to analyze hormonal data, weight changes, and changes in mRNA, as well as protein expression in male and female rats after restraint. One-way ANOVA was used to determine statistical significances for bilateral PVN lesions and effect of OVX using the STATISTICA software package (Tulsa, OK, USA). In the case of significance, ANOVA was followed by multiple pairwise comparisons according to the Newman–Keuls method. Grains/cell and cell number, as well as optical density data were expressed as percent of the male control to make the data from different hybridization and immunoautoradiographic procedures comparable. To achieve homogeneity of the variance, RR data for PrRP grains/cell and cell number values in the A1 cell group, RR data for PrRP/TH ratio in the NTS and prolactin concentration data were transformed using logarithms in the analysis. As the sham operations did not have any special effect on the brainstem's mRNA expression normalized data of control males and sham-operated males, as well as data of RR males and sham RR males were pooled for statistical analysis. Values are presented as means ± SEM. For the A1 cell group the analysis was made at rostrocaudal levels of the medulla, between the obex and 0.6 mm caudal to the obex. For the A2 cell group the analysis was made at the level of the obex ± 0.12 mm rostrocaudally.

Results

Weight and hormonal changes related to chronic repeated restraint

Body weight gains of RR animals lagged behind the controls both in males and females, which corresponds for a state of a chronic stress (Table 1). Other typical signs of the chronic stress, like adrenal mass increase and thymus weight loss (mg/body weight kg) were only observed in the males (Table 1). Serum corticosterone levels were elevated after RR in both genders and there was no measurable change in serum prolactin levels (Table 1).

PrRP and TH mRNA expression in the brainstem as a function of gender and repeated restraint

In agreement with former studies (Minami *et al.* 1999; Yamakawa *et al.* 1999), we found PrRP mRNA in three areas in the brain; in the A1 and A2 cell groups and in the DM of the hypothalamus.

Within the A1 catecholaminergic cell group (see Fig. 1, schematic drawing for illustration) both the basal PrRP mRNA expression/cell and the number of the PrRP mRNA-positive cells were higher in the females than in the males in the control (non-stressed) groups. Both parameters were significantly elevated in both genders following RR. However, this elevation was relatively smaller in the females, because of their higher basal PrRP mRNA levels (Fig. 2a and b). As PrRP and TH are coexpressed in neurons of the A1 cell group of the brainstem (Chen *et al.* 1999), we also examined the TH mRNA levels in this cell group. Unlike the basal PrRP

Table 1 Effect of chronic repeated restraint (RR) on weight and hormonal changes of male and female rats

	Body weight gain (g)	Relative adrenal weight (mg/bw kg)	Relative thymus weight (mg/bw kg)	Corticosterone (pmol/mL)	Prolactin (ng/mL)
Control-male	45.6 ± 2.5	145.8 ± 5.0	2002.6 ± 105.7	74.4 ± 17.4	2.7 ± 0.5
RR-male	22.3 ± 3.1*	181.6 ± 10.0*	1460.8 ± 16.4*	636.2 ± 56.4*	4.7 ± 1.1
Control-female	10.8 ± 1.8	322.2 ± 12.2	2011.7 ± 309.9	234.4 ± 71.6	2.2 ± 0.7
RR-female	4.0 ± 1.3#	319.4 ± 17.3	2088.5 ± 115.5	682.8 ± 118.3#	2.4 ± 0.6

Body weight (bw) gains of RR animals lagged behind the controls both in males and females, corresponding to a state of chronic stress ($p < 0.001$, $n = 8$). Other signs of chronic stress, such as relative (mg/bw kg) adrenal mass increase ($p < 0.05$, $n = 6$) and thymus weight loss ($p < 0.05$, $n = 5$) were typical only of males. RR had significant effect on plasma corticosterone levels both in males and females ($p < 0.001$), but not on plasma prolactin levels. Corticosterone measurements: $n = 7–9$, prolactin measurements: $n = 9–12$. *Significant versus control male, #significant versus control female, mean ± SEM.

mRNA expression, there was no gender difference in the basal TH mRNA expression/cell and the number of the TH-positive cells in control animals. However, similarly to the PrRP mRNA expression both parameters elevated significantly following RR, but in this case without gender-related differences (Fig. 2c). The relative changes in the PrRP grains/cell values in males, and the PrRP cell number values in both genders were higher than the relative changes in the TH grains/cell and cell number values (Fig. 2b and c).

Prolactin-releasing peptide-producing cells are also present in the dorsomedial medulla, colocalized with TH-positive neurons that belong to the A2 cell group (see Fig. 3, schematic drawing) (Minami *et al.* 1999; Yamakawa *et al.* 1999). Here, similarly to the A1 group we found a gender-related difference in the basal PrRP mRNA production of the individual cells, but not in the number of the PrRP mRNA-positive cells (Fig. 4a and b). The RR had no effect on PrRP mRNA production of females but both the grains/cell and the cell number values elevated in males (Fig. 4a and b).

Hence, in both investigated cell groups in the brainstem, females had higher basal PrRP mRNA expression along with a less sensitive PrRP mRNA response to RR compared with males. As only the catecholaminergic neurons in the A2 cell group colocalize with PrRP, and they are present in both the NTS and the dorsal motor vagal nucleus (DMX), we performed quantification of the TH mRNA signal separately in these two vagal nuclei (see Fig. 3, schematic drawing). There was no gender-related difference in the basal TH mRNA expression in either part of the A2 cell group. RR did not elicit significant elevation in these neurons (Fig. 4c).

As both in the A1 and in A2 neurons RR evoked a more enhanced alteration of the PrRP mRNA levels than that of the TH mRNA levels, we wondered, whether it also caused a change in the proportion of the neurons that express both PrRP and TH compared with the exclusively TH-expressing neurons in these cell groups. The fraction of both PrRP and TH mRNA colocalizing cells, among the only TH-expressing neurons in the A1 cell group was significantly higher in control females than that in control males (Figs 1 and 5a).

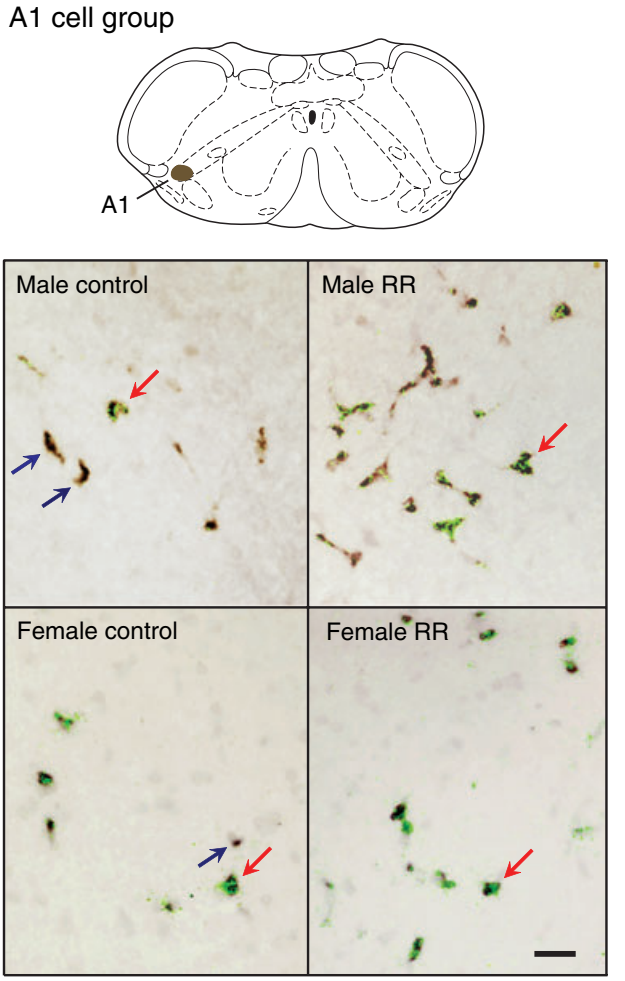

Fig. 1 Double *in situ* hybridization (ISH) for tyrosine hydroxylase (TH) and prolactin-releasing peptide (PrRP) mRNAs in the A1 cell group. A schematic drawing of a representative coronal section of the medulla (bregma −14.60 mm) illustrates the location of the A1 group. On the microphotographs, TH-positive cells (DIG-alkaline-phosphatase reaction product) are in brown, signals for PrRP ISH (silver grains) are shown in green. Red arrows show examples for double-labeled cells; blue arrows show examples for single labeled, TH mRNA-positive cells. RR, chronic repeated restraint. Scale bar: 50 μm.

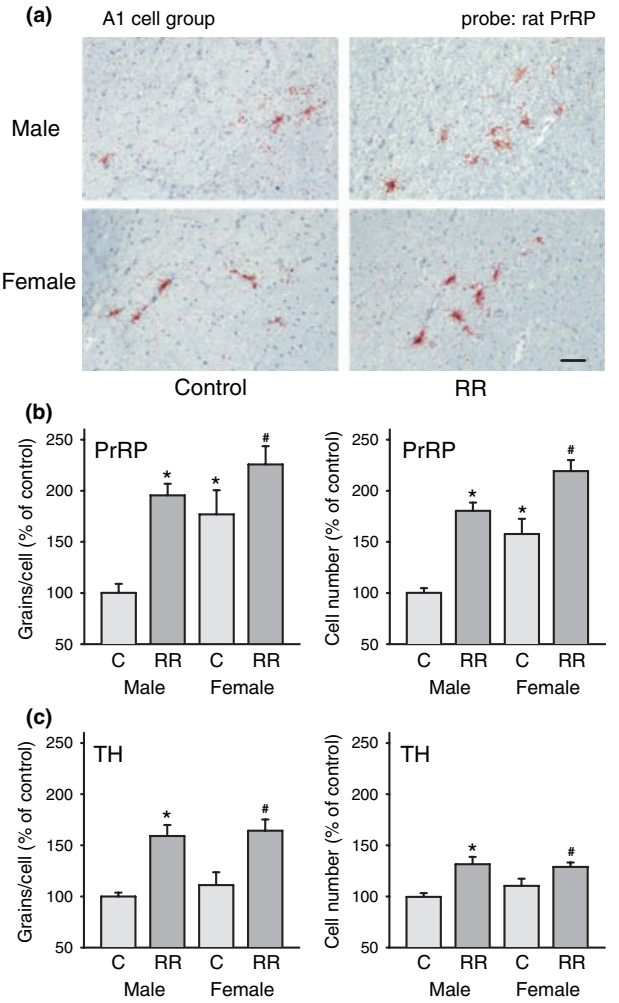

Fig. 2 Effect of chronic repeated restraint (RR) on prolactin-releasing peptide (PrRP) and tyrosine hydroxylase (TH) mRNA expression in the A1 cell group. (a) *In situ* hybridization (ISH) for rat PrRP mRNA. Sections were counter-stained with Giemsa solution, the ISH signal is shown in red. Scale bar: 50 μm. (b) Quantification of PrRP ISH, mean ± SEM. Relative grains/cell and cell number values expressed in the percent of male control are shown on the left and the right side, respectively. Grains/cell: control male versus control female and RR within males $*p < 0.001$, RR within females $\#p < 0.05$, $n = 9–16$. Cell number: control (C) male versus control female (*), RR within males (*) and RR within females $\#p < 0.001$, $n = 9–19$. (c) Quantification of TH ISH plotted the same way as on (b). The scaling on (b) and on (c) is the same. Grains/cell: RR within males (*) and RR within females $\#p < 0.001$, $n = 9–16$. Cell number: RR within males $*p < 0.001$, RR within females $\#p < 0.05$, $n = 9–16$. Pictures were taken and the analysis was made on similar sections at rostrocaudal levels of the medulla, between the obex and 0.6 mm caudal to the obex.

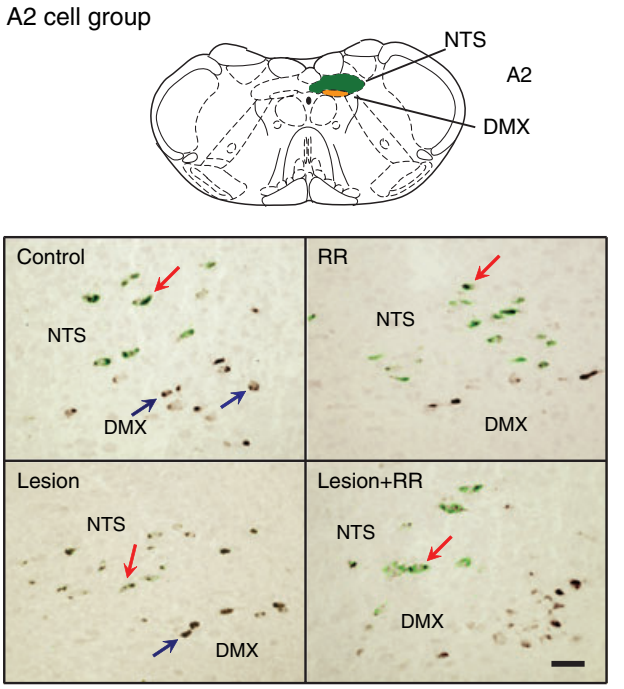

Fig. 3 Double *in situ* hybridization for tyrosine hydroxylase (TH) and prolactin-releasing peptide (PrRP) mRNAs in the A2 cell group in male rats. The schematic drawing above shows a representative coronal section of the medulla (bregma −14.08 mm) to illustrate the location of the A2 cell group and its NTS and DMX part. On the microphotographs, TH-positive cells (DIG-alkaline-phosphatase reaction product) are in brown, signals for PrRP *in situ* hybridization (ISH) (silver grains) are shown in green. Red arrows show examples for double-labeled cells; blue arrows show examples for single labeled, TH mRNA-positive cells. DMX, dorsal motor nucleus of the vagus; NTS, nucleus of the solitary tract; RR, chronic repeated restraint. Scale bar: 25 μm.

RR caused a rise in the PrRP/TH ratio in both genders, indicating that, in fact, A1 cells which do not express PrRP mRNA (or do it but below the detection level) under control conditions started to express PrRP mRNA in response to RR (Figs 1 and 5a). Relatively more cells started to coexpress PrRP mRNA with TH mRNA for RR in males than in females (Figs 1 and 5a). In the NTS, there was no gender-related difference between the PrRP/TH ratios of the control animals (Fig. 5b). There was no change in females to the RR here, but the PrRP/TH ratio became elevated in males after RR (Fig. 3, upper images; Fig. 5b).

In summary, we found two types of differences in the brainstem: one is cell group specific; the other one is gender specific. RR did not affect TH mRNA expression in A2 but elevated it in A1 neurons. Females reacted less sensitively to RR in both cell groups than males. It was common for both cell groups that the PrRP/TH mRNA ratio in the cells was increased in response to RR.

Effect of chronic repeated restraint on PrRP mRNA production of neurons in the hypothalamic dorsomedial nucleus

The third group of cells which produces PrRP in the rat brain is located in the DM of the hypothalamus (Fig. 6a). These cells do not colocalize with TH and we found no gender-related difference in their basal PrRP mRNA expression. RR

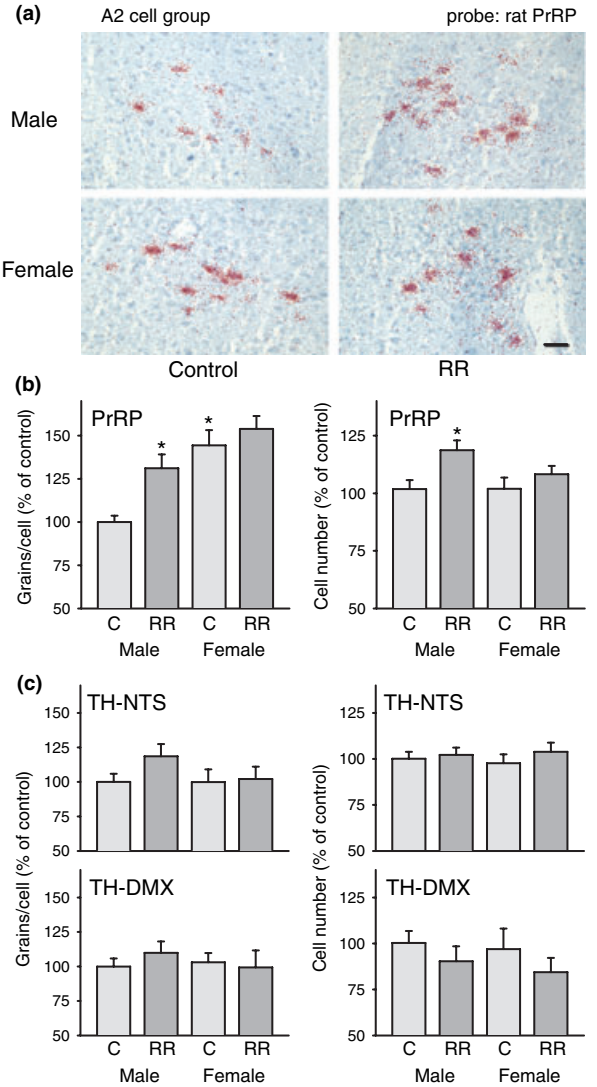

Fig. 4 Effect of chronic repeated restraint (RR) on prolactin-releasing peptide (PrRP) and tyrosine hydroxylase (TH) mRNA expression in the A2 cell group. (a) *In situ* hybridization (ISH) for rat PrRP mRNA. Sections were counter-stained with Giemsa solution, the ISH signal is shown in red. Scale bar: 25 μm. (b) Quantification of PrRP ISH, mean ± SEM. relative grains/cell and cell number values expressed in the percent of male control (C) are shown on the left and the right side, respectively. Grains/cell: control male versus control female and RR within males $*p < 0.001$, $n = 9–16$. Cell number: RR within males $*p = 0.003$, $n = 9–21$. (c) Quantification of TH ISH in the nucleus of the solitary tract (NTS) and in the dorsal motor nucleus of vagus (DMX) part of the A2 cell group, independently. The scaling on corresponding plots of (b) and (c) is the same. There is no significant difference, $n = 9–16$ for both the grains/cell and the cell number measurements. Pictures were taken and the analysis was made on similar sections at the level of the obex ± 0.12 mm rostrocaudally.

induced an increase in PrRP mRNA expression in both sexes to a similar extent, but only the grains/cell values changed significantly (Fig. 6a and b).

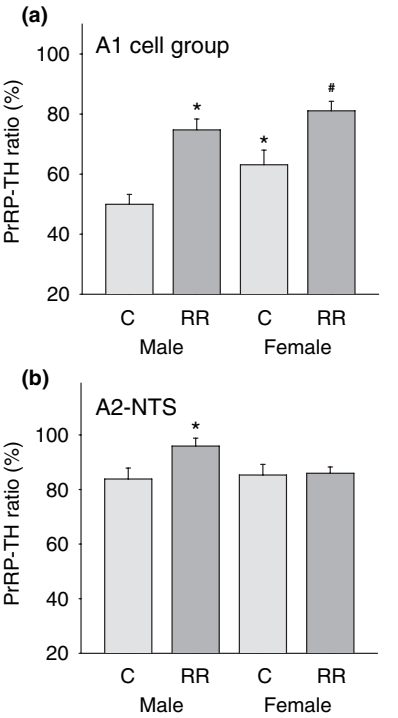

Fig. 5 Ratio of prolactin-releasing peptide (PrRP) and tyrosine hydroxylase (TH) mRNAs in the brainstem after chronic repeated restraint (RR). PrRP-positive cells in percentage of the TH-positive cells within the A1 cell group (a) and in the nucleus of the solitary tract (NTS) part of the A2 cell group (b) in male, female, control (C) and RR animals, mean ± SEM. Significant differences in (a): control male versus control female $*p < 0.05$, RR within males $*p < 0.001$, RR within females $\#p < 0.01$, $n = 9–16$. (b) Only RR within males is significant $*p < 0.01$, $n = 9–16$.

Effect of bilateral PVN lesions on chronic repeated restraint-evoked changes in PrRP and TH mRNA expression in the brainstem of male rats

The hypothalamic PVN is an integration center in the brain with bilateral neuronal connections to several brain areas including the A1 and A2 catecholaminergic cell groups in the medulla (Sawchenko and Swanson 1982; Luiten *et al.* 1985; Toth *et al.* 1999). Therefore, we performed bilateral PVN lesions *prior* to RR in male rats. We used male rats because they showed a more prominent reaction to RR both in the A1 and in the A2 areas, than females. Animals recovered from the adverse effects of the surgery by the time the chronic RR was applied, without developing long-term trophic changes in the HPA system, as reported earlier (Zelena *et al.* 2003). Interestingly, the bilateral PVN lesions influenced the basal PrRP and/or TH mRNA production of A2 neurons in the NTS, but not in the DMX. The grains/cell values dramatically decreased here, especially in case of PrRP mRNA, and this decrease was accompanied by a reduction of the number of PrRP mRNA-positive cells (Table 2). Although the A1 catecholaminergic cell group, like the A2, is known to have

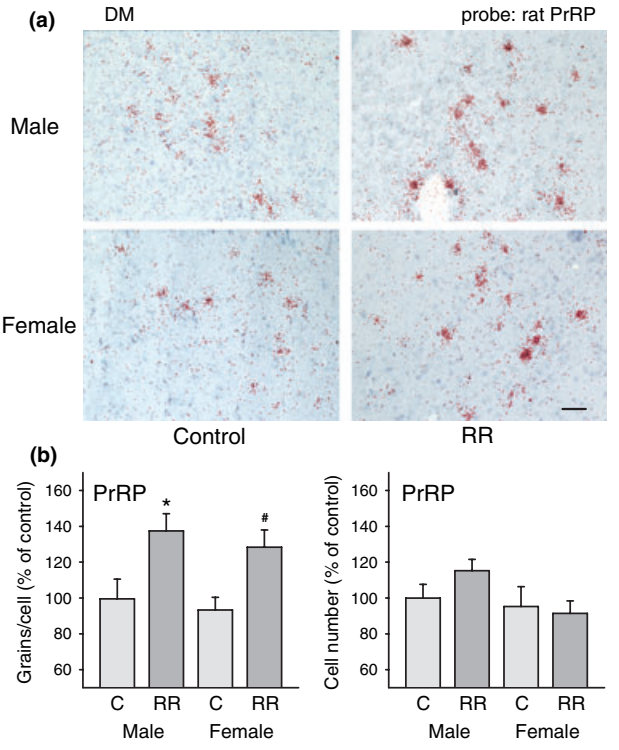

Fig. 6 Effect of chronic repeated restraint (RR) on prolactin-releasing peptide (PrRP) mRNA expression in the hypothalamic dorsomedial nucleus (DM). (a) *In situ* hybridization (ISH) for rat PrRP mRNA. Sections were counter-stained with Giemsa solution, the ISH signal is shown in red. Scale bar: 25 μm. (b) Quantification of PrRP ISH, mean ± SEM. Relative grains/cell and cell number values expressed in the percent of male control (C) are shown on the left and the right side, respectively. Grains/cell: RR within males (*) and RR within females #$p < 0.05$, $n = 10–16$. Cell number: there are no significant differences, $n = 11–17$. The pictures were taken and the analysis was made on similar sections at the rostrocaudal level between the stereotaxic coordinates P3400–P3600 μm from the bregma.

direct afferent and efferent connections with the PVN, the lesion of the nucleus by itself did not affect the PrRP or TH mRNA expression in the A1 cell group (Table 2).

The bilateral PVN lesions did not prevent the effects of RR in the A1 and in the A2 cell groups. RR evoked same kind of responses as we observed without the lesions (Table 2). The PrRP/TH ratio in the PVN lesion plus RR animals increased in the A1 cell group (Fig. 7a). In the NTS, the bilateral PVN lesions caused a reduction in the PrRP/TH ratio, but it has been increased after RR reaching the level of the controls (Figs 7b and 3, bottom images).

Changes in PrRP and TH protein levels in the brainstem, as a response to RR

To check whether the mRNA amounts were proportional to the protein levels, we repeated a part of these experiments and performed immuno-autoradiographic measurements for

Table 2 Effect of bilateral hypothalamic paraventricular nucleus (PVN) lesions on chronic repeated restraint (RR)-evoked prolactin-releasing peptide (PrRP) and tyrosine hydroxylase (TH) mRNA expression in the brainstem of male rats

	A1 – PrRP		A1 – TH		A2 – PrRP		A2 – TH			
					NTS		NTS		DMX	
	Grains/cell (%)	Cell number (%)	Grains/cell (%)	Cell number (%)	Grains/cell (%)	Cell number (%)	Grains/cell (%)	Cell number (%)	Grains/cell (%)	Cell number (%)
PVN lesion	108.9 ± 9.2	102.9 ± 7.4	105.3 ± 5.1	100.9 ± 8.4	51.3 ± 9.1*	83.2 ± 4.7*	63.9 ± 5.4*	92.4 ± 4.0	92.9 ± 10.2	105.2 ± 10.1
+RR	200.4 ± 16.0*	162.7 ± 10.0*	131.0 ± 5.9*	122.8 ± 4.6	88.3 ± 5.2#	102.9 ± 5.1#	84.6 ± 12.3	102.5 ± 1.8	111.3 ± 14.6	92.2 ± 5.1

Data are relative to the sham-operated control (100%). In the A1 cell group there was no significant change after bilateral PVN lesions either in the PrRP or in the TH mRNA expression. PVN lesions did not prevent the effect of RR, which resulted in an elevation of PrRP grains/cell, and cell number ($p < 0.001$) and TH grains/cell values ($p < 0.01$), $n = 8–11$ for PrRP and $n = 4–9$ for TH mRNA *in situ* hybridization measurements. In the nucleus of the solitary tract (NTS) part of the A2 cell group bilateral PVN lesions reduced the production of PrRP and TH mRNA ($p < 0.001$ and 0.01 vs. sham control, $n = 4–8$), as well as the number of PrRP-positive cells ($p < 0.05$ vs. sham control, $n = 8–12$), while there was not any change in TH mRNA expression in the dorsal motor nucleus of vagus part (DMX) of the A2 cell group ($n = 4–8$). The PVN lesions did not prevent either the stimulatory effect of RR on PrRP mRNA ($p < 0.01$) production of the cells, or the increase in the number of the PrRP mRNA-positive cells ($p = 0.014$), mean ± SEM. *Significant versus sham control, #significant versus PVN lesion.

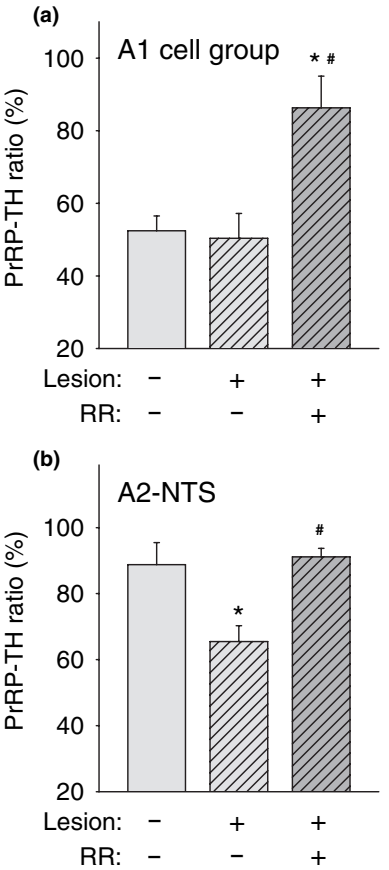

Fig. 7 Effect of bilateral paraventricular nucleus (PVN) lesions and chronic repeated restraint (RR) on ratio of prolactin-releasing peptide (PrRP) and tyrosine hydroxylase (TH) mRNAs in the brainstem. PrRP-positive cells in percentage of the TH-positive cells within the A1 cell group (a) and in the nucleus of the solitary tract (NTS) part of the A2 cell group (b) in sham-operated control (−;−), bilateral PVN lesioned (+;−) and bilateral PVN lesioned and RR (+;+) animals, mean ± SEM. (a) Only the effect of RR is significant versus the sham control (*) and versus the PVN lesion #$p < 0.01$, $n = 4–8$. (b) The effect of bilateral PVN lesions is significant versus the sham control *$p < 0.01$ and versus the PVN lesion and RR #$p < 0.05$, $n = 4–8$.

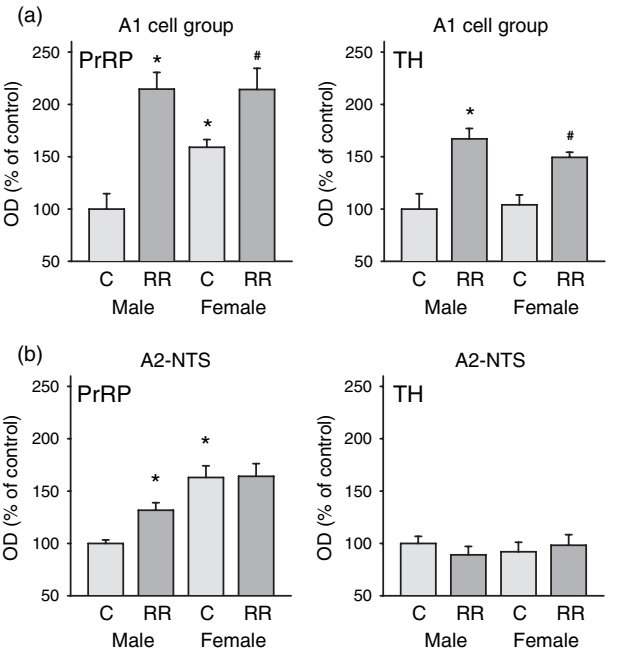

Fig. 8 Immunoautoradiographic measurements for prolactin-releasing peptide (PrRP) and tyrosine hydroxylase (TH) after chronic repeated restraint (RR). Immunoautoradiographic records for PrRP and TH in the A1 (a) and in the A2 (b) cell groups, mean ± SEM. Relative average optical density values for PrRP and TH expressed in the percent of male control (C) are shown on the left and the right sides, respectively. Note the same scaling for PrRP and TH ($n = 5–7$). (a) PrRP: control male versus control female and RR within males *$p < 0.05$ and $p < 0.001$, respectively. RR within females #$p < 0.05$. TH: RR within males (*) and RR within females (#) $p < 0.01$. (b) PrRP: control male versus control female and RR within males *$p < 0.001$, and $p < 0.05$, respectively. TH: there is no significant difference.

PrRP and TH. Kataoka *et al.* (2001) showed that PrRP mRNA levels in the NTS are higher in proestrus than that in diestrus or in male rats. Anderson *et al.* (2003) did not find any significant changes in PrRP expression in any area during the estrus cycle by real-time Taqman RT-PCR. Because of this controversy we used only females in diestrus or in metestrus.

As it can be seen on Fig. 8, PrRP and TH protein quantities in the different experimental groups were analogous to the appropriate mRNA measurements. Females had a higher basal PrRP levels than males both in the A1 and in the A2 cell groups (Fig. 8a and b, left), while there was no gender-related difference in the TH levels (Fig. 8a and b, right). In the A1 cell group, both PrRP and TH levels were elevated in response to RR in both sexes, and elevation of PrRP levels were higher than that in TH in males (Fig. 8a). The elevation of PrRP in the A1 cell group was smaller in females than in males (Fig. 8a, left). In the A2 cell group, RR-evoked elevation of PrRP only, and only in males (Fig. 8b).

Colocalization of PrRP with estrogen receptor α and β and effect of ovariectomy on PrRP expression in the brainstem

To understand the gender-related differences we found in the PrRP expression and response to RR, double immunostainings were performed for PrRP and ERα or β. In addition, the effect of OVX was also investigated on the PrRP expression in control rats. PrRP and ERα colocalized in the neurons of the A1 and A2 cell groups (Fig. 9a), but not in the PrRP-positive cells of the DM (not shown). PrRP and ERβ did not colocalize in any of the cell groups studied, although in the A2 cell group PrRP and ERβ immunopositive cells intermingled in the NTS (data not shown). OVX significantly decreased PrRP mRNA and protein expression both in the

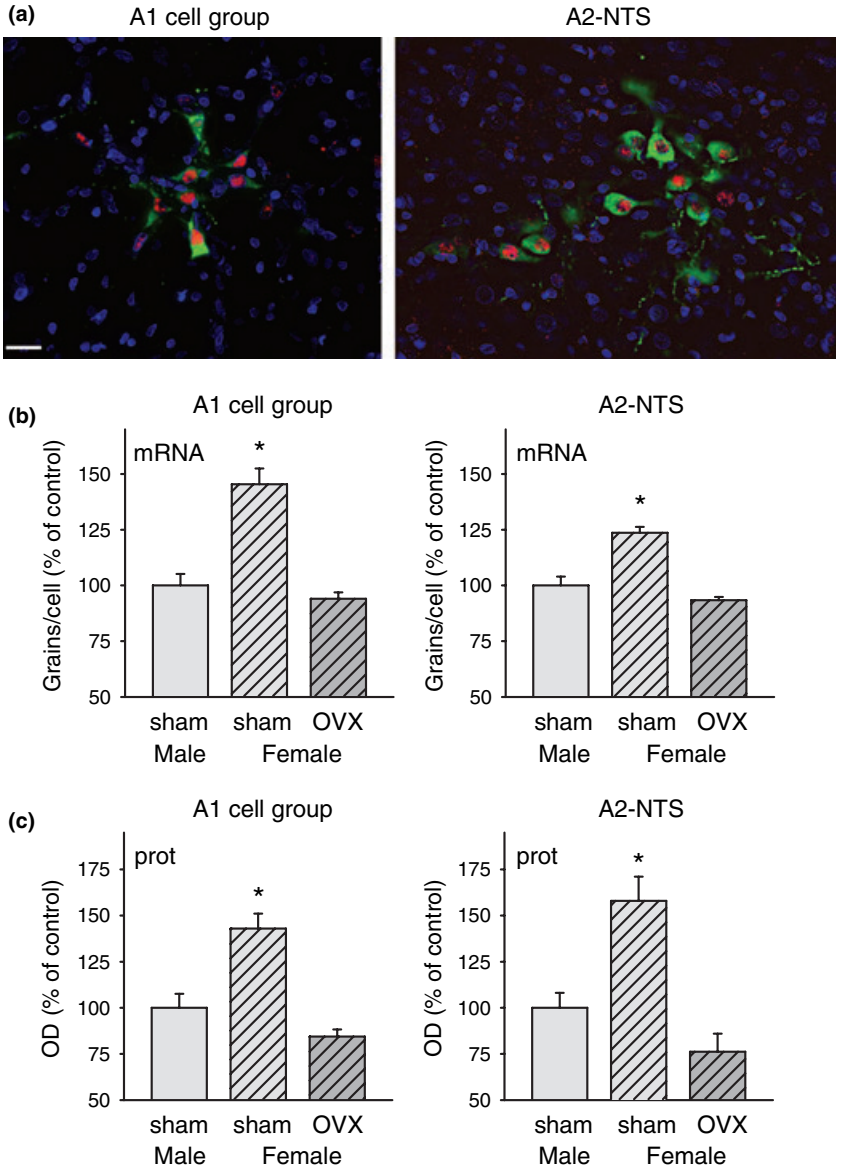

Fig. 9 Effect of ovariectomy (OVX) on prolactin-releasing peptide (PrRP) expression and colocalization of estrogen receptor α (ERα) and PrRP in the brainstem. (a) Double fluorescent immunostaining for ERα (red nuclei) and PrRP (green cytoplasmatic staining) in the neurons of the A1 (left) and A2 (right) cell groups. The sections were counter-stained with DAPI (blue). The pictures were taken and the analysis was made on similar sections at rostrocaudal levels in the medulla between the obex and 0.6 mm caudal to the obex and at obex ± 0.12 mm for the A1 and A2 cells, respectively. Scale bar: 25 μm. Quantification of PrRP ISH (b) and immunoautoradiography (c) after ovariectomy in the A1 and A2-NTS cell groups shown on the left and the right side, respectively, mean ± SEM. Relative grains/cell and average optical density values are expressed in the percent of male control. Sham male versus sham female on each panel $^*p < 0.001$, $n = 5–7$.

A1 and in the A2-NTS cell groups compared with the sham-operated females (Fig. 9b and c). These data suggest that estrogen acting probably through ERα plays an important role in the regulation of PrRP gene expression in the brainstem.

Discussion

Effect of chronic repeated restraint on PrRP expression in the brain

Previous data suggested the involvement of PrRP-producing neurons in acute stress (Maruyama *et al.* 2001; Morales and Sawchenko 2003; Zhu and Onaka 2003; Adachi *et al.* 2005; Mera *et al.* 2006). PrRP applied intracerebroventricularly elevated plasma ACTH and corticosterone levels through an effect on CRH neurons in the PVN (Matsumoto *et al.* 2000; Mera *et al.* 2006). We wondered if there was any change in PrRP mRNA and protein levels in response to a chronic stress situation. We applied RR stress in our experiments for three reasons: (i) as far as to our present knowledge, the role of PrRP in chronic stress situation has not been investigated, yet; (ii) it is an interesting question, as in chronic stress not only the HPA axis is activated, but the metabolism of the organism is also changed. Alterations in the metabolism are manifested, for example, in a reduced body weight of the rats, and PrRP was shown to be involved in the regulation of food intake and energy balance (Seal *et al.* 2001; Ellacott *et al.* 2002; Lawrence *et al.* 2002; Sun *et al.* 2005b); and (iii) we used 7 days of daily restraint stress because previously it proved to be an appropriate long and strong

stimulus to evoke the known signs and parameters typical to chronic stress in rats (Zelena *et al.* 2003).

Data presented here support our hypothesis that PrRP is involved in response to chronic stress. PrRP protein and/or PrRP mRNA levels were elevated in the three cell groups investigated in male rats following chronic stress. We also wondered what is the exact role of the elevated PrRP level in the DM and in the brainstem in response to chronic restraint. Reportedly, the DM participates in the regulation of body temperature (Zaretskaia *et al.* 2002), in the regulation of food intake (Bellinger and Bernardis 2002), and also in cardiovascular regulation (McDowall *et al.* 2006). PrRP has been suggested to play a role of all of these functions (Samson *et al.* 2000; Seal *et al.* 2001; Ellacott *et al.* 2002; Lawrence *et al.* 2002). It is also known that these functions are affected by chronic RR stress (Marti *et al.* 1994; Chung *et al.* 2000; Harris *et al.* 2002). Inhibition of feeding and the cardiovascular changes after chronic stress could be realized through the PrRP-producing neurons in the brainstem, as well (Hotta *et al.* 1991; Maruyama *et al.* 1999; Matsumoto *et al.* 2000; Horiuchi *et al.* 2002; Ueta *et al.* 2003; Sun *et al.* 2005b). Our finding of elevated PrRP levels 1 day after the last restraint suggests the possibility of another role for PrRP in the A1 and A2 cell groups under chronic stress. This new role is likely to be related to the brainstem catecholaminergic regulation considering our present results regarding the analysis of the PrRP–TH relationship in these cells (see below).

PrRP/TH ratio in the A1 and A2 catecholaminergic cell groups after chronic repeated restraint

Tyrosine hydroxylase mRNA expression was shown to be elevated in the neurons of the A1 and A2-NTS cell groups after different acute stressful stimuli and after chronic immobilization stress in male rats (Pacak 2000; Rusnak *et al.* 2001). In the present study, we found a significant elevation in TH and in the TH mRNA expression in the A1 but not in the A2 cell group after RR. PrRP expression increased in males in both cell groups, but this happened to a smaller extent in the A2 than in the A1 neurons. The A1 and A2 cells react to chronic stress in a stressor kind and strength-specific way (El Fazaa *et al.* 1999; Pacak 2000; Li *et al.* 2006; Mera *et al.* 2006).

Supporting our second hypothesis, there was a clear shift in the PrRP/TH ratio in favor of PrRP in the A1 and A2-NTS cell groups after RR (except in A2-NTS in females where there was no reaction at all, see discussion below). These shifts were demonstrated by the differences in the relative changes of the PrRP and TH mRNAs and proteins and also by the changes in the PrRP–TH ratio evoked by RR. The PrRP/TH colocalization ratio did not alter after acute water immersion–restraint stress (Maruyama *et al.* 2001) indicating that acute and chronic stress might have different effects on TH and PrRP signaling. The phenomenon seems to be similar to the response of the hypothalamic paraventricular neurons to chronic stress, where the number of CRH and AVP cosecreting cells, as well as the expression rate of AVP versus CRH are elevated (de Goeij *et al.* 1992; Bartanusz *et al.* 1993; Dallman 1993; Aguilera 1994; Ma and Lightman 1998). The mechanism might be similar in the present case if PrRP is less sensitive to glucocorticoid feedback than TH (Dallman 1993). There is no data in the literature confirming the existence of glucocorticoid responsive element (GRE) in the promoter region of the PrRP gene. A putative GRE sequence was identified by direct search between −4023 and −4009 bp of the rat PrRP gene (GeneID 63850) with high homology to the TH–GRE (unpublished data). Functional significance of this putative GRE site needs further studies. The elevated PrRP level may allude to a contribution in adaptation to the stress by helping to maintain elevated CRH and corticosterone levels. The goal of measuring hormone levels 24 h after the last restraint was to avoid the chance to measure the occurrent acute effect of the last restraint and determine habituation. Chronic RR caused a slight but significant elevation in the basal serum corticosterone level in the present experiments. The slightly elevated basal corticosterone level under chronic stress conditions facilitates ACTH response to a novel acute stressor, therefore important for the survival (Dallman 1993). The ACTH/corticosterone response evoked by intracerebroventricular administration of PrRP can be attenuated by CRH antagonist or antibody (Matsumoto *et al.* 2000; Samson *et al.* 2003; Mera *et al.* 2006; Ohiwa *et al.* 2007). Besides, PrRP can stimulate catecholamine synthesis in PC12 cells (Nanmoku *et al.* 2005) These indicate that the increased PrRP in chronic stress might contribute to the stress-induced facilitation of the HPA axis in two possible ways: (i) acting intrinsically at the level of the A1, A2-NTS cells by facilitating the noradrenergic input to the CRH/AVP neurons in the PVN, and/or (ii) acting directly at the level of the CRH/AVP cells facilitating the CRH/AVP expression. The fact that prolactin level did not increase in our experiments, as it happens usually after acute stress suggests habituation. This adds to the debate about the physiological role of PrRP in prolactin release (Sun *et al.* 2005a).

Gender-related differences in the PrRP expression

Repeated restraint evoked an elevation of the overall PrRP expression in the A1 cell group both in males and females, but in females the changes were milder, supporting our third hypothesis expecting a gender-related difference in PrRP levels in response to RR. In the A2-NTS cells PrRP expression increased only in males after RR. There was no gender-related difference in response to RR in the PrRP-expressing neurons of the DM. Thus, only the brainstem, and not the hypothalamic PrRP neurons indicated a gender difference. Interestingly, we found similar distinction in the distribution of the ERα expression being present in the nuclei

of the A1 and A2-NTS but not in the DM PrRP neurons. Similarly, the gender-related difference in the basal PrRP production was also restricted to the brainstem neurons Additionally, OVX abolished the higher basal PrRP expression in the brainstem of females, indicating an important role of estrogen in the regulation of the PrRP gene expression.

The chronic activation of the HPA axis leads to an elevated basal serum corticosterone level, as well as the appearance of all typical markers of the chronic stress. These markers include decreased body weight, decreased thymus, and increased adrenal weights (relative to body weight, i.e. mg/body weight kg) (Du Ruisseau *et al.* 1977; Blanchard *et al.* 1993). Male rats showed all of these signs in the present experiments. Female rats seemed less sensitive to RR as shown in PrRP expression in the brainstem and did not develop adrenal and thymus weight changes after 7 days of RR. This confirms the results of Lunga and Herbert (2004), who applied 1 h/day restraint for 10 days. It has been reported that in females the organ weight changes were characteristic after 14 repetitions of 1 h/day restraint, indicating that these changes might evolve at a slower rate in female rats than in males (Zelena *et al.* 2004). It seems that higher basal PrRP expression in the brainstem is accompanied by a higher basal corticosterone level (Atkinson and Waddell 1997; Galea *et al.* 1997) in females, and the less sensitive PrRP reaction in their brainstem is accompanied by a slower development of the markers of chronic stress.

Bilateral PVN lesions and chronic repeated restraint

Bilateral PVN lesions caused a significant decrease in PrRP and TH mRNA levels as well as in the number of PrRP-expressing cells in the A2 area in the NTS, without having any effect on the A2 cells in the DMX or on the cells of the A1 cell group. It has been reported, that the A2 cell group is consisted by a heterogeneous population of catecholaminergic neurons (Kalia *et al.* 1985). An adequate question is that the observed changes are due to the loss of PVN efferents that exerted positive effects on PrRP and TH expression or the retrograde degeneration of PrRP/TH containing axons from A2, and therefore the loss of those A2 neurons? In the present experiments the axons of A1 and A2 cells projecting to the PVN were mechanically cut by lesioning of the PVN, but the cut leaves several axon collaterals running to other directions intact. Thus, the A1 and A2 neuronal cell bodies may survive the operation. It is supposed, that, at least partly, tonic positive stimuli from PVN are responsible for maintaining the control level of PrRP and TH expressions in A2-NTS neurons. It also suggested that this positive effect may control the PrRP expression stronger than TH expression, as only the grains/cell values were reduced in the case of TH mRNA, while PrRP mRNA expression decreased more dramatically, far below the detection level that resulted in a reduction in the cell number values.

It is known that 70% of the NTS and 20% of the A1 neurons project to the PVN (Sawchenko and Swanson 1982). As there was no detectable decrease in the TH and PrRP mRNA expressions in the A1 cell group after bilateral PVN lesions, it is likely that not only the percentage of the efferent fibers toward the PVN is low in the A1 cell group, but A1 neurons might possess more axon collaterals branching toward other areas of the brain than the A2 neurons.

In our previous work we established that PVN lesions prevented RR-evoked changes, such as elevation of basal serum corticosterone level, body weight loss, and thymus weight reduction, as well as reduced RR-induced adrenal hypertrophy (Zelena *et al.* 2003). Therefore, the effects of PVN lesions on RR-induced weight and hormonal changes may be related to the reduced PrRP–TH ratio and impaired TH and PrRP signaling from the A2-NTS area toward the PVN. Work of Dayas *et al.* (2004) indicated that intact input from PVN was necessary for c-*fos* activation of the medullary catecholaminergic neurons in response to acute restraint stress and systemic immune challenge. Our results show that this intact input is not necessary for the up-regulation of TH and PrRP expressions after chronic RR. Under chronic situation some other upper autonomic center than PVN may play role in the regulation of A1 and A2 cell groups, or the ascending stress information that reaches the brainstem through neuronal and/or humoral pathways is the primary stimulus for inducing the TH and PrRP response.

Acknowledgements

We would like to thank for Dr Krisztina Kovács and Dr W. S. Young for the thorough and careful review of the manuscript and for Kinga Meltzer for technical help. PV is supported by Bolyai Fellowship. This work was supported by the Hungarian Science Research Fund (OTKA) T-043169 and T-043161.

References

Adachi S., Mochiduki A., Nemoto H., Sun B., Fujiwara K., Matsumoto H. and Inoue K. (2005) Estrogen suppresses the stress response of prolactin-releasing peptide-producing cells. *Neurosci. Lett.* **380**, 311–315.

Aguilera G. (1994) Regulation of pituitary ACTH secretion during chronic stress. *Front. Neuroendocrinol.* **15**, 321–350.

Anderson S. T., Kokay I. C., Lang T., Grattan D. R. and Curlewis J. D. (2003) Quantification of prolactin-releasing peptide (PrRP) mRNA expression in specific brain regions of the rat during the oestrous cycle and in lactation. *Brain Res.* **973**, 64–73.

Atkinson H. C. and Waddell B. J. (1997) Circadian variation in basal plasma corticosterone and adrenocorticotropin in the rat: sexual dimorphism and changes across the estrous cycle. *Endocrinology* **138**, 3842–3848.

Bartanusz V., Jezova D., Bertini L. T., Tilders F. J., Aubry J. M. and Kiss J. Z. (1993) Stress-induced increase in vasopressin and corticotropin-releasing factor expression in hypophysiotrophic paraventricular neurons. *Endocrinology* **132**, 895–902.

Bellinger L. L. and Bernardis L. L. (2002) The dorsomedial hypothalamic nucleus and its role in ingestive behavior and body weight regulation: lessons learned from lesioning studies. *Physiol. Behav.* **76**, 431–442.

Blanchard D. C., Sakai R. R., McEwen B., Weiss S. M. and Blanchard R. J. (1993) Subordination stress: behavioral, brain, and neuroendocrine correlates. *Behav. Brain Res.* **58**, 113–121.

Chen C., Dun S. L., Dun N. J. and Chang J. K. (1999) Prolactin-releasing peptide-immunoreactivity in A1 and A2 noradrenergic neurons of the rat medulla. *Brain Res.* **822**, 276–279.

Chung K. K., Martinez M. and Herbert J. (2000) c-fos expression, behavioural, endocrine and autonomic responses to acute social stress in male rats after chronic restraint: modulation by serotonin. *Neuroscience* **95**, 453–463.

Dallman M. F. (1993) Stress update: adaptation of the hypothalamic-pituitary–adrenal axis to chronic stress. *Trends Endocrinol. Metab.* **4**, 62–69.

Dayas C. V., Buller K. M. and Day T. A. (2004) Hypothalamic paraventricular nucleus neurons regulate medullary catecholamine cell responses to restraint stress. *J. Comp. Neurol.* **478**, 22–34.

Du Ruisseau P., Tache Y., Selye H., Ducharme J. R. and Collu R. (1977) Effects of chronic stress on pituitary hormone release induced by combined hemi-extirpation of the thyroid, adrenal and ovary in rats. *Neuroendocrinology* **24**, 169–182.

El Fazaa S., Somody L., Gharbi N., Kamoun A., Gharib C. and Gauquelin-Koch G. (1999) Effects of acute and chronic starvation on central and peripheral noradrenaline turnover, blood pressure and heart rate in the rat. *Exp. Physiol.* **84**, 357–368.

Ellacott K. L., Lawrence C. B., Rothwell N. J. and Luckman S. M. (2002) PRL-releasing peptide interacts with leptin to reduce food intake and body weight. *Endocrinology* **143**, 368–374.

Galea L. A., McEwen B. S., Tanapat P., Deak T., Spencer R. L. and Dhabhar F. S. (1997) Sex differences in dendritic atrophy of CA3 pyramidal neurons in response to chronic restraint stress. *Neuroscience* **81**, 689–697.

de Goeij D. C., Jezova D. and Tilders F. J. (1992) Repeated stress enhances vasopressin synthesis in corticotropin releasing factor neurons in the paraventricular nucleus. *Brain Res.* **577**, 165–168.

Harris R. B., Mitchell T. D., Simpson J., Redmann S. M. Jr, Youngblood B. D. and Ryan D. H. (2002) Weight loss in rats exposed to repeated acute restraint stress is independent of energy or leptin status. *Am. J. Physiol. Regul. Integr. Comp. Physiol.* **282**, R77–R88.

Hinuma S., Habata Y., Fujii R. *et al.* (1998) A prolactin-releasing peptide in the brain. *Nature* **393**, 272–276.

Horiuchi J., Saigusa T., Sugiyama N., Kanba S., Nishida Y., Sato Y., Hinuma S. and Arita J. (2002) Effects of prolactin-releasing peptide microinjection into the ventrolateral medulla on arterial pressure and sympathetic activity in rats. *Brain Res.* **958**, 201–209.

Hotta M., Shibasaki T., Yamauchi N., Ohno H., Benoit R., Ling N. and Demura H. (1991) The effects of chronic central administration of corticotropin-releasing factor on food intake, body weight, and hypothalamic-pituitary–adrenocortical hormones. *Life Sci.* **48**, 1483–1491.

Kalia M., Fuxe K. and Goldstein M. (1985) Rat medulla oblongata. II. Dopaminergic, noradrenergic (A1 and A2) and adrenergic neurons, nerve fibers, and presumptive terminal processes. *J. Comp. Neurol.* **233**, 308–332.

Kataoka Y., Iijima N., Yano T., Kakihara K., Hayashi S., Hinuma S., Honjo H., Tanaka M. and Ibata Y. (2001) Gonadal regulation of PrRP mRNA expression in the nucleus tractus solitarius and ventral and lateral reticular nuclei of the rat. *Mol. Brain Res.* **87**, 42–47.

Kiss J. Z., Mezey E. and Skirboll L. (1984) Corticotropin-releasing factor-immunoreactive neurons of the paraventricular nucleus become vasopressin positive after adrenalectomy. *Proc. Natl Acad. Sci. USA* **81**, 1854–1858.

Lawrence C. B., Ellacott K. L. and Luckman S. M. (2002) PRL-releasing peptide reduces food intake and may mediate satiety signaling. *Endocrinology* **143**, 360–367.

Li A. J., Wang Q. and Ritter S. (2006) Differential responsiveness of dopamine-beta-hydroxylase gene expression to glucoprivation in different catecholamine cell groups. *Endocrinology* **147**, 3428–3434.

Luiten P. G., ter Horst G. J., Karst H. and Steffens A. B. (1985) The course of paraventricular hypothalamic efferents to autonomic structures in medulla and spinal cord. *Brain Res.* **329**, 374–378.

Lunga P. and Herbert J. (2004) ^{17}Beta-oestradiol modulates glucocorticoid, neural and behavioural adaptations to repeated restraint stress in female rats. *J. Neuroendocrinol.* **16**, 776–785.

Ma X. M. and Lightman S. L. (1998) The arginine vasopressin and corticotrophin-releasing hormone gene transcription responses to varied frequencies of repeated stress in rats. *J. Physiol. (Lond.)* **510**, 605–614.

Makara G. B. and Kovacs K. J. (1997) Lesioning of the hypothalamic paraventricular nucleus inhibits ether-induced ACTH but not prolactin release. *Neurobiology (Bp)* **5**, 403–411.

Marti O., Marti J. and Armario A. (1994) Effects of chronic stress on food intake in rats: influence of stressor intensity and duration of daily exposure. *Physiol. Behav.* **55**, 747–753.

Maruyama M., Matsumoto H., Fujiwara K. *et al.* (1999) Central administration of prolactin-releasing peptide stimulates oxytocin release in rats. *Neurosci. Lett.* **276**, 193–196.

Maruyama M., Matsumoto H., Fujiwara K., Noguchi J., Kitada C., Fujino M. and Inoue K. (2001) Prolactin-releasing peptide as a novel stress mediator in the central nervous system. *Endocrinology* **142**, 2032–2038.

Matsumoto H., Maruyama M., Noguchi J. *et al.* (2000) Stimulation of corticotropin-releasing hormone-mediated adrenocorticotropin secretion by central administration of prolactin-releasing peptide in rats. *Neurosci. Lett.* **285**, 234–238.

McDowall L. M., Horiuchi J., Killinger S. and Dampney R. A. (2006) Modulation of the baroreceptor reflex by the dorsomedial hypothalamic nucleus and perifornical area. *Am. J. Physiol. Regul. Integr. Comp. Physiol.* **290**, R1020–R1026.

Mera T., Fujihara H., Kawasaki M. *et al.* (2006) Prolactin-releasing peptide is a potent mediator of stress responses in the brain through the hypothalamic paraventricular nucleus. *Neuroscience* **141**, 1069–1086.

Minami S., Nakata T., Tokita R., Onodera H. and Imaki J. (1999) Cellular localization of prolactin-releasing peptide messenger RNA in the rat brain. *Neurosci. Lett.* **266**, 73–75.

Morales T. and Sawchenko P. E. (2003) Brainstem prolactin-releasing peptide neurons are sensitive to stress and lactation. *Neuroscience* **121**, 771–778.

Nanmoku T., Takekoshi K., Fukuda T., Ishii K., Isobe K. and Kawakami Y. (2005) Stimulation of catecholamine biosynthesis via the PKC pathway by prolactin-releasing peptide in PC12 rat pheochromocytoma cells. *J. Endocrinol.* **186**, 233–239.

Ohiwa N., Chang H., Saito T., Onaka T., Fujikawa T. and Soya H. (2007) Possible inhibitory role of prolactin-releasing peptide for ACTH release associated with running stress. *Am. J. Physiol. Regul. Integr. Comp. Physiol.* **292**, R497–R504.

Pacak K. (2000) Stressor-specific activation of the hypothalamic-pituitary–adrenocortical axis. *Physiol. Res.* **49**, S11–S17.

Pacak K., Palkovits M., Kvetnansky R., Kopin I. J. and Goldstein D. S. (1993) Stress-induced norepinephrine release in the paraventricular nucleus of rats with brainstem hemisections: a microdialysis study. *Neuroendocrinology* **58**, 196–201.

Petrov T., Krukoff T. L. and Jhamandas J. H. (1993) Branching projections of catecholaminergic brainstem neurons to the paraventricular hypothalamic nucleus and the central nucleus of the amygdala in the rat. *Brain Res.* **609**, 81–92.

Rusnak M., Kvetnansky R., Jelokova J. and Palkovits M. (2001) Effect of novel stressors on gene expression of tyrosine hydroxylase and monoamine transporters in brainstem noradrenergic neurons of long-term repeatedly immobilized rats. *Brain Res.* **899**, 20–35.

Samson W. K., Resch Z. T. and Murphy T. C. (2000) A novel action of the newly described prolactin-releasing peptides: cardiovascular regulation. *Brain Res.* **858**, 19–25.

Samson W. K., Keown C., Samson C. K., Samson H. W., Lane B., Baker J. R. and Taylor M. M. (2003) Prolactin-releasing peptide and its homolog RFRP-1 act in hypothalamus but not in anterior pituitary gland to stimulate stress hormone secretion. *Endocrine* **20**, 59–66.

Sawchenko P. E. and Swanson L. W. (1982) The organization of noradrenergic pathways from the brainstem to the paraventricular and supraoptic nuclei in the rat. *Brain Res.* **257**, 275–325.

Sawchenko P. E., Swanson L. W. and Vale W. W. (1984) Co-expression of corticotropin-releasing factor and vasopressin immunoreactivity in parvocellular neurosecretory neurons of the adrenalectomized rat. *Proc. Natl Acad. Sci. USA* **81**, 1883–1887.

Seal L. J., Small C. J., Dhillo W. S., Stanley S. A., Abbott C. R., Ghatei M. A. and Bloom S. R. (2001) PRL-releasing peptide inhibits food intake in male rats via the dorsomedial hypothalamic nucleus and not the paraventricular hypothalamic nucleus. *Endocrinology* **142**, 4236–4243.

Serova L. I., Maharjan S. and Sabban E. L. (2005) Estrogen modifies stress response of catecholamine biosynthetic enzyme genes and cardiovascular system in ovariectomized female rats. *Neuroscience* **132**, 249–259.

Sun B., Fujiwara K., Adachi S. and Inoue K. (2005a) Physiological roles of prolactin-releasing peptide. *Regul. Pept.* **126**, 27–33.

Sun B., Nemoto H., Fujiwara K., Adachi S. and Inoue K. (2005b) Nicotine stimulates prolactin-releasing peptide (PrRP) cells and non-PrRP cells in the solitary nucleus. *Regul. Pept.* **126**, 91–96.

Toth Z. E., Gallatz K., Fodor M. and Palkovits M. (1999) Decussations of the descending paraventricular pathways to the brainstem and spinal cord autonomic centers. *J. Comp. Neurol.* **414**, 255–266.

Ueta Y., Ozaki Y., Saito J. and Onaka T. (2003) Involvement of novel feeding-related peptides in neuroendocrine response to stress. *Exp. Biol. Med. (Maywood)* **228**, 1168–1174.

Yamakawa K., Kudo K., Kanba S. and Arita J. (1999) Distribution of prolactin-releasing peptide-immunoreactive neurons in the rat hypothalamus. *Neurosci. Lett.* **267**, 113–116.

Young W. S. 3rd, Warden M. and Mezey E. (1987) Tyrosine hydroxylase mRNA is increased by hyperosmotic stimuli in the paraventricular and supraoptic nuclei. *Neuroendocrinology* **46**, 439–444.

Zaretskaia M. V., Zaretsky D. V., Shekhar A. and DiMicco J. A. (2002) Chemical stimulation of the dorsomedial hypothalamus evokes non-shivering thermogenesis in anesthetized rats. *Brain Res.* **928**, 113–125.

Zelena D., Mergl Z., Foldes A., Kovacs K. J., Toth Z. and Makara G. B. (2003) Role of hypothalamic inputs in maintaining pituitary–adrenal responsiveness in repeated restraint. *Am. J. Physiol. Endocrinol. Metab.* **285**, E1110–E1117.

Zelena D., Foldes A., Mergl Z., Barna I., Kovacs K. J. and Makara G. B. (2004) Effects of repeated restraint stress on hypothalamo-pituitary–adrenocortical function in vasopressin deficient Brattleboro rats. *Brain Res. Bull.* **63**, 521–530.

Zhu L. L. and Onaka T. (2003) Facilitative role of prolactin-releasing peptide neurons in oxytocin cell activation after conditioned-fear stimuli. *Neuroscience* **118**, 1045–1053.

Brain Structure and Function (2020) 225:969–984
https://doi.org/10.1007/s00429-020-02049-y

ORIGINAL ARTICLE

Colocalized neurotransmitters in the hindbrain cooperate in adaptation to chronic hypernatremia

Rita Matuska[1] · Dóra Zelena[2,3] · Katalin Könczöl[4] · Rege Sugárka Papp[5] · Máté Durst[4] · Dorina Guba[4] · Bibiana Török[2,6] · Peter Varnai[1] · Zsuzsanna E. Tóth[4]

Received: 17 June 2019 / Accepted: 13 February 2020 / Published online: 21 March 2020

Abstract

Chronic hypernatremia activates the central osmoregulatory mechanisms and inhibits the function of the hypothalamic–pituitary–adrenal (HPA) axis. Noradrenaline (NE) release into the periventricular anteroventral third ventricle region (AV3V), the supraoptic (SON) and hypothalamic paraventricular nuclei (PVN) from efferents of the caudal ventrolateral (cVLM) and dorsomedial (cDMM) medulla has been shown to be essential for the hypernatremia-evoked responses and for the HPA response to acute restraint. Notably, the medullary NE cell groups highly coexpress prolactin-releasing peptide (PrRP) and nesfatin-1/NUCB2 (nesfatin), therefore, we assumed they contributed to the reactions to chronic hypernatremia. To investigate this, we compared two models: homozygous Brattleboro rats with hereditary diabetes insipidus (DI) and Wistar rats subjected to chronic high salt solution (HS) intake. HS rats had higher plasma osmolality than DI rats. PrRP and nesfatin mRNA levels were higher in both models, in both medullary regions compared to controls. Elevated basal tyrosine hydroxylase (TH) expression and impaired restraint-induced TH, PrRP and nesfatin expression elevations in the cVLM were, however, detected only in HS, but not in DI rats. Simultaneously, only HS rats exhibited classical signs of chronic stress and severely blunted hormonal reactions to acute restraint. Data suggest that HPA axis responsiveness to restraint depends on the type of hypernatremia, and on NE capacity in the cVLM. Additionally, NE and PrRP signalization primarily of medullary origin is increased in the SON, PVN and AV3V in HS rats. This suggests a cooperative action in the adaptation responses and designates the AV3V as a new site for PrRP's action in hypernatremia.

Keywords Prolactin-releasing peptide · Noradrenaline · Nesfatin-1 · Restraint · Brattleboro rat · Stress

Introduction

Homeostatic regulation of plasma osmolality (275–290 mOsm/kg) is vital. Elevated osmolality develops primarily based on elevated extracellular [Na^+] level known as hypernatremia. Besides activating the central osmoregulatory system, hypernatremia also represents a serious stress for the organism that impairs the response of the hypothalamic–pituitary–adrenal (HPA) axis to a novel acute stressor (Amaya et al. 2001; Krause et al. 2017). The mechanism is still unclarified, therefore we focused our research on brain structures that participate in the control of both hypernatremia and stress-evoked responses, such as the A1 and A2 noradrenaline (NE) cell groups in the caudal ventrolateral (cVLM) and dorsomedial (cDMM) medulla oblongata.

Hypertonic saline administered by intravenous infusion evokes neuronal activation (Fos positivity) in the A1 and A2 NE cells specifically, as infusions of physiological

✉ Zsuzsanna E. Tóth
toth.zsuzsanna.emese@med.semmelweis-univ.hu

1 Department of Physiology, Semmelweis University, Budapest, Hungary

2 Behavioral Neurobiology, Institute of Experimental Medicine, Budapest, Hungary

3 Centre for Neuroscience, Szentágothai Research Centre, Institute of Physiology, Medical School, University of Pécs, Pécs, Hungary

4 Department of Anatomy, Histology and Embryology, Semmelweis University, Budapest, Hungary

5 Human Brain Tissue Bank and Microdissection Laboratory, Semmelweis University, Budapest, Hungary

6 Janos Szentagothai School of Neurosciences, Semmelweis University, Budapest, Hungary

or hypotonic NaCl solutions fail to activate these neurons (Hochstenbach and Ciriello 1995). NE is an essential transmitter for stimulating areas in the hypothalamus that govern the neuroendocrine, autonomic and behavioral responses for hypernatremia (Day 1989; Tanaka et al. 1997; Huang et al. 2000; Bourque 2008; Pedrino et al. 2012; da Silva et al. 2013; Sawchenko and Swanson 1981; Pacak et al. 1995). These areas receive their NE innervation primarily from the neurons of the A1, A2 cell groups and include the paraventricular (PVN) and supraoptic (SON) nuclei as well as the periventricular anteroventral third ventricle region (AV3V). The latter comprises the organum vasculosum laminae terminalis (OVLT), the median preoptic nucleus (MnPO) and the preoptic and anteroventral periventricular nuclei (Bourque 2008; Menani et al. 2014).

The neurons of the A1, A2 cell groups also convey stress-related stimuli that signal homeostatic perturbations (Liposits et al. 1986; Ulrich-Lai and Herman 2009; Gaillet et al. 1991) towards the HPA axis, namely towards the corticotropin-releasing hormone (CRH) producing cells in the parvocellular PVN. The PVN is innervated by NE fibers almost exclusively (94%) from the A1 and A2 cell groups (Sawchenko and Swanson 1981, 1982). Bilateral pharmacological lesions of the ascending medullary NE fibers lead to a 90% decrease of CRH released into hypophyseal portal vessels (Guillaume et al. 1987) and obliteration of the diurnal increment in plasma adrenocorticotropic hormone (ACTH) (Szafarczyk et al. 1985) under basal conditions. Similar lesions caused dramatically reduced ACTH and impaired corticosterone responses to acute ether or restraint stress (Gaillet et al. 1991; Pacak et al. 1995). Chemical ablation of the catecholaminergic terminals within the PVN also attenuated peak ACTH and corticosterone levels in response to acute restraint (Flak et al. 2014).

Despite these facts, the significance of the A1 and A2 cells in adaptation to chronic hypernatremia as well as in altered responsiveness of the HPA axis to acute restraint in hypernatremic animals has not been elucidated yet. Moreover, the A1 and A2 cells very intensely coexpress prolactin-releasing peptide (PrRP) and nesfatin-1/NUCB2 (nesfatin) (Chen et al. 1999; Toth et al. 2008; Konczol et al. 2010) together with NE. Therefore, we assume that cooperation of these substances may be relevant. Indeed, enhanced expression of different cotransmitters is a fundamental event in adaptation to chronic restraint stress (Ma et al. 1997; Amaya et al. 2001; Toth et al. 2008). PrRP cells comprise a large subpopulation of the A2 cells (~ 82%) in the nucleus of the solitary tract (NTS) and practically correspond to all A1 (~ 98%) neurons. They, therefore, coexpress tyrosine hydroxylase (TH, the rate-limiting enzyme of the NE synthesis) and PrRP (Chen et al. 1999; Toth et al. 2008). This feature helps to identify PrRP axons of medullary origin at the terminal fields, as the third PrRP cell population in the brain, which exists in the dorsomedial nucleus of the hypothalamus, is TH negative (Roland et al. 1999). PrRP is involved in various functions challenged by hypernatremia, like the cardiovascular regulation (Yamada et al. 2009) and the control of oxytocin (promotes sodium excretion) and vasopressin (AVP, stimulates water retention) release from the magnocellular cells of the SON and PVN (Maruyama et al. 1999; Uchida et al. 2010). PrRP neurons in the A1 and A2 cell groups are strongly activated (~ 90% Fos positivity) by water immersion-restraint stress, while PrRP-negative A2 neurons barely respond to this stimulus (Maruyama et al. 2001). Acute restraint upregulates PrRP mRNA expression of the A1 cell group (Mera et al. 2006; Konczol et al. 2010). PrRP cells synapse with CRH neurons in the PVN and central administration of PrRP induces Fos protein accumulation in CRH neurons as well as a CRH-mediated increase in the ACTH level (Seal et al. 2002; Maruyama et al. 2001). Although a synergistic effect of PrRP and NE was observed on ACTH (Maruyama et al. 2001) and AVP releases (Uchida et al. 2010), the contribution of PrRP to chronic hyperosmotic responses in the PVN, SON and AV3V has not been investigated yet and the origin of the PrRP fibers at these locations is unrevealed.

Nesfatin-1, the N-terminal fragment of the NUCB2 prohormone is expressed in several brain nuclei, for example, in the PVN and SON (Foo et al. 2008). The vast majority of the nesfatin neurons in the cVLM and cDMM are TH and PrRP coexpressing cells (Konczol et al. 2010). Nesfatin is not transported axonally, but acts locally by autocrine/paracrine fashion (Foo et al. 2008). Nesfatin has been attributed to similar autonomic and endocrine functions to PrRP (Konczol et al. 2010; Maejima et al. 2009; Yilmaz et al. 2015; Yosten and Samson 2009). As these effects were revealed by intracerebroventricular (icv) injections, the exact sites of actions are unknown. We earlier found, however, that acute restraint elevated nesfatin expression in the cVLM indicating its role in the stress response (Konczol et al. 2010).

Based on the above facts, we addressed the following questions: 1, whether the level of the stress caused by chronic hypernatremia may depend on the type of hypernatremia (i.e., eu- or hypervolemic, congenital or acquired); 2, whether the different types of chronic hypernatremia affect the responsiveness to acute restraint differentially; and 3, whether the expression of TH, PrRP and nesfatin in the cDMM and cVLM reflects the actual sensitivity of the HPA axis to acute restraint under chronic hypernatremic conditions. Additionally, we also examined the morphological basis for a putative interaction of NE and PrRP of medullary origin in the hypothalamus (PVN, SON, AV3V) in response to chronic hypernatremia. We used two kinds of models: (1) Brattleboro rats homozygous for diabetes insipidus (euvolemic, DI rats) due to hereditary AVP deficiency and (2)

Wistar rats receiving high salt (2% NaCl) solution instead of tap water (hypervolemic, HS rats) for 6 days.

Methods

Animals

The subjects of the study were adult (12–14 week old) male Wistar (Toxi-Coop Toxicological Research Center Zrt, Dunakeszi, Hungary) and homozygous Brattleboro rats (+/+ wild type; WT and −/− AVP deficient with diabetes insipidus; DI). The Brattleboro rats were maintained in a colony started from breeder rats from Harlan (Indianapolis, IN), as earlier described (Varga et al. 2016). The rats were housed in a controlled environment (23 ± 1 °C, 50–70% humidity, 12 h light starting at 07:00) and had free access to standard rodent chow and tap water, except otherwise indicated. Due to the extremely high level of urination caused by the diabetic condition, we changed sawdust bedding daily for all rats. Animals were anesthetized with ketamine (75 mg/bwkg) (Richter Gedeon Nyrt., Budapest, Hungary) and xylasine (15 mg/bwkg) (CP-Pharma, Burgdorf, Germany) given intramuscularly prior to perfusion fixation.

Experimental design

Experiment 1

The Brattleboro rats were divided into four groups: WT-control, DI-control, WT-restraint (R) and DI-R ($n = 7$/group). Bodyweight, food and water intake of rats were recorded daily in the morning for 5 consecutive days before the experiment started.

The Wistar rats were also assigned into four experimental groups: normal salt (NS)-control, high salt (HS)-control, NS-R and HS-R ($n = 8$/group). Animals in the HS groups received 2% NaCl solution instead of tap water for 6 days. Bodyweight, daily food and water intake of rats were measured on every 3rd day (starting on day zero) to minimize extra stress.

On the day of the experiments, all animals in the R groups were subjected to a single restraint stress as described below. Control subjects remained in their home cages. Blood from the tail vein was collected for hormonal measurements 1 h after restraint had started both from stressed and non-stressed animals. At the end of the restraint, all animals were sacrificed by decapitation. The thymi and adrenal glands were dissected out and their weights were measured. The brains were removed, frozen on dry ice and used for in situ hybridization histochemistry.

Experiment 2

The Wistar rats were assigned to two experimental groups, NS and HS ($n = 8$/group). Animals in the HS group received 2% NaCl solution instead of tap water for 6 days. At the end, animals were sacrificed either by decapitation ($n = 4$/group) or by transcardial perfusion with 4% paraformaldehyde in 0.1 M phosphate-buffered saline (PBS, pH = 7.4) ($n = 4$/group). The brains were removed and processed for western blot (fresh-frozen, $n = 4$/group) or immunohistochemistry (perfused-fixed, $n = 4$/group).

Restraint stress

Single, long-duration restraint was performed as previously described (Zelena et al. 2003). The animals were placed into transparent plastic tubes (5–6 cm inner diameter) having a 4-cm-long conical head part ending with a large breathing hole. Behind the body, the rear end of the tube was loosely packed with paper towels. This method allows restraint without any pain and minimizes temperature effects. Restraint lasted for 3 h in the morning (08:00–11:00) and was finished by transcardial perfusion or by decapitation of the animals.

In situ hybridization

Serial coronal sections (12 µm thick, 120 µm apart) of the brains were cut using a cryostat (Leica Microsystems, Nussloch, Germany) and mounted on Superfrost Ultra Plus slides (ThermoFisher Scientific, Budapest, Hungary). The slides were stored at − 80 °C until used.

Alternate series of sections from the caudal medulla oblongata were hybridized for either PrRP, TH or NUCB2. One series of hypothalamic sections was hybridized for PrRP receptor (PrRP-R alias GPR10). The S35-UTP-labeled (PerForm Hungaria Kft., Budapest, Hungary) riboprobes were prepared by in vitro transcription as described previously (Konczol et al. 2010; Toth et al. 2008). The specific sequences used for the hybridizations were: rat prepro-PrRP cDNA (10–240 bp of the coding sequence, accession # AB015418), rat TH cDNA (684–1068 bp of the coding sequence, accession # M23598) (Mezey et al. 1998), rat NUCB2 cDNA corresponding to the nesfatin-1 fragment (1–246 bp of the coding sequence, accession # DY314804) and the rat PrRP-R cDNA (189–636 bp of the coding sequence, accession # NM_139193) (Vas et al. 2013; Durst et al. 2019). The specificity of the cDNAs was verified by sequencing. Specificity of the probes was also controlled by performing experiments using sense probes failing to give any signals. After hybridizations, sections were apposed to BAS-MS imaging plates (Fuji Photo Film Co., LTD., Kanagawa, Japan, NJ) for 3 (PrRP, TH) or 7 (NUCB2) days. Data were read out by a Fujifilm FLA-8000 Image

Analyzer (Fujifilm Life Science, Stamford, CT). NUCB2 as well as PrRP-R labeled sections were dipped in Kodak NTB nuclear emulsion (Carestream Health Inc., Rochester, NY) for 2 and 6 weeks, respectively, according to the manufacturer's instructions and developed using Kodak developer and fixer (Sigma). The sections were stained with Giemsa and coverslipped using DPX (Sigma).

Quantitative analysis of the in situ hybridization signals

Radioactive in situ hybridization provides a linear relationship between the signal intensity and the mRNA expression level (Chen et al. 2012). The signals in the cVLM and cDMM (i.e. NTS) were evaluated on parallel series of sections, between 14.04 and 14.70 mm caudal from bregma (Paxinos and Watson 2007) corresponding to the most sensitive areas for restraint stress (Dayas et al. 2001). The rostrocaudal level of the sections was carefully matched between the animals. Optical densities (mean grey values) of the signals were measured in the phosphor imager recordings in at least four sections/animal using the same settings across animals. Background values measured in parallel were subtracted. NUCB2 signal in the cVLM was weak in the screen (see the Results), therefore, it was measured in darkfield images (Olympus BX60, UPlan FL 4x/0.13) made of the autoradiographic emulsion-coated sections (SPOT Xplorer 17.4 camera, Diagnostic Instruments Inc., Sterling Heights, MI). The amount of the silver grains over the individual cells was evaluated within identical ROIs and expressed as the area (pixels) covered by grains (Wittmann et al. 2015). The signal threshold for each cell was calculated as the mean pixel value of 2–3 background samples measured in the surrounding region. Only cells with pixel values above these criteria were included in the analysis. In all cases, the sections were evaluated bilaterally with the help of the ImageJ program (Wayne Rasband NIH, Bethesda, MD), as earlier described (Vas et al. 2013; Toth et al. 2008). The average/animal data were compared statistically. All measurements were made by an experimenter blind to the experimental settings.

Hormone measurements

Blood was collected in K-EDTA containing tubes on ice. After centrifugation, the plasma was stored at − 20 °C. ACTH and corticosterone levels were measured from unextracted plasma (50 and 10 µl, respectively) in duplicates with a radioimmunoassay, as described earlier (Zelena et al. 2003). The intra-assay coefficient of variation was 12.5% and 17.6% for ACTH and corticosterone measurements, respectively. All samples from one experiment were measured in one assay.

Microdissection of selected brain nuclei

Fresh frozen brains were cut into 200-µm-thick slices in a cryostat (Leica), mounted on pre-cooled, untreated glass slides (ThermoFisher) and stored at − 80 °C until used. The regions of the cVLM and cDMM, the SON, the PVN and the AV3V were dissected out guided by the Rat Brain Atlas (Paxinos and Watson 2007), using a modified Palkovits punch technique (Palkovits 1973). Briefly, for dissection, the slides were placed back into the cryostat and kept there during the whole procedure at – 10 °C. The individual nuclei were visualized using a head magnifier and removed from the sections using sterile punch needles with an inside diameter of 0.7 mm. The punch samples were collected immediately in ice cold Eppendorf tubes containing 100 µl of radioimmunoprecipitation assay buffer (RIPA, 50 mM TrisHCl, 150 mM NaCl, 1 mM EDTA, 1% Triton X-100, 0.1% SDS, 0.25% Na-deoxycholate, pH = 7.4) and a cocktail of protease and phosphatase inhibitors (ThermoFisher). Samples were homogenized, lysed and then stored at − 80 °C until used for western blot.

Western blot

Samples were centrifuged to separate cell debris and nuclei (20,000 *g*, 30 min at 4 °C). The protein concentrations in the supernatant were measured using the Pierce™ BCA Protein Assay Kit (ThermoFisher) according to the instructions of the manufacturer. Samples containing identical brain areas were diluted to equal final protein concentrations and denatured in 2 × Laemmli buffer (Bio-Rad Magyarország Kft., Budapest, Hungary). Proteins (10 µg/sample) were separated in a 13.5% SDS-PAGE gel with 10% stacking gel. After transferring onto PDVF membranes (Merck Millipore, Budapest, Hungary), the membrane-bound protein samples were blocked in 5% BSA for 1 h and subsequently exposed to one of the following primary antibodies: anti-nesfatin-1 (1–82) (Phoenix Europe GmbH, Karlsruhe, Germany, CAT# H-003–22, dilution 1:2000), anti-TH (Merck, CAT# AB152, dilution 1:1000), anti-TH phosphorylated at Ser31 (Sigma, CAT# SAB4300674, dilution 1:1000), anti-PrRP-R (ThermoFisher, CAT# PAS 75,372, dilution 1:1000), all made in rabbit, and then to anti-β-actin (Sigma, CAT# A1978, made in mouse, dilution 1:5000). Signals were visualized using HRP-conjugated goat anti-rabbit or mouse antibodies (Cell Signaling Technology Europe B.V., Frankfurt, Germany, dilution 1:5000) and Chemiluminescent HRP Substrate (Merck), or by fluorescently labeled goat anti-mouse IgG (AzureSpectra 700, Azure Biosystems, Dublin, CA, dilution 1:1000) and detected with the Azure c600 imaging system (Azure Biosystems). Densitometric analyses of the protein bands were performed with the help of the ImageJ

application. The average/animal data ($n = 4$) normalized to β-actin were compared statistically.

Immunohistochemistry

Serial coronal free-floating sections (50 µm-thick, 200 µm apart) from the hindbrain and from the hypothalamus were immunostained for PrRP. One series of hypothalamic sections from a control Wistar rat was double immunostained for PrRP and TH. The sections were incubated in 1% BSA containing 0.5% TX-100 (Sigma) in PBS for 1 h, to block non-specific binding sites in the tissues and to enhance penetration of the antibodies. The sections were then boiled using a microwave in 0.1 M citric acid (pH = 6.0), to perform antigen retrieval and eliminate endogenous HRP activity simultaneously (Toth and Mezey 2007). The rabbit anti-PrRP antibody (https://www.phoenixpeptide.com/products/view/Antibodies/H-008-52, Phoenix, dilution 1:8000) was applied for 2 days at 4 °C. Visualization was performed using the Vectastain-ABC-HRP Kit (Vector Laboratories, Burlingame, CA, CAT# PK 6100) and FITC-tyramide reaction (PerForm, CAT# NEL701A001KT). Double immunostained sections were then further incubated in mouse anti-TH (Millipore, Temecula CA, CAT# MAB318, https://www.merckmillipore.com, dilution 1:200) for 2 days at 4 °C, and in donkey anti-mouse AlexaFluor647 (ThermoFisher, dilution 1:100) for 2 h at room temperature. Control immunostainings were performed by omitting the primary antibodies from the reactions and showed no signals. The sections were mounted on precleaned slides and coverslipped with Vectashield mounting medium (Vector).

Evaluation of the PrRP immunostained sections

Hindbrain sections immunostained for PrRP were evaluated between 14.04 and 14.70 mm caudal from the bregma level. Hypothalamic sections were analyzed between the − 0.12 and + 0.24 mm, the 0.6–1.08 mm and the 1.3–1.8 mm relative levels to bregma, and contained the AV3V, the SON and the PVN, respectively (Paxinos and Watson 2007). Sections were scanned on a confocal laser scanning system using the same settings across the animals (Zeiss, LSM780, Plan-Apochromat 10×/0.45 M27, pixel size: 0.8303 µm^2, optical thickness: 25 µm). The number of PrRP-positive cells was counted in the cVLM and NTS in at least two sections per animal bilaterally, using the touch-count tool in the ImageJ application. The density of the immunoreactive fibers was determined in regions of interest (ROI: MnPO: 260 µm × 280 µm, PVN: 200 µm × 200 µm, SON: 40 µm × 40 µm) in two–three sections per animal, bilaterally. The area of the fibers within each ROI was determined with the help of the threshold function in the ImageJ application and divided with the area of the ROI. Measurements were made by an experimenter blind to the experimental settings. The average/animal data ($n = 4$) were compared statistically.

PrRP and TH coexpression analysis

Coexpression was measured in the above-mentioned hypothalamic areas in high magnification (Plan-Apochromat 60×/1.4 VC) confocal images (Bio-Rad Laboratories, Hemel Hempstead, UK). For each field 16–20 single optical sections were acquired at a z-separation of 2 µm (z-stack) from two sections/area bilaterally. Images with the most intense signals (at least 6/z-stack) were selected for analyses with the help of ImageJ application. Percentage data are expressed as means ± SEM obtained from the four z-stacks in each areas.

Statistics

Data analyses were performed by investigators blind to treatments. Statistical significances were calculated by employing the Sigmastat 3.5 application (Systat Software Inc., Chicago, IL). Student's *t* test (two-tailed) was used when comparing two groups with normal distribution of the data, otherwise Mann–Whitney *U* test was applied. Two-way ANOVA followed by Student–Newman–Keuls post hoc analysis was used for calculating statistical significance for four groups with two treatments. One-way ANOVA with repeated measures was used to analyze fluid and food intake values across the 6 days of HS or NS. Data were assessed for normality and equal variances before running ANOVA analyses. Results are expressed as means ± SEM values. Pearson method was used to calculate correlations. Differences between groups were considered statistically significant when $p < 0.05$.

Results

Body parameters, food and water intake

Lower bodyweight ($p < 0.05$) and higher plasma osmolalities ($p < 0.001$) were measured in DI animals compared to the age-matched WT peers. Despite the chronic hypernatremia, the relative adrenal and thymus weights were normal. DI rats consumed less food than WT rats ($p < 0.01$), but since they consumed according to their bodyweight, no alteration in the relative daily food intake was seen. The excessive absolute and relative daily water intake ($p < 0.001$ for both parameters) however, confirmed the diagnosis of diabetes insipidus (Table 1).

In Wistar rats, high salt intake for 6 days resulted in dramatic weight loss as opposed to weight gain observed in controls ($p < 0.001$). The plasma osmolality was elevated compared to non-challenged (NS) mates ($p < 0.001$),

Table 1 Body parameters, daily food and water intakes of homozygous (+/+ and −/−) Brattleboro rats

	WT	DI
Body weight (g)	408 ± 93	56* ± 15
Plasma osmolality (mOsm/L)	305 ± 43	35*** ± 2
Relative adrenal weight (g/bwkg)	97 ± 59	5 ± 9
Relative thymus weight (g/bwkg)	923 ± 82	815 ± 78
Food intake (g)	24 ± 1	21** ± 1
Relative food intake (g/bwkg)	66 ± 3	63 ± 3
Water intake (g)	31 ± 1	147*** ± 6
Relative water intake (g/bwkg)	76 ± 3	415*** ± 16
n	7	7

Food and water consumptions were measured for 5 consecutive days

Means ± SEM, Student's *t* tests, $p^{*} < 0.05$, $p^{**} < 0.01$ and $p^{***} < 0.001$ vs. WT

DI vasopressin-deficient genotype with diabetes insipidus, *WT* wild-type animals of the Brattleboro strain

Table 2 Effect of 2% NaCl solution (high salt; HS) intake for 6 days on body parameters of Wistar rats

	NS	HS
Bodyweight change (g)	49 ± 2	− 46*** ± 5
Plasma osmolality (mOsm/L)	304 ± 1	363*** ± 7
Relative adrenal weight (g/bwkg)	166 ± 8	219* ± 17
Relative thymus weight (g/bwkg)	2349 ± 139	944*** ± 102
n	8	8

Control subjects received tap water (normal salt; NS). Means ± SEM, Student's *t* tests, $p^{*} < 0.05$ and $p^{***} < 0.001$ vs. NS

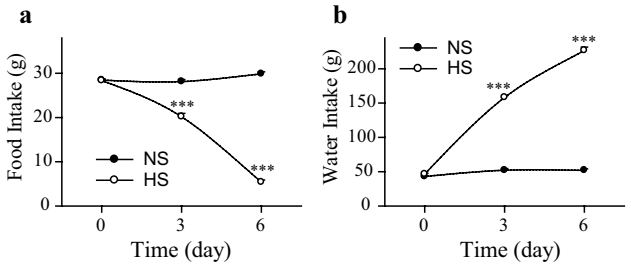

Fig. 1 Food (**a**) and fluid (**b**) consumptions of high salt loaded and normal Wistar rats. High salt solution intake evoked dramatic reduction and elevation in food and fluid consumption, respectively. Means ± SEM, Student's *t* tests, $p^{***} < 0.001$ vs. the same day values of non-salt loaded control rats, $n = 16$. *HS* 2% NaCl intake for 6 days, *NS* normal salt solution (tap water) drinking controls

or even DI rats ($p < 0.01$). HS rats suffered from chronic stress; they developed adrenal hypertrophy ($p < 0.05$) and extensive thymus involution ($p < 0.001$) during the

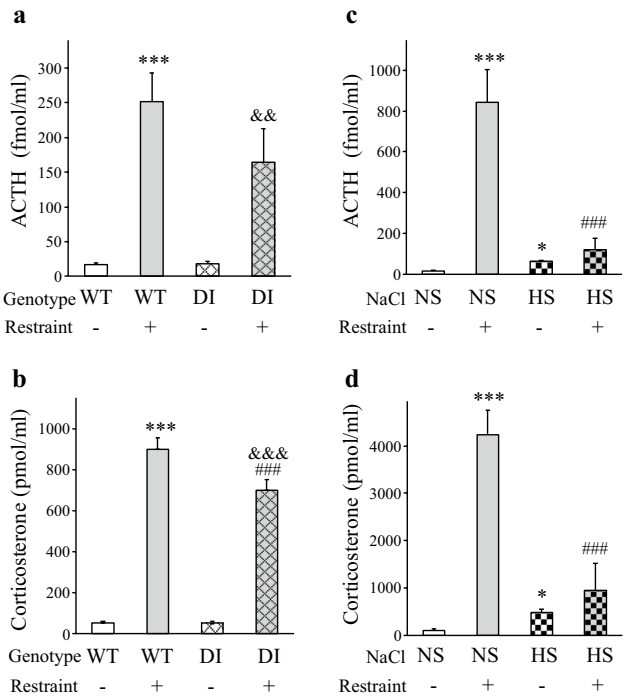

Fig. 2 Plasma adrenocorticotropic hormone and corticosterone concentrations in chronic hypernatremia and 1 h after acute restraint stress. ACTH (**a**) and corticosterone (**b**) levels in homozygous WT and DI Brattleboro rats. The basal hormone levels were similar between the WT and DI genotypes. The acute restraint (R) evoked large ACTH and corticosterone elevations in both genotypes, although the corticosterone response in the DI-R group was slightly reduced compared to the WT-R group. ACTH (**c**) and corticosterone (**d**) levels in the HS model. Chronic hypernatremia elicited by HS intake resulted in mild, but significant elevations in basal hormone levels. The acute restraint evoked large ACTH and corticosterone responses in the NS-R group. Hormonal responses were greatly inhibited in the HS-R group. Means ± SEM, Student's *t* test, $p^{*} \leq 0.001$ HS vs. NS control group, Two-way ANOVA, significance indicate the results of Student–Newman–Keuls post hoc tests, $p^{***} \leq 0.001$ vs. the WT or NS control groups, $p^{\#\#\#} \leq 0.001$ vs. the WT-R or NS-R group, $p^{\&\&\&} \leq 0.001$ and $p^{\&\&} \leq 0.01$ vs. the DI control group, DI model: $n = 7$; HS model: $n = 7$–8. *ACTH* adrenocorticotropic hormone, *DI* vasopressin-deficient genotype with diabetes insipidus, *WT* homozygous wild-type animals of the Brattleboro strain

treatment (Table 2). Food intake decreased ($p < 0.001$) (Fig. 1a), while fluid intake increased ($p < 0.001$) (Fig. 1b) gradually during HS intake.

Plasma ACTH and corticosterone concentrations

The basal ACTH and corticosterone levels were normal in DI rats suggesting the HPA axis was adapted to the congenital hypernatremia (Fig. 2a, b). The acute stress (restraint) evoked large ACTH (WT vs. WT-R: $p < 0.001$, DI vs DI-R: $p < 0.01$) and corticosterone (WT vs. WT-R and DI vs DI-R: $p < 0.001$) release. The corticosterone response was slightly

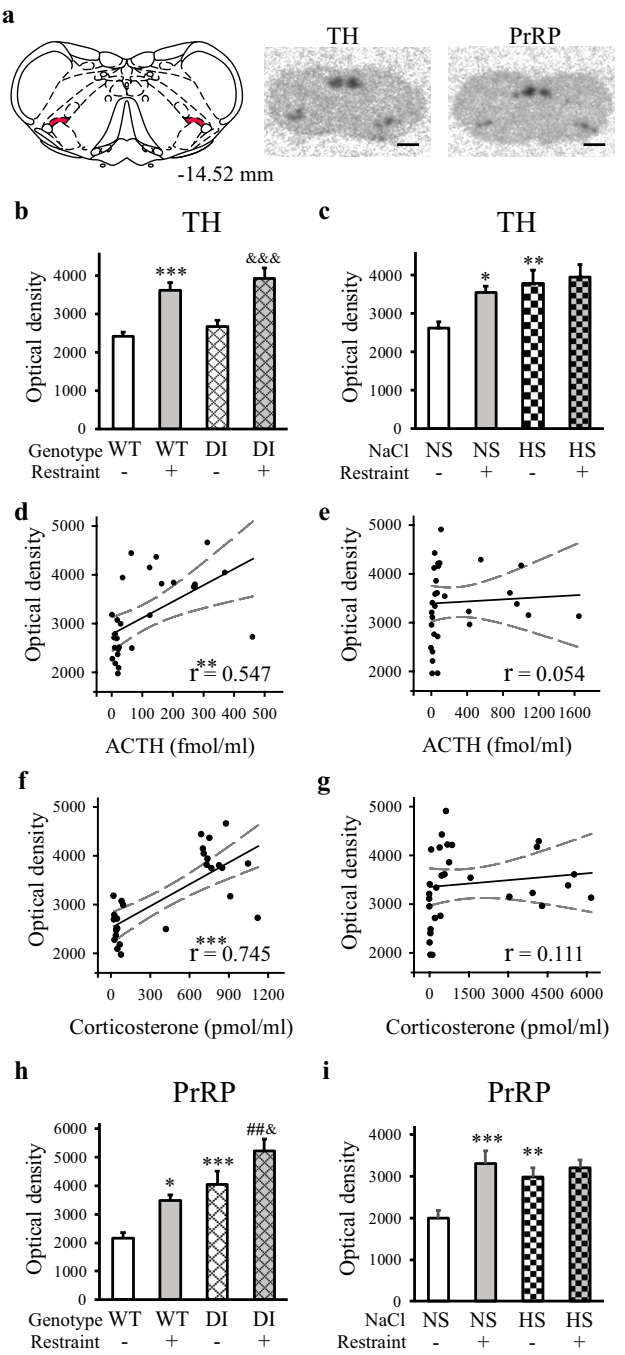

Fig. 3 Tyrosine hydroxylase and prolactin-releasing peptide mRNA levels in chronic hypernatremia and 3 h after acute restraint stress in the caudal ventrolateral medulla. **a** Location of the cVLM (left) and illustrative autoradiographic pictures (right). The red shaded regions in the drawing (Paxinos and Watson 2007) label the cVLM. The images display the in situ hybridization signals (dark spots) and were captured by storage phosphor screens. Distance from the bregma is indicated in millimeters. Scale: 4 mm. **b**, **c** TH mRNA. In Brattleboro rats, restraint evoked large increase, whereas the genotype had no effect (**b**). HS or restraint applied separately evoked TH mRNA level elevations in Wistar rats. Prior HS blunted the TH response for restraint (**c**). **d–g** Associations between the TH mRNA and ACTH or corticosterone levels. Both ACTH (**d**) and corticosterone (**f**) values showed strong relationships with TH mRNA levels in the DI model. There were no associations between these data (**e** and **g**, respectively) in the HS intake model. **h**, **i** PrRP mRNA. Both the DI genotype and restraint increased PrRP mRNA levels in Brattleboro rats, resulting in the largest reaction in the DI-R group (**h**). HS or restraint applied separately evoked PrRP mRNA level elevations in Wistar rats. Prior HS blunted the response for restraint (**i**). Bar graphs: means ± SEM, Two-way ANOVA, significance indicate the results of Student–Newman–Keuls post hoc tests, $p^{***} < 0.001$, $p^{**} < 0.01$, or $p^{*} < 0.05$ vs. WT or NS control groups, $p^{\#\#} < 0.01$ vs. WT-R animals, $p^{\&\&\&} < 0.001$ and $p^{\&} < 0.05$ vs. DI control rats, DI model: $n = 7$; HS model: $n = 8$. Correlation graphs: solid and dashed lines show linear regressions and 95% confidence intervals, respectively, see Pearson correlation coefficients (r) in the graphs, $p^{***} < 0.001$, $p^{**} < 0.01$, DI model: $n = 28$; HS model: $n = 31$. *PrRP* prolactin-releasing peptide, *TH* tyrosine hydroxylase, *cVLM* caudal ventrolateral medulla

subnormal in DI-R rats (WT-R vs. DI-R: $p = 0.001$) (Fig. 2a, b).

HS intake resulted in elevated basal ACTH and corticosterone levels (Student's t tests, $p \leq 0.001$ for both parameters) (Fig. 2c, d). The acute restraint evoked large ACTH and corticosterone release (NS vs. NS-R: $p < 0.001$ for both hormones), but the responsiveness of the HPA axis was greatly inhibited in the HS-R group (NS-R vs. HS-R: $p < 0.001$ for both hormones, HS vs. HS-R: no significant differences) (Fig. 2c, d).

Very high correlations were found between the ACTH and corticosterone values in both models (R_{DI} model = 0.827, $n = 28$; and R_{HS} model = 0.907, $n = 31$, $p < 0.00001$), indicating that the sensitivity of adrenal corticosterone secretion to plasma ACTH levels was maintained.

TH, PrRP and NUCB2 mRNA levels in the cVLM

In the cVLM (Fig. 3a), the basal amounts of TH mRNA were similar in the WT and DI rats (Fig. 3b), but differed between the NS and HS animals (NS vs. HS: $p < 0.01$) (Fig. 3c). The acute restraint evoked large increase in TH mRNA levels in the wild-type and DI Brattleboro rats (WT vs. WT-R and DI vs. DI-R: $p < 0.001$) (Fig. 3b), and in the normal Wistar rats (NS vs. NS-R: $p < 0.05$) (Fig. 3c). HS animals with elevated TH mRNA levels however, failed to react to restraint with TH mRNA increase (Fig. 3c). Therefore, TH mRNA levels correlated well with ACTH ($p < 0.01$) and corticosterone ($p < 0.001$) levels in the DI (Fig. 3d, f), but not in the HS intake model (Fig. 3e, g).

PrRP mRNA quantity was heightened by both DI (WT vs. DI: $p < 0.001$) and restraint (WT vs WT-R: $p < 0.05$), resulting in the highest mean value in the DI-R group (WT-R vs. DI.-R: $p < 0.01$, DI vs DI-R: $p < 0.05$) (Fig. 3h). PrRP mRNA changes in the HS model were similar to that of TH mRNA (NS vs. HS: $p < 0.01$ and NS vs. NS-R: $p < 0.001$). The PrRP mRNA response to the acute restraint was entirely impeded in the HS-R animals (Fig. 3i).

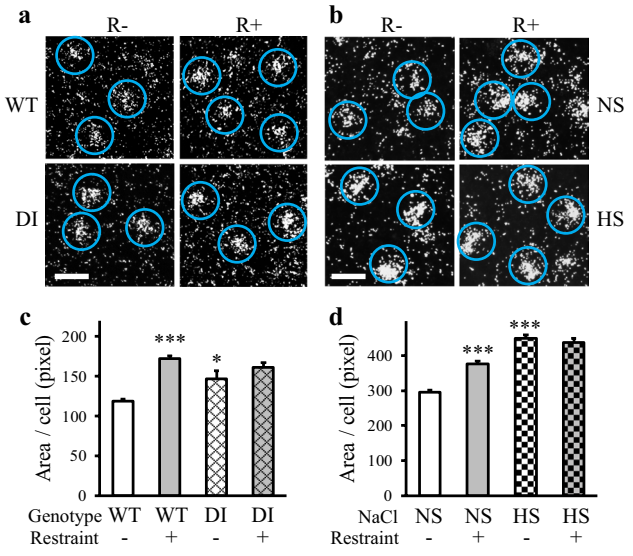

Fig. 4 NUCB2 mRNA levels in chronic hypernatremia and 3 h after acute restraint stress in the cVLM. **a**, **b** Illustrative darkfield microphotographs of the autoradiographic emulsion-coated sections displaying NUCB2 mRNA expressing cells encircled by blue ROIs. The in situ hybridization signals are seen as clusters of silver grains (white dots) over the cells. Scales: 40 µm **c**, **d** Chronic hypernatremia and restraint elevated NUCB2 mRNA levels in both models, when applied separately. No reactions were observed in the double challenged rats. Means ± SEM, two-way ANOVA, significance indicate the results of Student–Newman–Keuls post hoc tests, $p^{***} < 0.001$, $p^{*} < 0.05$ vs. WT or NS control rats, DI model: $n = 4$–5; HS model: $n = 8$

NUCB2 mRNA expressing cells were clearly visible in the emulsion-coated sections (Fig. 4a, b). The signal intensities were higher in hypernatremic animals (WT vs. DI: $p < 0.05$, NS vs. HS: $p < 0.001$), and in the restraint stressed groups (WT vs. WT-R and NS vs. NS-R: $p < 0.001$) compared to normal controls. Prior chronic osmotic stress inhibited the NUCB2 responses to restraint in both models (Fig. 4c, d).

TH, PrRP and NUCB2 mRNA levels in the cDMM

In the cDMM (Fig. 5a), TH, PrRP and NUCB2 mRNA levels were unaffected by acute restraint in both models (Fig. 5b–g). The amounts of TH mRNA were also normal in the hyperosmotic DI and HS rats (Fig. 5b, c).

PrRP mRNA values were increased in the DI rats (WT vs. DI and WT-R vs. DI-R: $p < 0.001$), (Fig. 5d), but they were reduced by HS intake (NS vs. HS: $p < 0.01$, NS-R vs. HS-R: $p < 0.001$) (Fig. 5e).

NUCB2 mRNA levels have changed similarly to that of PrRP mRNA in the Brattleboro rats and they were elevated by hyperosmolality (WT vs. DI: $p = 0.01$, WT-R vs. DI-R: $p < 0.05$) (Fig. 5f). HS intake also increased the

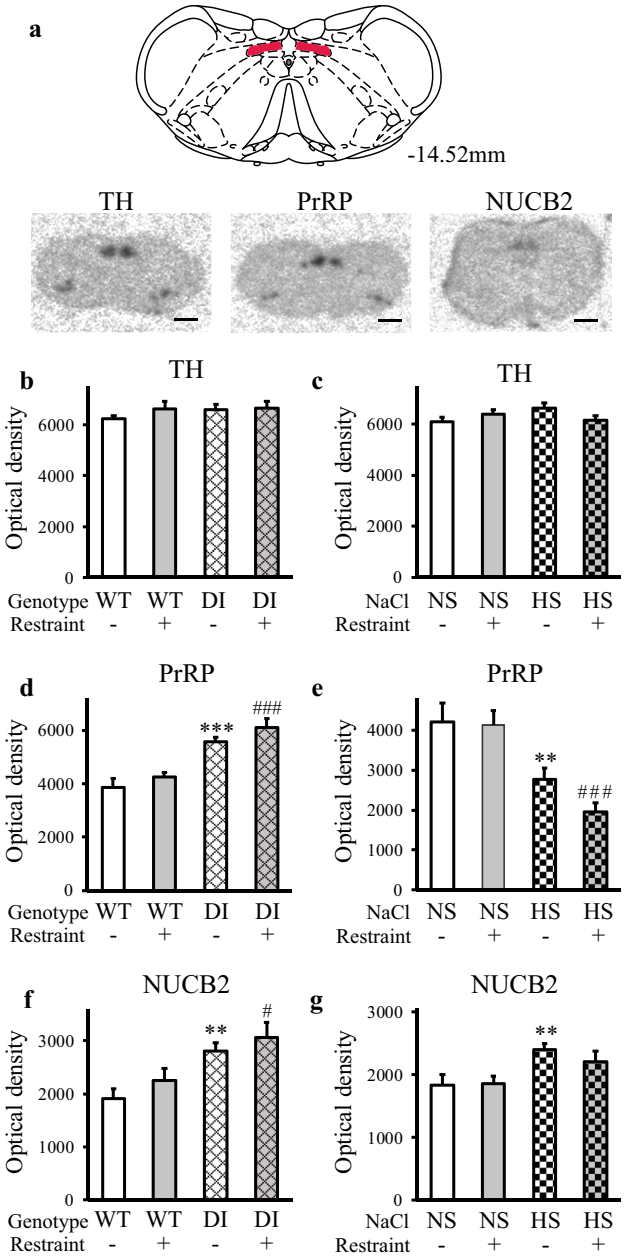

Fig. 5 TH, PrRP and NUCB2 mRNA levels in chronic hypernatremia and 3 h after acute restraint stress in the caudal dorsomedial medulla. **a** Location of the measured area within the cDMM (top) and illustrative autoradiographic pictures (bottom). The red shaded regions in the drawing (Paxinos and Watson 2007) label the measured area (nucleus of the solitary tract). The images display the in situ hybridization signals (dark spots), and were captured by storage phosphor screens. Distance from the bregma is indicated in mm. Scale: 4 mm. **b, c** TH mRNA. There were no alterations in either of the hypernatremia models; DI (**b**), HS intake (**c**). **d**, **e** PrRP mRNA. Increased levels were measured in the AVP deficient Brattleboro rats, independently of restraint (**d**). Depressed amounts of PrRP mRNA were detected in Wistar rats challenged by HS intake (**e**). Restraint had no effect in either of the models. **f**, **g** NUCB2 mRNA. Chronic hypernatremia elevated NUCB2 mRNA levels in both models. Restraint had no effect in either of the models. Means ± SEM, Two-way ANOVA, significance indicate the results of Student–Newman–Keuls post hoc tests, $p^{***} < 0.001$ and $p^{**} \leq 0.01$ vs. WT or NS control rats, $p^{\#\#\#} < 0.001$ and $p^{\#} < 0.05$ vs. WT-R or NS-R animals, DI model: $n = 7$ (**b**, **d**), $n = 4$–5 (**f**); HS model: $n = 8$. *cDMM*: caudal dorsomedial medulla

levels of NUCB2 mRNA (WT vs. HS: $p < 0.01$, NS-R vs. HS-R: $p = 0.085$) (Fig. 5g).

Chronic high salt intake evoked changes in protein expressions in the medulla and the hypothalamus

To better understand the molecular mechanisms of adaptation to chronic hypernatremia, we performed further investigations in the HS model. In harmony with the mRNA results, both TH ($p < 0.05$) and NUCB2 ($p < 0.05$) (43 kDa product) protein levels (measured by Western blot) were heightened by chronic HS intake in the cVLM (Fig. 6a). No alterations were measured in the amounts of these proteins in the cDMM (Fig. 6a). PrRP isoforms (PrRP31: 3.6 KDa, PrRP20: 2.6 KDa) were too small for western blot analysis. Therefore, the number of the PrRP-immunopositive cells was determined to evaluate expressional changes. The number of the PrRP-immunopositive cells was higher in the HS compared to NS group ($p < 0.05$) in the cVLM, in agreement with the mRNA measurements. However, in the cDMM, where we found reduced PrRP mRNA levels in the HS group, the number of the PrRP-immunopositive cells was maintained (Table 3).

PrRP and TH innervations were analyzed in the main osmoregulatory centers: the AV3V, PVN and SON. The PrRP fiber network was the richest in the PVN. More than two-thirds of the analyzed varicosities contained both TH and PrRP immunoreactivity in the AV3V and the PVN, and almost all were double labeled in the SON in control rats (Fig. 6b, c). Thus, the majority of the PrRP-positive fibers originated from the A1 or A2 cell groups. HS intake enhanced the density of the PrRP-positive fibers in all of the investigated regions ($p < 0.05$), (Table 3, Fig. 6d, e). Within the PVN, this was more obvious in the medial parvocellular region and less in the magnocellular parts of the nucleus, where the PrRP fiber network was poor (Fig. 6e). Several neurons expressed PrRP-R in the AV3V (mainly in the MnPO and in the anteroventral periventricular nucleus) and the medial parvocellular PVN. Neurons in the magnocellular PVN and SON failed to express PrRP-R (Fig. 6f). Chronic hypernatremia downregulated the amount of the PrRP-Rs (measured by Western blot) in the PVN ($p < 0.05$). The decrease in the AV3V did not reach the level of significance (Fig. 6g). Parallel with the increased PrRP innervation, TH phosphorylation at Ser31 (TH-Ser31) was upregulated in all of the HS samples (AV3V, SON: $p < 0.05$, PVN: $p < 0.001$) indicating a stimulated catecholamine release (Fig. 6g).

Discussion

Chronic hypernatremia triggers central reactions affecting the neuroendocrine, autonomous and behavioral circuits. NE and PrRP containing medullary axons target critical hypothalamic centers organizing these reactions and probably exert an enhanced signaling during chronic hypervolemic hypernatremia. Cooperation of NE and PrRP under this condition may represent a basis for the ongoing adaptation mechanisms. Contribution of nesfatin acting by autocrine/paracrine manner within the cVLM and cDMM is also suggested.

High salt solution intake for 6 days resulted in the development of typical, somatic signs of chronic stress due to the chronic, mild elevation of the resting plasma corticosterone level in adult rats. In contrast, genetically AVP deficient adult DI rats exhibited no somatic signs of chronic stress and normal basal plasma ACTH and corticosterone concentrations. The difference between the two models may explain the above findings. DI causes euvolemic hypernatremia, as an outcome of water loss through the kidneys, without high blood pressure (Sun 2006). In contrast, sodium overconsumption causes hypervolemic hypernatremia, elevated plasma AVP concentration and blood pressure (Choe et al. 2015). The plasma osmolality in the DI group was significantly lower than in the HS group. The mean corrected food intake of DI rats was normal. HS intake, however, caused dehydration-induced anorexia (Boyle et al. 2012). During the embryonic development, several alterations take place in the expression of different genes and neuronal pathways in DI rats to compensate for the lack of AVP (Scholer and Sladek 1981; Bundzikova et al. 2008; Pouzet et al. 2001; Yang and Coote 2007). Plasticity in response to challenges in adulthood is much more limited. All in all, HS intake represented a higher degree of homeostatic threat for the cardiovascular and osmotic control as well as the regulation of the energy balance. This definitely produced a higher level of stress in animals challenged by HS intake compared to DI rats.

Severe functional impairment of the HPA axis was displayed only when hypernatremia evoked serious chronic stress: the ACTH and corticosterone responses to acute restraint were absent in HS-R animals, while they were almost intact in the DI-R group. These hormonal responses to acute restraint greatly depend on the ascending medullary NE transmission towards the PVN (Gaillet et al. 1991; Pacak et al. 1995; Flak et al. 2014). Indeed, the acute restraint upregulated the expression of TH in the A1 cell group in the non-hypernatremic rats in both models (WT-R, NS-R). It seemed, however, that the type of hypernatremia affected the basal level of TH in the A1 cell group differentially (normal in DI and high in HS rats), and the level of TH determined

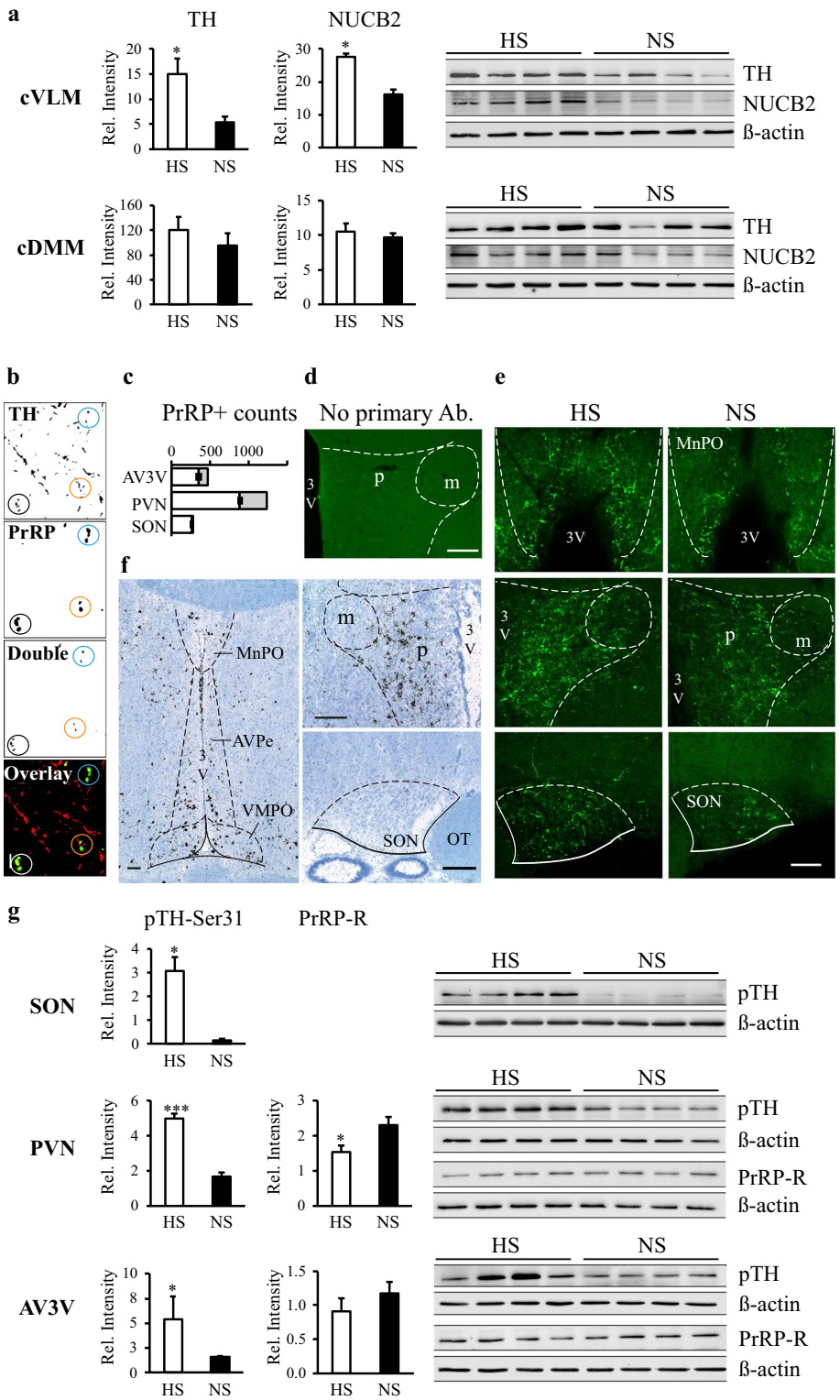

the responsiveness of the HPA axis for the acute restraint (normal in DI-R and blunted in HS-R rats). The correlation data between the TH and ACTH/corticosterone measurements confirmed this idea. Thus, a ceiling effect in the TH (the rate limiting enzyme for NE synthesis) expression may have contributed to the impaired HPA axis responsiveness.

The exhaustion of TH capacity in the A1 cell group in chronic HS intake occurs probably for complex reasons. Chronic HS intake challenges strongly the osmotic and

◂**Fig. 6** Chronic high salt intake induced changes in protein expressions. **a** Western blots and quantification of TH and NUCB2 signals in the cVLM and cDMM. Intensity values were normalized to β-actin. TH and NUCB2 protein levels were heightened in the cVLM, but not in the cDMM in response to HS intake. **b** Coexpression analysis of TH- and PrRP- immunoreactive profiles in normal Wistar rats. Illustrative, binary, confocal images (single optical layer) and the color-coded overlay picture (red: TH, green: PrRP, yellow: coexpression) of the same field within the SON. The identical circles feature identical elements. Double-labeled elements were calculated by the ImageJ program. Scale: 10 µm. **c** Quantitative results of the coexpression analysis. The number of PrRP-positive profiles were the highest in the PVN. Most of the counted profiles were double-labeled for TH and PrRP (white columns). The amount of the single PrRP-positive profiles were less than 30% in the AV3V and the PVN, and less than 10% in the SON (grey columns). **d**, **e** HS intake elicited changes in PrRP immunoreactivity. Control immunostaining for PrRP in the PVN (**d**). No signal is seen by omitting the primary antibody from the reaction. HS intake increased the density of PrRP-positive fibers in all investigated regions (**e**): the AV3V (MnPO, top), PVN (middle) and SON (bottom). Note, that PrRP fibers expand both in the parvo- and the magnocellular parts of the PVN during HS intake. Scale: 100 µm. **f** Pattern of the PrRP-receptor mRNA expression in the investigated hypothalamic areas. In situ hybridization signals (black silver grain clusters) in the AV3V region (left), the PVN (top right) and the SON (bottom right). Positive cells are present in the AV3V and the parvocellular PVN. Note, signals avoid the magnocellular PVN and the SON. The sections were counterstained with Giemsa. Scales: 100 µm. **g** Western blots and quantification of pTH-Ser31 and PrRP-receptor peptide levels in the hypothalamus. Intensity values were normalized to β-actin. The amounts of pTH-Ser31 increased in all measured regions in HS rats. PrRP-receptor level decreased in the PVN in response to HS. Means ± SEM, Student's *t* test, $p^{***} < 0.001$, $p^{*} < 0.05$ vs. NS group, $n = 4$. *Ab* antibody, *AV3V* anteroventral third ventricular area, *AVPe* anteroventral preoptic nucleus, *MnPO* median preoptic nucleus, *OT* optic tract, *PrRP-R* PrRP-receptor, *pTH-Ser31* phosphorylated TH at Ser31, *PVN* hypothalamic paraventricular nucleus, *m* magnocellular and *p* parvocellular parts of the PVN, *SON* supraoptic nucleus, *VMPO* ventromedial preoptic nucleus, *3V* third ventricle

cardiovascular regulations and NE of A1 origin is crucial for these functions (Day 1989; Fernandez-Galaz et al. 1994; Tanaka et al. 1997; Pedrino et al. 2008). It probably also plays an important role in the chronic activation of the HPA axis during hypernatremia, since the medullary catecholamine cell groups mediate HPA axis responses for stimuli that signal homeostatic perturbations (Ulrich-Lai and Herman 2009; Gaillet et al. 1991; Pacak et al. 1995; Ritter et al. 2003; Bienkowski and Rinaman 2008; Khan et al. 2011).

According to our data, PrRP and nesfatin may assist within certain limits when the need for NE is high. Moreover, the regulation of the TH, PrRP and nesfatin genes is coordinated. Both were upregulated by restraint and by chronic hypernatremia in the cVLM in both models. The acute restraint evoked PrRP response was in association with the TH capacity and the overload of the stress axis. Thus, it was maintained in the DI, but not the HS loaded rats. The nesfatin response to restraint was blunted by prior chronic hypernatremia in both models. Coordinated regulation of the genes coding TH, PrRP and nesfatin within the same cell can happen in several ways. Glucocorticoids exert central feedback in stress by regulating gene expression. Glucocorticoid signaling is altered in the A1 neurons by chronic stress (Kitayama et al. 1989), which may affect the expression of TH, PrRP and nesfatin. The expression of these genes may also be affected by neural inputs modulating the excitability of cells. Such inputs may arrive primarily from the cDMM, forwarding essential information from the peripheral baro- and osmoreceptors (Chan et al. 1995), and from the hypothalamus, exerting a descending control (Toth et al. 1999; Bourque 2008). Moreover, local regulatory short loops may be important in neuromodulation. Nesfatin is a good candidate acting by an autocrine/paracrine way (Foo et al. 2008). In vitro effects of nesfatin on the excitability of cDMM and PVN neurons have already been demonstrated (Price et al. 2008; Mimee et al. 2012).

During habituation to chronic salt loading, restraint and inflammatory stress upregulation of AVP was observed in the CRH neurons of the parvocellular PVN (Harbuz et al. 1992; Ma and Lightman 1998; Amaya et al. 2001; Toth et al. 2008). AVP may contribute to ACTH (and corticosterone) secretion acting on the anterior lobe of the pituitary via V1b receptors in synergism with CRH (Antoni 1993). Actually, the role of parvocellular AVP was emphasized in the development of the blunted ACTH response to acute stress (restraint) in Sprague-Dawley rats with chronic osmotic stimulation (water deprivation) (Grinevich et al. 2001). However, the ACTH response was just marginally impaired in DI rats with no AVP, compared to the HS intake rats. This controversy may also be due to the limitation of the knock-out model. Nevertheless, upregulation of PrRP in the NE neurons takes place during adaptation to chronic restraint in the medulla (Toth et al. 2008). By demonstrating the upregulation of the coexpressed neurotransmitters in the cVLM in chronic hypernatremia, we showed that this phenomenon is part of a general mechanism in habituation to chronic stressful stimuli.

The adaptation of the "healthy organism" to chronic hypernatremia has further been investigated in the HS model with aggressive alterations in the measured parameters and lacking the compensatory mechanisms that had been developed in the AVP-deficient rats throughout the ontogenesis.

TH, PrRP and NUCB2 protein levels were all elevated in the cVLM in the HS group compared to the NS group. This was in harmony with the mRNA data pointing to a balanced reaction to an increased demand. In the cDMM, discrepancies were found between the mRNA and protein data, pointing to an increased demand for PrRP and nesfatin that disturbed the dynamics between the synthesis and transport/release (Sterrenburg et al. 2011).

The increased NE and PrRP turnover during high salt loading was confirmed by the examination of the

Table 3 Prolactin-releasing peptide immunoreactivity in the different brain areas after high salt intake

	Cell number/section		Fiber density (μm²/100 μm²)			*n*
	cVLM	cDMM	AV3V	SON	PVN	
NS	6.3 ± 0.8	52.3 ± 3.7	1.2 ± 0.2	1.0 ± 0.1	4.2 ± 0.2	4
HS	10.8* ± 1.4	52.5 ± 5.4	3.0* ± 0.2	1.4* ± 0.1	10.2* ± 1.6	4

AV3V periventricular anteroventral third ventricle region, *cDMM* caudal dorsomedial, *cVLM* caudal ventrolateral medulla oblongata, *PVN* hypothalamic paraventricular nucleus, *SON* supraoptic nucleus. Means ± SEM, Student's *t* tests, $p^* < 0.05$ vs. NS controls

hypothalamic terminal fields. The elevated pTH-Ser31 levels pointed to an ongoing NE release (Dunkley et al. 2004; Haycock 1993; Daubner et al. 2011; Ong et al. 2012) in the SON, PVN and the AV3V in HS rats. Undoubtedly, since NE innervation of these areas arises almost exclusively from the A1 and A2 cell groups (AV3V: ~ 100%, PVN: 94%, SON: 89%), NE has been released primarily from the axons of the A1 and A2 cells (Sawchenko and Swanson 1981). The A1 and A2 neurons are practically identical to PrRP neurons (Chen et al. 1999), and a very high percentage of the PrRP-positive fibers was of A1 or A2 origin in the AV3V, PVN and SON. Together with the heightened density of PrRP-positive fibers found in the investigated hypothalamic regions in the HS group, these results provide convincing evidence that the sustained NE release is linked with PrRP corelease.

Regarding the known cooperation between NE and PrRP in the AVP and ACTH release (Maruyama et al. 2001; Uchida et al. 2010), as well as in habituation to chronic stress (Toth et al. 2008), we assume that PrRP acts synergistically with NE in the different responses to chronic hypernatremia. Coordinated or independent PrRP release, however, from the non-NE PrRP cells located in the dorsomedial nucleus cannot be excluded.

Several central behavioral, autonomic and hormonal reactions are triggered by the increased plasma sodium level. These include the generation of thirst, reducing sodium appetite, increasing renal sodium excretion and water retention, elevation of blood pressure and parallel activation of renal sympatho-inhibition (Bourque 2008; Dos Santos Moreira et al. 2017). Noradrenergic inputs to the SON, PVN and the AV3V from the A1 and A2 cell groups are essential to trigger these reactions (Fernandez-Galaz et al. 1994; Pedrino et al. 2005, 2008, 2012; Dos Santos Moreira et al. 2017). Based on our results, the central role of PrRP in all these functions is therefore emerging.

In the parvocellular PVN, not only the density of the PrRP fibers was enhanced, but the receptors were also downregulated, further confirming the augmentation of PrRP release in HS rats. This highlights the putative role of PrRP in the control of the dehydration-induced anorexia (in addition to the already discussed regulation of the HPA axis). Both food intake and bodyweight of HS rats were reduced. PrRP acts as an anorexigen, which is mediated by CRH neurons in the parvocellular PVN (Lawrence et al. 2004). Negative energy balance (e.g. food restriction, lactation) therefore downregulates the expression of PrRP (Lawrence et al. 2000). In dehydration-induced anorexia, however, central mechanisms might be turned on to reduce food intake, which is a way to compensate the excessive salt intake (Boyle et al. 2012). Thus, expression of PrRP is expected to be increased, which is in harmony with our results.

In the magnocellular PVN and SON, PrRP innervation was weak, but inducible by HS intake. PrRP-Rs were present barely. Still, a single dose of icv. PrRP is able to stimulate the release of magnocellular oxytocin and AVP (Maruyama et al. 1999; Uchida et al. 2010). As oxytocin regulates natriuresis and AVP regulates water conservation by the kidneys as well as increases blood pressure, both hormones substantially control the hypernatremia-evoked responses. Although direct action of PrRP mainly on oxytocin neurons is possible (Maruyama et al. 1999), our data indicate that PrRP stimulates hormone release from the magnocellular neurons via an indirect pathway.

We recognized the AV3V as a new site for PrRP's action. The AV3V exhibited a significant amount of PrRP-Rs and a great network of PrRP-positive fibers. In addition, PrRP innervation of the MnPO was enhanced by HS intake. The AV3V supervises the release of AVP and oxytocin (Honda et al. 1990; Yamaguchi and Yamada 2008; Tanaka et al. 1997) and plays a decisive role in the processing of autonomic responses elicited by HS intake (Pedrino et al. 2005; Bourque 2008). Therefore, it may serve as a relay center toward the magnocellular system. The effect of PrRP on the blood pressure (Samson et al. 2000; Yamada et al. 2009) was shown to be greatly mediated by neuropeptide FF2 receptors in the parvocellular PVN (Ma et al. 2009). However, according to our data the AV3V may also mediate this action via PrRP-Rs. Indeed, a polymorphism of the PrRP-R, the only cognate receptor of PrRP, has been associated with lower blood pressure in humans (Bhattacharyya et al. 2003).

In summary, we have found that the level of stress caused by chronic hypernatremia depended on the type of hypernatremia, affected the responsiveness to acute restraint differentially, and that the sensitivity of the HPA

axis to acute restraint was reflected by the expression pattern in the cVLM. An interaction of NE and PrRP of medullary origin in the hypothalamus (PVN, SON, AV3V) in response to chronic hypernatremia was revealed and the AV3V was identified as a new site for PrRP's action.

Acknowledgements Open access funding provided by Semmelweis University (SE). Special thanks for Judit Kerti and Szilvia Deak for their technical contribution to the study.

Funding This work was supported by NKFIH K 115422 (ZET) and NKFIH K 120311 (ZD) and the Excellence Program (Semmelweis University).

Compliance with ethical standards

Conflict of interest The authors declare that they have no conflict of interest.

Ethics approval This article does not contain any studies with human participants performed by any of the authors. All applicable international, national, and/or institutional guidelines for the care and use of animals were followed. All procedures performed in studies involving animals were in accordance with the ethical standards of the institution or practice at which the studies were conducted. Experiments were performed according to the European Communities Council Directive (86/609/EEC/2 and 2010/63/EU) and were supervised by the Animal Care and Use Committee of the Institute of Experimental Medicine, Hungarian Academy of Sciences, Budapest, Hungary (22.1/3895/003/2009 and 22.1/533/3/2011) and Semmelweis University (PEI/001/1775–2/2015 and PE/EA/1563–7/2017) in accordance with legal requirements of the European Community (Decree 86/609/EEC).

References

Amaya F, Tanaka M, Hayashi S, Tanaka Y, Ibata Y (2001) Hypothalamo-pituitary-adrenal axis sensitization after chronic salt loading. Neuroendocrinology 73(3):185–193. https://doi.org/10.1159/000054635

Antoni FA (1993) Vasopressinergic control of pituitary adrenocorticotropin secretion comes of age. Front Neuroendocrinol 14(2):76–122. https://doi.org/10.1006/frne.1993.1004

Bhattacharyya S, Luan J, Challis B, Schmitz C, Clarkson P, Franks PW, Middelberg R, Keogh J, Farooqi IS, Montague C, Brennand J, Wareham NJ, O'Rahilly S (2003) Association of polymorphisms in GPR10, the gene encoding the prolactin-releasing peptide receptor with blood pressure, but not obesity, in a UK Caucasian population. Diabetes 52(5):1296–1299

Bienkowski MS, Rinaman L (2008) Noradrenergic inputs to the paraventricular hypothalamus contribute to hypothalamic-pituitary-adrenal axis and central Fos activation in rats after acute systemic endotoxin exposure. Neuroscience 156(4):1093–1102. https://doi.org/10.1016/j.neuroscience.2008.08.011

Bourque CW (2008) Central mechanisms of osmosensation and systemic osmoregulation. Nat Rev Neurosci 9(7):519–531. https://doi.org/10.1038/nrn2400

Boyle CN, Lorenzen SM, Compton D, Watts AG (2012) Dehydration-anorexia derives from a reduction in meal size, but not meal number. Physiol Behav 105(2):305–314. https://doi.org/10.1016/j.physbeh.2011.08.005

Bundzikova J, Pirnik Z, Zelena D, Mikkelsen JD, Kiss A (2008) Response of substances co-expressed in hypothalamic magnocellular neurons to osmotic challenges in normal and Brattleboro rats. Cell Mol Neurobiol 28(8):1033–1047. https://doi.org/10.1007/s10571-008-9306-x

Chan RK, Peto CA, Sawchenko PE (1995) A1 catecholamine cell group: fine structure and synaptic input from the nucleus of the solitary tract. J Comp Neurol 351(1):62–80. https://doi.org/10.1002/cne.903510107

Chen C, Dun SL, Dun NJ, Chang JK (1999) Prolactin-releasing peptide-immunoreactivity in A1 and A2 noradrenergic neurons of the rat medulla. Brain Res 822(1–2):276–279

Chen CC, Wada K, Jarvis ED (2012) Radioactive in situ hybridization for detecting diverse gene expression patterns in tissue. J Vis Exp. https://doi.org/10.3791/3764

Choe KY, Han SY, Gaub P, Shell B, Voisin DL, Knapp BA, Barker PA, Brown CH, Cunningham JT, Bourque CW (2015) High salt intake increases blood pressure via BDNF-mediated downregulation of KCC2 and impaired baroreflex inhibition of vasopressin neurons. Neuron 85(3):549–560. https://doi.org/10.1016/j.neuron.2014.12.048

Daubner SC, Le T, Wang S (2011) Tyrosine hydroxylase and regulation of dopamine synthesis. Arch Biochem Biophys 508(1):1–12. https://doi.org/10.1016/j.abb.2010.12.017

Day TA (1989) Control of neurosecretory vasopressin cells by noradrenergic projections of the caudal ventrolateral medulla. Prog Brain Res 81:303–317

Dayas CV, Buller KM, Crane JW, Xu Y, Day TA (2001) Stressor categorization: acute physical and psychological stressors elicit distinctive recruitment patterns in the amygdala and in medullary noradrenergic cell groups. Eur J Neurosci 14(7):1143–1152. https://doi.org/10.1046/j.0953-816x.2001.01733.x

da Silva EF, Freiria-Oliveira AH, Custodio CH, Ghedini PC, Bataus LA, Colombari E, de Castro CH, Colugnati DB, Rosa DA, Cravo SL, Pedrino GR (2013) A1 noradrenergic neurons lesions reduce natriuresis and hypertensive responses to hypernatremia in rats. PloS One 8(9):e73187. https://doi.org/10.1371/journal.pone.0073187

Dos Santos Moreira MC, Naves LM, Marques SM, Silva EF, Rebelo AC, Colombari E, Pedrino GR (2017) Neuronal circuits involved in osmotic challenges. Physiol Res 66(3):411–423

Dunkley PR, Bobrovskaya L, Graham ME, von Nagy-Felsobuki EI, Dickson PW (2004) Tyrosine hydroxylase phosphorylation: regulation and consequences. J Neurochem 91(5):1025–1043. https://doi.org/10.1111/j.1471-4159.2004.02797.x

Durst M, Konczol K, Balazsa T, Eyre MD, Toth ZE (2019) Reward-representing D1-type neurons in the medial shell of the accumbens nucleus regulate palatable food intake. Int J Obes (Lond) 43(4):917–927. https://doi.org/10.1038/s41366-018-0133-y

Fernandez-Galaz C, Dyer RG, Herbison AE (1994) Analysis of brainstem A1 and A2 noradrenergic inputs to the preoptic area using microdialysis in the rat. Brain Res 636(2):227–232

Flak JN, Myers B, Solomon MB, McKlveen JM, Krause EG, Herman JP (2014) Role of paraventricular nucleus-projecting norepinephrine/epinephrine neurons in acute and chronic stress. Eur J Neurosci 39(11):1903–1911. https://doi.org/10.1111/ejn.12587

Foo KS, Brismar H, Broberger C (2008) Distribution and neuropeptide coexistence of nucleobindin-2 mRNA/nesfatin-like immunoreactivity in the rat CNS. Neuroscience 156(3):563–579. https://doi.org/10.1016/j.neuroscience.2008.07.054

Gaillet S, Lachuer J, Malaval F, Assenmacher I, Szafarczyk A (1991) The involvement of noradrenergic ascending pathways in the stress-induced activation of ACTH and corticosterone secretions is dependent on the nature of stressors. Exp Brain Res 87(1):173–180

Grinevich V, Ma XM, Verbalis J, Aguilera G (2001) Hypothalamic pituitary adrenal axis and hypothalamic-neurohypophyseal responsiveness in water-deprived rats. Exp Neurol 171(2):329–341. https://doi.org/10.1006/exnr.2001.7784

Guillaume V, Conte-Devolx B, Szafarczyk A, Malaval F, Pares-Herbute N, Grino M, Alonso G, Assenmacher I, Oliver C (1987) The corticotropin-releasing factor release in rat hypophysial portal blood is mediated by brain catecholamines. Neuroendocrinology 46(2):143–146. https://doi.org/10.1159/000124811

Harbuz MS, Rees RG, Eckland D, Jessop DS, Brewerton D, Lightman SL (1992) Paradoxical responses of hypothalamic corticotropin-releasing factor (CRF) messenger ribonucleic acid (mRNA) and CRF-41 peptide and adenohypophysial proopiomelanocortin mRNA during chronic inflammatory stress. Endocrinology 130(3):1394–1400. https://doi.org/10.1210/endo.130.3.1537299

Haycock JW (1993) Multiple signaling pathways in bovine chromaffin cells regulate tyrosine hydroxylase phosphorylation at Ser19, Ser31, and Ser40. Neurochem Res 18(1):15–26

Hochstenbach SL, Ciriello J (1995) Plasma hypernatremia induces c-fos activity in medullary catecholaminergic neurons. Brain Res 674(1):46–54

Honda K, Negoro H, Dyball RE, Higuchi T, Takano S (1990) The osmoreceptor complex in the rat: evidence for interactions between the supraoptic and other diencephalic nuclei. J Physiol 431:225–241

Huang W, Sved AF, Stricker EM (2000) Vasopressin and oxytocin release evoked by NaCl loads are selectively blunted by area postrema lesions. Am J Physiol Regul Integr Comp Physiol 278(3):R732–740. https://doi.org/10.1152/ajpregu.2000.278.3.R732

Khan AM, Kaminski KL, Sanchez-Watts G, Ponzio TA, Kuzmiski JB, Bains JS, Watts AG (2011) MAP kinases couple hindbrain-derived catecholamine signals to hypothalamic adrenocortical control mechanisms during glycemia-related challenges. J Neurosci 31(50):18479–18491. https://doi.org/10.1523/jneurosci.4785-11.2011

Kitayama I, Cintra A, Janson AM, Fuxe K, Agnati LF, Eneroth P, Aronsson M, Harfstrand A, Steinbush HW, Visser TJ et al (1989) Chronic immobilization stress: evidence for decreases of 5-hydroxy-tryptamine immunoreactivity and for increases of glucocorticoid receptor immunoreactivity in various brain regions of the male rat. J Neural Transm 77(2–3):93–130

Konczol K, Bodnar I, Zelena D, Pinter O, Papp RS, Palkovits M, Nagy GM, Toth ZE (2010) Nesfatin-1/NUCB2 may participate in the activation of the hypothalamic-pituitary-adrenal axis in rats. Neurochem Int 57(3):189–197. https://doi.org/10.1016/j.neuint.2010.04.012

Krause EG, Pati D, Frazier CJ (2017) Chronic salt-loading reduces basal excitatory input to CRH neurons in the paraventricular nucleus and accelerates recovery from restraint stress in male mice. Physiol Behav 176:189–194. https://doi.org/10.1016/j.physbeh.2017.03.038

Lawrence CB, Celsi F, Brennand J, Luckman SM (2000) Alternative role for prolactin-releasing peptide in the regulation of food intake. Nat Neurosci 3(7):645–646. https://doi.org/10.1038/76597

Lawrence CB, Liu YL, Stock MJ, Luckman SM (2004) Anorectic actions of prolactin-releasing peptide are mediated by corticotropin-releasing hormone receptors. Am J Physiol Regul Integr Comp Physiol 286(1):R101–107. https://doi.org/10.1152/ajpregu.00402.2003

Liposits Z, Sherman D, Phelix C, Paull WK (1986) A combined light and electron microscopic immunocytochemical method for the simultaneous localization of multiple tissue antigens. Tyrosine hydroxylase immunoreactive innervation of corticotropin releasing factor synthesizing neurons in the paraventricular nucleus of the rat. Histochemistry 85(2):95–106

Ma XM, Lightman SL (1998) The arginine vasopressin and corticotrophin-releasing hormone gene transcription responses to varied frequencies of repeated stress in rats. J Physiol 510(Pt 2):605–614

Ma XM, Levy A, Lightman SL (1997) Emergence of an isolated arginine vasopressin (AVP) response to stress after repeated restraint: a study of both AVP and corticotropin-releasing hormone messenger ribonucleic acid (RNA) and heteronuclear RNA. Endocrinology 138(10):4351–4357. https://doi.org/10.1210/endo.138.10.5446

Ma L, MacTavish D, Simonin F, Bourguignon JJ, Watanabe T, Jhamandas JH (2009) Prolactin-releasing peptide effects in the rat brain are mediated through the Neuropeptide FF receptor. Eur J Neurosci 30(8):1585–1593. https://doi.org/10.1111/j.1460-9568.2009.06956.x

Maejima Y, Sedbazar U, Suyama S, Kohno D, Onaka T, Takano E, Yoshida N, Koike M, Uchiyama Y, Fujiwara K, Yashiro T, Horvath TL, Dietrich MO, Tanaka S, Dezaki K, Oh IS, Hashimoto K, Shimizu H, Nakata M, Mori M, Yada T (2009) Nesfatin-1-regulated oxytocinergic signaling in the paraventricular nucleus causes anorexia through a leptin-independent melanocortin pathway. Cell Metab 10(5):355–365. https://doi.org/10.1016/j.cmet.2009.09.002

Maruyama M, Matsumoto H, Fujiwara K, Noguchi J, Kitada C, Hinuma S, Onda H, Nishimura O, Fujino M, Higuchi T, Inoue K (1999) Central administration of prolactin-releasing peptide stimulates oxytocin release in rats. Neurosci Lett 276(3):193–196

Maruyama M, Matsumoto H, Fujiwara K, Noguchi J, Kitada C, Fujino M, Inoue K (2001) Prolactin-releasing peptide as a novel stress mediator in the central nervous system. Endocrinology 142(5):2032–2038. https://doi.org/10.1210/endo.142.5.8118

Menani JV, Vieira AA, Colombari DSA, De Paula PM, Colombari E, De Luca LA, Jr. (2014) Frontiers in Neuroscience Preoptic-Periventricular Integrative Mechanisms Involved in Behavior, Fluid-Electrolyte Balance, and Pressor Responses. In: De Luca LA, Jr., Menani JV, Johnson AK (eds) Neurobiology of Body Fluid Homeostasis: Transduction and Integration. CRC Press/Taylor & Francis (c) 2014 by Taylor & Francis Group, LLC., Boca Raton (FL),

Mera T, Fujihara H, Kawasaki M, Hashimoto H, Saito T, Shibata M, Saito J, Oka T, Tsuji S, Onaka T, Ueta Y (2006) Prolactin-releasing peptide is a potent mediator of stress responses in the brain through the hypothalamic paraventricular nucleus. Neuroscience 141(2):1069–1086. https://doi.org/10.1016/j.neuroscience.2006.04.023

Mezey E, Eisenhofer G, Hansson S, Hunyady B, Hoffman BJ (1998) Dopamine produced by the stomach may act as a paracrine/autocrine hormone in the rat. Neuroendocrinology 67(5):336–348. https://doi.org/10.1159/000054332

Mimee A, Smith PM, Ferguson AV (2012) Nesfatin-1 influences the excitability of neurons in the nucleus of the solitary tract and regulates cardiovascular function. Am J Physiol Regul Integr Comp Physiol 302(11):R1297–1304. https://doi.org/10.1152/ajpregu.00266.2011

Ong LK, Sominsky L, Dickson PW, Hodgson DM, Dunkley PR (2012) The sustained phase of tyrosine hydroxylase activation in vivo. Neurochem Res 37(9):1938–1943. https://doi.org/10.1007/s11064-012-0812-3

Pacak K, Palkovits M, Kopin IJ, Goldstein DS (1995) Stress-induced norepinephrine release in the hypothalamic paraventricular nucleus and pituitary-adrenocortical and sympathoadrenal activity: in vivo microdialysis studies. Front Neuroendocrinol 16(2):89–150. https://doi.org/10.1006/frne.1995.1004

Palkovits M (1973) Isolated removal of hypothalamic or other brain nuclei of the rat. Brain Res 59:449–450. https://doi.org/10.1016/0006-8993(73)90290-4

Paxinos G, Watson C (2007) The rat brain in stereotaxic coordinates, 6th edn. Elsevier, London, Amsterdam

Pedrino GR, Nakagawa Sera CT, Cravo SL, Colombari DS (2005) Anteroventral third ventricle lesions impair cardiovascular responses to intravenous hypertonic saline infusion. Auton Neurosci Basic Clin 117(1):9–16. https://doi.org/10.1016/j.autneu.2004.09.005

Pedrino GR, Rosa DA, Korim WS, Cravo SL (2008) Renal sympathoinhibition induced by hypernatremia: involvement of A1 noradrenergic neurons. Auton Neurosci Basic Clin 142(1–2):55–63. https://doi.org/10.1016/j.autneu.2008.06.006

Pedrino GR, Freiria-Oliveira AH, Almeida Colombari DS, Rosa DA, Cravo SL (2012) A2 noradrenergic lesions prevent renal sympathoinhibition induced by hypernatremia in rats. PloS One 7(5):e37587

Pouzet B, Serradeil-Le Gal C, Bouby N, Maffrand JP, Le Fur G, Bankir L (2001) Selective blockade of vasopressin V2 receptors reveals significant V2-mediated water reabsorption in Brattleboro rats with diabetes insipidus. Nephrol Dial Transpl 16(4):725–734

Price CJ, Hoyda TD, Samson WK, Ferguson AV (2008) Nesfatin-1 influences the excitability of paraventricular nucleus neurones. J Neuroendocrinol 20(2):245–250. https://doi.org/10.1111/j.1365-2826.2007.01641.x

Ritter S, Watts AG, Dinh TT, Sanchez-Watts G, Pedrow C (2003) Immunotoxin lesion of hypothalamically projecting norepinephrine and epinephrine neurons differentially affects circadian and stressor-stimulated corticosterone secretion. Endocrinology 144(4):1357–1367. https://doi.org/10.1210/en.2002-221076

Roland BL, Sutton SW, Wilson SJ, Luo L, Pyati J, Huvar R, Erlander MG, Lovenberg TW (1999) Anatomical distribution of prolactin-releasing peptide and its receptor suggests additional functions in the central nervous system and periphery. Endocrinology 140(12):5736–5745. https://doi.org/10.1210/endo.140.12.7211

Samson WK, Resch ZT, Murphy TC (2000) A novel action of the newly described prolactin-releasing peptides: cardiovascular regulation. Brain Res 858(1):19–25

Sawchenko PE, Swanson LW (1981) Central noradrenergic pathways for the integration of hypothalamic neuroendocrine and autonomic responses. Science 214(4521):685–687

Sawchenko PE, Swanson LW (1982) The organization of noradrenergic pathways from the brainstem to the paraventricular and supraoptic nuclei in the rat. Brain Res 257(3):275–325

Scholer J, Sladek JR Jr (1981) Supraoptic nucleus of the Brattleboro rat has an altered afferent noradrenergic input. Science 214(4518):347–349

Seal LJ, Small CJ, Dhillo WS, Kennedy AR, Ghatei MA, Bloom SR (2002) Prolactin-releasing peptide releases corticotropin-releasing hormone and increases plasma adrenocorticotropin via the paraventricular nucleus of the hypothalamus. Neuroendocrinology 76(2):70–78. https://doi.org/10.1159/000064427

Sterrenburg L, Borch A, Peeters BW, Pinter O, Zelena D, Roubos EW, Kozicz T (2011) Acute ether stress differentially affects corticotropin-releasing factor and urocortin 1 in the Brattleboro rat. Brain Res 1398:21–29. https://doi.org/10.1016/j.brainres.2011.04.047

Sun Z (2006) Genetic AVP deficiency abolishes cold-induced diuresis but does not attenuate cold-induced hypertension. Am J Physiol Renal Physiol 290(6):F1472–1477. https://doi.org/10.1152/ajprenal.00430.2005

Szafarczyk A, Alonso G, Ixart G, Malaval F, Assenmacher I (1985) Diurnal-stimulated and stress-induced ACTH release in rats is mediated by ventral noradrenergic bundle. Am J Physiol 249(2 Pt 1):E219–226. https://doi.org/10.1152/ajpendo.1985.249.2.E219

Tanaka J, Hayashi Y, Watai T, Fukami Y, Johkoh R, Shimamune S (1997) A1 noradrenergic modulation of AV3V inputs to PVN neurosecretory cells. Neuroreport 8(14):3147–3150

Toth ZE, Mezey E (2007) Simultaneous visualization of multiple antigens with tyramide signal amplification using antibodies from the same species. J Histochem Cytochem 55(6):545–554. https://doi.org/10.1369/jhc.6A7134.2007

Toth ZE, Gallatz K, Fodor M, Palkovits M (1999) Decussations of the descending paraventricular pathways to the brainstem and spinal cord autonomic centers. J Comp Neurol 414(2):255–266

Toth ZE, Zelena D, Mergl Z, Kirilly E, Varnai P, Mezey E, Makara GB, Palkovits M (2008) Chronic repeated restraint stress increases prolactin-releasing peptide/tyrosine-hydroxylase ratio with gender-related differences in the rat brain. J Neurochem 104(3):653–666. https://doi.org/10.1111/j.1471-4159.2007.05069.x

Uchida K, Kobayashi D, Das G, Onaka T, Inoue K, Itoi K (2010) Participation of the prolactin-releasing peptide-containing neurones in caudal medulla in conveying haemorrhagic stress-induced signals to the paraventricular nucleus of the hypothalamus. J Neuroendocrinol 22(1):33–42. https://doi.org/10.1111/j.1365-2826.2009.01935.x

Ulrich-Lai YM, Herman JP (2009) Neural regulation of endocrine and autonomic stress responses. Nat Rev Neurosci 10(6):397–409. https://doi.org/10.1038/nrn2647

Varga J, Ferenczi S, Kovacs KJ, Csano A, Prokopova B, Jezova D, Zelena D (2016) Dissociation of adrenocorticotropin and corticosterone as well as aldosterone secretion during stress of hypoglycemia in vasopressin-deficient rats. Life Sci 166:66–74. https://doi.org/10.1016/j.lfs.2016.10.011

Vas S, Adori C, Konczol K, Katai Z, Pap D, Papp RS, Bagdy G, Palkovits M, Toth ZE (2013) Nesfatin-1/NUCB2 as a potential new element of sleep regulation in rats. PloS One 8(4):e59809. https://doi.org/10.1371/journal.pone.0059809

Wittmann G, Mohacsik P, Balkhi MY, Gereben B, Lechan RM (2015) Endotoxin-induced inflammation down-regulates L-type amino acid transporter 1 (LAT1) expression at the blood-brain barrier of male rats and mice. Fluids Barriers CNS 12:21. https://doi.org/10.1186/s12987-015-0016-8

Yamada T, Mochiduki A, Sugimoto Y, Suzuki Y, Itoi K, Inoue K (2009) Prolactin-releasing peptide regulates the cardiovascular system via corticotrophin-releasing hormone. J Neuroendocrinol 21(6):586–593. https://doi.org/10.1111/j.1365-2826.2009.01875.x

Yamaguchi K, Yamada T (2008) Roles of forebrain GABA receptors in controlling vasopressin secretion and related phenomena under basal and hyperosmotic circumstances in conscious rats. Brain Res Bull 77(1):61–69. https://doi.org/10.1016/j.brainresbull.2008.04.009

Yang Z, Coote JH (2007) Paraventricular nucleus influence on renal sympathetic activity in vasopressin gene-deleted rats. Exp Physiol 92(1):109–117. https://doi.org/10.1113/expphysiol.2006.034884

Yilmaz MS, Altinbas B, Guvenc G, Erkan LG, Avsar O, Savci V, Kucuksen DU, Arican I, Yalcin M (2015) The role of centrally injected nesfatin-1 on cardiovascular regulation in normotensive and hypotensive rats. Auton Neurosci Basic Clin 193:63–68. https://doi.org/10.1016/j.autneu.2015.07.009

Yosten GL, Samson WK (2009) Nesfatin-1 exerts cardiovascular actions in brain: possible interaction with the central melanocortin

system. Am J Physiol Regul Integr Comp Physiol 297(2):R330–336. https://doi.org/10.1152/ajpregu.90867.2008

Zelena D, Mergl Z, Foldes A, Kovacs KJ, Toth Z, Makara GB (2003) Role of hypothalamic inputs in maintaining pituitary-adrenal responsiveness in repeated restraint. Am J Physiol Endocrinol Metab 285(5):E1110–1117. https://doi.org/10.1152/ajpendo.00219.2003

Neurobiology of Disease

Prolactin-Releasing Peptide Contributes to Stress-Related Mood Disorders and Inhibits Sleep/Mood Regulatory Melanin-Concentrating Hormone Neurons in Rats

Szilvia Vas,[1,2] Rege S. Papp,[3] Katalin Könczöl,[4] Emese Bogáthy,[1] Noémi Papp,[1] Csaba Ádori,[5] Máté Durst,[4] Klaudia Sípos,[4] Klementina Ocskay,[4] Imre Farkas,[6,7] Flóra Bálint,[7] Szilamér Ferenci,[8] Bibiána Török,[9,10] Anita Kovács,[10] Evelin Szabó,[10] Dóra Zelena,[9,10] Krisztina J. Kovács,[8] Anna Földes,[11] Erzsébet Kató,[12] László Köles,[11,12] György Bagdy,[1,2,13] Miklós Palkovits,[3,4] and Zsuzsanna E. Tóth[4]

[1]Department of Pharmacodynamics, Semmelweis University, Budapest, 1089, Hungary, [2]MTA-SE Neuropsychopharmacology and Neurochemistry Research Group, Semmelweis University, Budapest, 1089, Hungary, [3]Human Brain Tissue Bank and Laboratory, Semmelweis University, Budapest, 1094, Hungary, [4]Laboratory of Neuroendocrinology and In Situ Hybridization, Department of Anatomy, Histology and Embryology, Semmelweis University, Budapest, 1094, Hungary, [5]Department of Neuroscience, Karolinska Institutet, Stockholm, 17177, Sweden, [6]Laboratory of Reproductive Neurobiology, Institute of Experimental Medicine, Eötvös Loránd Research Network, Budapest, 1083, Hungary, [7]Laboratory of Endocrine Neurobiology, Institute of Experimental Medicine, Eötvös Loránd Research Network, Budapest, 1083, Hungary, [8]Laboratory of Molecular Neuroendocrinology, Institute of Experimental Medicine, Eötvös Loránd Research Network, Budapest, 1083, Hungary, [9]Laboratory of Behavioral and Stress Studies, Institute of Experimental Medicine, Eötvös Loránd Research Network, Budapest, 1083, Hungary, [10]Institute of Physiology, Medical School, University of Pécs, Centre for Neuroscience, Szentágothai Research Center, Pécs, 7624, Hungary, [11]Department of Oral Biology, Semmelweis University, Budapest, 1089, Hungary, [12]Department of Pharmacology and Pharmacotherapy, Semmelweis University, Budapest, 1089, Hungary, and [13]NAP2-SE New Antidepressant Target Research Group, Budapest, 1085, Hungary

Stress disorders impair sleep and quality of life; however, their pathomechanisms are unknown. Prolactin-releasing peptide (PrRP) is a stress mediator; we therefore hypothesized that PrRP may be involved in the development of stress disorders. PrRP is produced by the medullary A1/A2 noradrenaline (NA) cells, which transmit stress signals to forebrain centers, and by non-NA cells in the hypothalamic dorsomedial nucleus. We found in male rats that both PrRP and PrRP-NA cells innervate melanin-concentrating hormone (MCH) producing neurons in the dorsolateral hypothalamus (DLH). These cells serve as a key hub for regulating sleep and affective states. *Ex vivo*, PrRP hyperpolarized MCH neurons and further increased the hyperpolarization caused by NA. Following sleep deprivation, intracerebroventricular PrRP injection reduced the number of REM sleep-active MCH cells. PrRP expression in the dorsomedial nucleus was upregulated by sleep deprivation, while downregulated by REM sleep rebound. Both in learned helplessness paradigm and after peripheral inflammation, impaired coping with sustained stress was associated with (1) overactivation of PrRP cells, (2) PrRP protein and receptor depletion in the DLH, and (3) dysregulation of MCH expression. Exposure to stress in the PrRP-insensitive period led to increased passive coping with stress. Normal PrRP signaling, therefore, seems to protect animals against stress-related disorders. PrRP signaling in the DLH is an important component of the PrRP's action, which may be mediated by MCH neurons. Moreover, PrRP receptors were downregulated in the DLH of human suicidal victims. As stress-related mental disorders are the leading cause of suicide, our findings may have particular translational relevance.

Key words: **GABA(A) receptor; MCH; mental disorders; sleep; stress; suicide**

Received Nov. 15, 2021; revised Aug. 31, 2022; accepted Sep. 30, 2022.

Author contributions: S.V., R.S.P., K.K., E.B., N.P., C.A., M.D., K.S., K.O., I.F., F.B., S.F., B.T., A.K., E.S., D.Z., A.F., E.K., L.K., and M.P. performed research; S.V., R.S.P., K.S., I.F., A.K., E.S., K.J.K., and Z.E.T. analyzed data; S.V., C.A., and Z.E.T. wrote the first draft of the paper; S.V. and Z.E.T. edited the paper; S.V. and Z.E.T. wrote the paper; G.B. and Z.E.T. designed research.

This work was supported by Hungarian Brain Research Program Grants 2017-1.2.1-NKP-2017-00002 and KTIA_13_NAPA-II/14; and National Development Agency Grant KTIA_NAP_13-1-2013-0001 and NKFI K 115422. Project TKP2021-EGA-25 has been implemented with the support provided by the Ministry of Innovation and Technology of Hungary from the National Research, Development and Innovation Fund, financed under the TKP2021-EGA funding scheme. We thank Judit Kerti, Szilvia Deák, and Ágnes Ruzsits for the indispensable technical assistance; and Jacqueline Casey for excellent contribution in proofreading the final draft.

The authors declare no competing financial interests.

Correspondence should be addressed to Zsuzsanna E. Tóth at toth.zsuzsanna.emese@med.semmelweis-univ.hu.

https://doi.org/10.1523/JNEUROSCI.2139-21.2022

Significance Statement

Treatment resistance to monoaminergic antidepressants is a major problem. Neuropeptides that modulate the central monoaminergic signaling are promising targets for developing alternative therapeutic strategies. We found that stress-responsive prolactin-releasing peptide (PrRP) cells innervated melanin-concentrating hormone (MCH) neurons that are crucial in the regulation of sleep and mood. PrRP inhibited MCH cell activity and enhanced the inhibitory effect evoked by noradrenaline, a classic monoamine, on MCH neurons. We observed that impaired PrRP signaling led to failure in coping with chronic/repeated stress and was associated with altered MCH expression. We found alterations of the PrRP system also in suicidal human subjects. PrRP dysfunction may underlie stress disorders, and fine-tuning MCH activity by PrRP may be an important part of the mechanism.

Introduction

Chronic or repeated exposure to stress may cause serious mental health conditions, such as anxiety, post-traumatic stress disorder (PTSD), and major depressive disorder (Smoller, 2016). Dysregulation of the hypothalamus-pituitary-adrenal (HPA) axis, the stress axis, as well as mood and sleep disturbances are typical symptoms in patients, which develop by unknown mechanisms (Goldstein and Walker, 2014; Bao and Swaab, 2019).

Serotonin and noradrenaline (NA) reuptake inhibitor (SNRI) antidepressants are commonly used to treat major depressive disorder, anxiety, and PTSD, although treatment resistance to conventional SNRIs occurs frequently (Voineskos et al., 2020). Neuropeptides, which can modulate neurotransmitter levels in the brain (neuromodulators), may offer alternative antidepressant targets (Mantas et al., 2022). Here, we designate prolactin-releasing peptide (PrRP)/prolactin-releasing hormone (PRLH) as a novel candidate known to be involved in the regulation of stress, sleep, and mood (Dodd and Luckman, 2013). PrRP may act in part by affecting melanin-concentrating hormone (MCH) producing cells in the dorsolateral hypothalamus (DLH). Our hypothesis is based on the following.

PrRP neurons are in a decisive position for transmitting stress-related signals toward higher brain centers and influence the efficacy of noradrenergic transmission. The adaptive response of the HPA axis to homeostatic stressors and peripheral inflammation depends on the integrity of the ascending pathway from the medullary A1/A2 noradrenergic cell groups (Pacak et al., 1995). PrRP is expressed exclusively in the A1/A2 cell groups (Chen et al., 1999) and the hypothalamic dorsomedial nucleus (DM) (Dodd and Luckman, 2013). PrRP cells respond to various psychogenic stressors, such as conditioned-fear stimuli, foot shock, restraint, inflammatory stress, etc. (Ohiwa et al., 2007; Dodd and Luckman, 2013). PrRP-deficient mice fail to increase plasma ACTH following reexposure to a conditioned fear stimulus (Yoshida et al., 2014). Serving key role in stress, PrRP stimulates the release of ACTH (Maruyama et al., 2001) and corticosterone (Mera et al., 2006) *in vivo*, and substantially potentiates the ACTH-stimulatory effect of NA (Maruyama et al., 2001).

PrRP also affects the sleep–wake cycle, although the available literature is contradictory (Zhang et al., 2001; Lin et al., 2002). *Ex vivo* studies suggest that the reticular nucleus of the thalamus may mediate some effects of PrRP on the sleep–wake cycle (Lin et al., 2002), where PrRP alias PRLH receptor (PRLHR) expression is high, but PrRP axons are absent (Dodd and Luckman, 2013). In contrast, PrRP fibers innervate the DLH (Dodd and Luckman, 2013). The DLH is populated by MCH cells (Verret et al., 2003), which cells are considered a key regulatory hub of sleep and mood, moreover, participate in the control of stress-response (Smith et al., 2006; Diniz and Bittencourt, 2017; Bandaru et al., 2020). A series of data highlights MCH dysfunction underpinning the pathophysiology of anxiety, depression, and PTSD (Chaki et al., 2005; Chung et al., 2011; Torterolo et al., 2015; Concetti et al., 2020). Although antagonists of MCH1 receptor (MCH1R) have shown promise as antidepressant drugs (Chung et al., 2011; Johansson and Löfberg, 2015), the exact mechanism of how MCH contributes to stress-related mental disorders remains to be elucidated. MCH neuronal activity during acute stress (foot shock) was necessary for subsequent coping with contextual fear (Izawa et al., 2019) and for cued fear extinction (Concetti et al., 2020). Controversially, the administration of MCH in a repeated stress paradigm (learned helplessness [LHe]) impaired the animals' ability to cope adequately with a second foot shock, resulting in helpless behavior (Urbanavicius et al., 2019). Thus, it appears that proper control of MCH signaling is critical in preventing the adverse effects of chronic/repeated stress.

We applied an array of histologic and electrophysiological methods, as well as depression models, and analyzed human PrRP receptor expression in the DLH of suicidal subjects. Our data reveal that the PrRP system may contribute to the development of stress-related mental disorders because of defects in PrRP signaling caused by chronic/repeated stress. We propose that PrRP regulates the function of MCH neurons; furthermore, PrRP signaling in the DLH is impaired in animal models of depression and in suicidal humans.

Materials and Methods

Animals

The experimental animals were male Wistar rats (Toxi-Coop), housed and kept under standard laboratory conditions with 12/12 h light/dark cycle (lights on at 6:00 A.M., unless otherwise stated). We used males to exclude sex effects on the data, as PrRP expression varies depending on female gonadal hormone levels (Tóth et al., 2008). Rats were 10-12 weeks old, unless otherwise indicated. All experiments were performed in accordance with the National Institutes of Health's "Principles of Laboratory Animal Care" (NIH Publications No. 85-23, revised 1985), international standards (European Community Council Directive, 86/609/EEC, 1986, 2010), and specific national laws (the Hungarian Governmental Regulations on animal studies 40/2013). The experiments were approved by the National Scientific Ethical Committee on Animal Experimentation, the Ethical Review Board of the Semmelweis University (PE/EA/1563-7/2017, PE/EA/850-2/2016, PTE/84 033-6/2020), and the Animal Welfare Committee of the Institute of Experimental Medicine (PE/EA/43-4/2019) and met the guidelines of the Animal Hygiene and Food Control Department, Ministry of Agriculture, Hungary and the European Communities Council Directive recommendations for the care and use of laboratory animals (2010/63/EU).

For brain surgeries and transcardial perfusions, anesthesia was given to rats by intramuscular injection of a ketamine (50 mg/kg)/xylazine

(4 mg/kg) (Richter Gedeon) cocktail. Animals were decapitated or were perfusion-fixed with 4% paraformaldehyde in 0.1 M PBS, pH 7.4. Brains were removed quickly, frozen and stored at −80°C. Perfusion-fixed brains were cryoprotected in 20% sucrose solution before freezing.

Immunohistochemistry (IHC)

For IHC, standard chromogenic or fluorescent immunohistochemical methods were applied (Table 1) using serial coronal 50-µm-thick free-floating sections. When ISH and IHC were combined, 20-µm-thick slide-mounted sections were used. Primary antibodies were applied after serum (1% BSA or 3% NDS, supplemented with 0.1% Triton X-100) and endogenous peroxidase (3% H_2O_2, all from Merck Life Science) activity blocking steps. Secondary antibody-conjugated peroxidase activity was eliminated by using 3% H_2O_2 solution supplemented with 0.01% Na-azide. Microwave treatment (5 min) was performed in 0.1 M citric acid (pH 6.0, Merck) for antigen retrieval, prevention of nonspecific cross reactions of antibodies, and/or for blocking HRP enzyme activity (Tóth and Mezey, 2007). Multiple detections were performed sequentially. The following reagents were used:

Primary antibodies. Primary antibodies are as follows: rabbit anti-cFos (catalog #ABE 457, Merck); anti-pro-MCH (catalog #sc-28931, raised in rabbit or sc-14509, raised in goat, Santa Cruz Biotechnology); rabbit anti-Orexin A (aa:14-33, catalog #R-104-100, Novus Biologicals); rabbit anti-PrRP (catalog #H-008-52, Phoenix Pharmaceuticals); and mouse anti-TH (catalog #MAB318, Millipore).

Detection reagents. Detection reagents include the following: AlexaFluor-488-conjugated Donkey Anti-Rabbit IgG (catalog #A21206), AlexaFluor-594-conjugated Donkey Anti-Mouse IgG (catalog #A21203), AlexaFluor-647-conjugated Donkey Anti-Goat IgG (catalog #A32849), AlexaFluor-568-conjugated streptavidin (catalog #S11226), and Tyramide Signal Amplification (TSA) Kits (catalog #T20912, T20920, T20925) (Fisher Scientific; Invitrogen); biotinylated donkey anti-rabbit IgG (catalog #711-065-152) and peroxidase-conjugated Donkey Anti-Goat IgG (catalog #705-035-003) (Jackson ImmunoResearch Laboratories, Izinta Trading); biotinylated goat anti-rabbit IgG (catalog #BA-1000, Vector Laboratories); DAB (catalog #D12384), extravidin-horseradish peroxidase (catalog #E2886) (Merck); and Fluorescein Tyramide Reagent Pack (catalog #SAT701B, PerkinElmer Life and Analytical Sciences).

Analysis of PrRP and TH coexpression in the varicosities in the rat hypothalamus

Serial coronal sections from perfusion-fixed naive rats ($n = 2$) were triple-immunolabeled for MCH, PrRP, and TH (see above). Confocal *z*-stack images were acquired bilaterally through a 63× lens objective (see Imaging) from three sections per animal containing the highest density of MCH cells. The *z* separation was adjusted to 3 µm to avoid capturing the same varicosity twice. The number of $PrRP^+$ varicosities were determined in the perifornical area (PFA) (20 *z* stacks) and the lateral hypothalamus (LH) (17 *z* stacks) in the single optical sections (1 AU, ROI size: 135 × 135 μm^2). TH positivity of the same profiles was analyzed in a separate channel, using the multipoint tool in the ImageJ 1.32j software (Wayne Rasband; National Institutes of Health). The percentage of PrRP-TH coexpression was calculated for each optical section and used for the statistical analysis.

ISH

Radioactive ISH was used for localization of the PRLHR and Neuropeptide FF receptor 2 (NPFF2R) mRNAs ($n = 2$ rats), and for measuring PrRP mRNA levels in sleep-deprived animals. Hybridizations were performed using serial coronal 12-µm-thick fresh frozen and 20-µm-thick perfusion fixed sections, as described previously (Tóth et al., 2008) using [^{35}S]UTP-labeled (Per-Form Hungaria) antisense riboprobes. The probes were generated by *in vitro* transcription (MAXIscript Kit, Fisher Scientific) according to the manufacturer's instructions using the following rat cDNA sequences: PrRP (10-240 bs, GenBank AB015418) and PRLHR (189-636 bs, GenBank NM_139193) cloned into pBC KS^+ vector (Addgene), as well as NPFF2R (112-796 bs, GenBank AF268900.1) cloned into pGemT Easy vector (Promega). The specificity of the cDNA fragments was verified by sequencing and assessed by BLAST screening of the rat genome (https://blast.ncbi.nlm.nih.gov/Blast.cgi). For signal detection, the sections were apposed to a BAS-MS imaging plate (Fuji PhotoFilm) for 5 d. The signals were read out by a Fujifilm FLA-8000 Image Analyzer. The sections were dipped into Kodak NTB autoradiographic emulsion (Agar Scientific), exposed for 5 d (PrRP ISH) or 6 weeks (PRLHR and NPFF2R ISHs), developed using Kodak Dektol developer and Fixer (Sigma-Aldrich), and were counterstained with Giemsa (Sigma), except when processed for IHC before ISH signal detection.

Table 1. Summary of the immunohistochemical reactions[a]

Figure	Primary/host	Detection
1*A*	1.[b] PrRP/rabbit 1:10,000 2. MCH/rabbit 1:10,000	Biotinylated goat anti-rabbit IgG 1:1000, EA-HRP 1:2000 1. DAB-Ni 2. DAB
1*B*	1.[b] PrRP /rabbit 1:10,000 2. TH/mouse 1:200	1. Biotinylated goat anti-rabbit IgG 1:1000, EA-HRP 1:2000, FITC tyramide 2. AlexaFluor-594-donkey anti-mouse IgG, 1:500
1*C*	1. MCH/goat 1:500 2.[b] PrRP/rabbit 1:10,000 3.[c] TH/mouse 1:1000	1. HRP-donkey anti-goat IgG 1:1000, Pacific Blue tyramide (from TSA KIT T20920) 2. TSA KIT T20925 with goat anti-rabbit-HRP and AlexaFluor-594 tyramide 3 TSA KIT T20912 with goat anti-mouse-HRP and AlexaFluor-488 tyramide
1*E*	1. MCH/rabbit 1:1000, or orexin/rabbit 1:1000	Biotinylated goat anti-rabbit IgG 1:1000, EA-HRP 1:2000, DAB
4*A*,*B*	1.[b] PrRP/rabbit 1:10,000	Biotinylated goat anti-rabbit IgG 1:1000, EA-HRP 1:2000 1. DAB
4*D*	1. cFos/rabbit 1:20,000 2.[b] MCH/goat 1:500 3. PrRP/rabbit 1:10,000	1. TSA KIT T20925 with goat anti-rabbit-HRP and AlexaFluor-594 tyramide 2. AlexaFluor-647-donkey anti-goat IgG, 1:500 3. Biotinylated donkey anti-rabbit IgG 1:1000, EA-HRP 1:2000, FITC tyramide
5*C*	1. MCH/rabbit 1:1000 2. intracellular biocytin	1. AlexaFluor-488-donkey anti-rabbit IgG, 1:500 AlexaFluor-568-SA, 1:500
6*F*	1.[b] cFos/rabbit 1:20,000 2. PrRP/rabbit 1:10,000	Biotinylated goat anti-rabbit IgG 1:1000, EA-HRP 1:2000 1. DAB-Ni 2. DAB
6*H*	1.[b] PrRP/rabbit 1:10,000	TSA KIT T20925 with goat anti-rabbit-HRP and AlexaFluor-594 tyramide
6*I*	1. MCH/goat 1:500	AlexaFluor-647-donkey anti-goat IgG, 1:500

[a]EA, Extravidin; SA, streptavidin.
[b]Microwave pretreatment in 0.1 M citric acid (pH 6.0, Merck) for 5 min.
[c]Preincubation in 3% H_2O_2 solution containing 0.01% sodium azide in PBS for 15 min.

Brain slice electrophysiology

Whole-cell patch-clamp experiments were conducted using acute rat brain slices from 30-d-old rats ($n = 20$) to evaluate the effect of PrRP 12-31 (3.5 µM, #P7357, Merck) on MCH neurons and to test the effect of PrRP on the NA (10 µM, #A9512, Merck) evoked responses. Rats were anesthetized by 1% Isoflurane (Baxter) 1-2 h after lights on. After decapitation, the brain was removed and 250 µm thick coronal slices containing the DLH (bregma −1.43 mm) were generated with a Leica VT-1000S vibratome (Leica Microsystems) in ice-cold, reduced sodium aCSF equilibrated with 95% O_2 and 5% CO_2, (composition in mM as follows: saccharose 205, KCl 2.5, $NaHCO_3$ 26, $MgCl_2$ 5, NaH_2PO_4 1.25, $CaCl_2$ 1, glucose 10). The upper part of the slice was dissected just above the mammillothalamic tract to avoid influence of thalamic neurons expressing PRLHR (Ibata et al., 2000). Then the slices were incubated in aCSF (composition in mM as follows: NaCl 130, KCl 3.5, $NaHCO_3$ 26, $MgSO_4$ 1.2, NaH_2PO_4 1.25, $CaCl_2$ 2.5, glucose 10) for 1 h at room temperature. Recordings were conducted in aCSF at 33°C using an Axopatch-200B patch-clamp amplifier, Digidata-1322A data acquisition system, and pCLAMP 10.4 software (also used

for analyses of data, Molecular Devices) under a BX51WI IR-DIC Olympus microscope. The patch electrodes (OD = 1.5 mm, thin wall, Hilgenberg) were pulled with a Flaming-Brown P-97 puller (Sutter Instruments), the resistance was 2-3 MΩ. The intracellular pipette solution contained the following (in mM): K-gluconate 130, KCl 10, NaCl 10, HEPES 10, $MgCl_2$ 0.1, EGTA 1, Mg-ATP 4, Na-GTP 0.3 and biocytin (1.5 mg/ml, all from Merck).

Cells in the PFA were injected with hyperpolarizing/depolarizing square-step-pulses (duration: 900 ms, amplitudes: −30 and 30 pA, respectively) in current-clamp mode. MCH neurons were identified by their characteristic ion current responses (van den Pol et al., 2004) and by *post hoc* IHC for MCH and detection of biocytin. Ion currents were recorded in voltage-clamp mode at −70 mV holding potential. Resting potentials (V_{rest}) were recorded in current-clamp mode at 0 pA holding current in the absence/presence of TTX (660 nM, Bio-Techne R&D Systems). TTX was added 10 min before recordings started and then it was continuously present in the aCSF bath solution. Measurements started with initial control recordings. Either PrRP 12-31 or NA (3.5 μM, #P7357 and 10 μM, #A9512, respectively, Merck) was added in single boluses into the recording chamber. When added together (PrRP + NA), NA was applied immediately after PrRP. Consecutive applications of NA and PrRP + NA were performed, when V_{rest} returned to the baseline. When the α2-adrenergic receptor antagonist yohimbine (2 μM, #1127, Bio-Techne) or the GABA(A) receptor antagonist picrotoxin (100 μM, #1128, Tocris) was applied, they were continuously present in the bath solution from the 10th min before NA administration. Slices were fixed in 4% paraformaldehyde overnight and processed for fluorescence detection of MCH and biocytin.

Brain surgeries

Implantation of EEG electrodes. Stainless-steel screw electrodes were implanted over the left frontal cortex (stereotaxic coordinates: 2.0 mm lateral to the midline and 2.0 mm anterior to bregma) and over the left parietal cortex (2.0 mm lateral to midline and 2.0 mm anterior to λ) for frontoparietal EEG recordings. An occipital electrode as a ground was also implanted. A pair of EMG electrodes (stainless-steel spring electrodes covered by silicon rubber) was placed into the neck muscles.

Intracerebroventricular (ICV) cannulation. A polyethylene guide cannula (0.58 mm inner diameter, Intramedic PE-50, Clay Adams, Thomas Scientific) was inserted into the right lateral ventricle under stereotaxic control (−0.8 mm caudal to bregma, 2.0 mm lateral to midline, 4.0 mm ventral to the surface of the skull). EEG electrodes were implanted at the same time, when needed. Rats were allowed to recover and were handled for at least 7 d.

EEG recording and analysis

The effects of ICV-injected saline and different doses of PrRP12-31 (1.6, 4.0, and 10 nmol/5 μl, Merck) on the sleep–wake stages were investigated. Injections were given to awake rats at the beginning of the light phase (lights on at 10:00 A.M.) in a crossover design with 3 d washouts between the treatments ($n = 8$). EEG recordings were compared among the different doses of PrRP and saline.

Rats were placed and kept individually during the study in glass recording chambers (35 × 35 × 40 cm), while attached to a flexible recording cable to allow free movement. The recorded EEG/EMG signals (Vital Recorder software, Kissei Comtec) were amplified (5000 and 10,000 times for EEG and EMG, respectively), and were subjected to analog filtering (<0.5 Hz and >60 Hz). Analog/digital conversion was performed at a sampling rate of 128 Hz. During the whole period of the recordings (24 h), rats were undisturbed, and had access to food and water *ad libitum*. Sleep-EEG analysis was performed in 10 s periods (epochs) using the automatic detection function of Sleep Sign for Animal software (Kissei) based on conventional criteria (Kantor et al., 2004) followed by visual assessment by experienced EEG scorers.

The following sleep–wake stages were differentiated; wakefulness: EEG signal is characterized by low-amplitude activity at β (14-29 Hz) and α (10-13 Hz) frequencies, with high EMG and intense locomotor activity; non-REM sleep (NREMS): EEG is characterized by high-amplitude slow cortical waves (0.5-4 Hz) interrupted by spindles (10-12 Hz), with reduced EMG activity and minimal motor activity; REM sleep (REMS): EEG is characterized by low-amplitude and high-frequency activity with regular theta waves (5-9 Hz), accompanied by silent EMG and motor activity with occasional twitching (Kantor et al., 2004). Power spectral analysis was computed for consecutive 10 s epochs at the frequency range of 0.5-60 Hz (fast Fourier transformation routine, Hanning window, frequency resolution: 0.25 Hz). Adjacent 0.25 Hz bins were summed into 1 Hz bins. Bins are marked by their upper limits (2 Hz refers to 1.25-2.00 Hz). The values of consecutive epochs, separately in wakefulness, NREMS, and REMS were averaged for the first 60 min after treatment. Epochs that contained artifacts or transition between sleep–wake stages were excluded from the power spectral analysis.

Sleep deprivation

REMS deprivation (SD) was performed using the flower pot method, as described previously (Vas et al., 2013). Rats (250-350 g) were sleep-deprived for 72 h starting at lights on (at 10:00 A.M.) on small (SP, diameter: 6.5 cm) or large platforms (LP, diameter: 13 cm) surrounded by water or kept in their home cages (HC) as controls. REMS is eliminated on SP because rats fell into the water because of muscle atony during REMS, whereas LP enables REMS. Thus, LP-kept rats serve as stress controls. Platform sizes and rat weights were chosen based on our previous work (Kitka et al., 2009) and other studies (Maloney et al., 1999; Verret et al., 2003; Machado et al., 2004) validating the method. After 72 h, subgroups of SD rats were allowed to have recovery sleep (2 h) (SPR, LPR) in their HCs.

Rats were killed and the brains were used for quantitative ISH (5 groups, $n = 5$/group) or IHC (5 groups, $n = 3$/group). Additional animals were used for EEG analysis of the recovery sleep (3 h, SPR and LPR groups, $n = 6$/group). Bodyweight change and food intake during the 72 h were measured for the cohort used for PrRP mRNA and protein analysis ($n = 8$/group). EEG recordings during the sleep recovery period were compared with the undisturbed baseline recordings of each rat (1-3 h after lights on, under the same conditions).

Measurement of PrRP mRNA expression levels in SD animals

Fresh frozen brains were cut into 12-μm-thick serial coronal sections in a cryostat, mounted onto Superfrost UltraPlus slides (Fisher Scientific), and stored at −80°C. PrRP mRNA was localized in the sections by radioactive ISH providing a linear relationship between the signal intensity and the mRNA expression level (Chen et al., 2012). Optical densities (mean gray values) of the individual nuclei were measured from the storage phosphor recordings in the A1 and A2 cell groups and between 14.04 and 14.70 mm, as well as in the DM between 3.36 and 4.08 mm caudal to bregma (Paxinos and Watson, 2007) with Image J 1.32j software. Data were determined in three and two consecutive sections in the brainstem and the hypothalamus, respectively, selected from the centers of the investigated areas. The same nuclei were evaluated by applying the same settings both across the sections and across the animals. Background values were measured in parallel and subtracted. In the A1 and DM, where optical densities showed significant differences among the groups, we determined mRNA expression levels also within the individual cells from darkfield microscopic images of autoradiographic emulsion-coated sections as described previously (Tóth et al., 2008). Microphotographs were captured through a 10× objective lens on an Olympus BX60 microscope (Olympus Hungary) from one representative section per animal (see Imaging). The silver grains were selected using the threshold tool in the ImageJ software. The amount of the silver grains over the individual cells was evaluated within identical ROIs and expressed as the area (pixels) covered by grains (Wittmann et al., 2015). In all cases, the signal threshold was set to be >3 times the mean value of two or three background samples measured in the surrounding region. All measurements were performed bilaterally.

Counting of PrRP-immunopositive cells in SD animals
PrRP-immunolabeled cells were visualized on serial coronal sections using DAB as chromogen. Microphotographs were captured through a 10× objective lens on an Olympus microscope (see Imaging). Cells were counted bilaterally in three sections showing the strongest signals in A1 and A2 cell groups, as well as in one or two sections in the DM using the touch count tool in the ImageJ 1.32j software.

Counting of MCH and cFos-immunopositive cells
Cells were visualized on serial coronal sections using Ni-DAB for cFos and DAB for MCH as chromogens. cFos, MCH, and double-labeled cells were counted bilaterally in four sections within 100 × 300 μm^2 ROIs, placed over the PFA or LH using the touch count tool in the ImageJ 1.32j software.

LHe paradigm
The LHe was performed as described previously (Otrokocsi et al., 2017) with slight modifications. Automated soundproof shuttle-boxes interfaced with a computer running Med-PC IV software (Med Associates) were used for the experiment. The shuttle-boxes consisted of two identical compartments and were equipped with photobeam sensors, stimulus light, a tone generator, stainless-steel grid floor, and a guillotine door between the compartments. The paradigm consisted of a training and a test session. On the morning of the experimental day, rats were placed individually in the left or right compartment of the shuttle-box with the guillotine door closed and left to explore for 5 min. The training session lasted for 40 min. Rats in the shocked group ($n = 10$) received 120 trials of 5 s cue (light and tone stimuli) followed by an inescapable (closed door), uncontrollable electric foot shock at 0.4 mA with random duration ranging from 5 to 15 s and unpredictable intershock intervals. Control animals ($n = 5$) did not receive the cues and foot shocks but were otherwise treated similarly. The test session started 7 d later by returning the animals to their previously assigned compartment. All rats received 30 trials of 5 s cues during which the guillotine door was open, followed by an unexpected and escapable foot shock (0.4 mA intensity, 10 s duration with random intershock intervals). Escape during stimulus or escape during shock was scored if the animal crossed the door during cue presentation or the 10 s shock, respectively. Escape latency was measured. Escape failure was scored on the animal not crossing the door during the trial. Animals were classified as being LHe-resilient or LHe-susceptible ("helpless") by applying the *k*-means clustering ($k = 2$) method (Marques et al., 2022). The analysis was applied on the escape failure and escape latency data pairs ($n = 15$). The results were validated by applying the mean + 2 SDs criterion for the escape failure data. Bodyweight and food intake were measured immediately before the training and the test sessions, so the bodyweight change, and food intake were calculated over the 7 d (between the two sessions). Fecal discharge during sessions was counted. Rats were decapitated 24 h after testing between 11:00 A.M. and 12:00 A.M. Trunk blood was collected, the plasma was separated by centrifugation and stored at −80°C for corticosterone RIA (Zelena et al., 2003). The brains were frozen and processed for microdissection and subsequent RT-PCR.

Microdissection of rat brain tissue
Fresh frozen brains were cut into 300-μm-thick slices in a cryostat and mounted on untreated glass slides (Fisher Scientific). The regions containing the DLH, DM, A1, and the A2 cell groups were identified using a head magnifier, with reference to the Rat Brain Atlas (Paxinos and Watson, 2007). The areas were removed from the sections bilaterally using sterile punch needles with an inside diameter of 0.7 mm. The sections were kept frozen in the cryostat throughout the whole procedure. The samples were collected in RNase/DNase-free tubes (Eppendorf) containing NucleoZOL (Macherey-Nagel), homogenized and stored at −80°C.

RIA
Corticosterone was measured in 10 μl unextracted plasma, as described previously (Zelena et al., 2003). Assay sensitivity was 1 pmol. The intra-assay coefficient of variation was 7.5%. All the samples were measured in one assay.

Lipopolysaccharide (LPS) treatments
Rats were treated with intraperitoneal injections of LPS (1 mg/BW kg, O55:B5, Merck) or pyrogen-free saline. Animals in Cohort 1 were killed for IHC (Table 1) 3 or 24 h ($n = 3$/group) and for RT-PCR 3 h ($n = 5$/group) after treatments. Cohort 2 was assessed in the forced swim test (FST) 24 h after LPS (LPS: $n = 6$, control: $n = 5$).

Quantitative evaluation of the immunofluorescence PrRP and MCH signals
Sections immunostained for PrRP and MCH from control and 24 h LPS-treated animals were selected and matched according to their rostro-caudal levels. Confocal images from the PFA and LH were acquired through a 10× lens objective (see Imaging). Measurements were performed using the ImageJ 1.32j software. The PrRP fibers were separated from the background using the threshold tool. Density of the fibers was determined as the area (pixels) covered by fibers within a 100 × 300 μm^2 ROI, placed over the PFA or LH. The total corrected cellular fluorescence in the MCH-immunostained neurons was calculated by measuring the integrated density of the cell and subtracting the background (area of measured cell × mean fluorescence of background readings) (McCloy et al., 2014). The cell bodies were outlined, and the relevant parameters were measured along with three adjacent background readings using the same outline. Only in focus-plane cells (20 cells/image) were evaluated. Data obtained from bilateral measurements of two PrRP and one MCH-immunostained sections from each animal were used for the statistical analysis.

FST
Rats were placed individually in a cylinder (diameter: 18 cm, height: 61 cm) filled (up to 30 cm) with water at 27°C-28°C, during the light phase between 10:00 AM and 2:00 PM (Porsolt et al., 1978; Slattery and Cryan, 2012). Tests (6 min) were performed 24 h following a training session (15 min). PrRP (4 nmol) was given ICV to rats 30 min before the test session. LPS was given to rats in a separate experiment right after the training session. Behavior of the animals ($n = 6$ and $n = 5$ for treatment and control [saline] groups, respectively) was recorded by a camcorder and analyzed later by an observer blinded to the treatment groups using Solomon Coder software (https://solomoncoder.com). During the test, the time spent floating (immobility), struggling, and swimming was determined. Floating was scored when the general activity of the animal was minimized to occasional and small movements of legs or tail necessary to keep the nose above the water. Struggling was considered when the animal was permanently breaking the water surface by intense movements of forepaws usually directed against the walls. Swimming was defined as making active swimming motions, more than necessary to merely keep the head above water (Mlynarik et al., 2007). Immobility (floating) time (%) during the test was rated as passive coping behavior. Each animal was dried and returned to its cage after sessions. Bodyweight and food intake between the sessions were measured.

Human subjects and microdissection of human brain tissue
DLH tissue samples from postmortem control ($n = 7$) and suicidal ($n = 8$) male subjects were provided by the Human Brain Tissue Bank (Semmelweis University, Budapest, Hungary). We included only males in the study to avoid possible sex bias in the data (Tóth et al., 2008) and to be consistent with our animal studies. Clinical information and permission from the patient or the next of kin for the use of the brain tissue for research purposes had been previously received. The medical history of the subjects was obtained from medical or clinical records, and from pathologic and neuropathological reports. Demographic characteristics and available relevant clinical and neuropathological information of the cohort are provided in Table 2. The tissues were stored at −80°C until dissection and later kept frozen throughout the whole procedure. Tissue samples were removed from the brains at the rostral mammillary level from 1.0- to 1.5-mm-thick coronal sections cut by an electric slicer. The regions were identified using the human brain atlas (Mai et al., 2015) and a stereomicroscope with prechilled stage. The

Table 2. Demographic, clinical, and postmortem characteristics of the control and suicide subjects[a]

Case no.	Age (yr)	Sex	Postmortem interval (h)	Cause of death	Neuropathology	Sample
Control						
1	49	Male	2	Cardiac insufficiency	Negative	LHA
2	52	Male	4.5	Myocardial infarction	Negative	LHA
3	54	Male	2	Myocardial infarction	Negative	LHA
4	55	Male	1	Myocardial infarction	NA	LHA
5[b]	55	Male	6	Myocardial infarction	Negative	LHA
6	73	Male	6	Myocardial infarction	NA	LHA
Mean ± SEM	56.3 ± 3.5		3.6 ± 0.9			
Suicide						
1	31	Male	8	Hanging	NA	LHA
2	35	Male	6	Hanging	Negative	LHA
3[b]	40	Male	10	Hanging	Negative	LHA
4	41	Male	4	Hanging	Negative	LHA
5	42	Male	2	Hanging	NA	LHA
6	47	Male	6	Hanging	Negative	LHA
Mean ± SEM	39.3 ± 2.3*		6 ± 1.2			
Control						
1	49	Male	2	Cardiac insufficiency	Negative	DHA
2	54	Male	2	Myocardial infarction	Negative	DHA
3	55	Male	1	Myocardial infarction	NA	DHA
4[b]	55	Male	6	Myocardial infarction	Negative	DHA
5	73	Male	6	Myocardial infarction	NA	DHA
6	81	Male	5	Ischemic heart failure	NA	DHA
Mean ± SEM	61.2 ± 5.2		3.7 ± 0.9			
Suicide						
1	35	Male	6	Hanging	Negative	DHA
2[b]	40	Male	10	Hanging	Negative	DHA
3	41	Male	4	Hanging	Negative	DHA
4	47	Male	6	Hanging	Negative	DHA
5	62	Male	2.5	Hanging	NA	DHA
6[b]	65	Male	10	Hanging	Negative	DHA
Mean ± SEM	48.3 ± 5.1		6.4 ± 1.3			

[a]The subjects were without known treatment with psychotropic medications except Patient 7 (risperidone, donepezil-hydrochloride, paroxetine all prescribed for dementia). Tissue samples were obtained from the DHA and LHA.
[b]Subjects with blood alcohol test. All test results were negative.
*$p < 0.05$, compared with control group (Mann–Whitney U statistic = 10.000 T = 74.000); $n = 6$/group.

samples were removed by using sterile punch needles with inside diameter of 1.0 mm (Palkovits, 1973), collected in RNase/DNase-free tubes (Eppendorf) and stored immediately at −80°C and used for RT-PCR analyses.

Samples were collected in accordance with the Ethical Rules for Using Human Tissues for Medical Research in Hungary (HM 34/1999) and the Code of Ethics of the World Medical Association (Declaration of Helsinki) and approved by institutional ethics committees of the Semmelweis University. Human brain microdissection procedures were approved by the Regional and Institutional Committee of Science and Research Ethics of Scientific Council of Health (34/2002/TUKEB-13 716/2013/EHR, Budapest, Hungary) and the Code of Ethics of the World Medical Association (Declaration of Helsinki). The study was performed in the course of an approved study by the Ethical Committee of the Semmelweis University.

RT-PCR

Total RNA was isolated using a GeneJET RNA Purification Kit. RNA quality and quantity were determined with a NanoDrop 2000 Microvolume Spectrophotometer and in the human samples also by examining the ribosomal RNA bands on agarose gels. cDNAs were prepared using a High Capacity cDNA Reverse Transcription Kit. Amplifications were performed on an ABI StepOnePlus Real-Time PCR system using TaqMan Universal Master Mix II and commercially available TaqMan assays (Table 3). (All above were purchased from Fisher Scientific.) Expression levels were normalized to GAPDH in the rat samples and to acidic ribosomal protein P0 in the human samples. Samples were measured in technical parallels. Relative fold changes were calculated by the comparative CT method ($2^{-\Delta\Delta Ct}$).

Table 3. Catalog numbers of the Fisher Scientific TaqMan assays used for RT-PCRs[a]

Target	Human	Rat
PRLHR	Hs00244685_s1	Rn01411250_s1
NPFF2R	Hs01003259_m1	Rn00576846_m1
PrRP	—	Rn00573653_m1
pro-MCH	—	Rn00561766_g1
TNFα	—	Rn01525859_g1
GAPDH	HS99999905_m1	Rn01775763_g1
RPLPO	HS99999902_m1	—

[a]RPLPO, Ribosomal protein large P0.

Amplifications were not detected in the no-template and a reverse transcriptase minus reactions.

Imaging

Light microscopic examinations were performed using an Olympus BX60 microscope equipped with a SPOTXplorer digital CCD camera (Diagnostic Instruments). Pictures were taken using UPlanFL 4×/0.13, 10×/0.30, or 20×/0.50 objectives. Confocal images were acquired on an LSM 780 confocal laser-scanning microscope (Zeiss). For PrRP and MCH quantitative measurements, pictures were captured using a 10×/0.45 M27 objective with pinhole size 6.5 and 1 AU, respectively. MCH coexpression with biocytin was investigated using 63×/1.4 Oil DIC M27 objective with pinhole size 1.47 AU. For the quantitative analysis of PrRP and TH coexpression and for the illustrative pictures of the MCH neurons, single optical sections were captured using a Plan-

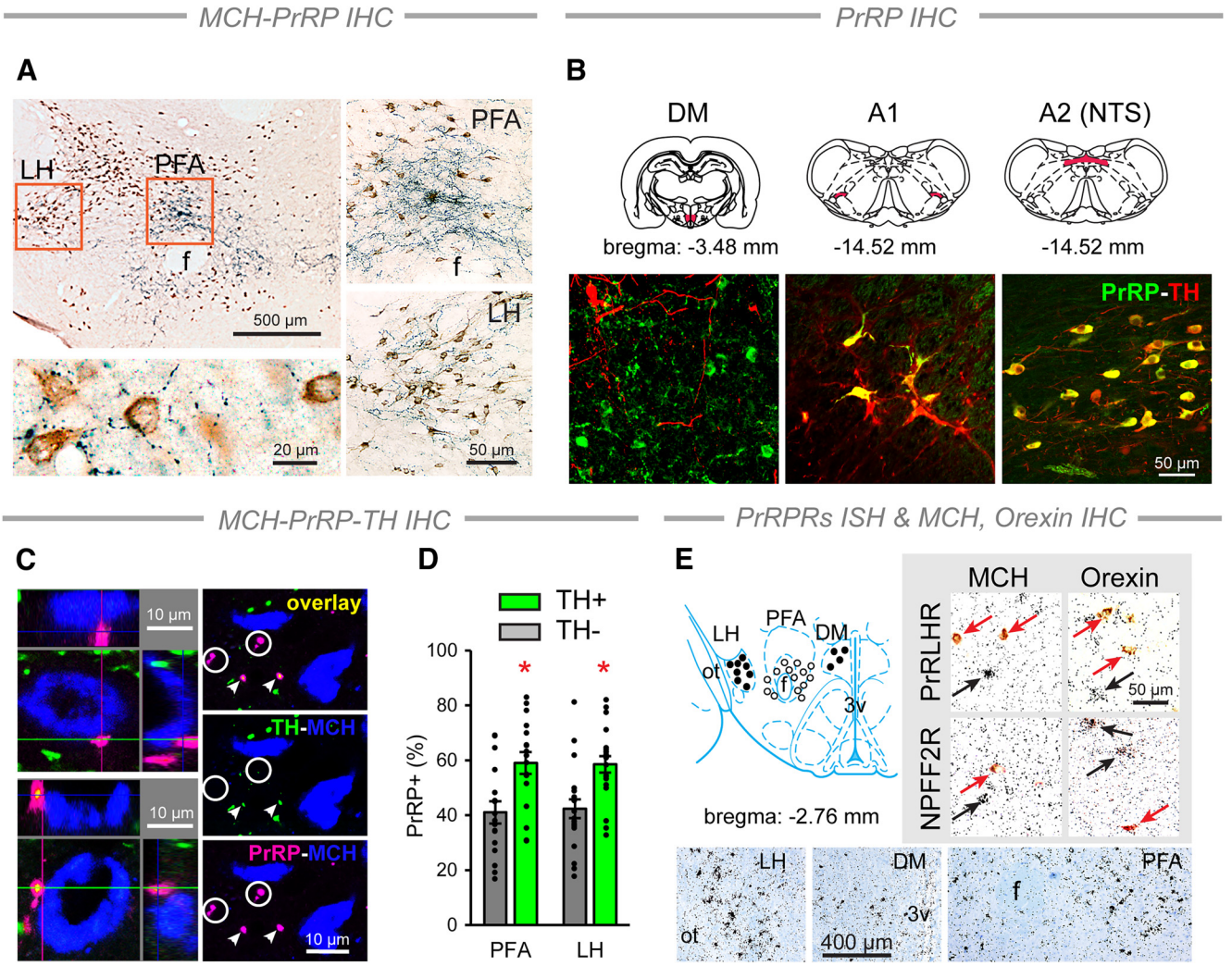

Figure 1. Anatomical relationship between PrRP and MCH neurons in the DLH. ***A***, Double IHC. Top left, Dense PrRP fiber (blue) network surrounds the MCH cells (brown) mainly in the PFA and LH. Right, The PFA and the LH (framed on ***A***) at higher magnification. Bottom left, Multiple PrRP$^+$ axonal varicosities contact the perikarya and dendrites of MCH neurons. ***B***, Noradrenergic and non-noradrenergic PrRP cell populations. Top, Location of the PrRP cells (red) in the hypothalamic DM, and in the A1 and A2 (within the NTS) NA cell groups. Double immunolabeling of TH (red) and PrRP (green) producing cells confirms the catecholamine content of medullary PrRP cells (yellow) (Chen et al., 1999; Tóth et al., 2008). PrRP cells in the DM lack TH. ***C***, Confocal images of triple-labeled sections. Left, Both TH$^-$ (top) and TH$^+$ (green, bottom) PrRP$^+$ terminals (magenta) form close contacts with MCH (blue) neurons. Right, TH$^-$ (circles) and TH$^+$ (arrowheads) axonal varicosities of PrRP$^+$ fibers were analyzed in separate channels. ***D***, Quantitative analysis of the different types of PrRP$^+$ profiles in the DLH. Error bars indicate mean ± SEM. Two-way ANOVA, TH: $F_{(1,70)} = 22.46$, $p < 0.001$. Student-Newman-Keuls multiple comparison test, TH$^+$ versus TH$^-$: *$p = 0.001$, $n = 20$ (PFA) and *$p = 0.002$, $n = 17$ (LH). ***E***, Top left, Location of cells expressing PrRP receptors (PrRPRs): NPFF2R (closed circles) and PRLHR (open circles). Bottom, NPFF2R-expressing cells in the LH and DM as well as PRLHR-expressing cells in the PFA detected by radioactive ISH. The autoradiography shows black silver grain conglomerations over the positive cells. The sections were counterstained by Giemsa (blue). Top right, MCH- and orexin-immunopositive neurons (red arrows) do not express PRLHR and NPFF2R (black arrows). f, Fornix; ot, optic tract; 3v, third ventricle. The schematic drawings of the coronal sections are from the Paxinos atlas (Paxinos and Watson, 2007).

Apochromat 63×/1.4 Oil DIC M27 objective with z separation of 3 and 1 µm, respectively. In case of the MCH staining, the stacks were z-projected in the ImageJ 1.32j software. Contrast and sharpness of the illustrative images were adjusted in Adobe Photoshop CS 8.0. Multipanel figures were assembled in Adobe Illustrator CS3.

Experimental design and statistical analysis

The statistical evaluations were performed using Sigmastat 3.5 application (Systat Software). The size of the experimental groups was determined based on the literature of the field and our previous experience. Each experiment presented in the paper was repeated in multiple animals ($n = 3$-8/groups, see relevant sections). In all experiments, relevant animals were allocated to experimental groups randomly. Data analysis was performed blinded to experimental groups in all cases where the results would have been biased otherwise (in case of more than one treatment groups and manual data analysis). Statistical significance was accepted when $p < 0.05$. Data are expressed as mean ± SEM, except ΔCt data that are shown using box-and-whiskers plots. Paired or unpaired Student's t tests (two-sided) were used for the comparison of two groups with normal distribution of data; otherwise, we applied Mann–Whitney U statistics. When more than two groups were compared, one- or two-way ANOVA or repeated-measures ANOVA were conducted, depending on the experimental setup. Pearson's correlation was used to examine correlations with normal distribution of the data.

Results

Both medullary and hypothalamic PrRP neurons project to the DLH

The interaction between PrRP and MCH neurons requires an appropriate anatomic basis; therefore, we first performed morphologic studies. Our IHC findings revealed that PrRP$^+$ axonal terminals distribute within the DLH. Numerous PrRP$^+$ axonal

terminals established close appositions with MCH$^+$ neurons. This was seen mostly within two areas of the DLH, namely, the PFA and the LH (Fig. 1*A*). Confocal microscopy analysis confirmed the catecholamine content (TH positivity) of the medullary PrRP cells, which were located in the A1 and A2 cell groups. In A2, they were distributed in the nucleus of the solitary tract (NTS) (Chen et al., 1999; Tóth et al., 2008). PrRP neurons in the DM were, however, negative for TH (Fig. 1*B*). MCH-, PrRP-, and TH-triple-labeled sections showed the existence of intimate contacts between the A1/A2- and DM-originated PrRP$^+$ varicosities and MCH$^+$ neurons (Fig. 1*C*, left). When counting 711 and 579 PrRP$^+$ varicosities in the PFA and LH, respectively, ~60% of the varicosities contained TH in both investigated areas (Fig. 1*C*,*D*).

To see whether MCH neurons express PrRP receptors, we performed ISH combined with IHC. PRLHR mRNA-expressing cells were restricted to the PFA. NPFF2R, which mediates some effects of PrRP (Ma et al., 2009), was detected in the dorsal periventricular region in the DM and in a narrow field of the rostral LH adjacent to the optic tract (Fig. 1*E*, left and bottom). Importantly, the receptor-expressing cells were negative for MCH, which excludes the possibility that the intimate contacts between PrRP$^+$ and MCH$^+$ neuronal elements are direct synaptic contacts. Orexin cells, which are also a major cell population of the DLH (Kitka et al., 2011; Vas et al., 2013), did not express PrRP receptors either (Fig. 1*E*, top, right).

ICV PrRP injection promotes sleep

Since there is a strong relationship between stress, sleep, and mood (van Dalfsen and Markus, 2018; Steiger and Pawlowski, 2019), and the DLH is a critical site of sleep–wakefulness regulation (Bonnavion et al., 2016), next we examined the effect of ICV PrRP administration on the sleep–wake cycle. PrRP (0, 1.6, 4, and 10 nmol) injection at the beginning of the passive phase (Fig. 2*A*) elicited an acute sleep-promoting effect by increasing the amount of NREMS and decreasing NREMS latency. Both effects ceased within 30 min and were significant with the higher doses of PrRP only (Fig. 2*B*,*C*). Lower doses of PrRP (1.6 and 4.0 nmol) also affected the quantitative EEG spectra during NREMS by reducing the power of the δ (1-4 Hz) frequency range (Fig. 2*D*). The amount of wakefulness diminished gradually along with the increasing doses of PrRP (Fig. 2*E*). The amount of REMS was nearly zero in the short period of PrRP's effects; therefore, the effects of PrRP on REMS and REMS latency could not be investigated using this experimental setup (Fig. 2*F*,*G*).

PrRP expression is associated with sleep–wake stages

To challenge MCH neurons that are known to be involved in promoting REMS (Bandaru et al., 2020), we used the flower pot SD paradigm, which eliminates REMS completely, and enhances the REMS pressure (i.e., the need for REMS, Fig. 3*A*) (Maloney et al., 1999; Verret et al., 2003; Machado et al., 2004). During the recovery sleep following 72 h SD, REMS was recovered in the SPR rats, by producing twice as much REMS compared with the baseline, whereas the amount of NREMS decreased. The LPR group revealed no change in the sleep parameters versus the baseline (Fig. 3*B*).

Despite consuming a similar amount of food to HC rats (Fig. 3*C*, top), both SP and LP rats lost weight compared with HC animals (Fig. 3*C*, bottom). This effect was independent of the size of the platforms.

The SP- but not the LP-induced SD increased the amount of PrRP mRNA in the DM, and this was normalized during recovery (Fig. 3*D*). Additionally, both SP and LP conditions elevated

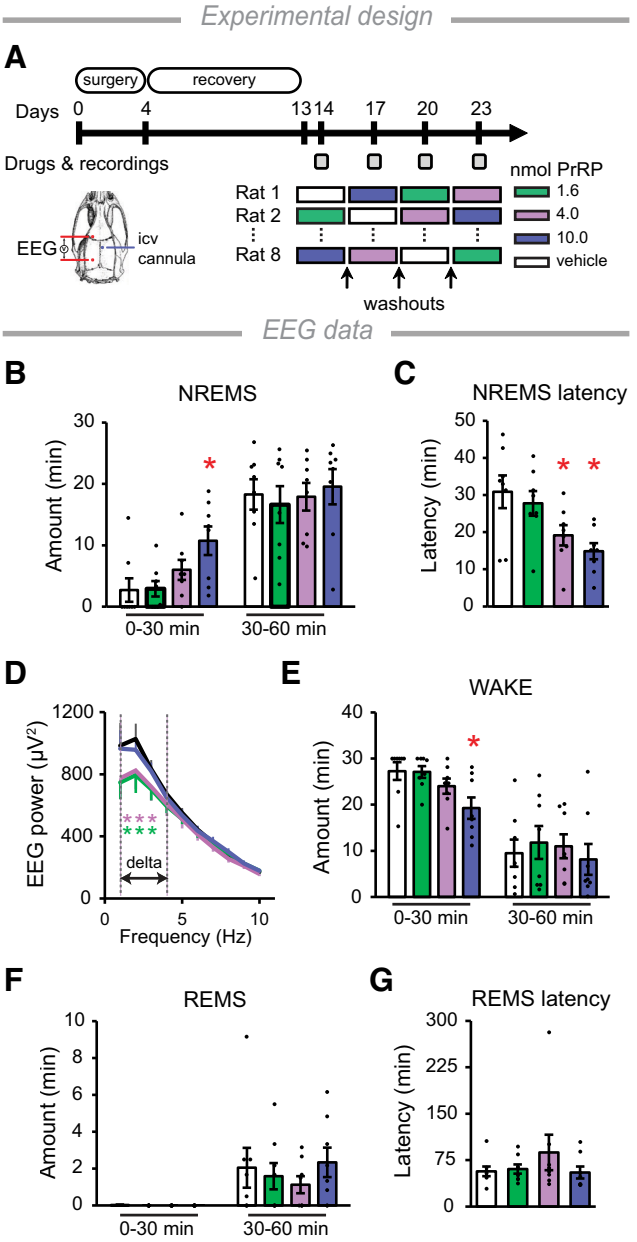

Figure 2. Effects of PrRP on EEG parameters. ***A***, Schematic and timeline of the experiment. Frontoparietal EEG was recorded on the left (red). Different doses of PrRP, or vehicle (saline), were injected intracerebroventricularly (ICV) through a chronically implanted cannula (blue) into the right ventricle, at the beginning of passive (light) phase using a crossover design. Gray squares represent the days when treatments and recordings were performed. ***B***, The amount of NREMS. Zero is the time point of the drug administration. One-way repeated-measures ANOVA 0-30 min, $F_{(3,21)} = 5.14$, $p = 0.008$. ***C***, NREMS latency. One-way repeated-measures ANOVA, $F_{(3,21)} = 6.56$, $p = 0.003$. ***D***, EEG δ power (1-4 Hz) during the first hour after injections. Two-way repeated-measures ANOVA, treatment × frequency interaction: $F_{(9,63)} = 2.86$, $p = 0.007$. ***E***, Time spent awake. One-way repeated-measures ANOVA, $F_{(3,21)} = 5.09$, $p = 0.008$. ***F***, The amount and (***G***) the latency of REMS. For *post hoc* analysis, Bonferroni multiple comparison tests were performed. *$p < 0.05$ versus vehicle; $n = 8$/group. Error bars indicate mean ± SEM.

PrRP mRNA levels remarkably in the A1 cell group, which remained high during the recovery sleep. Neither the SP- nor the LP-induced SD altered the expression of PrRP mRNA in the NTS (Fig. 3*D*). PrRP protein levels showed parallel alterations in the relevant experimental groups to the PrRP mRNA levels (Figs. 3*E*, 4*A*). Measurements at the cellular level showed that changes in the expression of PrRP mRNA in both the DM (Fig. 4*A*) and

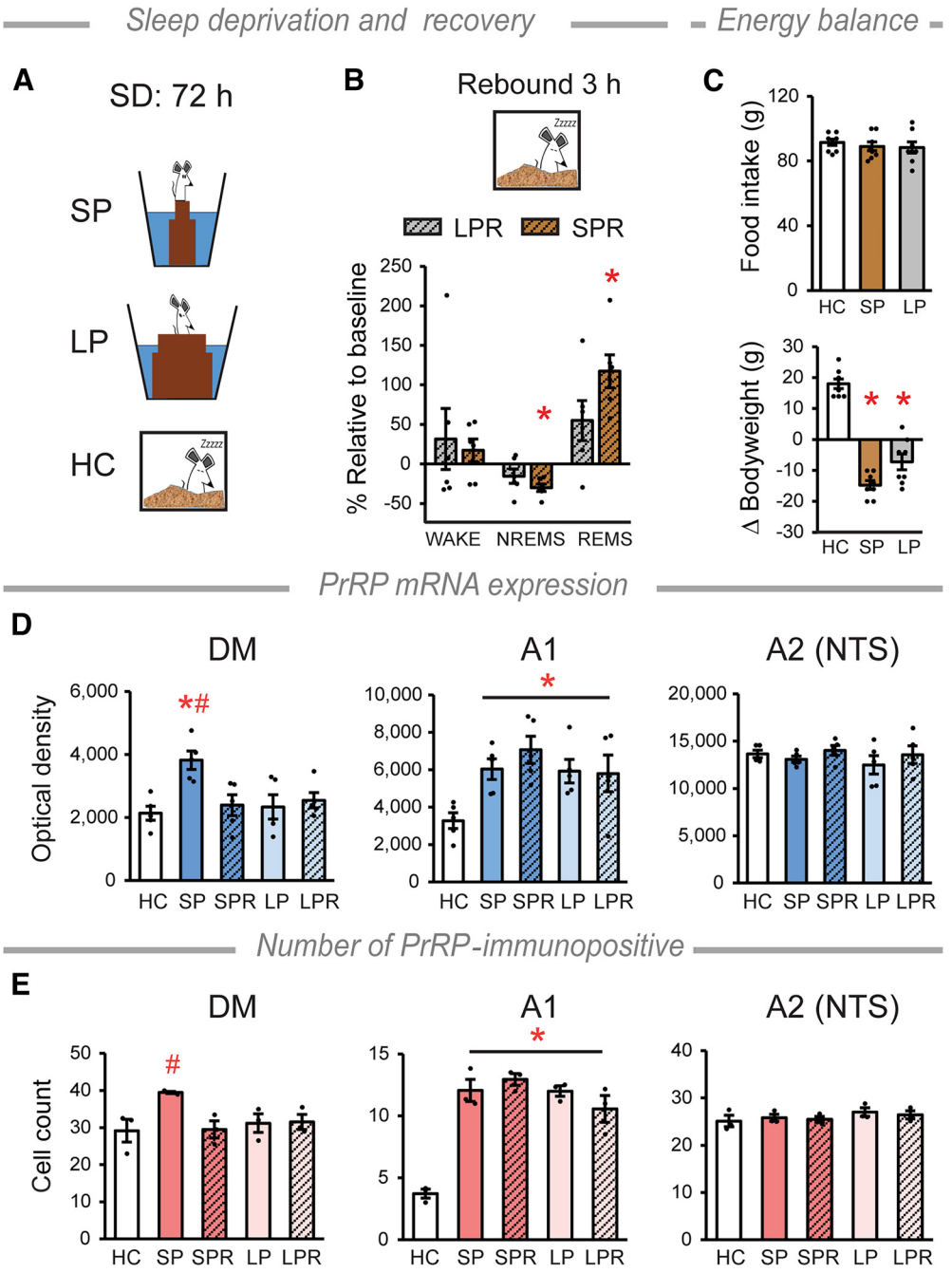

Figure 3. PrRP expression varies with the amount of sleep. ***A***, Schematic of SD method. Rats were placed individually on round platforms surrounded by water. REMS is eliminated on SP because rats fell into the water because of muscle atony during REMS, whereas LP enables REMS. Thus, LP-kept rats serve as stress controls (Maloney et al., 1999; Machado et al., 2004; Kitka et al., 2009). ***B***, Sleep parameters during the recovery sleep. The amount of NREMS decreases, while the amount of REMS increases significantly in the SP rebound (SPR), but not in the LP rebound (LPR) group, compared with baseline recorded for each rat. Two-way repeated-measures ANOVA, vigilance state × pot interaction: $F_{(2,15)} = 31.6$, $p < 0.0001$, NREMS $^{*}p < 0.0001$ and REMS $^{*}p = 0.0002$; $n = 6$/group. ***C***, Food intake (top) and bodyweight change (bottom) during SD. Kruskal–Wallis test, $H_2 = 17.19$, $p < 0.001$, $^{*}p < 0.05$ versus HC; $n = 8$/group. ***D***, PrRP mRNA expression levels in the DM, the A1 and A2 (NTS) cell groups. Graphs represent the quantitative results measured as optical densities of the ISH signals. DM: one-way ANOVA, $F_{(4,20)} = 4.96$, $p = 0.006$, SP versus HC $^{*}p < 0.01$, SP versus all the other groups $^{\#}p \leq 0.01$. A1 cell group: one-way ANOVA, $F_{(4,20)} = 4.16$, $p = 0.013$, all groups versus HC $^{*}p < 0.05$. NTS: no alterations were detected, $n = 5$/group. ***E***, Number of PrRP-immunopositive cells. DM: one-way ANOVA, $F_{(4,10)} = 3.54$, $p = 0.048$, SP versus SPR and LPR $^{\#}p < 0.05$, SP versus HC and LP $p = 0.053$ and $p = 0.061$, respectively. A1 cell group: one-way ANOVA, $F_{(4,10)} = 28.11$, $p < 0.001$, all groups versus HC $^{*}p < 0.001$. There was no change in the NTS. $n = 3$/group. Error bars indicate mean ± SEM. For multiple comparisons, the Holm–Sidak method (***B***) and the Student-Newman-Keuls (***C–E***) test were used.

the A1 cell group (Fig. 4*B*) were because of the elevated expression of the PrRP mRNA within the individual cells.

PrRP inhibits REMS-active MCH neurons *in vivo*

Our flower pot experimental data provided evidence for the active participation of the endogenous PrRP in the sleep–wake regulation. Additionally, it provided a useful experimental setup for the functional investigation of the morphologically established circuits between PrRP and MCH neurons. Evoking rebound sleep after SD by the flower pot method is a powerful way to activate the majority of MCH neurons in the DLH, which can be detected by cFos IHC (Verret et al., 2003; Kitka et al., 2011). To see whether

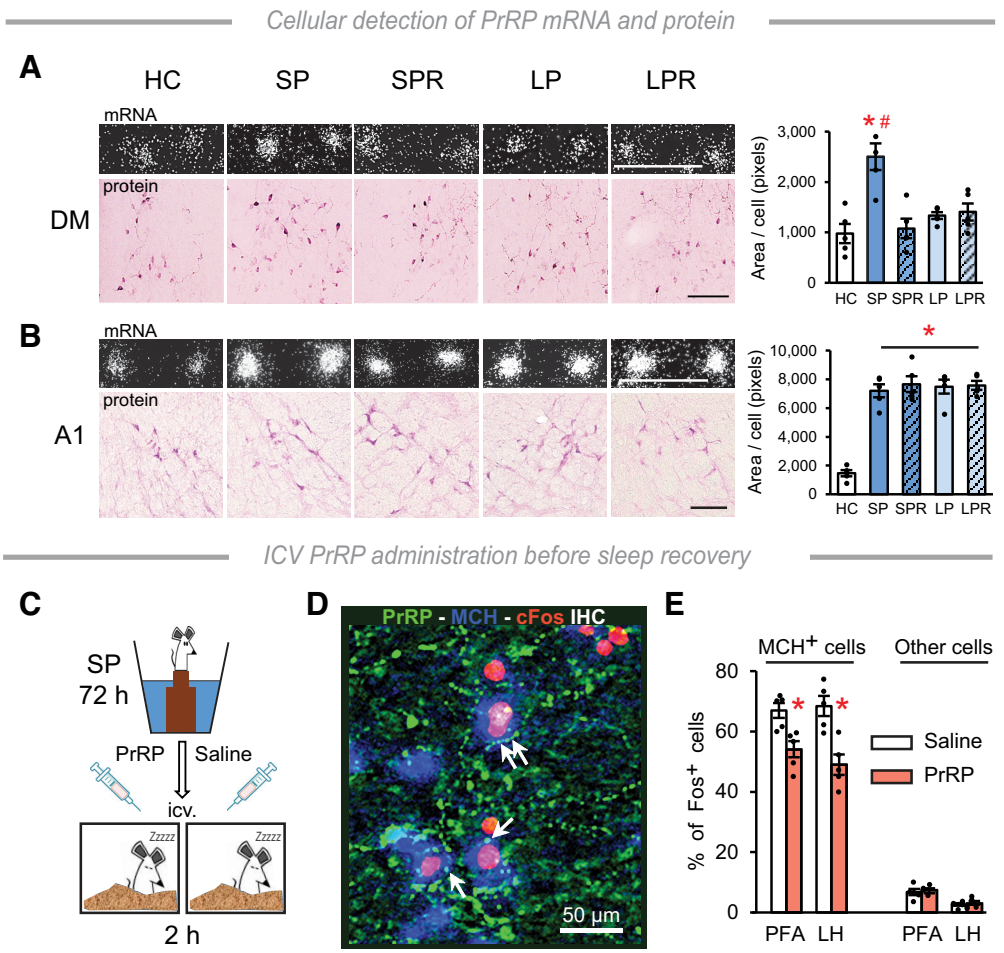

Figure 4. Cellular changes after SD. ***A***, ***B***, Detection of PrRP mRNA and protein in the cells in the DM and the A1 cell group, respectively. Top, left, Darkfield pictures: autoradiography of PrRP mRNA-labeled cells. The density of the silver grains (white spots) over the positive cells changes in proportion to the amount of mRNA. Bottom, left, Immunohistochemical detection of $PrRP^+$ neurons. Scale bars, 100 µm. Right, Graphs represent the results of the mRNA level measurements at cellular level. Data are expressed as the area covered by silver grains over the individual cells. One-way ANOVA, DM: $F_{(4,24)} = 10.53$, $p < 0.001$, A1: $F_{(4,24)} = 40.15$, $p < 0.001$, Student-Newman-Keuls multiple comparison test, $^*p < 0.001$ versus HC, $^{\#}p < 0.001$ versus all other groups; $n = 5$/group. ***C***, PrRP (4 nmol/5 µl) or saline (5 µl) was administered ICV into SP-deprived rats prior of recovery sleep. ***D***, MCH (blue), cFos (red), and PrRP (green) triple fluorescence IHC showed close contacts between $PrRP^+$ fibers and MCH^+ neurons, which were activated by REMS rebound. ***E***, Percentages of MCH^+ and non-MCH^+ neurons exhibiting cFos signal in the PFA and LH in animals treated with PrRP, or saline. Two-way ANOVA, effect of treatment: $F_{(1,16)} = 28.73$, $p < 0.001$; $n = 5$/group. Student-Newman-Keuls multiple comparison test, $^*p < 0.01$ versus saline. Error bars indicate mean ± SEM.

PrRP affects the function of REMS-active MCH neurons, SP rats were injected with PrRP (4 nmol, ICV), or vehicle just before recovery sleep (Fig. 4*C*). We found that PrRP fibers frequently formed close contacts with $cFos^+/MCH^+$ neurons (Fig. 4*D*). In the PrRP-treated rats, the ratio of $cFos^+/MCH^+$ neurons was significantly lower compared with controls in both the PFA and LH (Fig. 4*E*, left). The percentage of other types of $cFos^+$ cells was unaffected by the PrRP treatment (Fig. 4*E*, right).

PrRP hyperpolarizes MCH neurons and greatly increases the effect of NA *ex vivo*

To characterize the observed effect of PrRP on MCH neurons, we performed whole-cell patch-clamp experiments using brain slices from 30-d-old rats. At this age, the MCH neuronal system is fully developed (Risold et al., 2009), and the MCH cell population appears similar to those in adults (Fig. 5*A*, left). MCH neurons in the PFA (Fig. 5*A*, right) were identified by their characteristic electrophysiological responses to current steps (Fig. 5*B*) as follows: (1) adaptation of firing during the depolarizing step; (2) absence of spontaneous spikes at resting state; (3) absence of rebound depolarization at the end of the hyperpolarizing step; and (4) absence of sag at the beginning of the hyperpolarizing step (van den Pol et al., 2004). Identity of the measured MCH neurons was also confirmed by *post hoc* IHC (Fig. 5*C*).

PrRP (3.5 µM) evoked an outward current in the MCH cells, starting within 15 s after its application (I_{max}: 36.06 ± 2.45 pA, duration: 28.00 ± 4.67 s) (Fig. 5*D*). PrRP hyperpolarized MCH neurons in the absence of the voltage-gated Na-channel blocker TTX with a 4.66 ± 0.48 mV change in the resting potential (ΔV_{rest}) and with a duration of 27.42 ± 3.71 s (Fig. 5*E*). This effect was not observed in the presence of TTX (Fig. 5*F*).

We also investigated the interaction between PrRP and NA. As expected (van den Pol et al., 2004), NA (10 µM) hyperpolarized the patched MCH neuron repeatedly (Fig. 5*G*, left, Fig. 5*H*). When PrRP (3.5 µM) was added just before the third application of NA, the response was almost doubled. Meanwhile, the mean durations of the triggered V_{rest} changes were unaltered (Fig. 5*G*, left, Fig. 5*H*). In the presence of TTX (Fig. 5*G*, right, Fig. 5*H*), the response to NA was similar to that observed in the absence of TTX. PrRP did not modify the NA-triggered response in the presence of TTX (Fig. 5*G*, right, Fig. 5*H*). The response to NA was completely blocked in the presence of the α2-adrenergic receptor antagonist yohimbine (2 µM, Fig. 5*I*) (van den Pol et al., 2004).

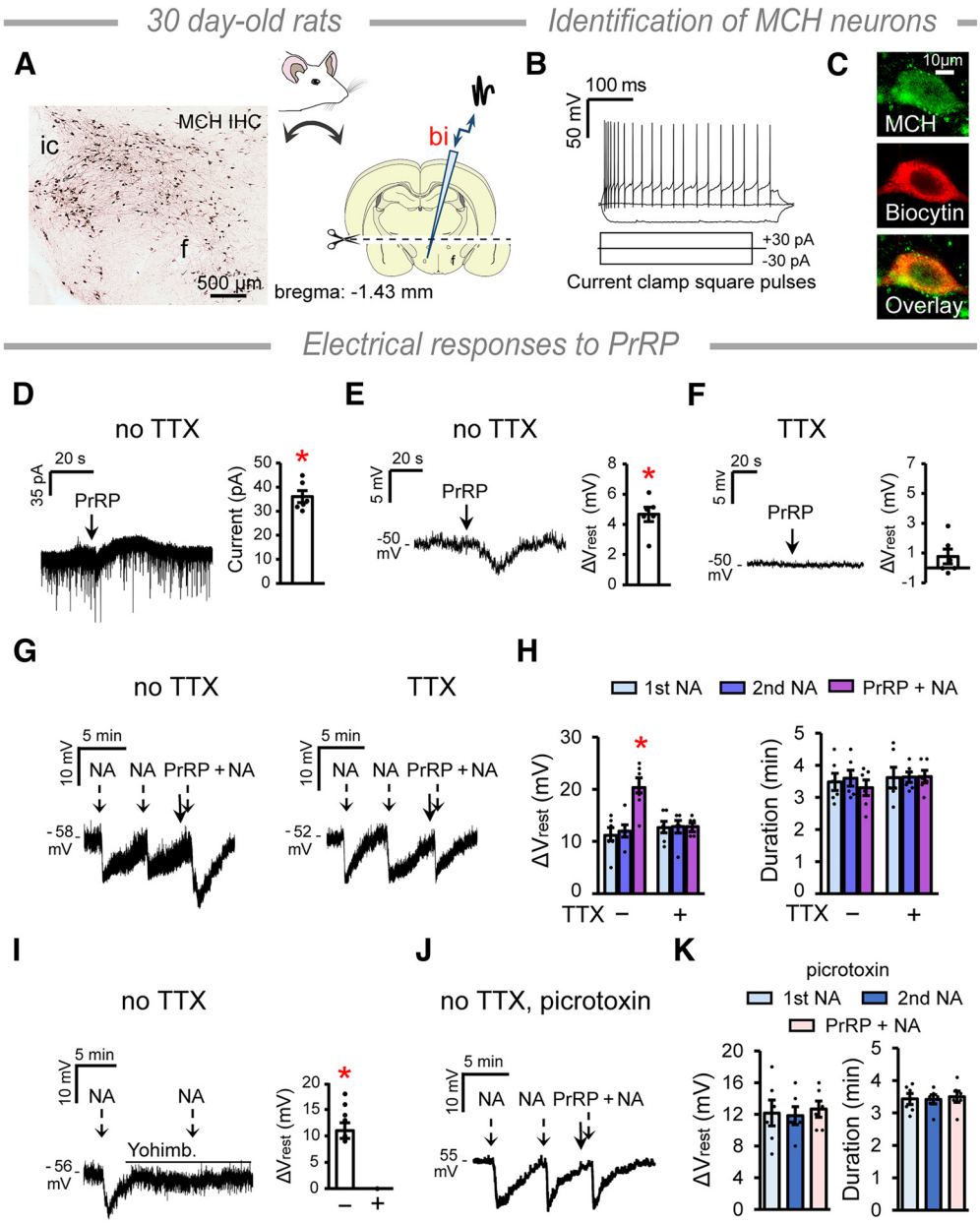

Figure 5. PrRP inhibits the MCH neurons. ***A***, Left, Immunohistochemical detection of MCH neurons in 30-d-old rats. Right, Schematics (Paxinos and Watson, 2007) of the brain slice preparation for patch-clamp recording. Acute coronal slices containing the hypothalamus were used with the thalamus, and the cortex removed. Neurons in the PFA were patched using a biocytin (bi) filled electrode. ***B***, Electrophysiological identification of the MCH neurons was performed by their response to current steps (van den Pol et al., 2004). ***C***, Identity of the measured cells was confirmed by *post hoc* IHC. ***D***, PrRP (3.5 µM) elicits a transient outward current in MCH neurons in the absence of TTX. Student's *t* test (paired), $t = 14.745$, $df = 5$, $^*p = 0.000$. ***E***, Membrane potential changes (ΔV_{rest}) of MCH neurons in response to PrRP in the absence of TTX. Student's *t* test (paired), $t = 9.785$, $df = 5$, $^*p = 0.000$. ***F***, There is no response to PrRP in the presence of TTX. ***G***, ΔV_{rest} in response to repeated administration of NA (10 µM, dashed arrows), and after pretreatment with PrRP (solid arrow) in the absence (left) and presence of TTX (right). ***H***, Graphs summarize the effects of PrRP on the NA-induced responses. One-way repeated-measures ANOVA. ΔV_{rest} no TTX: $F_{(2,10)} = 32.6$, $p < 0.001$, Holm–Sidak multiple comparison tests, PrRP+NA versus first and second NA, $^*p < 0.0001$. ***I***, ΔV_{rest} in response to NA in the absence (−) and presence (+) of the α2-adrenergic receptor antagonist yohimbine (2 µM, horizontal line above the recording). Student's *t* test, $t = 8.900$, $df = 5$, $^*p = 0.000$. ***J***, ΔV_{rest} in response to repeated administration of NA (dashed arrows), and after pretreatment with PrRP (solid arrow) in the presence of the GABA(A) receptor antagonist picrotoxin (100 µM) and absence of TTX. ***K***, Graphs summarize the effects shown in ***J***. Error bars indicate mean ± SEM. $n_{cells} = 6$ for all except $n_{cells} = 4$ in ***F***. One or two cells/animal were measured in independent experiments.

Next, we used the same experimental setup to identify the cell type mediating the inhibitory effect of PrRP on MCH neurons. This time, we used bath-applied picrotoxin (100 µM), a GABA(A) receptor antagonist. We assumed that PrRP acts via inhibitory interneurons in the PFA, because PRLHR is a Gq-coupled receptor (Dodd and Luckman, 2013) and is highly expressed by GABAergic cells in the reticular nucleus of the thalamus (Lin et al., 2002). Indeed, whereas NA elicited similar responses in MCH neurons than previously, PrRP failed to modify the effect of NA in the presence of picrotoxin and absence of TTX (Fig. 5*J*,*K*). Together, our findings revealed a presynaptic, GABA(A) receptor mediated, inhibitory effect of PrRP on MCH neurons, which substantially adds to the postsynaptic action of NA. The presence of close contacts between MCH neurons and PrRP varicosities may therefore suggest that PrRP receptors are located at the GABAergic terminals innervating MCH cells.

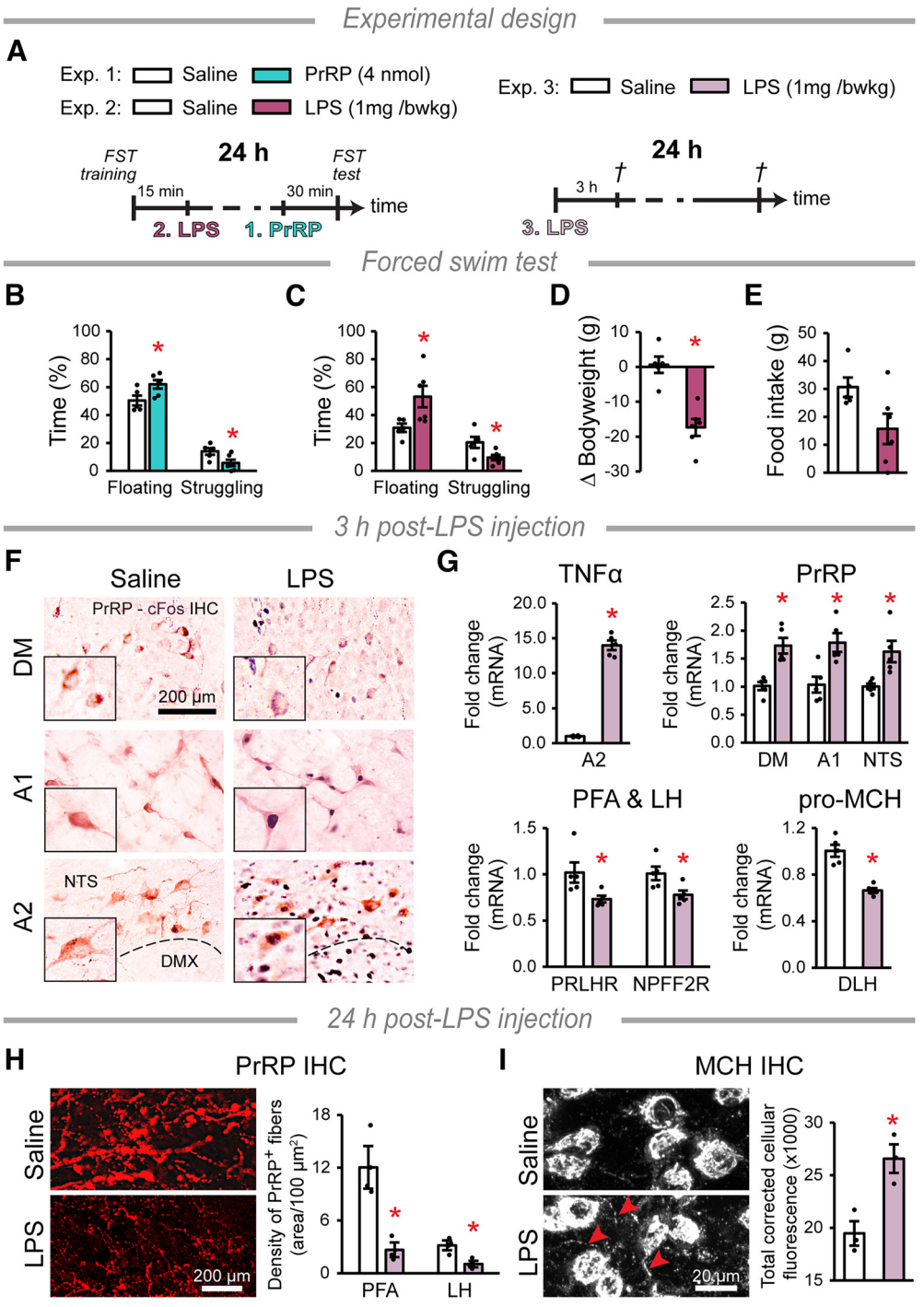

Figure 6. Evaluation of the inflammation-induced depression model. ***A***, Timelines of the experiments. LPS was added intraperitoneally to induce inflammation. PrRP was injected intracerebroventricularly. Control rats received saline. ***B, C***, Exp. 1. and 2, respectively: Student's *t*-tests, $df = 9$, saline: $n = 5$, treated: $n = 6$. Percentage of the time spent passively ("floating") and actively ("struggling") in the FST 30 min after (***B***) PrRP (floating: $^*p = 0.036$, struggling: $^*p = 0.035$, $t = -2.459$ and $t = 2.484$, respectively) or 24 h after (***C***) LPS treatments (floating: $^*p = 0.034$, struggling: $^*p = 0.030$, $t = -2.499$ and $t = 2.576$, respectively). ***D***, Bodyweight change ($t = 5.213$, $^*p = 0.001$) and (***E***) food intake ($p = 0.056$) during the 24 h after the LPS injections. ***F***, PrRP cell (brown) activation 3 h after LPS treatment. The cFos nuclear signal (black) appears in the activated neurons. The inserts show PrRP neurons at higher magnification. DMX: dorsal motor nucleus of the vagus nerve. ***G***, Exp. 3: Student's *t*-tests, $df = 8$, $n = 5$/group. Relative mRNA levels of TNFα ($^*p = 0.001$, $t = 37.153$, measured in the A2 cell group), PrRP (DM: $^*p = 0.001$, $t = 4.759$, A1: $^*p = 0.008$, $t = 3.501$, NTS: $^*p = 0.005$, $t = 3.814$), PrRP receptors (PRLHR and NPFF2R: $^*p = 0.02$, $t = -2.898$ and $t = -2.890$, respectively) and pro-MCH ($^*p = 0.001$, $t = -6.854$) 3 h post-LPS treatment. ***H***, Exp. 3: Student's *t*-tests, $df = 4$, $n = 3$/group. PrRP immunopositivity in DLH axons 24 h after treatments. The image illustrates the PFA. The bar graph shows the density of PrRP$^+$ fibers in the area (PFA: $^*p = 0.021$, LH: $^*p = 0.034$, $t = 3.675$ and $t = 3.168$). ***I***, MCH immunopositive cells in the PFA 24 h after treatments. The arrowheads point to axonal processes. The bar graph shows the total cellular fluorescence measured in the MCH neurons, Student's *t*-test, $t = -3.989$ $df = 4$, $^*p = 0.016$, $n = 3$/group, error bars indicate mean ± SEM.

Overload of PrRP neurons underlines increased passive coping in FST

To determine whether previous exposure to PrRP ("artificial stress") affects subsequent coping with stress, we administered ICV PrRP to rats 30 min before subjecting them to FST (Fig. 6*A*, Experiment 1). The effect of ICV PrRP on ACTH release ceases after 10 min (Seal et al., 2002), in line with the effects of PrRP on the EEG, which worn off within 30 min. Post-PrRP animals

showed increased immobility ("floating") and decreased active coping ("struggling") behavior compared with the control group (Fig. 6*B*). The percentage of time spent swimming was unaltered (saline: 20.2 ± 4.5%; PrRP: 18.0 ± 4.5%).

Next, we used LPS treatment to induce inflammatory stress in rats (Fig. 6*A*, Experiment 2). LPS has long-term effects, first triggering a surge of pro-inflammatory cytokines and sickness behavior, leading to the development of "depression-like" behavior in the late phase (24 h) (Frenois et al., 2007; Dantzer, 2009). Compared with controls, LPS-treated rats spent more time "floating" and less time "struggling" in the FST 24 h after the treatment (Fig. 6*C*), with no alteration in the percentage of time spent swimming (saline: 30.4 ± 4.6%, LPS: 22.9 ± 7.0%). The LPS-treated rats lost weight (Fig. 6*D*), although their 24 h food intake (Fig. 6*E*) was not significantly different from controls.

We then investigated the LPS-induced effects on the brain (Fig. 6*A*, Experiment 3). A high number of PrRP cells in the A1 and A2 cell groups were cFos^{+} in the LPS-treated animals 3 h after injection (Fig. 6*F*). At the same time, the mRNA expression of the pro-inflammatory cytokine, TNFα, was strongly upregulated by LPS in the A2 cell group (Fig. 6*G*). The expression of PrRP mRNA was also increased in all PrRP-producing cell groups, while the expression of PrRP receptors and pro-MCH was decreased in DLH (Fig. 6*G*). One day following LPS treatment, PrRP immunopositivity was severely depleted in axons in the PFA and LH (Fig. 6*H*). Meanwhile, MCH protein levels were elevated in the neuronal perikarya (Fig. 6*I*).

Normal PrRP signaling in the DLH may be protective against the development of LHe

To further examine the role of PrRP in regulation of mood, we applied the LHe paradigm (Fig. 7*A*). Helpless behavior developed in 50% of the stressed rats (LHe-susceptible rats). This was clearly indicated by the number of missed escapes (Fig. 7*B*) and the escape latency (Fig. 7*C*). The escape behavior of LHe-resilient animals was normal.

Fecal discharge is a reliable marker of acute stress in rats (Bindra and Thompson, 1953). LHe-susceptible and LHe-resilient animals produced an equally high number of fecal pellets because of the inescapable shock received during the "training." Nonshocked controls showed no signs of acute stress (Fig. 7*D*). The escapable shock received 1 week later ("test") was a moderate level of acute stress for all animals equally (Fig. 7*D*).

Blood corticosterone concentrations were elevated 24 h after the test session in both the LHe-susceptible and LHe-resilient rats, indicating that the training induced chronic activation of the HPA axis (Fig. 7*E*). The level of chronic stress was mild, reflected by the comparable bodyweight gain (Fig. 7*F*) and food intake (Fig. 7*G*) among the groups. Importantly, although HPA activity between the LHe-susceptible and LHe-resilient rats was similar, helpless behavior developed only in the LHe-susceptible rats.

The relative expression of PrRP mRNA in the DM doubled specifically in LHe-susceptible rats (Fig. 7*H*). In the A1 cell group, PrRP mRNA level was remarkably elevated in both LHe-susceptible and LHe-resilient rats, with a near-significant difference between

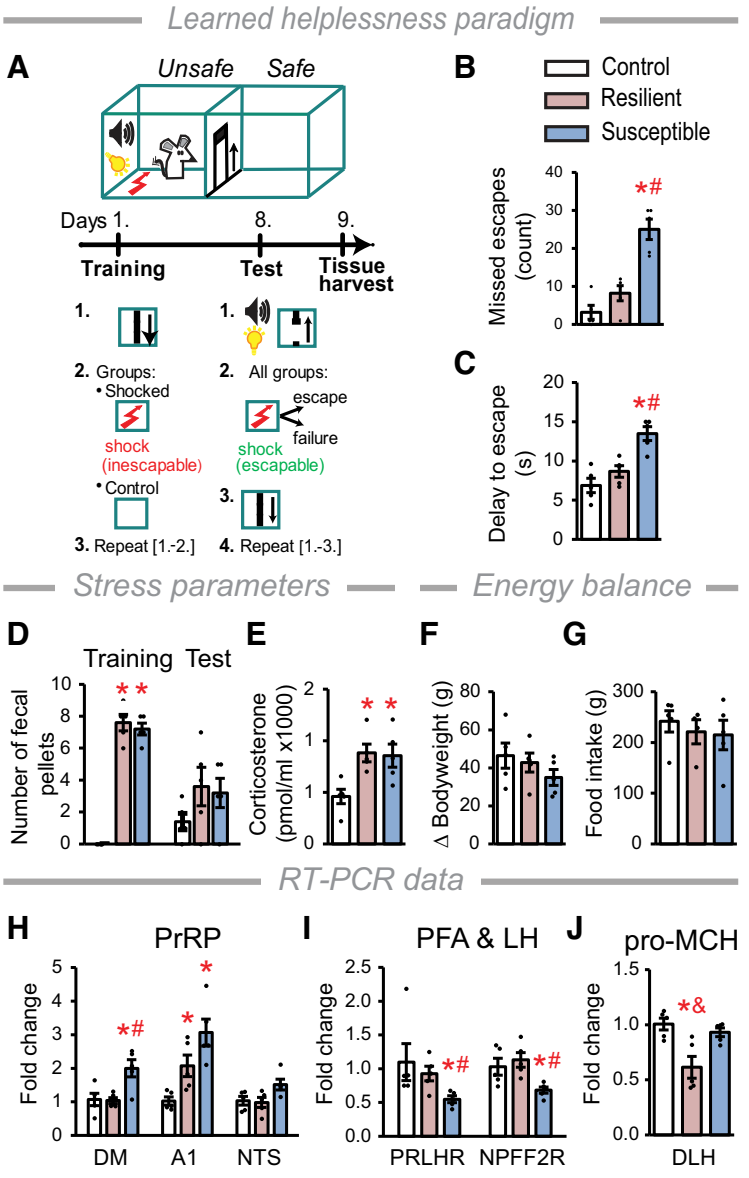

Figure 7. Rats with helpless behavior show altered PrRP and MCH signaling. ***A***, Schematic of the LHe paradigm. During the training, one group of animals is exposed to a series of uncontrollable and inescapable foot shock (two-chamber cage, door closed). During the test, all animals receive a series of foot shock, with prior light and sound cues provided while the door opens. ***B***, Number of missed escapes, $F_{(2,12)} = 27.02$, $p < 0.001$. $^{*}p < 0.001$ versus control. $^{\#}p < 0.001$ versus LHe-resilient. ***C***, Delay to escape, $F_{(2,12)} = 16.06$, $p < 0.001$. $^{*}p < 0.001$ versus control. $^{\#}p = 0.002$ versus LHe-resilient. ***D***, Number of fecal pellets, $F_{(2,12)} = 137.2$, $p < 0.001$. $^{*}p < 0.001$ versus control. ***E***, Corticosterone levels 24 h after the test session, $F_{(2,12)} = 6.82$, $p = 0.011$. $^{*}p = 0.016$, $^{*}p = 0.01$ versus control, for LHe-resilient and LHe-susceptible, respectively. ***F***, Bodyweight change and (***G***) food intake between the training and the test. ***H–J***, Relative mRNA levels 1 d after the test. ***H***, PrRP: DM: $F_{(2,12)} = 6.04$, $p = 0.015$. $^{*}p = 0.025$ versus control. $^{\#}p = 0.012$ versus LHe-resilient. A1 cell group: $F_{(2,12)} = 16.82$, $p < 0.001$. $^{*}p < 0.004$, $^{*}p = 0.001$ versus control for LHe-resilient and LHe-susceptible rats, respectively. $p = 0.053$ LHe-resilient versus LHe-susceptible. NTS: $F_{(2,12)} = 3.29$, $p = 0.073$. ***I***, PrRP receptors in the DLH: PRLHR: $F_{(2,12)} = 5.14$, $p = 0.024$. $^{*}p = 0.028$ versus control. $^{\#}p = 0.029$ versus LHe-resilient. NPFF2R: $F_{(2,12)} = 7.24$, $p = 0.009$. $^{*}p = 0.015$ versus control. $^{\#}p = 0.009$ versus LHe-resilient. ***J***, pro-MCH: $F_{(2,12)} = 8.63$, $p = 0.005$. $^{*}p = 0.006$ versus control. $^{\&}p = 0.006$ versus LHe-susceptible. Statistics for RT-PCR were calculated from the ΔCt values. Error bars indicate mean ± SEM; $n = 5$/group. One-way ANOVA and Student-Newman-Keuls multiple comparison test were used for all statistics.

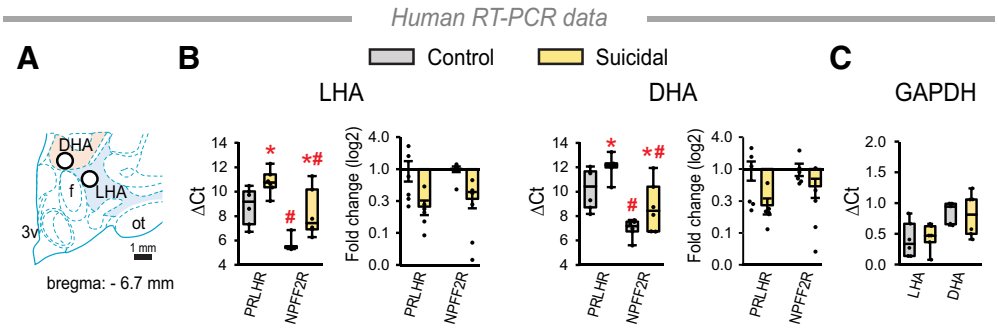

Figure 8. Relative mRNA expression of PrRP receptors in the LHA and DHA in control and suicidal human subjects. ***A***, Schematic of the right human hypothalamus (Mai et al., 2015). White circles represent the size and location of the areas within the LHA (blue) and DHA (beige), from which tissue samples were taken for RT-PCR. f, Fornix; ot, optic tract; 3v, third ventricle. ***B***, RT-PCR data (ΔCt and fold change) of PrRP receptors. $LHA_{receptors}$: $F_{(1,10)} = 27.71$, $p < 0.001$. $^{\#}p < 0.001$ versus PRLHR within both groups and LHA_{groups}: $F_{(1,10)} = 14.70$, $p = 0.003$. $^{*}p = 0.048$ versus controls within both receptors. $DHA_{receptors}$: $F_{(1,10)} = 23.05$, $p < 0.001$. $^{\#}p < 0.001$ versus PRLHR within both groups and DHA_{groups}: $F_{(1,10)} = 12.51$, $p = 0.05$. $^{*}p = 0.023$ and $^{*}p = 0.005$ versus controls within PRLHR and NPFF2R, respectively. ***C***, RT-PCR data of GAPDH. There is no significant difference between the control and suicidal samples. Two-way repeated-measures ANOVA: ***B***, $n = 6$/group; ***C***, $n = 5$ or 6/group. One control DHA sample was excluded for technical reasons. Statistics for all RT-PCR data were calculated using the ΔCt values. Symbols label the results of the Student-Newman-Keuls multiple comparison tests. Bar graphs represent mean ± SEM. Box (indicating the first and third quartiles) and whisker (extending to the minimum and maximum data points) plots are used for showing ΔCt data.

the two groups. The relative expression of PrRP mRNA was statistically unchanged in the NTS (Fig. 7*H*). Meanwhile, PRLHR and NPFF2R expressions in the LH and PFA were considerably downregulated exclusively in the LHe-susceptible group (Fig. 7*I*), suggesting that the development of helpless behavior could definitely be linked to the malfunction of the PrRP system in the DLH. Along with this, the expression level of pro-MCH mRNA was markedly downregulated in the LHe-resilient group, but not in the LHe-susceptible group compared with nonshocked controls (Fig. 7*J*), pointing to a possible link between PrRP signaling and MCH function.

PrRP receptor expression is downregulated in suicidal individuals

To support the potential translational relevance of our data obtained in animal models, we measured the relative mRNA expressions of PRLHR and NPFF2R in postmortem tissue samples from suicidal and control males. Samples were obtained from the lateral hypothalamic area (LHA) and dorsal hypothalamic area (DHA) (Fig. 8*A*), which correspond to the LH and PFA in rats, respectively (Krolewski et al., 2010). Both PrRP receptors were expressed in the investigated areas with a predominance of NPFF2R mRNA. We detected a remarkable downregulation of both receptors in the suicidal group (Fig. 8*B*). We note that suicidal individuals were younger than controls in case of LHA samples (Table 2); however, there was no correlation between the ages and ΔCt values of the subjects (Table 4). We also measured the expression of another housekeeping gene, GAPDH, in the samples to verify the selectivity of our results. The expression levels of GAPDH did not differ between the control and suicidal groups in any of the investigated areas (Fig. 8*C*).

Table 4. Correlation analysis data between mRNA levels of the PrRP receptors (ΔCt values) and the age of human subjects[a]

	LHA				DHA			
	PRLHR		NPFF2R		PRLHR		NPFF2R	
	Control	Suicidal	Control	Suicidal	Control	Suicidal	Control	Suicidal
Pearson's *r*	−0.704	0.580	−0.366	0.083	−0.529	0.004	0.717	0.652
p	0.119	0.220	0.476	0.875	0.280	0.994	0.108	0.160

[a]Significance was calculated with $p < 0.05$; $n = 6$.

Discussion

Our study points to the potential involvement of the PrRP system in the pathophysiology of stress-related mental disorders. We also show a link between failures of the PrRP signaling and dysregulation of the MCH system, known to be involved in the pathomechanism of depression, anxiety, and PTSD (Chaki et al., 2005; Lagos et al., 2011; Torterolo et al., 2015; Concetti et al., 2020). We find downregulation of PrRP receptors in DLH of suicidal individuals, highlighting the possible clinical relevance of our findings.

Emotional brain function is causally and bidirectionally related to sleep (Goldstein and Walker, 2014). Most antidepressants impact sleep, and SD may elicit antidepressant effects (Steiger and Pawlowski, 2019). Thus, getting a better understanding of common mechanisms that regulate both sleep and mood has a fundamental importance. PrRP applied at the beginning of the passive phase produced a brief NREMS-promoting effect against the high sleep pressure in awake rats, in concordance with Zhang et al. (2001). One limitation of our study is that we might have detected a longer-lasting effect of PrRP if it had been administered during the active phase, when sleep propensity is low. Interestingly, the increase in NREMS was accompanied by a decrease in δ power. Similar effects were observed after treatment with diazepam, a classic benzodiazepine drug that acts as a nonselective agonist on different GABA(A) receptor subtypes and has a subtype-specific spatial distribution (Rudolph et al., 2001; Kopp et al., 2004). Our data thus suggest that the effects of PrRP are mediated, at least in part, by GABA. Consistent with this, PrRP inhibited MCH neurons through a GABA(A) receptor-mediated mechanism in our experiments. In addition, PrRP also acts on GABAergic cells in the reticular nucleus of the thalamus (Lin et al., 2002).

Our *ex* and *in vivo* results suggest that PrRP inhibits MCH neurons and substantially adds to the inhibitory effect of NA on MCH neurons. This is in line with earlier data reporting the cooperation of PrRP and NA to elicit ACTH release (Maruyama et al., 2001). The release of neuropeptides during neuronal firing varies with time and depends also on the firing pattern of the

neuron (Cropper et al., 2018). Therefore, it is possible that the PrRP to NA ratio changes in the proximity of the MCH neurons depending on the actual activity of PrRP and PrRP-NA neurons. We hypothesize that PrRP may be an ideal molecule to fine-tune the activity of MCH neurons, by enabling and maintaining it within appropriate limits.

The expression of neuropeptides is dynamic, and their release is followed by *de novo* synthesis in the cell body (Hokfelt et al., 2000). We identified a PrRP cell population in the DM, in which the expression of PrRP was upregulated (suggesting release) by SD when most of the MCH neurons are usually inhibited (van den Pol et al., 2004; Blanco-Centurion et al., 2016). However, MCH neurons are critical to promote REMS, and the number of actively firing MCH cells increases over time during NREMS and peaks during REMS (Blanco-Centurion et al., 2019). The active state of MCH neurons during REMS recovery (Verret et al., 2003; Hassani et al., 2009) was associated with the downregulation of PrRP in the DM in our study. Together with the fact that ICV PrRP injection reduced the number of $cFos^+$ MCH neurons during REMS recovery, and the number of $cFos^+$ MCH neurons correlates with the number of REMS episodes (Kitka et al., 2011), it is likely that PrRP is involved in the inhibition of REMS under certain challenged conditions. Since REMS-active MCH neurons regulate hippocampus-dependent forgetting of contextual fear-related memories (Izawa et al., 2019), PrRP may influence the development of stress-related mental disorders associated with hippocampal dysfunction by modulating MCH activity (Cominski et al., 2014; Wingenfeld and Wolf, 2014). In addition, the majority of REMS-active MCH neurons are also active during exploratory behavior (Blanco-Centurion et al., 2019), which changes with anxiety (Heinz et al., 2021). Further, PrRP expression was elevated in the A1 cell group in all treatment groups in the SD experiment, suggesting a stress-related reaction on the platforms. This is in harmony with the key role of the A1 cell group in the activation of the HPA axis (Buller et al., 2001; Tóth et al., 2008) that essentially modulates sleep as well (Buckley and Schatzberg, 2005).

We postulated the involvement of PrRP in the development of repeated/chronic stress-evoked mental disorders based on different types of animal models. In the FST experiment, we activated the PrRP neurons (Dodd and Luckman, 2013) 30 min after the ICV administration of PrRP. The PrRP receptors were presumably inactivated by the time of the test, since GPCRs, like receptors of PrRP, undergo a ligand-stimulated desensitization/internalization (Luttrell and Lefkowitz, 2002; Madsen et al., 2012). This happens within several minutes *in vivo*, rendering the cell to be insensitive for hours (Scherrer et al., 2006). Indeed, the acute effects of ICV PrRP were no longer detectable than 30 min (Seal et al., 2002), and previous exposure to PrRP led to impaired running stress-stimulated ACTH release (Ohiwa et al., 2007). This experiment, therefore, directly linked previous exposure to PrRP to increased passive coping, suggesting that PrRP dysfunction may underlie the development of stress disorders.

We observed a depletion of PrRP immunoreactivity in axons innervating the DLH 24 h after LPS injection in the LPS-induced depression model (Frenois et al., 2007; Dantzer, 2009). There had been a prolonged PrRP release in the area: we detected downregulation of PrRP receptors in the DLH, and upregulation of PrRP expression (Hokfelt et al., 2000; Luttrell and Lefkowitz, 2002), while most of the medullary PrRP cells were still cFos-positive 3 h after LPS injection, indicating active firing of neurons (Barth et al., 2004). Others reported that cFos positivity of neurons in the medulla was detected up to 6 h following LPS treatment (Frenois et al., 2007). After an initial decrease, MCH immunoreactivity increased 24 h after treatment. This experiment also confirmed that impaired PrRP signaling may be associated with behavioral despair.

The role of neuroinflammation in the pathophysiology stress disorders has been highlighted recently (Echeverria et al., 2016). PrRP-NA neurons in the NTS represent the first interface between the vagus-mediated peripheral signals in the brain, as vagal afferents innervate most noradrenergic cells directly (Appleyard et al., 2007). The importance of the vagus-mediated peripheral signals is further supported by the finding that stimulation of the vagus nerve has anti-inflammatory and anti-depressant effects (Liu et al., 2020).

Using the LHe model, we designated the stress-induced PrRP overload in the DLH as one of the mechanisms potentially responsible for the susceptibility to LHe. PrRP overload could also affect the function of MCH cells. Foot shock activates the medullary PrRP neurons (Morales and Sawchenko, 2003). MCH neurons are also activated by foot shock, and inhibition of this activity causes a relapse into excessive cued fear response (freezing) for weeks (Concetti et al., 2020). Therefore, if the training-induced PrRP overactivation inhibited the optimal function of MCH cells in LHe-sensitive animals, they may have exhibited an enhanced fear response during the test.

On the other hand, acute, pretest MCH treatment increased the helpless behavior of previously shocked rats compared with nonshocked controls in the LHe paradigm (Urbanavicius et al., 2019). Chronic downregulation of MCH expression in LHe-resilient animals, therefore, may have been protective against the enhanced sensitivity to MCH in the test eliciting MCH cell activation. Importantly, PrRP receptors were not downregulated in the DLH in the LHe-resilient animals, in contrast to LHe-susceptible rats. Given the role of PrRP as a potential negative regulator of MCH cell activity, it is possible that the chronic/repeated stress-induced impairment of PrRP signaling contributes to failure of downregulation of MCH in LHe-sensitive rats. Together with MCH hypersensitivity, this may lead to a reduced ability to cope with stressful situations. Since the development of helpless behavior and symptoms in the LHe model are reminiscent of those of human depression (Wang et al., 2017), PrRP receptor downregulation found in the corresponding hypothalamic areas in suicidal individuals may have a fundamental significance. Although the etiology of suicide is complex, stress-related mental disorders underlie almost all cases, with depression being at the forefront (van Heeringen and Mann, 2014; Bryan, 2016; Bachmann, 2018).

Based on our multiple correlative data, we suggest that repeated/chronic stress leads to PrRP overload, and dysfunction of the PrRP system, consequently increasing the risk of developing stress-induced mental disorders. Dysregulation of MCH activity may also contribute to the development of these mental disorders and is likely to be associated with PrRP dysfunction in the DLH. Further work is needed to verify this hypothesis.

SNRI antidepressants are widely used to treat stress-related mental disorders, although the side effects and frequent inefficacy limit their benefits (Voineskos et al., 2020). Development of antidepressant drugs with a combined effect on monoaminergic and peptidergic systems may open new directions. Compounds targeting the GPCRs, such as PrRP receptors, are optimal for this purpose and may have a great therapeutic potential in the future (Mantas et al., 2022).

References

Appleyard SM, Marks D, Kobayashi K, Okano H, Low MJ, Andresen MC (2007) Visceral afferents directly activate catecholamine neurons in the solitary tract nucleus. J Neurosci 27:13292–13302.

Bachmann S (2018) Epidemiology of suicide and the psychiatric perspective. Int J Environ Res Public Health 15:1425.

Bandaru SS, Khanday MA, Ibrahim N, Naganuma F, Vetrivelan R (2020) Sleep–wake control by melanin-concentrating hormone (MCH) neurons: a review of recent findings. Curr Neurol Neurosci Rep 20:55.

Bao AM, Swaab DF (2019) The human hypothalamus in mood disorders: the HPA axis in the center. IBRO Rep 6:45–53.

Barth AL, Gerkin RC, Dean KL (2004) Alteration of neuronal firing properties after in vivo experience in a FosGFP transgenic mouse. J Neurosci 24:6466–6475.

Bindra D, Thompson WR (1953) An evaluation of defecation and urination as measures of fearfulness. J Comp Physiol Psychol 46:43–45.

Blanco-Centurion C, Liu M, Konadhode RP, Zhang X, Pelluru D, van den Pol AN, Shiromani PJ (2016) Optogenetic activation of melanin-concentrating hormone neurons increases non-rapid eye movement and rapid eye movement sleep during the night in rats. Eur J Neurosci 44:2846–2857.

Blanco-Centurion C, Luo S, Spergel DJ, Vidal-Ortiz A, Oprisan SA, Van den Pol AN, Liu M, Shiromani PJ (2019) Dynamic network activation of hypothalamic MCH neurons in REM sleep and exploratory behavior. J Neurosci 39:4986–4998.

Bonnavion P, Mickelsen LE, Fujita A, de Lecea L, Jackson AC (2016) Hubs and spokes of the lateral hypothalamus: cell types, circuits and behaviour. J Physiol 594:6443–6462.

Bryan CJ (2016) Treating PTSD within the context of heightened suicide risk. Curr Psychiatry Rep 18:73.

Buckley TM, Schatzberg AF (2005) On the interactions of the hypothalamic-pituitary-adrenal (HPA) axis and sleep: normal HPA axis activity and circadian rhythm, exemplary sleep disorders. J Clin Endocrinol Metab 90:3106–3114.

Buller K, Xu Y, Dayas C, Day T (2001) Dorsal and ventral medullary catecholamine cell groups contribute differentially to systemic interleukin-1beta-induced hypothalamic pituitary adrenal axis responses. Neuroendocrinology 73:129–138.

Chaki S, Funakoshi T, Hirota-Okuno S, Nishiguchi M, Shimazaki T, Iijima M, Grottick AJ, Kanuma K, Omodera K, Sekiguchi Y, Okuyama S, Tran TA, Semple G, Thomsen W (2005) Anxiolytic- and antidepressant-like profile of ATC0065 and ATC0175: nonpeptidic and orally active melanin-concentrating hormone receptor 1 antagonists. J Pharmacol Exp Ther 313:831–839.

Chen C, Dun SL, Dun NJ, Chang JK (1999) Prolactin-releasing peptide-immunoreactivity in A1 and A2 noradrenergic neurons of the rat medulla. Brain Res 822:276–279.

Chen CC, Wada K, Jarvis ED (2012) Radioactive in situ hybridization for detecting diverse gene expression patterns in tissue. J Vis Exp 62:3764.

Chung S, Parks GS, Lee C, Civelli O (2011) Recent updates on the melanin-concentrating hormone (MCH) and its receptor system: lessons from MCH1R antagonists. J Mol Neurosci 43:115–121.

Cominski TP, Jiao X, Catuzzi JE, Stewart AL, Pang KC (2014) The role of the hippocampus in avoidance learning and anxiety vulnerability. Front Behav Neurosci 8:273.

Concetti C, Bracey EF, Peleg-Raibstein D, Burdakov D (2020) Control of fear extinction by hypothalamic melanin-concentrating hormone-expressing neurons. Proc Natl Acad Sci USA 117:22514–22521.

Cropper EC, Jing J, Vilim FS, Weiss KR (2018) Peptide cotransmitters as dynamic, intrinsic modulators of network activity. Front Neural Circuits 12:78.

Dantzer R (2009) Cytokine, sickness behavior, and depression. Immunol Allergy Clin North Am 29:247–264.

Diniz GB, Bittencourt JC (2017) The melanin-concentrating hormone as an integrative peptide driving motivated behaviors. Front Syst Neurosci 11:32.

Dodd GT, Luckman SM (2013) Physiological roles of GPR10 and PrRP signaling. Front Endocrinol (Lausanne) 4:20.

Echeverria V, Grizzell JA, Barreto GE (2016) Neuroinflammation: a therapeutic target of cotinine for the treatment of psychiatric disorders? Curr Pharm Des 22:1324–1333.

Frenois F, Moreau M, O'Connor J, Lawson M, Micon C, Lestage J, Kelley KW, Dantzer R, Castanon N (2007) Lipopolysaccharide induces delayed FosB/DeltaFosB immunostaining within the mouse extended amygdala, hippocampus and hypothalamus, that parallel the expression of depressive-like behavior. Psychoneuroendocrinology 32:516–531.

Goldstein AN, Walker MP (2014) The role of sleep in emotional brain function. Annu Rev Clin Psychol 10:679–708.

Hassani OK, Lee MG, Jones BE (2009) Melanin-concentrating hormone neurons discharge in a reciprocal manner to orexin neurons across the sleep–wake cycle. Proc Natl Acad Sci USA 106:2418–2422.

Heinz DE, Schottle VA, Nemcova P, Binder FP, Ebert T, Domschke K, Wotjak CT (2021) Exploratory drive, fear, and anxiety are dissociable and independent components in foraging mice. Transl Psychiatry 11:318.

Hokfelt T, Broberger C, Xu ZQ, Sergeyev V, Ubink R, Diez M (2000) Neuropeptides: an overview. Neuropharmacology 39:1337–1356.

Ibata Y, Iijima N, Kataoka Y, Kakihara K, Tanaka M, Hosoya M, Hinuma S (2000) Morphological survey of prolactin-releasing peptide and its receptor with special reference to their functional roles in the brain. Neurosci Res 38:223–230.

Izawa S, Chowdhury S, Miyazaki T, Mukai Y, Ono D, Inoue R, Ohmura Y, Mizoguchi H, Kimura K, Yoshioka M, Terao A, Kilduff TS, Yamanaka A (2019) REM sleep-active MCH neurons are involved in forgetting hippocampus-dependent memories. Science 365:1308–1313.

Johansson A, Löfberg C (2015) Novel MCH1 receptor antagonists: a patent review. Expert Opin Ther Pat 25:193–207.

Kantor S, Jakus R, Balogh B, Benko A, Bagdy G (2004) Increased wakefulness, motor activity and decreased theta activity after blockade of the 5-HT2B receptor by the subtype-selective antagonist SB-215505. Br J Pharmacol 142:1332–1342.

Kitka T, Katai Z, Pap D, Molnar E, Adori C, Bagdy G (2009) Small platform sleep deprivation selectively increases the average duration of rapid eye movement sleep episodes during sleep rebound. Behav Brain Res 205:482–487.

Kitka T, Adori C, Katai Z, Vas S, Molnar E, Papp RS, Toth ZE, Bagdy G (2011) Association between the activation of MCH and orexin immunorective neurons and REM sleep architecture during REM rebound after a three day long REM deprivation. Neurochem Int 59:686–694.

Kopp C, Rudolph U, Tobler I (2004) Sleep EEG changes after zolpidem in mice. Neuroreport 15:2299–2302.

Krolewski DM, Medina A, Kerman IA, Bernard R, Burke S, Thompson RC, Bunney WE Jr, Schatzberg AF, Myers RM, Akil H, Jones EG, Watson SJ (2010) Expression patterns of corticotropin-releasing factor, arginine vasopressin, histidine decarboxylase, melanin-concentrating hormone, and orexin genes in the human hypothalamus. J Comp Neurol 518:4591–4611.

Lagos P, Urbanavicius J, Scorza MC, Miraballes R, Torterolo P (2011) Depressive-like profile induced by MCH microinjections into the dorsal raphe nucleus evaluated in the forced swim test. Behav Brain Res 218:259–266.

Lin SH, Arai AC, España RA, Berridge CW, Leslie FM, Huguenard JR, Vergnes M, Civelli O (2002) Prolactin-releasing peptide (PrRP) promotes awakening and suppresses absence seizures. Neuroscience 114:229–238.

Liu CH, Yang MH, Zhang GZ, Wang XX, Li B, Li M, Woelfer M, Walter M, Wang L (2020) Neural networks and the anti-inflammatory effect of transcutaneous auricular vagus nerve stimulation in depression. J Neuroinflammation 17:54.

Luttrell LM, Lefkowitz RJ (2002) The role of beta-arrestins in the termination and transduction of G-protein-coupled receptor signals. J Cell Sci 115:455–465.

Ma L, MacTavish D, Simonin F, Bourguignon JJ, Watanabe T, Jhamandas JH (2009) Prolactin-releasing peptide effects in the rat brain are mediated through the Neuropeptide FF receptor. Eur J Neurosci 30:1585–1593.

Machado RB, Hipólide DC, Benedito-Silva AA, Tufik S (2004) Sleep deprivation induced by the modified multiple platform technique: quantification of sleep loss and recovery. Brain Res 1004:45–51.

Madsen KL, Thorsen TS, Rahbek-Clemmensen T, Eriksen J, Gether U (2012) Protein interacting with C kinase 1 (PICK1) reduces reinsertion rates of interaction partners sorted to Rab11-dependent slow recycling pathway. J Biol Chem 287:12293–12308.

Mai JK, Majtanik M, Paxinos G (2015) Atlas of the human brain, Ed 4. Amsterdam: Elsevier Science.

Maloney KJ, Mainville L, Jones BE (1999) Differential c-Fos expression in cholinergic, monoaminergic, and GABAergic cell groups of the pontomesencephalic tegmentum after paradoxical sleep deprivation and recovery. J Neurosci 19:3057–3072.

Mantas I, Saarinen M, Xu ZD, Svenningsson P (2022) Update on GPCR-based targets for the development of novel antidepressants. Mol Psychiatry 27:534–558.

Marques DB, Ruggiero RN, Bueno-Junior LS, Rossignoli MT, Leite JP (2022) Prediction of learned resistance or helplessness by hippocampal-prefrontal cortical network activity during stress. J Neurosci 42:81–96.

Maruyama M, Matsumoto H, Fujiwara K, Noguchi J, Kitada C, Fujino M, Inoue K (2001) Prolactin-releasing peptide as a novel stress mediator in the central nervous system. Endocrinology 142:2032–2038.

McCloy RA, Rogers S, Caldon CE, Lorca T, Castro A, Burgess A (2014) Partial inhibition of Cdk1 in G2 phase overrides the SAC and decouples mitotic events. Cell Cycle 13:1400–1412.

Mera T, Fujihara H, Kawasaki M, Hashimoto H, Saito T, Shibata M, Saito J, Oka T, Tsuji S, Onaka T, Ueta Y (2006) Prolactin-releasing peptide is a potent mediator of stress responses in the brain through the hypothalamic paraventricular nucleus. Neuroscience 141:1069–1086.

Mlynarik M, Zelena D, Bagdy G, Makara GB, Jezova D (2007) Signs of attenuated depression-like behavior in vasopressin deficient Brattleboro rats. Horm Behav 51:395–405.

Morales T, Sawchenko PE (2003) Brainstem prolactin-releasing peptide neurons are sensitive to stress and lactation. Neuroscience 121:771–778.

Ohiwa N, Chang H, Saito T, Onaka T, Fujikawa T, Soya H (2007) Possible inhibitory role of prolactin-releasing peptide for ACTH release associated with running stress. Am J Physiol Regul Integr Comp Physiol 292:R497–R504.

Otrokocsi L, Kittel Á, Sperlágh B (2017) P2X7 receptors drive spine synapse plasticity in the learned helplessness model of depression. Int J Neuropsychopharmacol 20:813–822.

Pacak K, Palkovits M, Kopin IJ, Goldstein DS (1995) Stress-induced norepinephrine release in the hypothalamic paraventricular nucleus and pituitary-adrenocortical and sympathoadrenal activity: in vivo microdialysis studies. Front Neuroendocrinol 16:89–150.

Palkovits M (1973) Isolated removal of hypothalamic or other brain nuclei of the rat. Brain Res 59:449–450.

Paxinos G, Watson C (2007) The rat brain in stereotaxic coordinates, Ed 6. Amsterdam: Elsevier.

Porsolt RD, Anton G, Blavet N, Jalfre M (1978) Behavioural despair in rats: a new model sensitive to antidepressant treatments. Eur J Pharmacol 47:379–391.

Risold PY, Croizier S, Legagneux K, Brischoux F, Fellmann D, Griffond B (2009) The development of the MCH system. Peptides 30:1969–1972.

Rudolph U, Crestani F, Möhler H (2001) GABA(A) receptor subtypes: dissecting their pharmacological functions. Trends Pharmacol Sci 22:188–194.

Scherrer G, Tryoen-Tóth P, Filliol D, Matifas A, Laustriat D, Cao YQ, Basbaum AI, Dierich A, Vonesh JL, Gavériaux-Ruff C, Kieffer BL (2006) Knockin mice expressing fluorescent delta-opioid receptors uncover G protein-coupled receptor dynamics in vivo. Proc Natl Acad Sci USA 103:9691–9696.

Seal LJ, Small CJ, Dhillo WS, Kennedy AR, Ghatei MA, Bloom SR (2002) Prolactin-releasing peptide releases corticotropin-releasing hormone and increases plasma adrenocorticotropin via the paraventricular nucleus of the hypothalamus. Neuroendocrinology 76:70–78.

Slattery DA, Cryan JF (2012) Using the rat forced swim test to assess antidepressant-like activity in rodents. Nat Protoc 7:1009–1014.

Smith DG, Davis RJ, Rorick-Kehn L, Morin M, Witkin JM, McKinzie DL, Nomikos GG, Gehlert DR (2006) Melanin-concentrating hormone-1 receptor modulates neuroendocrine, behavioral, and corticolimbic neurochemical stress responses in mice. Neuropsychopharmacology 31:1135–1145.

Smoller JW (2016) The genetics of stress-related disorders: PTSD, depression, and anxiety disorders. Neuropsychopharmacology 41:297–319.

Steiger A, Pawlowski M (2019) Depression and sleep. Int J Mol Sci 20:607.

Torterolo P, Scorza C, Lagos P, Urbanavicius J, Benedetto L, Pascovich C, López-Hill X, Chase MH, Monti JM (2015) Melanin-concentrating hormone (MCH): role in REM sleep and depression. Front Neurosci 9:475.

Tóth ZE, Mezey E (2007) Simultaneous visualization of multiple antigens with tyramide signal amplification using antibodies from the same species. J Histochem Cytochem 55:545–554.

Tóth ZE, Zelena D, Mergl Z, Kirilly E, Várnai P, Mezey E, Makara GB, Palkovits M (2008) Chronic repeated restraint stress increases prolactin-releasing peptide/tyrosine-hydroxylase ratio with gender-related differences in the rat brain. J Neurochem 104:653–666.

Urbanavicius J, Fabius S, Roncalho A, Joca S, Torterolo P, Scorza C (2019) Melanin-concentrating hormone in the locus coeruleus aggravates helpless behavior in stressed rats. Behav Brain Res 374:112120.

van Dalfsen JH, Markus CR (2018) The influence of sleep on human hypothalamic-pituitary-adrenal (HPA) axis reactivity: a systematic review. Sleep Med Rev 39:187–194.

van den Pol AN, Acuna-Goycolea C, Clark KR, Ghosh PK (2004) Physiological properties of hypothalamic MCH neurons identified with selective expression of reporter gene after recombinant virus infection. Neuron 42:635–652.

van Heeringen K, Mann JJ (2014) The neurobiology of suicide. Lancet Psychiatry 1:63–72.

Vas S, Ádori C, Könczöl K, Kátai Z, Pap D, Papp RS, Bagdy G, Palkovits M, Tóth ZE (2013) Nesfatin-1/NUCB2 as a potential new element of sleep regulation in rats. PLoS One 8:e59809.

Verret L, Goutagny R, Fort P, Cagnon L, Salvert D, Léger L, Boissard R, Salin P, Peyron C, Luppi PH (2003) A role of melanin-concentrating hormone producing neurons in the central regulation of paradoxical sleep. BMC Neurosci 4:19.

Voineskos D, Daskalakis ZJ, Blumberger DM (2020) Management of treatment-resistant depression: challenges and strategies. Neuropsychiatr Dis Treat 16:221–234.

Wang Q, Timberlake MA 2nd, Prall K, Dwivedi Y (2017) The recent progress in animal models of depression. Prog Neuropsychopharmacol Biol Psychiatry 77:99–109.

Wingenfeld K, Wolf OT (2014) Stress, memory, and the hippocampus. Front Neurol Neurosci 34:109–120.

Wittmann G, Mohácsik P, Balkhi MY, Gereben B, Lechan RM (2015) Endotoxin-induced inflammation down-regulates L-type amino acid transporter 1 (LAT1) expression at the blood-brain barrier of male rats and mice. Fluids Barriers CNS 12:21.

Yoshida M, Takayanagi Y, Onaka T (2014) The medial amygdala-medullary PrRP-synthesizing neuron pathway mediates neuroendocrine responses to contextual conditioned fear in male rodents. Endocrinology 155:2996–3004.

Zelena D, Mergl Z, Foldes A, Kovács KJ, Tóth Z, Makara GB (2003) Role of hypothalamic inputs in maintaining pituitary-adrenal responsiveness in repeated restraint. Am J Physiol Endocrinol Metab 285:E1110–E1117.

Zhang SQ, Inoué S, Kimura M (2001) Sleep-promoting activity of prolactin-releasing peptide (PrRP) in the rat. Neuroreport 12:3173–3176.

AKOYA BIOSCIENCES®

Opal Multiplex IHC Assay Development Guide and Image Acquisition Information

Phenoptics Research Solutions

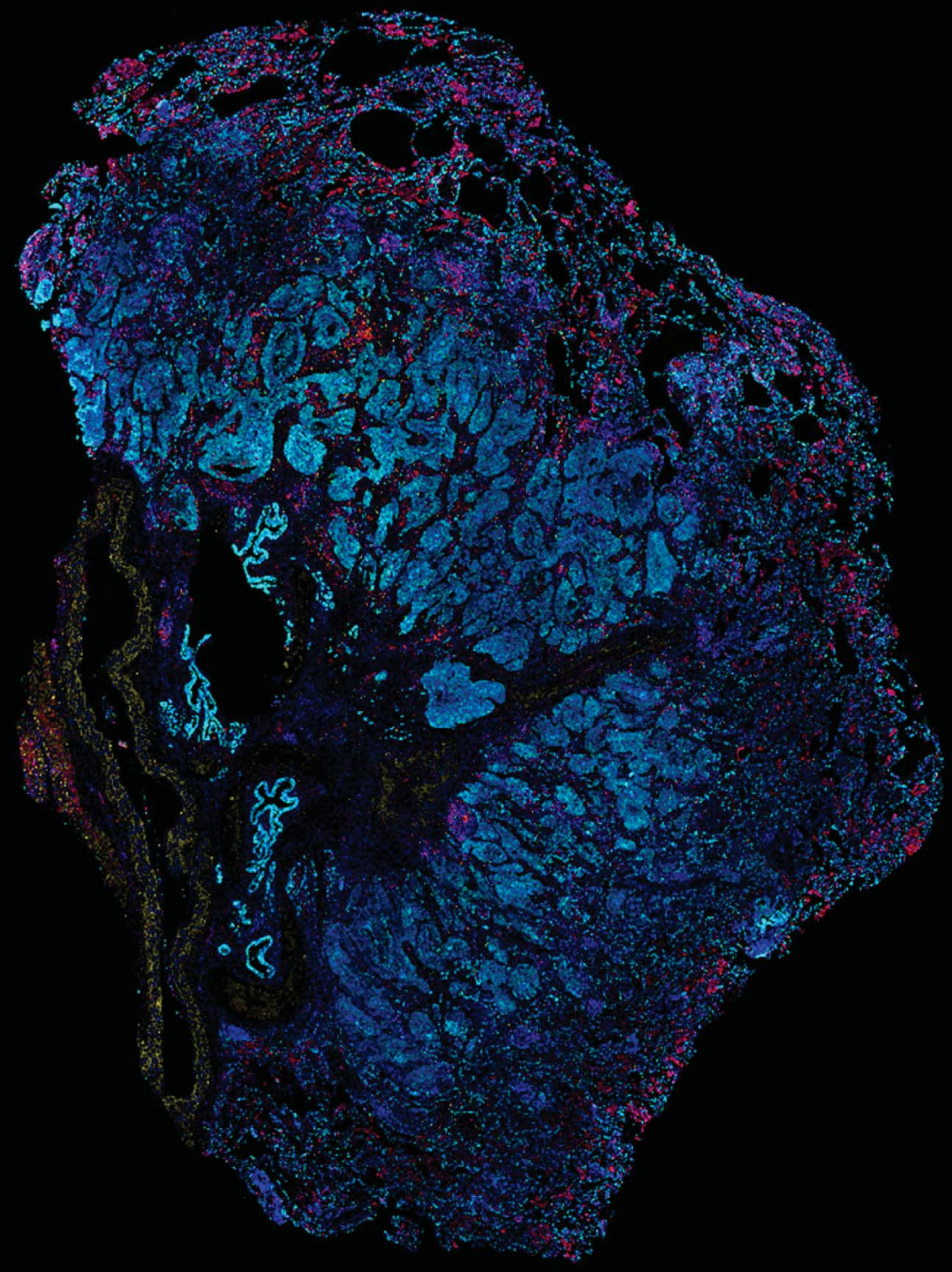

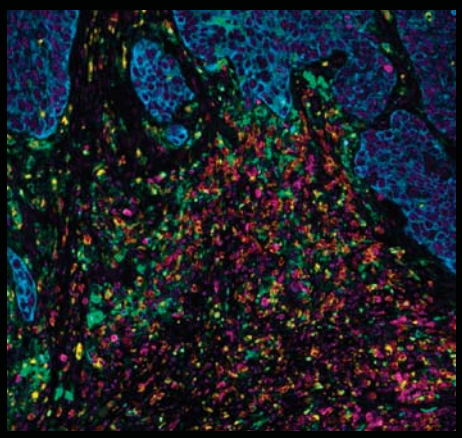

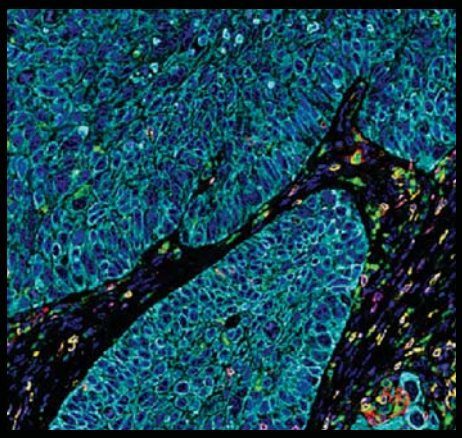

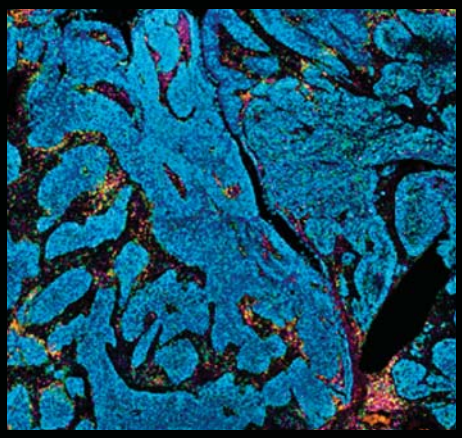

Preface

Welcome to the world of Phenoptics and Opal reagents!

This guide will act as your reference for all things pertaining to our Opal product line, including assay development and optimization using both manual and automated techniques, product notes for each imaging system, an image analysis guide, and frequently asked questions/ troubleshooting. The goal of this document is to act as a starting point for new Opal users to help guide them in their set-up of their first panel, and to assist veteran Opal users with integration of the new Opal Polaris 480 and 780 fluorophores.

We are continually updating our Opal staining methodology, as well as adding exciting new reagent platforms to help improve the Phenoptics workflow while simultaneously extending its performance capabilities. As such, please be advised that this is a living document that will be continually updated with new insights and information. We recommend that you regularly check our website for updates.

We strongly advise all research laboratories who are integrating Opal into their multiplex IHC workflow to consider utilizing the information provided in this guide to become confident in Opal immunohistochemistry assay development, fluorescence imaging using the Vectra or Mantra platforms, and image analysis using inForm, Visiopharm, or HALO.

As always, if you have any issues or concerns during the Opal optimization process, please do not hesitate to reach out to us at **support@akoyabio.com** so we may assist you.

Happy staining!

Phenoptics 2.0 – An Overview

What is Phenoptics? Akoya's Phenoptics workflow enables imaging and analysis of up to eight immunofluorescent markers plus DAPI within intact tissue sections. Quantitative analysis of multiple cellular phenotypes and cell-to-cell interactions can be observed within their native spatial constructs, a feat that can be extremely difficult to observe by other imaging modalities. The complete Phenoptics workflow incorporates three aspects: Opal reagents, image acquisition hardware, and tissue analysis software (Figure 1).

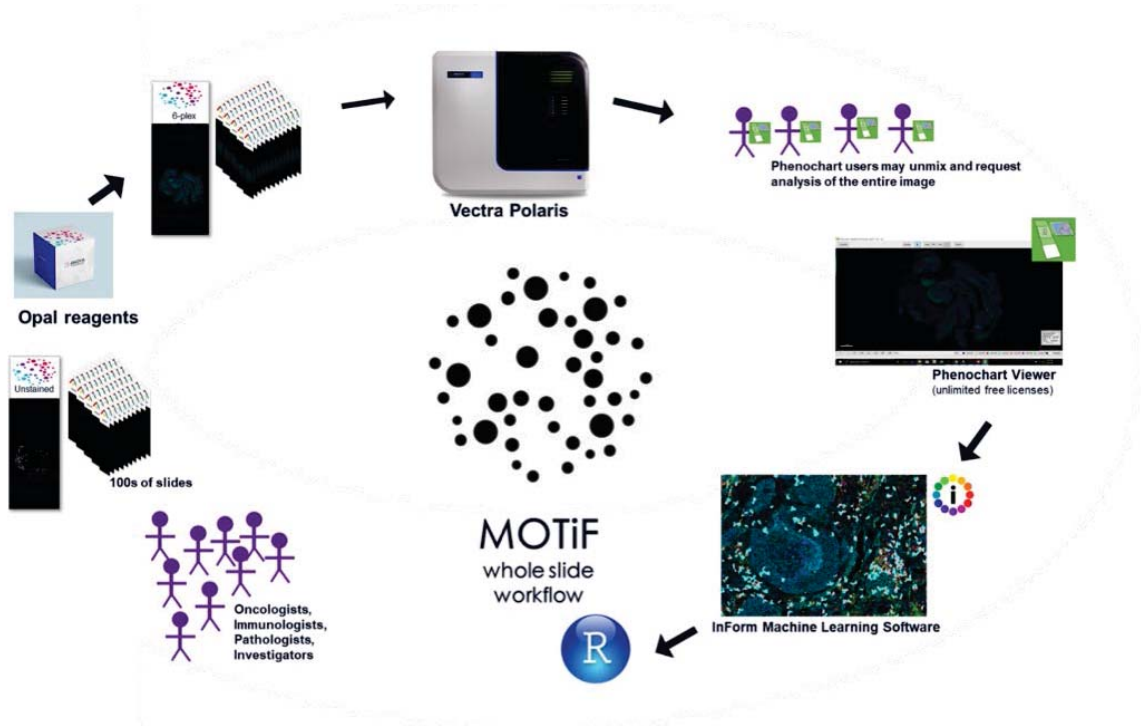

FIGURE 1. MOTiF Whole Slide Workflow. Our MOTiF™ technology generates unmixed whole slide scans of up to 7-colors in less than 10 minutes. Images captured using our MOTiF technology allow for files to be annotated in Phenochart and directly opened in inForm for quantitative analysis.

Opal Assay Kits and Reagents

Opal allows for the use of any standard unlabeled primary antibody, including multiple antibodies raised in the same species. The Opal polymer HRP is applied after, using Tyramide Signal Amplification (TSA) to amplify IHC detection by covalently depositing fluorescent molecules in close vicinity to that targeted antigen. After labeling is complete, antibodies are removed in a manner that does not disrupt the Opal fluorescence signal, allowing for the next target to be detected without antibody

References

1. Toth, Zsuzsanna E., and Eva Mezey. "Simultaneous visualization of multiple antigens with tyramide signal amplification using antibodies from the same species." Journal of Histochemistry & Cytochemistry 55.6 (2007): 545-554. (http://jhc.sagepub.com/ content/55/6/545.short)
2. Stack, Edward C., Chichung Wang, Kristin A. Roman, and Clifford C. Hoyt. "Multiplexed immunohistochemistry, imaging, and quantitation: A review, with an assessment of Tyramide signal amplification, multispectral imaging and multiplex analysis." Methods70, no. 1 (2014): 46-58. (http://www.sciencedirect.com/ science/article/pii/S1046202314002837)
3. Uhlén, Mathias, et al. "Tissue-based map of the human proteome." Science 347.6220 (2015): 1260419. (http://www.proteinatlas.org/)
4. GeneCards®: The Human Gene Database (http://www.genecards.org)

Additional Resources

Please visit www.akoyabio.com/support for additional resources, including FAQs and publications.

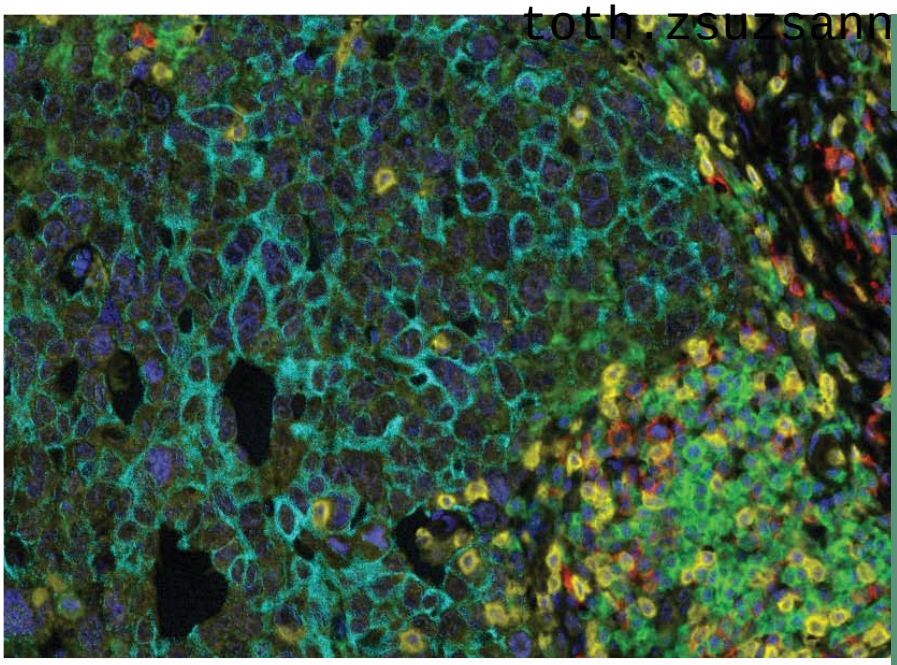

Pseudo-color composite of a breast cancer section, labeled for killer T cells (CD8, yellow), helper T cells (CD4, green), B cells (CD20, red), epithelial cells (cytokeratin, aqua) and DAPI (blue).

APPLICATION NOTE

Multiplex Biomarker Imaging

Highlights

- Immune response revealed through the characterization of infiltrating and stromal lymphocytes in FFPE tissue
- Opal™ multiplex staining using unlabeled primary antibodies from the same species and TSA Plus signal amplification
- Rapid automated analysis of whole sections using Vectra
- Quantitative results from breast cancer T and B cell panel (CD4, CD8, CD20, cytokeratin, DAPI) using inForm

Cancer Immunology: Capturing Immune Status in FFPE Sections

Introduction

Recent successes with experimental drugs targeting PD-L1 and PD-1, and adoptive immunotherapy are two examples of the tremendous potential to leverage the host's immune system to fight cancer. However, interactions between host cells, invading tumor cells and immune cells are quite complex, and are not adequately characterized by conventional single-stain immunohistochemical staining of tissue sections or by flow cytometry of disaggregated fresh tissues. In particular inflammatory cells can operate in conflicting ways, with both tumor-supporting and tumor-killing subclasses. The balance between the conflicting inflammatory responses in tumors is likely to prove instrumental in prognosis and, quite possibly, in therapies[1]. Capturing the spatial arrangements of immune, normal and malignant cells in intact tissue sections, to accurately characterize immune status, is made possible with highly multiplexed immunofluorescence labeling and multispectral imaging, offering opportunities for new assays to guide immunotherapy approach, and to monitor response. This application note describes recent advances towards an integrated approach combining highly multiplexed labeling (up to 10 labels), automated staining, imaging-based analysis to capture expression and contextual information, and data mining.

PerkinElmer
For the Better

Multiplexed staining is accomplished by use of the Opal method. Opal is based on a method published by Tóth and Mezey[2] and involves use of tyramide signal amplification (TSA) for covalent deposition of fluorophores followed by microwave treatment (MWT) to remove primary and secondary antibodies. Labels are added sequentially using a repetitive process that is simple relative to typical multicolor immunohistochemical methods. This approach allows use of any number of unlabeled primary antibodies from the same species in multiplexed assays. Labeling is specific, robust and balanced and the workflow is amenable to routine implementation.

In this study, the capability is demonstrated on control samples (tonsil) and a cohort of clinical breast cancer samples, by comparing automated and visual assessments, to perform a method proof-of-concept. However, this general methodology is extendible to a whole range of markers (up to 10 in a panel) and can combine both immune markers and other cancer, cell signaling or tumor-microenvironment markers.

Methods

A multiplexed assay for tumor-inflitrating lymphocytes for breast cancer was tested and validated on de-identified excess clinical samples, including a tonsil sample for method development, and applied to four de-identified breast cancer samples from the University of Pennsylvania Hospital. The Opal staining method involves serial application of TSA-amplified immunofluorescence labels for CD4, CD8, CD20, cytokeratin, and a DAPI counterstain. Prior to immunofluorescence labeling, all four antigens are retrieved with a single microwave step. Each labeling cycle (shown in Figure 1) consists of application of a primary antibody, a secondary antibody conjugated to horse radish peroxidase (HRP), and TSA conjugated to a fluorophore. After each TSA-fluorophore conjugate is applied, the sample is processed with the microwave again to strip primary and secondary antibodies, leaving TSA-fluorophore constructs which are covalently bound and very resilient to microwave exposure.

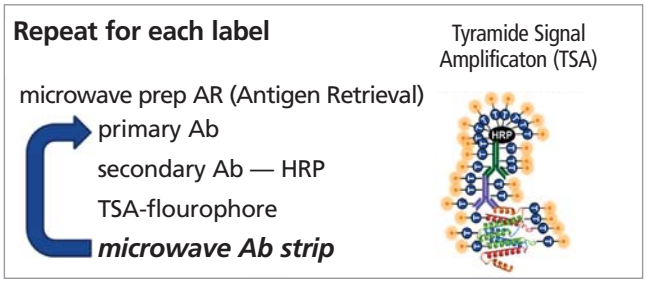

Figure 1. Same-species serial TSA immunofluorescence labeling

The fluorophores used are shown in Table 1. Because antibodies are stripped with each cycle, species interference issues are avoided, and all antibodies can be of the same species (e.g., rabbit-monoclonal antibodies), as is the case in this assay. Detailed staining protocols are available upon request.

Image acquisition and analysis

- Samples were imaged using the Vectra® multispectral slide analysis system from PerkinElmer to automatically acquire 25 fields of interest per slide. The automated workflow consists of a 4x survey of the entire slide involving the capture of a whole-slide 4x image, automated pattern recognition detection of tumor areas, and a sampling algorithm to select the 25 20x fields for multispectral imaging and analysis only from areas of interest on the sample.
- The multispectral images were analyzed using inForm® Tissue Finder™ pattern recognition software from PerkinElmer to:
  - spectrally unmix the DAPI, CD4, CD8, CD20, and cytokeratin signals and remove tissue autofluorescence;
  - segment tissue into regions of tumor and stroma;
  - and phenotype cells into categories of cancer cells, killer T cells, helper T cells, and B cells.
- Cell phenotype maps were produced from the cell segmentation data retaining spatial arrangements.
- All imagery was then carefully assessed by a pathologist for segmentation and cell phenotyping accuracy, and for distinguishing inter- versus intra-epithelial cells.

Table 1. Label-fluorophore conjugation

Marker	Cell Type	Fluorophore
CD4	Helper T cell	Fluorescein
CD8	Killer T cell	Cyanine 3
CD20	B cell	Cyanine 5
Cytokeratin	Epithelial cell	Coumarin
Counterstain	Nuclei	DAPI

Imagery and data of tonsil samples used in assay development and optimization are shown in Figures 2 and 3.

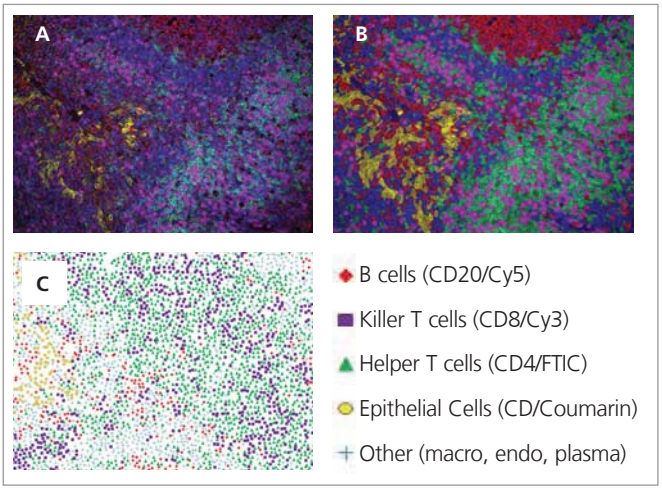

Figure 2. (A)Unmixed composite of a multispectral image from a tonsil biopsy section. (B) Image with inForm automated segmentation finding B cells (CD20+) in red, Killer T cells (CD8+) in purple, Helper T cells (CD4+) in green, Epithelial cells (CK) in yellow, and other cells in blue. (C) A cell phenotype map created from the spatial information obtained in the segmentation data.

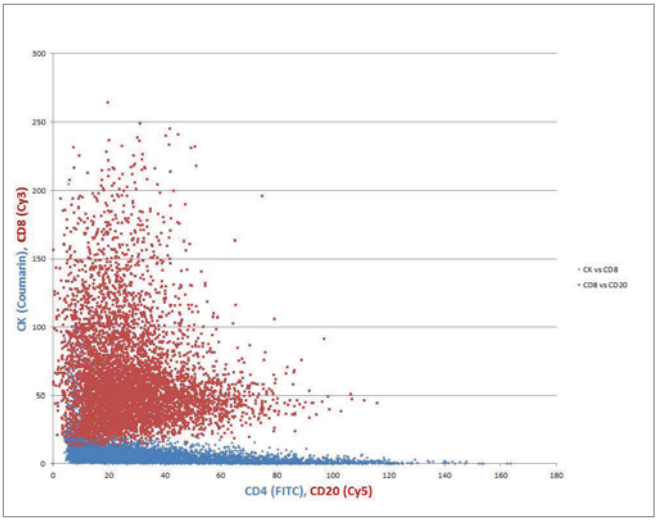

Figure 3. Per-cell expression levels from tonsil biopsy analysis plotting CK vs CD8 and CD4 vs CD20.

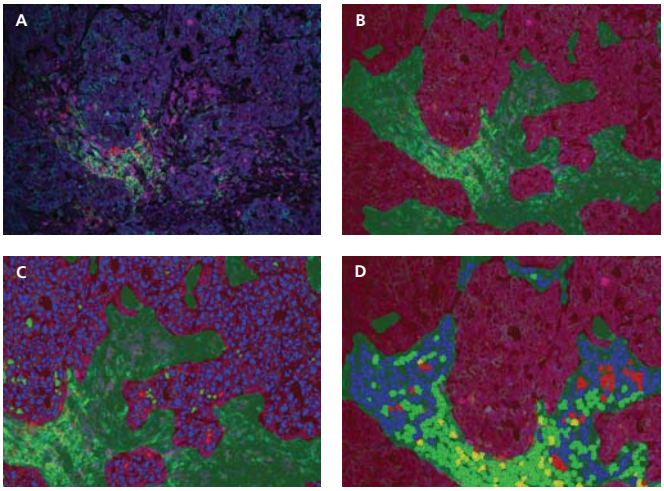

Figure 4. Example 20x field from one of the four breast cancer samples. (A) Unmixed composite image from multispectral data separating CD4, CD8, CD20, cytokeratin, and DAPI from each other and from autofluorescence. (B) Image after inForm analysis with automated tissue segmentation separating tumor (in red) from stroma (in green), (C) tumor cells segmented and scored with CD8+ only cells shown in red, CD4+ only cells shown in green, cells double positive for both CD8 and CD4 shown in yellow, and double negative cells in blue, and (D) same as in (C) but for cells in stroma regions.

Table 2. Results from image analysis of breast cancer imagery

Killer T cells (CD8+)		
Case #	% in tumor	Density (/sq mm)
#21	8.1%	574
#22	0.6%	31
#23	1.7%	99
#24	6.1%	482
Helper T cells (CD4+)		
Case #	% in tumor	Density (/sq mm)
#21	0.9%	67
#22	0.0%	0
#23	0.4%	25
#24	0.0%	10

Results

Labeling of tonsil samples demonstrated specificity and sensitivity estimated by a pathologist to be greater than 95% accurate (Example 20x field shown in Figure 4). On breast cancer samples, comparable accuracy was achieved. More importantly however, in the breast cancer samples, distinguishing inter- and intra-epithelial immune cells was estimated to be nearly perfect, despite significant inflammation in non-epithelial areas immediately adjacent to tumor, in some samples. Tumor T cell, killer/CD8 and helper/CD4 densities are shown in Table 2.

Conclusions

The approach shows reliable detection of phenotypes and accurate segmentation of tumor and stromal regions, to accurately assess how immune cells are interacting with the tumor mass, such as tumor infiltration to combat the cancer. These results support the feasibility of a practical and viable clinical workflow, in which immune response assessment is automated by computer and results are reviewed by pathologists to assure data quality.

The methodology shown in this example can be extended to a whole range of immune cell and other cancer markers and can be expanded to up to eight or nine fluorophores. In the field of cancer immunology in particular this is of great importance in exploring the role of immune cells in the tumor microenvironment.

References

[1] Hanahan, D. & Weinberg, R.A. Hallmarks of cancer: the next generation. Cell 144, 646-674 (2011).

[2] Toth, Z. E., & Mezey, E. Simultaneous visualization of multiple antigens with tyramide signal amplification using antibodies from the same species. Journal of Histochemistry & Cytochemistry, 55(6), 545-554 (2007).

PerkinElmer, Inc.
940 Winter Street
Waltham, MA 02451 USA
P: (800) 762-4000 or
(+1) 203-925-4602
www.perkinelmer.com

PerkinElmer®

011313B_01 PKI

Manual

Multiplex IHC

Research Use Only. Not for use in diagnostic procedures.

Opal™ 4-Color Manual IHC Kit 50 slides
Opal™ 7-Color Manual IHC Kit 50 slides

Product Information

Storage	Store dry Opal reagent at -20 ºC. Upon reconstituting in DMSO, store at 2–8ºC. Store remaining kit components at 2–8ºC
Stability	See kit label on outside of box for expiration date
Application	The Opal 4 or 7-Color Manual IHC Kits are intended for multiplex fluorescent IHC.
Safety Note	DMSO is classified as hazardous and combustible. Some reagents in this kit contain Proclin® 300 that is classified as corrosive to metals and skin, a skin and eye irritant, and hazardous to the aquatic environment. DAPI is considered corrosive to the skin and an irritant to the eye. All other reagents are classified as nonhazardous. It is strongly recommended to wear disposable gloves and safety glasses while working with the items in this kit. Thorough washing of hands after handling is also recommended.
Quality Control	We certify that QC results of these reagents meet our quality release criteria.
Slide Number	When using this kit's recommended TSA dilution of 1:100, it will enable a 4- or 7-color assay on 50 slides.

What is the Opal Method?

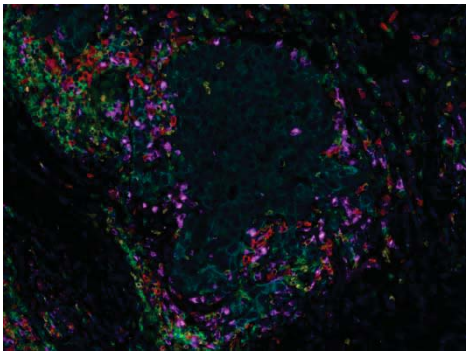

Human breast cancer tissue was stained with CD4, CD8, CD20, FoxP3, CD68, and PanCK using the Opal 7-color Automation Kit on a BOND RX automated IHC & ISH stainer. Image was captured using the Vectra 3.0 automated quantitative pathology imaging system and image analysis was performed using inForm software.

The Opal workflow allows simultaneous detection of multiple biomarkers in tissue. This Opal protocol was written specifically for a 4 or 7-Color IHC in formalin-fixed paraffin-embedded (FFPE) tissue*. The approach involves detection with Opal reactive fluorophores, followed by microwave treatment (MWT) for: removal of primary and secondary antibodies[1]; removal of any non-specific staining; and reduction of tissue auto-fluorescence. The Opal signal is largely unaffected by MWT and antibody removal. After MWT, another round of staining can be performed for additional target detection without risk of antibody cross reactivity.

Opal allows staining of multiple IHC targets using unlabeled primary antibodies raised in the same species[2]. Combining Opal with multispectral imaging and analysis enables simultaneous, quantitative results for up to 6 biomarkers in fluorescence, even with co-localized markers, plus nuclear counterstain (DAPI). **Fluorescent multispectral imaging (usually with the Mantra™ or Vectra® systems) is required for successful analysis of more than 4 Opal fluorophores at once.**

***Please contact us if you would like to work with other types of samples. PerkinElmer provides assistance with assay development and offers multiplex Opal IHC and IF services. Visit: www.perkinelmer.com/Opal.**

Rinse slides in the appropriate AR buffer.

Step 7: Microwave treatment
Place slides in an Opal Slide Processing Jar and fill it completely with the appropriate AR buffer. Loosely cover the jar with lid, place it in microwave for 45 sec at 100% power; may require optimization as described).Microwave for an additional 15 mins at 20% power. Allow slides to cool down at room temperature before proceeding (15 – 30 min). Importantly, do not let slides dry out. Rinse slides in distilled water followed by TBST.

This microwave step strips the primary-secondary-HRP complex allowing introduction of the next primary antibody. For detection of the next target, restart the protocol at Step 3: Blocking.

If all targets have been detected, continue to Step 8.

Step 8: Counterstain and Mount
Apply DAPI Working Solution for 5 min at room temperature in a humidity chamber. Wash the slides for 2 min in TBST buffer and then for 2 min in water. Coverslip slides with mounting medium (i.e. ProLong® Diamond Antifade Mountant (Thermofisher)).. *(Note: do not counterstain monoplex slides to be used for spectral library development.)*

Imaging and Analysis

Visualization of 7-color Opal slides can be performed using Mantra or Vectra Quantitative Pathology Imaging Systems. The systems use multispectral imaging for quantitative unmixing of many fluorophores and tissue autofluorescence, enabling advanced analysis including *in situ* cellular phenotyping. For more information, please see: http://www.perkinelmer.com/quantitative-pathology.

Important Notes:

1. All standard Vectra or Mantra epi-fluorescent cubes should be used for imaging Opal slides: DAPI, FITC, CY3, Texas Red, and CY5.
2. If the Opal fluorophores are not found in the Stain Store Manager in your version of inForm, please visit http://www.perkinelmer.com/resources/software-downloads.xhtml to download the latest inForm update that contains the novel Opal stains. If you believe that you have the latest version of inForm and you still cannot find the stains in the store manager, please contact your Field Application Specialist.

References

[1] Toth, Zsuzsanna E., and Eva Mezey. "Simultaneous visualization of multiple antigens with tyramide signal amplification using antibodies from the same species." *Journal of Histochemistry & Cytochemistry* 55.6 (2007): 545-554

[2] Stack, E.C., Wang, C., Roman, K., and Hoyt, C.C. “Multiplexed immunohistochemistry, imaging, and quantitation: a review, with an assessment of Tyramide signal amplification, multispectral imaging and multiplex analysis.” *Methods*: (2014) doi:10.1016/j.ymeth.2014.08.016.